Structure and function of the chikungunya virus nsP3 protein and implication in alphavirus biology

Vasiliya Kril

Université Paris Cité

École doctorale **Hématologie, Oncogenèse et Biothérapies** (ED 561)

Génomes, biologie cellulaire et thérapeutique (UMR 7212 / U 944)

Équipe **Biologie des Virus Émergents**

Structure and function of the chikungunya virus nsP3 protein and implication in alphavirus biology

Par **Vasiliya KRIL**

Thèse de doctorat de **Biothérapies et Biotechnologies**

Dirigée par **Ali AMARA**

Présentée et soutenue **publiquement**

le 08/12/2023

Devant un jury composé de :

Caroline GOUJON, CR-HDR, Université de Montpellier	Rapportrice
Yves GAUDIN, DR, Université Paris-Saclay	Rapporteur
Nolwenn JOUVENET, DR, Université Paris Cité	Examinatrice
Félix REY, DR, Université Paris Cité	Examinateur
Laurence BRIANT, DR, Université de Montpellier	Examinatrice
Juan REGUERA, DR, Université Aix-Marseille	Membre invité
Ali AMARA, DR, Université Paris Cité	Directeur de thèse

Index

INDEX **2**
ACKNOWLEDGMENTS **6**
SUMMARY **10**
RESUME **12**
FIGURES INDEX **14**
ABBREVIATIONS **18**
INTRODUCTION **21**
CHAPTER I. ARBOVIRUSES **22**

A. EMERGING VIRUSES 22
B. FOCUS ON EMERGING ARBOVIRUSES 24

CHAPTER II. ALPHAVIRUSES **26**

A. PHYLOGENY AND GEOGRAPHICAL DISTRIBUTION 26
B. TRANSMISSION CYCLE 28
C. ARTHRITOGENIC ALPHAVIRUSES 29

CHAPTER III: CHIKUNGUNYA DISEASE **31**

A. CHIKUNGUNYA VIRUS, A RE-EMERGING HUMAN PATHOGEN OF GLOBAL HEALTH CONCERN 31
1. Discovery *31*
2. Transmission cycles and Epidemiology *32*
3. Mechanisms of re-emergence *33*
B. PHYSIOPATHOLOGY AND IMMUNOLOGY 36
1. Acute disease *36*
2. Chronic disease *37*
3. Immunological aspects of CHIKV disease *38*
C. A KEY ROLE OF THE MUSCULOSKELETAL TISSUE IN CHIKV PATHOGENESIS 40
D. CURRENT STRATEGIES TO FIGHT CHIKV INFECTION 42
1. Vector control *42*
2. Vaccine development *43*
3. Therapeutic strategies *44*
4. Antiviral strategy *45*

CHAPTER IV: CHIKUNGUNYA VIRUS LIFE CYCLE **46**

A. CHIKUNGUNYA VIRUS STRUCTURE AND GENOME ORGANIZATION 46
B. CHIKV LIFE CYCLE 48
1. CHIKV entry into target cells *49*
i Receptor-mediated entry 49
ii Endocytosis and fusion 50
2. Viral replication *51*

3. Structural proteins synthesis, viral assembly and egress 52
i Structural proteins synthesis 52
ii RNA packaging and nucleocapsid formation 54
iii Virion assembly and budding 55

CHAPTER V: ROLE OF THE CHIKV NON-STRUCTURAL PROTEINS IN VIRAL REPLICATION AND INHIBITION OF HOST IMMUNE RESPONSES 57

A. CHIKV NON-STRUCTURAL PROTEINS 57
B. NSP PROCESSING AND MATURATION OF THE REPLICASE COMPLEX 57
C. CHIKV NSP AND HOST CELLULAR RESPONSE TO VIRAL INFECTION 60
1. Inhibition of host cell transcription 60
2. Counteracting antiviral immunity 61
3. Host cell translational shutoff 62

CHAPTER VI: ARCHITECTURE OF CHIKV REPLICATION COMPLEX 63

A. RNA VIRUSES REARRANGE CELLULAR MEMBRANES TO FORM REPLICATIVE ORGANELLES 63
B. CHIKUNGUNYA VIRUS SPHERULES 65
1. Minimal replicase complex required for spherule formation 65
2. nsP1 dodecameric-ring gate the entry of CHIKV spherules 66
3. Cryo-EM structure of CHIKV replicative spherules 68

CHAPTER VII: CHIKV NSP3, AN ENIGMATIC PROTEIN ESSENTIAL FOR CHIKV INFECTION AND PATHOGENESIS 73

A. NSP3 ORGANIZATION 73
1. Macrodomain (MD) 73
2. Alphavirus Unique Domain (AUD) 74
3. Hypervariable domain (HVD) 76
B. NSP3 FUNCTIONS DURING ALPHAVIRUS REPLICATION 77
1. CHIKV genome replication and transcription 77
2. Stress granule disassembly 78
3. Interacting hub for host factors involved in viral replication and host-adaptation 81
4. nsP3 form stable cytoplasmic granules of unknown function 82
C. G3BP PROTEINS: ANTIVIRAL PURPOSE, PROVIRAL ROLE 85
1. G3BP organization 85
2. G3BP1 assembles stress granules and amplifies innate immunity signaling 86
3. G3BP proteins are directly involved in CHIKV replication 87
D. FHL1 IS A MAJOR HOST FACTOR FOR CHIKV TROPISMS AND PATHOGENESIS 88
1. FHL1 organization and expression 88
2. FHL1 expression and importance in muscle tissue development 89
3. FHL1 is a major host factor for CHIKV infection in vitro and in vivo 91

THESIS OBJECTIVES 95

RESULTS **97**

A. THE ALPHAVIRUS NSP3 PROTEIN FORMS HELICAL SCAFFOLDS DRIVING VIRAL REPLICATION AND PARTICLE ASSEMBLY (SUBMITTED, UNDER REVISION) 97

B. DECIPHERING THE MOLECULAR MECHANISMS OF THE FHL1-NSP3 INTERACTION AND ITS IMPLICATIONS IN CHIKV INFECTION REPLICATION 143

DISCUSSION AND PERSPECTIVES **170**

A. STRUCTURE AND FUNCTION OF THE ALPHAVIRUS NSP3 171

1. nsP3 helical scaffolds are involved in vRC formation 171

2. Cytoplasmic nsP3 aggregates 177

B. MOLECULAR MECHANISMS OF FHL-1 MEDIATED CHIKV INFECTION 187

1. FHL1 interactions with the nsP3 HVD and implication in infection 187

2. Investigating the molecular mechanisms of FHL1-mediated CHIKV infection 189

3. FHL1 usage and CHIKV tropism and pathogenesis 193

C. CONCLUDING REMARKS 194

REFERENCES **196**

ANNEXES **244**

RESUME DETAILLE **301**

Remerciements

Je souhaite tout d'abord remercier le Dr Ali Amara de m'avoir donné l'opportunité d'intégrer son équipe et de travailler sur un sujet de recherche qui m'a passionnée du début à la fin. Malgré les difficultés rencontrées, nous avons, je le crois, su tirer le meilleur de cette collaboration, aussi bien sur le plan scientifique que sur le plan humain. Sans écoute, confiance et bienveillance, il n'y a ni réussite, ni épanouissement professionnel, et encore moins de vocations suscitées.

Je souhaite aussi remercier le Pr Constance Delaugerre. Je te remercie pour ta considération, ton implication dans mon projet et tes précieux conseils. Tu as toujours répondu présente et pour cela, je te suis extrêmement reconnaissante. Merci !

Je remercie du fond du cœur le Dr Caroline Goujon et le Dr Yves Gaudin pour le temps accordé à la relecture de mon mémoire de thèse. Je remercie le Dr Nolwenn Jouvenet, le Pr Félix Rey, le Dr Laurence Briant ainsi que le Dr Juan Reguera d'examiner ce travail. Ces mots sont écrits à quelques semaines de la soutenance et malgré l'appréhension, je suis impatiente de pouvoir discuter avec vous tous. Ce sera passionnant !

Je souhaite remercier le Pr Alessia Zambrolini, le Dr François Bontems ainsi que le Dr Stéphane Emiliani, qui ont suivi l'évolution de mon travail au cours de ces quatre années de thèse. Merci de votre implication, de vos encouragements et de vos conseils !

Dr Laurent Meertens, je suis profondément reconnaissante pour ton appui et ta présence. Je ne te cache pas ma petite déception lorsque tu m'as dit : « NON, je ne veux pas être ton directeur de thèse ! Et de toute manière, je n'ai pas mon HDR ! » Tu n'as pas voulu être mon directeur de thèse, mais tu as été ce qui se rapproche le plus d'un mentor. Tu ne liras peut-être jamais ces mots, mais je crois que tu as le potentiel d'encadrer des étudiants, de les faire évoluer et même de susciter des passions ! À la seule condition d'accepter de t'investir et de penser à l'étudiant non pas comme à des petites mains pour faire des manips, mais comme à un esprit scientifique qui ne demande qu'à apprendre et à se développer. Chacune de nos conversations scientifiques a été un moteur pour moi ! Même si à chaque fois que je proposais quelque chose, tu répondais « Oui, mais… ». Je te souhaite un avenir professionnel brillant, j'espère que tu monteras ton équipe un jour dans laquelle j'aurais une place ! Laisse-moi rêver un peu !!!

Chers et chères collègues (présents ou passés) de l'équipe BVE, merci de votre soutien inconditionnel ! Vous avez cru en moi, vous avez été là pour moi à chaque instant.

Copine Céline, cela ne fait même pas un an que j'ai la chance de travailler avec toi et sache que tu as été mon plus grand coup de cœur professionnel et amical. Je crois que le monde a besoin de personnalités comme la tienne. Merci d'avoir cru en moi, d'avoir travaillé d'arrache-pied avec moi pour faire ce papier, d'avoir écouté mes colères, mes complaintes, mes euphories et les quelques idées scientifiques. Ce fut un BONHEUR IMMENSE de travailler avec toi ! J'espère ne pas te perdre et avoir l'occasion de retravailler avec toi un jour. Que ce soit à la paillasse ou à un bar à fêta, j'espère que ton avenir sera doux, heureux, stimulant et rempli d'AMOUR !!!!

Copain Luc, je pense avec beaucoup d'émotion à toi. Tu es arrivé ici pour ton stage de master et bientôt tu arrives à la fin de ta thèse. C'est un réel bonheur pour moi de t'avoir vu évoluer. Tu as avancé et tu continues à avancer, à t'améliorer. Je te remercie pour cette admiration (certes sans réel fondement) que tu as toujours

montrée à mon égard, c'est ce que j'ai toujours ressenti dans nos échanges. Peu importe ce qui t'attend après ta thèse, je crois que cette expérience t'a appris à exiger toujours plus de toi, à encaisser la déception et à relativiser. N'arrête jamais de cultiver tout cela. J'espère que notre amitié ne s'arrêtera pas à la fin de ma thèse ici avec vous.

Dimitri, il m'est difficile de restreindre mes mots pour qu'ils puissent tenir dans un seul paragraphe. Tu en doutes souvent, je crois, mais tu es une personne admirable. A part cela « Oui Dimitri, tu as toujours raison ! » Je souhaite témoigner ici toute ma gratitude pour ton implication, tes encouragements et ta foi, presque religieuse, en mes capacités ! Je te remercie pour les cafés et les brainstormings qui ont nourri ma réflexion et mon projet ! Nos échanges m'ont fait rêver et m'ont toujours donné l'impression que tout était possible. Merci pour tout ! Mes mots ne sont pas à la hauteur de tout ce que tu as fait pour moi, mais ils sont sincères et empreints de beaucoup d'émotion.

Laurine, merci pour ton investissement dans notre projet ! Sans toi, le travail aurait été bien plus difficile ! Je te remercie du fond du cœur pour ta sollicitude !

Marie, je sais que nous ne sommes pas très proches, mais je te remercie du fond du cœur pour toutes les discussions qu'on a pu avoir ensemble ! Et même les coups de gueule ! Au moins, on ne s'ennuie pas !

Erwan, pour moi tu es toujours notre Master2 chéri ! Je regrette profondément ton expérience décevante ici… J'espère que des opportunités s'ouvriront à toi. En fait, je n'en doute pas, tu es un esprit préparé ! Tu réussiras ! Merci pour ton implication et surtout pour ta bonne humeur et ta philosophie de vie ! Tu es plus intéressant et enrichissant que bien des personnes ! Crois en toi !

Laura, je souhaite te témoigner toute ma gratitude, mon respect et mon admiration. Je n'ai pas eu l'occasion de beaucoup te côtoyer, mais j'espère avoir encore de multiples occasions d'échanger avec toi ! Je te souhaite le meilleur et j'espère que tu trouveras enfin un endroit (professionnel) qui te donnera la place que tu mérites ! Merci à toi !

Fanny, tu n'es plus vraiment dans cette équipe, mais tu es pour toujours ma collègue et amie qui sait aller droit au but et me remettre les idées en place ! Avec toi, j'ai fait les meilleures expériences, celles du dimanche, qui étaient le fruit d'une imagination débordante. Si seulement on pouvait travailler comme ça, librement, je suis persuadée que des innovations, on en aurait à la pelle !!! Merci à toi, pour les pauses clope/café/brainstorming ! Je te souhaite un avenir professionnel à la hauteur de tes rêves… et un chalet en Suisse !

Je souhaite remercier du fond du cœur ma Claudita d'amour. Tu es un exemple de courage et de résilience. Merci de m'avoir soutenue, de m'avoir fait comprendre avec bienveillance que je ne dois pas toujours prendre tout à cœur, on s'épuise à force ! Malgré cela, j'éprouve un sentiment de colère à l'égard de ces personnes, dans notre monde professionnel, qui ont profité de ta gentillesse et ton dévouement. J'espère que tu trouveras, toi aussi, un endroit qui saura te valoriser. Tu es brillante et une vraie Super Woman.

Je remercie Alexis, Athéna et Sarah pour leur soutien. Athéna, malgré nos coups de gueule, je suis heureuse de t'avoir rencontrée. Alexis, j'ai toujours admiré ta philosophie et ton détachement quant aux choses négatives de la vie. Tu retombes toujours sur tes pattes ! Sarah, toi et moi, nous avons formé une alpha-équipe très efficace et pleine de bonne humeur. Merci pour toute l'aide que tu m'as apportée et ta contribution à ce projet de thèse malgré les conditions difficiles. J'espère que tous trois, vous avez trouvé le bonheur et l'équilibre professionnel. Encore merci du fond du cœur.

Je remercie Lamine et Lucie qui m'ont accueillie dans cette équipe alors que j'étais une toute jeune étudiante, pas très dégourdie ! Lamine, je te remercie tout particulièrement de m'avoir encadrée lors de mes premières expériences qui sont gravées à jamais dans ma mémoire.

Je remercie tout particulièrement Kadidja, qui même sous l'eau, m'a toujours aidée et a énormément facilité mon quotidien au laboratoire ! Merci à toi. Je remercie également Hadidja, Hélène, Lucie, Thassadite et Renaud sans qui ce laboratoire ne pourrait tourner.

Je souhaite remercier chaleureusement Pascale et Emmanuelle, qui m'ont toujours encouragée et soutenue. Pascale, je te suis profondément reconnaissante pour ta bienveillance, ton optimisme et tes conseils toujours mesurés.

Je remercie toutes les personnes qui ont participé de près ou de loin à mon projet de thèse. Tout particulièrement je remercie Niclas et Cristelle, ainsi que toute l'équipe de la plateforme technologique de l'IRSL.

Je remercie pour leur contribution à ce projet le Pr. Marc Lecuit ainsi que son équipe, avec une pensée émue pour le Dr Thérèse Couderc qui nous a quittée récemment. Je remercie aussi François Bontems ainsi qu'Andres Ferino Irriarte pour leur collaboration.

Je remercie toute l'équipe de la plateforme Nanoimaging de l'Institut Pasteur et tout particulièrement Anna, Stéphane et Jan.

———

Cette thèse n'aurait jamais pu exister sans le soutien inconditionnel de mon mari, Rémi, de ma mère, Anna, et de ma grande sœur, Yoanna. Vous ne pouvez pas imaginer à quel point je vous aime. Merci d'avoir traversé cette épreuve avec moi. Merci d'avoir supporté mes absences, mon égoïsme et mes coups de colère. Maman, je te suis éternellement reconnaissante d'avoir fait ce choix difficile de quitter la Bulgarie pour venir vivre en France. Merci de t'être battue pour nous offrir la meilleure des vies ! Tu as su dépasser toutes les peurs et tous les obstacles. Ma réussite est la tienne. Je tenais à te remercier d'avoir su m'encourager, même si tu avais peur de cet investissement, parfois déraisonné, dans ma thèse. Il paraît qu'il n'y a pas de parents parfaits, ni d'éducation parfaite. Je crois que tu nous as donné, à Yo et à moi, ta part de perfection.

Je souhaite aussi remercier tout particulièrement Philippe. Tu as une place très particulière dans ma vie. Tu n'es pas mon père et pourtant c'est bien ce que tu représentes pour moi. Merci de ton investissement dans ma vie en général, et mon avenir professionnel en particulier. Je trouve toujours les conseils dont j'ai besoin auprès de toi. Je t'aime profondément. Merci !

Ma sœur chérie, merci mille fois pour tout ce que tu as fait pour moi. A commencer par cette brillante idée que tu as eue de me rapatrier à Paris pour que je puisse y faire des brillantes études ! C'est l'occasion de témoigner mon amour à mon beau-frère : King Julian, merci pour ton implication dans mon avenir professionnel, merci pour ton soutien ! Le souvenir de la recherche d'appartement, de glace McDo, d'appareils à raclette et d'aspirateur d'âme ne me quittera jamais ! Je suis heureuse que tu fasses partie de notre famille. Je souhaite écrire un petit mot pour mon neveu, Thomas, qui a à peine 1 an. Yo, Ju, vous avez créé un petit garçon merveilleux qui remplit nos existences d'amour !! J'ai hâte de savoir quel caractère de cochon vous lui avez refilé !

À mon mari, mon amour. Je n'ai pas les mots pour t'exprimer ma reconnaissance, ma gratitude. Cette thèse, je la dédie à toi. Tu as été le pilier dont

j’avais besoin pour traverser cette aventure. Tu m’as soutenue sans jamais douter de mes capacités. Tu as su me protéger de moi-même, de mes travers, lorsque je me laissais absorber un peu trop. Toi et moi, nous venons d’atteindre la ligne d’arrivée et nous sommes tous les deux épuisés. C’est une dure épreuve pour un couple, mais « la paix arrive » …Je suis heureuse et honorée d’être devenue ta femme. Je t’aime et je te remercie pour tout.

Je suis éternellement reconnaissante à mes amis qui ont, chacun et chacune, contribué à ma réussite et mon épanouissement au cours de ces années. Je remercie tout particulièrement Claire, Thomas, Amandine, Stéphane, Lionel, Sam, Mélissa, Corentin, Thibaud. Claire, je te remercie du fond du cœur pour ta présence, ton amitié, tes encouragements, ton soutien inconditionnel. Tu as su trouver à chaque instant les mots justes pour faire taire mes doutes et mes peurs. Thomas et Amandine, merci de votre présence et tous ces apéros où on refaisait le monde ! J’ai une pensée émue pour votre petite fille qui vient de naître, la merveilleuse Alba. Je vous souhaite un bonheur sans limites. Je vous aime. Dr2 Stéphane Marot, je te remercie pour ton aide sur tous les plans. Depuis le stage de M2 et les pauses café, on ne s’est jamais éloignés ! Tu es un soutien professionnel et émotionnel sans failles ! Je suis honorée de compter parmi tes amis. Nos discussions ont toujours été une source inépuisable de bonne humeur, d’enthousiasme et de motivation. Merci ! Lionel et Sam, cette dernière année vous m’avez vue (et supportée) dans tous mes états. Je vous remercie de votre soutien et votre amitié. Je vous aime. Mélissa, Corentin, Thibaud je suis heureuse de vous avoir rencontrés et d’avoir pu partager avec vous les galères de thèse ! Corentin, je te remercie tout particulièrement de m’avoir toujours incluse dans les groupes et sorties depuis le M2. Je te remercie aussi pour ces belles conversations et rêves que nous avons partagés pour le futur : une science collaborative et ouverte. Thibaud, je te remercie d’avoir partagé avec moi tes galères, et m’avoir laissé la possibilité d’en faire autant. Tu soutiens ta thèse le 7 décembre et j’espère que tu es fier de cette bataille que tu as menée. Je te souhaite un avenir professionnel épanouissant, tu le mérites ! Je vous aime les amis !

Ces remerciements sont bien trop longs mais absolument nécessaires. Ces quelques pages seront mon pense-bête qui me rappellera tout ce que vous avez fait pour moi.

Summary

Structure and function of the chikungunya virus nsP3 protein and implication in alphavirus biology

Alphaviruses, such as the chikungunya virus (CHIKV), are a group of arthropod-borne RNA viruses that represent an ongoing challenge to medicine and public health. CHIKV is epidemiologically the most prevalent alphavirus and has spread globally. It re-emerged in the last decades, causing multiple outbreaks around the globe. In humans, CHIKV infection can lead to highly incapacitating arthritis and musculoskeletal diseases that can persist weeks to months after the initial infection. Despite a considerable effort to develop treatments, no approved antivirals or vaccines exist. Understanding the fundamental mechanisms governing the CHIKV infectious cycle represents a major challenge in developing new antiviral strategies. CHIKV, like all alphaviruses, encodes seven proteins necessary for viral propagation. Among them, the nsP3 protein is the most enigmatic protein encoded by CHIKV. NsP3 plays a critical role in the synthesis of viral RNA, in the regulation of the immune response, and allows the recruitment of numerous cellular factors important for viral pathogenesis. A particular aspect of nsP3 is to form in infected cells cytoplasmic granules whose structural organization and function are poorly understood.

The general objective of this thesis is to explore the function of nsP3 during the CHIKV life cycle. The first part of this work describes the cryo-electron microscopy structure of purified CHIKV nsP3 at 2.35 Å resolution (collaboration with Dr. Juan Reguera, ASMB, Marseille). Our results showed that nsP3 assembles into tubular structures made by the helical arrangement of its alphavirus unique domain (AUD), which acts as an oligomerization module. The relevance of these oligomers has been validated in the infectious context in multiple cell lines. We showed that nsP3 tubular assemblies are a hallmark of alphaviruses. Disruption of nsP3 oligomerization by mutagenesis of AUD residues has major consequences on the formation of viral replication complexes, RNA synthesis, and infectious particle production. We also showed that nsP3 tubes accumulate viral genomic RNA and capsid proteins, suggesting that these structures could be essential in the later steps of the CHIKV infectious life cycle.

The second part of this thesis aims to provide fundamental insights into the

function of FHL1, a host factor that binds the hypervariable domain (HVD) of nsP3 and plays an important role in CHIKV tropism and pathogenesis. In collaboration with Pr. Félix Rey's team, we determined the structure of the FHL1-nsP3 complex using NMR and identified the precise region of the nsP3 that interacts with FHL1. Functional studies showed that viruses lacking the FHL1-binding domain have strong defects in replication in mammalian cells.

Moreover, we found that CHIKV stains from distinct lineages use FHL1 for efficient infection. Interestingly, we observed that CHIKV strains associated with severe musculoskeletal disease highly depend on FHL1 expression, highlighting a link between FHL1 usage and CHIKV disease severity. Altogether, the results obtained during this PhD provide essential insights into the function of the CHIKV nsP3 during infection. The major discovery is an unexpected nsP3-dependent molecular organization required for alphavirus infection, raising the possibility of targeting this process for therapeutic intervention.

Key-words : Chikungunya, alphavirus, nsP3, replication complexes, host factors, FHL1

Résumé

Structure et fonction de la protéine nsP3 du virus chikungunya et son impact sur la biologie des alphavirus

Les alphavirus, tels que le virus du chikungunya (CHIKV), constituent un groupe de virus transmis par des arthropodes et d'importance en santé publique. Le CHIKV est l'alphavirus le plus prévalent. Il a ré-émergé au cours des dernières décennies, provoquant de multiples épidémies à travers le monde. Chez l'homme, l'infection par CHIKV peut conduire à une arthrite très invalidante et à des maladies musculosquelettiques, qui peuvent persister de quelques semaines à plusieurs mois après l'infection aigüe. En dépit des efforts considérables pour développer des traitements, aucun antiviral ou vaccin approuvé n'existe. Comprendre les mécanismes fondamentaux régissant le cycle infectieux du CHIKV représente en enjeu important dans le développement de stratégies antivirales nouvelles. Le CHIKV, comme tous les alphavirus, codent sept protéines qui sont indispensables au bon déroulement de son cycle de vie. Parmi elles, la protéine nsP3 est la protéine la plus énigmatique. Celle-ci joue un rôle essentiel dans la synthèse de l'ARN viral, dans la régulation de la réponse immunitaire et permet le recrutement de nombreux facteurs cellulaires importants pour la pathogénèse virale. Une particularité de nsP3 est de former dans les cellules infectées des granules cytoplasmiques dont l'organisation structurale et la fonction sont à ce jour inconnues.

L'objectif général de cette thèse est d'explorer la fonction de nsP3 pendant le cycle infectieux du CHIKV. La première partie de ce travail décrit la structure de la nsP3 purifiée en cryo-microscopie électronique (cryo-EM) à une résolution de 2,35 Å (en collaboration avec le Dr Juan Reguera, ASMB, Marseille). Nos résultats montrent que nsP3 s'assemble en structures tubulaires induite par l'arrangement hélicoïdal de son domaine central AUD, qui agit comme un module d'oligomérisation. La pertinence de ces oligomères a été validée dans le contexte infectieux sur plusieurs lignées cellulaires. Nous avons montré que les assemblages tubulaires de nsP3 sont une caractéristique des alphavirus. La perturbation de l'oligomérisation de nsP3 par mutagenèse des résidus d'AUD a des conséquences majeures sur la formation des complexes de réplication, la synthèse de l'ARN et la production de particules

infectieuses. Nous avons également montré que les tubes de nsP3 accumulent l'ARN génomique viral et les protéines de capside, suggérant que ces structures pourraient être essentielles dans les étapes ultérieures du cycle viral.

La deuxième partie de cette thèse vise à fournir des perspectives fondamentales sur la fonction de FHL1, une protéine cellulaire interagissant avec nsP3, importante pour le tropisme et la pathogenèse du CHIKV. En collaboration avec l'équipe du Pr Félix Rey, nous avons déterminé la structure du complexe FHL1-nsP3 en résonance magnétique nucléaire (RMN) et identifié la région précise de nsP3 liant FHL1. Les études fonctionnelles ont montré que les virus dépourvus du domaine de liaison à FHL1 présentent d'importants défauts de réplication dans les cellules de mammifères. De plus, nous avons constaté que les souches de CHIKV provenant de lignées distinctes utilisent FHL1. De manière intéressante, nous avons remarqué que les souches de CHIKV associées à des maladies musculosquelettiques sévères dépendent fortement de l'expression de FHL1, soulignant un potentiel lien entre l'utilisation de FHL1 et la gravité de la maladie due au CHIKV.

Dans l'ensemble, les résultats obtenus au cours de cette thèse fournissent des informations essentielles sur la fonction de nsP3 du CHIKV lors de l'infection. La découverte majeure est une organisation moléculaire inattendue dépendante de nsP3, requise pour l'infection par les alphavirus, ouvrant la possibilité de cibler ce processus pour le développement de futures thérapeutiques.

Mots-clés : Chikungunya, alphavirus, nsP3, compléxes de réplication, facteurs cellulaires, FHL1

Figures index

Introduction

Figure 1	Viral emergence	8
Figure 2	Emergence mechanisms for arboviruses	15
Figure 3	Phylogenetic tree of the alphaviruses produced using Bayesian methods and mid-point rooted.	16
Figure 4	World map showing the spread of CHIKV and its main vectors Ae. albopictus and aegypti.	25
Figure 5	Overview of innate immune signaling pathways impacting CHIKV and other alphavirus infection	28
Figure 6	Muscle stem cell (satellite cells) (MuSC) mediated skeletal muscle regeneration.	31
Figure 7	CHIKV virion structure and envelop protein organization	36
Figure 8	CHIKV genome organization: CHIKV genomic organization and viral proteins	37
Figure 9	Overview of CHIKV replicative cycle	38
Figure 10	CHIKV entry in a target cell.	41
Figure 11	Structural polyprotein processing.	42
Figure 12	Model of multi-site alphavirus genome packaging.	45
Figure 13	P1234 processing and viral RNA synthesis:	
Figure 14	CHIKV proteins counteract the host-cell antiviral immunity	51
Figure 15	Fundamental principles regarding the organization of replication organelles in viral replication	54
Figure 16	Polyrpotein processing and spherule formation	55
Figure 17	CHIKV nsP1 andnsP1- dodecameric ring organization	57
Figure 18	mRNA capping mechanism during alphavirus infection	57
Figure 19	Comparison of nodavirus RCs and crowns to those of alphaviruses	58

Figure 20 Comparison of the molecular architecture of active and inactive CHIKV replicase complexes 60
Figure 21 Model for alphavirus spherule biogenesis and RNA synthesis 61
Figure 22 Domain organization of Alphavirus nsP3 protein 62
Figure 23 Structure of CHIKV nsP3 macrodomain (MD) 64
Figure 24 Structure of SINV AUD 65
Figure 25 Simplified schematic representation of alphaviruses' HVD features 67
Figure 26 Stress granules are cellular immune and stress signaling platforms 69
Figure 27 Model of virus infection-induced SG assembly and disassembly regulated by nsP3 ADP-ribosylhydrolase activity. 70
Figure 28 Schematic representation of nsP3 established proviral functions 73
Figure 29 G3BP1 and G3BP2 protein organization 75
Figure 30 FHL1 gene and protein organization 79
Figure 31 Structure of FHL1 isoforms 80
Figure 32 FHL1 is an important determinant for CHIKV tropism and pathogenesis in the mice model: 82
Figure 33 FHL1 protein is required for replicative spherule formation. 82
Figure 34 FHL1 protein directly interacts with CHIKV nsP3-HVD domain and is recruited within nsP3 cytoplasmic condensates 84
Figure 35

The alphavirus nsP3 protein forms helical scaffolds driving viral replication and particle assembly (submitted, under revision)

Figure 1 Structure of CHIKV nsP3 helical scaffolds (HSs)
Figure 2 Superposition of nsP3 HSs on tomographic reconstructions of membrane-associated CHIKV RCs

Figure 3 CHIKV nsP3 assembles into tubular structures that define the architecture of alpha-granules.

Figure 4 nsP3 helical scaffolds are required for CHIKV replication and infectious particle production

ED Figure 1 CHIKV nsP3 purification and electron microscopy analysis

ED Figure 2 Flowchart of the image processing pipeline for nsP3.

ED Figure 3 Analysis of charge distribution on the AUD helical scaffolds.

ED Figure 4 Sequence alignment of the AUD from different alphaviruses

ED Figure 5 NsP3 alpha-granules and alphavirus infection

ED Figure 6 NsP3 HS formation requires nsP2-nsp3 precursor cleavage

ED Figure 7 NsP3 tubular structure characterization

ED Figure 8 The AUD mediates nsP3 oligomerization

ED Figure 9 Role of nsP3 helical scaffolds during CHIKV infection

Deciphering the molecular mechanisms of the FHL1-nsP3 interaction and its implications in CHIKV infection replication

Figure 1 Impact of FHL1-binding site deletion or mutation on CHIKV replication in human cells.

Figure 2 FHL1-interacting region on CHIKV HVD cover the R4 sequence, as well as CD2AP and BIN1/Amph2 binding motif

Figure 3 HVD-R5 motif is involved into FHL1 recruitment to nsP3 complexes and in CHIKV infection in different cell type

Figure 4 CHIKV dependency on FHL1 varies between the viral strains in

human cells

Figure 5 FHL1 and G3BPs depletion dramatically impair CHIKV replication in HAP1 cells

Figure 6 FHL1 and G3BPs play distinct role during CHIKV replication cycle

Figure 7 FHL1 is possibly involved into nsP3 aggregates formation in infectious conditions.

Figure 8 Characterization of FHL1 interactome

Figure 9 Functional validation of FHL1-interacting partners during CHIKV infection

Discussion and perspectives

Figure 1 Structure of inactive vRC

Figure 2 nsP3 forms a supporting crown below nsP1-dodecameric ring of vRC

Figure 3 Comparison of SGs and nsP3-assemblies ultrastructure

Figure 4 nsP3-tubular assemblies contain nsP2 and capsid but not nsP1 and E2 viral proteins

Figure 5 Overview of nsP3-tubular assemblies' potential functions during alphavirus replication

Figure 6 nsP3 tubular assemblies' purification and interactome analysis

Figure 7 Experimental approach for CHIKV non-infectious virus particle production and in situ characterization of nsP3-tubes by cryo-electron tomography.

Figure 8 Cryo-electron tomography of nsP3-tubular structures in CHIKV single-round particles infected Vero cells

Figure 9 FHL1 as a scaffold for CHIKV interaction with the actin cytoskeleton.

Figure 10 Model for FHL1-mediated repressing of HERC5 and its subsequent impact on viral infection

Figure 11 FHL1-hijacking and sequestration by CHIKV-nsP3 might be involved in impaired muscle cell regeneration and differentiation

Abbreviations

Ae.	Aedes
AUD	Alphavirus Unique Domain
BFV	Barmah Forest Virus
cGAMP	Cyclic GMP-AMP
cGAS	cGAMP synthase
CHIKV/F	Chikungunya virus/fever
Cp	Capsid protein
CPV-I	Cytopathic vacuoles type I
CPV-II	Cytopathic vacuoles type II
CSE	Cis-acting sequence elements
DENV/F	Dengue virus/fever
dsRNA	Double-stranded RNA
E1-A226V	Substitution in the E1 envelop protein at position 226
E1/E2	Envelop proteins
ECSA	East-Central-South African
EEEV	East Equine Encephalitis virus
eEF	Eukaryotic translation elongation factor
eIF	Eukaryotic translation initiation factor
ER	Endoplasmic reticulum
FMRP	Fragile X mental retardation protein
G3BP	RasGAP-associated endoribonuclease
GAGs	Glycosaminoglycans
gRNA	Genomic RNA
HVD	Hypervariable domain
IFIT-1	Interferon-induced protein with tetratricopeptide repeats 1
IFN-I	Interferon Type-I
IL-6	Interleukin 6
In-vRO	Invagination type replication organelles
IOL	Indian Ocean Lineage
IRF3	Interferon regulatory factor 3
LLPT/S	Liquid-liquid phase separation/transition

MAR	Monomeric ADP-ribose
MAVS	Mitochondrial antiviral signaling
MAYV	Mayaro virus
MD	Macrodomain
MDA5	Melanoma differentiation-associated protein 5
mRNPs	Messenger ribonucleoproteins
MuSC	Muscle steam cells/satellite cells
NC	Alphavirus nucleocapsid
NF-κB	Nuclear Factor-kappa B
NHP	Non-human primates
NSAIDs	Nonsteroidal anti-inflammatory drugs
nsP1	Non-structural protein 1
nsP2	Non-structural protein 2
nsP3	Non-structural protein 3
nsP4	Non-structural protein 4
NW	New World alphaviruses
NW	New World alphaviruses
ONNV	O'nyong-nyong virus
ORF	Open reading frame
OW	Old World alphaviruses
PAR-CLIP	Photoactivatable ribonucleoside crosslinking and immunoprecipitation
PARPs	Poly-ADP-ribose polymerases
Pr-vRO	Protrusion-type replication organelles
PRNT	Plaque-reduction neutralizing test
PRR	Pattern recognition receptors
PSs	Packaging signals
RA	Rheumatoid arthritis
RIG-I	Retinoic acid-inducible gene I
RRV	Ross River virus
RT-PCR	Reverse Transcriptase Polymerase Chain Reaction
SFV	Semliki Forest virus
sgRNA	Sub-genomic RNA

SGs	Stress granules
SINV	Sindbis virus
STAT1	Signal transducer and activator of transcription 1
STING	Stimulator of interferon genes
TIA1	T cell internal antigen 1
TIAR	TIA1-related protein
TLR	Toll-like receptors
TNF-α	Tumor necrosis factor-alpha
UPR	Unfolded protein response
UTR	Untranslated regions
VBD	Vector-borne diseases
VEEV	Venezuelan Equine Encephalitis virus
VLP	Virus-like particles
vRC	Viral replicase complex (applied here to alphaviruses vROs)
vRO	Viral replication organelles
WA	West Africa strain
WEEV	West Equine Encephalitis virus
WHO	World Health Organization

Introduction

Chapter I. Arboviruses

A. Emerging viruses

An emerging virus is the causative agent of a new or previously uncharacterized infection disease in a given population that can potentially cause outbreaks (Y. K. Choi 2021). Occasionally, a known pathogen displaying new geographical distribution, expanded host range, or an increase in disease could be defined as an emerging or re-emerging pathogen. In human populations, emerging viruses are often pathogens that circulate within non-human hosts (e.g., wild or domesticated animals) and are accidentally transmitted to humans (zoonotic infection) (Rall et al. 2015). Viral emergence is a complex phenomenon depending on multiple parameters such as: environmental changes, ecological disturbances and, population density and distribution (Figure 1A) (Rall et al. 2015). All these interconnected parameters are key players in virus-host interactions. There are four general types of virus-host interactions: *stable*, *evolving*, *resistant* and *dead-end* (Rall et al. 2015). It is worth noting that these groups are not fixed and static, but instead describe the continuous and dynamic interactions between viral and host populations (Figure 1) (Rall et al. 2015). In *stable* interactions both viral and host population survive and can reproduce. Although this state seems optimal for the viral population, as it maintains it in the ecosystem, it remains dynamic and fragile.

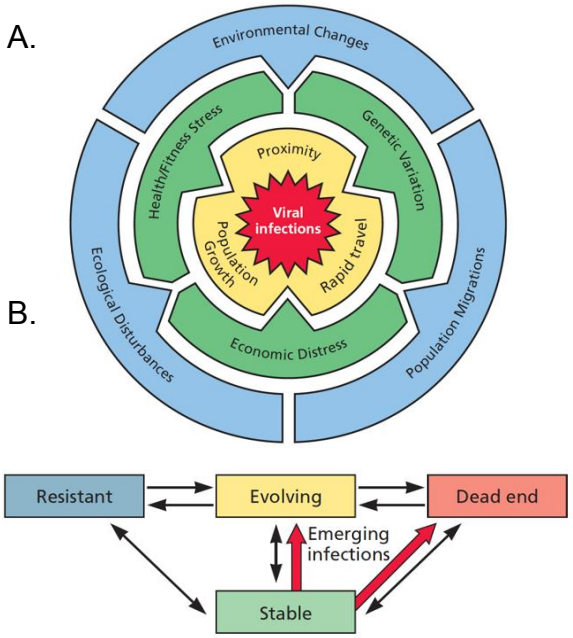

Figure 1: Viral emergence. *A. The intricated parameters are shaping viral-host interactions. B. Four groups of virus-host interactions. From (Rall et al., 2015)*

In some cases, such as smallpox, measles or herpes simplex viruses, stable interactions can be permanent if there is one and only natural host for a given viral population (Rall et al. 2015). Although this interaction appears to be optimal, it actually leads to a constraint in viral population evolution, threatening its survival if there are any ecological or environmental changes. For instance, smallpox has been successfully eradicated when a worldwide immunization of human population has

been achieved (Strassburg 1982). On the other hand, some viruses establish stable interactions with multiple host species. That is the case of arboviruses (arthropod-borne viruses) that efficiently reproduce in some insects, mammals, and birds (Madewell 2020).

The three other groups derive from stable interactions when disturbed by ecological or environmental changes (Rall et al. 2015). *Evolving* interactions describe the passage of a virus from an "experienced" to a "naïve" population in the same or new host-species, with more or less dramatic consequences on the viral and the host-population. Historical example is the introduction of smallpox and measles by the Europeans in the Americas in 1520, devastating the native population that had never experienced these pathogens (Y. K. Choi 2021; Oldstone 2020). It is estimated that 3.5 million Aztecs died from smallpox within two years, far more than from conquistadors' bullets (Y. K. Choi 2021; Oldstone 2020). Those who survived smallpox, perished from measles brought in the same time by the European belligerent. In our modern times humanity is still not immune to viral emergence (Y. K. Choi 2021; Oldstone 2020). Another contemporary example is the accidental introduction of West Nile virus (WNV) in New York City in 1999 (Mackenzie, Gubler, et Petersen 2004). WNV is a flavivirus discovered in Uganda in 1937, that had never been reported on the American continent (Mackenzie, Gubler, et Petersen 2004).

Alike *evolving* interactions, *dead-end* interactions can derive from a *stable* interaction (Rall et al. 2015). Instead of transmitting efficiently between the members of a new host species, the virus either kills its host or, if the new host survives, it isn't efficiently transmitted to the members of the new species (Rall et al. 2015). *Dead-end* interactions are often a consequence of cross-species infections and are frequently observed with arthropod-borne viruses (e.g., West Nile virus): the virus establishes stable interactions with its arthropod host, but occasionally the latter can transmit the pathogen to a new species (e.g.; humans) with severe consequences. Several animal species play a critical role in the transmission to humans of highly pathogenic viruses (Rall et al. 2015). Rodents and bats could be persistently infected by multiple RNA viruses (e.g., of the *Bunyaviridae* or *Arenaviridae* families for rodents, *Paramyxoviridae* or *Filoviridae* families for bats) with mild or no pathological effect. A viral population is maintained in those animals that efficiently excrete viral particles in their secretions (urine, saliva, feces), thus transmitting the virus to new members. Whereas humans are not the natural host species for those viruses, they can be

infected by direct contact with animals' excretions. Unfortunately, the outcome of these infections is often lethal, making humans a dead-end host. Finally, some hosts can efficiently block viral infection because host cells are not susceptible or permissive to viral infection, or because the host defense mechanisms are too strong and efficiently limit viral propagation.

B. Focus on emerging arboviruses

During the last 75 years, emerging zoonoses have been responsible for the most of the emerging infections affecting humans, with billions of human illness cases, millions of deaths per year and a long-lasting threat to human health (Lloyd-Smith et al. 2009). Many emerging zoonotic viruses are transmitted to humans by hematophagous insects (mosquito such as *Aedes*, *Anopheles*, *Culex*; sandflies, ticks) (Madewell 2020).These are designed as arboviruses (arthropod-borne viruses), of which the vast majority are RNA viruses belonging to the genera *Alphavirus, Flavivirus, Orthobunyavirus, Nairovirus, Phlebovirus, Orbivirus, Vesiculovirus and Thogotovirus* (Mayer, Tesh, et Vasilakis 2017). In the last decades, arboviruses spread more widely and rapidly through the globe. According to the World Health Organization (WHO), approximately 17% of infectious diseases and around 700,000 deaths each year globally are attributed to vector-borne diseases (VBDs), which encompass arboviruses (« Vector-Borne Diseases » s. d.). Several factors contribute to this trend, including increased air travel and uncontrolled mosquito populations (Y. K. Choi 2021; Gould et al. 2017). Dengue (flavivirus) is the most widespread arbovirus, causing over 90 million cases and 40 000 deaths per year (Kading, Brault, et Beckham 2020). Other arboviruses such as Chikungunya virus (alphavirus, 693 000 cases/year), Zika virus (flavivirus, 500 000 cases/year), or Yellow Fever virus (flavivirus 130 000 cases/year) are also a major public health concern (Kading, Brault, et Beckham 2020; Madewell 2020).

Arboviruses can emerge through various mechanisms (Scott C. Weaver et al. 2018) (Figure 2). First, some viruses directly spill over from their natural wildlife cycles (enzootic cycle) to infect humans, as observed with WNV during its expansion into the Americas (Mackenzie, Gubler, et Petersen 2004). Secondly, some viruses undergo secondary amplification in domesticated animals, as seen with Japanese encephalitis, Venezuelan equine encephalitis, and Rift Valley fever viruses (reviewed in (Scott C. Weaver et al. 2018)). In a third mechanism, the virus passes from an enzootic cycle

to a human-vector-human cycle or urban cycle. Humans become the amplification hosts, and the transmission cycle is mediated by anthropophilic mosquitoes such as *Aedes aegypti or Aedes albopictus*. This urban emergence has been witnessed in viruses such as Dengue, yellow fever, chikungunya, and Zika which are among the most prevalent human arboviruses (Scott C. Weaver et al. 2018).

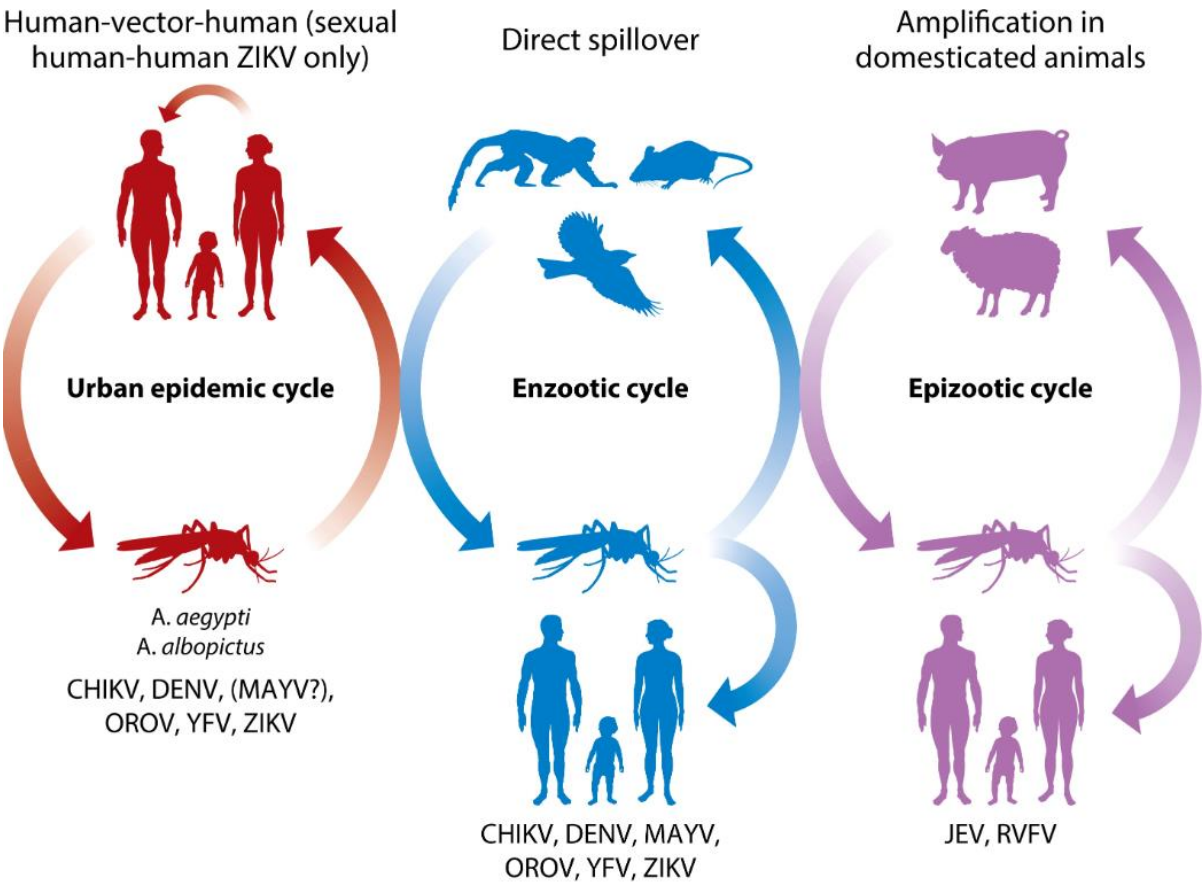

Figure 2: Emergence mechanisms for arboviruses. *All the reviewed viruses are transmitted by mosquito, with the exception of urban transmission of OROV, which involves Culicoides spp. midges. Viruses that have historically emerged in urban areas often utilize non-human primates as enzootic hosts and then infect humans through direct spillover. The abbreviations used in the figure are as follows: CHIKV for chikungunya virus, DENV for dengue virus, JEV for Japanese encephalitis virus, MAYV for Mayaro virus, OROV for Oropouche virus, RVFV for Rift Valley fever virus, YFV for yellow fever virus, and ZIKV for Zika virus. From (Scott C. Weaver et al. 2018)*

Chapter II. Alphaviruses

Alphaviruses, that belong to the *Togaviridae* family, are characterized by a strong impact on human and animal health. Some alphavirus species cause encephalitis in horses, but can also infect humans with fatal outcome (Lundberg, Carey, et Kehn-Hall 2017). This is the case of the Venezuelan Equine Encephalitis virus (VEEV) which belongs to the New World encephalitic alphaviruses. On the other hand, Chikungunya virus (CHIKV) for instance is the most impactful human alphavirus that caused multiple outbreaks in the last decades. CHIKV belongs to the Old World arthritogenic alphaviruses.

A. Phylogeny and geographical distribution

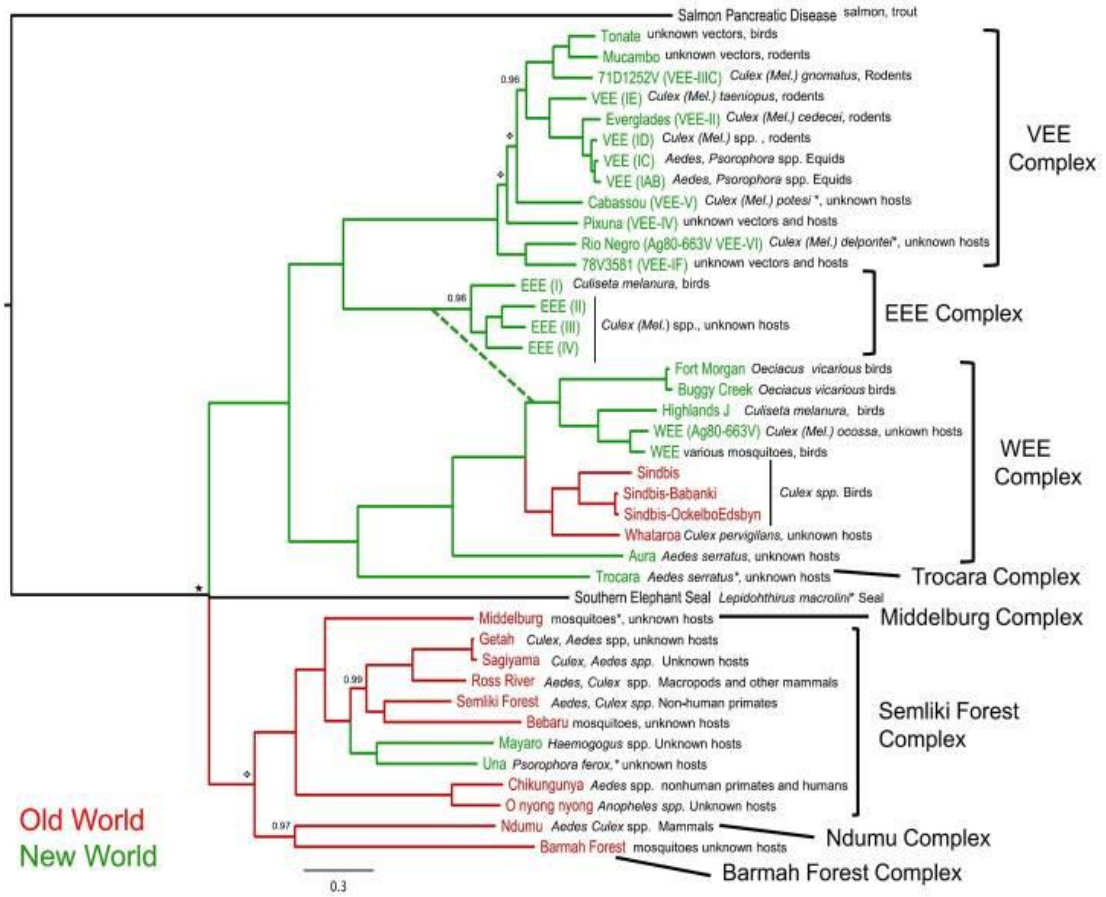

Figure 3: Phylogenetic tree of the alphaviruses produced using Bayesian methods and mid-point rooted. *Vectors and vertebrate hosts are printed next to virus labels. The tree includes representatives from all species and was constructed using the structural protein E2, 6 K and E1 genes. The dashed line indicates the point at which ancestral SINV and EEEV recombined to form the recombinant WEEV ancestor. All posterior probabilities were 1 unless shown. Nodes with a ❖ symbol had posterior probabilities less than 0.9 and nodes with a ★ had no posterior support. From (Scott C. Weaver et al. 2012)*

Alphaviruses belong to the Baltimore classification Group IV (Berman 2012), containing a positive single-stranded RNA genome [(+) ssRNA]. Initially, the identification of seven antigenic complexes of mosquito-borne alphaviruses was accomplished by assessing the levels of cross-reactivity among them (Calisher et al. 1980). These complexes were named as EEE, VEE, WEE, Semliki Forest, Barmah Forest, and Middelburg complexes (Calisher et al. 1980). However, since the 1980s, genomic sequence comparisons have largely replaced antigenic analyses. As a result, some newly described alphaviruses like Trocara virus have been categorized into complexes based on genetic data (Powers et al. 2001). Consequently, the current classification of the alphavirus family, comprising eight complexes, is a combination of both antigenic and genetic classification approaches (Powers et al. 2001). Except for two aquatic alphaviruses (southern elephant seal virus and salmon pancreas disease virus), all the members are arthropod-borne viruses (Powers et al. 2001). They circulate between hematophagous mosquitoes and vertebrate hosts, including human and nonhuman primates, equids, birds, amphibians, reptiles, rodents, and pigs (R. Chen et al. 2018) (Figure 3).

Alphaviruses are distributed world-wide, occupying all continents except Antarctica. They can be also classified into Old World or New World alphaviruses according their geographical origin and distribution (Figure 3). The Barmah Forest, Ndumu, Middelburg, and Semliki Forest complexes occur almost exclusively in the Old World (OW), and originated from the African continent (Powers et al. 2001; Forrester et al. 2012; Azar et al. 2020). On the other hand, New World alphaviruses (NW) (VEEV, EEEV, WEEV complexes) originated in the Americas (Figure 3). OW alphaviruses are generally associated with arthritogenic disease in humans, whereas NW alphaviruses lead to neurological disease (Suhrbier, Jaffar-Bandjee, et Gasque 2012; Zacks et Paessler 2010). It is important to emphasize that the classification doesn’t perfectly reflect the evolution of the different viruses. For instance, phylogenetic studies classify Sindbis virus (SINV) as a member of the WEEV antigenic complex, whereas its geographical distribution classifies it as an OW alphavirus (Calisher et al. 1980). Further studies demonstrated that a recombinant event occurred between the envelope genes of a SINV ancestor with those of an EEEV ancestor, led to the emergence of the WEEV complex (S C Weaver et al. 1997), suggesting a common geographical distribution in the past. Furthermore, whereas OW alphaviruses are considered as arthritogenic and NW alphaviruses – as encephalitic, the Mayaro

virus interrogates the origin of these alphaviruses as it circulates in South America but is associated to arthritic disease (Auguste et al. 2015). Whether encephalitic NW alphaviruses have evolved from the OW alphaviruses or, inversely, is not clear. Some phylogenetic studies positioned the two aquatic alphavirus species at the base of the phylogenetic trees, suggesting an aquatic origin of alphaviruses, followed by movements both east and west, thus resulting in the Old and New World ancestors of the mosquito-borne viruses (Powers et al. 2001; Forrester et al. 2012).

B. Transmission cycle

Most alphaviruses circulate between mosquitoes and avian or mammalian reservoirs, and/or amplification hosts (S.C. Weaver, Klimstra, et Ryman 2008). Spillover events from the enzootic cycle can occur when humans enter the sylvatic cycle or amplification increases virus circulation. Secondary amplification involving domestic animals in close proximity to humans could accelerate spillover events. This is the case of VEEV hosts (S.C. Weaver, Klimstra, et Ryman 2008). Finally, an urban cycle can occur when humans become amplification hosts. This transmission cycle relies on anthropophilic mosquitoes. CHIKV for instance, is the only alphavirus that circulates in the enzootic cycle between non-human primates and sylvatic primatophilic mosquitoes (*Ae. furcifer-taylori, Ae. africanus, Ae. luteocephalus and Ae. neoafricanus*) (Jupp et McIntosh 1990; McIntosh 1988; S.C. Weaver, Klimstra, et Ryman 2008; Scott C. Weaver et al. 2012), and in an urban cycle, where it circulates between anthropophilic *Aedes aegypti* and *Aedes albopictus* mosquitoes and humans (S.C. Weaver, Klimstra, et Ryman 2008; Scott C. Weaver et al. 2018; Lambrechts, Scott, et Gubler 2010).

Alphaviruses transmission starts when a female mosquito feeds on a viremic vertebrate host. Following the blood meal, the virus migrates to the midgut, undergoing replication (Scott C. Weaver, Chen, et Diallo 2020). However, during the blood digestion process, the midgut epithelium releases a peritrophic matrix that can obstruct virus entry (Dong et al. 2017), serving as the initial barrier known as the *midgut infection barrier* (Dong et al. 2017). Overcoming this bottleneck is crucial for the establishment of effective infection and transmission. Once the virus crosses this barrier, it replicates and escapes into the hemocoel (Naomi L. Forrester, Coffey, et Weaver 2014). The hemocoel is vital in disseminating the virus and infecting other secondary tissues (Naomi L. Forrester, Coffey, et Weaver 2014) . The final step in the

transmission cycle involves the infection and the replication cycles within the salivary glands until sufficient viral loads are reached to infect vertebrate hosts. All these steps, from crossing the midgut epithelium to replicating in the salivary glands, determine the vector competence for a specific virus (Dong et al. 2017; Lim et al. 2018).

C. Arthritogenic alphaviruses

Arthritogenic alphaviruses comprise chikungunya virus (CHIKV), Ross River virus (RRV), Barmah Forest virus (BFV), O'nyong-nyong virus (also known as Igbo Ora), the Sindbis group of viruses and Mayaro virus. In contrast to arboviruses such as flaviviruses (for which asymptomatic care represents more than 90% of the infections), alphaviruses are symptomatic in most cases (Suhrbier, Jaffar-Bandjee, et Gasque 2012). For instance, CHIKV infection is symptomatic between 70% and 97% of the time (Suhrbier, Jaffar-Bandjee, et Gasque 2012; Bartholomeeusen et al. 2023; Renault et al. 2007).

Infections with alphaviruses are characterized by a brief viremia of 5-7 days, rapidly controlled by the IFNα/β response and neutralizing antibodies (Schwartz et Albert 2010; Suhrbier, Jaffar-Bandjee, et Gasque 2012). A strong inflammatory immune response probably accounts for the acute symptoms: fever, polyarthralgia and polyarthritis, rash, and myalgia (reviewed in Suhrbier 2019). Although usually self-limiting, chronic rheumatic manifestations have been reported following the resolution of acute disease for arthritogenic alphaviruses (except ONNV). Protracted arthralgia was well documented for Sindbis virus (Kurkela et al. 2005), RRV (Suhrbier et Mahalingam 2009), and CHIKV disease (Hawman et al. 2013; Hoarau, Jaffar Bandjee, et al. 2010; McCarthy, Davenport, et Morrison 2019; Poo et al. 2014). For instance, CHIKV arthritic disease is reported to remain unresolved after six months to 3 years in 1.6–57% of patients (depending on the study) (Suhrbier, Jaffar-Bandjee, et Gasque 2012). Viremia typically increases a few days before the onset of symptoms. Direct diagnosis can be done through RT-PCR or virus isolation (Levi et Vignuzzi 2019). However, RT-PCR may not detect the virus after seven days of symptom onset for CHIKV and MAYV, with virus isolation being efficient for an even shorter duration (Levi et Vignuzzi 2019; Suhrbier 2019; Bartholomeeusen et al. 2023). These diagnostic tools are highly specific between and within viral families but are not always applicable in practice. Indirect diagnosis is achieved using serological tests to detect IgM and IgG antibodies. Although these antibodies appear later than viremia, they are more

persistent (Centers for Disease Control and Prevention (CDC) 2006; Natrajan, Rojas, et Waggoner 2019). For CHIKV, IgM can appear as early as two days after symptom onset and is usually positive after a week. IgM levels typically decrease after three months but can persist for over six months in some cases. IgG usually becomes detectable 7-14 days after the onset of illness and remains present for a long time (Figure 4). The main challenge with serological methods is the potential for cross-reactivity among alphaviruses. This makes it difficult to identify the specific arthritogenic alphavirus involved, especially in regions where multiple alphaviruses co-circulate. Consequently, the plaque-reduction neutralizing test (PRNT) is considered the gold standard for diagnostics.

Chapter III: Chikungunya disease

A. Chikungunya virus, a re-emerging human pathogen of global health concern

1. Discovery

In 1952, an unknown disease occurred on the Makonde Plateau (Newala and Masasi Districts) in the Southern Province of Tanganyika, along the border between Mozambique and Tanganyika (the mainland part of modern Tanzania) (M. C. Robinson 1955; Lumsden 1955; Ross 1956). A hallmark of the infection was the particularly severe joint pains responsible for the contorted posture of affected people (M. C. Robinson 1955; Lumsden 1955; Ross 1956). The local term "*chikungunya,*" derived from the Makonde root verb "*kungunyala*," meaning "to walk bent over," was given to the disease (M. C. Robinson 1955; Lumsden 1955; Ross 1956). Chikungunya fever shares several clinical characteristics with dengue fever (DENF), but the latter does not circulate on the Makonde Plateau. Observations made on one hundred and fifteen patients in the hospital and other infected people in the villages showed that after an incubation period of 3 to 12 days, infected people experienced a sudden disease onset with rapid temperature rise, varying between 38.8°C and 40.5°C disease (M. C. Robinson 1955; Lumsden 1955; Ross 1956). After an apyrexial period, most of the patients experienced a second pic of fever and the appearance of maculo-papular eruption (M. C. Robinson 1955; Lumsden 1955; Ross 1956). Unlike dengue fever, patients suffering from CHIKF experienced joint pain "frightening in its severity," aggravated with movements (M. C. Robinson 1955). The patient follow-up has also revealed that pains were persistent without any other disease symptoms in most affected people. For some, severe joint pains last up to 4 months (M. C. Robinson 1955).

The findings from epidemiological and environmental investigations conducted by W. H. R. Lumsden and Dr. R. W. Ross indicate that the causative agent of CHIKF (Chikungunya fever) is transmitted by blood-sucking insects. In the specific region of the Makonde Plateau, which is densely populated but lacks accessible water sources, water storage in houses has led to a significant presence of *Aedes aegypti* and *Culex fatigans* mosquitoes (Lumsden 1955; Ross 1956). Further studies on the agent's behavior found in acute sera and mosquito pools demonstrated its lethality when

inoculated into baby mice (Lumsden 1955; Ross 1956). The agent could not be filtered through a Seitz filter, could be passaged indefinitely in brain suspension, and mice injected with passaged strains showed symptoms within two days (Lumsden 1955; Ross 1956). Bacteriological cultures did not exhibit growth when exposed to these filtrates, and microscopic analysis failed to identify any particles (Ross 1956). These observations strongly suggested that the causative agent of CHIKF is a virus transmitted by mosquitoes, likely a strain of dengue virus. Subsequent serological and antigenic studies classified the virus as an Alphavirus closely related to Sindbis and Semliki forest virus (Monath 2020; Spence et Thomas 1959).

2. Transmission cycles and Epidemiology

CHIKV was shown to be circulating on an enzootic or sylvatic transmission cycle between arboreal*, canopy-dwelling Aedes (Ae.) spp.* vectors and diverse nonhuman primates (NHP) presented in forested regions of sub-Saharan Africa (Azar et al. 2020; R. Chen et al. 2018; Weinbren, Haddow, et Williams 1958; Jupp et McIntosh 1990). CHIKV was isolated from wild *Ae. africanus* mosquitoes in Uganda in 1958 (Weinbren, Haddow, et Williams 1958). Further studies have shown that inoculated monkeys developed viremia and subsequently produced neutralizing antibodies (S. D. Paul et Singh 1968; Weinbren, Haddow, et Williams 1958). Additionally, between 1972 and 1986, an extensive study in Senegal (West Africa) isolated 185 CHIKV strains from 13 forest mosquito species such as *Ae. furcifer-taylori* and *Ae. Luteocephalus*, which are likely the major sylvatic vectors in Senegal. Viral isolation and serological studies have confirmed the role of NHP (such as African green monkeys, bushbabys, guenons, or Guinea baboons) as viral reservoirs (Traore-Lamizana et al. 1999). Phylogenetic and sequencing studies demonstrated that CHIKV strains circulating in sub-Saharan Africa are a part of two enzootic clades termed *East-Central-South Africa (ESCA)* and *West Africa (WA***)** (Brault et al. 2000; Volk et al. 2010). CHIKV sylvatic cycle consists of a periodic amplification of the virus, which circulates actively between wild forest mosquitoes and NHP, mainly (Traore-Lamizana et al. 1999). Silent intervals of 3 to 5 years punctuate the enzootic cycle, likely related to the monkey population's immune status. Several studies suggest that a second wild transmission cycle involving squirrels, rodents, and birds contributes to maintaining the virus in the endemic region during silent intervals. At the same time, NHPs are protected (Traore-Lamizana et al. 1999). Occasional spillovers of sylvatic CHIKV occur in humans, causing small outbreaks in the enzootic areas, likely due to

Ae. furcifer (in West and South Africa) and *Ae. africanus* (East and Central Africa) (Diallo et al. 2012; Jupp et McIntosh 1990; Traore-Lamizana et al. 1999).

CHIKV presence outside the African continent was clearly documented in Thailand in 1959 (Hammon, Rundnick, et Sather 1960). Further studies demonstrated that *Ae. aegypti* was involved in an endemic, urban transmission of CHIKV in the Southeast Asia, causing moderate-in-size outbreaks (Hammon, Rundnick, et Sather 1960). Subsequently, CHIKV was recorded in Cambodia and India in the early 60s (Halstead et Udomsakdi 1966; Inoue et al. 2003; Marchette et al. 1978; Wolfe et al. 2001).There is no clear evidence for an Asian enzootic transmission cycle of CHIKV. Although studies have reported seropositive NHP and other vertebrates in Southeast Asia (Halstead et Udomsakdi 1966; Inoue et al. 2003; Marchette et al. 1978; Wolfe et al. 2001), CHIKV strains were successfully isolated only from domestic vectors (Halstead et Udomsakdi 1966), suggesting that CHIKV likely originated from Africa and was introduced in Southeast Asia afterward (Brault et al. 2000). We can't rule out the possibility of a spillback from the urban to an enzootic transmission cycle. CHIKV genotype circulating in Asia (Asian lineage) have likely diverged from the enzootic ECSA lineage at the end of the eighth century and is maintained mainly in Eastern Asia's urban transmission cycle, causing periodic outbreaks (Scott C. Weaver et Forrester 2015) (23). Since the Barsi outbreak in 1973, the long absence of CHIKV epidemics lead to the hypothesis of CHIKV extinction in India and South-East Asia (Burke at al., 1985; Pavri, 1986; Neogi et al., 1995).

3. Mechanisms of re-emergence

CHIKV gets particular attention in 2004, when a new ESCA strain has emerged in coastal Kenya (Mombassa and Lamu Island) (Chretien et al. 2007; Onyango et al. 2008)**,** and has spread to the Indian Ocean islands, causing an urban epidemic with unprecedented attack rates (Kariuki Njenga et al. 2008) (Onyango et al. 2008; Sang et al. 2007). The largest documented outbreak occurred in La Réunion island and has provided valuable information about CHIKV transmission, evolution and associated pathology. Between March 2005 and April 2006, the surveillance system has reported around 244,000 cases, with an estimated attack rate of 35% (Renault et al. 2007; Gérardin et al. 2008; Josseran et al. 2006). To date, no death is clearly imputable to CHIKV infection. A case fatality-rate for chikungunya disease was roughly estimated at ≈1/1000 cases following the evaluation of 260 excess deaths during La Réunion island epidemic (Renault et al. 2007; Josseran et al. 2006). Simultaneously, CHIKV

spread to other Indian Ocean territories (Seychelles, Mauritius, Madagascar) and finally reached India. After a gap of 32 years, India's CHIKV outbreak caused 1.3 million cases in 13 states (Yergolkar et al. 2006; Arankalle et al. 2007). Since 2008, autochthonous transmission has been recorded in Italy (2007) and South France (2014) (Angelini et al. 2008; Delisle et al. 2015). A third major outbreak occurred in December 2013 on the Caribbean Saint Martin Island. Rapidly, the virus spread to more than 50 countries in South and Central America, causing at least 1 million infections (Cassadou et al. 2014; Van Bortel et al. 2014). Few autochthonous cases were recorded in Florida (2014). Since 2014, more than 2.9 million infections have been reported in the US country. Today, > 100 countries where CHIKV has been notified and > 10 million cumulative cases of CHIKV fever have been recorded (Bartholomeeusen et al. 2023; Nsoesie et al. 2016). Aedes distribution is a crucial determinant for future outbreaks of CHIKV (and other arboviruses) species vectors worldwide. Local outbreaks of Chikungunya, Dengue, or Zika viruses were shown to follow within 5-15 years of infestation of an urban area *by Ae. aegypti and Ae. albopictus* (Messina et al. 2014; Kraemer et al. 2015). The factors involved in *Ae.* species propagation to naïve regions is multiple. Climate change is of particular concern. *Ae. aegypti* is anticipated to expand significantly within its tropical territory and move into adequately temperate areas in the USA and China (Bartholomeeusen et al., 2023). However, it is expected to largely avoid spreading in Europe, except for the southern regions of Italy and Turkey. On the other hand, *Ae. albopictus*, whose dormant eggs enable survival in colder winters, is projected to establish its presence across Europe, the northern USA, highland regions of South America, and eastern Africa (Messina et al. 2014; Kraemer et al. 2015; Oliveira et al. 2021).

The unprecedented magnitude of the 2005-2007 Indian Ocean islands and South East Asia outbreaks has raised questions about the origin of the virus and the determinants of its emergence. A comparison of full-genome sequences demonstrated a 99.9% sequence similarity between the Indian and Reunion strains, indicating that the Indian epidemic strain originates from the ECSA and not from the Asian clade (33). The extent of this epidemic led to the consideration of a new fourth lineage – the Indian Ocean Lineage (IOL) derived from an ECSA enzootic strain (Volk et al. 2010; Scott C. Weaver et al. 2012; Wahid et al. 2017).

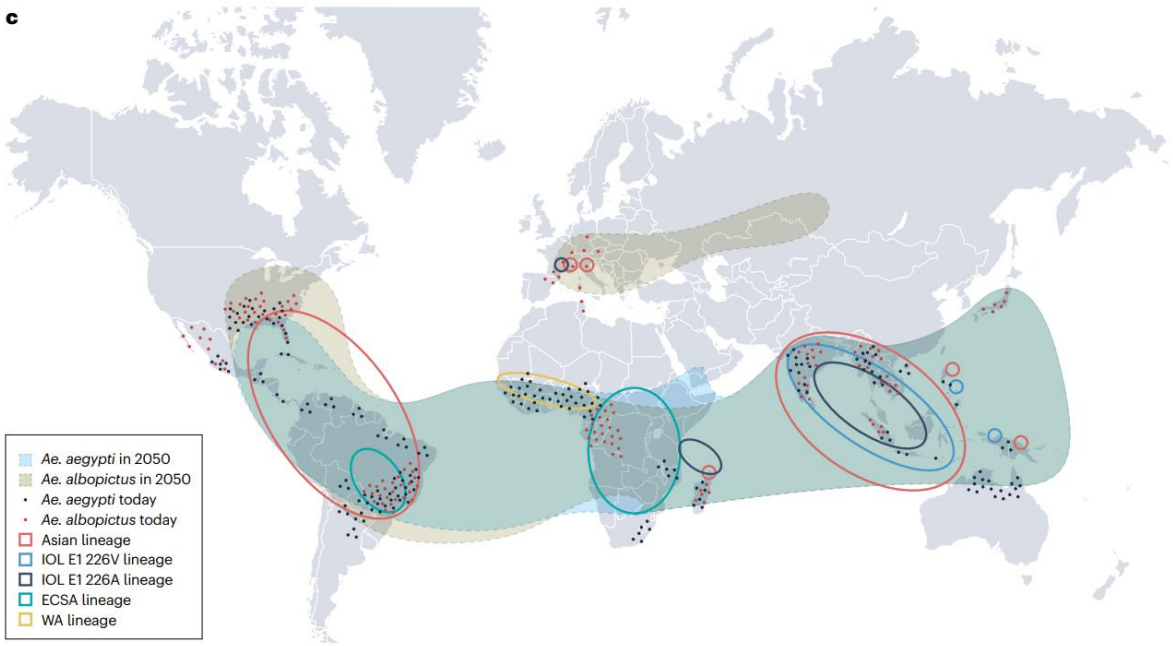

Figure 4: World map showing the spread of CHIKV and its main vectors, Aedes albopictus, and aegypti. *Color dots represent the actual distribution of both vectors. Colored area shading illustrates the potential vector global spread by 2050.*

Before the Indian Ocean (IO) outbreak, the CHIKV interhuman transmissions were mainly due to the *Ae. aegypti* vector, established in tropical and subtropical regions of the globe (Tsetsarkin et Weaver 2011). However, the mosquito responsible for the interhuman transmissions that occurred on La Réunion island was the Asian tiger mosquito, *Ae. albopictus* that previously has never been associated with alphavirus outbreaks (Tsetsarkin et al. 2007). Phylogenetic analysis of several CHIKV isolates from different regions during the Indian Ocean epidemic, identified the independent acquisition of a common alanine to valine substitution in the E1 envelop protein at position 226 (*E1-A226V*). This mutation was directly associate to an adaptation to the *Ae. albopictus* vector, and plausibly explains how CHIKV caused an epidemic on a territory lacking its typical vector *Ae. aegypti*. Indeed, reverse genetics and viral competition experiments demonstrating that the single E1-A266V mutation was responsible for an increase in CHIKV infectivity for *Ae. albopictus*, without changing viral fitness in its primary vector *Ae. aegypti* (Tsetsarkin et al. 2007). Further studies demonstrated that this mutation led to more efficient CHIKV oral infectivity for midgut epithelial cells (40 to 100-fold), thus leading to better dissemination in the *Ae. albopictus* salivary glands and enhanced transmission to a vertebrate host (Vazeille et al. 2007; Tsetsarkin et al. 2007; Arias-Goeta et al. 2013).

Interestingly, the first Southeast Asian outbreak (Malaysia, 2006) was associated to the Asian genotype strain that has been circulating for more than 60

years. Although *Ae. albopictus* is native to that region of the globe, *Ae. aegypti* played a major role in the Asian CHIKV strain transmission until 2007. Strikingly, between 2007 and 2009, a shift in the viral genotypes was observed, with the IOL strain progressively replacing the Asian endemic CHIKV strain. Since the Indian Ocean outbreaks demonstrated that the single E1-A226V substitution greatly enhances CHIKV transmission by *Ae. albopictus*, one can reasonably question why this mutation had not been selected during more than 60 years of transmission. This could be partially explained by identifying epistatic mutations within the E1-protein sequence (Tsetsarkin et al. 2009). Epistatic mutations are genetic changes that interact with one another, influencing an organism's overall phenotype or characteristics (Tsetsarkin et al. 2009). The Asian lineage possesses a tryptophan residue at position 98 of its E1 glycoprotein (E1-98T) that negatively affects E1-226V mutation, thus restricting the adaptability of this genotype to *Ae. albopictus* and its emergence in Asia. This inability has likely facilitated the IOL strains to colonize the Ae. albopictus transmission cycle niche in Southeast Asia (Tsetsarkin, Chen, et Weaver 2016; Tsetsarkin et Weaver 2011). Conversely, E1-A98T and E2-I211T substitutions were demonstrated to positively impact the CHIVK strains harboring the A226V mutation by increasing the infectivity in *Ae. albopictus*, favoring CHIKV emergence and (Tsetsarkin, Chen, et Weaver 2016; Tsetsarkin et Weaver 2011).

B. Physiopathology and Immunology

1. Acute disease

The infection cycle starts in the dermis, following the bite of an infected mosquito, where the virus-containing saliva is deposited. Initial replication in the dermis produces infectious virions that reach the bloodstream or spread to draining lymph nodes. Subsequently, CHIKV targets multiple organs and tissues: the liver, spleen, muscles, and joints. The acute phase of the disease is characterized by the rash, fever, and joint/muscle pain triad (Suhrbier et Mahalingam 2009), with a particularly high viremia accompanied by a robust innate immune response (Waggoner et al. 2016; Matusali et al. 2019; Poo et al. 2014; Teo et al. 2012). Innate response drives an abrupt onset of fever 4-7 days post-infection (B. et al. 2019; Dutta et al. 2014). Viremia resolves often in a week. The prominent symptom of CHIKV acute infection is highly invalidating joint pain (92% of cases) with symmetrical arthralgia affecting primary distal joints, as well as myalgia (52% of cases) (Bartholomeeusen et

al. 2023). This condition persists in >50% of patients for 1 month (Bartholomeeusen et al. 2023; B. J. Paul et Sadanand 2018; Poo et al. 2014). Severe disease manifestations, including encephalitis and encephalopathy, renal failure, toxic hepatitis, and myocarditis, have been reported during the 2005-2006 Indian Ocean islands outbreaks, as well as during the Caribbean epidemic between 2013-2015 Gérardin et al. 2016).

2. Chronic disease

The post-acute phase of Chikungunya fever encompasses the period from 21 days to 3 months after the onset of symptoms (Simon et al. 2015). When the clinical manifestations, with arthralgias being a prominent feature, persist for more than 3 months, Chikungunya fever is classified as the chronic form of (Hoarau, Bandjee, et al. 2010; Simon et al. 2015). Estimating the proportion of patients progressing to the chronic form of Chikungunya fever is challenging and appears to be influenced by factors such as patient age and/or CHIKV genotype. However, approximately 40–80% of patients are believed to experience chronic disease (Hoarau, Jaffar Bandjee, et al. 2010; Amaral, Bilsborrow, et Schoen 2020; Heath et al. 2018; Sissoko et al. 2009). In addition to the chronic arthralgia observed in up to 79% of patients with a protracted disease, long-term sequelae include depression, chronic fatigue (Duvignaud et al. 2018; Suhrbier 2019), and neurological disorders (Mehta et al. 2018; Brizzi 2017).

During acute infection, higher viral loads, as well as symptoms like arthralgias, body aches, and weakness, are associated with an increased risk of developing chronic arthralgias (Hoarau, Bandjee, et al. 2010; Heath et al. 2018; Amaral, Bilsborrow, et Schoen 2020). However, it's important to note that replicative virus has not been detected in these cases (Hoarau, Jaffar Bandjee, et al. 2010; Heath et al. 2018; Sissoko et al. 2009). Moreover, individuals with pre-existing osteoarthritis are more susceptible to being affected by chronic arthralgias (Sissoko et al. 2009). The reported prevalence of joint pain outbreaks may vary and could be influenced by the duration of follow-up. However, most estimates suggest that around one-quarter of patients are affected by joint pain even one year after the initial infection (Heath et al. 2018; Sissoko et al. 2009; Manimunda et al. 2010; Rodríguez-Morales et al. 2016).

3. Immunological aspects of CHIKV disease

The strong immune response, that accounts for CHIKV disease, is triggered by the entry and replication of CHIKV. This response involves specialized immune receptors called pattern recognition receptors (PRRs), such as Toll-like receptors 3, 7, and 8 (TLR-3, -7, and -8) and retinoic acid-inducible gene I (RIG-I)-like receptors (RLR). These receptors recognize various intermediate replication forms of the (+) ss RNA virus. The activation of PRRs initiates a complex signaling cascade that can involve the mitochondrial antiviral signaling (MAVS) pathway, leading to the activation of Nuclear Factor-kappa B (NF-κB) and interferon regulatory factor 3 (IRF3) pathways (Schwartz et Albert 2010; Suhrbier 2019). This results in the release of pro-inflammatory cytokines like interleukin 6 (IL-6) and tumor necrosis factor-alpha (TNF-α), which play a significant role in establishing an inflammatory state. These cytokines also control the recruitment of antigen-presenting cells to the site of infection and

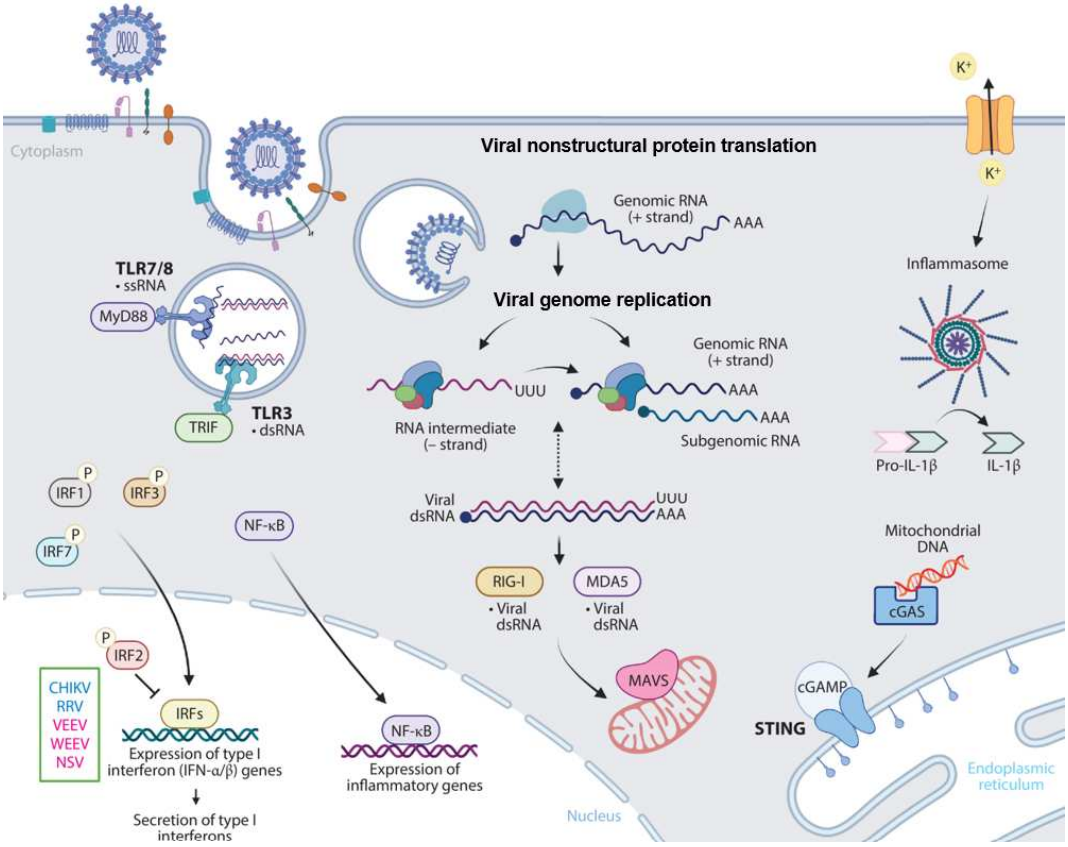

Figure 5: Overview of innate immune signaling pathways impacting CHIKV and other alphavirus infections. *Endosomal PRRs (TLR3, TLR7, and TLR8) recognize PAMPs and signal through distinct adaptor proteins (e.g., MyD88 and TRIF). TLR activation and secondary signaling through potassium efflux activate the inflammasome. Viral RNA transcription in the cytoplasm leads to the formation of dsRNA, which can trigger cytoplasmic PRRs, RIG-I, and MDA5 to interact with MAVS on the mitochondrial membrane. cGAS can recognize endogenous or foreign DNA released during infection, leading to the activation of STING. These recognition events initiate the translocation of IRFs and NF-κB into the nucleus and regulation of type I interferons and proinflammatory gene expression. Abbreviations: cGAMP, cyclic GMP-AMP; cGAS, cGAMP synthase; dsRNA, double-stranded RNA; IRF, interferon regulatory factor; MAVS, mitochondrial antiviral-signaling protein; NF-κB, nuclear factor kappa B; PAMP, pathogen-associated molecular pattern; PRR, pattern recognition receptor; ssRNA, single-stranded RNA; STING, stimulator of interferon genes; TLR, Toll-like receptor. Adapted from Kafai, Diamond, et Fox 2022.*

induce the transcription of type I interferon genes (IFN) (Chirathaworn, Chansaenroj, et Poovorawan 2020) (Chow et al. 2011; Poo et al. 2014; Suhrbier 2019). IFNβ and subtypes of IFNα are crucial in controlling CHIKV infection in mammals (Rudd et al. 2012; Poo et al. 2014; Suhrbier 2019).

Experiments using IFNα receptor knock-out (*IFNAR*^{KO}) mice showed that they succumbed to CHIKV infection within two days, while all wild-type mice survived for 20 days after infection (Couderc et al. 2008). Neonates with immature RIG-I response or impaired interferon regulatory factor (IRF) 7 activation are at higher risk of developing severe disease (Danis et al. 2008; Rudd et al. 2012; Marr et al. 2014). Elderly individuals with reduced TNF receptor-associated factor 3 and IRF8 expression, which are required for RIG-I signaling, control less efficiently CHIKV infection (Molony et al. 2017). Although interferons are essential for limiting viral infection, excessive pro-inflammatory cytokines during CHIKV infection can increase disease severity (Chirathaworn, Chansaenroj, et Poovorawan 2020). For instance, challenging mice with polyinosinic:polycytidylic acid (mimicking double-strand RNA), a potent inducer of type I IFN production, induces arthritis with comparable proinflammatory gene expression profile as observed in CHIKV arthropathy (Prow et al. 2017). Finally, it is noteworthy that the antiviral activity of IFN cytokines is temperature-dependent, optimal at 37°C. This explains, at least in part, why CHIKV replicates more efficiently in peripheral joints than elsewhere in the organism (Prow et al. 2017). Despite a robust and rapid immune response, CHIKV effectively evades the cellular antiviral control (Akhrymuk, Kulemzin, et Frolova 2012; Bae, Lee, et Myoung 2020; Göertz et al. 2018; Rathore, Ng, et Vasudevan 2013; Jelke J. Fros et Pijlman 2016). In fibroblasts, for instance, the translational shut-off induced by CHIKV proteins, as well as the viral-induced apoptosis, lead to CHIKV-dissemination and a pick of viremia during the acute phase (White et al. 2011; Sourisseau et al. 2007).

Proinflammatory cytokines and chemokines secretion induced by viral replication leads to the recruitment of immune cells. These include monocytes, NK cells, neutrophils, and T cells, which help limit the infection but also participate in inflammation and tissue damage (Teo et al. 2012; Poo et al. 2014; Suhrbier 2019). For instance, monocytes and macrophages, which are involved in inflammation resolution and disease clearance (Ikeda et al. 2018), are also sites of CHIKV replication and persistence (Labadie et al. 2010; Zaid et al. 2018; 2020). Indeed, studies in nonhuman primates demonstrated viral RNA persistence in synovial macrophages (Labadie et al.

2010). In vitro experiments conducted in RAW264 cells, a murine macrophage cell line, have indicated that macrophages infected with the CHIKV produce inflammatory cytokines such as TNF and IL-6 (Nayak et al. 2019). Additionally, investigations using mouse models of chikungunya arthritis and the analysis of peripheral blood mononuclear cells from patients, have pointed towards the involvement of the NOD-, LRR- and pyrin domain-containing 3 (NLRP3) inflammasome, and consequently, the release of IL-1β and IL-18, during CHIKV infection (W. Chen et al. 2017). It's worth noting that a small-molecule inhibitor that prevents NLRP3 activation has shown the ability to reduce CHIKV-induced inflammation in mice (Guo et al. 2018). Interestingly, NLRP3 is also implicated in the development of rheumatoid arthritis (RA), as high levels of NLRP3 activation have been reported in monocytes/macrophages that infiltrate the synovial tissue of RA patients (Guo et al. 2018).

Mechanisms of CHIKV chronic disease are poorly understood. It was proposed that chronic inflammation is simply a prolongation of the acute inflammatory state, and that chronic CHIKV arthritis is not linked to active viral replication (Chang at al. 2018). In addition, patient experiencing chronic CHIKV disease, exerted aberrant immune response with higher levels of IL-6 than those that had recovered from acute infection (Gardner et al. 2010; Chow et al. 2011). In joint tissues, IL-6 lead to the activation of RANKL and inhibition of osteoprotegrin (OPG), which directly impair osteoblast functioning and bone mineralization (Chow et al. 2011; Noret et al. 2012; Sharp et al. 2021). Persistent CHIKV arthralgia is also linked to higher amounts of IL-17 which is a bone resorption-associated cytokine (Chow et al. 2011).

C. A key role of the musculoskeletal tissue in CHIKV pathogenesis

Like other arthritogenic alphaviruses, CHIKV displays a large cell and tissue tropism in vertebrates. Indeed, CHIKV efficiently replicates in endothelial cells, fibroblasts from almost all organs, and brain cells (Abraham et al. 2013; 2017; Abere et al. 2012; Briant et al. 2014; Bernard et al. 2015). However, the induced rheumatic disease mainly reflects CHIKV capacity to establish a productive infection in cells from joint and muscle tissues (Sourisseau et al. 2007; Wikan et al. 2012; Young et al. 2019). Within joints, cells such as chondrocytes, osteoblasts, and bone marrow mesenchymal stem cells, which give rise to osteogenic cells, are susceptible to CHIKV infection (Hoarau, Jaffar Bandjee, et al. 2010; Phuklia et al. 2013; Roy et al. 2020). The infection

causes cellular damage, contributing to CHIKV-induced arthritis and joint pain. For instance, when osteogenic cells are infected, their ability to mineralize and repair is impaired, leading to dysregulated bone homeostasis observed in patients (Roy et al. 2020). In muscles, CHIKV replication is prominent, as evidenced by the presence of viral antigens and signs of necrosis, vacuolization, and fibrosis in patients with acute and chronic CHIKV disease (Ozden et al. 2007). In vitro studies showed that muscle fibroblasts, satellite cells, and myoblasts (muscle progenitors) are highly susceptible to CHIKV infection (Couderc et al. 2008; Ozden et al. 2007; Lohachanakul et al. 2015).

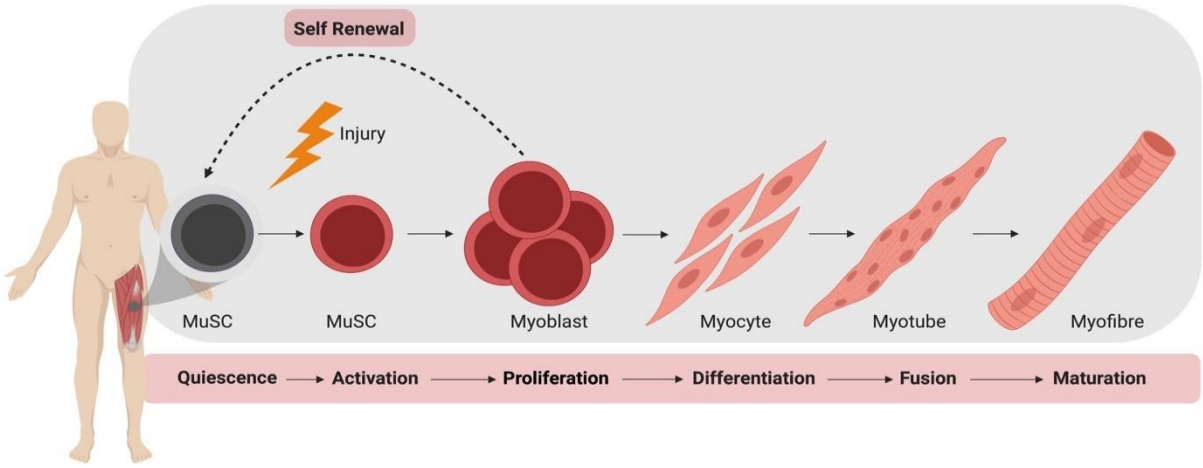

Figure 6:Muscle stem cell (satellite cells) (MuSC) mediated skeletal muscle regeneration. *Following injury, quiescent MuSCs are activated and undergo rapid proliferation, followed by differentiation into myocytes, which fuse and mature to generate new muscle fibers.*

Initially, it was believed that fully differentiated myotubes are less affected by CHIKV infection (Ozden et al. 2007). However, recent research has shown that murine skeletal muscle fibers can be efficiently infected, impacting the severity of CHIKV infection in mice (Roberts et al. 2017; Lentscher et al. 2020; Rohatgi et al. 2014). Some studies have suggested that different strains of CHIKV may vary in their ability to infect muscle cells and induce myopathic syndromes, but this has not been definitively proven (Lohachanakul et al. 2015; Roberts et al. 2017; Lentscher et al. 2020; Rohatgi et al. 2014). For example, an isolate from the Reunion Island outbreak was found to cause more severe muscle disease in neonatal mice compared to an isolate from Senegal that circulated in 1983 (Rohatgi et al. 2014). While both strains spread from the site of infection to distal muscle by infecting connective tissue fibroblasts, the epidemic strain replicates more efficiently in myofibers, leading to increased muscle disease characterized by severe myonecrosis (Rohatgi et al. 2014). It is not entirely clear whether the increased muscle pathology is solely due to a more robust immune

response, as no significant differences were observed in the induction of type I interferon (IFN-I) and proinflammatory cytokines such as IL-1β or IL-6 (Rohatgi et al. 2014).

Recent studies have demonstrated the importance of viral replication in muscle cells for CHIKV pathogenesis (Lentscher et al. 2020; Young et al. 2019). Researchers engineered a CHIKV strain that has restricted replication in muscles by incorporating sequences, complementary to a skeletal muscle cell-specific microRNA called miR-206 (Lentscher et al. 2020). This microRNA is expressed in skeletal muscle progenitor satellite cells, significantly induced upon differentiation, and stably expressed throughout the life of the muscle fiber (G. Ma et al. 2015). Using this genetically modified virus, it was shown that viral replication in skeletal muscle cells does not significantly affect overall viral titers or the global inflammatory status. However, it does result in reduced muscle damage, as reflected by diminished necrosis and local induction of IL-6, IL-1β, TNFα, and IP10, which are biomarkers of disease severity in humans and mice (Lentscher et al. 2020; Nair et al. 2017).

Overall, the pathogenesis of CHIKV is closely linked to the regulation of the immune response following infection, but also to its propensity to highly replicate in the musculoskeletal tissue. Further studies about viral and cellular determinants involved into CHIKV replication and pathogenesis are needed to completely understand the induced pathology. A question of great interest is to what extent viral products can persist in infected tissues, and how this persistence could trigger a chronic inflammatory state, thus participating to the establishment of chronic musculoskeletal disease.

D. Current strategies to fight CHIKV infection

1. Vector control

Vector control is one of the pillars of CHIKV and arboviruses fighting. Mass spraying of chemical insecticides or using mechanical methods to protect houses from mosquito entering and to eliminate standing waters are first-line solutions to improve vector control. However, using toxic chemicals is not always possible regarding human health and environmental considerations, and outdoor insecticide spraying is not efficient on indoor resting *Ae. spp.* mosquitoes (Wahid et al. 2017; Perich et al. 2000). Furthermore, vector resistance to chemical insecticides is an additional argument favoring the development of other strategies. Such strategies include vector trapping,

resulting in vector capture, death, and/or sterilization of vectors (Barrera 2022). For example, inactivated yeast-interfering RNA tablets were developed and placed in water inside trap containers to kill mosquito larvae. Finally, to control the transmission of human-health-threatening viral pathogens, genetic control technologies are currently developed to control or modify mosquito populations. For instance, replacing the existent mosquito population with mosquitoes infected with the intracellular parasite *Wolbachia* is a valuable strategy to reduce arboviruses transmission (G.-H. Wang et al. 2021).

2. Vaccine development

From a vaccine-based prevention perspective, after more than 60 years of vaccine research, a CHIKV vaccine might be soon approved. A CHIKV vaccine would elicit rapid and durable immunity and provide protection against the different CHIKV variants. The primary goal of the vaccination must be to decrease morbidity associated to viral infection, meaning that it must be highly safe and tolerable. Finally, because CHIKV infects low- and middle-income countries, the approved vaccine must be affordable, easy to store and to ship. Promisingly, seroepidemiological studies conducted after natural CHIKV infections suggest that the levels of neutralizing antibodies, which can persist for years, are likely indicative of the level of protection a vaccinated individual may have against future infections (Milligan et al. 2019; Bartholomeeusen et al. 2023).The most advanced CHIKV vaccine in development is VLA1553, a live-attenuated, single-dose vaccine (Schneider et al. 2023). This vaccine was developed on the CHIKV-LR2006-OPYI strain isolated from the epidemic on the Reunion Island in 2006 (Schneider et al. 2023). Despite that near 100% of the participants from a randomized controlled trial have met the imposed threshold for seroprotection following one dose, and have tolerated the vaccine, care must be taken. Indeed, live-attenuated vaccines cause more often systemic reactogenicity. For VLA1553 vaccine, high fever, transient arthralgia and arthritis have been reported (reviewed in (Bartholomeeusen et al. 2023). The same observations were made for the live-attenuated 181/25 CHIKV vaccine, with ~8% of vaccinated participants experienced mild, transient arthralgias (Edelman et al. 2000). Due to this reactogenicity, 181/25 vaccine development was halted.

Live vaccines are unsuitable for specific at-risk groups, such as pregnant individuals or those with weakened immune systems. An alternative to live-attenuated vaccines is a VLP-based product. Virus-like particles, or VLPs, consist of essential

viral proteins that naturally form structures resembling the virus but lack the ability to reproduce. VLP vaccines offer simpler manufacturing processes, convenient storage and transport, and a well-established track record of safety (Mohsen et Bachmann, 2022). In 2022, a phase II trial was conducted involving PXVX0317, a virus-like particle (VLP) combined with aluminum hydroxide adjuvant (Bennett et al. 2022). This investigation revealed a significant enhancement in the neutralization response following the initial injection. Seropositivity rates rapidly increased within just 7 days and reached 100% by day 57. Notably, a single high dose resulted in a swift, approximately tenfold rise in neutralizing antibodies within a week and a nearly hundredfold increase at 28 days, with a sustained elevation lasting up to approximately two years. Furthermore, administering a booster dose 18 months after the initial active injection elicited a robust memory response (Bennett et al. 2022). Regarding side effects, joint pain was reported in 6% of participants following the initial vaccination, whereas joint pain was observed in 12% of volunteers who received VLA1533 (Wressnigg et al. 2020). Currently, the single high-dose regimen is undergoing testing in a phase III clinical trial, and PXVX0317 has been granted FDA Fast Track designation.

3. Therapeutic strategies

From a therapeutic perspective, analgesic and/or nonsteroidal anti-inflammatory drugs (NSAIDs) remain the primary treatment choices for managing the symptoms of arthritogenic alphaviral diseases. The systemic use of corticosteroids during the acute phase of chikungunya fever (less than 3 weeks) is not recommended (Simon et al. 2015). However, in cases where non-steroidal anti-inflammatory drugs (NSAIDs) or opioids are contraindicated or ineffective, low doses of corticosteroids may be considered during the post-acute phase. The administration of corticosteroids is most beneficial in the post-acute and chronic phases (more than 3 months after infection), particularly for patients exhibiting joint inflammation (such as tenosynovitis, synovitis, or tunnel syndrome), neurological symptoms, or inflammation in other significant areas (Amaral, Bilsborrow, et Schoen 2020). Additionally, they can be combined with additional pain relievers (both level 1 and level 2) if NSAIDs prove resistant or ineffective.

4. Antiviral strategy

Numerous potential drug candidates targeting various viral enzymatic functions have been documented. These candidates encompass both novel chemical compounds derived from nature and those that inhibit the capping, macrodomain, and capsid protease functions of nsPs (Abdelnabi et Delang 2020; Battisti, Urban, et Langer 2021; Skidmore et Bradfute 2023). Despite these promising findings, none of the compounds have undergone *in vivo* testing or entered preclinical assessment. In contrast, during a drug repurposing screen, the FDA-approved drugs *novobiocin* and *telmisartan* were identified as potential CHIKV protease inhibitors. However, their actual antiviral efficacy in vivo is yet to be determined (Tripathi et al. 2020).

Broad-spectrum nucleobase analogs like *favipiravir* and *sofosbuvir*, which target CHIKV RNA-dependent RNA polymerase activity, have demonstrated some *in vivo* potential against CHIKV. Sofosbuvir, a drug effectively used in hepatitis C virus infections, holds particular promise for clinical relevance (Delang, Abdelnabi, et Neyts 2018; Ferreira et al. 2019). Furthermore, approaches aimed at targeting the viral entry pathway, particularly the interaction between the viral envelope and the MXRA8 receptor using recombinant Fc-MXRA8 fragments or combinations of neutralizing monoclonal antibodies, have displayed potential in animal models, with a reduced risk of off-target effects. Other therapeutic avenues under investigation involve targeting host cell pathways that either support or suppress viral replication. These strategies include manipulating fatty acid synthesis, cholesterol trafficking pathways, regulating endosome acidification to hinder virus entry, inhibiting nucleobase biosynthesis, or employing immunomodulatory therapies to stimulate an interferon response (Abdelnabi et Delang 2020; Skidmore et Bradfute 2023; Battisti, Urban, et Langer 2021). While some promising broad-spectrum candidate compounds exhibit antiviral activity against multiple viruses, it is essential to anticipate off-target toxic effects due to potential disruptions of cellular pathways. Nevertheless, comprehensive preclinical and clinical evaluations for these compounds remain outstanding (Bartholomeeusen et al. 2023; Ekchariyawat et al. 2015; Wong et Chu 2018; Abdelnabi et Delang 2020; Skidmore et Bradfute 2023).

Chapter IV: Chikungunya virus life cycle

A. Chikungunya virus structure and genome organization

CHIKV virions are spherical particles of roughly 70nm in diameter with an icosahedral symmetry of triangulation T = 4 (Sun et al. 2013; Mangala Prasad et al. 2022; Voss et al. 2010). Viral envelop proteins (E1/E2) organize in 80 trimeric glycoprotein spikes, each spike formed by three E1-E2 heterodimers and embedded within a host-cell derived lipid bilayer (membrane) (Sun et al. 2013; Mangala Prasad et al. 2022; Voss et al. 2010). E2 is required for attachment factors and receptor recognition. It harbors three immunoglobulin-like domains (A, B, and C) exposed at the virion surface and targeted by the neutralizing antibodies (Voss et al. 2010; Fong et al. 2014; Smith et al. 2015). A transmembrane domain anchors E2 into the viral membrane, and a cytoplasmic domain mediates interactions with the nucleocapsid. E1 is a pH-dependent, type-II fusion protein anchored in the viral membrane by a transmembrane helix (Voss et al. 2010; Yap et al. 2017). It is organized into three domains, I, II, and III, with a fusion loop within the domain II, which is responsible for the fusion of the viral envelope with the cell membrane (Figure 10) (Voss et al. 2010; Yap et al. 2017). Underneath the membrane, 240 copies of capsid protein form a well-ordered icosahedral capsid protecting the viral single-stranded RNA genome.

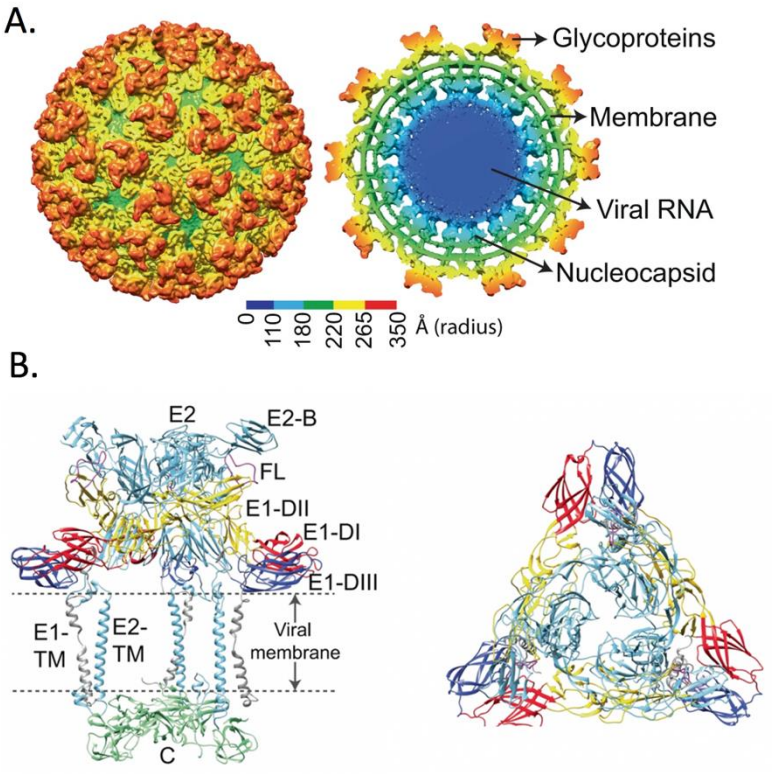

Figure 7: CHIKV virion structure and envelop protein organization. *A, Surface view (left) and cross-sectional view (right) of UV-inactivated CHIKV strain S27. Cryo-EM density map is colored according to radius. B, Side view of ribbon structure of the trimeric surface glycoprotein heterodimers in contact with the inner capsid protein as observed in the wild-type virion (PDB ID: 3J2W). Bottom panel, Top view of the trimeric E1-E2 heterodimers on wild-type CHIKV. (Mangala Prasad et al.*

CHIKV genome is an 11.8kb single-stranded RNA molecule of positive polarity that resembles cellular mRNA as it is 5'capped and 3' polyadenylated (Khan et al. 2002). These features enable viral genome translation by the cell machinery immediately after its release in the cytosol of the infected cell (Khan et al. 2002). The genomic RNA (gRNA) contains two open reading frames, encoding a non-structural polyprotein (5'-ORF1) and a structural-polyprotein (3'-ORF2). In addition, gRNA molecules contain several nucleotide sequences, named *cis*-acting sequence elements (CSEs), located in the 5' and 3' untranslated regions (UTR) as well as between the two ORFs (subgenomic promotor). These structures play multiple functions in viral RNA replication, transcription of the subgenomic RNA (sgRNA), and viral RNA packaging into newly formed viral particles (D. Y. Kim et al. 2011). The presence of stem-loops structures at the very start of the 5'UTR region, was also demonstrated as involved into gRNA protection from cellular interferon-induced proteins (e.g., IFIT1), thus allowing viral gRNA translation by the cellular machinery (Reynaud et al. 2015).

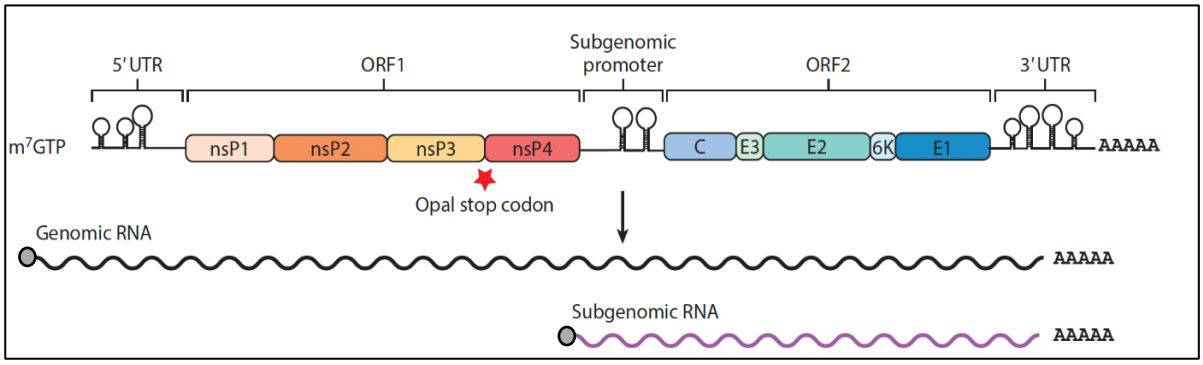

Figure 8: CHIKV genome organization: CHIKV genomic organization and viral proteins. *The CHIKV genome comprises a 5'capped and 3'-polyadenylated positive-stranded RNA molecule divided into two ORFs. Expression of ORF1 and ORF2, encoding for the nonstructural and structural polyproteins, is controlled by the genomic promoter in the 5'UTR and the internal subgenomic promoter, respectively. Genome replication and transcription are cis-regulated by RNA stem-loops, referred to as conserved sequence elements, located in the 5'UTR, subgenomic promoter, and 3' UTR regions. CHIKV replication results in the accumulation of full-length RNA used as a genome for CHIKV progeny assembly. Subgenomic RNA is transcribed and used as a template for translating structural polyproteins. From Kril et al.2021*

The 5'-ORF1 encodes the non-structural (ns) polyprotein involved into the synthesis of the viral machinery, also called *replicase complex,* required for genome replication and transcription (J. H. Strauss et Strauss 1994; Merits et al. 2001; Rausalu et al. 2016). The individualization of the non-structural proteins (nsP) *nsP1, nsP2, nsP3 and nsP4* result from the sequential processing of the polyprotein, mediated by the protease activity of the viral nsP2 (J. H. Strauss et Strauss 1994; Merits et al. 2001; Rausalu et al. 2016). The nsP possess specific enzymatic activities as well as accessory functions, crucial for viral replication and host-cell response regulation.

CHIKV structural proteins form the virion and are translated from the subgenomic viral RNAs and also expressed as a polyprotein, that is processed by viral and cellular proteases. Three main structural proteins are expressed: capsid, E1 and E2 viral glycoproteins. Two supplementary small structural proteins are also synthesized E3 and 6K, that play stabilization and regulation functions involved into viral glycoproteins assembly and particle budding.

B. CHIKV life cycle

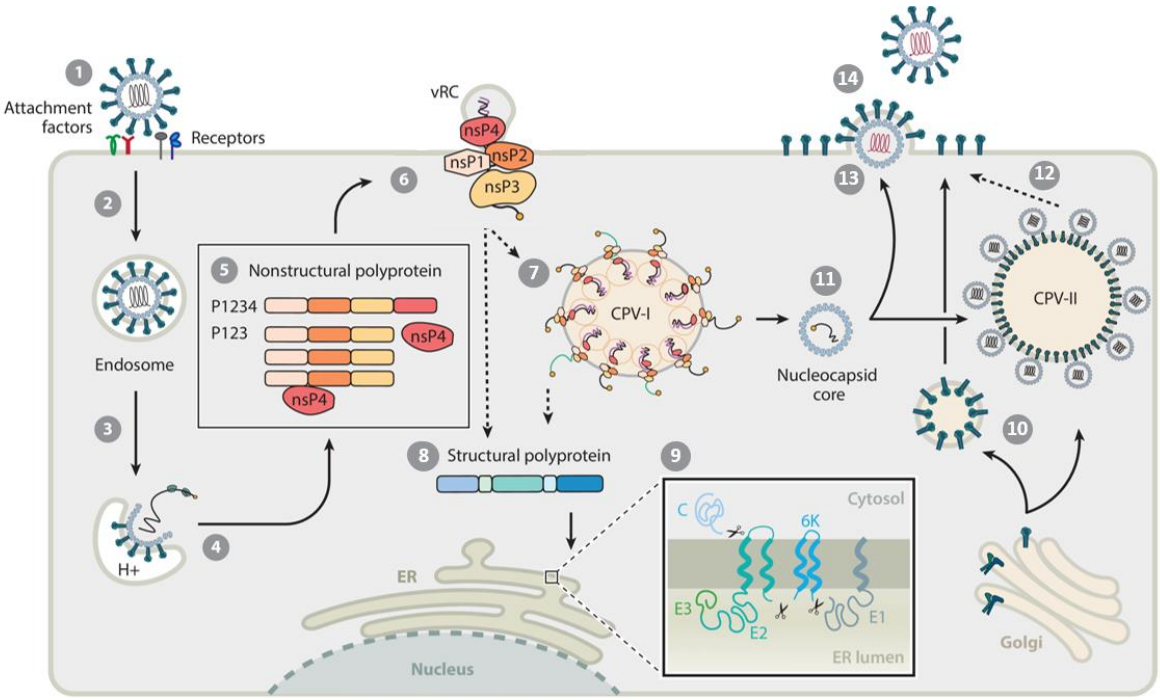

Figure 9: Overview of CHIKV replicative cycle. *1, CHIKV entering the host cell is mediated by viral glycoproteins E1/E2 with receptor and attachment factors on the cell surface. 2. The virus is internalized through endocytosis and transported to endosomes. 3. The acidic environment in the endosome triggers fusion between the viral and endosomal membranes. 4, The viral C protein is released into the cytoplasm and undergoes uncoating. 5, The CHIKV genome is translated to produce P123 and P1234 polyproteins. 6, nsP4, along with P123 and an RNA template, forms a complex that reshapes the cell membrane to create replication organelles called spherules. 7, Replication compartments may undergo endocytosis and fusion with endo-lysosomes to form CPV-I, where active spherules are located. 8, Structural proteins are translated from subgenomic RNA and translocated to the endoplasmic reticulum. 9, autocatalytic processing releases Capsid protein, while host proteases mature E glycoproteins and 6K protein. 10, Mature E glycoproteins and 6K protein are trafficked to the plasma membrane via the secretory pathway. 11, the capsid protein and the RNA genome assemble at the plasma membrane into an icosahedral nucleocapsid. 12, Viral assembly occurs primarily at the plasma membrane, where mature E glycoproteins and nucleocapsids are targeted. 13, The capsid protein and E2 glycoprotein interaction promote CHIKV particle budding and release. 14, Assembled nucleocapsids and E glycoproteins can also be recruited to CPV-II, contributing to viral assembly and budding. Figure adapted from Kril et al. 2021*

As an arthropod virus, alphaviruses establish a replicative cycle in invertebrates and mammalian cells. Whereas in mammalian cells, the replicative cycle is cytopathic, mosquito cells support persistent viral infection (Jose, Taylor, et Kuhn 2017). In both hosts, alphaviruses achieve their replication exclusively in the cytosol. Following receptor interaction and entry into the cell, the viral genome is released into the cytoplasm, where nsP1-4 are directly translated and addressed to the plasma membrane, along with the incoming genomic RNA (gRNA)(J. H. Strauss et Strauss

1994; K. H. Kim et al. 2004; Jose, Taylor, et Kuhn 2017). Viral RNA synthesis occurs into membrane invaginations named spherules, formed through the synergic activity of the non-structural proteins and host-factors (J. H. Strauss et Strauss 1994; Jose, Taylor, et Kuhn 2017; Rupp et al. 2015; Girard et al. 2023; Tan, Chmielewski, Yien Law, et al. 2022; Laurent et al. 2022). These spherules could be internalized in mammalian cells, forming cytopathic vacuoles (CPV-1) where viral synthesis continues (Jose, Taylor, et Kuhn 2017; Reis et al., 2022). In contrast, in persistently infected mosquito cells, viral replication organelles are established on large endolysosomal vesicles and not transported to the plasma membrane. Furthermore, viral replication and assembly sites seem to have dual localization in infected mammalian cells (spherule/CPV-1 and CPV-2/plasma membrane, respectively). In infected mosquito cells, nucleocapsids and glycoproteins are found on the large vesicles containing the replicative spherules, suggesting that replication and assembly sites are not segregated (Jose, Taylor, et Kuhn 2017). These structural differences may account for establishing a persistent viral infection in mosquito cells (Jose, Taylor, et Kuhn 2017). In the following sections, the different steps of the CHIKV replication cycle in mammalian cells are discussed more deeply.

1. CHIKV entry into target cells

i Receptor-mediated entry

The identity of the cellular receptor responsible for CHIKV entry was unknown until Zhang and colleagues (R. Zhang et al. 2018) conducted a genome-wide screening using CRISPR/Cas9 and identified *Mxra8* (also known as limitrin, DICAM, or ASP3) as a CHIKV entry factor. Mxra8 is an adhesion molecule primarily found on epithelial and mesenchymal cell types targeted by CHIKV, such as dermal and synovial fibroblasts, osteoblasts, chondrocytes, and skeletal muscle cells (R. Zhang et al. 2018; 2019). Mxra8 is not specific to CHIKV, and it is used by other arthritogenic alphaviruses such as Mayaro virus, Ross River virus and O'nyong-nyong virus (R. Zhang et al. 2018). However, encephalitic alphaviruses use different sets of receptors (Clark et al. 2022; H. Ma et al. 2020). Structural studies have shown that Mxra8 interacts with the envelope spike of CHIKV through a complex 3:3 binding interaction involving both the E2 and E1 proteins (Basore et al. 2019; Song et al. 2019). This interaction facilitates virus attachment and internalization into the cell (Basore et al. 2019; Song et al. 2019). Increasing the expression of Mxra8 in cells that are normally

less susceptible to CHIKV infection allows viral entry (R. Zhang et al. 2018). Conversely, blocking the Mxra8-CHIKV interaction using CRISPR-Cas9 to deplete the Mxra8 gene, neutralizing antibodies, or fusing extracellular domains of Mxra8 with an immunoglobulin Fc fragment (Mxra8-Fc) inhibits infection in both mouse and human cells, and reduces CHIKV pathogenesis in mice (R. Zhang et al. 2018; 2019). This indicates that Mxra8 is important for optimal infection, dissemination, and joint-related pathogenesis. Although Mxra8 plays a crucial role in CHIKV infection and pathogenesis, CHIKV infection has been observed in murine or human cells lacking Mxra8 (R. Zhang et al. 2018; 2019). Additionally, the limited dependence on Mxra8 of the epidemic CHIKV strains (IOL, LR-2006 strains) compared to the Asian lineage strains, strongly suggests that other CHIKV receptors exist and remain to be discovered (R. Zhang et al. 2018; Y.-N. Zhang et al. 2019; Song et al. 2019; A. S. Kim et Diamond 2022). Additionally, glycosaminoglycans (GAGs), a family of negatively charged polysaccharides, interact with a positively charged domain in the E2 protein and have been proposed to enhance CHIKV infection by promoting E1/E2 dissociation (McAllister et al. 2020; Sahoo et Chowdary 2019). Recent genome-wide screens have identified GAGs biosynthesis enzymes as critical factors for CHIKV infectivity (Tanaka et al. 2017). The requirement for GAGs binding appears to be inversely correlated with Mxra8 dependency, suggesting that GAG binding may compensate for CHIKV strains with limited interaction with Mxra8 (strains from the IOL)(McAllister et al. 2020). However, viral entry can still occur to some extent in the absence of both GAGs and Mxra8 (McAllister et al. 2020). Several other cell factors have also been reported to facilitate CHIKV entry and broad tropism, including C-type lectins (DCSIGN and L-SIGN), immunoglobulin and mucin domain-containing proteins 1 and 4 (hTIM1 and hTIM4), and the AXL receptor (Klimstra et al. 2003; Jemielity et al. 2013; Moller-Tank et Maury 2014). These factors may contribute to the complex mechanism underlying CHIKV entry and its ability to infect various cell types.

ii **Endocytosis and fusion**

Following receptor recognition, CHIKV is essentially internalized via clathrin-mediated endocytosis (CME) which is the main route for cargo internalization and widely used by many enveloped viruses (Bernard et al. 2010; Hoornweg et al. 2016; R. C. H. Lee et al. 2013) (Figure 9A). CHIKV is addressed to the endosomal compartment from the clathrin-coated vesicles, where the fusion step between the viral envelope and the endosomal membrane takes place (Voss et al. 2010; L. Li et al.

2010). Indeed, as the endosomal acidification progresses due to the vacuolar ATPase proton pump, the low pH triggers major conformational changes of the E2-E1 heterodimers, leading to the exposure of the E1-fusion loop and its insertion into the endosomal membrane (Long Li et al. 2010; Bernard et al. 2010; Hoornweg et al. 2016; Sahoo et Chowdary 2019; A. S. Kim et Diamond 2022). Cryo-electron tomography studies coupled with sub-tomogram averaging analysis recently characterized the different stages of the CHIKV fusion process which starts with the attachment of the exposed E1-loop (Mangala Prasad et al. 2022). Subsequently, E1 molecules assemble into homotrimers that insert into the target membrane, leading to the tightly docking of both viral and cellular lipid bilayers. Finally, membrane fusion leads to the formation of a pore that allows the release of an intact nucleocapsid (Figure: 9D-G) (Mangala Prasad et al. 2022).

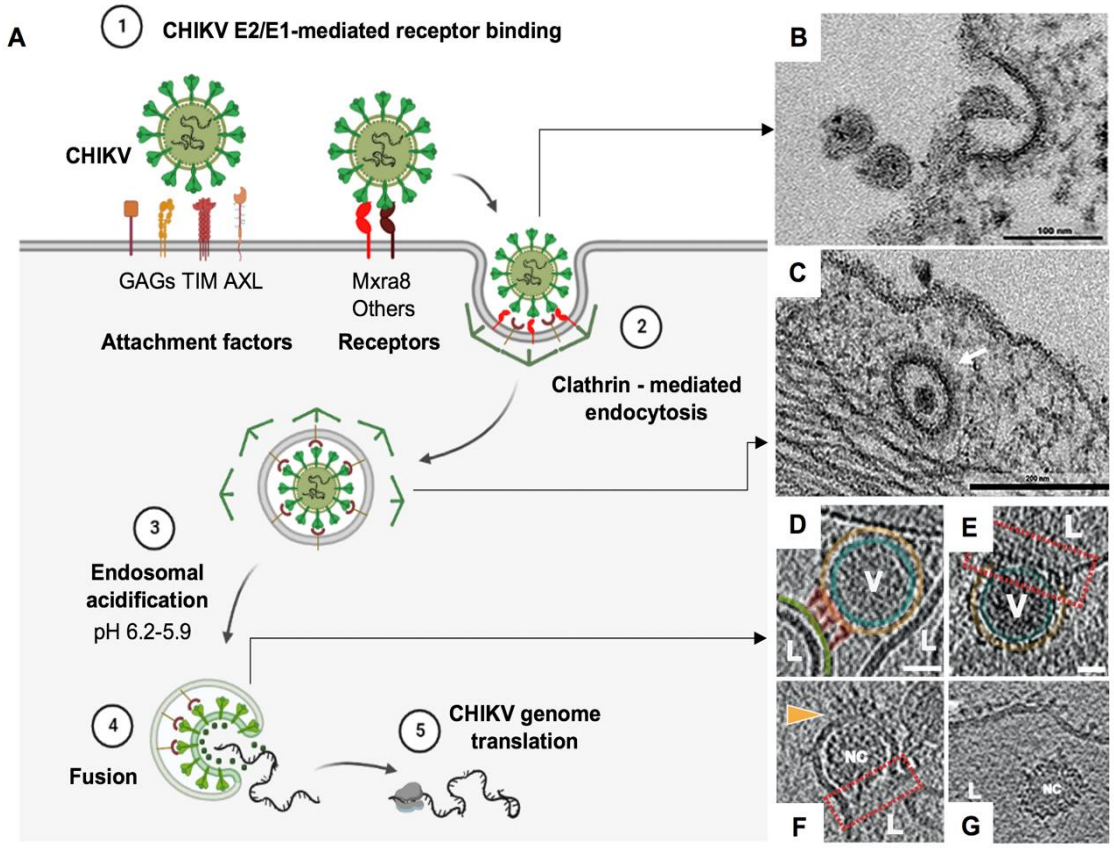

Figure 10: CHIKV entry in a target cell. *A, simplified schematic representation of CHIKV receptor mediated binding on cell surface (1), clathrin-mediated endocytosis (2), endosomal acidification triggering glycoproteins conformation change and E1-fusion loop exposure (3) leading to endosomal and viral membrane fusion. B, represents electron micrograph of A formed endosome coated with clathrin (white arrow). D-G, Tomograms showing the different steps of viral (orange)/liposome (green) membrane fusion: viral glycoprotein attachment and E1-homotrimers (red cone-shaped complexes) formation, E, membrane insertion and opposing membrane superposition, F, hemifusion pore formation (red) and G, nucleocapsid release. V; virus, L; liposome, NC; nucleocapsid. Adapted from (Reis et al., s. d.; Mangala Prasad et al. 2022)*

2. Viral replication

Upon viral fusion, the nucleocapsid disassembles in the cytoplasm and releases the single-stranded positive viral RNA genome. The 5'-ORF1, which encodes the non-structural polyprotein (P1234/P123+nsP4), is directly translated by the cellular machinery, resulting in the non-structural polyprotein formation. Following translation, P1234 is sequentially processed by the protease activity encoded by the nsP2 and the four nsP (nsP1, nsP2, nsP3 and nsP4) are fully individualized (E. G. Strauss et al. 1992; Merits et al. 2001; Saisawang et al. 2015; Bartholomeeusen et al. 2018). These proteins compose the enzymatic machinery, called viral replicase complex (vRC) in charge with viral genome replication and transcription (J. H. Strauss et Strauss 1994). Viral replicase complex, along with viral RNA, is addressed at the plasma membrane by unknown mechanisms, to form replicative membrane spherules where RNA synthesis takes place (J. H. Strauss et Strauss 1994; Jose, Taylor, et Kuhn 2017; Rausalu et al. 2016). Within these spherules, negative-stranded full-length RNA is generated, serving as template for new positive RNA synthesis. Subsequently, P123 undergoes a series of steps to generate the four mature non-structural proteins (nsPs), causing a transition in the replication complex's function towards synthesizing a genome of positive-stranded RNA (40S) and subgenomic RNA (26S). The major steps of replicase processing and activation, and spherule formation are deeply discussed in the next chapters.

3. Structural proteins synthesis, viral assembly and egress

i Structural proteins synthesis

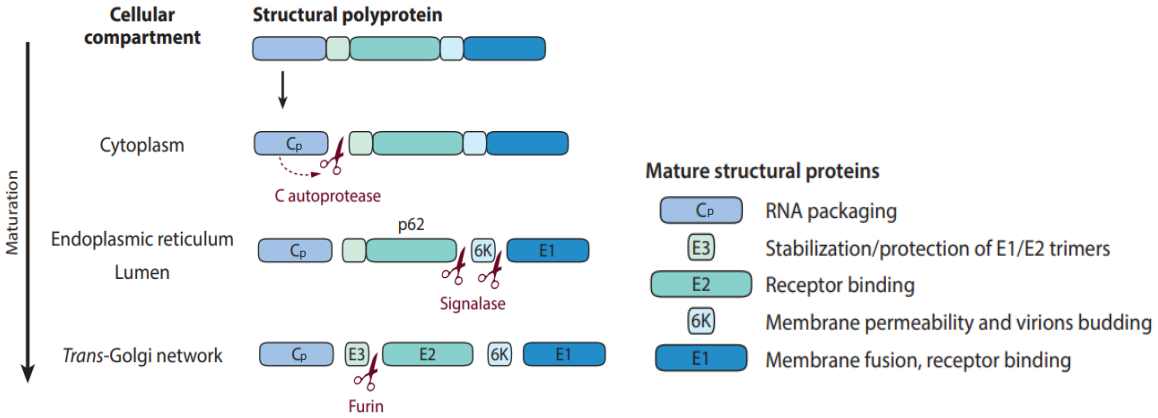

***Figure 11: Structural polyprotein processing**. The structural precursor is first maturated by the C protein that possesses cis-proteolytic activity and then by cellular proteases (signalases and furin), resulting in the production of E1, E2, and E3 glycoproteins and 6K protein, all contributing to viral particle assembly and budding. From Kril et al., 2021*

Following synthesis of the subgenomic 26S RNA, alphaviral protein production is shifted towards the synthesis of the structural proteins required for virion assembly

(Vasiljeva et al. 2003; A. Lulla, Lulla, et Merits 2012; K. H. Kim et al. 2004; J. H. Strauss et Strauss 1994). Structural proteins are expressed as a polyprotein that is first processed by the autoproteolytic activity of the viral capsid (Melancon et Garoff 1987; Mendes et Kuhn 2018). The latter is released in cytoplasm, whereas the remaining polyprotein (pE3-E2-6K-E1) is translocated and inserted into the endoplasmic reticulum (ER) membrane for processing (Mendes et Kuhn 2018; Zheng et Kielian 2013; Kalkkinen et al. 1980).

CHIKV capsid protein (Cp) is a small ~260 amino acid protein organized into two distinct domains. The C-terminal domain structure reveals a chymotrypsin-like protease capable of a single-cleavage event that releases the protein (Mendes et Kuhn 2018; H.-K. Choi et al. 1991). The highly positive-charged N-terminal domain could be divided into two regions. Region I contains a putative secondary structure or helix I, embedded in a low-complexity sequence enriched in basic residues, involved into capsid dimerization through coiled-coil interactions. Region II contains the RNA-binding motif that recognizes the viral gRNA for packaging (Mendes et Kuhn 2018; Perera et al. 2001). An additional N-terminal ribosome binding site recruit ribosome that are thought to trigger viral uncoating and immediate gRNA translation following viral entry and membrane fusion.

Once translocated into the endoplasmic reticulum, the envelop polyprotein is processed by a cellular signal peptidase (Liljeström et Garoff 1991). The release of the 6K protein is thought to be involved into the E3/E2 (also named p62 precursor) association with E1 into an immature non-fusogenic trimeric spike complex that traffics through the secretory pathway (Sanz et Carrasco 2001; Yap et al. 2017). The sequential processing of the E3/E2 precursor is a critical step ensuring correct maturation and infectivity of the future virions (Uchime, Fields, et Kielian 2013). E3/E2 remains as a precursor associated to the E1 protein, therefore locking the E2-domain B at the interface between E2 and E1, blocking E1-fusion loop, and preventing premature fusion in the ER or trans-Golgi network (Mulvey et Brown 1996; Uchime, Fields, et Kielian 2013; Liljeström et Garoff 1991). Once in the Golgi apparatus, E3 is released from E2 following furin-like protease cleavage, without disturbing E2/E1 heterodimer which can be primed upon acidic exposure (X. Zhang et al. 2003). Mature alphavirus E2/E1 complex are transported to the plasma membrane where it anchors in the lipid bilayer through transmembrane domains. Three mature E2/E1 complexes assemble into homotrimeric fusogenic spike with intra-spike and inter-spike

interactions mediated by E2 and E1 respectively (Voss et al. 2010; Yap et al. 2017). E3 was suggested to undergo weak interactions with E2 following its cleavage, and it was proposed to be part of the virion for some alphavirus.

ii RNA packaging and nucleocapsid formation

Packaging and assembly are finely regulated steps leading to a selective encapsulation of the full-length genomic RNA over the sgRNA which is produced in 3-4-fold greater amounts (Rümenapf, Strauss, et Strauss 1994). Different studies suggested that alphavirus genomes contain specific sequences named packaging signals. (PSs) are RNA conserved regions that allow viral genome to be encapsulated into new virions (E Frolova, Frolov, et Schlesinger 1997; D. Y. Kim et al. 2011; Mendes et Kuhn 2018; R. S. Brown et al. 2020). The presence of PSs was thought to be critical, since during alphavirus replication cycle, different RNA species are synthesized and only full-length viral RNA must be packaged into new virions. For CHIKV (and other viruses from the Semliki Forest clade), PSs are found within the nsP2 gene, whereas for other alphaviruses such as SINV, PSs are structured as eight stem loops within the nsP1 gene (E Frolova, Frolov, et Schlesinger 1997). However, it was demonstrated that PSs defective viruses are still able to grow, meaning that packaging occurs in absence of those signals, likely due to electrostatic interactions of the N-terminal domain of the Cp with the RNA (E Frolova, Frolov, et Schlesinger 1997; D. Y. Kim et al. 2011). Recently, a study combining biotinylation system to efficiently retrieve capsid protein with PAR-CLIP (photoactivatable ribonucleoside crosslinking and immunoprecipitation) method, successfully mapped Cp interactions with SFV genome with a nucleotide precision (R. S. Brown et al. 2020). In addition to already known PSs, these results identified multiple gRNA specific sites that bound to the capsid and promote gRNA packaging (R. S. Brown et al. 2020). The proposed model suggests a multi-site genome packaging process starting with Cp specific interaction with gRNA high affinity sites, resulting in a stable Cp:gRNA interaction (1). Non-specific interactions could also occur with other RNAs but with lower affinity, rendering the binding instable. As Cp protein accumulates it engages in lower affinity interactions that likely contribute to genome compaction through charge neutralization and Cp-Cp oligomerization (2). Finally, the nucleocapsid (NC) is completed containing one copy of gRNA surrounded by a shell formed by 60 asymmetric units composed of 4 proteins for a total of 240 copies of Cp arranged into icosahedral symmetry (3) (R. S. Brown et al. 2020) (Figure: 12).

Although we have accumulated valuable knowledge about viral RNA packaging mechanisms, the specific subcellular location of NC assembly is still unknown. Live imaging of alphavirus infected cells (SINV) demonstrated that during the infectious cycle, Cp is found as a part of different complexes in distinct subcellular compartments (Zheng and Kielian 2013). A first complex was detected at the plasma membrane, where Cp was found with the envelop proteins (Zheng et Kielian 2013). The fact that those complexes are not visible in budding-defective viruses, confirm that these are site for virion assembly and budding (Zheng et Kielian 2013). In addition, small and highly motile Cp puncta enriched with the E2 envelop protein were observed in the

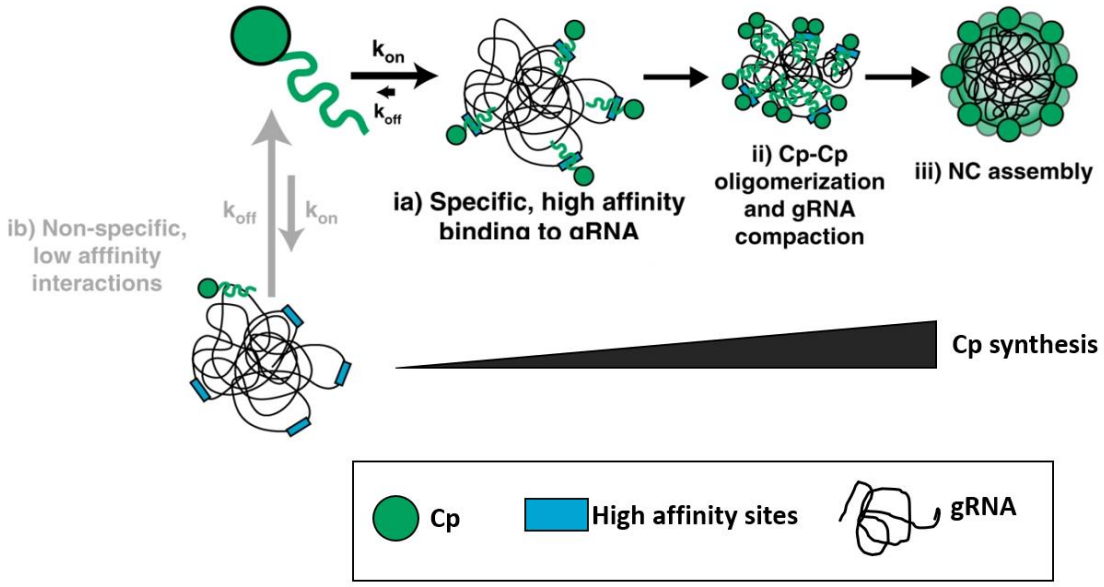

Figure 12: ***Model of multi-site alphavirus genome packaging.*** *Adapted from (Brown et al. 2020)*

cytoplasm (Zheng and Kielian 2013). These suggest that Cp or complete NC interact with envelope proteins before reaching the plasma membrane. Finally, an intriguing complex containing Cp, nsP3 protein and the host factor G3BP was described, forming cytoplasmic irregular spherical aggregates (Zheng and Kielian 2013. Since the nsP3-G3BP interaction was already reported as a viral mechanism to counteract cellular stress-granules (see Chapter VII), it was proposed that Cp protein can play additional, non-structural function, supporting viral replication (Zheng and Kielian 2013).

iii Virion assembly and budding

In a recent study, researchers gained valuable insights into the budding process of newly produced CHIKV particles. They discovered that budding sites were present directly at the basal layer of the plasma membrane (PM) or on virus-induced filopodia (Chmielewski et al. 2022). The budding process initiates with both vertical interactions (between nucleocapsid (NC) and mature spike) and lateral interactions (between

spikes) that induce membrane bending (Chmielewski et al. 2022). This cascade of conformational changes affects both NC and spikes, ultimately leading to the formation of the fully mature NC, which bends the PM to create the final new VP (Chmielewski et al. 2022). The maturity and arrangement of spikes in the PM play a critical role in both the assembly and budding processes (Chmielewski et al. 2022). The study demonstrated that when spikes were blocked into non-mature forms using antibodies, they could not effectively interact with the NC and other membrane-anchored spikes, preventing the formation of the complete viral envelope (Chmielewski et al. 2022). For the final release step, it was proposed that the interaction between the NC and spikes in the inner part of the virion was sufficiently strong to drive the membrane scission and facilitate the release of the newly formed viral particles (Chmielewski et al. 2022).

Chapter V: Role of the CHIKV non-structural proteins in viral replication and inhibition of host immune responses

A. CHIKV non-structural proteins

Each nsP protein possesses specific functions involved in RNA replication and transcription. Together, the four nsP form the enzymatic complex called replicase complex, responsible for RNA synthesis and spherule biogenesis (Chapter VI). The principal known nsP functions are summarized below (Table 1). Besides their role in viral RNA synthesis, the nsP counteract the cellular intrinsic immune response for optimal viral infection (Akhrymuk, Kulemzin, et Frolova 2012; Bae, Lee, et Myoung 2020; J. J. Fros et al. 2012; Jayabalan et al. 2021a; Göertz et al. 2018). These functions are summarized in *section C.*

Table 1: Alphavirus non-structural protein functions

	Length (aa)	Functions involved into RNA synthesis	References
nsP1	535	Adressing replicase complex to plasma membrane through membrane interactions and anchoring RNA-capping through methyltransferase (MTase) and guanylyltransferase (GTase)	Laakkonen et al. 1998; N. Zhang, Zhao, et Zhang 2019; Bakhache et al. 2020; R. Jones et al. 2021
nsP2	798	Nucleoside triphosphatase, helicase, and RNA-dependent 5´- triphosphatase activities (N-terminal part of the protein) Protease activity (C-terminal domain) required for the non-structural polyprotein processing	Merits et al. 2001; Vasiljeva et al. 2003; Rausalu et al. 2016)
nsP3	530	Phosphoprotein ADP- and polyADP-ribose binding and hydrolase activity Recruitment of host-cell proteins	Teppor et al. 2021; Leung et al. 2018; Cristea et al. 2006; Meshram et al. 2018
nsP4	611	RNA-dependent RNA-polymerase Terminal adenylyl-transferase activities	Y. F. Wang, Sawicki, et Sawicki 1994a; Tomar et al. 2006; M. W. Chen et al. 2017

B. nsP processing and maturation of the replicase complex

During infection, two ns polyproteins could be synthesized, P123 and P1234, depending on the presence of an opal codon stop located at the C-terminus of the

nsP3 sequence, thus restricting the synthesis of the viral RNA-dependent RNA-polymerase nsP4 (J. H. Strauss et Strauss 1994). For CHIKV, most of the clinical isolates contain the opal stop codon, even though it was demonstrated that some laboratory-adapted CHIKV strains have an opal-to-arginine substitution resulting in the expression of P1234 precursor(J. H. Strauss et Strauss 1994; J. E. Jones et al. 2017). The impact of the opal-to-arginine mutation on viral fitness and replication remains elusive. There is some evidence showing that an opal-to-arginine mutation within an infectious CHIKV clone from Sri Lanka doesn't impact viral replication in vitro (on human or mosquito cells) but is associated with decreased virulence in vivo in the mice model (decreased footpad swelling, delayed proinflammatory response and decreased inflammatory cell infiltration in the infected joints) (J. E. Jones et al. 2017).

Efficient CHIKV infection requires the synthesis, in a specific order, of different RNA species: (1) a negative RNA genome, which will serve as a template for the production, (2) the full-length gRNA, and (3) the sgRNA. The full-length gRNA will serve either for the translation of new replicase complexes (P1234), or will be packaged within the nucleocapsid (Bartholomeeusen et al. 2018; Ahola et Merits 2016; Hellström et al. 2017). The sgRNAs produce the structural proteins necessary to form new infectious particles (Melancon et Garoff 1987; Mendes et Kuhn 2018). Viral replication and transcription are achieved by the replicase complex (RC), which is formed by the cleavage products of the P1234 precursor. Template preferences and enzymatic activities of the RC entirely depend on the processing intermediates of the P1234 precursor (Bartholomeeusen et al. 2018; Ahola et Merits 2016; Hellström et al. 2017). This proteolysis is mediated by the nsP2-protease domain (Salonen et al. 2003). Early studies suggested that the alphavirus nsP2-protease domain was similar to papain-like *proteases*, harboring a catalytic dyad consisting of cysteine and histidine residues, recognizing specific residues around the cleavage sites within the P1234 (Merits et al. 2001; Vasiljeva et al. 2003). Despite some discrepancies between the studies concerning the active site motif of CHIKV-nsP2 protease domain (Saisawang et al. 2015), *in vitro* and cell-based experiments demonstrated that cysteine at position 478 (Cys478) and tryptophan at position 479 (Trp479) residues that are well conserved among alphaviruses are critical for nsP2 protease activity (Rausalu et al. 2016).

The first cleavage event occurs in-*cis* at the site 3^4 (between nsP3 and nsP4), leading to the individualization and activation of nsP4: the viral RNA-dependent RNA polymerase (Figure 13). This early replicase *P123+ns4* is short-lived and utilizes the positive gRNA as a template for synthesizing a full-length negative viral RNA (Rausalu et al. 2016; Hardy et Strauss 1989; Utt et al. 2015). This antigenome is present in a duplex with the gRNA, forming a double-strand RNA replicative intermediate (Figure 13)(Hardy et Strauss 1989). The early replicase is inefficient in synthesizing positive RNA species (Hardy et Strauss 1989), and a second irreversible cleavage event mediated by nsP2 in-*trans* occurs rapidly at the 1^2 site (between nsP1 and nsP2). Consequently, negative-strand RNA synthesis depends on the continuous translation of the viral replicase complex (Rausalu et al. 2016; Vasiljeva et al. 2003). The second cleavage generates the *nsP1-P23-nsP4* complex that mainly drives the synthesis of the full-length gRNA, and in a lesser extent sgRNA species (Figure 13). Finally, the viral nsP3 is released from the P23 intermediate, thus leading to the fully processed replicase complex nsP1+nsP2+nsP3+nsP4 synthesizing sgRNAs (Figure 13). This sequential processing ensures that, in early steps of the infectious cycle, important amounts of genomic RNA are synthesized, then at the later steps, the production of sgRNA ensures the expression of structural proteins and the packaging of newly synthesized viral genomes.

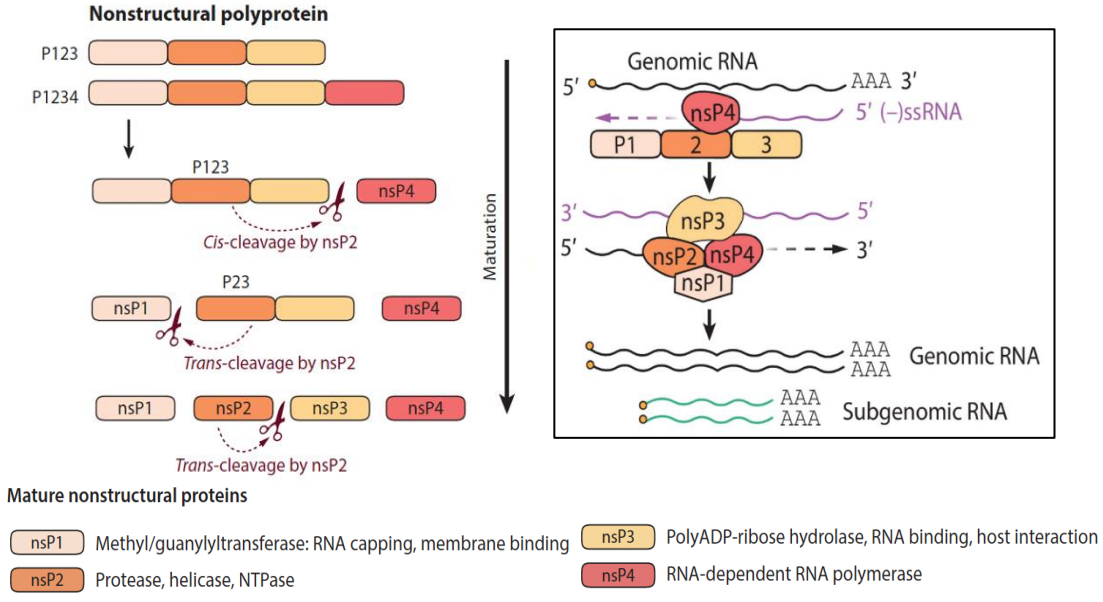

Figure 13: P1234 processing and viral RNA synthesis: *A leaky opal stop codon at the end of the nsP3 sequence directs the translation of a partial nonstructural polyprotein (P123). P123 and P1234 are sequentially processed in cis- and trans-reactions by the cysteine protease nsP2 to produce mature nsPs (nsP1–4), forming the replication complex. P123+nsP3 can synthesize the negative viral RNA, which serves as a template for synthesizing new positive RNAs. nsP1+P23+ nsP4 and nsP1+nsP2+nsP3+nsP4 can synthesize genomic RNA and subgenomic RNA. Adapted from Kril et al. 2021*

Alterations of P1234 processing have been widely investigated for other alphaviruses (SINV, SFV). The acceleration of P1234 proteolysis by the introduction of point mutations within the nsP2-protease domain was demonstrated to be lethal for SINV (E. G. Strauss et al. 1992). Interestingly, mutants incapable of 2^3 processing are more efficient in gRNA synthesis than the wildtype alphaviruses (K. H. Kim et al. 2004; Gorchakov, Frolova, et al. 2008). However, these mutants can't develop spreading infection and cytopathic effect in IFN-type I production and signaling competent cells (Gorchakov, Frolova, et al. 2008). These results point out the importance of nsP function outside the viral replicase complex, mainly in the regulation of the host cell immune response to viral infection

C. CHIKV nsP and host cellular response to viral infection

In vertebrate cells, alphavirus infection induces profound metabolic changes in global transcriptional and translational shutoff, leading to a rapid cytopathic effect. These changes are efficient viral strategies to evade the host cell's innate antiviral immunity and promote viral protein synthesis instead of the host cell. The following sections discuss CHIKV proteins and the mechanisms involved in these functions. It is important to remember that most of the knowledge is inferred from SINV and SFV studies.

1. Inhibition of host cell transcription

In CHIKV-infected cells, nsP2 is found near the plasma membrane and in the nucleus, where it can translocate early after infection due to a noncanonical nuclear localization motif (Utt et al. 2015; Jelke J. Fros et al. 2013). Inside the nucleus, nsP2 targets the Rpb1 catalytic subunit of RNA polymerase II for proteasomal degradation, effectively shutting down cellular gene transcription and preventing the activation of innate immune genes (Akhrymuk, Kulemzin, et Frolova 2012) (Figure 14). This nsP2-mediated degradation of Rpb1 does not depend on nsP2's enzymatic activities but is hindered by a specific mutation in the nsP2 C-terminus (Bouraï et al. 2012; Jelke J. Fros et al. 2013; Utt et al. 2015; Akhrymuk, Kulemzin, et Frolova 2012). Overexpression of SINV-nsP2 alone is sufficient to inhibit cellular transcription and to induce cell death (Frolov et al. 2009).

2. Counteracting antiviral immunity

Aside from the primary mechanism of evading the cellular antiviral response through Rpb1 degradation, it appears that nsP2 can also disrupt IFN signaling in a way unrelated to general transcriptional shutoff. The nuclear fraction of nsP2 prevents the nuclear accumulation of *signal transducer and activator of transcription 1* (STAT1) by promoting its re-export into the cytoplasm through the chromosome region maintenance 1–mediated pathway. This activity involves the nsP2 methyltransferase-like domain (Göertz et al. 2018) (Figure 14). Finally, a study also suggested that nsP2, along with E1 and E2, antagonize the MDA5 and RIG-I- mediated induction of NF-κB promotor activity, thus inhibiting type-I IFN synthesis (Bae, Lee, et Myoung 2020).

nsP1 was also found to antagonize cellular immune response by interacting with STING, an adaptor protein of the cGAS-STING pathway that is involved in the DNA-induced type-I IFN-transcription (S. Hu et al. 2019; Webb et al. 2020). The nsP1/STING interaction leads to inhibition of the signaling pathway, but also to increased expression of palmitoylated nsP1(Webb et al. 2020), thus favoring CHIKV replication. The cGAS-STING pathway is also restricted by CHIKV capsid protein which mediates cGAS degradation via a autophagic dependent mechanisms (Webb et al. 2020).

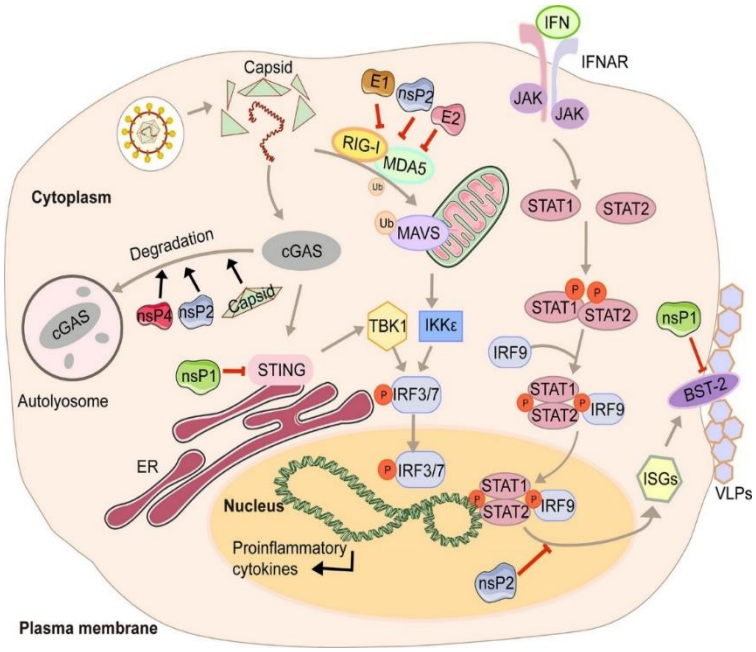

Figure 14: CHIKV proteins counteract the host-cell antiviral immunity.

In addition to nsP1 and nsP2, CHIKV nsP3 protein is also proposed to play an important role in cellular antiviral immunity. Indeed, nsP3 protein is involved into the disruption of stress granules (SGs). During viral infection, SGs form signaling platforms that coordinate and favor the antiviral response (Yoneyama, Jogi, et Onomoto 2016). The nsP3 mechanisms involved into SGs disassembly and cellular immunity counteraction are further discussed in the next chapter.

3. Host cell translational shutoff

Alphaviruses genomes harbor a 5' Cap and a 3' poly(A), which allows the direct translation of the non-structural ORF following viral genome release in the cytosol of the infected cell (J. H. Strauss et Strauss 1994). NsP synthesis relies on the translational cell machinery, which is tightly regulated. The eukaryotic translation initiation factor eIF2 is one of the main regulators of cell translation. The phosphorylation of its α subunit prevents eIF2 recycling between successive rounds of protein synthesis, thus inhibiting the cap-dependent protein synthesis (Clemens 2001; McInerney et al. 2005). eIF2α could be phosphorylated by four different cellular kinases activated upon cellular stress: Protein kinase R (PKR) senses double-stranded RNA, PKR-like ER kinase (PERK) senses unfolded proteins in the ER, whereas GCN2 and HRI are activated by nutrient starvation and heme deficiency, respectively (Jelke J. Fros et Pijlman 2016). During the early steps of CHIKV infection, the replicative double-strand RNA intermediate is sensed by cellular PKR, leading to eIF2α phosphorylation and translation shutoff (Clavarino et al. 2012). Furthermore, viral replication also triggers the endoplasmic reticulum (ER) stress response, also known as unfolded protein response (UPR), mainly after the accumulation of envelope proteins in the ER (Jelke J. Fros et al. 2015). During UPR, PERK activates following self-dimerization and phosphorylation. Activated PERK induces eIF2α phosphorylation and translational shutoff. Although CHIKV nsP4 protein was identified to inhibit eIF2α phosphorylation, thus avoiding translational inhibition (Rathore, Ng, et Vasudevan 2013), multiple studies demonstrated that alphaviruses, including CHIKV, efficiently allow eIF2α phosphorylation. (Gorchakov et al. 2004; Gorchakov, Frolova, et Frolov 2005; Ventoso et al. 2006; White et al. 2011; Jelke J. Fros et al. 2015). In addition, CHIKV nsP2 was also demonstrated to induce the eukaryotic translation elongation factor 2 (eEF2) phosphorylation by increasing cellular cAMP concentration. cAMP is a second messenger that activates several signaling pathways, including the PKA and eEF2 kinases, of which the latter phosphorylates eEF2 and decreases protein synthesis (Treffers et al. 2023). Interestingly, alphaviruses sgRNA are efficiently translated into structural proteins even when eIF2α is phosphorylated and host-cell protein synthesis is shutdown (White et al. 2011; Jelke J. Fros et al. 2015).

Chapter VI: Architecture of CHIKV replication complex

A. RNA viruses rearrange cellular membranes to form replicative organelles

A hallmark of positive-strand RNA viruses replication is the rearrangement of cellular membranes in so called viral replication organelles (vROs) (Belov et van Kuppeveld 2012; Wolff et Bárcena 2021; Neufeldt et Cortese 2022).These structures constitute an elaborate environment concentrating viral and host factors required for RNA synthesis, but also protecting the dsRNA-intermediate from cellular RNases and the detection of cytosolic RNA sensors that could trigger the intrinsic cellular immunity (D. Paul et Bartenschlager 2013; Risco et al. 2014).

In the recent years, the technological advances that comes with the three-dimensional (3D) imaging methods (volume scanning electron microscopy and (cryo)electron tomography), successfully resolved the special organization of numerous positive-stranded RNA viruses replication organelles (Figure 15) (Belov et van Kuppeveld 2012; Wolff et Bárcena 2021; Neufeldt et Cortese 2022). vROs are classified into two major morphotypes: the protrusion type replication organelles (Pr-vRO) and the invagination type replication organelles (In-vRO) (Figure 15). Pr-vRO are conserved among a large range of animal and plant viruses (Wolff et Bárcena) 2021. Important human pathogens such as Hepatitis C (HCV) and coronaviruses (SARC-CoV and MERS) induce Pr-vRO upon infection. Pr-vRO are dynamic and complex in terms of structure. Indeed, protrusions can form single membrane vesicles or tubules, that eventually mature into double or multiple-layered membrane structures as the infection progresses (Wolff et al. 2020). In addition, in contrast with In-vROs which can form within multiple cellular membranes, Pr-vROs seem to be exclusively linked to organelles of the secretory pathway (Wolff et al. 2020). The In-vROs type consists in the invagination of cellular membranes (plasma membrane, mitochondria, endoplasmic reticulum) into spherules of 40-90nm of size that are connected to the cytosol by a membrane channel gated by a pore-like structure allowing the selective movement of molecules and export of synthesized RNAs (Ertel et al. 2017; Unchwaniwala et al. 2021; Laurent et al. 2022; Tan, Chmielewski, Yien Law, et al. 2022). A variety of genetically diverse viruses, infecting plants (Tomato Bushy stunt

virus (Tombusvirus), insects and vertebrates (Dengue virus (Flavivirus) and Chikungunya virus (Alphavirus) use this compartmentalization strategy to provide a suitable microenvironment for viral RNA synthesis.

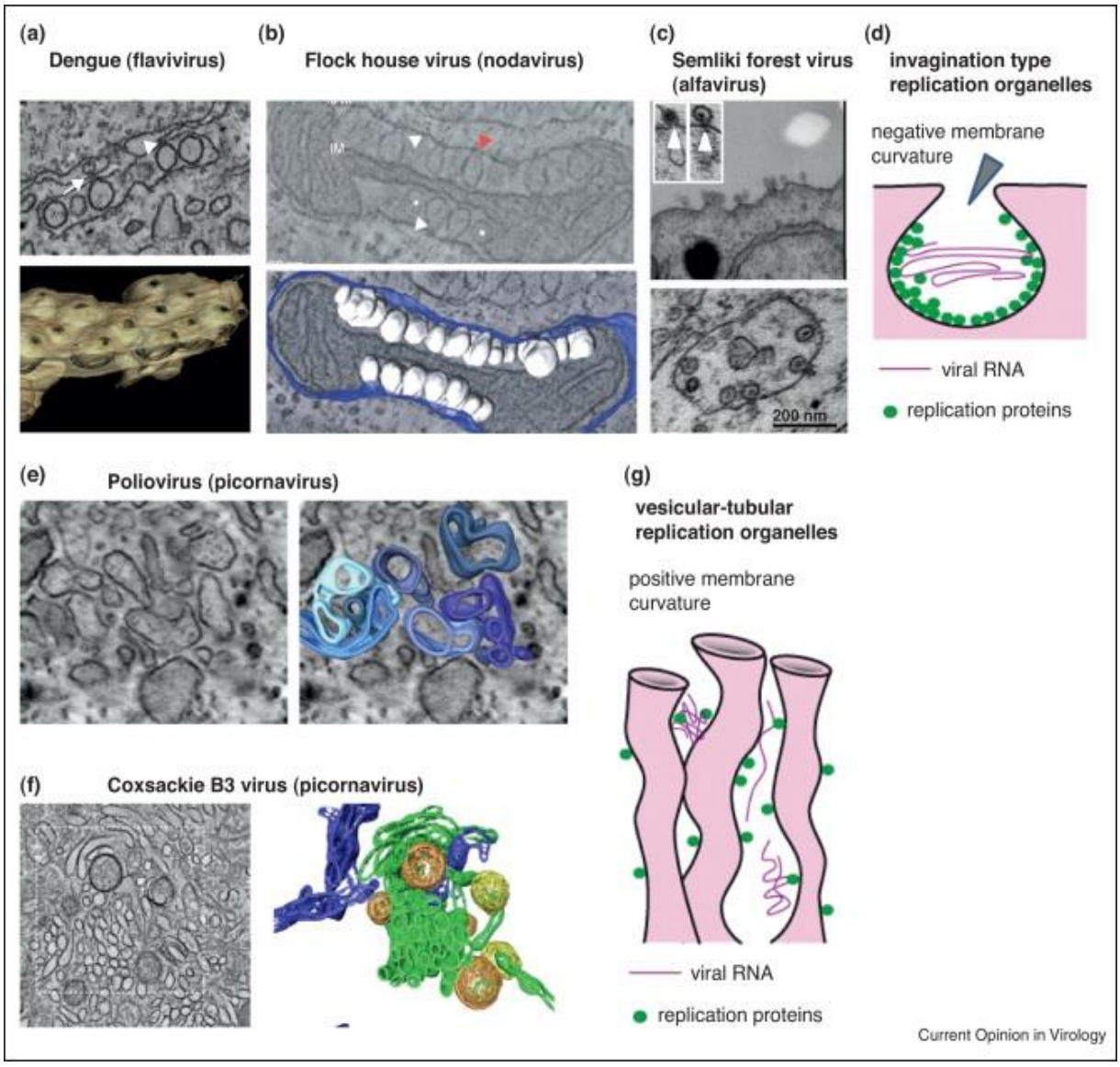

Figure 15: Fundamental principles regarding the organization of replication organelles in viral replication *can be summarized as follows: a) Replication organelles exhibit invagination, displaying a negative membrane curvature typical for viruses resembling Flaviviruses and Alphaviruses. Arrowheads indicate the connection of the inner compartment with the cytoplasm. An electron microscopy (EM) image and tomography reconstruction demonstrate Dengue virus-induced replication structures on ER membranes. b) Replication structures induced by Flock house virus on the outer mitochondrial membrane display invagination and negative membrane curvature. Illustrated through an EM image and tomography reconstruction. c) At the early stage of Semliki Forest virus infection, spherules are formed on the plasma membrane with negative curvature, subsequently translocated inside the cytoplasm. d) A schematic representation illustrates the invagination-spherule replication organelle organization, emphasizing negative membrane curvature. e-g) Replication organelles for viruses resembling Picornaviruses demonstrate vesicular-tubular structures characterized by positive membrane curvature. EM images and tomography reconstructions depict early replication structures of poliovirus and Coxsackie B3 virus. A schematic representation outlines the vesicular-tubular replication organelle organization.* ***From Belov et van Kuppeveld, 2012***

B. Chikungunya virus spherules

1. Minimal replicase complex required for spherule formation

CHIKV, like all alphaviruses, remodels the host plasma membrane into spherules of ~50nm of size that concentrates viral nsPs, genomic RNA and negative-strand RNA intermediate (E. I. Frolova et al. 2010; Tan et al. 2022). Despite the accumulated structural data of individual alphavirus nsPs protein domains, their organization and topology within the vROs, as well as the precise mechanisms of spherule biogenesis, are still poorly understood. Studies using alphavirus *trans*-replication systems (Figure 16 A) investigated the minimal viral components required for spherules biogenesis (Spuul et al. 2011; Hellström et al. 2016; Kallio et al. 2016). In *trans*-replication systems, the replicase complex encoded within the P1234 precursor and the RNA template are expressed from separate DNA plasmids, facilitating the dissection of the replicase complex (RC) molecular functions (Figure 16 A). Indeed, by using a SFV

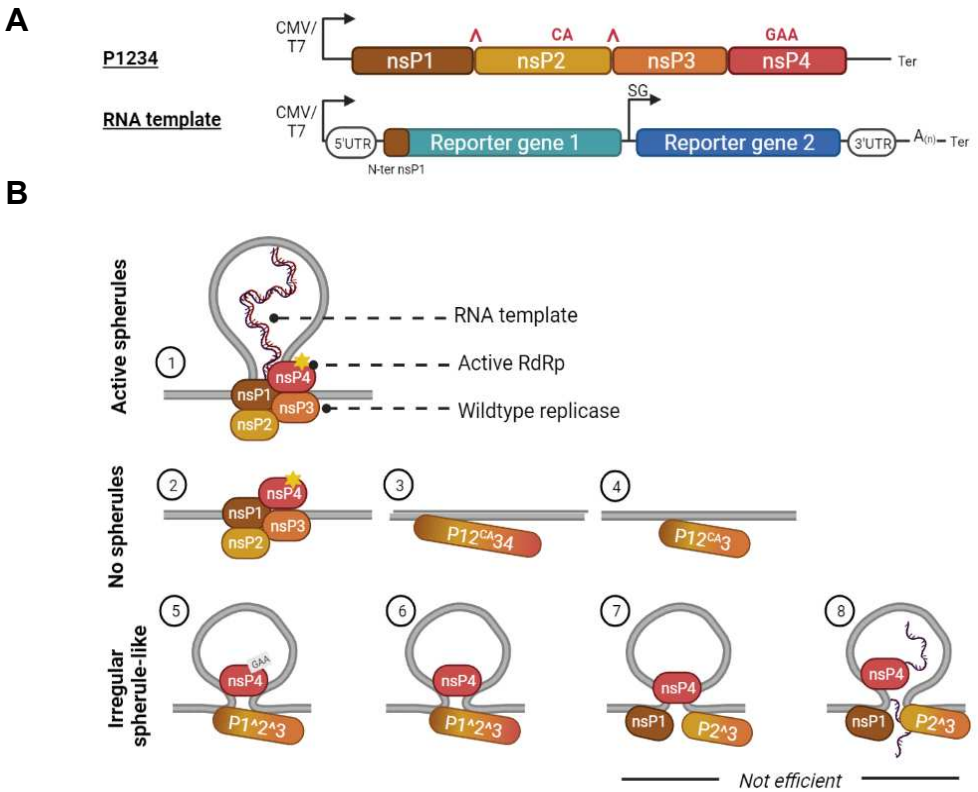

Figure 16: Polyprotein processing and spherule formation. *A, CHIKV trans-replicase system: Upper panel, schematic presentation of a CMV promoter-based expression constructs of CHIKV replicase. Lower panel, CMV promoter-based constructs expressing template RNAs. The 5' and 3' UTRs are from CHIKV; N-ter nsP1—region encoding for the 77 N-terminal amino acid residues of nsP1; SG—CHIKV SG promoter. Non-structural and structural polyproteins CDSs are replaced with reporter genes. B, Minimal replicase processing for spherule biogenesis: 1. Active replicative spherules formation requires the expression of all four nsPs from a polyprotein which is sequentially processed by viral nsP2 protease, viral RNA and active RNA-dependent RNA polymerase (nsP4). Either in absence of viral template (2), unprocessed nsP4 (3) or complete absence of nsP4 (4), no spherules are observed. Partially processed P123+nsP4 are able to form irregular spherules-like, independently of the polymerase activity (5 and 6). The processing of P23 is not a prerequisite for spherule-like formation (7 and 8).*

and SINV *trans*-replication systems, it was demonstrated that in addition to the wildtype RC, alphavirus spherules biogenesis requires an active RdRp and a suitable RNA template, suggesting that RNA synthesis and spherule biogenesis are concomitant and interdependent events (Spuul et al. 2011; Hellström et al. 2016; Kallio et al. 2016) (Figure 16 B). Further studies based on the same molecular system harboring mutations within the cleavage sites of the P1234 demonstrated that partially processed replicase alone could generate spherules in the presence or absence of an RNA template. Thus, the nsP4 must be released from the polyprotein, which can be provided as uncleaved P123 or as a combination of nsP1+P23, the latter being less efficient in spherule formation in the absence of RNA template (Figure 16 B) (Hellström et al. 2017).

2. nsP1 dodecameric-ring gate the entry of CHIKV spherules

nsP1 is involved in the RCs anchoring to the plasma membrane where the replicative spherules are formed (Spuul et al. 2007; Hellström et al. 2017), as well as in the formation of membrane protrusions or filopodia (Laakkonen et al. 1998). This protein is the only viral nsP to interact with and deform cellular membranes (Laakkonen et al. 1998; N. Zhang, Zhao, et Zhang 2019; Bakhache et al. 2020; R. Jones et al. 2021). The presence within the nsP1 of palmitoylated cysteine residues was shown to be important for nsP1-targeting the plasma membrane. Additionally, it was demonstrated that palmitoylated cysteines resulted in the CHIKV-nsP1 co-segregation with cholesterol-rich detergent-resistant membrane microdomains (DRMs), also called lipid rafts (Bakhache et al. 2020). An amphipathic region that structures as an α-helix upon binding to negatively charged lipids led to the establishment of a model suggesting that nsP1 is primarily targeted to the plasma membrane through the α-helix, then cysteines' palmitoylation is mediated by two zinc finger Asp-His-His-Cys (DHHC) domain-containing palmitoyl transferase (ZDHHC2 and ZDHHC19), that tighten the interaction between nsP1 and the membrane (Laakkonen et al. 1998; Spuul et al. 2007; N. Zhang, Zhao, et Zhang 2019). Recent studies successfully purified the active membrane-associated nsP1 complexes from insect and mammalian cells (R. Jones et al. 2021; K. Zhang et al. 2021). Three-dimensional (3D) Cryo-electron microscopy data revealed that twelve copies of nsP1 form a crown-shaped ring structure associated with the membrane (R. Jones et al. 2021; Girard et al. 2023). The ring

complex consists of three essential domains: the capping domain, known as the crown, the waist domain, responsible for forming a pore, allowing the passage of small proteins and particles, and the skirt, which associates with the membrane (Figure 17).

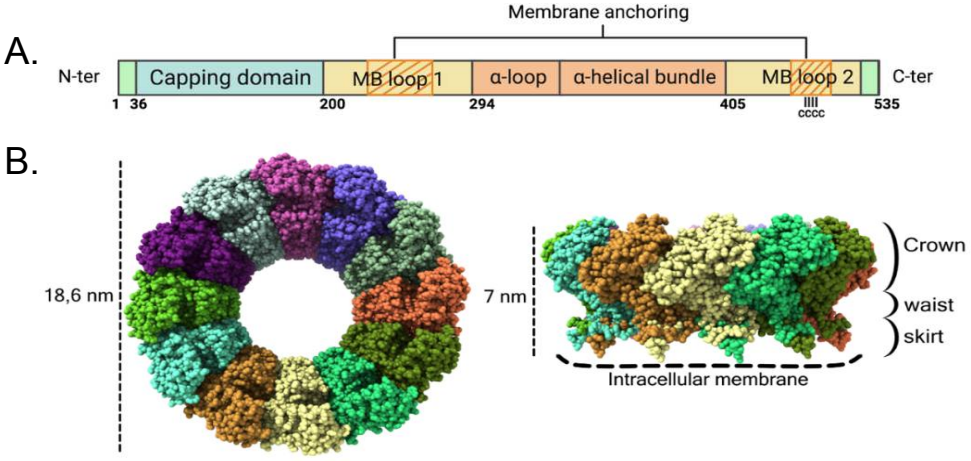

Figure 17: CHIKV nsP1 andnsP1- dodecameric ring organization. *A, Simplified representation of nsP1 domains. B, Atomic structure of the pores of the chikungunya nsP1 virus with the different monomers shown in different colors. Each atom is represented as a sphere. On the left side of the image the pore is shown from the cytoplasmic view and on the right from a side view. The dimensions of the pore are indicated on the left, the crown, waist and ski Art regions are indicated on the right and the contact sites with the membrane are indicated at the bottom by dashed lines. Adapted from (« Cryo-EM Structures of the Chikungunya Virus NsP1 Reveal Capping Rings as Functional Gates of Membranous Viral Factories » s. d.)*

Structural analysis suggested that the interaction with the membrane and the process of oligomerization play a crucial role in activating the nsP1 capping enzyme (R. Jones et al. 2021). This activation occurs through the stabilization of the capping domain's conformation and the formation of a catalytic pocket that includes the GTP-binding domain and the SAM-binding domain (R. Jones et al. 2021; K. Zhang et al. 2021; R. Jones et al. 2023). The capping pathway is unique to Alphaviruses as it begins with the N7 methylation of a guanosine triphosphate (GTP) molecule, followed by the covalent linkage of an m7GMP group to a conserved histidine in nsP1 and the transfer of this cap structure to a diphosphate RNA that requires the activity of viral nsP2 protein (R. Jones et al. 2021; 2023). The stoichiometry of the nsP1 complex suggests that it acts as a bioreactor that can simultaneously cap up to 12 RNA molecules, thus contributing to the exceptionally high alphavirus replication rates (R. Jones et al. 2021).

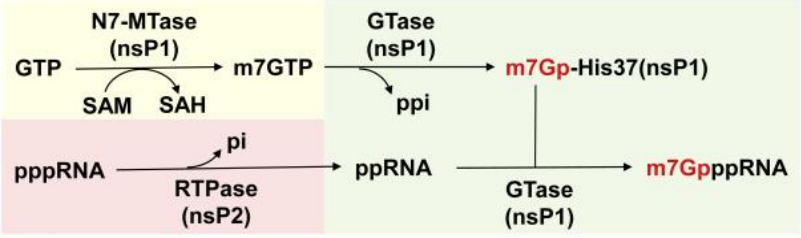

Figure 18: mRNA capping mechanism during alphavirus infection. *Step 1 (pink box) nsP2 RTPase catalyzes the removal of the γ-phosphate from the 5' triphosphorylated RNA. Step 2 (yellow bow) sP1 MTase catalyzes the N7 methylation of the GTP. Step 3 (green box) nsP1 GTase catalyzes the formation of the cap-0 structure. From (K. Zhang et al. 2021).*

The presence of a protein complex organized in a ring-shape structure gating the entry of the replicative organelles (RO) has already been described for other positive-strand RNA viruses such as the Flock House nodavirus (FHV) (Unchwaniwala et al. 2021). In contrast to alphaviruses, FHV remodels the outer mitochondrial membrane to form replicative vesicles that grow between the outer and inner mitochondrial membranes (Figure 19). Cryo-ET showed that the ~50 nm spherule invaginations are gated on their cytosolic face with a crown-like protein structure, forming a pore connecting the spherule interior with the cytosol. Sub-tomogram averaging demonstrated that each crown contains a 12-fold symmetric, cupped, inner turret of ~19 nm diameter, with 12 flanking projections at ~35 nm diameter. Further studies identified that this crown is formed by the multifunctional protein A (Ertel et al. 2017).

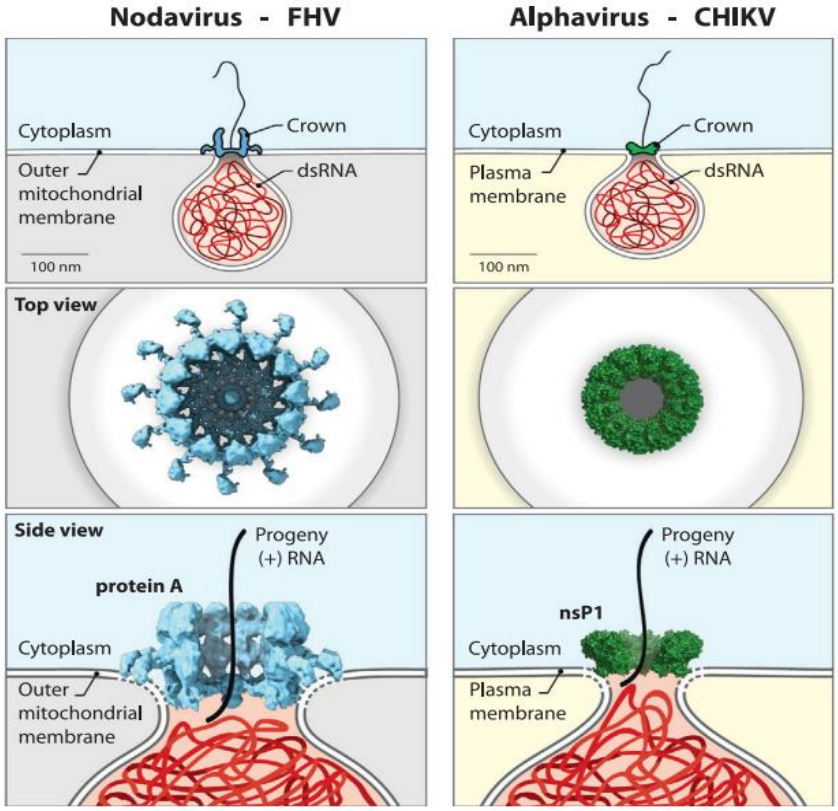

Figure 19: Comparison of nodavirus RCs and crowns to those of alphaviruses. *Left column: the spherule RNA replication complexes of nodaviruses are crowned by 12-fold symmetric crown complex of protein A. Right column: In the absence of other viral proteins, exogenously expressed alphavirus nsP1, which contains RNA capping domains similar to those of the nodavirus crown basal region, assembles into a 12-mer ring that is proposed to reside atop alphavirus spherules similarly to the basal ring of the nodavirus crown Adapted from (Unchwaniwala et al. 2021).*

3. Cryo-EM structure of CHIKV replicative spherules

Expression of different combinations of nsPs and interaction studies, as well as nsP4 mutagenic assays, revealed that all nsPs potentially interact with each other (Cristea et al. 2006; Bouraï et al. 2012; Lark, Keck, et Narayanan 2018; Tan et al. 2022; Yin et al. 2023). However, the spatiotemporal organization of nsPs leading to

spherule biogenesis and the synthesis of the different RNA species is not completely revealed. Recent works performed independently by Tan et al. 2022 and Laurent et al. 2022, brought valuable insights into the molecular basis of CHIKV RC biogenesis and genome replication. The *in vitro* purification of CHIKV RC followed by RNA elongation assays demonstrated that nsP1 is required for efficient nsP4 polymerase activity (nsP1+nsP4 complex) and that nsP2 further potentializes RNA elongation by the nsP1+2+4 complex, suggesting that the core RNA replicase is formed by nsP1+2+4. Even though the insoluble nature of nsP3 made it impossible to test in vitro, several studies demonstrated that nsP3 is essential for efficient viral replication (Y. F. Wang, Sawicki, et Sawicki 1994; Schulte et al. 2016; Meshram et al. 2018; Teppor, Žusinaite, et Merits 2021). The nsP3 role in CHIKV replication is discussed in detail in *Chapter VII*. The cryo-EM structure of nsP1+2+4 replicase core at 2.8Å demonstrated that nsP4 likely gets activated upon proper folding within the central of the nsP1-dodecameric ring previously described (Tan et al. 2022). In addition, 10 of the 12 nsP1-subunits recruit flexible loops to hook onto nsP4, thus stabilizing the polymerase within the center of the pore and enhancing its activity (Tan et al. 2022). One molecule of nsP2 was also described within the nsP1 ring, with a part of the helicase domain at the interface with nsP4 and nsP1, whereas the protease domain, whose structure is not solved, is projected outside facing the cytoplasmic side of the complex (Tan et al. 2022).

The biological relevance of the in vitro reconstituted RC core was further validated by cryo-electron tomography (cryo-ET) performed on CHIKV-infected cells (Figure 20) (Tan et al. 2022). Interestingly, in addition to RCs positioned at the neck of spherules, ring-like complexes docked mainly on thin membrane extensions were observed (Tan et al. 2022). The latter were smaller in size and not associated with RNA or membrane invagination. Sub-tomogram averaging revealed that this non-replicative complex was the RC core constituted by the nsP1-ring, the nsP4 polymerase and the helicase domain of nsP2 (Tan et al. 2022). In contrast, at the neck of *bona fide* replicative spherules, the RC display additional cytoplasmic ring structure enclosing contiguous linear density consistent with viral RNA exported from the spherule to the cytoplasm. This additional ring-structure likely supports the high negative membrane curvature and viral replication, as in its absence no spherules are formed (Figure 20).

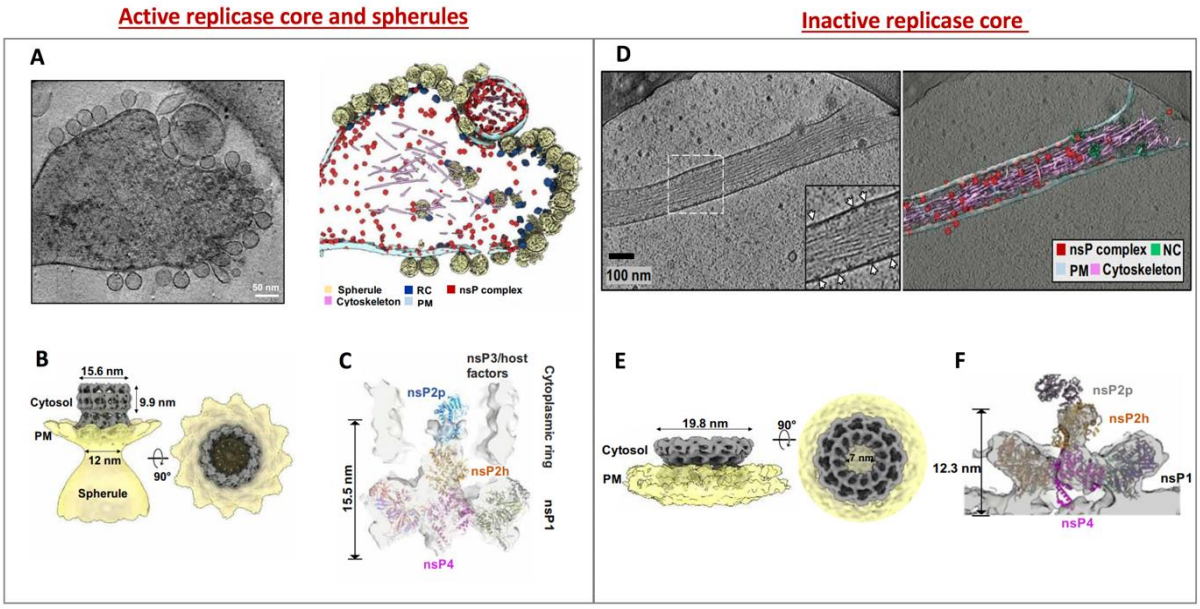

Figure 20: Comparison of the molecular architecture of active and inactive CHIKV replicase complexes. A-C Active CHIKV replication complexes. *A Tomographic slice of cell periphery depicting CHIKV RNA replication spherules at the PM. Scale bar, 50 nm, and Corresponding 3D segmentation of cellular features. CHIKV spherule 3D volume is determined by subtomogram averaging with imposed C12 symmetry. (E) The RC core complex (nsP1 + 2 + 4) is fitted into the C1 subtomogram average map of the RC. A cytoplasmic ring as observed in (C), likely made of nsP3, RNA, and host factors remain loosely connected to the nsP1 ring, which is bound at the neck of the spherule. The extra density above the nsP2h region is likely to be the C-terminal protease of nsP2, stabilized or restrained by the cytoplasmic ring.* ***D-F Inactive replicase core****: D (left), Tomographic slice of cell periphery depicting a filopodia-like membrane protrusion structure extended from the PM. White arrows point to the membrane-associated nsP complexes. Scale bar, 100 nm. D (right) Corresponding 3D segmentation of cellular features. E, CHIKV nsP complex 3D volume determined by subtomogram averaging with imposed C12 symmetry. F, The RC core complex (nsP1 + 2 + 4) is fitted into the C1 subtomogram average map of the nsP complex. Note that the cytoplasmic ring as observed in Fig. 3C is absent in this inactive nsP complex. Consequently, there is no density observed for the C-terminal protease of nsP2. From Tan et al. 2022.*

Since viral nsP3 is known to localize to active replicative spherules (Götte, Liu, et McInerney 2018; Y. F. Wang, Sawicki, et Sawicki 1994), the model proposes that the cytoplasmic ring-shaped structure may be composed by nsP3 and additional host factors (Tan et al. 2022). Interestingly, the independent study conducted by Laurent et al., also demonstrated the presence of a cytoplasmic ring or crown-like structure above the nsP1-dodecameric ring, that was proposed to be composed by nsP2 recruited to the plasma membrane by nsP1 in a concentration- dependent manner (Laurent et al. 2022). Whereas single-particle cryo-EM and in situ cryo-ET provided valuable information about viral replicase organization and spherule biogenesis, little is known about the host factors involved into this critical step. Viral nsP3 protein is proposed as a major determinant for cellular factors recruitment at the plasma membrane to allow membrane remodeling and spherule formation. Furthermore, how the different capped positive RNA species exit the spherules and reach either site for translation or sites for RNA packaging into nucleocapsid is poorly understood.

A model for spherule biogenesis and viral RNA synthesis can be built (Figure 21): P1234 or P123+nsP4 replicates reach the plasma membrane and anchor to it through the nsP1. Viral RNA is also addressed to PM by unknown mechanisms. If the P1234 polyprotein is produced, it must be processed to liberate the fully active RdRp nsP4. It is thought that this processing changes replicase topology, activating spherule biogenesis and the synthesis of the negative RNA strand, which serves as a template for the synthesis of new positive single-stranded viral RNAs. This early replicase complex is further processed into a short-lived nsP1+P23+nsP3 complex, thought to synthesize positive gRNA. Because of the full processing of nsP1, one can speculate that at this stage, the nsP1-dodecameric ring is completely formed and active for RNA capping. Finally, the last processing releases nsP3 from nsP2, leading to a full active replicase that synthesizes mainly subgenomic RNAs. The precise topology of nsP3 is not reported, but it was proposed to form a cytoplasmic crown supporting nsP1-ring.

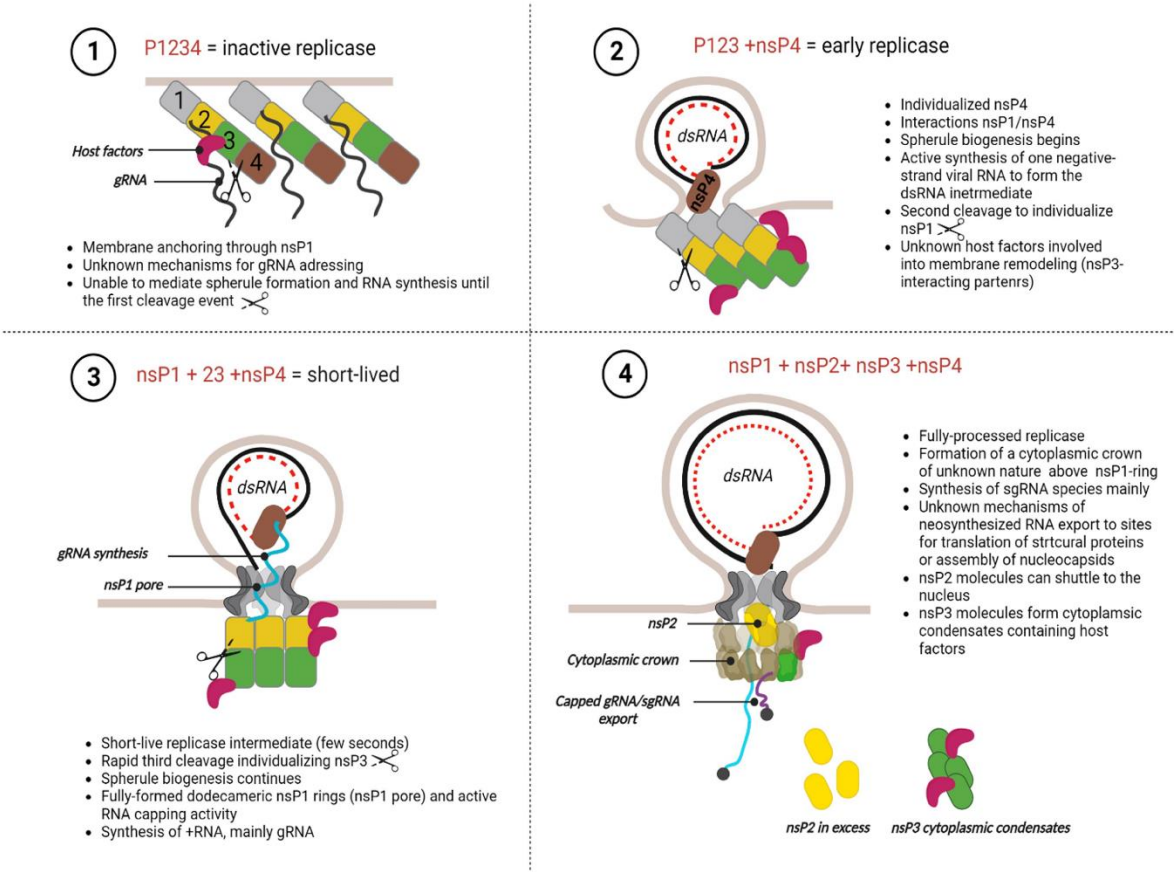

Figure 21: Model for alphavirus spherule biogenesis and RNA synthesis

Regarding the newly synthesized genomic and subgenomic RNA species, it is still unknown by what mechanisms the different RNA species are sorted. Indeed, the newly synthesized genomic RNA could serve either for translation of new non-structural polyprotein or for packaging into nucleocapsids for further particle assembly.

In addition, the sub-genomic RNA must be taken in charge by the translation machinery for the synthesis of structural proteins. Another recent study investigating CHIKV-vRC in their cellular context by *in situ* cryogenic-electron microscopy (Girard et al. 2023), confirm replicative spherules are mostly maintained at the plasma membrane rather than being internalized (Girard et al. 2023). In addition, the obtained tomograms showed vRC associated to filaments resembling viral RNA, tightly linked to ribosome-like structures, which suggested that the sites of viral replication and viral protein synthesis are likely nearby (Girard et al. 2023).

Chapter VII: CHIKV nsP3, an enigmatic protein essential for CHIKV infection and pathogenesis

A. nsP3 organization

Alphavirus nsP3 is a phospho-protein, organized into an N-terminal, highly conserved Macrodomain, a Central Alphavirus Unique/ Zinc finger binding domain, and a C-terminal, intrinsically disordered hypervariable domain (Figure 22). The following sections discuss nsP3 domain structure and functions in detail.

Figure 22: Domain organization of alphavirus nsP3 protein

1. Macrodomain (MD)

The MD, first described as an X-domain (X for unknown function) found within the polyprotein of alpha-, corona- and rubiviruses (Gorbalenya, Koonin, et Lai 1991), is a highly conserved protein domain present in all kingdoms of life (Rack, Perina, et Ahel 2016). MDs consist of 130-190 amino acids folds, associated with ADP-ribose function and metabolism. ADP-ribosylations are a post-translational modification controlling various cellular processes, including DNA repair, transcription and stress response. ADP-ribose is covalently attached to cellular proteins by poly-ADP-ribose polymerases (PARPs) (reviewed in Gupte, Liu, et Kraus 2017). Since multiple PARPs are induced by interferon, it is proposed that ADP-ribosylation is involved into the cellular antiviral response (Fehr et al. 2020). For instance, ZIKA virus NS1 and NS3 are ADP-ribosylated by cellular PARP12 which leads to their degradation and therefore ZIKA virus replication inhibition (Lili Li et al. 2018). Most macrodomains bind to monomeric ADP-ribose (MAR) and its derivatives, including ADP-ribose-1″-phosphate (Appr1p), O-acyl-ADP-ribose, and the terminal ADP-ribose of poly(ADP-ribose) (PAR), as well as protein-conjugated MAR or PAR (i.e., MARylated or PARylated proteins (Leung, McPherson, et Griffin 2018). In addition to bind ADP-ribose, a subset of MDs is able to hydrolyze ADP-ribose derivatives (C. Li et al. 2016). Viral macrodomains present a great structural conservation, suggesting a crucial role during viral replication which could be involved into antiviral immunity inhibition (Rack, Perina, et Ahel 2016).

Structural studies of CHIKV MD showed a central twisted six-stranded β sheet surrounded by three helices on one side and one on the other (Figure 23A) (Malet et al. 2009). CHIKV-MD was found to bind to monomeric ADP-ribose (MAR) and poly(ADP-ribose) (PAR) and possess ADP-ribose-1'' phosphate phosphatase activity, converting ADP-ribose-1''-phosphate to ADP-ribose (Figure 23B,C) (Malet et al. 2009). Mutations abolishing both binding and hydrolase activities resulted in attenuated replication, and virulence in mice (McPherson et al. 2017). Interestingly, VEEV MDs exerts the same activities as CHIKV MDs, whereas the SFV MDs is not able to bind monomeric-ADP-riboses, suggesting that MDs shares some functional properties but are not identical (Malet et al. 2009; Neuvonen et Ahola 2009).

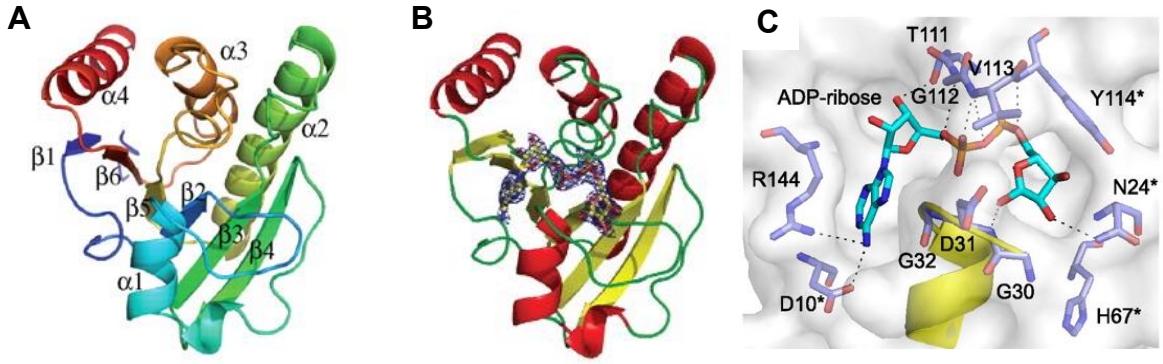

Figure 23: Structure of CHIKV nsP3 macrodomain (MD): *A, Representation of CHIKV macro domain in a purple-to-red gradient (from N terminus to C terminus). Secondary structure elements are labeled on the CHIKV macro domain. B, ADP-ribose binding site of the CHIKV macro domain. B, representation of the CHIKV macro domain with helices, strands, and loops colored, respectively, in red, yellow, and green. ADP-ribose is displayed in sticks with carbons in yellow, oxygens in red, nitrogens in blue, and phosphorus in orange. C, The CHIKV macro domain is complex with ADP-ribose. ADP-ribose is shown in cyan. Residues interacting with ADP-ribose in the CHIKV macro domain are shown in blue, and mutated residues are indicated with an asterisk. From Malet et al. 2009.*

2. Alphavirus Unique Domain (AUD)

The AUD is also a highly conserved protein domain, with around 50% of identical amino acid residues between CHIKV and SINV (Gao et al. 2019). The domain is also referred as a Zinc finger binding domain (ZBD). Indeed, the most comprehensive AUD structural data is available from the uncleaved P23 precursor of SINV (Shin et al. 2012). It demonstrates that the AUD contains an antiparallel α-helical bundle, two parallel β-strands and a previously unknown zinc (Zn)-binding site. Zn ion is coordinated by four cysteines, absolutely conserved between all alphaviruses AUD. C263 and C265 are located in the loop between the two α-helices, whereas C288 and C306 are positioned at the end of the two parallel β-strands (Figure 24).

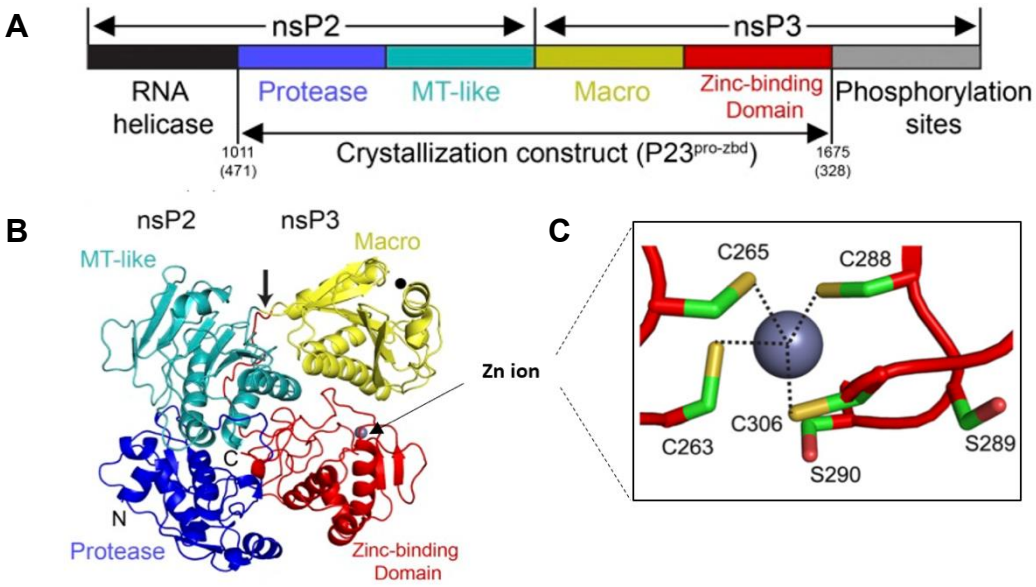

Figure 24: Structure of SINV AUD. *(A) Schematic representation P23 precursor domain organization. The crystallization construct consists of four domains: protease (blue) and methyltransferase-like (teal) domains of nsP2 and the macro (yellow) and zinc-binding (red) domain of nsP3, encompassing amino acids 1011–1675 of the SINV P1234 polyprotein. Amino acid numbering provided from the amino terminus of nsP2 and nsP3 are also noted in parentheses. (B) Ribbon diagram of P23pro-zbd colored according to A. A gray sphere with black arrow head denotes the position of the zinc ion. The P2/3 cleavage site, nsP2 protease active site, and ADP ribose–binding site are labeled with an arrow, asterisk (*), and filled circle, respectively. (C) Stick representation of the AUD Zn-finger binding domain: the gray sphere represents Zn ion, the four cysteines coordinating the Zn and two highly conserved serine residues. Adapted from Shin et al., 2012.*

Interestingly, no structurally similar metalloprotein folds have been described in other organisms so far. Site directed mutagenesis of all four conserved cysteines residues revealed a critical role of Zn-binding domain for propagative viral infection (Shin et al. 2012). In addition those mutants failed to express the viral protein, suggesting a structural role of the Zn ion (Shin et al. 2012). In the same study, the purification of P23 allowed to pull-down great amounts of RNA and basic residues-enriched patches were found in great proximity to the Zn-binding site extending to the nsP2 (Shin et al. 2012). In line with these observations, and the fact that zinc metalloproteins are also involved in nucleic acid-binding and gene regulation, it was proposed that the basic interface extending across nsP2 and nsP3 is involved into viral RNA binding (Shin et al. 2012; Berg 1990). Very little is known about the AUD proviral function during CHIKV (and alphavirus) replication.

3. Hypervariable domain (HVD)

In contrast with the rest of the nsP3 protein, the hypervariable domain (HVD) displays high variability of sequence among alphaviruses (Figure 25) (E. G. Strauss et al. 1988). HVD is largely of low complexity or intrinsically disordered domain, with no predicted secondary structure (Meshram et al. 2018). Partial deletions in the HVD have only minor effects on viral replication and productive infection, thus making it an ideal location for tag insertions (N. J. Foy et al. 2013; Remenyi et al. 2017). Since the HVD is an intrinsically disordered domain, it was suggested to mediate multiple protein-protein interactions required for viral infection (N. J. Foy et al. 2013; Meshram et al. 2018; Babu 2016). Indeed, despite the high sequence variability of Alphaviruses HVDs, a number of conserved linear motifs were mapped and proposed to recruit distinct sets of cellular proteins (Gorchakov, Garmashova, et al. 2008; D. Y. Kim et al. 2016; Frolov et al. 2017; Meshram et al. 2018). The conserved motifs HVD motifs mediating host factor interactions are discussed in section B.3.

The HVD is also the only phosphorylated replicase protein. A formal demonstration of HVD phosphorylation was brought for SINV, SFV and VEEV, where the phosphorylated sites were mapped to Ser/Thr residues in the beginning of the HVD sequence (G. Li et al. 1990; Peränen et al. 1988; Vihinen et Saarinen 2000; Niall J. Foy et al. 2013). A deletion of SINV-HVD phosphorylation sites didn't result in dramatic reduction in viral replication and infectivity, suggesting that HVD-phosphorylation is not critical for the replication cycle. In contrast, phosphorylation sites deletion attenuated SFV in vivo, and VEEV replication was affected in mosquito cells but not in mammalian cells (G. Li et al. 1990; Vihinen et Saarinen 2000; Niall J. Foy et al. 2013). These findings suggest that despite common phosphorylation sites, inferences from one alphavirus to other should not be made. This was further validated recently with the study of CHIVK and ONNV phosphorylation sites. In contrast with the other alphaviruses, CHIKV nsP3 phosphorylation sites were throughout the HVD. Interestingly, their complete elimination resulted in total loss of viral infectivity (Teppor, Žusinaite, et Merits 2021). Peränen and colleagues put forward a hypothesis suggesting that phosphorylation could potentially play a regulatory role in RNA synthesis (Peranen et al. 1988). They also observed that the portion of nsP3 associated with RNA polymerase activity in the P15/membrane fraction exhibited a higher level of phosphorylation compared to the nsP3 in the S15/cytosolic fraction (Peranen et al. 1988). It is important to note, that some phosphorylated residues are

found within HVD-motifs required for the recruitment of host factors, thus whether the lethal phenotype is due to phosphorylation profile or to an impairment of interaction with essential host factors is not clear.

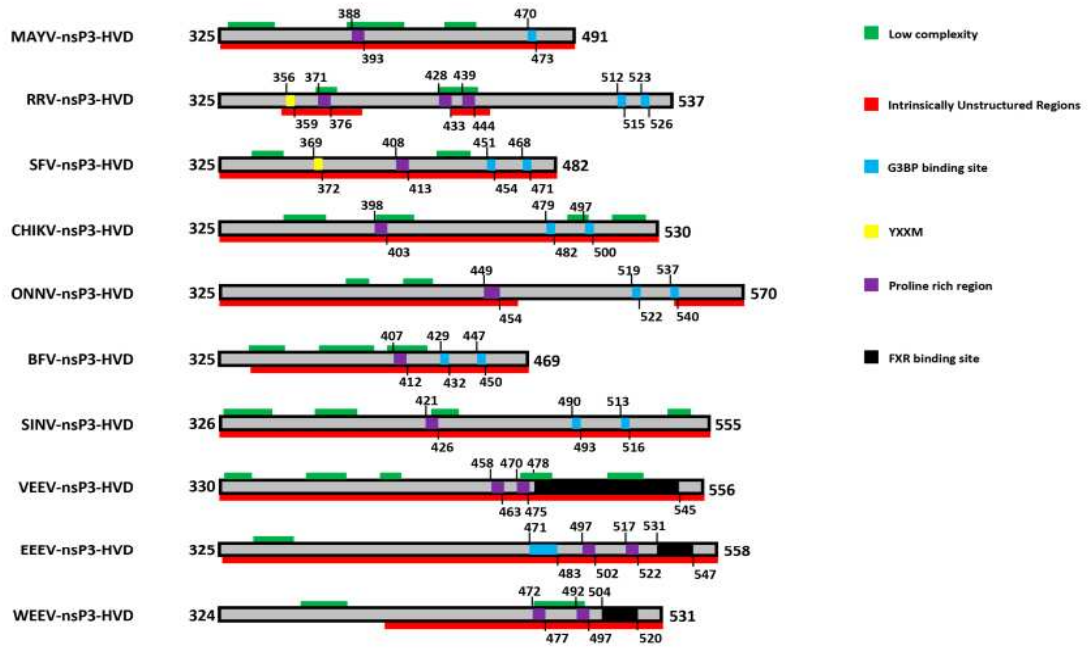

Figure 25: Simplified schematic representation of alphaviruses' HVD features *From Götte et al, 2018.*

B. nsP3 functions during alphavirus replication

1. CHIKV genome replication and transcription

As mentioned in the previous chapters, nsP3 is a major component of the replicase complex. While the roles of nsP1, nsP2 and nsP4 are well-documented in the literature, the function of nsP3 and particularly its AUD domain in viral genome replication and spherule biogenesis remains to be fully characterized.

The AUD is highly conserved among alphaviruses, suggesting a crucial role during virus replication. As described previously, the structural analysis of SINV-P23 precursor (Shin et al. 2012) demonstrated that the AUD contains a zinc-finger binding motif that is a part of larger domain with putative RNA-binding. Mutagenesis of the cysteine residues coordinating the zinc ion, was shown to completely abolish viral replication in all cell types (G. Shin et al. 2012; Gao et al. 2019). So far, there is only one functional study bringing insights about AUD importance during viral replication (Gao et al. 2019). Indeed, mutagenesis of CHIKV AUD (Gao et al. 2019), based on the structure of the P23 precursor of SINV (Shin et al. 2012), provided original information on the role of the AUD during genome replication and transcription.

Indeed, 10 AUD residues exposed at the surface of the protein and absolutely conserved among alphaviruses were mutated in a CHIKV subgenomic replicon system to test their importance during the replication step. Each mutation's phenotype was analyzed in human, rodent, or mosquito cell lines. Mutation of the two cysteine residues coordinating the zinc ion (C262A/C264A) that are proposed to be involved in RNA-binding (Shin et al. 2012) and residues adjacent to the zinc-binding cysteines (V260A/P261A), completely abolished CHIKV replicon amplification in all cell lines. Two other basic residues exposed at the AUD surface (R243 and K245) completely abrogate replication in mammalian cells, whereas in mosquito cells, these mutations reverted to wild type. Thus, these residues are likely involved in the replication process in vertebrate and invertebrate hosts. Another residue of great interest -M219, was demonstrated to be involved in the RNA interference response in mosquito cells. Altogether, this study described for the first time the importance of the nsP3 AUD domain in adapting CHIKV to its different hosts.

One particular AUD mutant, harboring P-to-A substitution at position 247 and V-to-A substitution at position 248 (referred to as P247A/V248A mutant), was of great interest in this study (Gao et al. 2019). The P247A/V248A mutant could not replicate in human Huh or Huh7.5 cells, whereas its replication was impaired in human rhabdomyosarcoma cell line and rodent and mosquito cells. Mechanistic experiments showed that the P247A/V248A mutant was competent in viral entry and virus particle release but exhibited a major defect in virus assembly. Further investigations suggested that these double mutations affect the ability of the AUD to recognize the subgenomic promotor from the negative viral RNA strand, leading to impaired synthesis of sgRNA species and, thus to a defect in structural protein synthesis (Gao et al. 2019). Finally, this mutant shows an impaired localization of viral replicative complexes, nsP3, and capsid protein, suggesting that the nsP3 protein is likely coordinating the replication and the assembly steps at the plasma membrane of infected cells.

2. Stress granule disassembly

During the early phase of infection, the positive-stranded RNA virus synthesizes a dsRNA replicative intermediate that triggers Protein Kinase R (PKR) phosphorylation and activation. PKR activation leads to eIF2α phosphorylation and inhibition of host mRNA translation (Gorchakov et al. 2004). Inhibition of cellular translation results in

the formation of stress granules (SG), non-membranous dynamic aggregates of translationally silent messenger ribonucleoproteins (mRNPs) (Marc D. Panas et al. 2012; McInerney et al. 2005; Jayabalan et al. 2021a). SGs form through liquid-liquid phase transition (LLPT), thought to be initiated by long stretches of messenger RNA, not engaged in the translation process. The accumulated RNAs serve as a scaffold for multiple RNA-binding proteins, including RasGAP-associated endoribonuclease 1 (G3BP1), T cell internal antigen 1 (TIA1), TIA1-related protein (TIAR), Caprin1, and fragile X mental retardation protein (FMRP), as well as ribosomal subunits (40S ribosome subunit) (Beckham et Parker 2008; Ivanov, Kedersha, et Anderson 2019; Jayabalan et al. 2021a). These proteins contain intrinsically disordered regions (IDRs) that establish weak interactions and drive LLPT, thus promoting SGs assembly (Lin et al., 2015; Molliex et al., 2015; Tourrière et al. 2003; Gilks et al. 2004; Mazroui et al. 2006), The sole overexpression of G3BP proteins for instance, can induce SGs formation even without any stress (Kedersha et Anderson 2007).

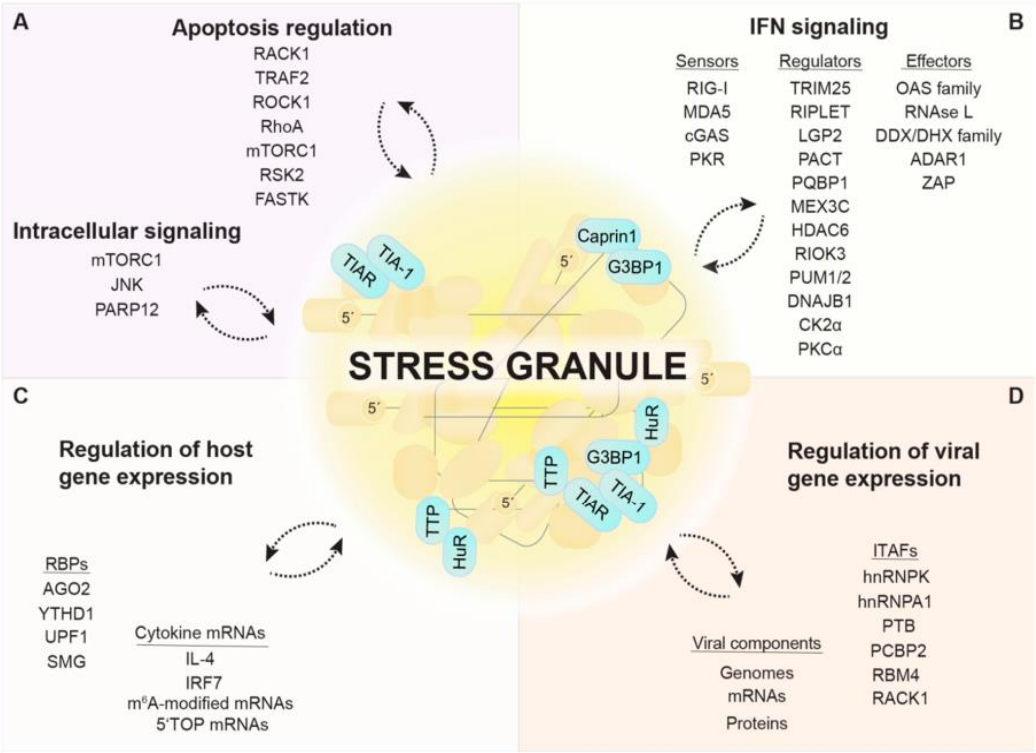

Figure 26: Stress granules are cellular immune and stress signaling platforms. *SGs serve as immune and signaling hubs formed through phase separation, concentrating regulatory proteins that participate in apoptosis induction and various intracellular signaling pathways (A) and IFN signaling (B). SGs prefer certain RBPs and cellular mRNAs, such as cytokine mRNAs (C). Additionally, SGs house viral components and ITAFs responsible for controlling viral gene expression (D). It's important to note that the composition of SGs varies significantly based on stress conditions and cell types. Notably, many components have been identified in SGs during metabolic or environmental stress, but their role in the context of viral infection remains unexplored. The localization and function of specific SG components rely on their interaction with particular SG core proteins, highlighted in turquoise. From (Eiermann et al. 2020).*

SG formation is highly regulated by posttranslational modifications of its constituents, including ADP-ribosylation SGs (Duan et al. 2019; Catara et al. 2017). The non-covalent interaction between ADP-ribose and proteins triggers their addressing to SGs (Duan et al. 2019; Catara et al. 2017). In humans, ADP-ribosylation is mediated by a family of ADP-ribosyltransferases named poly-(ADP-ribose) polymerases (PARPs). Overexpression of PARPs induces SGs formation, whereas the overexpression of PAR-glycohydrolase (PARG) disassembles SGs (Leung et al. 2011; Duan et al. 2019).

In the late steps of the infection, it was proposed that alphaviruses disassemble SGs through the sequestration of G3BP proteins via the C-terminal Hypervariable domain of the nsP3 (J. J. Fros et al. 2012; Marc D. Panas et al. 2015; 2012). However, in a recent work performed by Jayabalan and colleagues, it was demonstrated that nsP3, by its sole interaction with G3BPs proteins, is not sufficient to disassemble cellular SG (Jayabalan et al. 2021a). The viral domain involved in this activity was shown to be the MD, which can trigger alone the suppression of these condensates, despite persistent eIF2α phosphorylation (Jayabalan et al. 2021a). This is consistent with the recent evidence showing that the MD possesses an ADP-ribose (mono- and poly-ADP ribose) binding and mono-ADP-ribosylhydrolase activities (McPherson et al. 2017; Eckei et al. 2017; Abraham et al. 2018). In addition, mutant nsP3 unable to interact with G3BPs protein was still able to disassemble SG (Jayabalan et al. 2021a), showing that the nsP3-HVD interaction with G3BP proteins is not required for SG inhibition. Thus, it is proposed that nsP3 regulates SG formation, disassembly and composition through both its HVD-G3BPs binding capacities and its MD- ADP-ribose hydrolase activity. As nsP3 accumulates through the course of infection, the nsP3-MD binds and hydrolyze ADP-ribose modifications onto G3BP1 and likely other SGs components. This leads to the disassembly of SGs at the later stages of infection, and prevents the formation of new ones (Jayabalan et al. 2021a)

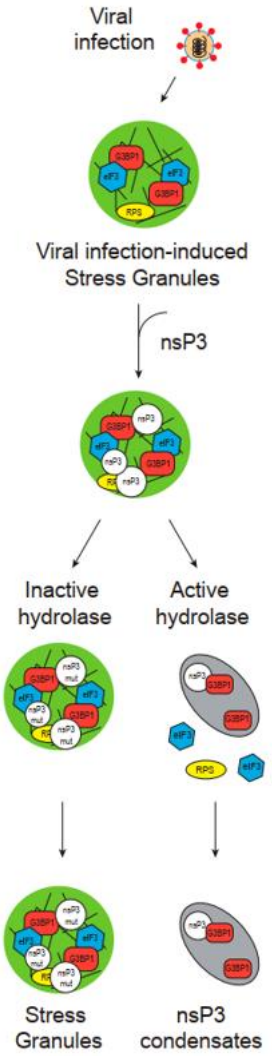

Figure 27: Model of virus infection-induced SG assembly and disassembly regulated by nsP3 ADP-ribosylhydrolase activity. *From Jayabalan et al. 2021*

(Figure 27). It is proposed that prevention of SGs formation might be important to release translation initiation factors and allow the viral structural proteins synthesis.

3. Interacting hub for host factors involved in viral replication and host-adaptation

Affinity-purification and mass-spectrometry approaches, phage display screens, genetic screens or hypothesis-driven approaches demonstrated that nsP3 recruits multiple host factors involved into viral replication (Cristea et al. 2006; Gorchakov, Garmashova, et al. 2008; Neuvonen et al. 2011; Abere et al. 2012; Mazzon et al. 2018; Götte, Liu, et McInerney 2018; Meertens et al. 2019). A substantial part of nsP3-interactants was found to be recruited through the HVD of the viral protein. HVD-interactants which have been validated, either for their interaction or for their proviral function, are shown in Table 2.

Table 2: Major alphavirus nsP3-interacting host factors and their putative proviral functions

	Host factors	Known HVD-biding motif	Cellular functions	Proviral functions	References
SH3-domain containing proteins	BIN1/ Amphiphysine2	P[I/V][P/A]PPR	• Src-homology 3 (SH3)-domain containing proteins • SH3-domain: involved in protein/ protein interactions multiple signaling pathways, membrane curvature, trafficking and cytoskeleton regulation	• Recruited to dsRNA-containing viral complexes • Putative functions in viral replication and spherule biogenesis	Kaneko, Li, et Li 2008; Mutso et al. 2018; Meshram et al. 2018; Neuvonen et al. 2011; Tossavainen et al. 2016
	CD2AP SH3KBP1	Motif 1: P[I/V][P/A]PPRGRNLTVT Motif 2: PMASVR			
DExH-box Helicase	DHX9	*ND*	• Unwind DNA and RNA-secondary structures • RNA metabolism (transcription, splicing, ribosome biogenesis) • Interferon secretion	• Negative impact on RNA synthesis • Enhencing viral non-structural polyprotein synthesis	S. Zhang et Grosse 1997; Suisheng Zhang et Grosse 2004; Z. Zhang et al. 2011; S. Li et al. 2011; Matkovic et al. 2018
NAP1 proteins	NAP1L1 NAP1L4	Motif 1: TTMELSHPPISFGAP Motif 2: DDLTDSDWSTCPDTDD	• Histones transport into the nucleus • Nucleosome formation • Modifying chromatin structure • Govern essential cellular functions like transcription and the progression of the cell cycle	• Interaction with phosphorylated HVD • Stimulate viral replication	Y.-J. Park et Luger 2006 Meshram et al. 2018; Dominguez et al. 2021;
G3BP- and FXR-family proteins	G3BP1 & G3BP2 (Old World alphaviruses) FXR-1 & FXR-2 (New World alphaviruses)	G3BP: Two FGDF motifs in C-terminal HVD FXR: Agenet-like domain binding motif	• Ras-GAP SH3 domain-binding protein • Formation of stress granules (involved into cell reponse to stress) • Homo-oligomerization, Rna interaction	• Viral RNA synthesis • Putative role as a molecular switch from gRNA translation to replication • Clustering of replicative spherules • Ribosome interactions	Cristea et al. 2006, Gorchakov, Garmashova, et al. 2008; Marc D. Panas et al. 2012; D. Y. Kim et al. 2016; Frolov et al. 2017; Schulte et al. 2016
FHL proteins	FHL1 FHL2	FHL1: VTCD...QAPP FHL 2: *ND*	• Four and a half LIM-domain containing proteins • Mediate protein/protein interactions • Actin cytoskeleton reorganization • Muscle tissue development and homeostasis	• Requiered for efficent CHIKV and ONNV replication • Likely involved in viral RNA synthesis	Meshram et al. 2018; Meertens et al. 2019; Lukash et al. 2021

Among them, G3BP proteins and FHL1 display the most important phenotypes regarding CHIKV replication *in vitro* and/or in *vivo*. Indeed, G3BP proteins are used by several alphaviruses and were demonstrated to be essential only for CHIKV replication (J. J. Fros et al. 2012; Scholte et al. 2015; D. Y. Kim et al. 2016; Götte et al. 2019). Four-and-a-half LIM domain protein 1 (FHL1), has been recently identified as an important CHIKV host factor required for viral tropism and pathogenesis. The role of

these two cellular factors is discussed in the following sections.

4. nsP3 form stable cytoplasmic granules of unknown function

Once synthesized, alphavirus nsP3 is found as a part of distinct protein complexes, either with other nsPs or in interaction with multiple host factors (Cristea et al. 2006; Götte, Liu, et McInerney 2018; Meshram et al. 2018). Cell fractionation studies demonstrated that in contrast with SFV-nsP3, which is in great part associated with the membrane pallet along with nsP1 and nsP4, the majority of CHIKV-nsP3 was retrieved in the cytosolic fraction of the infected cells (Albulescu et al. 2014; Peranen et al. 1988). Imaging analysis of nsP3 subcellular localization during infection demonstrated that a fraction of nsP3 is a part of vRC, either at the plasma membrane or in the CPV-I (Gorchakov, Garmashova, et al. 2008; Elena Frolova et al. 2006; Wang, Sawicki, et Sawicki 1994b). However, a substantial part of the nsP3 pool was also found in large cytoplasmic aggregates (or granules) either in infection conditions or overexpression experiments. nsP3 granules morphology was proposed to depend on the recruitment of host factors (Marc D. Panas et al. 2012; Remenyi et al. 2017; Jayabalan et al. 2021).

As discussed in the previous sections, while CHIKV-nsP3 disassembles SG, it forms other cytoplasmic condensates containing SGs RNA-binding proteins (G3BP1, TIA-1, TIAR, HuR) but not the translation initiation factors (eIF3b, eIF3i, RACK1…). These nsP3-enriched condensates are a hallmark of alphaviruses. (Gorchakov, Garmashova, et al. 2008; J. J. Fros et al. 2012; D. Y. Kim et al. 2016a; Jayabalan et al. 2021a; Nowee et al. 2021). Interestingly, these condensates are formed under the expression of nsP3 alone in stressed or unstressed cells (Jayabalan et al. 2021). Furthermore, nsP3-condensates are not sensitive to cycloheximide, a translation elongation inhibitor, disassembling SGs. Those nsP3 granules appear to be different in nature from *bona fide* SGs. Our knowledge about these nsP3 condensates is limited.

Multiple imaging studies of CHIKV-infected cells demonstrated the accumulation of the nsP3-binding proteins within cytoplasmic structures (e.g., G3BPs, BIN1, FHL1). Live-cell imaging of SNAP-tag nsP3 encoding CHIKV replicon system coupled to 3D high resolution microscopy, allowed to characterize more in details the different nsP3 complexes formed during infection in Huh7 cells. Sub-diffraction multicolor microscopy, validated the presence of nsP3/G3BPs-enriched round

cytoplasmic granules of different sizes. These granules exhibited several interesting characteristics: (i) they contained nsP3 and G3BP1/2, (ii) they were positioned adjacent to double-stranded RNA foci and nsP1-positive structures, and (iii) they were close to the nuclear membrane and the nuclear pore complex protein Nup98. Furthermore, these granules could persist for extended periods, ranging from hours to days. They also accumulated newly synthesized proteins and displayed varied movement speeds as they traversed the cytoplasm (Remenyi et al. 2018). We and others demonstrated that another major nsP3-interacting partner is sequestrated within these granules, the Four-and-a-half LIM domain protein 1 (FHL1) (Meertens et al. 2019; Lukash et al. 2020). So far, the proviral role of these condensates and their implication in viral pathogenesis is still elusive. In addition, nsP3-enriched "rod-like" structures were described as transient complexes that likely evolved into large spherical granules associated with lipid droplets and in proximity with viral nsP1 protein (Remenyi et al. 2017). Interestingly, the nsP3 rod-like structures have also been reported in other cell types (mouse myoblasts, glial cells, dermal fibroblasts) during transient replication and late stages of infection (Scholte et al. 2015; Roberts et al. 2017).

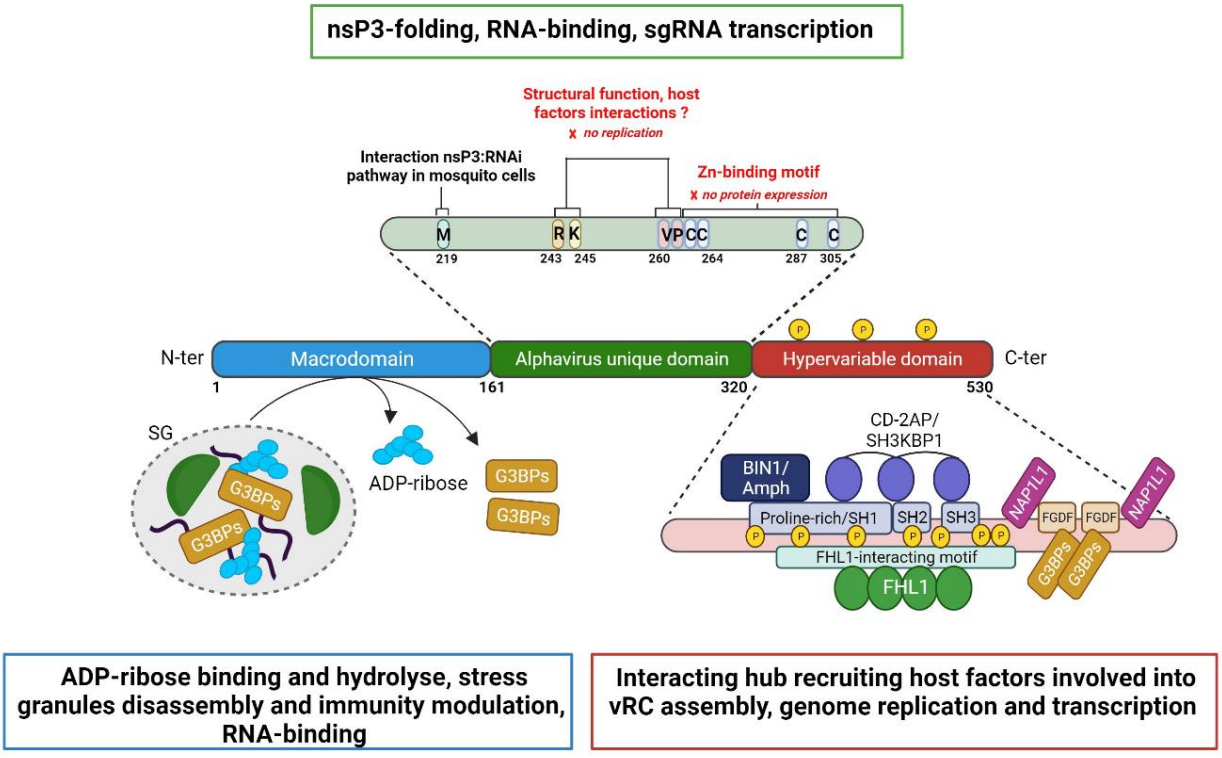

Figure 28: Schematic representation of nsP3 established proviral functions

Altogether, nsP3 is a versatile protein playing multiple and critical functions during the viral cycle (Figure 28). Each domain exerts specific activities and allows efficient viral replication. The MD modulates the cellular stress and antiviral response through its ADP-ribose binding and hydrolase activities. This activity is further potentialized by the ability of the HVD to recruit and interact with multiple host factors. These factors are required for different steps, such as efficient viral replication complexes (vRC) formation and antiviral response antagonism. The established data suggest that: **(1)** CHIKV replication is not dependent on individual members of host protein families; instead, it relies redundantly on all family members or even representatives from different families that share similar domains, such as the SH3 domain-containing proteins. **(2)** The interaction between CHIKV-HVD and G3BP family members is crucial for viral RNA replication, and any changes in these interactions render the virus nonviable. **(3)** Extensive mutagenesis of HVD, aimed at preventing binding to all host factors except G3BPs, also leads to the abolition of CHIKV replication. **(4)** To restore viability, CHIKV variants must possess at least one of the binding motifs in HVD and those that interact with G3BPs. However, these variants replicate less efficiently than the wild-type virus. These findings indicate a significant level of redundancy in the functions of different host factor families and their collective contributions to CHIKV RNA replication. Nevertheless, this redundancy also complicates the understanding of binding sites and the specific roles of individual host proteins in vRC formation and function.

Finally, the AUD domain is likely directly involved in viral RNA replication and subgenomic RNA transcription. Despite extended research, it still needs to be determined what are the precise molecular mechanisms behind these multiple roles. A question of great interest concerns the proviral role of nsP3 granules, which are not active viral replication complexes. How these granules are formed, their precise composition, and whether they are involved in specific steps of the viral cycle remain unsolved. Finally, the accumulated data concerning SINV or SFV nsP3, widely used as models for alphavirus infection, are insufficient to understand CHIKV infection, as CHIKV-nsP3 displays significant differences with the other nsP3. Thus, it remains of great importance to study specifically this protein.

C. G3BP proteins: antiviral purpose, proviral role

Multiple studies demonstrated that Old Word alphaviruses possess a repeated FGDG motif in the C-terminal part of the HVD domain. This motif binds the cellular G3BP-1 and -2 (Ras-GAP SH3 domain-binding protein) (Cristea et al. 2006, Gorchakov, Garmashova, et al. 2008; Marc D. Panas et al. 2012; D. Y. Kim et al. 2016; Frolov et al. 2017; Schulte et al. 2016). It is known that perturbation of SFV-HVD interaction with G3BPs causes SFV attenuation but not complete lethality. In contrast, disrupting CHIKV-HVD interaction with G3BPs results in essentially non-viable viruses (D. Y. Kim et al. 2016; Schulte et al. 2016). These observations suggest that despite recruiting the same host factors, the proviral mechanisms could differ events between closely related alphaviruses.

1. G3BP organization

There are three isoforms of G3BP: G3BP1 and two splice variants, G3BP2a and G3BP2b (collectively referred to as G3BP). G3BP1 and G3BP2a share approximately 66% amino acid identity and have a similar domain structure. All G3BP isoforms consist of the following domains arranged from the N- to C-terminus: a nuclear transport factor 2 (NTF2)-like domain, an acidic domain, a proline-rich region with several PxxP motifs, an RNA recognition motif (RRM), and an arginine-/glycine-rich domain (RGG) (Irvine et al. 2004; Matsuki et al. 2013; Jayabalan, Griffin, et Leung 2023).

Figure 29: G3BP1 and G3BP2 protein organization

The N-terminal domain of G3BP contains specific motifs that enable them to interact with other proteins, while the C-terminal domains are responsible for binding nucleic acids (Figure 29). For instance, the NTF2L domain of G3BP interacts with *FGDF* sequence motifs found in numerous proteins, and the PxxP domain interacts with SH3 motifs. On the other hand, the RRM domain plays a crucial role in binding to RNA, and the RGG domain not only enhances RNA binding but also facilitates interactions with other proteins. Except the structured NTF2-like and RRM domains,

G3BPs are intrinsically disordered (Peiguo Yang et al. 2020). This property is involved into the protein-protein and protein-RNA interactions abilities of G3BPs (Peiguo Yang et al. 2020). In some instances, the functions of G3BP1 and G3BP2 show redundancy, but this is not always the case (Kedersha et al. 2016). For example, when G3BP1 expression and function are knocked down, the expression of G3BP2 increases to compensate for the loss, but the reverse is not observed (Scholte et al. 2015; Kedersha et al. 2016).

2. G3BP1 assembles stress granules and amplifies innate immunity signaling

As mentioned in the previous section, G3BP are components of stress granules (SG), as it is involved into SG nucleation and assembly (Kedersha et al. 2016). Indeed, G3BP organizes a core interaction network with cytoplasmic free RNAs, and functions as a molecular switch that triggers RNA-dependent liquid-liquid phase separation (LLPs) (Peiguo Yang et al. 2020). The C-terminal RGG-domain of G3BP binds the 40S ribosomal subunit which is thought to participate in SG assembly (Kedersha et al. 2016). Additionally, G3BP proteins are capable to interact with cellular proteins with antagonistic properties in SG assembly (Kedersha et al. 2016). G3BP interaction with Caprin-1 protein promotes SG assembly, whereas G3BP binding to USP10 disassembles SG (Kedersha et al. 2016). This binding is mediated by the NTF2-like domain which interacts with the FGDF motif of USP10, also found within the HVD sequence of Alphaviruses nsP3. In addition to form the core of SG, G3BP1 regulates the early innate response through protein- and nucleic acids-binding. Through its RGG domain, G3BP1 binds the RIG-I helicase domain and viral dsRNA to prevent RIG-I degradation, thus promoting IFN-β response (S. S.-Y. Kim, Sze, et Lam 2019). G3BP1 also interacts with cGAS, leading to the formation of large protein complexes. This interaction efficiently primes cGAS which is thus able to better bind cytosolic DNA (Z.-S. Liu et al. 2019). G3BP1/cGas binding activates cellular PKR and the downstream DNA-induced interferon production (Z.-S. Liu et al. 2019; S. Hu et al. 2019).

G3BPs are targeted by many viral families and can play both antiviral and proviral roles (reviewed in Jayabalan, Griffin, et Leung 2023). Indeed, given their propensity to trigger SGs formation and to amplify the early innate response to infection, G3BPs appear to be efficient antiviral factor (Jayabalan, Griffin, et Leung 2023; Z.-S. Liu et al. 2019; S. S.-Y. Kim, Sze, et Lam 2019). For instance,

Picornaviridae et *Coronaviridae* are negatively regulated by G3BPs (Ruggieri et al. 2012; H. Liu et al. 2022). Overexpression of G3BP1 reduces viral replication, protein synthesis, and virus production, while G3BP1 knockdown enhances viral replication. Both viral families have evolved to counteract G3BP1-induced antiviral response, either by mediating G3BP1 cleavage or sequestration (Ruggieri et al. 2012; H. Liu et al. 2022; Jayabalan, Griffin, et Leung 2023).

Old World Alphavirus also evolved to exploit G3BPs (Scholte et al. 2015; D. Y. Kim et al. 2016a). It is well-established that these viruses interact with the NTF2-like domain of G3BPs through two FGDF motifs found in the C-terminal of the nsP3-HVD (M. D. Panas, Ahola, et McInerney 2014; Marc D. Panas et al. 2015; Schulte et al. 2016). Structural studies of the NTF2-like domain of G3BP1 in complex with a nsP3-peptide from SFV showed that FGDF motif binds to a hydrophobic groove on the NTF2-like domain of G3BP1 (Kristensen 2015). Furthermore, NTF2-like domain forms dimers, and both N-ter and C-ter FGDF motifs bind to G3BP1 monomers on separate dimers, thus inducing the formation of poly-complex (Götte et al. 2019). SFV mutants with either one FGDF motif or none, are attenuated suggesting that nsP3:G3BP1 poly-complexes are involved in viral replication (Marc D. Panas et al. 2012; Schulte et al. 2016). Since G3BPs are essential elements for SGs formation, it was generally admitted that the nsP3 interaction with G3BPs leads to the sequestration of G3BPs and SG disassembly, thus counteracting host cell translational shutoff and antiviral immunity. As it was discussed in the previous chapter, SG disassembly was recently demonstrated to be the outcome of the MD-ADP-ribosylhydrolase activity, more than the HVD-G3BPs interaction, suggesting that the formation of nsP3:G3BPs poly-complexes play another, proviral function during alphavirus infection. In contrast to SFV, which still replicates without G3BPs interactions, CHIKV mutants unable to interact with G3BPs are not viable (D. Y. Kim et al. 2016; Schulte et al. 2016). The same phenotype is observed in CRISPR/Cas9 G3BPs knock-out cell lines (D. Y. Kim et al. 2016). These observations also point out an additional function of this host factor.

3. G3BP proteins are directly involved in CHIKV replication

It was hypothesized that G3BPs, through their ability to bind RNA and ribosomal subunits, can be critical factors in the switching from initial viral translation to viral genome replication by clearing the incoming viral RNA from ribosomes (Scholte et al. 2015). Another hypothesis postulates that nsP3:G3BPs poly-complexes are involved in building pre-replication complexes that recruit gRNA to replication (D. Y. Kim et al.

2016a). Results from immunostaining and *in situ* hybridization followed by confocal microscopy experiments in CHIKV-infected cells are consistent with these assumptions (D. Y. Kim et al. 2016). In the early steps of the infection cycle, nsP3:G3BPs complexes are found without viral RNA species at the plasma membrane (1). These are thought to be P123 polyprotein complexes containing G3BPs and targeted to the plasma membrane. Then, complexes containing nsP3, G3BPs, and single-stranded RNA are visible, suggesting a complex ready to replicate viral RNA (2). Finally, fully functional nsP3:G3BPs:dsRNA complexes are observed (3) (D. Y. Kim et al. 2016b). Lastly, mutagenetic analysis investigating the importance of each of the G3BP domains during CHIKV replication demonstrated that the G3BP-RGG domain is also required for efficient replication. Immunoprecipitation assays showed that this domain forms a G3BP:nsP3:40S ribosomal subunit complexes machinery (Götte et al. 2019). These data and electron microscopy results further suggested that G3BPs could be involved in clustering replicative spherules (via the NTF2-like domain) and recruitment of the host-cell translational machinery (Götte et al. 2019). Despite the accumulating data, it is still unclear how G3BP mediates viral infection and why CHIKV exerts complete dependency on GB3P.

D. FHL1 is a major host factor for CHIKV tropisms and pathogenesis

As discussed in ***Chapter III***, despite a large cell and tissue tropism, CHIKV-induced pathology mainly reflects the virial capacity to strongly replicate in joints and muscle tissues (Sourisseau et al. 2007; Briant et al. 2014; Bernard et al. 2015; Ekchariyawat et al. 2015; Young et al. 2019; Meertens et al. 2019 *(Research paper in annex*). However, the molecular determinants that dictate CHIKV tropism for the musculoskeletal tissue are unknown. Indeed, none of the cellular proteins and pathways co-opted by CHIKV and mentioned above could explain this cell and tissue preference. In a CRISPR/cas9 genetic screen performed by our team to describe new host-factors involved in CHIKV infection, we identified the Four-and-a-half LIM domain protein 1 (FHL1) as an important CHIKV host dependency factor.

1. FHL1 organization and expression

As its name implies, FHL1 is organized into a N-terminal half LIM domain, followed by four complete LIM domains (Figure 30). First identified in 1988, LIM domains are protein-interaction domains composed of a cysteine-rich amino acid sequence (Schmeichel et Beckerle 1994). Indeed, a consensus sequence of a LIM domain is

about 55 amino acids with eight highly conserved residues, either cysteine or histidine, located at defined intervals (Schmeichel et Beckerle 1994). The abundance and spacing of the cysteine residues in the LIM motifs were reminiscent of a metalloprotein. Further, studies identified that each LIM domain coordinates two Zn(II) ions (Michelsen et al. 1993). Two Zn-finger modules are always separated by a two-residue spacer, which is essential for LIM-domain function (Schmeichel et Beckerle 1997). LIM domains are quite abundant in eukaryotes. In humans, for instance, roughly 135 LIM domain encoding sequences scattered through 58 genes have been identified (Kadrmas et Beckerle 2004). These proteins can comprise exclusively LIM domains. LIM modules can be connected to other domains such as homeodomains, catalytic domains, or other protein-binding domains (reviewed in (Kadrmas et Beckerle 2004). LIM domains don't possess proper enzymatic activity but mediate different biological functions by interacting with target proteins. Through the binding to their partners, LIM domain proteins are involved in multiple biological processes, mainly cytoskeletal functions and the control of gene expression, meaning that their subcellular

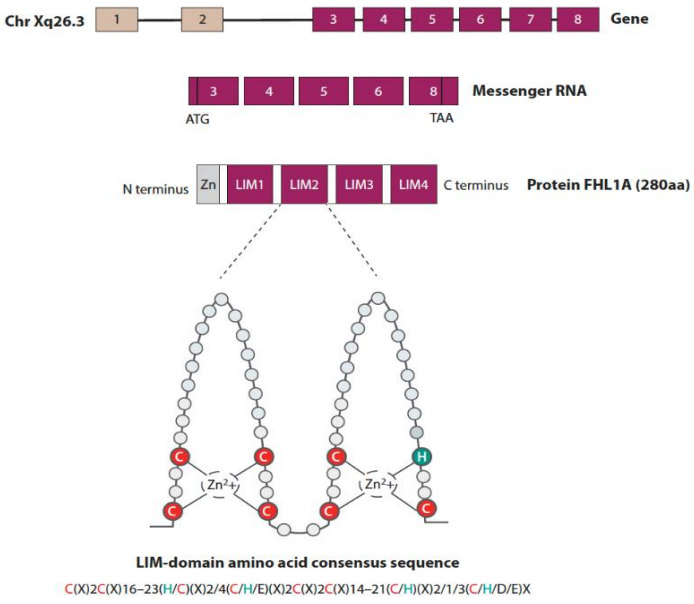

Figure 30: FHL1 gene and protein organization. *FHL1A is encoded by human chromosome Xq26.3 and is expressed with high levels in striated muscle cells and fibroblasts. Exons 1 and 2 (beige boxes) are noncoding; exons 3 to 8 (purple boxes) encode the full-length FHL1 protein, organized into an N-terminal half LIM domain followed by four complete LIM domains. Each domain consists of two zinc-finger motifs, proposed to be a protein/protein binding interface ensuring the assembly of multimeric protein complexes. The LIM domain amino acid consensus sequence is indicated. From (Kril et al. 2021).*

localization could be dual, either cytoplasmic and nuclear.

2. FHL1 expression and importance in muscle tissue development

FHL1, the founding member of the FHL protein family which also contains FHL2, FHL3 and FHL5 in humans, was originally identified in skeletal muscle and designed skeletal muscle LIM protein (SLIM) (Shathasivam, Kislinger, et Gramolini 2010; Morgan et al. 1995). Apart from FHL5, which is exclusively expressed in

spermatids of adult testes, all FHL proteins are expressed in muscles: FHL1 and FHL3 are most abundant in skeletal muscles (Morgan et Madgwick 1999), and FHL2 is highly expressed in cardiac muscle (Kong et al. 2001).

In addition to the full-length FHL1, also named FHL1A, alternate splice isoforms were identified (Figure 31). These isoforms do not display the classical FHL1 structure. Indeed, isoform B of FHL1 (called also SLIMMER) lacks the last LIM domain (LIM4) and in place, encodes three functional nuclear import sequences, a putative nuclear export sequence, and a region that binds RBP-Jκ. FHL1C is the shorter variant (22kDa) and contains the first two and a half LIMs and a putative RBP-Jk binding region in its C-terminus (Shathasivam, Kislinger, et Gramolini 2010; Wei et Zhang 2020). Both isoforms B and C are also expressed in muscle cells, but their subcellular localization could differ from isoform A (Shathasivam, Kislinger, et Gramolini 2010; Wei et Zhang 2020). FHL1A is predominantly cytoplasmic, linked to focal adhesions and actin cytoskeleton in myoblasts and myotubes. It can also shuttle to the nucleus promoting myoblast adhesion, spreading, and migration (P. A. Robinson et al. 2003). FHL1B is found in the nucleus of undifferentiated myoblasts and later in the cytoplasm of differentiated myotubes (S. Brown et al. 1999). FHL1 plays a crucial role in cell signaling, connecting the actin cytoskeleton and transcriptional machinery. It is recruited to focal adhesions by Kindlin-2 and translocates to the nucleus upon phosphorylation by cytosolic tyrosine kinase Src (X. Wang et al. 2018).

Figure 31: Structure of FHL1 isoforms. *FHL1A contains four complete and an N-terminal half LIM domain. FHL1B contains the N-terminal three and a half LIM domains identical to FHL1A. In place of LIM4 domain, there are three nuclear localization signals (NLS), a nuclear export sequence (NES), and a binding site for RBP-Jκ. FHL1C comprises the N-terminal two and a half LIM domains of isoforms A and B, followed by a C-terminal RBP-Jκ-binding domain.*

FHL1 expression is linked to muscle tissue hypertrophy and early muscle differentiation, as overexpression in mice promotes myoblast differentiation and hypertrophic myotube formation (McGrath et al. 2003; Cowling et al. 2008). Fhl1 gene knockout in zebrafish disrupts skeletal muscle structure and function (Keßler et al. 2018). In mice, FHL1 depletion contributes to age-related muscle pathologies (Domenighetti et al. 2014). Silencing FHL1 in chicken myoblasts hinders myogenic differentiation and myotube development (Han et al. 2020). FHL1 also regulates

autophagy by interacting with LC3, affecting apoptosis levels; these findings align with the roles of other LIM-domain proteins like MLP and FHL2 in the autophagy pathway (Rachid et al. 2015; Liu et al. 2019). Finally, FHL1A promotes muscle hypertrophy by interacting with the calcineurin/NFATc1 pathway and enhancing transcription of hypertrophic genes (Cowling et al. 2008). Additionally, it plays a role in sarcomere assembly, competing with myosin for binding to MyBP-C and impacting sarcomere functionality (McGrath et al. 2006). FHL1A's direct influence on myogenesis was evident in fhl1-knockout mouse myoblasts, which failed to form myotubes, while reintroducing the fhl1 gene rescued myotube formation (Domenighetti et al. 2014)

Recent research has heavily focused on FHL1-related myopathies, attributed to abnormalities in the FHL1 gene. These myopathies include X-linked myopathy (Quinzii et al. 2008), muscular dystrophy, myofibrillar myopathy (Y.-E. Park, Kim, et Shin 2019), inflammatory myopathy (Albrecht et al. 2015), and reducing body myopathy (Z. Hu et al. 2019). Mutations in FHL1, particularly in distal exons (5-8), are linked to Emery-Dreifuss muscular dystrophy (EDMD), a rare disorder characterized by joint contractures, muscle weakness, and cardiac issues (Gueneau et al. 2009; Borch et al. 2022). Mutations often result in significant loss of protein expression. In reducing body myopathies (RBM), FHL1 mutations affect Zn (II)-ion binding, leading to cytotoxic protein aggregates within myotubes and impaired differentiation (Wilding et al. 2014). These aggregates sequester NFATc1, disrupting its role in regulating hypertrophic gene transcription (Wilding et al. 2014).

3. FHL1 is a major host factor for CHIKV infection in vitro and in vivo

Except one study which identified by mass spectrometry FHL1 as a potential nsP3-binding (Meshram et al. 2018), FHL1 has never been described as proviral factor so far. In our work (Meertens et al. 2019), we demonstrated that FHL1 is a major host factor involved into cell susceptibility to CHIKV infection. Indeed, naturally CHIKV-susceptible human cell lines (HAP1, HEK-293T) invalidated for *fhl1* expression, become less susceptible to viral infection. Conversely, ectopic expression of FHL1 in cells that are naturally resistant to viral infection (BeWo, HepG2), restore the susceptibility to CHIKV. Interestingly, FHL1 is selectively used by CHIKV and its closest relative, ONNV. Other alphaviruses are not dependent on FHL1 expression. The importance of FHL1 during CHIKV infection was further strengthened by the results demonstrating that CHIKV was unable to efficiently replicate in primary cells isolated from patients suffering from the Emery-Dreifuss muscular dystrophy,

harboring a mutation responsible for FHL1 -protein degradation (Meertens et al. 2019). In these cells, ectopic expression of FHL1 confers permissiveness to CHIKV, highlighting the major role of FHL1 in CHIKV tropism (Meertens et al. 2019).

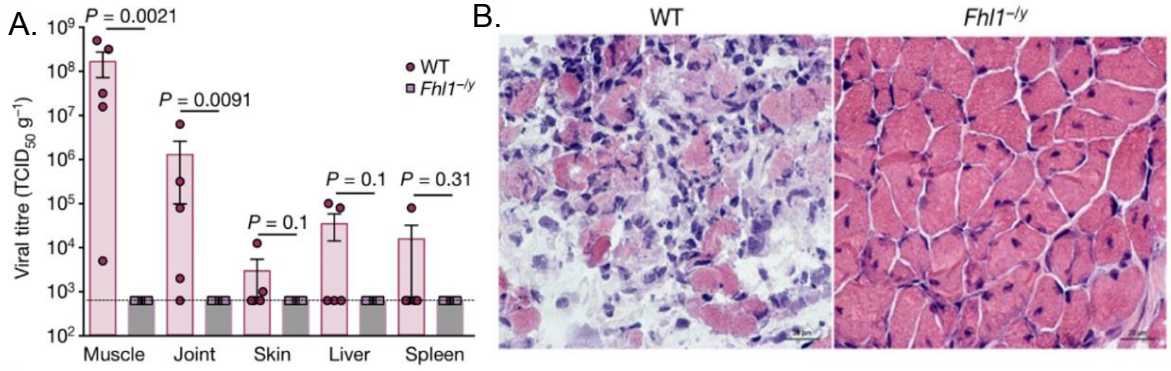

Figure 32: FHL1 is an important determinant for CHIKV tropism and pathogenesis in the mice model: *(A, B) Wild-type (WT) and Fhl1 KO (FHL1-null) newborn mice were injected with CHIKV by intradermal route and sacrificed 7-day post-inoculation. (A) Quantification of viral titers in tissues of WT and Fhl1 KO mice. (B) Hematoxylin and eosin staining of transversal section of skeletal muscle in CHIKV-infected mice.*

Further in vivo analysis demonstrated that FHL1 is a relevant host determinant for CHIKV infection and pathogenesis (Figure 32). 9-day-old newborn control and $fhl1^{ko}$ were inoculated with CHIKV and viral loads were monitored at 7 days post inoculation in different tissue types. Whereas joints and muscles were highly infected in WT littermates, viral titers were below the detection threshold for FHL1-null mice. Furthermore, histology and immunohistochemistry analysis demonstrated necrosis of muscle fibers of the skeletal muscle of WT mice, whereas FHL1-deficient mice muscle exerted no detectable pathology. These results validated that FHL1 is a key player in CHIKV tropism and pathogenesis (Meertens et al. 2019). A work published recently by W.H. Ng and colleagues also validated our findings in $FHL1^{-/-}$ mouse model and further demonstrated that CHIKV unable to mediate interactions with FHL1 was avirulent in vivo. Finally, this work also showed that inoculated mice were protected from disease upon challenge with CHIKV and ONNV, and that the

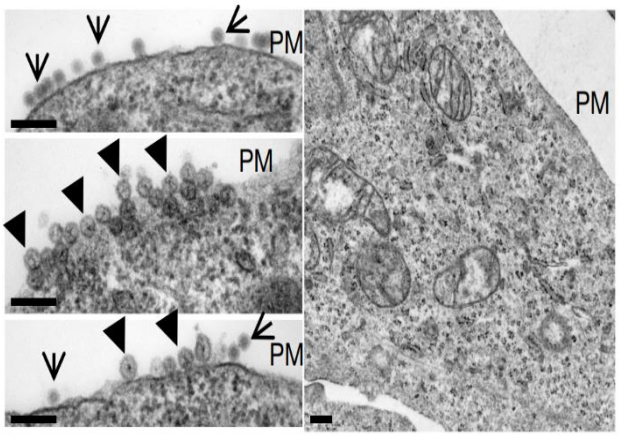

Figure 33: FHL1 protein is required for replicative spherule formation. *Transmission electron microscopy of control and ΔFHL1 HAP1 cells challenged with CHIKV21 at 24 h after infection.*

protective effect was also observed in RRV- and MAYV- challenged mice. Altogether these data confirm the importance of FHL1 in CHIKV replication, tropism and disease, and highlighted its potential as a therapeutic strategy (Ng et al. 2023).

From functional perspective, we demonstrated that FHL1 is involved in the early steps of viral infection by regulating negative-strand RNA synthesis. Electron microscopy investigations demonstrated that in the absence of FHL1, CHIKV replicative spherules couldn't be formed at the plasma membrane (Figure 33). Biochemical analysis also demonstrated that FHL1 directly interacts with the nsP3 protein through the nsP3-HVD domain (Figure 34A-B). Interestingly, FHL1 was also found within nsP3-cytoplasmic granules, G3BPs, and other interacting partners (Figure 34A-B). The comparison of CHIKV and ONNV HVD sequences with those of other alphaviruses led to the identification of a region of 32 amino acids (residue 424 to 456) involved in nsP3-FHL1 binding (Figure 34A). Deleting this region abolished nsP3/FHL1 interaction, and CHIKV lacking this interacting motif exerted a strong defect in viral replication (Meertens et al. 2019). In addition to FHL1, we demonstrated that FHL2, which is also a four-and-a-half LIM domain protein expressed in skeletal muscles, can restore, to some extent, CHIKV infection in FHL1-knockout cells. These suggest a redundant function between both proteins.

Another group also validated FHL1/nsP3-HVD interaction through the Nuclear Magnetic Resonance (NMR) strategy (Lukash et al. 2020). NMR can identify alterations in the nearby electronic environment caused by binding interactions, providing insights into the specific regions of a protein involved in a binding interface. The HVD-interacting region established in this study contains the previously identified HVD sequence (residue 424 to 456) but also overlaps in the N-terminal part with one of the CD2AP-interacting motifs. Whereas it was demonstrated that HVD/CD2AP interaction is not dependent on FHL1, it is still unknown if there is any additive proviral function of the HVD/CD2AP/FHL1 complex (Lukash et al. 2020).

Interestingly Lukash and colleagues reported that several cell lines which do not express FHL1, such as Huh7.5 or HepG2, are susceptible to CHIKV infection. Furthermore, CHIKV infection in *fhl1*-knockout HEK-293T cells replicates significantly less than in WT cells, but is still viable. The discrepancies observed between this study and ours on the importance of the effect of FHL1 depletion on CHIKV replication, which is more important in our experiments, could be explained in part by the CHIKV-strain used for the infection experiments. Indeed, our work demonstrated that in contrast to

epidemiological CHIKV strain from Reunion Island, the enzootic West African strain didn't show the same level of dependence on FHL1. In the study performed by Lukash and colleagues, the CHIKV strain used was the attenuated CHIKV 181/clone 25, a live-attenuated derivative of Southeast Asian human isolate strain AF15561 (Gorchakov et al. 2012). In addition, the tested cell lines expressed FHL2, although at low levels, which can restore to some extent viral infection.

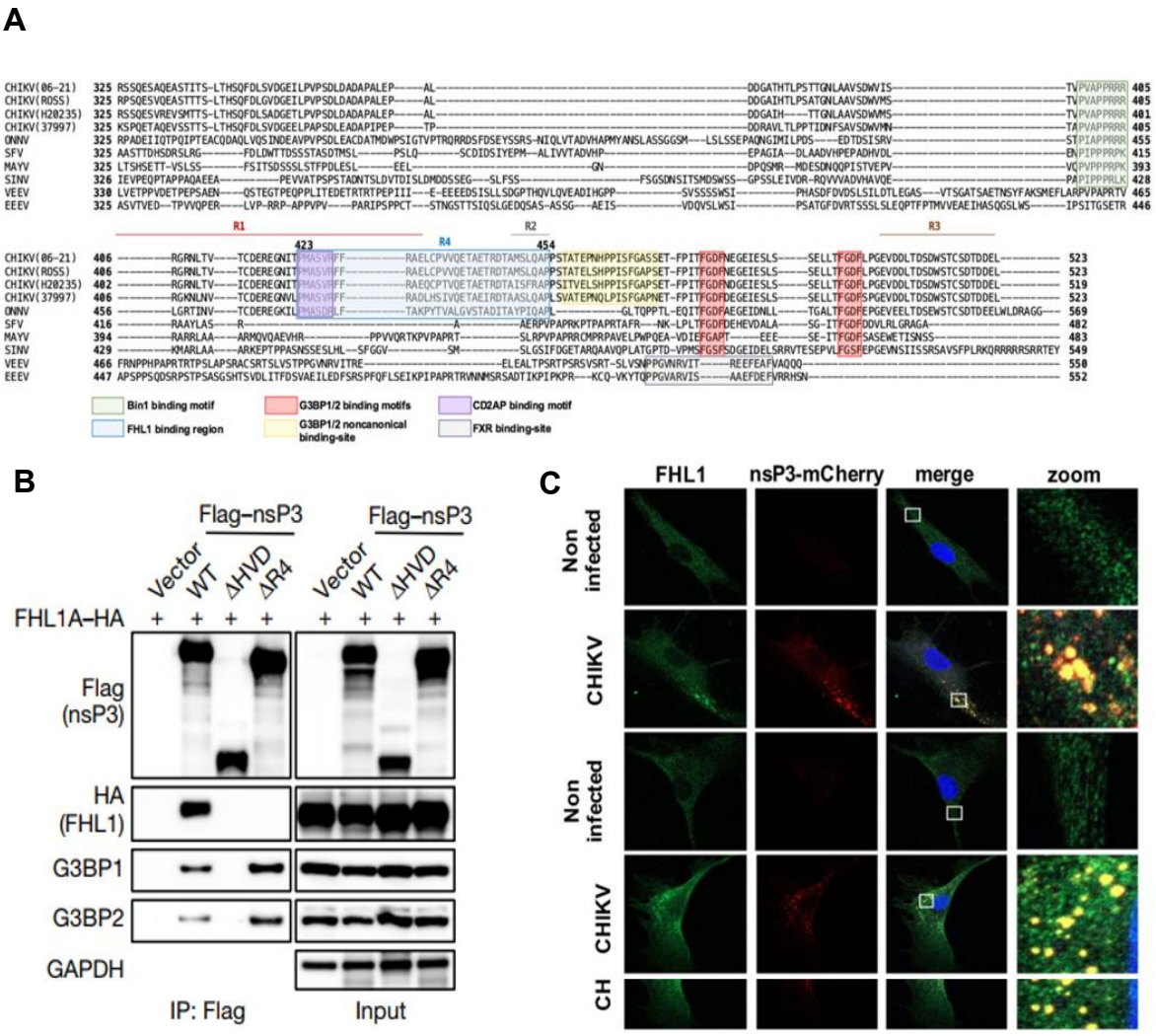

Figure 34: FHL1 protein directly interacts with CHIKV nsP3-HVD domain and is recruited within nsP3 cytoplasmic condensates. *A, Alignment of HVD from different CHIKV strains and different alphaviruses. HVD-motifs involved into BIN1, CD2AP, G3BP and FHL1 binding are depicted in colored boxes. B, HEK293T cells were co-transfected with plasmids encoding haemagglutinin (HA)-tagged FHL1A (FHL1A–HA) and Flag-tagged wild-type CHIKV nsP3, CHIKV nsP3(ΔHVD) or CHIKV lacking the amino acid region 423–454 (ΔR4). Proteins from cell lysates were immunoprecipitated with anti-Flag beads followed by immunoblot analysis with Flag, HA and G3BP1 and G3BP2 antibodies. C, Confocal microscopy of the colocalization of CHIKV nsP3 with FHL1 in fibroblasts inoculated with CHIKV nsP3–mCherry (MOI of 2), fixed 48 h after infection and stained with anti-FHL1 antibody. Adapted from Meertens et al. 2019.*

Thesis Objectives

Chikungunya virus is a re-emerging arthropod-borne virus that caused several outbreaks in the last decades. It belongs to arthritogenic alphaviruses, a group of positive single-stranded RNA viruses causing musculoskeletal disease that can persist for months. Although substantial advances in understanding CHIKV biology and physiopathology, no efficient antiviral treatments are available. A hallmark of alphaviruses is the formation of viral replication complexes (vRC) at the plasma membrane of infected cells, which shelter viral RNA synthesis. One of the viral proteins required for vRC formation and RNA replication is the non-structural protein 3 (nsP3). Multiple studies reported the critical role of nsP3 in viral replication and host cell response regulation. nsP3 mediates multiple interactions with host proteins such as FHL1 and G3BP through its hypervariable domain, allowing alphavirus adaptability to different hosts. In the late stages of the infectious cycle, it organizes cytoplasmic condensates. It also counteracts the cellular antiviral response by disassembling stress granules via its macrodomain (MD). Despite recent advances, nsP3 remains the most enigmatic viral protein, and its precise role in vRC formation, RNA synthesis, and host response regulation remains unclear.

The first part of my thesis aims to characterize the structure and function of alphavirus nsP3 using CHIKV-nsP3 as a model. In collaboration with Dr. Juan Reguera's *team Architecture and Function of Biological Macromolecules laboratory (AFMB, UMR7257),* we sought to determine the structural organization of the *in vitro* purified CHIKV nsP3 by single-particle cryo-electron microscopy approach. The results revealed the helical arrangement of the nsP3 through its alphavirus-unique domain. In the second part of this study, we sought to determine the relevance of nsP3 oligomers during CHIKV infection. Imaging approaches by confocal and electron microscopy were applied to decipher CHIKV nsP3 organization and composition in situ. Finally, by generating a panel of nsP3 mutants unable to oligomerize, we aimed to assess the impact of nsP3-oligomerization on the establishment of efficient viral replication and productive viral spreading.

The second part of my thesis assessed the importance of CHIKV nsP3 and FHL1 interaction, a major CHIKV host dependency factor previously identified by our group. Collaborative work with Pr. Félix Rey group Structural Virology (Pasteur Institute) applied a nuclear magnetic resonance (NMR) approach to identify the nsP3

domain mediating FHL1-binding. Next, we generated CHIKV mutant viruses unable to mediate FHL1-binding and assessed their replicating ability. By developing human cell lines knocked out for nsP3-major interacting factors, we validated the importance of FHL1 for different CHIKV strains. Multiple functional studies using CHIKV replicon systems, imaging approaches, and biochemical approaches aimed to understand better how FHL1 enables CHIKV replication and productive spreading.

Results

A. The alphavirus nsP3 protein forms helical scaffolds driving viral replication and particle assembly (submitted, under revision)

Chikungunya virus (CHIKV) is a re-emerging Old-World alphavirus, causing debilitating musculoskeletal disorder, which persist from weeks to months. Despite many efforts to understand CHIKV life cycle and develop new antiviral treatments or vaccines, we still lack comprehension of the fundamental aspects of CHIKV replication and persistence. Four viral proteins called non-structural proteins (nsPs) orchestrate viral replication. Among them, the nsP3 is the most enigmatic alphavirus protein, that is absolutely required for virus infection. nsP3 is localized in replication complexes (vRC) formed at the plasma membrane of infected cells, where it participates to RNA synthesis. Furthermore, nsP3 also accumulates in cytoplasmic granules of unknown function.

In this study we aimed to characterize nsP3 structure and function during CHIKV replication. A collaboration with Dr Juan Reguera (Viral Macromolecular Complexes team, AFMB, Marseille, France) and Dr Michael Hons (EMBL) permitted to characterized the cryo-electron microscopy structure of purified CHIKV-nsP3. The obtained structure revealed that nsP3-Alphavirus Unique Domain (AUD) is a unique oligomerization module that triggers the formation of nsP3 helical scaffolds *in vitro*. These nsP3-helices organize into a structure similar to the putative cytoplasmic crown observed above the nsP1-capping pores at the vRC neck. With the help of Dr. Beate Kümmerer, Dr Céline Amadori and Laurine Couture, I validated the functional importance of these structures, demonstrating that nsP3 cytoplasmic granules are a hallmark of alphaviruses and are highly-ordered tubular networks recruiting nsP3-interacting factors (FHL1, G3BP), viral capsid proteins and genomic RNA. Mutations in the AUD that disturb nsP3-oligomerization, significantly impacts RNA synthesis, capsid protein sub-cellular localization and infectious particles production.

Altogether, these results suggest that AUD-oligomerization is a critical step to ensure nsP3 activities, which includes viral RNA synthesis and vRC formation. In addition, nsP3-cytoplasmic tubes, formed in the late stage of the viral cycle and containing viral RNA, capsid protein and proviral host-factors, might be a microenvironment for the formation of new infectious particles.

ABSTRACT

Alphaviruses, including chikungunya virus (CHIKV), are a group of positive-stranded RNA viruses that represent an ongoing challenge to medicine and public health. Alphaviruses replicate their genome within spherules that house the viral replication complexes (RCs) at the plasma membrane. RCs are made of four nonstructural proteins (nsP1 to 4) translated as a polyprotein P1234 which is self-cleaved by a viral protease nsP2 [1]. Proteolytic processing acts as a molecular clock triggering the transition from the synthesis of dsRNA intermediate to the synthesis of new progeny of viral genomic and sub genomic RNAs. However, how polyprotein processing regulates other viral functions is poorly understood. Additionally, the mechanisms of newly synthetized RNA trafficking from the viral spherules to the cytoplasm for packaging into virions remain unknown. Here, we show that the nsP3, an enigmatic alphavirus-encoded protein[2,3], has a critical role in the coordination of viral replication and particle assembly. Cryo-electron studies showed that, upon the cleavage at nsP2-nsP3 junction, nsP3 assembles into tubular structures made by the helical arrangement of its alphavirus unique domain which acts as an oligomerization module. NsP3 helical scaffolds are essential for the formation of mature RCs by establishing a crown structure above de nsP1-dodecameric ring at the neck of the viral spherules. As the infection progresses, nsP3 proteins organize into cytoplasmic tubular structures containing viral genomic RNA, capsid and host factors required for productive infection. CHIKV harboring mutations in the AUD which prevent or disturb nsP3 helices have a strong defect in viral replication, assembly and release, respectively. Altogether, our results reveal an unexpected nsP3-dependent molecular organization required for alphavirus replication and subsequent assembly, raising the possibility of targeting this process for therapeutic intervention.

MAIN TEXT

Many alphaviruses, including CHIKV, are emerging and re-emerging mosquito-borne viruses that represent a significant threat to human health due to the current context of global warming[4]. Alphaviruses cause neurological and arthritogenic diseases in humans than can persist months to years after the initial infection. No efficient vaccine or therapeutic means against alphaviruses are available, highlighting the urgent need to provide fundamental knowledge about their biology. Alphavirus genome is a single-stranded positive RNA organized in two open reading frames (ORFs) [5,6]. The 5' ORF encodes the P1234 polyprotein that is processed to generate four non-structural proteins (nsP1- to 4) involved in viral replication and immune evasion [5,6]. The 3' ORF is transcribed into a sub-genomic positive-stranded RNA and encodes the structural proteins important for virus assembly and budding [5,6]. The mechanisms of alphavirus replication and virion assembly are poorly understood. Alphavirus infection induces invaginations of the plasma membrane called spherules that house the viral replication complex (vRC) which consist in the double stranded viral RNA (dsRNA), the viral non-structural proteins nsP1 to 4 and cellular factors. [5,6]. These virus-induced organelles create an optimal micro-environment for the synthesis of new capped and polyadenylated genomic RNAs and subgenomic RNAs and protect the dsRNA replication intermediates from host immune responses. Structural studies showed that the nsP1, which mediates viral RNA capping, gates the replication organelles by forming a dodecameric pores that associate with the spherule neck[7]. Reconstitution of the alphavirus RC showed that nsP1 associated with one nsP4 (RNA dependent RNA polymerase) at the center of the pore [8]. Recent tomographic reconstructions of spherule necks in infected cells confirmed this architecture and also identified a tubular structure at the cytoplasmic side where the nascent RNA would be directed [8,9]. The

82 newly synthetized viral RNA is exported from the spherules to the assembly sites to
83 form the nucleocapsid in the cytosol. Tomographic studies of particle budding showed
84 how preformed viral capsids containing gRNA reach the cell membrane, resulting on
85 the budding of the virions[10]. However, the molecular mechanisms by which the nascent
86 viral gRNA at the RCs traffics to the sites of assembly and is subsequently
87 encapsulated into virions, as well as the role of viral components in this temporal and
88 spatial process remain elusive.
89 The nsP3 is probably the most fascinating alphavirus-encoded protein. NsP3 is
90 composed of three domains, a macrodomain (MD) which recognizes and hydrolyses
91 ADP ribosylated proteins, a conserved Alphavirus Unique Domain (AUD) required for
92 RNA synthesis [11], and a hypervariable domain (HVD) mediating extensive host
93 interactions important for viral replication and adaptation to the host [2,5].The structure
94 and function of nsP3 has remained elusive over the years. nsP3 is generated after the
95 processing of the P1234 precursor by the viral protease nsP2. The only structural
96 information available of nsP3 derives from an uncleaved form of Sindbis virus nsP2-3
97 construct showing a mysterious conformation with the AUD interacting with the
98 protease domain of nsP2 conferring a U shape to the polyprotein[12]. During the early
99 phase of infection, nsP3 localizes at the cytoplasmic side of the viral spherules and is
100 important for RNA synthesis [6], however its precise organization within the vRC is not
101 understood. As the infection progresses, nsP3 assembles into enigmatic cytoplasmic
102 granules (referred here as “alpha-granules”) that are an hallmark of alphavirus
103 infection. Alpha-granules are distinct from vRC and are believed to sequester the Ras
104 GTPase-activating protein-binding proteins (G3BPs) to inhibit the formation of
105 cytoplasmic stress granules [13] and consequently host cell translation. However, how

these enigmatic structures are organized and how they regulate alphavirus life cycle remain elusive.

Here, we provide major insights into the mechanism of alphavirus replication and assembly. We describe the cryo-EM structure of CHIKV nsP3 at 2,35 Å resolution. We show that, upon proteolytic cleavage of the P1234 polyprotein, nsP3 polymerize via its AUD to generate unprecedented helical scaffolds (HSs). These scaffolds form the cytoplasmic crown above nsP1-capping pore at the neck of vRC, thus enabling vRC formation and RNA synthesis. As the infection progreses, nsP3 HSs assemble into tubular structures also define the internal architecture of alpha-granules, which act as platform for infectious particles production.

Atomic structure of alphavirus nsP3 helical scaffolds. We expressed the CHIKV nsP3 in Hi-5 insect cells (see methods). Purification of nsP3 by consecutive affinity and size exclusion chromatography at 0.5 M NaCl yielded both monomeric and high molecular-weight nsP3 species. Unexpectedly, analysis by negative staining electron microscopy revealed that the latter correspond to tubular macro-complexes harboring a well-defined internal cavity delimited by a weakly structured matrix and surrounded by a jelly-like shield (Extended Data Fig.1 a, b). The nsP3 monomers can re-assemble *in vitro* by lowering low salt concentration (Extended data Fig1 c). We also determined the structure of the nsP3 tubes by cryo-electron microscopy (cryo-EM) at 2.52 Å resolution (EMD: 17729, Extended data Fig.2 and Table S1). Local refinement allowed to reach 2.36 Å on which we refined the AUD structure from an Alphafold2 prediction (EMD: 17678; PDB: 8PHZ, Extended data Fig.2, Table S1 and supplementary information) and reconstitute the helical assembly (PDB: 8PK7). We found that the tubes are made by a helical arrangement of the nsP3 AUD with an axial rise of 2.782

131 Å and a helical twist of -164.175 ° (Extended Data Fig.2, methods and supplementary
132 information). Lateral views clearly reveal the existence of two-start parallel helixes (hA
133 and hB) with a right-handed arrangement of the AUD (Fig. 1). Each helix has 11.37
134 protomers per turn (Fig. 1 a,b). The assembly generates interstitial positively charged
135 pores connecting the negatively charged inner cavity with the exterior (Extended data
136 Fig.3). This charge distribution would allow the flow of nucleic acids inside and their
137 exit through the interstitial pores following the negative to positive charge gradient.
138 Although barely visible in the structure due to their high flexibility, the N-terminal MD
139 and the C-terminal HVD, are clearly projected to the outside of the tubular structure
140 (Fig.1a). Refinement using a larger mask yielded a lower resolution map of the helical
141 particles (2.98 Å resolution, EMD: 17730) with discernable globular appendices that
142 can be assigned to the MD by main-chain connectivity (Fig. 1b). The MD of each nsP3
143 protomer is lying on the next AUD (A n+1) of the same helix. A 3D focused classification
144 provided one 3D class clearly showing the beginning of the HVD interacting with the
145 MD of the n-1 protomer (Fig. 1c, Extended Data Fig.2, EMD: 17730). Because of the
146 low resolution of the map (6.84 Å) we could not deduce the exact position of contacts
147 between the MD and HVDs, which are connected to the AUD through long flexible
148 linkers. Beside these limitations, the structure clearly shows that MD-MD and HVD-MD
149 interactions build a flexible and structured shield on the exterior of the tube which
150 contributes to the interprotomer interactions.
151 **The nsP3 AUD is an oligomerization module activated by the nsP2-3 polyprotein**
152 **cleavage.** The AUD core is a hallmark of alphavirus nsP3 proteins and on the light of
153 the helical structure its folding acquires a new sense (see Fig. 1d and sequence
154 alignment in Extended Data Fig.4). It consists of four alpha helixes (α1-α4) with
155 extensions at the N and C terminus acting as oligomerization modules (C and N O-

156 modules) which are responsible for lateral and axial contacts with the AUD of
157 neighboring protomers, respectively. The lateral and axial interfaces bury 320 Å^2 and
158 530 Å^2 of surface area, respectively (Fig. 1e). The O-modules are rich in positively
159 charged residues and hold the core of neighboring complexes both contacting with two
160 regions including residues Y200 to K222 and R243 to P257 (Fig. 1f). The R243 to P257
161 region contains a loop flanked by C246 and P257 residues (O-loop) rich in acidic
162 residues which adopts a slightly different conformation as compared to the predicted
163 Alphafold2 [14] structure, consistent with previous structures reported on Sindbis virus
164 (SINV)[12] (Fig. 1g). The O-loop mediates extensive interactions with both N- and C O-
165 modules from hA n-1 and hB n-protomers, respectively. Even if no stable salt bridges
166 are observed in the structure, the charge distribution is suggestive of an interaction of
167 electrostatic nature (Extended data Fig. 3) which is in line with findings that high salt
168 concentrations promote filament disassembly *in vitro* (Extended data Fig.1 c). In
169 addition, a network of hydrogen bonds woven by residues A251, S254, V211, Y200
170 with residues H207, Y266, K304, Q301 and K302 of hB n-protomer seals the axial
171 contacts. Likewise, residues M219, K222, D249 and C246 coordinate h-bonds with
172 R187, A185, G203 and R205, stabilizing the lateral interface (Fig. 1f).
173 The cleavage of the P1234 precursor at the boundary between nsP2 and nsP3 is
174 important for viral infection and pathogenesis [6,12]**. I**nterestingly, the superposition of
175 AUD domains of HSs and uncleaved nsP2-nsP3 protein reveals that in the uncleaved
176 polyprotein the O-loop is completely buried by the nsP2 protease domain preventing
177 HSs formation (Fig. 1g). Therefore, nsP2 protease- mediated cleavage of the nsP2-3
178 junction might release the O-loop and trigger the nsP3 AUD scaffold formation (Fig.
179 1g, see section nsP3 helical scaffolds form tubular structures that define the
180 architecture of alpha-granules).

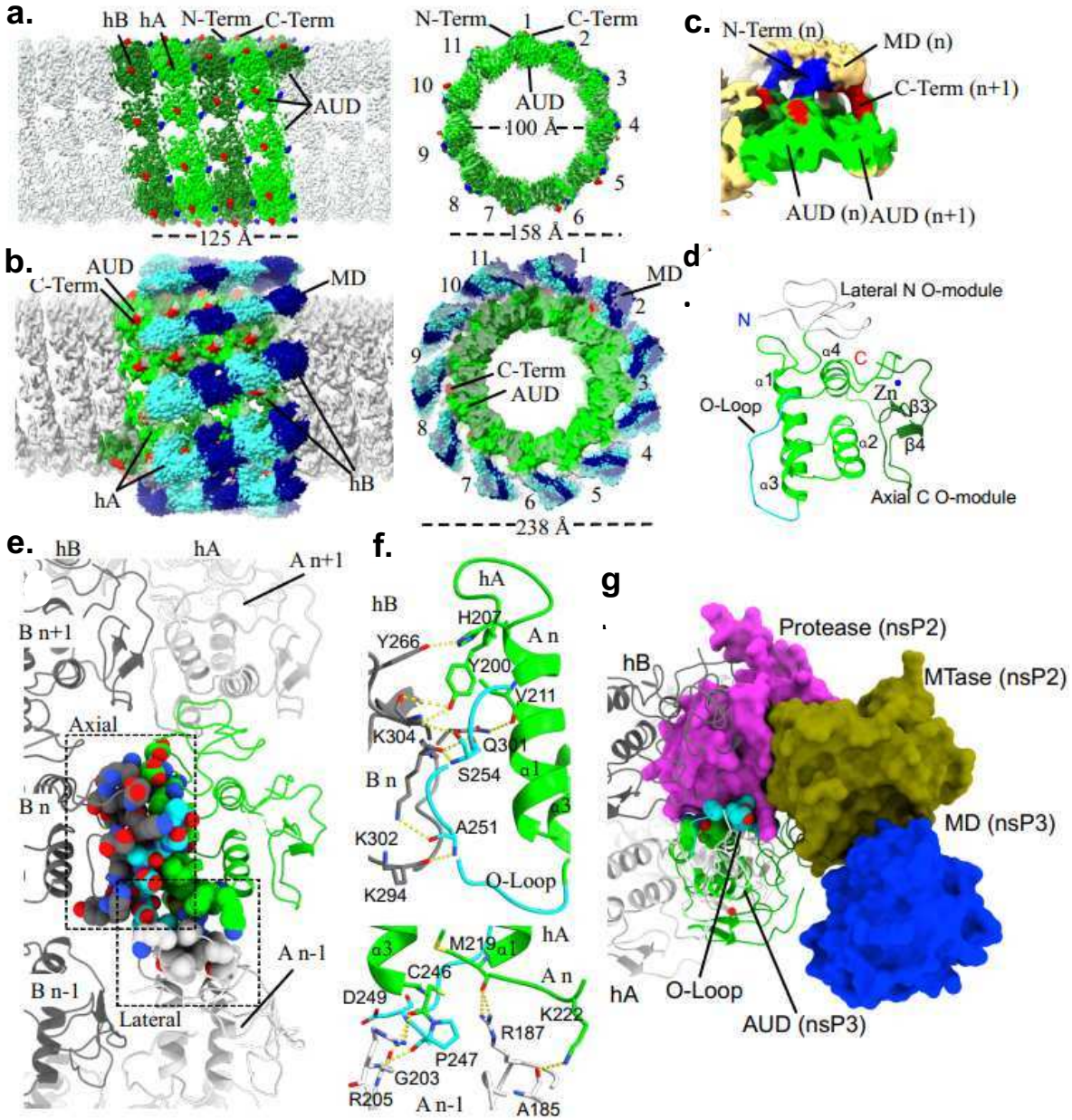

Figure 1. Structure of CHIKV nsP3 helical scaffolds (HSs). a, Cryo-EM map of nsP3 HSs at 2.5 Å resolution (EMD: 17729) is represented in light grey. The left panel shows a longitudinal view of the scaffold with two turns of the two-start helix of AUD domains (hA and hB) colored in light and dark green, respectively. The N and C terminus of each protomer are colored in blue and red, respectively. The right panel shows a transversal section of the same structure, 11 protomers per turn are visible, the dimensions of the internal and external diameter of the AUD scaffold are indicated. **b**, same representation of the cryo-EM map calculated with a larger mask at 2.98 Å resolution (EMBD: 17730) colored in dark grey. Additional densities corresponding to the MD are visible and colored in cyan and blue for the hA and hB, respectively. The right panel shows the transversal section of the structure as in a. The outer diameter of the scaffold including the MDs is indicated. **c**, Cryo-EM map after local 3D classification at 6.4 Å resolution (EMBD: 17730) is shown in yellow. The AUDs are colored in light green and labeled. The N and C terminus of the AUD are colored in blue and red respectively. This map shows the connection of the AUD N terminus with the density corresponding to the MD, and also the interaction of the beginning of the HVD at the C terminus of the nearby AUD n+1 contacting the protomer n MD. **d**, Cartoon representation of the AUD domain with the oligomerization modules (O-modules) which mediate lateral and axial contacts colored in light grey and dark green, respectively, and labeled. The oligomerization loop, which mediates contacts in both axial and lateral interface, is colored in cyan and labeled. **e**, The interprotomer interactions are shown in the context of the helical scaffold. The two helices of AUD, hA and hB, are represented in light and dark cartoons and labeled. The AUD An is colored in green and the residues mediating interprotomer contacts are shown in spheres and colored as in panel d. The residues mediating contacts from Bn and A n-1 protomers are also shown in spheres. The axial (Bn/An) and lateral (An/An-1) interfaces are indicated by dashed line squares. **f**. Detailed representation of axial and lateral contacts between AUDs are shown in the upper and bottom panels, respectively. AUDs are labeled, represented in cartoon and colored as in panel e. The residues mediating interprotomer contacts are shown in sticks and labeled. Hydrogen bonds are shown by yellow dashed lines. **g**, Superposition of the Alphafold2 predicted structure of the uncleaved nsP2-3 on the nsP3 HSs. One turn of the helical scaffold is shown in dark and light grey cartoon (for hA and hB respectively). The model is superposed in the hA AUD of the helix. It is shown with nsP2 protease surface colored in magenta, the MTase domain in olive green, the nsP3 MD domain in blue and the AUD in green cartoons. The protease domain completely blocks the axial contacts of the helical scaffold in the nsP2-3 uncleaved structure.

NsP3 helical scaffolds are part of the viral replication complex. NsP3 is a component of the vRC [6]. Tomographic reconstruction of CHIKV spherule necks revealed the vRC architecture with a molecular pore delineated by a nsP1 dodecamer ring connected to a larger tubular structure (crown) in its cytoplasmic side [8,9]. Superposition of nsP3 HSs into the crowns shows similar dimensions and shape [8,9] (Fig. 2). The tomographic reconstruction of the vRC reported by Laurent et al.[9] shows perimetral volumes which correlate well in the superposition with the nsP3 MDs (Fig. 2a). This perimetral volumes are lost in Tan et al [8] (Fig. 2b). For both tomographic reconstructions a 12-fold symmetry (C12) was imposed to the calculated volumes which is consistent with nsP1 capping pores. However, this conflicts with the helical symmetry that we find now for nsP3 scaffolds (with 11.37 nsP3 protomers per turn). Interestingly, mismatched symmetries of ring-like complexes as the observed in icosahedral viruses vortex and bacterial flagellar rotors are associated to dynamic processes essential for virus assembly and DNA packing or bacterial motion, respectively[15,16]. One can speculate that symmetry mismatches between the nsP1 capping pores and nsP3 scaffolds might underlie motions between both modules occurring during transcription and replication.

Helical arrangements of nsP3 AUD form tubular structures that define the architecture of alpha-granules. In infected cells, CHIKV nsP3 accumulates in large cytoplasmic alpha-granules that do not co-localize with the dsRNA and are distinct from vRCs [2,3,17,18] (Extended data Fig 5a,b). During the early phases of infection, the alpha-granules appear globular and spherical (Extended data Fig 5a-d) while assembling into irregular internal structures up to 0.8 μm long at later stages.

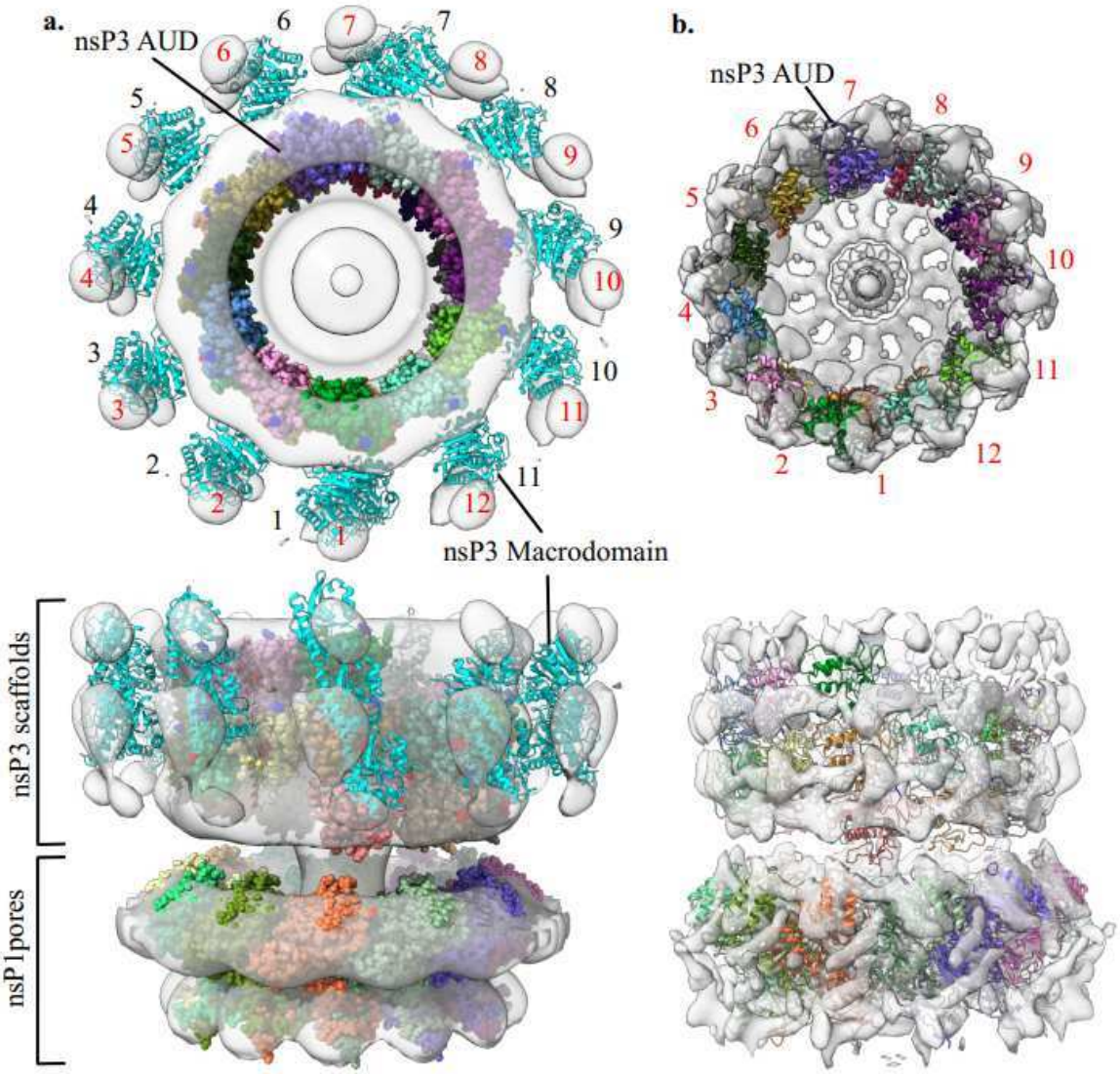

Figure 2. Superposition of nsP3 HSs on tomographic reconstructions of membrane-associated CHIKV RCs. **A**, Superposition of nsP1 capping pores and the nsP3 scaffolds on the tomographic reconstruction of CHIKV RCs. Top and lateral views are shown in the top and bottom panels respectively. The volume is shown as a transparent grey surface. nsP1 and nsP3 AUDs are colored by protomer and shown in spheres, the MDs of nsP3 are shown in cartoon and colored in cyan. Their position with respect to the AUDs was determined based on their fitting on the map shown in Fig. 1.b (EMD: 17730). The tomographic volume was calculated applying a 12-fold symmetry and consequently has 12 outer volumes on the region which are shown numbered [9]. The superposition shows the consistent matching in size and shape of AUD helices with the rings above the nsP1 capping pores and the outer spherical volumes have a partial matching with the MDs positions found in HSs. However, the structure of the nsP3 helical scaffold have 11,37 protomers per turn instead of 12, slightly breaking the symmetry with the nsP1 pores and the volume reconstructions. Superposition allows to confidently assign the central ring above nsP1 to the AUDs and the peripheral volumes to the MDs. **b**. same representation of the superposition of capping pores and nsP3 scaffolds on the volume of RCs reported by Tan et al.[8] . The volume reaches higher resolution and only shows electron density for the AUD region of the nsP3 scaffold. The volume was also calculated imposing C-12 symmetry.

206 (Extended data Fig 5 b-d). Alpha-granule formation is a hallmark of alphavirus biology
207 (Extended data Fig 5e). Of note, alpha-granules length and morphology varies
208 depending on the CHIKV strain or lineage (Extended data Fig 5c-d). An average of 40
209 alpha-granules are formed per cell after 24 h post-infection. Of note, the expression of
210 nsP3 alone, independently of the presence of other viral components, is sufficient to
211 induce alpha-granule formation. (Extended data Fig 5e).
212 Consistent with Fig.1g, alpha-granule formation depends on nsP2-nsP3 processing.
213 Indeed, expression of the P1234 precursor harboring mutations affecting the nsP2-
214 nsP3 cleavage[19,20] prevents assembly of alpha-granules (Extended data Fig 6).
215 Transmission electron microscopy studies performed on either CHIKV-infected
216 primary fibroblasts or cells stably expressing nsP3 revealed that the alpha-granules
217 are made by a honeycomb arrangement of tubular structures consistent in size and
218 shape with nsP3 HSs (Fig 3a, Extended data Fig.7a). Immunogold labeling of nsP3
219 confirmed the identity of these scaffolds (Extended data Fig.7b). NsP3 tubular
220 structures are found in cells either infected by several alphaviruses such as Mayaro
221 virus (MAYV) or O'Nyong Nyong virus (ONNV) or in cells transfected with plasmids
222 encoding Eastern Equine Encephalitis virus (EEEV), MAYV or ONNV nsP3 (Extended
223 data Fig.7c). Confocal and electron microscopy studies show that the nsP3 tubes
224 contain G3BPs [3] and FHL1 [21] , two host factors that bind the nsP3 HVD (Extended
225 data Fig.7d-e). Considering the density of nsP3 scaffolds in the granules (400 helices
226 /μm^2) and the number of nsP3 protomers per µm in the HSs (3870 nsP3/µm), we
227 estimate that 1.55 million nsP3 protomers would be present in 1 μm^3 of alpha-granules.
228 This indicates that nsP3 tubular structures are formidable molecular traps sequestering
229 host factors important for infection.

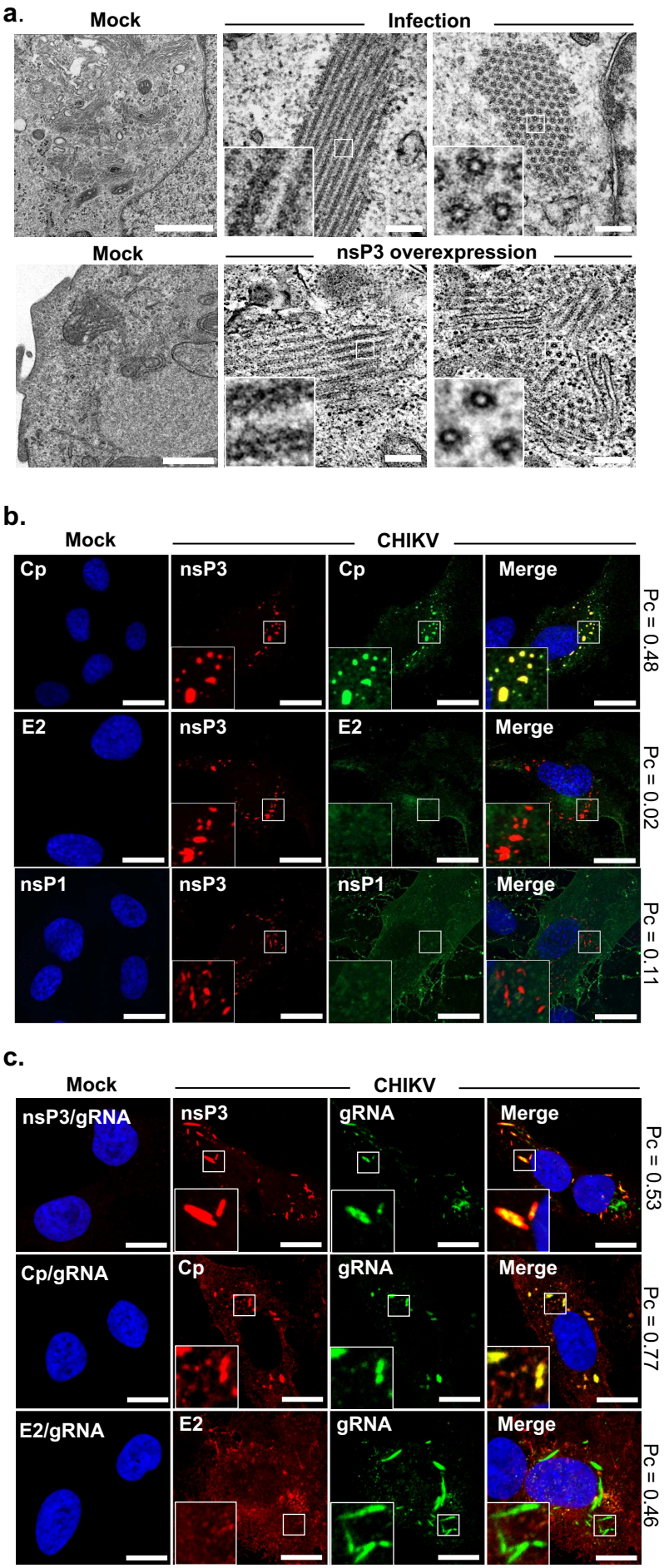

Figure 3. CHIKV nsP3 assembles into tubular structures that define the architecture of alpha-granules. **a,** Transmission electron microscopy of human fibroblasts infected with CHIKV 21 strain (MOI of 10) for 24 h (upper panel) or stably expressing the CHIKV nsP3 (lower panel). Longitudinal (left) and transversal (right) views of the nsP3 tubes are shown. Images are representative of two independent experiments. Scale bars, 500nm (mock panels) and 200 nm (infection and nsP3-overexpression panels). **b,** Human fibroblasts were infected with CHIKV nsP3-mCherry (MOI of 10) for 24h. Cells were immunostained for capsid, E2 or nsP1 viral proteins. Co-localization analysis were performed using JACoP plugin implemented in ImageJ [32]. Scale bars, 20 μm. Images are representative of 3 independent experiments. **c,** Human fibroblasts were infected as described in **a.** Cells were fixed and immunostained for nsP3, capsid or E2 viral proteins (red channel). CHIKV genomic RNA was detected following incubation with CHIKV specific fluorescent RNA probes (green channel). Co-localization analysis were performed as described in b. Scale bars, 20 μm. Images are representative of 2 independent experiments.

Importantly, in infected cells, most of the nsP3 alpha-granules colocalize with both viral capsid (Fig. 3b, Extended data Fig.7f) and the viral genomic RNA (Fig. 3c) but contain neither E2 nor nsP1 proteins (Fig 3b-c), indicating that they are the site of passembly of the viral nucleocapsids. This idea is in line with a study describing the imaging of alphavirus capsid protein during virus replication in living cells [22]. Since the tubular structures of *in vitro*-purified or *in vitro*-assembled nsP3 (Extended data Fig.1) do not show any honeycomb arrangement, one can speculate that host or viral factors besides nsP3 could mediate this organization through interactions with the exposed MD or HVD. This unique nsP3 mediated internal architecture, combining solid ordered scaffolds with intrinsically disordered regions, challenges our current understanding of the architecture of biomolecular condensates[23] .

NsP3 helical structures are important for both CHIKV RNA replication and infectious virion production. The nsP3 AUD has an intrinsic oligomerization capacity and forms filaments when expressed in human cells (Extended data Fig. 8a, b). Consistently, nsP3 molecules lacking the AUD domain do not form alpha-granules and are diffusively distributed in the cell cytoplasm when compared to WT or nsP3 deleted from the MD or HVD (Extended data Fig. 8a). We generated a panel of structure-based mutations aiming to disturb nsP3 oligomerization in the context of the AUD alone (Extended data Fig. 8c) or the full nsP3 Extended data Fig. 8d). We expressed the nsP3 variants by transfection in U2OS cells and investigated their ability to form filaments and alpha- granules (Extended data Fig. 8c-d). All the nsP3 mutants were similarly expressed but presented different phenotypes (Extended data Fig. 8e). Mutants R187A/R205A, A252P, P255A, R187A, S254A/S255A, H207A, Q301A, A250W, D249G/A250G/D251G showed AUD filaments and nsP3 alpha-granule

255 formation like their WT counterpart (Extended data Fig. 8 c-d). Interestingly, the AUD
256 or nsP3 proteins harboring K302A/V303A or P247A/V248A mutations are
257 homogeneously distributed through the cytoplasmic with a strong reduction of alpha-
258 granule formation (Fig. 4a-b, Extended data Fig. 8 c-d). Finally, the Y200A mutant
259 failed to form alpha-granules and presented a homogeneous distribution in the cell
260 cytoplasm (Fig. 4a-b, Extended data Fig.8 c-d). We next purified the recombinant
261 K302A/V303A, P247A/V248A and Y200A nsP3 mutants as monomers and tested their
262 *in vitro* oligomerization capacity by negative staining electron microscopy in
263 comparison with WT nsP3. At the same protein concentration (0.2 mg/ml),
264 K302A/V303A and P247A/V248A nsP3 molecules showed altered oligomerization
265 properties with the formation of long aggregates and a weak formation of scaffolds,
266 respectively. In agreement with the observations in cells, the nsP3 Y200A mutant was
267 unable to form tubes (Fig. 4c, Extended data Fig. 9 a,d). To investigate the role of nsP3
268 HSs during viral infection, we introduced the most disruptive AUD mutations
269 (K302A/V303A, P247A/V248A and Y200A) in a full length CHIKV Renilla Luc (Rluc)
270 molecular clone [21]. We transfected *in vitro* transcribed viral RNA into 293T or U2OS
271 cells (Fig. 4d, Extended data Fig. 9) and monitored viral replication by measuring the
272 Rluc accumulation in cell lysates as a function of time (Fig. 4d). The Y200A mutation,
273 which prevents the formation of nsP3 helices, abolished viral replication, recapitulating
274 the phenotype of the replication-deficient CHIKV containing a GDD to GAA mutation
275 in the viral RNA-dependent-RNA polymerase nsP4 (Fig.4d Extended data Fig. 9b-c).
276 Viruses expressing the K302A/V303A or P247A/V248A mutations showed significant
277 reduction in viral replication in 293T (Fig. 4d)). Importantly, both mutant viruses also
278 formed smaller plaques than their WT counterparts, accompanied by a drastic
279 reduction in viral titer in plaque assays, indicating a strong impairment of infectious

280 virus particle release (Fig. 4 e,f, Extended data Fig. 9d-e). To further analyze the effects
281 of AUD mutations on CHIKV life cycle, we introduced the corresponding them into a
282 CHIKV replicon system that contain two luciferase reporter genes. A renilla luciferase
283 (RLuc) is fused in frame within the C-terminal hypervariable domain of nsP3, and a
284 firefly luciferase (FLuc) replaces the structural protein. RLuc activity allows to evaluate
285 at early time points both transfection efficiency and input RNA translation. Fluc activity
286 reflects the synthesis and translation of sub-genomic RNA, which happens only when
287 replication occurs. Kinetic curves showed that the initial translation of the incoming
288 RNA is not affected for all the AUD mutant tested (Rluc activity between 0- and 4-hours
289 post-transfection) (Fig. 4h). Interestingly, the Y200A has a strong defect in viral
290 replication with a kinetic curve similar to the GAA replication-dead mutant, (Fig. 4h-i).
291 However, P247A/V248A and K302A/V303A were still able to replicate, albeit to a lower
292 level that the WT RNA (Fig. 4h-i). To further characterize the phenotype of the AUD
293 mutants, we analyzed nsP3, nsP2 and the capsid protein expression in transfected
294 cells by western blot. As a control, a complete inhibition of nsP2, nsP3 and Capsid
295 proteins expression was observed for Y200A and the GAA mutants (Fig. 4g). NsP2
296 and nsP3 protein synthesis was detectable in cells transfected with the P247A/V248A
297 and K302A/V303A mutant, but a lower level than the WT (Fig. 4i). However, for both
298 mutants, capsid protein synthesis was barely detectable, suggesting a defect in sub-
299 genomic RNA synthesis.
300 Interestingly, both K302A/V303A and P247A/V248A mutated viruses displayed an
301 altered intracellular distribution of the structural capsid protein and a strong reduction
302 in nsP3/capsid foci formation when compared to the WT virus (Extended data Fig. 9
303 f,g). Overall, these data show that partial perturbations of the nsP3 scaffold assembly
304 affects alpha-granule formation, with drastic consequences on viral RNA synthesis,

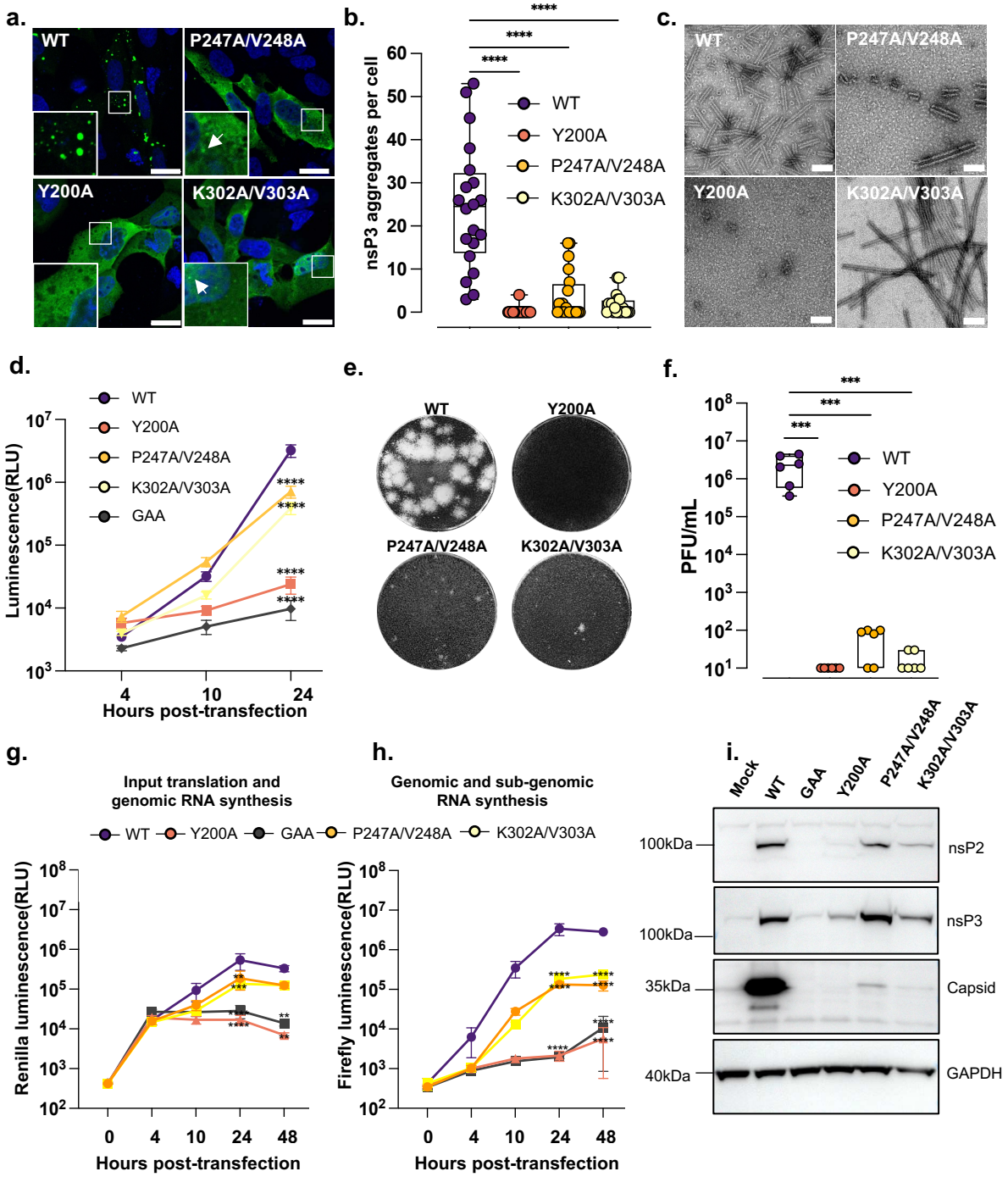

Figure 4. nsP3 helical scaffolds are required for CHIKV replication and infectious particle production. a-b, Characterization of nsP3 AUD mutants. U2OS cells were transfected with plasmids encoding FLAG-tagged wild-type CHIKV nsP3 or mutants harboring substitutions of amino acids involved in AUD-AUD contacts (Y200A, P247A/V248A, and K302A/V303A). **a,** At 48 h after transfection, cells were fixed and nsP3 sub-cellular localization was assessed by immunofluorescence using an anti-FLAG mAb. Images were acquired by confocal microscopy and are representative of 2 independent experiments. White arrows indicate the presence of nsP3 aggregates. Scale bars, 20 μm. **b**. The number of nsP3 aggregates per cell was assessed using ImageJ. Each symbol represents one cell. (n= 20 cells for each condition). One-way ANOVA with Dunnett's multiple comparison test (****P<0.0001). **c,** Negative staining micrographs of nsP3 *in vitro* assembly experiments after incubation at 0.1M NaCl for 1h showing the assembly of HSs WT, absence of HSs formation for Y200A mutant, and in comparison, with the wt, reduced formation of HSs for the P247A/V248A mutant and formation of long collapsed HSs for the K302A/V303A mutant. White scale bars are 100 nm long. **d-g**, HEK293T cells were transfected with the indicated CHIKV *in vitro*-transcribed and capped RNA expressing Renilla luciferase (Rluc). **d,** RLuc activity was monitored at indicated time points. GAA, replication deficient mutant. RLU, relative light units. Data are mean ± s.e.m. n = 3 independent experiments performed in quadruplicate. Two-way ANOVA with a Dunnett's multiple comparison test (****P<0.0001). **e.f,** Viral titer in the supernatant of infected cells (24 h post-infection) were measured by plaque assay. Images representative of WT (supernatant dilution at 1/1000) and mutant virus plaques (at supernatant dilution of 1/2). (**e**) and bar graph showing the corresponding viral titers (**f**) are shown. Data are mean ± s.e.m. n = 3 independent experiments performed in duplicate. One-way ANOVA with a Dunnett's multiple comparison test (***P=0.0003). g. h-i. HEK293T cells were transfected with *in vitro* transcribed and capped CHIKV dual luciferase replicon RNA to assess initial viral translation and replication**,** h. RLuc activity and i. Fluc activity were monitored at indicated time points. GAA, replication deficient mutant. RLU, relative light units. Data are mean ± s.e.m. n = 2 independent experiments performed in quadruplicate. Two-way ANOVA with a Dunnett's multiple comparison test (****P<0.0001; ***P =0.0003; **P= 0.0012.). i. HEK239T cells were transfected with *in vitro* transcribed and capped full-length WT or mutant CHIKV RNA. Cells were harvested 48h post-transfection, lysated and total protein were extracted and separated by SDS-PAGE. CHIKV nsP2, nsP3, capsid and cellular GAPDH proteins expression was assessed by westernblot using specific antibodies.

capsid protein localization and subsequent particle production. Inhibiting scaffold assembly (Y200A mutation) causes a total lack of viral replication. Together, these data suggest that nsP3 oligomerization is required for efficient viral RNA synthesis and viral particle production.

Conclusion. In this study, we show that CHIKV nsP3 auto-assembles into HSs important for viral infection. To our knowledge, nsP3 tubular structures represent a new form of viral biomolecular condensates that contribute to the spatiotemporal organization of alphavirus replication cycle, connecting RNA synthesis with virion assembly. We propose that, during the early steps of infection, nsP3 helical assemblies form a cytoplasmic crown that supports vRC and RNA synthesis. These results are consistent with the vRC model provided recently by cryo-electron tomography (Tan et al., 2022) that observed inactive nsP complexes anchored at the plasma membrane, lacking a cytoplasmic crown. Furthermore, the nascent RNA would go through the nsP3 scaffold and interact with the positively charged pores being expelled for transcription (e.g. sgRNA) or retained for packaging (e.g. gRNA) through perhaps recognition of specific gRNA packaging signals[24]. As infection progresses, free nsP3 accumulates into alpha-granules (as occurs in nsP3 overexpression experiments) organized by a highly-ordered networks of helical tubular scaffolds that recruit host factors, viral gRNA and capsid proteins. We propose that in addition to its direct role in vRC formation and activity, nsP3-induced tubular networks might be microenvironments that shelter and transport newly synthesized positive RNAs to sites where packaging could be initiate. Further in situ cryo-electron tomography studies are required to determine the three-dimensional architecture of nsP3 tubes in infected cells and decipher how these structures orchestrate viral replication complexes formation and particle production. Beyond, the inner architecture of alpha-granules also

challenges our current understanding of the structural organization of non-membranous organelles by combining both intrinsically disordered regions and highly defined helical scaffolds.

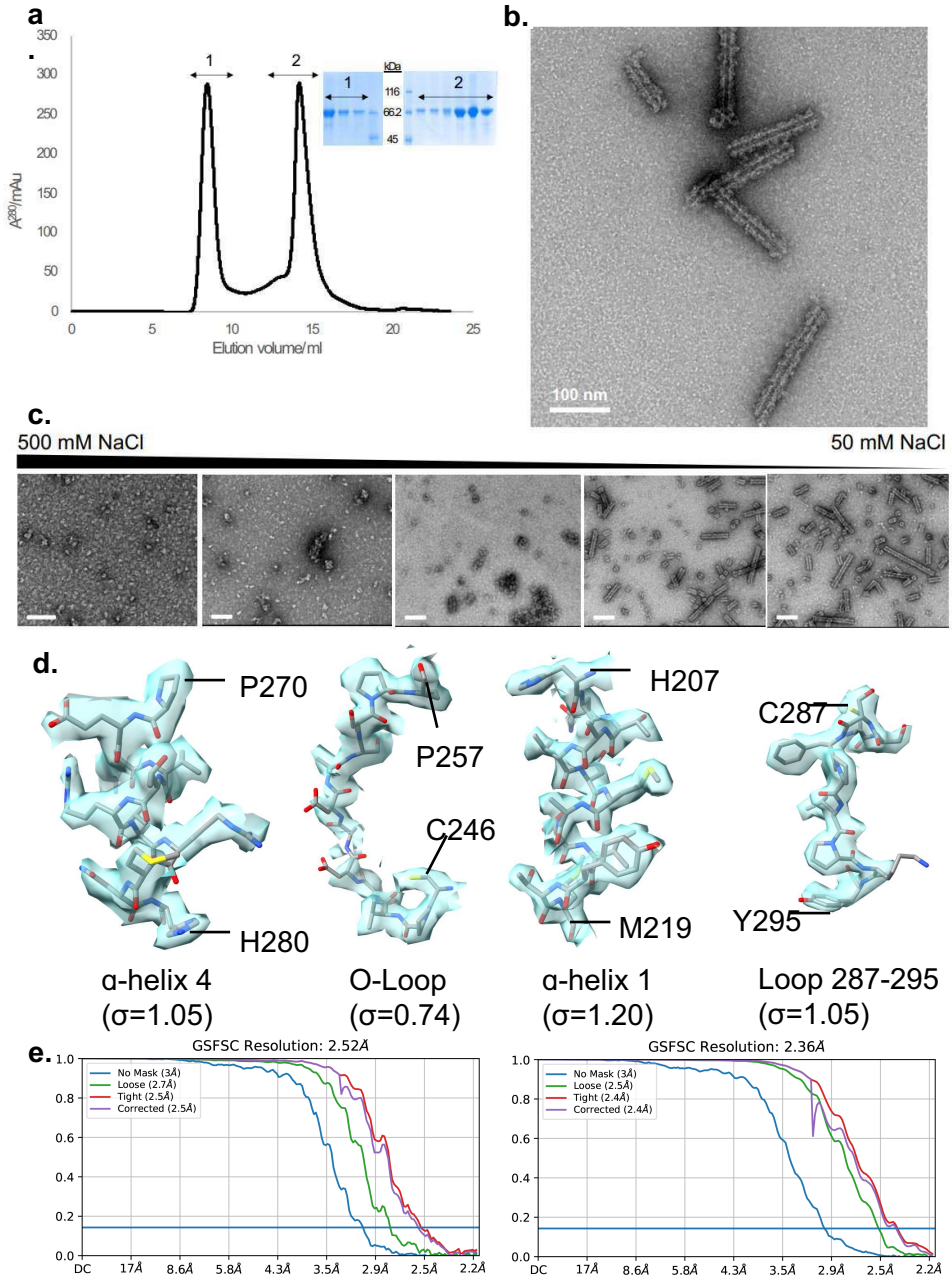

Extended Data Fig. 1. **CHIKV nsP3 purification and electron microscopy analysis a**. Size exclusion chromatography profile of nsP3 protein expressed in insect cells after nickel affinity chromatography at 0.5 M NaCl. Two picks are obtained, one at high molecular weight (1) and another consistent with monomeric nsP3 (2). The inset shows an SDS-PAGE of the indicated fractions for both peaks 1 and 2 showing the nsP3 migrated at the expected molecular weight in both cases (61kDa). **b**, Negative staining TEM micrograph of the sample from the peak 1 of panel a, showing the tubular structures formed by nsP3. **c**. The monomeric nsP3 was diluted to 0.2 mg/ml in buffers with decreasing NaCl concentration and equilibrated for 1h at. 4°C. The nsP3 assemblies start to appear at 200 M NaCl concentration. **d**. Representative fragments of electron density maps (EMD: 17678) are showed in transparent cyan at the specified sigma. The refined model (PDB: 8PHZ) is represented in sticks and colored by atom. The first and last residues for each fragment are labeled. **e.** Fourier shell correlation curves for the helical refinement and the focused refinement maps in the left and right panels respectively (EMD: 17729 and EMD: 17678, respectively).

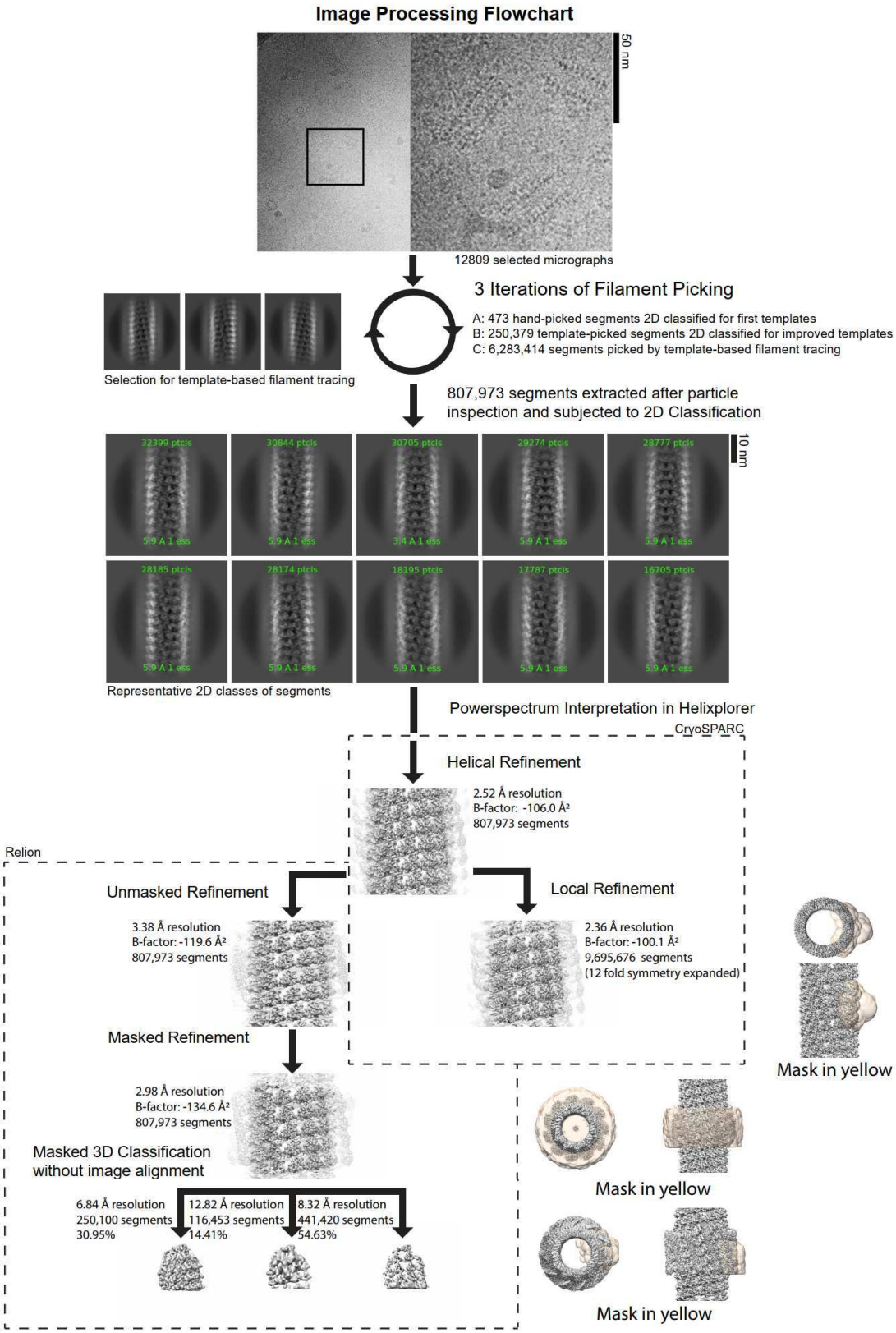

Extended Data Fig. 2. Flowchart of the image processing pipeline for nsP3. A representative micrograph section is shown with two different magnifications with exemplary nsp3 particle segments. The iterative segment picking workflow is illustrated. Particles are extracted and representative class averages are shown. Helical parameters were defined in helixplorer software (https://rico.ibs.fr/helixplorer, see supplementary information). Unmasked and masked refinement were performed in cryoSPARC and Relion with subsequent local classification procedures. 3D maps are represented in greyscale with two different thresholds to show both the densities of AUDs and macrodomains. Final maps are shown with annotated overall resolutions and B-factors. Used software packages are indicated. For a detailed description of the image processing pipeline, see methods, Table 1 and supplementary information.

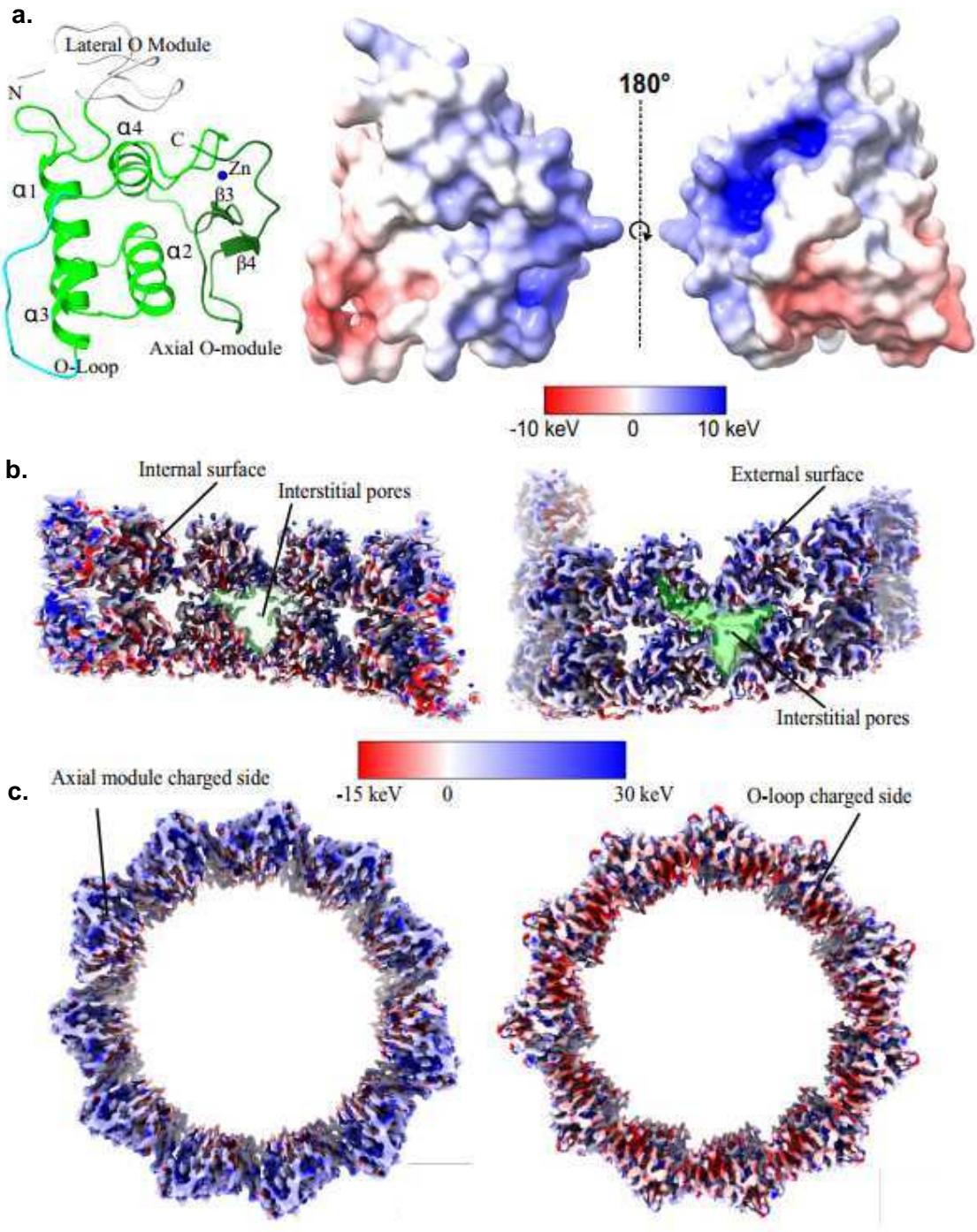

Extended Data Fig. 3. **Analysis of charge distribution on the AUD helical scaffolds**. **a**, Surface charges representation of two sides of the AUD monomer. The monomer on the left panel is represented as in Fig. 1d with the same orientation as the monomer in the central panel. The O-loop displays negative surface charges while the axial O-module, partly including the Zn finger, displays positive charges. **b**, a section through the diameter of the scaffold shows the charge distribution of the interior which is rather neutral, equally combining positive and negative charges. The right panel shows the surface of the positively charged surface of the tubes. The positively charged interstitial pores of the helices connect with the external positive charged surface suggesting that naked RNA could transit the pores and bind the scaffold surface. **c**. same representation of the bottom and top of the HSs with positively and negatively charges, respectively, showing the electrostatic nature of the AUD oligomerization and helix formation. The surface electrostatics were calculated using APBS (https://www.poissonboltzmann.org/) on the ranges indicated by the scale-bars for panel a, and bc respectively.

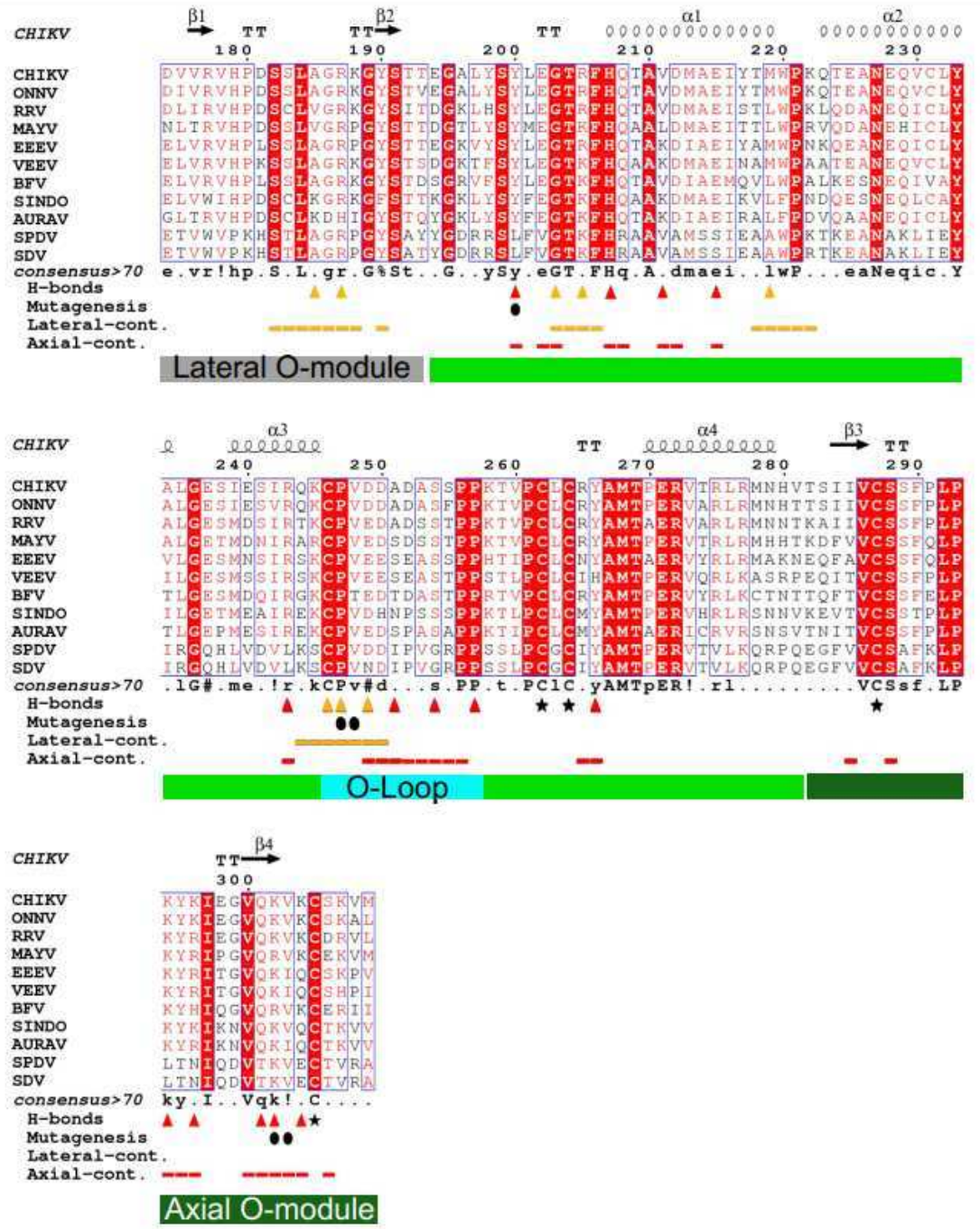

Extended Data Fig. 4. **Sequence alignment of the AUD from different alphaviruses.** ESPript3 sequence alignment representation of CHIKV (UniProt: Q8JUX6), O'nyong-nyong virus (ONNV) (UniProt: P13886), Ross river virus (RRV) (UniProt: P13887), Mayaro virus (MAYV) (UniProt: Q8QZ73), Eastern equine encephalitis virus (EEEV) (UniProt: Q4QXJ8), Venezuelan equine encephalitis virus (VEEV) (UniProt: P36327), Barmah forest virus (BFV) (UniProt: P87515), Sindbis virus (SINDO) (UniProt: P03317), Aura virus (AURAV) (UniProt: Q86924) and Sleeping disease virus (SDV) (UniProt: Q8JJX1). The secondary structures of the AUD are indicated in the top and residue numbering corresponds to CHIKV. At the bottom the consensus sequence is displayed, the residues maintaining hydrogen bonds in the lateral and axial interfaces are indicated by yellow and red triangles, respectively, and cysteine residues coordinated with the Zn atom are labelled by stars. Those residues maintaining contacts in the lateral and axial interfaces are indicated by yellow and red bars, respectively. The contacts were calculated by the PISA server and alignment done with TCoffee (EBI). The mutated residues in this study with drastic effects on replication and alpha-granule formation are indicated by black dots. The regions forming the O-modules and O-loop are indicated by thick bars at the bottom of the alignment following the same colour code as in Fig. 1d.

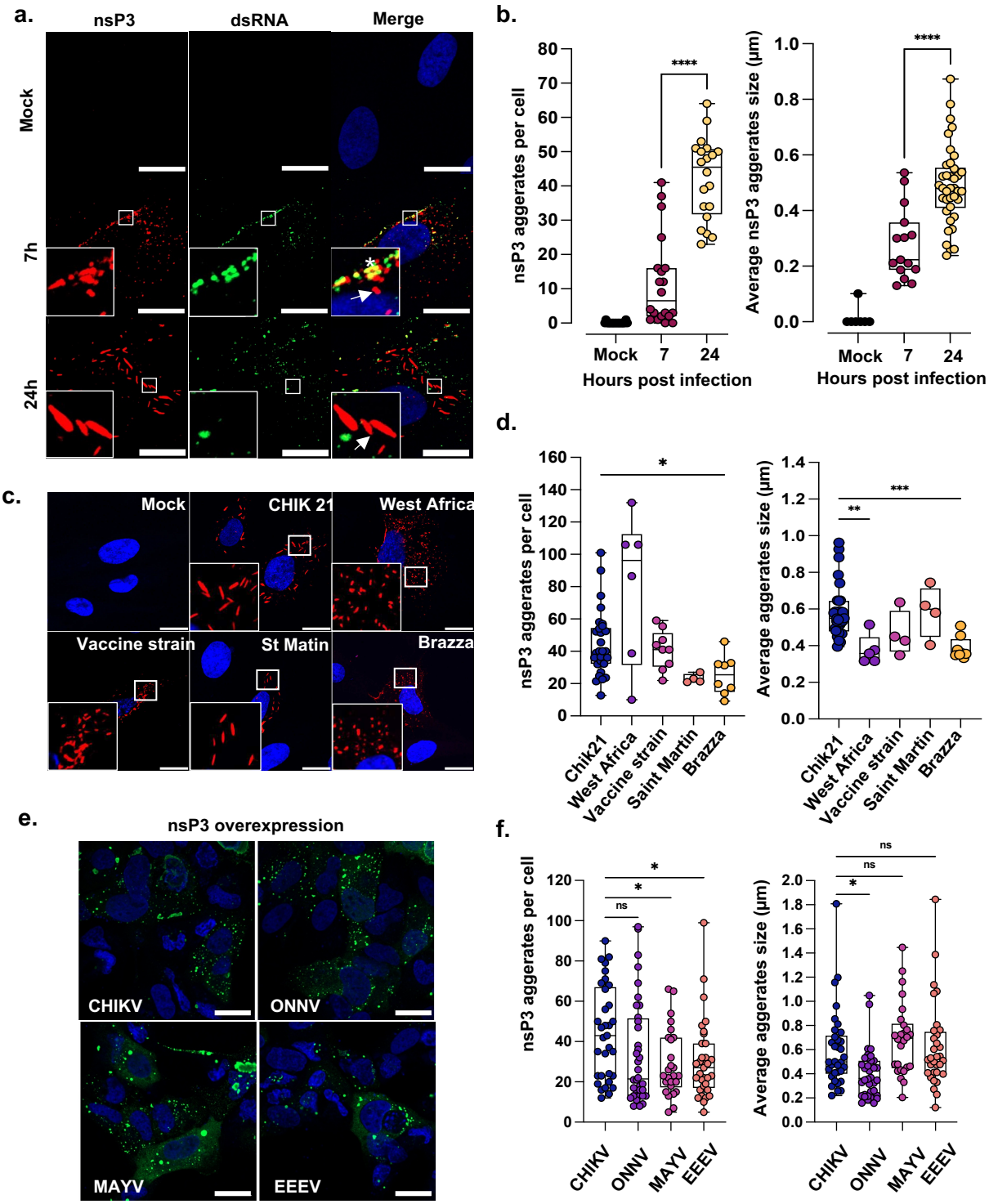

Extended Data Figure 5. NsP3 alpha-granules and alphavirus infection. a,b, Human fibroblasts were inoculated with the CHIK21 strain for 7 h (MOI of 10) or 24 h (MOI 2). Mock and infected cells were co-stained with a mouse anti-dsRNA mAb and rabbit anti-nsP3 Ab. Representative images were acquired by confocal microscopy and are shown. Replicative complexes (asterisk) and nsP3 alpha-granules (arrow) are shown. Co-localization analysis were performed as described in Fig 3b. Images are representative from 2 independent experiments. Scale bars, 20 µm. **b.** nsP3-aggregates were quantified following image segmentation by signal thresholding. Graph bar showing the number of nsP3-aggregates per cell (left) and the average aggregate size (right) from two independent biological replicates (n=20 cells in mock, n=20 cells at 7 h.p.i and n=20 cells at 24 h.p.i). h.p.i, hours post-infection. One-way ANOVA with a Dunnett's multiple comparison test. Significant differences denoted by **** $P < 0.0001$, ** P = 0.0012. **c,d,** Human fibroblasts were inoculated either with CHIKV21, West Africa, vaccine strain 181/25, Saint Martin or Brazza CHIKV strains for 24 h. **c,** nsP3 alpha-granule was detected using anti- nsP3 specific Ab and images were acquired by confocal microscopy. Data are representative from 2 independent experiments. **d,** The number of alpha-granule per cell (left plot) and the average aggregate size (right plot) were quantified as in (**b**) (n=30 cells in CHIKV21, n=6 cells for West Africa, n=9 cells for Vaccine strain, n=4 cells for St Martin and n=8 cells for Brazza strain). One-way ANOVA with Kruskal-Wallis multiple comparisons test. Significant differences denoted by *** $P = 0.0008$, ** $P = 0.0053$, * $P=0.0350$. e. U2OS cells were transfected for 48 hours with FLAG-tagged CHIKV-nsP3, ONNV-nsP3, MAYV-nsP3 or EEEV-nsP3 expressing plasmids. Alpha-granules were detected by confocal microscopy following anti-FLAG immunostaining. Images are representative from 2 independent experiments. Scale bars, 20 µm. **f.** The number of aggregates per cell (left plot) and the average aggregate size (right plot) were quantified as in (**b**) (n=24 cells in CHIKV, n=18 cells in ONNV, n=12 cells in MAYV and n=12 cells in EEEV). One-way ANOVA with a Dunnett's multiple comparison test. Significant differences denoted by *P =0.0251.

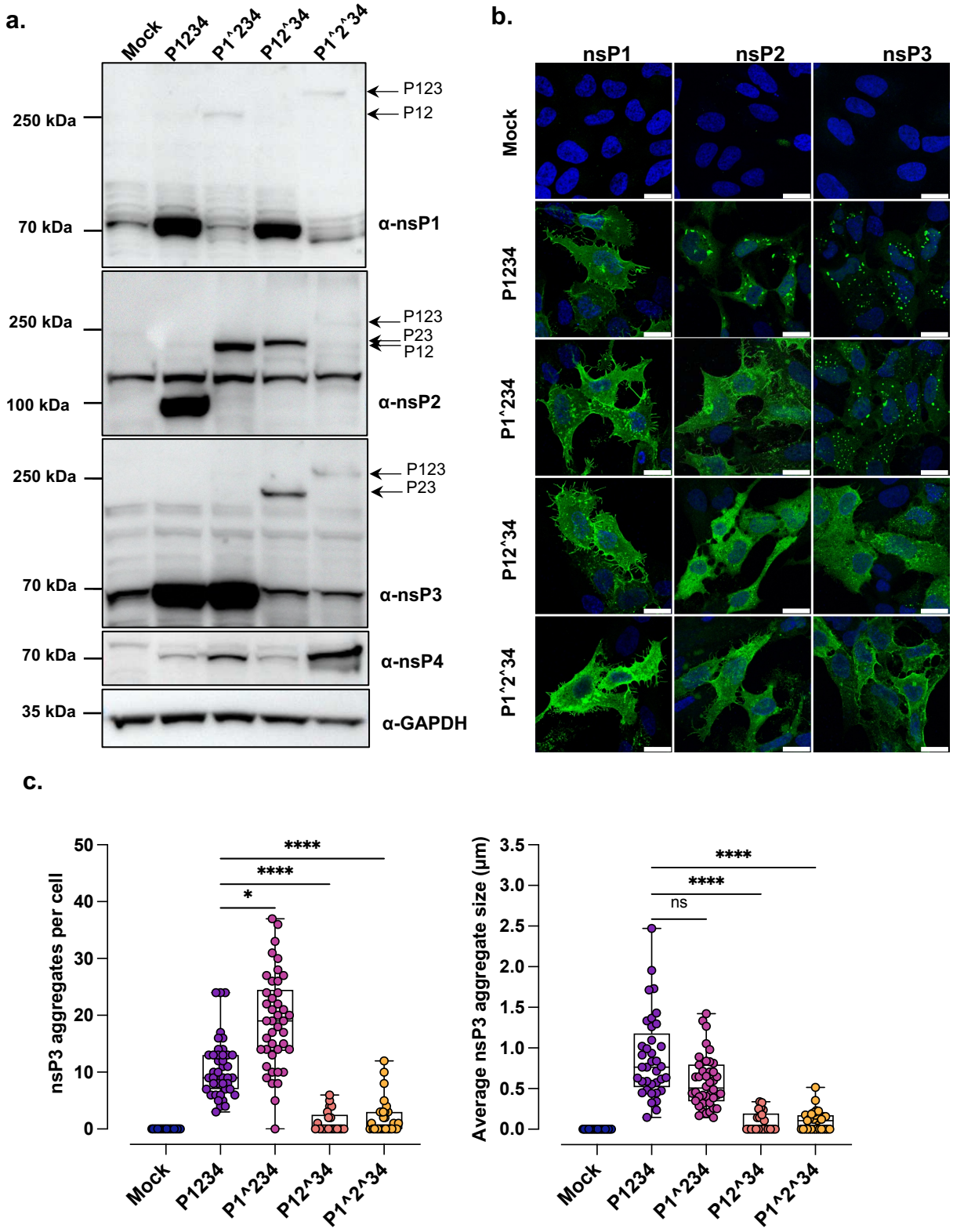

Extended Data Figure 6. NsP3 HS formation requires nsP2-nsp3 precursor cleavage. **a-c,** U2OS cells were transfected with a plasmid encoding the polyprotein precursor (P1234) or cleavage-deficient mutants (^ indicates the uncleavable sites). **a**, Cell lysates were separated by SDS-PAGE and non-structural proteins processing was ascertained by immunoblot analysis with nsP1, nsP2, nsP3, nsP4 or GAPDH antibodies. **b**, The subcellular localization of nsP1, nsP2 and nsP3 was assessed by immunofluorescence at 48 h post-transfection. **a,b,** data shown are representative of 2 independent experiments. **c,** Graph bar showing the number of nsP3 aggregates per cell (left) and the average aggregate size (right) from two independent biological replicates (n=20 cells in mock, n=43 cells for P1234, n=42 cells in P1^234, n=21 cells in P12^34 and n=31 cells in P1^2^34). One-way ANOVA with Kruskal-Wallis multiple comparisons test. Significant differences denoted by **** $P < 0.0001$, * P=0.0232.

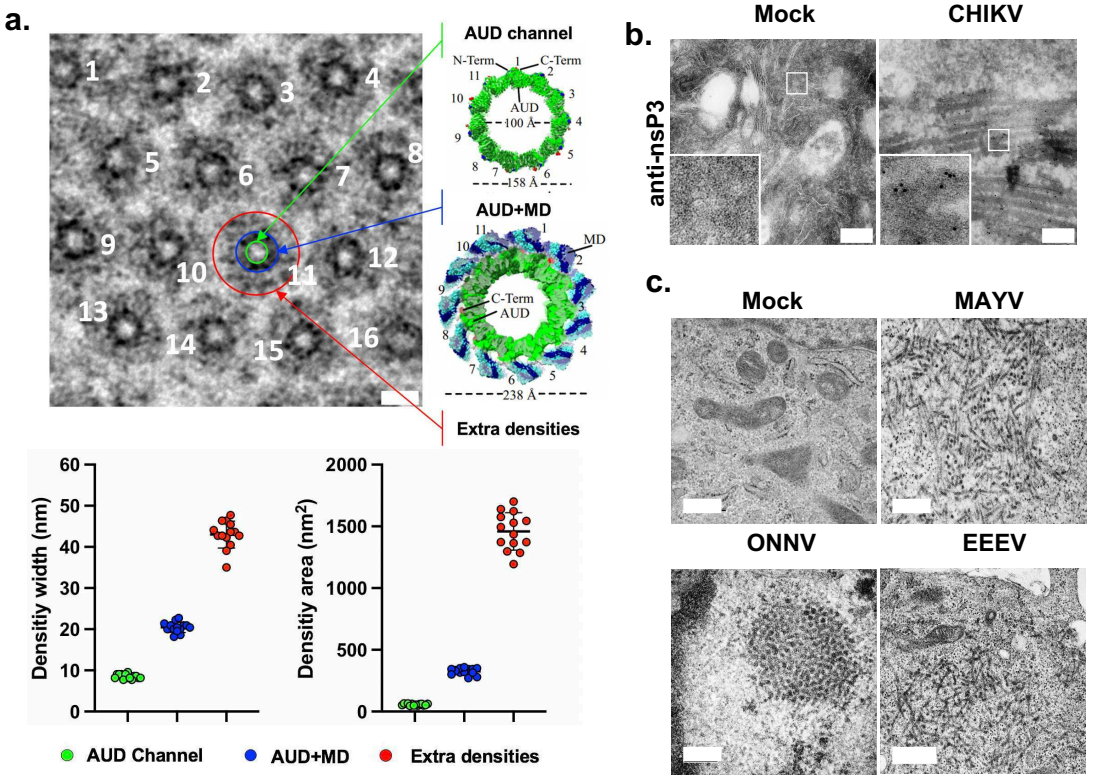

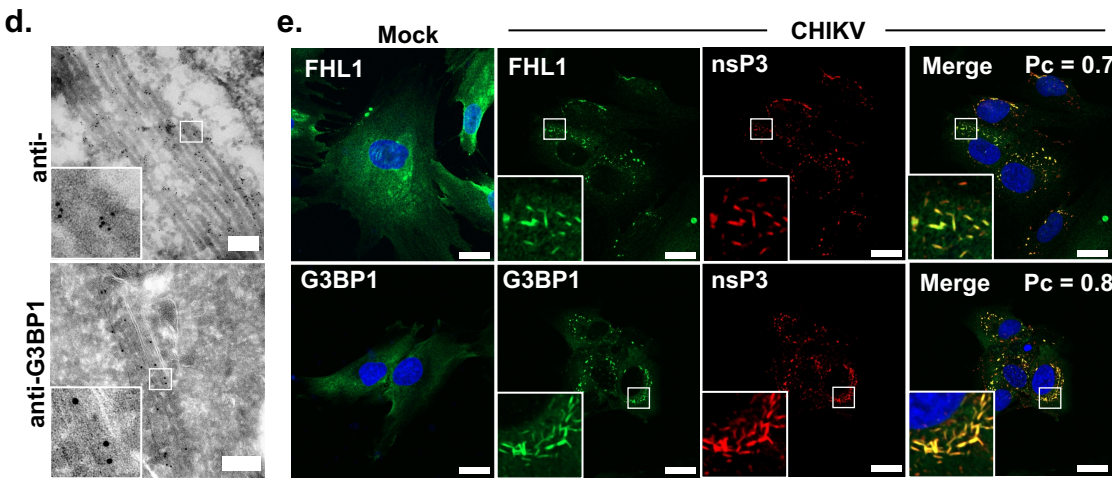

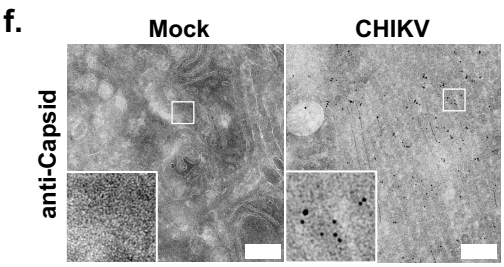

Extended Data Figure 7. NsP3 tubular structure characterization. a, The left panel shows a micrograph corresponding to a section of alpha granules perpendicularly cutting a bundle of HSs. A 0.2 μm² is depicted. The right panel shows the interior of the rectangle magnified. 16 HSs are present and numbered within the 0.2 μm² square. The scaffold numbered as 13 is superposed to three concentric circles of the dimensions obtained for the HSs (see Fig. 1) including the internal channel (green circle), the MDs (blue circle), the and external density around the tube (red circle) with 10 nm, 20 nm and around 40 nm 15.8 nm and of diameter, respectively. Circles diameter and area were calculated with ImageJ for each one of the 16 HSs in the image (bottom panels) **b.** Transmission electron microscopy of CHIKV-infected fibroblasts following immunogold labeling with an anti-nsP3 antibody. Scale bars, 200 nm. **c**. Transmission electron microscopy of human fibroblasts. **c** Transmission electron microscopy of human fibroblasts transfected with empty plasmid (mock) or MAYV, OONV or EEEV nsP3 plasmids. Scale bars, 500nm. d. Transmission electron microscopy of CHIKV infected human dermal fibroblasts following immunostaining using gold anti-FHL1 or -G3BP1 Ab, showing that nsP3 tubular structures contain FHL1 and G3BP. Scale bars, 200 nm. **e**, Human fibroblasts were inoculated with CHIK-nsP3-mCherry virus at MOI of 5 for 24 hours and immunostained for FHL1 and G3BP1 expression. Images were acquired by confocal microscopy (nsP3-mCherry in red, FHL1 and G3BP1 in green). Co-localization analysis were performed as described in Fig 3b. Pearson's coefficients (Pc) are shown for each staining (n>15 cells). Scale bars, 20 μm. **f**. Transmission electron microscopy of CHIKV-infected fibroblasts following immunogold labeling with an anti-capsid antibody. Scale bars, 200 nm. (**a-e**) Images are representative of 2 independent experiments.

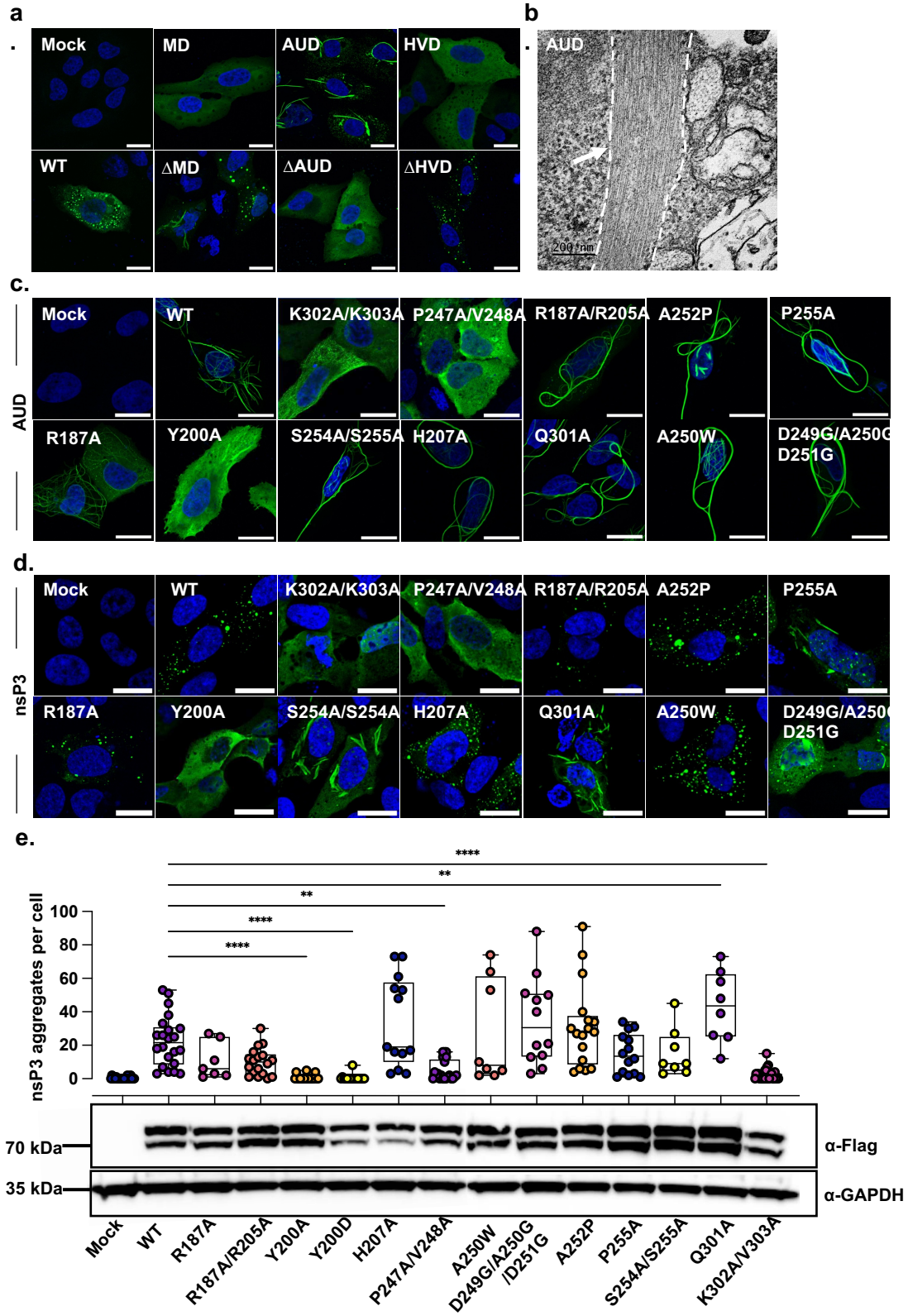

Extended Data Figure 8. The AUD mediates nsP3 oligomerization. a. U2OS cells were transfected with plasmids encoding FLAG-tagged CHIKV nsP3, nsP3 Macrodomain (MD), nsP3 Alphavirus unique domain (AUD), nsP3 Hypervariable domain (upper panels), or CHIKV nsP3 deleted for one of these domains (ΔMD, ΔAUD or ΔHVD) (lower panels). At 48h after transfection, cells were fixed and stained with FLAG antibody. Images were acquired by confocal microscopy. Scale bars, 20 μm. Images are representative of 2 independent experiments. **b,** Transmission electron microscopy of U2OS cells stably expressing the nsP3 AUD domain. White arrow and dashed lines show long filamentous structures specific to AUD-transfected cells. Scale bars, 200 nm. **c,** U2OS cells were transfected with either FLAG-tagged wild-type nsP3 AUD or a panel of nsP3 AUD constructs harboring mutations of residues proposed to mediate interprotomer contacts (*see figure 1*). AUD filaments formation was assessed 48 h after transfection by immunostaining with FLAG antibody. Images were acquired by confocal microscopy and are representative of 2 independent experiments. Scale bars, 20 μm. **d-f,** U2OS cells were transfected with the full-length FLAG-tagged CHIKV nsP3 carrying the AUD mutations shown in (**c**). **d,** The ability of each mutant to form cytoplasmic aggregates was assessed by immunostaining with FLAG antibody. Images are representative of 2 independent experiments. Scale bars, 20 μm. **e,** Graph bar showing the number of nsP3-aggregates per cell from 2 independent experiments (n ≥ 15 cells). One-way ANOVA with a Dunnett's multiple comparison test. Significant differences denoted by **** $P < 0.0001$, **P = 0.0021. **f,** NsP3 expression in U2OS transfected cells.

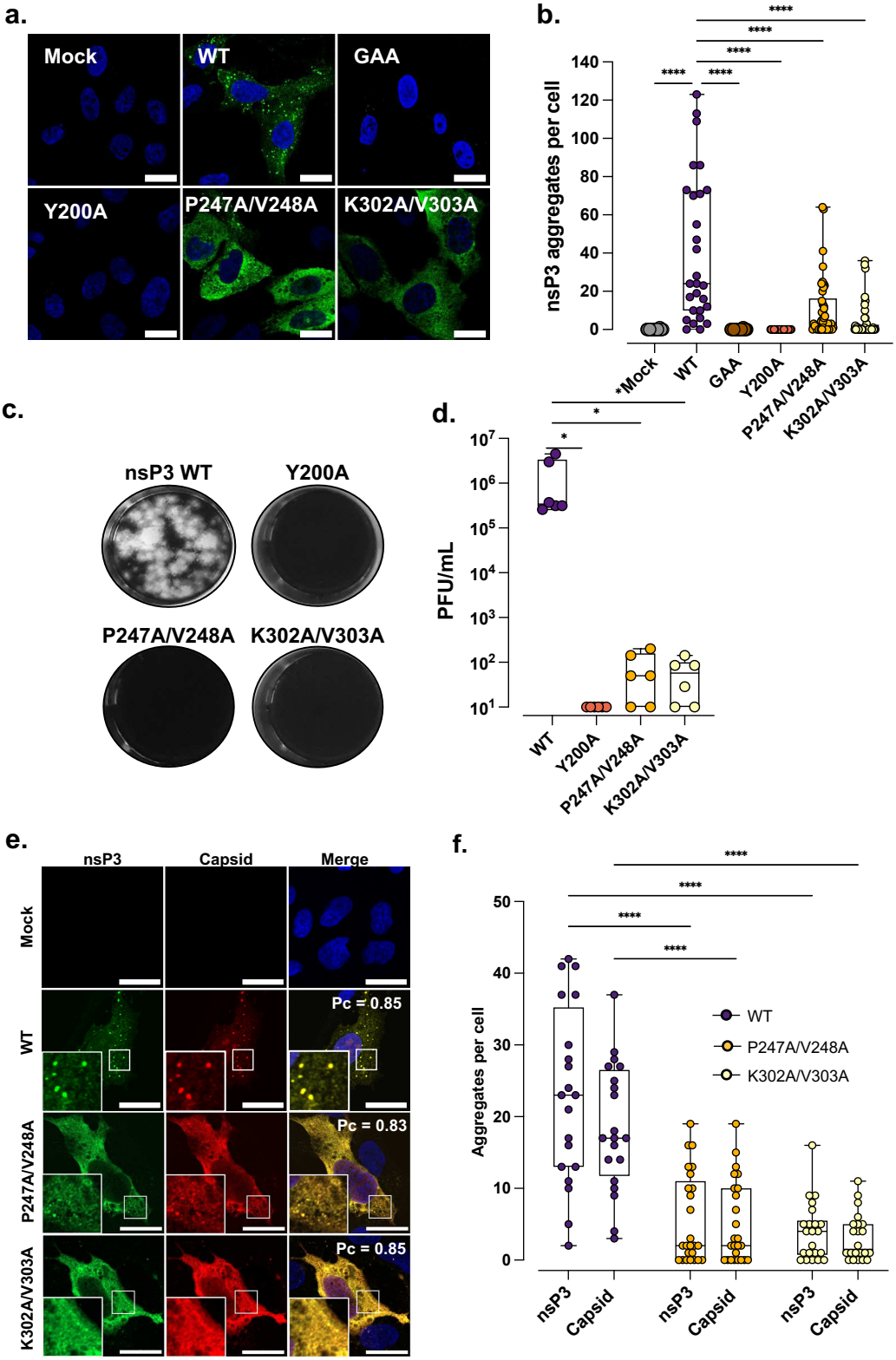

Extended Data Figure 9. Role of nsP3 helical scaffolds during CHIKV infection a-f, U2OS cells were transfected with the indicated CHIKV capped *in vitro* transcribed RNA. GAA, replication deficient mutant. **a,** U2OS were fixed and immunostained with nsP3-specific Ab to assess the nsP3 sub-cellular localization by confocal microscopy. **b,** Graph bar showing the quantification of nsP3 aggregates per cell from two independent biological replicates (n≥15) using ImageJ. Significant differences denoted by ****P <0.0001. **c,d,** Supernatant of infected cells were collected at 24 h post transfection and viral titers were measured by plaque assay on VeroE6 cells. Images representative of WT and mutant viruses' plaques (**c**) and bar graph showing the corresponding viral titers (**d**) are shown. Data are mean ± s.e.m. n = 3 independent experiments performed in duplicate. One-way ANOVA with a Dunnett's multiple comparison test (*P =0.0174). **e,** At 48 h post-transfection, the subcellular localization of nsP3 and capsid proteins was monitored by immunofluorescence. Images were acquired by confocal microscopy. Images are representative of 2 independent experiments. **f**, Quantification of CHIKV capsid and nsP3 alpha-granules per cell using ImageJ from two independent biological replicates (n=20 cells in WT, n=24 cells in P247A/V248A, and n=22 cells in K302A/V303A). Two-way ANOVA with a Dunnett's multiple comparison test (****P<0.0001).

METHODS

Recombinant expression and purification of CHIKV nsP3 protein.

Nsp3 was expressed in Hi5^{TM} cells (Thermofisher) using BactoBac system (Thermofisher). The coding sequence of nsp3 (corresponding to residues 1334-1863 of the non-structural polyprotein sequence from the S27 African prototype (Uniprot ID Q8JUX6) was synthesized by Gen9 as a codon optimized gene and subcloned into a pFastBac vector (Thermofisher) with a C-terminal hexahistidine tag. Site directed mutagenesis was performed on the pFB-nsP3 construct by Q5 Site-Directed Mutagenesis Kit Quick Protocol (NEB) and the whole nsP3 sequence was verified by sanger sequencing. Recombinant bacmids and viruses were produced in YFP-DH10 Bac cells and Sf21 cells, respectively according to the manufacturer's protocols (Thermofisher). For protein expression, Hi5 cells were grown in suspension at a density of 0.5-1.0x 10^6 ml^{-1} and then infected with baculoviruses at 2% volume of the culture. Cells were harvested at day 2-3 post cell arrest. Cells were resuspended in buffer A (20mM Tris pH 8, 500mM NaCl, 2mM TCEP, 5% glycerol, 20mM imidazole) supplemented with 2mM PMSF, 10 μg/ml DNAse and 5 mM $MgSO_4$, and lysed by sonication. Lysates were centrifuged at 18,000g for 1h to remove unbroken cells and debris. The clarified lysate was incubated with Ni-NTA resin (GE Healthcare) in batch at 4°C for 30 minutes. Resin was washed with 10 column volumes of lysis buffer and the protein eluted over 1.5 column volumes with buffer A containing 500mM imidazole. Elution fractions containing the protein were pooled and concentrated (Amicon 30k MW C/O) for size exclusion chromatography. Samples were applied to a Supedex 200 10/300 increase column (GE Healthcare) pre-equilibrated with the size exclusion buffer: 20 mM HEPES pH = 8.0 ; 500 mM NaCl; 5 % glycerol and 2 mM TCEP.

Grid preparation for cryo-EM imaging

Quantifoil grids R2/1 were treated with plasma glow discharge (Quorum) two times for 25 seconds at 15mA with a 2 min pause between the pulses. 3.5µl of Purified nsP3 protein at 1mg/ml in freezing buffer (100mM NaCl, 20mM HEPES pH7.5 and 2mM TCEP) were applied on the prepared grids and left to incubate for 1 min for binding at RT. The grid was transferred in Leica GP plunge freezer and then blotted for 10s from the back side. Grids were plunged into liquid ethane and then transferred and stored in liquid nitrogen until the imaging session. For data collection on nsP3 grids we used the Titan Krios microscope in ESRF CM01 beamline [25] at Grenoble, France. Vitrified nsP3 grids were loaded into the microscope equipped with a Gatan K3 direct electron detector and a Gatan Bioquantum LS/967 energy filter. Cryo-EM data were acquired with EPU software (FEI) at a nominal magnification of ×81,000, with a pixel size of 1.06 Å and a total dose of 42 e/Å^2 (see Table S1). 13,046 image frames were acquired in super-resolution mode with a flux of 18.1 electrons per square-pixel, fractionated into 40 frames with a defocus range from −0.6 µm to −2.6 µm. Using the CM01 real-time processing setup, within the SCIPION wrapper [26] , the imported movies were drift-corrected using MotionCor2 and CTF parameters were estimated using Gctf for real-time evaluation. Further data processing was conducted using the cryoSPARC suite [27] and Relion4.

Cryo-EM Image processing: 13,046 motion-corrected and dose-weighted micrographs were imported into cryoSPARC for further processing and CTF estimated. After exposure curation 12809 micrographs remained. Combining manual picking plus two rounds of 2D classification template picking we obtained an initial set of templates for template-based filament tracing. Filament tracing was performed with a segment diameter of 130 Å and a distance of 32.5 Å based on measurements within 2D classes and resulted in 6,283,414 particle images. Subsequent picking inspection (NCC score

> 0.180, local power 83.0-108.0, curvature, 0.0012 (1/ Å) and sinuosity <1.18) reduced the selection to 831,539 particles (5,451,875 particles excluded). 807,973 particles were extracted with an extraction crop size of 408 pixels and 2D-classified into 200 classes. Helical refinement without prior estimation of helical twist and helical rise was not successful. Accordingly, helical twist and rise estimates were found by power spectrum analysis in helixplorer software (https://rico.ibs.fr/helixplorer/helixplorer/ see supplementary information). Helical parameters were refined during 3D reconstruction and converged to a twist of -164.175 degrees and a helical rise of 2.782 Å. The map refined to a nominal 2.52 Å resolution (according to 0.143 threshold) and a B-factor of 106.0 (EMD: 17729). Symmetry expansion (Point group symmetry: C1, helical twist (degrees): -164.175, helical rise (Å): 2.782, helical symmetry order: 12 of all final particles in this map was performed. Symmetry expanded particles (9,695,676 particles) were used in local refinement with a local mask covering an 3x3 array of 9 helical domains and a protruding central domain to cover the potential macrodomain resulted in a map of a nominal 2.36 Å resolution and slightly improved side chains (EMD: 17678).

807,973 non-subtracted particles and reference maps from cryoSPARC were imported from cryosparc into Relion. A first round of unmasked refinement was performed followed by masked refinement giving rise to better defined protruding densities of the potential macrodomain (EMD: 17730). For that a cylindrical mask covering the 30% central section of the helix and the protruding densities was designed from the helix. Different sets of masked 3D classification variants were tested (varying class size, with and without alignment, with and without particle subtraction). Here a smaller mask covering only a threefold array of two neighboring AUD and the protruding density was

used. The best class was derived from non-particle subtracted classification into 3 classes (supplementary map in EMD: 17730).

Model building, refinement and analysis.

The first model of the whole nsP3 was obtained using ColabFold [28] (see supplementary information). The predicted model AUD domain fitted perfectly in the maps with the exception of the O loop which was traced by hand using Coot. A model with five AUD including one protomer and four neighbor contacting protomers was done using Coot and real-space refined using Phenix on the 2,35 Å resolution map (PDB: 8PHZ and EMD: 17678 respectively). The HVD and MD conformations predicted by Alphafold2 where incompatible with the helix formation, in consequence for the interpretation of the MD densities at low resolution the MD was placed manually and fitted into density using ChimeraX. The biological assembly with 120 protomers forming the helix was calculated extending the helical symmetry with ChimeraX setting an axial rise of 2.782 Å and a helical twist of -164.175 ° on the helical reconstruction map at 2.53 Å resolution (PDB: 8PK7, EMD: 17729). For the analysis of interprotomer contacts we used the PISA server (https://www.ebi.ac.uk/pdbe/pisa/). We applied a cutoff of 3.5 Å for assigning H bonds as indicated in Extended Data Fig. 3.

Cell culture. HEK293T (ATCC, CRL-3216), Vero E6 (gift of Marc Lecuit, Pasteur Institute Paris, France), BHK-21 (ATCC, CCL-10) and U2OS cells (gift of Andres Merits, University of Tartu, Estonia) were cultured in DMEM supplemented with 10% FBS, 1% penicillin–streptomycin, and 25 mM HEPES. Fibroblast BJ-5ta cells (ATCC, CRL-4001) were cultured in DMEM supplemented with 20% Gibco Media 199, 10% FBS, 1% penicillin–streptomycin, 25 mM HEPES and 10 µg/mL Hygromycin D. All cell

433 lines were cultured at 37 °C in 5% CO2. All cell lines were routinely tested to be free
434 of mycoplasma contamination.
435
436 **Virus strains and production**. CHIKV21 (strain 06-21 from Reunion Island) was
437 previously described [29] and obtained from Philippe Despres (Institut Pasteur, Paris,
438 France). CHIKV West Africa (strain 37997), CHIKV St Martin (H20235 2013 Asian),
439 MAYV (strain TC 625) and ONNV (strain Dakar 234) were obtained from the European
440 Virus Archive (EVA) collection. Viruses were propagated with limited passages on Vero
441 E6 cells. CHIKV 181/25 molecular clone (gift from Dr Gofinnet Christine, Institute of
442 Virology Charité, Berlin, Germany) was derived from the parental Asian strain
443 AF155561 and attenuated by two amino acid substitutions in the E2 glycoprotein [30].
444 Recombinant CHIKV nsP3-mCherry and CHIKV-Rluc molecular clones were derived
445 from CHIKV isolate obtained during the Mauritius outbreak in 2006 (GenBank
446 accession no. FJ959103) [31]. To generate infectious viruses from CHIKV molecular
447 clones, capped viral RNAs were generated from the NotI-linearized CHIKV plasmids
448 using a mMESSAGE mMACHINE SP6 or T7 Transcription Kit (Thermo Fischer
449 Scientific) according to manufacturer's instructions. Resulting RNAs were purified by
450 phenol:chloroform extraction and isopropanol precipitation, resuspended in water,
451 aliquoted and stored at -80°C until used. Thirty μg of purified RNAs were transfected
452 in BHK21 with lipofectamine 3000 reagent and supernatants harvested 72 hours later
453 were used for viral propagation on Vero E6 cells.
454 All virus stocks were purified through a 20% sucrose cushion by ultracentrifugation at
455 80,000g for 2 hours at 4°C. Pellets were resuspended in HNE1X pH7.4 (Hepes 5 mM,
456 NaCl 150 mM, EDTA 0.1 mM), aliquoted and stored at -80°C. Viral titers were
457 determined on Vero E6 cell by plaque assay and are expressed as PFU per mL and

458 also by flow cytometry as previously described [21]. Briefly, Vero E6 cells were incubated
459 for 1 h with 100 μL of 10-fold serial dilutions of viral stocks. The inoculum was then
460 replaced with 500 μL of culture medium and the percent of E2 expressing cells was
461 quantified by flow cytometry at 8 hpi. Virus titers were calculated using the following
462 formula and expressed as FACS Infectious Units (FIU) per mL. [Titer (FIU/mL) =
463 (average % of infection) x (number of cells in well) x (dilution factor) / (mL of inoculum
464 added to cells)].
465 **Plasmid constructions.** All N-terminal FLAG-tagged full-length nsP3 constructs
466 derived from CHIKV Sri Lanka/2006/SL15649 strain (Accession number:
467 MK028838.1), the nsP3 macrodomain (MD; aa A1-T160), the alphavirus unique
468 domain (AUD; aa Q161-Y324) and the hypervariable domain (HVD; aa R325-L523)
469 were synthesized and cloned into pcDNA 3.1 (-) mammalian expression vector by
470 GenScript. The WT FLAG-tagged nsP3 and FLAG-tagged AUD constructs were
471 subcloned into a pLVX-EF1a-IRES-puromycin (Takara) using NotI and BamHI
472 restriction enzymes. pMC-GTU CHIKV P1234 WT and mutant replicase plasmids were
473 described elsewhere[19] and kindly provided by Pr. Andres Merits (University of tartu,
474 Estonia). FLAG-tag ONNV-nsP3 (isolate UVRI0804, accession number: ON595759.1),
475 FLAG-tag MAYV-nsP3 (isolate Haiti-1/2014, accession number: KY985361.1) and
476 FLAG-tag EEEV-nsP3 (isolate USA/R131399b/2019, accession number:
477 MT782295.1) were synthesized and cloned into pcDNA 3.1 (-) mammalian expression
478 vector by GenScript.
479 To establish pCHIKV with an Rluc gene insertion in the nsP3 gene (pCHIKV-Rluc), two
480 PCR fragments were amplified from pCHIKV-M [31]. Part of the CHIKV nsp3 sequence
481 was amplified using primers 5009F (5'-TGACCACAACGTGCCATCGCG-3') and
482 Bo426 (5' cggggtcgtacaccttggaagccatCAAGCTTTCGATTTCTCCTTCGTTG-3'), and

a CHIKV sequence encoding parts of nsP3 and nsP4 was amplified using Bo427 (5'-gtgctgaagaacgagcagGAgtcactaTCTTCTGAGCTACTAACTTTCGG-3') and Bo409 (5'-GACTTCCTCCAGGGTGTTCACC-3'). Finally, the Rluc gene was amplified from phRL-CMV (Promega) using primers Bo425 (5'-CAACGAAGGAGAAATCGAAAGCTTGatggcttccaaggtgtacgaccccg-3') and Bo428 (5'-CCGAAAGTTAGTAGCTCAGAAGAtagtgacTCctgctcgttcttcagcac-3'). The three fragments were fused by PCR amplification using the outer primer pairs 5009F and Bo409. The resulting fragment was cut with NheI and AgeI and fused together with an NgoMIV-NheI fragment derived from pCHIKV-M into pCHIKV-M digested with NgoMIV-AgeI. For pCHIKV-Rluc mutants Y200A, two PCR fragments encompassing the desired change were amplified from pCHIKV-Rluc using primers Bo408 (CACCACGTGCTCCTGGTCAGTG) and Bo1646 (5'-tcccttctagaGCtgagtacagtg -3') or Bo1645 (5'-cactgtactcaGCtctagaaggga-3') and Bo409 (see above). The resulting fragments were fused together using the outer primers Bo408 and Bo409. For P247A/V248A and K302A/V303A mutants, the primers encompassing the mutations (Bo1646 and Bo1645) were replaced by Bo1651 (5'-ggcagaaatgcGCTGCTgatgatgcaga-3') and Bo1652 (5'-tctgcatcatcAGCAGCgcatttctgcc-3'), or Bo1654 (5'-ttagagcatttTGCTGCttgcactcctt-3') and Bo1653 (5'-acgcatcatctGcAcccaaaactgt-3') respectively. The PCR fragments containing the mutations were cut with SacII and AgeI and fused together with a BamHI - SacII derived fragment of pCHIKV-RLuc into pCHIKV-Rluc cut with BamHI and AgeI.

Lentiviral production. Lentiviral plasmids containing FLAG-tagged full-length nsP3 or AUD were packaged as previously described [21]. Supernatants were collected 48 h and

72 h after transfection, cleared by centrifugation (750g for 10 min), filtered using a 0.45-µm filter and purified through a 20% sucrose cushion by ultracentrifugation (80,000g for 2 h at 4 °C). Pellets were resuspended in HNE 1X pH 7.4, aliquoted and stored at −80 °C. Fibroblasts were transduced by spinoculation (750g for 2 h at 33 °C) using these lentiviruses and selected with puromycin (2 µg/mL).

Antibodies. The following primary antibodies were used: anti-Flag M2 mouse monoclonal antibody (F1804, Sigma), anti-dsRNA J2 mouse monoclonal antibody (Scicons), anti-nsP1, anti-nsP2, anti-nsP3 and anti-Capsid rabbit polyclonal antibodies (in-house from Andres Merits's laboratory), anti-CHIKV E2 mouse monoclonal antibody (3E4), anti-GAPDH mouse monoclonal antibody (SC-47724, Santa Cruz Biotechnology), anti-FHL1 mouse monoclonal antibody (MAB5938, R&D Systems) and anti-G3BP1 mouse monoclonal antibody (H-10 sc-365338, Santa Cruz Biotechnology). The following secondary antibodies were used: Alexa Fluor 488-conjugated goat anti-rabbit IgG (A11034, Invitrogen), Alexa Fluor 488-conjugated goat anti-mouse IgG (A11001, Invitrogen), Alexa Fluor 647-conjugated donkey anti-rabbit IgG (A31573, Invitrogen), Alexa Fluor 647-conjugated donkey anti-mouse IgG (A31571, Invitrogen), Alexa Fluor 594-conjugated donkey anti-rabbit IgG (21207, Invitrogen), peroxydase-conjugated donkey anti-rabbit IgG (711-035-152, Jackson ImmunoResearch), and anti-mouse/HRP (P0260, Dako Cytomotion).

Immunofluorescence. For nsP3 aggregates characterization in infectious context, human fibroblasts (1.1 x 10^4 cells per well) were grown on Lab-Tek CC2 chamber slides (Nunc) for 24 hours. Cells were inoculated with CHIKV21 or CHIKV nsP3-mCherry at the indicated MOIs. For immunofluorescence in the context of transient

transfection, U2OS (3 x 10^5 cells) were grown on Lab-Tek CC2 chamber slides for 24 hours. Cells were transfected with 250 ng of DNA expression plasmid using jetOPTIMUS® DNA Transfection Reagent (PolyPlus) according to the manufacturer's instructions. At 7 and 24 hpi, or after 48 h of transfection, cells were washed with PBS and fixed with 2% (v/v) of PFA diluted in PBS for 15 min at room temperature. Fixed cells were washed with PBS for 5 min, then incubated with 0.1 mM of glycine in PBS for 30 min at room temperature. Cells were permeabilized and blocked with 0.1% Triton X-100 and 3% (w/v) BSA in PBS for 45 min. Cells were incubated for 1 h at room temperature with primary antibodies, and washed with PBS. Cells were labelled with corresponding Alexa Fluor-conjugated secondary antibodies (1 $\mu g.ml^{-1}$) for 30 min at room temperature. All antibodies were diluted in PBS supplemented with 3% (w/v) BSA. Slides were mounted with ProLong Gold antifade reagent containing DAPI for nuclear staining (Thermo Fisher Scientific). Fluorescence microscopy images were acquired using a LSM 800 confocal microscope with the following objectives: Plan-Apochromat 63x/1.40 Oil DIC M27 and Plan-Apochromat 40x/1.3 Oil DIC (UV) VIS-IR M27 (Zeiss).

RNA-Fluorescent In Situ Hybridization. A pool of 48 Custom Stellaris™ RNA FISH Probes was designed against the 5' open reading frame of CHIKV (strain LR2006-OPY1, GenBabk: DQ443544.2) by utilizing the Stellaris RNA FISH Probe Designer (LGC, Biosearch Technologies, Petaluma, CA) available online at www.biosearchtech.com/stellarisdesigner. Each probe was labelled with Quasar™ 570 dye (LGC, Biosearch Technologies, Petaluma, CA) and hybridized to CHIK21-infected human fibroblasts, according to the manufacturer's instructions available online at www.biosearchtech.com/stellarisprotocols. Briefly, following viral protein

558 immunostaining (see section ‘Immunofluorescence’), cells were washed three times
559 with PBS and fixed with 2% (v/v) of PFA diluted in PBS for 10 min at room temperature.
560 Cells were washed twice in PBS and incubated with Stellaris Wash Buffer A at room
561 temperature for 10 min. Cells were incubated with RNA probes diluted at 0.125 nM
562 final concentration in hybridization buffer supplemented with 0.5 mM vanidyl
563 ribonucleoside complex, for 16 h in humidified chamber at 37°C. Cells were first
564 washed in Stellaris Wash buffer A for 30 min at 37°C, and then with Stellaris Wash
565 buffer B for 10 min. Slides were mounted with ProLong Gold antifade reagent
566 containing DAPI for nuclear staining (Thermo Fisher Scientific). Of note, all buffers and
567 reagents used were RNase-free. Fluorescence microscopy images were acquired
568 using a LSM 800 confocal microscope (Zeiss).
569
570 **Genomic viral RNA, viral replicon transfection and viral infection analysis.** To
571 assess wildtype and mutant CHIKV RNA replication, we transfected HEK293T cells
572 with capped genomic viral RNA generated from pCHIKV-Rluc molecular clones (see
573 ‘Virus strains and production) or capped replicon RNA encoding Renilla luciferase
574 reporter gene fused in the C-terminal part of viral nsP3, and Firefly luciferase reporter
575 gene expressed under the viral sub-genomic reporter gene Cells were plated on 48
576 well plates (5 x 10^4 cells) and transfected with 50 ng of purified RNA using the
577 Lipofectamine MessengerMax reagent according to the manufacturer’s instructions
578 (Thermo Fisher Science). Only for genomic viral RNA-transfected cells, at 3 h after
579 transfection, medium was removed and fresh medium was added. At specific time
580 intervals, cell supernatant was collected and frozen at -80°C for plaque assay on
581 VeroE6 cells.Genomic RNA and replicon RNA-transfected cells were washed once
582 with PBS and lysed with Passive lysis buffer. Lysates were kept at −20 °C until all

samples were collected. Luciferase activity was measured using the Renilla Luciferase Reporter Assay system (Promega) on a TriStar2 LB 942 with 20 μL of cell lysate, 20 μL of substrate and 2 s integration time. Each experiment was performed in quadruplicate. For replicon-transfected cells, both signals were measured using the Dual Luciferase Reporter Assay system (Promega, E1910) following manufacturer's instructions.

Immunoblot. U2OS (3 x 10^6 cells) were grown on 6-well plates for 24 hours. Cells were transfected with 2.5 μg of DNA expression plasmid using jetOPTIMUS® DNA Transfection Reagent (PolyPlus) according to the manufacturer's instructions. At 48 h after transfection, cells were washed with PBS, collected with cell scrapper and pelleted by centrifugation (400g for 5 min). Cell pellets were lysed in Pierce™ IP Lysis Buffer (Thermo Fisher Scientific) containing Halt™ Protease and Phosphatase Inhibitor Cocktail (Thermo Fischer Scientific) for 30 min at 4°C. Equal amount of protein, determined by DC™Protein Assay (BioRad), were prepared in LDS Sample Buffer 4X (Pierce™) containing 25 mM dithiothreitol (DTT) and heated at 95°C for 5 min. Samples were separated on Bolt™ 4-12% Bis-Tris gels in Bolt® MOPS SDS Running Buffer (Thermo Scientific), and proteins were transferred onto a PVDF membrane (BioRad) using the Power Blotter system (Thermo Fischer Scientific). Membranes were blocked with PBS containing 0.1% Tween-20 and 5% non-fat dry milk and incubated overnight at 4°C with primary antibody. Staining was revealed with corresponding horseradish peroxidase (HRP)-coupled secondary antibodies and developed using SuperSignal™ West Dura Extended Duration Substrate (Thermo Fisher Scientific) following manufacturer's instructions. The signals were acquired through Fusion Fx camera (VILBERT Lourmat).

Transmission electron microscopy

Cells were fixed for 24 h in 1% glutaraldehyde, 4% paraformaldehyde, (Sigma, St-Louis, MO) in 0.1 M phosphate buffer (pH 7.2). Samples were then washed in phosphate-buffered saline (PBS) and post-fixed for 1 h by incubation with 2% osmium tetroxide (Agar Scientific, Stansted, UK). Cells were then fully dehydrated in a graded series of ethanol solutions and propylene oxide. Impregnation step was performed with a mixture of (1:1) propylene oxide/Epon resin (Sigma) and then left overnight in pure resin. Samples were then embedded in Epon resin (Sigma), which was allowed to polymerize for 48 hours at 60°C. Ultra-thin sections (90 nm) of these blocks were obtained with a Leica EM UC7 ultramicrotome (Wetzlar, Germany). Sections were stained with 2% uranyl acetate (Agar Scientific), 5% lead citrate (Sigma) and observations were made with a transmission electron microscope (JEOL 1011, Tokyo, Japan).

Immunogold labelling of cryosections

Cells were fixed for 2 hours with 4% paraformaldehyde in phosphate buffer (pH 7.6), washed with PBS (pH 7.6) for 2 x 5 min and centrifuged at 300g for 10 min. After removing the supernatant, cell pellets were included in gelatin 12% and infused with sucrose 2.3 M overnight at 4°C. 80 nm ultra-thin cryosections were made a −120°C on a LEICA FC7 cryo-ultramicrotome. Ultra-thin sections were retrieved with Methylcellulose 2%/Sucrose 2.3 M mixture (1:1) and collected onto formvar/carbon coated nickel grids. After removal of gelatine at 37°C, sections were incubated on drops of either 1:100 anti-nsP3 rabbit serum, anti-Capsid rabbit serum, anti-FHL1 monoclonal or anti-G3BP1 monoclonal antibody diluted in PBS. After six washes of five minutes each, grids were incubated on drops of PBS containing 1:30 gold-conjugated goat anti-rabbit or anti-mouse Ab (6 nm) (Aurion, Wageningen,

Netherlands). Grids were finally washed with six drops of PBS (five minutes each), post-fixed in 1% glutaraldehyde and rinsed with three drops of distilled water. Contrasting step was performed by incubating grids on drops of uranyl acetate 2% / methylcellulose 2% mixture (1:10). The sections were imaged in a transmission electron microscope at 100 kV (JEOL 1011).

Image processing and analysis. All confocal microscopy images were processed and analyzed with ImageJ (version: 2.9.0/1.53t). For aggregate quantification, cell boundaries were traced to delimitate each signal-positive cell. Aggregates' channel was extracted and automatic signal thresholding was applied to locate objects of interest. Images were binarized and Image J "*Analyze particles*" macro was used to quantify aggregates based on size (0.05-5 µm) and circularity (0.01-1) discrimination. For colocalization analysis, images were processed and Pearson's coefficient was calculated using BIOP JACoP plugin as described in https://imagej.net/plugins/jacop).

Statistical analysis. Graphical representation and statistical analyses were performed using Prism 9 software (GraphPad software). Unless otherwise stated, results are shown as mean ± s.e.m. from at least two independent experiments in duplicates. Differences were tested for statistical significance one-way or two-way ANOVA with multiple comparison post hoc test.

REFERENCES

1. Lulla, V. *et al.* Timeliness of Proteolytic Events Is Prerequisite for Efficient Functioning of the Alphaviral Replicase. *J Virol* **92**, e00151-18 (2018).
2. Götte, B., Liu, L. & McInerney, G. M. The Enigmatic Alphavirus Non-Structural Protein 3 (nsP3) Revealing Its Secrets at Last. *Viruses* **10**, 1–26 (2018).
3. Fros, J. J. *et al.* Chikungunya Virus nsP3 Blocks Stress Granule Assembly by Recruitment of G3BP into Cytoplasmic Foci. *Journal of Virology* **86**, 10873–10879 (2012).
4. Gould, E. A. & Higgs, S. Impact of climate change and other factors on emerging arbovirus diseases. *Trans R Soc Trop Med Hyg* **103**, 109–121 (2009).
5. Kril, V., Aïqui-Reboul-Paviet, O., Briant, L. & Amara, A. New Insights into Chikungunya Virus Infection and Pathogenesis. *Annu Rev Virol* **8**, 327–347 (2021).
6. Ahola, T., McInerney, G. & Merits, A. Alphavirus RNA replication in vertebrate cells. *Adv Virus Res* **111**, 111–156 (2021).
7. Jones, R., Bragagnolo, G., Arranz, R. & Reguera, J. Capping pores of alphavirus nsP1 gate membranous viral replication factories. *Nature* **589**, 615–619 (2021).
8. Tan, Y. B. *et al.* Molecular architecture of the Chikungunya virus replication complex. *Sci Adv* **8**, eadd2536 (2022).
9. Laurent, T. *et al.* Architecture of the chikungunya virus replication organelle. *Elife* **11**, e83042 (2022).
10. Chmielewski, D., Schmid, M. F., Simmons, G., Jin, J. & Chiu, W. Chikungunya virus assembly and budding visualized in situ using cryogenic electron tomography. *Nat Microbiol* **7**, 1270–1279 (2022).
11. Gao, Y., Goonawardane, N., Ward, J., Tuplin, A. & Harris, M. Multiple roles of the non-structural protein 3 (nsP3) alphavirus unique domain (AUD) during Chikungunya virus genome replication and transcription. *PLoS Pathog* **15**, e1007239 (2019).
12. Shin, G. *et al.* Structural and functional insights into alphavirus polyprotein processing and pathogenesis. *Proc Natl Acad Sci U S A* **109**, 16534–16539 (2012).
13. Meshram, C. D. *et al.* Multiple Host Factors Interact with Hypervariable Domain of Chikungunya Virus nsP3 and Determine Viral Replication in Cell-Specific Mode. *J. Virol.* (2018) doi:10.1128/JVI.00838-18.
14. Jumper, J. *et al.* Highly accurate protein structure prediction with AlphaFold. *Nature* **596**, 583–589 (2021).
15. Fang, Q. *et al.* Structural morphing in a symmetry-mismatched viral vertex. *Nat Commun* **11**, 1713 (2020).
16. Johnson, S. *et al.* Symmetry mismatch in the MS-ring of the bacterial flagellar rotor explains the structural coordination of secretion and rotation. *Nat Microbiol* **5**, 966–975 (2020).
17. Kim, D. Y. *et al.* New World and Old World Alphaviruses Have Evolved to Exploit Different Components of Stress Granules, FXR and G3BP Proteins, for Assembly of Viral Replication Complexes. *PLoS Pathog.* **12**, e1005810 (2016).
18. Remenyi, R. *et al.* Persistent Replication of a Chikungunya Virus Replicon in Human Cells Is Associated with Presence of Stable Cytoplasmic Granules Containing Nonstructural Protein 3. *J. Virol.* **92**, (2018).
19. Bartholomeeusen, K. *et al.* A Chikungunya Virus trans-Replicase System Reveals the Importance of Delayed Nonstructural Polyprotein Processing for Efficient Replication Complex Formation in Mosquito Cells. *J Virol* **92**, e00152-18 (2018).

20. Vasiljeva, L. *et al.* Regulation of the sequential processing of Semliki Forest virus replicase polyprotein. *J Biol Chem* **278**, 41636–41645 (2003).
21. Meertens, L. *et al.* FHL1 is a major host factor for chikungunya virus infection. *Nature* **574**, 259–263 (2019).
22. Zheng, Y. & Kielian, M. Imaging of the alphavirus capsid protein during virus replication. *J Virol* **87**, 9579–9589 (2013).
23. Banani, S. F., Lee, H. O., Hyman, A. A. & Rosen, M. K. Biomolecular condensates: organizers of cellular biochemistry. *Nat Rev Mol Cell Biol* **18**, 285–298 (2017).
24. Brown, R. S., Anastasakis, D. G., Hafner, M. & Kielian, M. Multiple capsid protein binding sites mediate selective packaging of the alphavirus genomic RNA. *Nat Commun* **11**, 4693 (2020).
25. Kandiah, E. *et al.* CM01: a facility for cryo-electron microscopy at the European Synchrotron. *Acta Crystallogr D Struct Biol* **75**, 528–535 (2019).
26. de la Rosa-Trevín, J. M. *et al.* Scipion: A software framework toward integration, reproducibility and validation in 3D electron microscopy. *J Struct Biol* **195**, 93–99 (2016).
27. Punjani, A., Rubinstein, J. L., Fleet, D. J. & Brubaker, M. A. cryoSPARC: algorithms for rapid unsupervised cryo-EM structure determination. *Nat Methods* **14**, 290–296 (2017).
28. Mirdita, M. *et al.* ColabFold: making protein folding accessible to all. *Nat Methods* **19**, 679–682 (2022).
29. Schuffenecker, I. *et al.* Genome microevolution of chikungunya viruses causing the Indian Ocean outbreak. *PLoS Med.* **3**, e263 (2006).
30. Levitt, N. H. *et al.* Development of an attenuated strain of chikungunya virus for use in vaccine production. *Vaccine* **4**, 157–162 (1986).
31. Kümmerer, B. M., Grywna, K., Gläsker, S., Wieseler, J. & Drosten, C. Construction of an infectious Chikungunya virus cDNA clone and stable insertion of mCherry reporter genes at two different sites. *J. Gen. Virol.* **93**, 1991–1995 (2012).
32. Bolte, S. & Cordelières, F. P. A guided tour into subcellular colocalization analysis in light microscopy. *Journal of Microscopy* **224**, 213–232 (2006).

ACKNOWLEDGMENTS

A.A.’s lab received fundings from the French Government’s Investissement d’Avenir program, Laboratoire d’Excellence “Integrative Biology of Emerging Infectious Diseases” (grant n°ANR-10-LABEX-62- IBEID), the Fondation pour la Recherche Medicale (FRM équipe - EQU202003010193), the Agence Nationale de la Recherche (project CHIKHOST ANR-20-CE15-0029, project COALITION ANR-20-CE92-0054 and project CHIK MacANR-22-CE11 0023), INSERM transfert and l’Association Française pour la Myopathie (AFM, grant *23270)*. J.R ’s team was supported by grants of the Agence Nationale de la Recherche (project CHIKmac ANR-22-CE11-0023-01 and project CoMemRep ANR-20-COV3-0004) and the Fondation Bettencourt Shueller (AGDI-531281), ATIP-Avenir grant (CNRS/INSERM). B.M.K received funding from the Deutsche Forschungsgemeinschaft (DFG, German Research Foundation, Project ID 369799452-TRR237). We thank the European Synchrotron Radiation Facility for provision of beam time on CM01. We used the Integrated structural biology facility (PBSIM) at the AFMB supported by French Infrastructure for Integrated Structural Biology (FRISBI) (ANR-10-INBS-0005). V.K is supported by a fellowship from University de Paris Cité. A.K. is supported by a CENTURI PhD fellowship financed by "Investissements d’Avenir" program (ANR-16-CONV-0001) and from Excellence Initiative of Aix-Marseille University - A*MIDEX. The authors are grateful Andres Merits (University of Tartu, Estonia) for providing us anti-nsP1-4 antibodies and CHIKV P1234 plasmids. The authors thank Olivier Schwartz, Alessia Zamborlini and all the Amara’s and Reguera ‘s lab for critical readings of the manuscript and helpful discussions.

AUTHORS' CONTRIBUTIONS

A.A and J.R designed and coordinated the research. VK performed all the infection and functional studies. V.K generated and characterized the FLAG-tagged nsP3, AUD plasmids and lentiviruses. V.K performed RNA-FISH experiments, confocal microscopy, image processing and analysis and western blot studies. M.H. carried out the data collection, processing and volume reconstructions with the input of A.D. for helical reconstruction. L.M and J.B.G performed the first experiments that allowed the identification of nsP3 tubes in CHIKV-infected cells. L.M participated in the functional and infection studies and manuscript preparation. L.C produced and titrated the CHIKV and alphavirus stocks used in this work. C.A generated the *in vitro* transcribed CHIKV viral RNA and participate in the transfection experiments and infection studies. J.B.G and P.R. performed the EM experiments. A.T and B.M.K. generated the CHIKV RLuc molecular clones. R.J and C.Z isolated, identified and biochemically characterized the nsP3 tubes. A.K. produced the nsP3 mutants in Hi-5cells and performed the *in vitro* assembly studies. D.P. vitrified the samples for cryo-EM. J.R did the model building, analysis and refinement. V.K, A.A. and J.R. wrote the initial manuscript draft and the other authors contributed to its editing in its final form.

COMPETING INTEREST STATEMENT: The authors declare no competing financial interests.

MATERIAL & CORRESPONDENCE. Requests should be addressed to Dr Ali Amara (ali.amara@inserm.fr) and Dr Juan Reguera (juan.reguera@inserm.fr)

B. Deciphering the molecular mechanisms of the FHL1-nsP3 interaction and its implications in CHIKV infection replication

This chapter aims to provide insights into the molecular mechanisms by which FHL-1 mediates CHIKV infection. The first part of this work aims to characterize the structural basis of FHL1 nsP3 interaction. NMR studies performed by Andrès Ferrino Irirarte, François Bontems, and Félix Rey at the Pasteur Institute showed that FHL1 interacts with a 69 amino acid long sequence within the CHIKV nsP3 HVD that overlaps with the binding sites of BIN-1 and CD2AP, two other host factors involved into CHIKV cycle. Functional investigations indicate that the R5 region fails to interact with FHL1 and is important for CHIKV infection.

The second part investigates FHL1 usage by pathogenic and non-pathogenic CHIKV strains and dissects the molecular mechanisms involved in its proviral effect. Our data showed that FHL1 is an important CHIKV host dependency factor. All the CHIKV strains are highly dependent on FHL1 in primary fibroblasts, one of the main CHIKV target cells. FHL1 acts at a post-entry step of the viral life cycle and plays a distinct function from that of G3BP during CHIKV RNA amplification. However, the molecular details still remain to be elucidated.

Finally, the third part of the study aims to investigate whether FHL1 could act as an adaptor protein that recruits additional host factors for optimal infection. The FHL1 affinity purification approach, followed by mass spectrometry analysis, gave us interesting insights into FHL1 interactome in the context of infection. We found that FHL1 interacts with components of the actin-cytoskeleton (spectrins, myosins, actin-binding proteins) and antimicrobial immunity regulators (HERC5, PKR). Functional validation by siRNA screen identified the SPTBN1 protein (beta spectrin) as a potential CHIKV dependency factor, whose role must be further validated.

1) Results

a. Structure of the nsP3 HVD/FHL1 interactions by Nuclear Magnetic Resonance *(Dr. Andres Ferrino Iriarte, Dr. François Bontems and Pr. Felix Rey)*

Our previous data identified a specific 30 amino acid region (residue 424 to 456, named *R4* in the study) important for FHL1 nsP3 HVD interaction (Figure 1A). A recent NMR study performed by another group (Lukash et al. 2020) confirms our data and indicates that FHL1-binding domains overlap with one CD2AP-interacting motifs (PMASVR amino acid motif). To validate the importance of the R4 sequence CHIKV infection, we generated, in collaboration with Dr Beate M. Kümmerer (Institute of Virology, University of Bonn Medical Centre, Bonn, Germany), a CHIKV molecular clone harboring mutation in nsP3 R4 region (ΔR4 and R4*) (Figure 1) and investigate their replicative properties in FHL1-positive and KO cells. Figure 1 shows that ΔR4 and R4* viruses could replicate to some extent in WT cells, albeit at not WT level (Figure 1B). In contrast, WT, ΔR4, and R4* replication was strongly impaired in FHL1^{KO} (Figure 1B). These results showed that the R4 region is important but not critical to mediate CHIKV replication in 293T cells. This suggests that the FHL1-binding motif extends beyond the R4 regions.

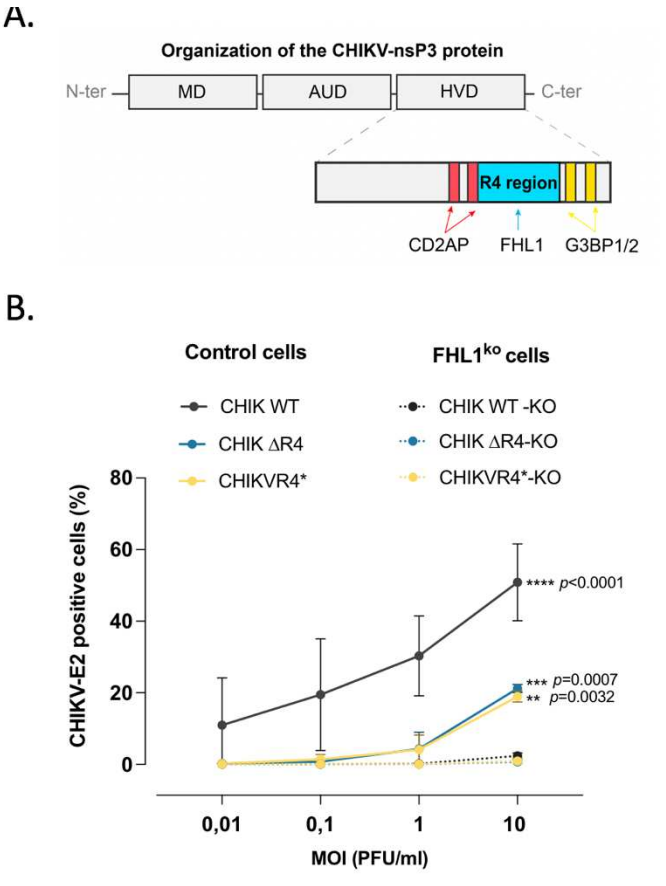

Figure 1. Impact of FHL1-binding site deletion or mutation on CHIKV replication in human cells. *A. Schematic presentation of FHL1-interacting site localization on the nsP3-HVD domain. B. E2 protein expression in control or FHL1^{KO} cells infected with the WT, ΔR4, and R4* at different MOIs. Data are mean ± s.d. n = 2 independent experiments performed in duplicate*

To gain further insights into FHL1-nsP3 interaction, our lab has started collaborating with Pr Félix REY 's lab to solve the structure of the FHL1-nsP3 complex. X-ray crystallography is not straightforward because the nsP3 HVD is unstructured, and FHL1 is organized as a chain of beads, with each LIM domain connected flexibly to its flanking domains. Proteins of this type cannot form well-ordered crystals diffracting X-rays sufficiently well. The strategy was to use Nuclear Magnetic Resonance (NMR) to characterize any potential interaction of the individual LIM domains with the HVD. The experiments described below were performed by Dr. Andres Ferrino Iriarte and Dr. Francois Bontemps in Pr Félix Rey's laboratory. Applied to protein analysis, the two-dimensional NMR ^{1}H-^{15}N-HSQC method correlates the chemical shift of a ^{15}N atom from a given residue's backbone amide group to the chemical shift of its directly bound proton. Chemical shift, expressed in part per million (ppm), is the difference in resonant frequencies of two nuclei of a molecule. The chemical shift value of each nucleus is specific and depends on the local molecular and electron environment. The obtained 2D spectrum is a diagram of peaks, each peak representing the ^{15}N—^{1}H of a unique amino acid of the protein. Further complex analysis is required to assign the protein's NMR signals (spectrum peaks) to specific residues. Based on this, the same information can be extracted for a given protein in complex with its known ligand. In the obtained spectrum, chemical shift perturbations are observed for each residue involved in the ligand interaction. Thus, one can identify the interacting interface of two proteins by comparing the free- or apo-and bound-state 2D 1H-15N HSQC spectra. Figure 2A (right panel) reports the 2D ^{1}H-^{15}N HSQC spectrum of CHIKV HVD in a free state and (left panel) the assigned HVD residues to each peak. The acquisition of the same spectrum but in the presence of increasing concentrations of full-length FHL1 (called titration experiments) demonstrated that 69 HVD amino acids, spanning from residue 390 to residue 458, are involved in this interaction (Figure 2C). Interestingly, NMR data shows that this region (called now R5 region) is even bigger than we and Lukash et al. 2020 identified and also overlaps with the BIN1/Amph2-and CD2AP-binding motifs.

Finally, by performing the same titration experiments with the individual LIM domains of FHL1 instead of the entire protein, it was demonstrated that each LIM domain interacts with around 15 HVD amino acids in an antiparallel manner (Figure 2C).

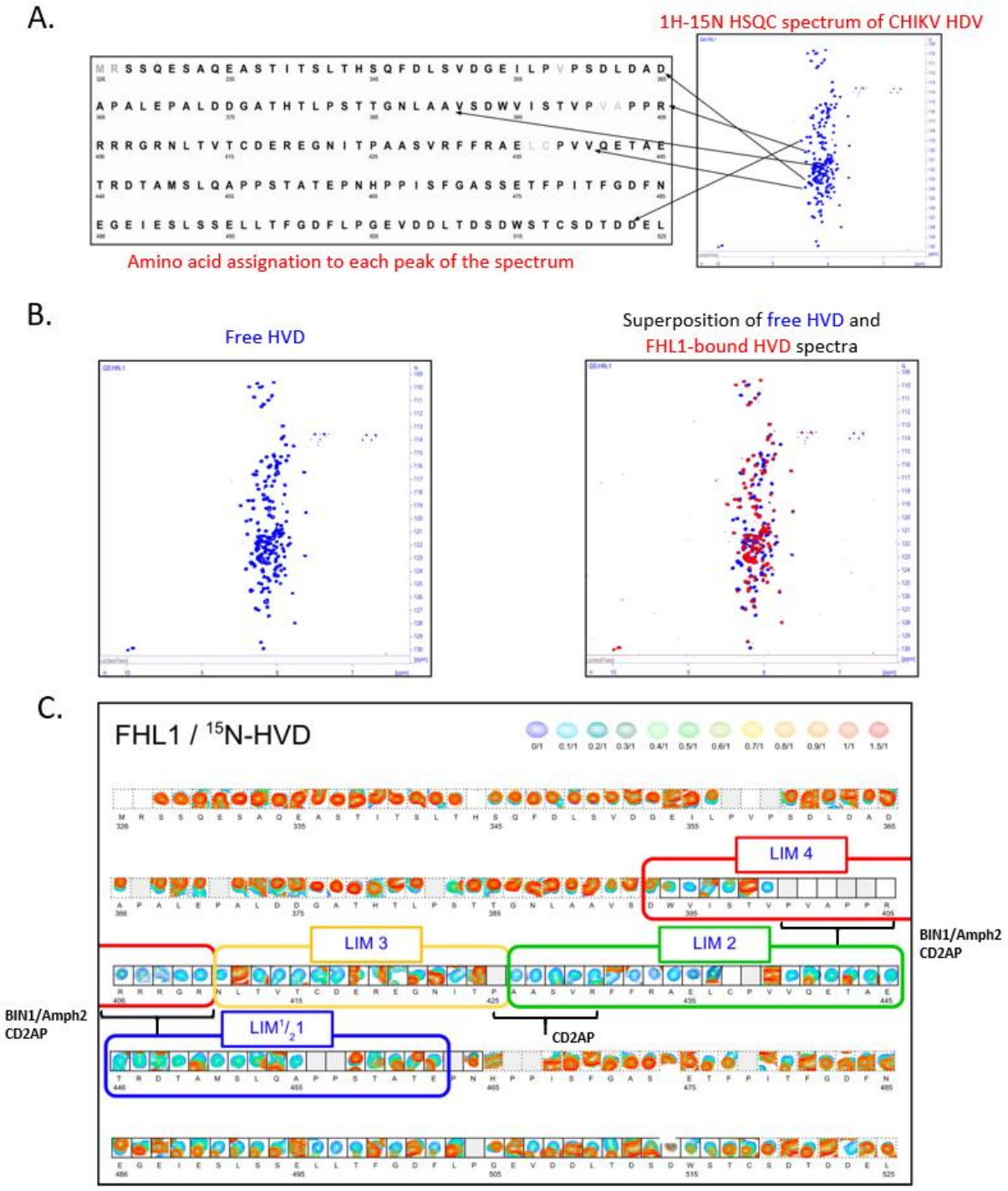

Figure 2: FHL1-interacting region on CHIKV HVD cover the R4 sequence, as well as CD2AP and BIN1/Amph2 binding motifs. *The precise residues involved into FHL1 interaction were revealed by NRM-2D ^{1}H-^{15}N HSQC approach. A. Free-state HVD ^{1}H-^{15}N HSQC spectrum is shown on the left. A specific residue of the HVD sequence was assigned to each peak of the spectrum (right). B The same spectrum is shown on the left. Superposition of free-state HVD and HVD plus full length FHL1 spectra, demonstrating chemical shift perturbation of residues involved into the interaction (right). C. Superposition of all spectra obtained from the titration experiments with increasing concentrations of FHL1. HVD residues interacting with each LIM domain of FHL1 are mapped.* ***All the experiments and corresponding results are adapted from Andres Ferrino Iriarte PhD thesis.***

b. Impact of the FHL-1 binding region on CHIKV infection (*work performed by Dr Céline Amadori, post-doctoral researcher in Amara's lab)*

We then performed functional experiments to validate that the R5 region is important for nsP3/FHL1 interaction. Since immunoprecipitation assays were inconclusive in our hands, we chose another experimental approach based on the ability of nsP3 to recruit FHL1 and the other host factors into large cytoplasmic aggregates, easily observed by microscopy. U2OS cells were transiently transfected with a pcDNA3.1 expression vector encoding WT or ∆R5 CHIKV nsP3. 48 hours post-transfection, cells were fixed and co-stained with anti-nsP3 and anti-FHL1 or anti-G3BP1 specific antibodies. Since we know that both FHL1 and G3BP1 are recruited to nsP3 cytoplasmic granules, we assumed that if nsP3 ∆R5 is no longer able to mediate FHL1-binding, the subcellular localization of the cellular protein will remain unchanged, whereas G3BP1 recruitment to nsP3-cytoplasmic aggregates will be preserved. Indeed, the immunofluorescence experiments showed that nsP3-∆R5 can still form aggregates, colocalizing with G3BP1 (Figure 3B), but can no longer recruit FHL1 (Figure 3A).

To evaluate the importance of the R5 sequence in CHIKV replication, we generated a CHIKV Renilla luciferase (CHIKV-Rluc) molecular clone deleted for the R5 region (collaboration with Beate Kummerer). In vitro, transcribed RNA from WT, ∆R5, and the replication-dead (GAA) CHIKV were transfected into several cell lines: U2OS, 293T, Vero, and BHK21. Their ability to replicate was monitored by quantifying the Renilla luciferase activity in cell lysates 48 hours post-transfection (Figure 3C). When compared to the WT, the replication of the ∆R5 CHIKV virus was dramatically impaired in two human FHL1-expressing cell lines tested, U2OS and 293T cells. The same phenotype was observed in Vero cells which lack FHL1 but express FHL2 (Lukash et al., 2020). We can't rule out the possibility that the R5 region also recruits FHL2, explaining why the ∆R5 virus failed to efficiently replicate in these cells. We can neither exclude the possibility that in Vero cells, the ∆R5 virus also depends on BIN1, CD2AP, or additional host factors to replicate. Finally, both WT and ∆R5 viruses efficiently propagated in BHK21, a hamster cell line that expresses very low levels of FHL1 and FHL2.

These results showed that the R5 motif is involved in recruiting FHL1 to nsP3 foci, but it is not a prerequisite for nsP3 aggregation. This region is also required for CHIKV replication in cells expressing FHL proteins.

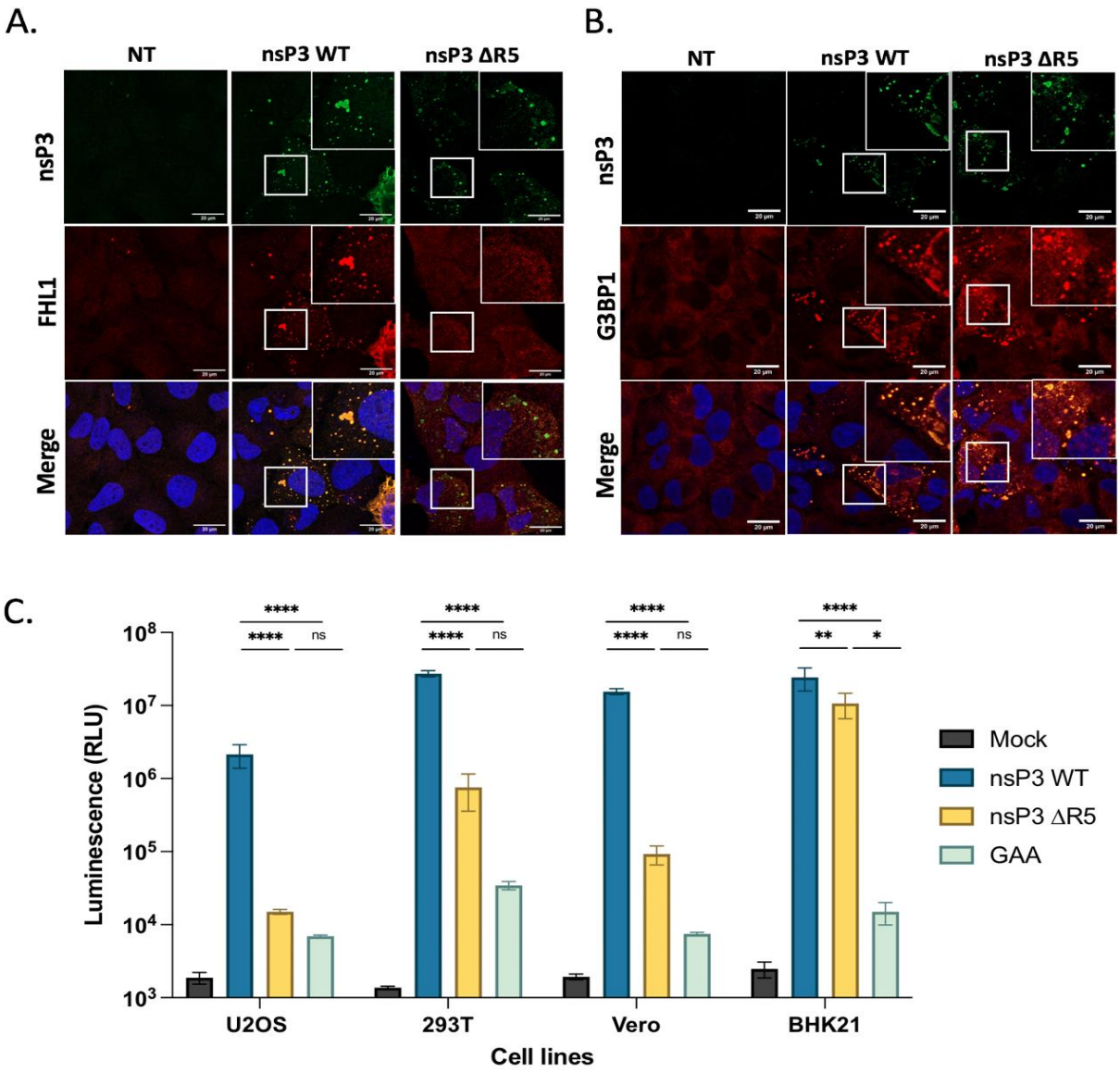

Figure 3: HVD-R5 motif is involved into FHL1 recruitment to nsP3 complexes and in CHIKV infection in different cell types. *A, B, U2OS cells were transfected with pcDNA 3.1 plasmids expressing either WT or ΔR5 CHIKV-nsP3 for 24 hours. Subcellular localization of nsP3 and endogenous FHL1 (A) or G3BP1 (B) was analyzed following specific antibody staining and immunofluorescence images acquisition with a confocal LSM800 Zeiss microscope. C, Different cell lines were transfected with CHIKV-Renilla luciferase molecular clones harboring either WT or mutant ΔR5 nsP3 sequence. Viral replication was monitored at 48h post-transfection. CHIKV harboring defective nsP4 (GDD-to-GAA mutation) was used as replication-dead control. Data are mean ± s.e.m. n = 2 independent experiments performed in quadruplicate. Two-way ANOVA with a Dunnett's multiple comparison test (****P<0.0001, **P<0.0039, *P<0.02).*

c. FHL1 usage by CHIKV strains

In this section, we have investigated the FHL1 usage by a panel of CHIKV strains in a cell line edited or not for FHL1 expression or in immortalized human fibroblasts derived from an EDMD patient harboring FHL1 deficiency (collaboration with Dr Gisele Bonne, Institut de Myologie, La Pitié Salpétrière, Paris) (Figure 4A). To that purpose, cells were infected with CHIKV strains belonging to the Asian lineage (strain St Martin H20235,2013), the East, Central, and South African (ECSA) lineage (strains Ross and Brazza (MRS1 2011), the Indian Ocean lineage (Reunion island epidemic CHIK21 strain) as well as the sylvatic West Africa enzootic lineage (strain M-899) and the attenuated 181/25 (Asian lineage, attenuated strain) for 24h at different MOIs (Figure 4B). Viral infection was monitored by flow cytometry following cell fixation and CHIKV envelope E2 protein immunostaining (Figure 4B, C). In both cell types, the epidemic CHIKV 21 strain (Indian Ocean lineage) and attenuated 181/25 (Asian lineage, attenuated strain) exert the highest replication level as at the highest MOI, more than 60 % of control cells were efficiently infected. St Martin and Brazza CHIKV strains, which belong to the Asian and ECSA lineage, respectively, showed a delay in the infection as less than 40% of control cells were infected at the highest MOI (Figure 4B, C). Finally, the West Africa lineage strain, isolated from the *Aedes furcifer* mosquito, showed a plateau of infection with a maximum of 40% of cells infected at 48h (MOI 0.016). This could be explained by the fact that the West Africa strain didn't circulate within the human population. Depletion of FHL1 in the two cellular contexts leads to a drastic reduction of CHIKV infection (Figure 4B, C). This phenotype was more pronounced for the epidemic CHIKV 21 strain, for which less than 2% of FHL1 deficient cells were infected at saturation in control cells. All the strains efficiently infect primary fibroblasts, but their replicative capacities were strongly affected in fibroblasts lacking FHL-1 expression (Figure 4C). The attenuated 181/25 strain can still replicate in $FHL1^{KO}$ HAP-1 cells but to a significantly less extent than in WT cells. Finally, as reported in our previous study, the West African strain also demonstrated a reduced dependency on FHL1 in HAP1 cells (Meertens et al. 2019 see in annex).

Our data confirm that FHL1 is important for CHIKV infection, particularly in human fibroblasts, one of the main immunocompetent cells targeted by the virus. FHL1 seems also to be differentially used by pathogenic and non-pathogenic CHIKV strains. For instance, the CHIKV-21 strain isolated from a patient infected during the

2005–2006 CHIKV outbreak on Reunion Island highly depends on FHL1 for infection in vitro and induces severe muscular pathology in mice (Meertens et al. 2019). Conversely, the requirement for FHL1 was less pronounced for the sylvatic CHIKV 37997 strain from the West African genotype or the attenuated CHIKV 181/25 strain (Lukas et al. 2021), which are less pathogenic in mice (see discussion).

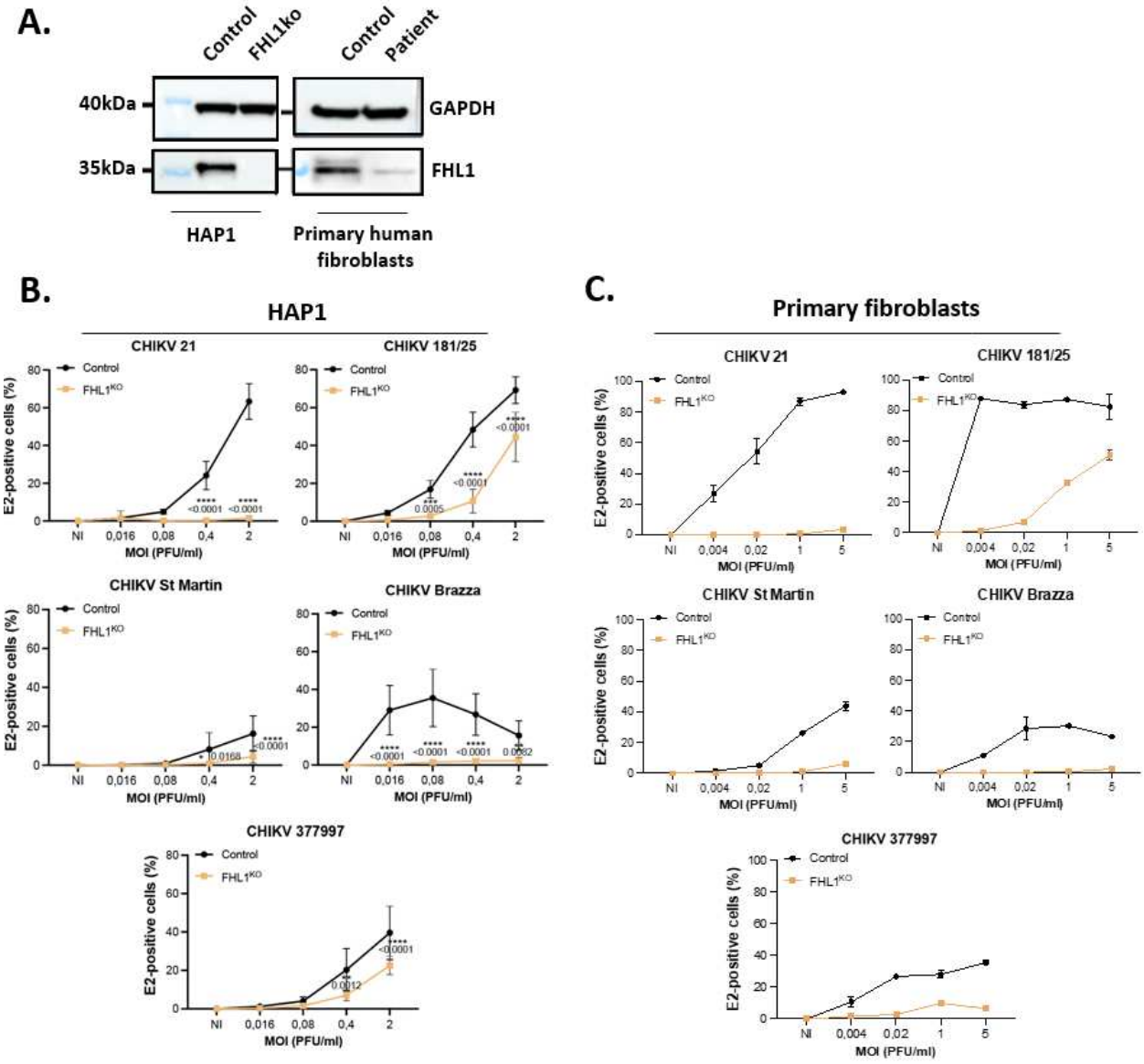

Figure 4: CHIKV dependency on FHL1 varies between the viral strains in human cells. *A. Westernblot validation of FHL1 expression in control and FHL1KO HAP1 cell lines, and in control or patient primary human fibroblasts suffering from a fhl1-gene mutation leading to a drastic decrease of protein expression. B. HAP1 control and FHL1 KO cells and C. control and primary human fibroblasts were infected for 24h with different CHIKV strains at different multiplicity of infection (MOIs). For HAP1 cells, data are mean infection mean ± s.d. n = 3 independent experiments performed in duplicate. One-way ANOVA with a Dunnett's multiple comparison test. For fibroblasts infection, only one experiment was performed in duplicate. CHIKV 21 (Reunion Island epidemic, IOL lineage), Saint Martin (Asian lineage), Brazza (ECSA lineage), 181/25 (attenuated CHIKV strain from Asian*

d. Impact of FHL1, G3BPs, CD2AP and BIN-1 depletion on CHIKV infection

As introduced in the previous chapter, the nsP3 HVD domain is an interacting module that recruits several host factors, including FHL1, DHX9, SH3-domain containing proteins such as Bin1/Amphiphysin 2 and CD2AP, Ras GTPase-activating protein-binding protein 1 and 2 (G3BP1 and G3BP2) and Nucleosome Assembly Protein 1 Like 1 and 4 (NAP1L1 and NAP1L4) (Figure 5A). HVD mutagenesis and structural NMR studies allowed the mapping of some of these host factors with the HVD (Meertens et al. 2019; Agback et al. 2019; Neuvonen et al. 2011; Tossavainen et al. 2016; Schulte et al. 2016; Dominguez et al. 2021), however, except for FHL1 and G3BPs, the contribution of these molecules in CHIKV infection is unclear. NMR and biochemical studies suggested that CD2AP and FHL1 could form a tripartite interacting complex in vitro (Lukash et al. 2020), but no cooperative effect was observed between CD2AP and FHL1-binding (Lukash et al. 2020).

To obtain further insights into FHL1, CD2AP, and Bin1 function in CHIKV infection, we generated human HAP1 knockout cells for each host cell factor, and gene editing was validated by western blot (Figure 5B). Intriguingly, whereas FHL1, CD2AP, or Bin1 knockout didn't affect the expression of the other proteins, knockout of both G3BP1 and G3BP2 genes visibly reduced the expression of Bin1/Amph2 and FHL1. A similar phenotype was observed in U2OS cells knocked out for the expression of both G3BP1 and 2, where FHL1 protein expression was drastically reduced (data not shown). Cells were infected with CHIKV 21 for 24h. Viral infection was monitored by FACS using the anti-E2 monoclonal antibody (Figure 5C). Infection curves demonstrated that CD2AP depletion alone didn't impact CHIKV replication when compared to FHL1- or G3BP1/2 knockout cells. However, at the highest MOI (MOI of 10 and 20), viral infection was observed in FHL1 knock-out cells, whereas CHIKV was not viable in G3BP1/2 ko cells. Double depletion of FHL1 and CD2AP had a slight additive effect compared with $FHL1^{KO}$ cells. Finally, BIN1/Amph2 depletion demonstrated a slight but significant reduction (roughly 20%) in CHIKV E2 production. A triple FHL1/CD2AP/BIN1 depletion is ongoing, and it remains to be characterized. Notably, NAP1L1/L4 knockout cells couldn't be generated as the depletion of these factors exerts a cytotoxic effect. Thus, the contribution of NAP1 during CHIKV infection is difficult to investigate.

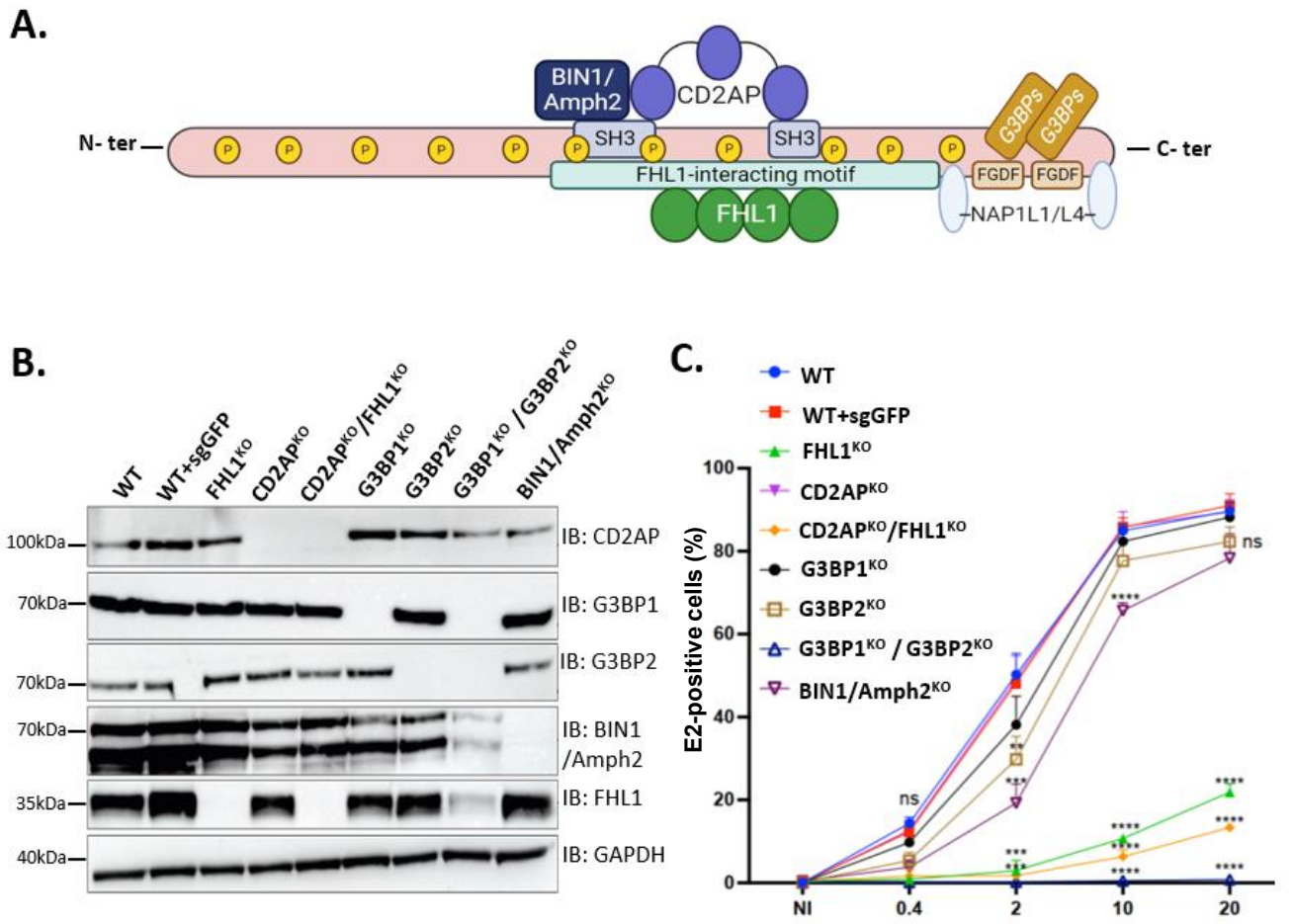

Figure 5: FHL1 and G3BPs depletion dramatically impair CHIKV replication in HAP1 cells. A*, schematic presentation of CHIKV nsP3-HVD with mapped host-factors binding sites. CD2AP protein bind to two distinct SH3 domains, overlapping BIN1 and FHL1-binding sites. G3BPs bind to two FGDF motifs in the very C-terminal part of the HVD. NAP1L1/L4 binding motifs are found on both sides of G3BPs-binding sites. Phosphorylation sites are scattered across the HVD domain and likely influence host factors binding.* ***B****, Westernblot analysis of HVD- interacting host factors expression in control and knockout HAP1 cell lines.* ***C****, control and knockout HAP1 cells were inoculated with CHIKV21 for 24 hours at different multiplicity of infection (MOI). Viral infection was monitored by FACS following E2-protein specific staining. Data are mean ± s.d. n = 3 independent experiments performed in duplicate. One-way ANOVA with Tukey's multiple comparison test. ****P < 0.0001. P, phosphorylation site; BIN1/Amph2, Bridging Integrator-1 et Amphiphysin-2; CD2AP, CD2-associated protein; FHL1, Four-and-a-half LIM domain protein 1; G3BPs, RasGAP SH3 domain–binding proteins; FGDF, G3BPs-binding site NAP1L1/L4, Nucleosome assembly protein 1-like 1 and 4.*

e. Distinct roles of FHL1 and G3BPs during CHIKV infection

To dissect the role played by FHL1 and G3BPs during CHIKV infection, we transfected *in vitro* transcribed full-length CHIKV RNA or CHIKV replicon RNA in WT, FHL1^{KO,} or G3BP^{KO} HAP-1 cells (Figure 6A). CHIKV replicons are alphavirus mini-genomes lacking structural proteins. They harbor only the viral replicative machinery and can't spread in contrast to the full-length RNA genome. Full-length CHIKV and CHIKV replicon RNA molecules used in this study encode a luciferase reporter gene inserted into the C-terminal part of nsP3-HVD to monitor RNA amplification as a function of time. Without FHL1 or G3BPs, the transfected full-length CHIKV RNA molecule failed to propagate efficiently compared to WT HAP-1 cells. These results confirmed that both FHL1 and G3BPs act at a post-entry step and are important for establishing efficient viral replication and amplification. In cells transfected with the CHIKV replicon system, efficient replication was observed in FHL1^{KO} cells, albeit at significantly lower levels than in WT cells (Figure 6B). In contrast, no viral replication was observed in G3BPs^{KO} cells (Figure 6B). These data suggested that G3BPs are directly involved in the priming of the replication process. Indeed, the negative impact of G3BPs depletion is observed as soon as 4h post-transfection. It is possible that G3BPs are required for the establishment of viral replication complexes and further RNA synthesis. In contrast, a slight but significant reduction of viral amplification was observed in FHL1^{KO} cells but after 6h post-transfection, suggesting a distinct proviral function during CHIKV replication. Interestingly, our previously published results demonstrated that the synthesis of the replicative dsRNA intermediate, required for the synthesis of new positive genomes, was drastically impaired in FHL1^{KO} cells compared to WT cells at 6 hours post-infection. It is of great importance to note that the alphavirus replicative cycle is very rapid (Reis et al. 2022; Singer et al. 2021). Indeed, dsRNA synthesis occurs as soon as 1h post-entry, and the first viral particles are released around 3h post-infection (Reis et al. 2022; Singer et al. 2021). This suggests that at 6h post-infection, viral replication complexes are already formed. One hypothesis could be that FHL1 is not required for replicative complex formation and RNA synthesis, but it indirectly controls viral genome synthesis.

Confocal experiments were done in CHIKV-infected fibroblasts at 7 pi, great proximity of nsP3 and G3BP1-stainings, and partial colocalization with vRCs (detected here using dsRNA-specific antibody) (Figure 6C). G3BPs and nsP3 also form cytoplasmic granules in infected cells that do not contain viral dsRNA intermediate

and, thus, are inactive vRCs. In contrast, FHL1-staining didn't clearly co-localize with dsRNA on the plasma membrane, suggesting that it is not recruited on vRC or that very few FHL1-molecules are localized within the vRC and could not be detected by confocal microscopy. This is also an indirect argument suggesting a distinct role of FHL1 and G3BP during CHIKV infection.

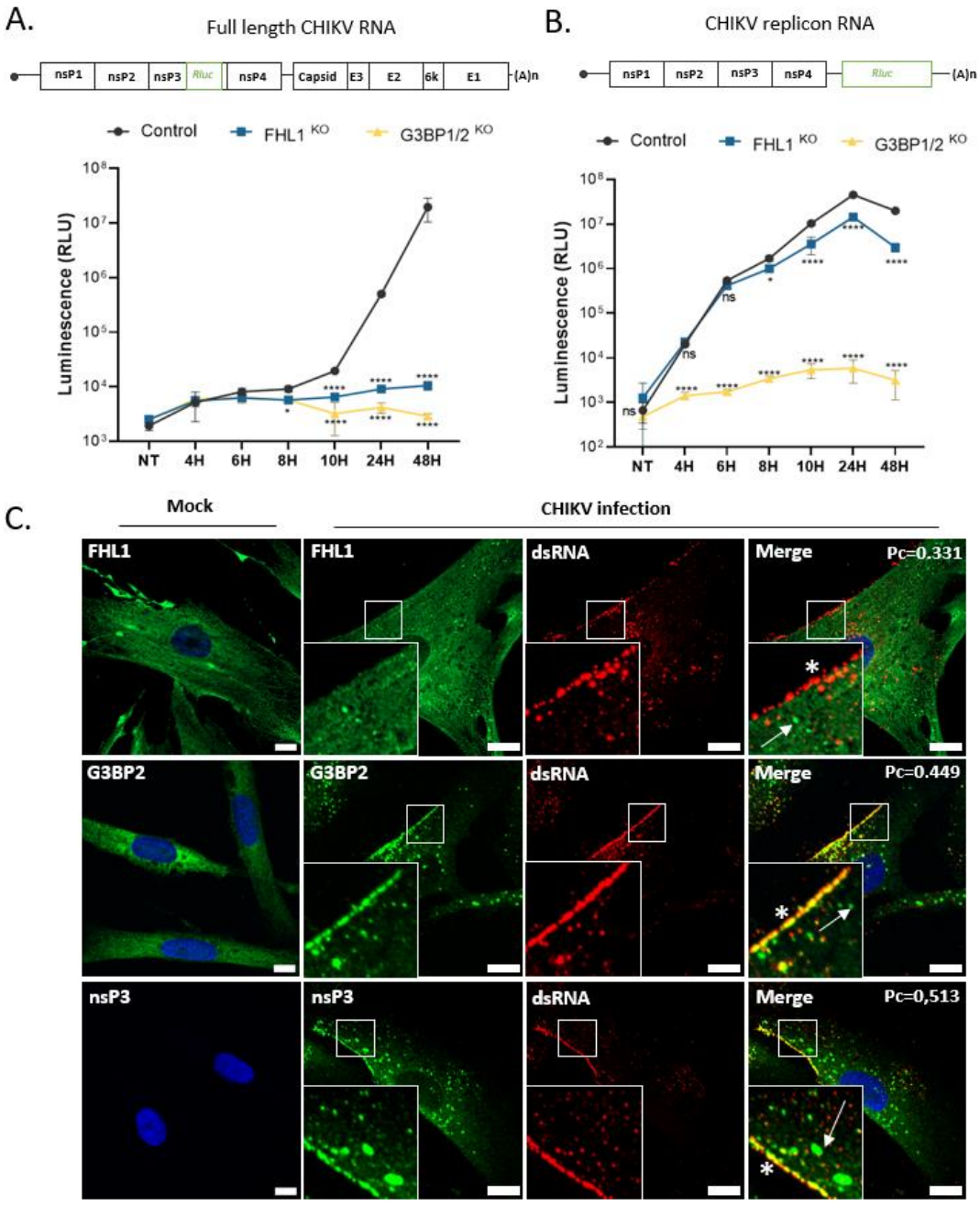

Figure 6: FHL1 and G3BPs play distinct role during CHIKV replication cycle. A*, Control, FHL1KO and G3BPs KO HAP1 cells were transfected with in vitro transcribed full-length CHIKV molecular clone encoding a Renilla luciferase reporter gene, inserted in the C-terminal part of the HVD. Viral replication is monitored through the Rluc activity at the indicated time points* ***B****, the same cells were transfected with in vitro transcribed CHIKV replicon molecule, expressing Rluc through the subgenomic viral promoter. Rluc activity reflecting viral replication was monitored at the indicated time points. RLU, relative light units.* ***C****, immortalized human dermal fibroblasts were inoculated with CHIK21 strain at MOI 100 for 7 hours. Colocalization of FHL1, G3BP2 or nsP3 with viral replication complexes was assessed following protein staining with specific antibody staining, and viral replication complexes were stained with anti-dsRNA monoclonal antibody. Representative images were obtained by confocal microscopy using LSM800 Zeiss microscope. Co-localization analysis were performed*

We then investigated the impact of FHL1 and G3BP depletion on nsP3-protein expression and subcellular localization (Figure 7). For this, we stably express the 3XFlag version of nsP3 in WT, FHL1 ^{KO,} or G3BP^{KO} cells. FHL1 and G3BP1/2 proteins' expression was analyzed by western blot. It is important to note that WT HAP1 cells expressing nsP3 exerted a reduced FHL1 band on the western blot (Figure 7A). Conversely, in FHL1^{KO} cells, nsP3-band was of greater intensity. Altogether, these results reasonably suggested that co-expression of FHL1 and nsP3 lead to the formation of protein complexes insoluble in standard lysis-buffer conditions. Finally, as observed previously (data not shown), double knockout of G3BP1/2 proteins leads to reduced FHL1 expression in mock-transfected cells (Figure 6A). This phenotype was not cell clone-specific as all the double G3BP1/2 ^{KO} HAP1 clones obtained exerted a reduction in FHL1 expression (data not shown). Moreover, the same phenotype was observed in G3BP1/2^{KO} U2OS cells (data not shown). This phenotype has never been discussed in CHIKV literature before, although double G2BP1/2 ^{KO} cell lines such as U2OS are widely used in Alphavirus research. Altogether, in these experimental conditions, we can't conclude about a putative role of FHL1 in nsP3-expression or stability. Then, we evaluated nsP3 subcellular localization in WT, FHL1 ^{KO,} or G3BP^{KO} cells by confocal microscopy. In all three nsP3-expressing cell lines, nsP3-cytoplasmic granules were observed, suggesting that nsP3 is expressed and the protein's subcellular localization was preserved in the absence of both FHL1 and G3BP1/2 factors (Figure 6B). Altogether, these data suggest that FHL1 is not involved in nsP3 stability or cytoplasmic aggregation process. However, we can't rule out the possibility that FHL1 proviral role is linked to the nsP3 cytoplasmic granules.

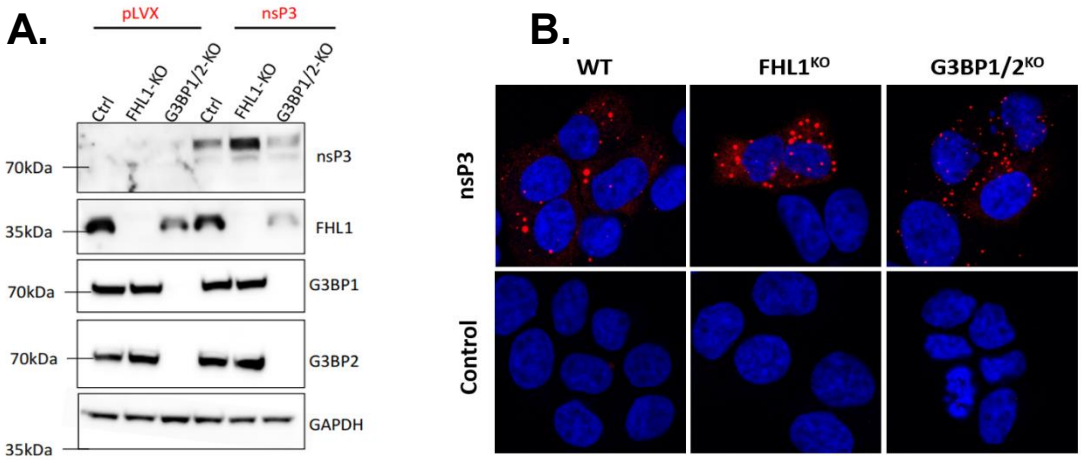

Figure 7: FHL1 is possibly involved into nsP3 aggregates formation in infectious conditions. *A. nsP3-protein expression in WT, FHL1KO and G3BP1/2KO HAP1 cells stably expressing CHIKV-nsP3. B. The same cells were analyzed by immunofluorescence to assess nsP3 cytoplasmic aggregates formation in absence of FHL1 or G3BP1/2 proteins.*

f. Mapping FHL1 interactome during CHIKV infection

FHL1 contains four-and-a-half highly-conserved LIM domains, each having two zinc fingers arranged in tandem. LIM domains typically act as a conserved scaffold for multi-protein complex assembly (actin cytoskeleton organization, activation of transcription factors involved in muscle homeostasis, autophagy). One can speculate that FHL1 is hijacked by CHIKV to act as a scaffolding protein that orchestrates the recruitment of host proteins required for optimal infection. To test this hypothesis, we established the FHL1-interactome in mock and CHIKV-infected cells by affinity-purification approach coupled with a mass spectrometry analysis (AP-MS). These experiments were performed by Dr. Lamine Hafirassou (alumni post-doctoral researcher in Amara's lab) and are reported in Figure 8A-D. Briefly, FHL1-HA was immunoprecipitated using HA-antibody coupled magnetic beads, following cell lysis and protein extraction, either from mock or CHIKV-infected 293T cells for 24h. The retained protein complexes were eluted by competition with HA-peptide, separated by SDS-PAGE, and visualized by silver staining. Finally, samples from three independent experiments were subjected to mass spectrometry (MS) analysis performed at Taplin Biological Mass Spectrometry Facility (Harvard Medical School) (Figure 8A). The raw AP-MS data were analyzed with SAINT express, a statistical method to probabilistically score protein-protein interactions (Teo et al.,2014). NsP proteins were efficiently co-purified with FHL1, with an important distribution along the nsP3 sequence. This suggests that we have indeed isolated FHL1/nsP3 complexes. Interestingly, nsP1 and nsP2, but not nsP4, were also purified. The absence of nsP4 might be due to its rapid degradation by the ubiquitin-dependent N-end rule pathway (de Groot et al. 1991). We also identified peptides corresponding to the CHIKV structural protein (Figure 8B).

We additionally identified 43 proteins that co-purified with FHL1, with a probability score >0.8 following SAINT express analysis. This list was analyzed with DAVID 6.8 to identify statistical enrichment for specific Gene Ontology (GO) terms from the "biological process" category (Figure 8C). In line with the literature and the previous experiments, FHL1 was found in a complex with G3BP1, G3BP2 and CD2AP (major interactants of CHIKV nsP3), thus validating our experimental approach. In addition, FHL1 was found to interact with components of the actin-cytoskeleton such as spectrins (SPTBN1, SPTBN2, SPTAN1, MYH9, MYH10, MYH14, FLII, ADD2,

KIF2A). This is encouraging, given the data published in the literature demonstrating that FHL1 is found within a complex with MYH10 (non-muscle myosin) and ACTG1 (gamma-actin) both involved in a wide range functions such as cell morphology, motility, differentiation and even apoptosis (L. Wang et al. 2013).

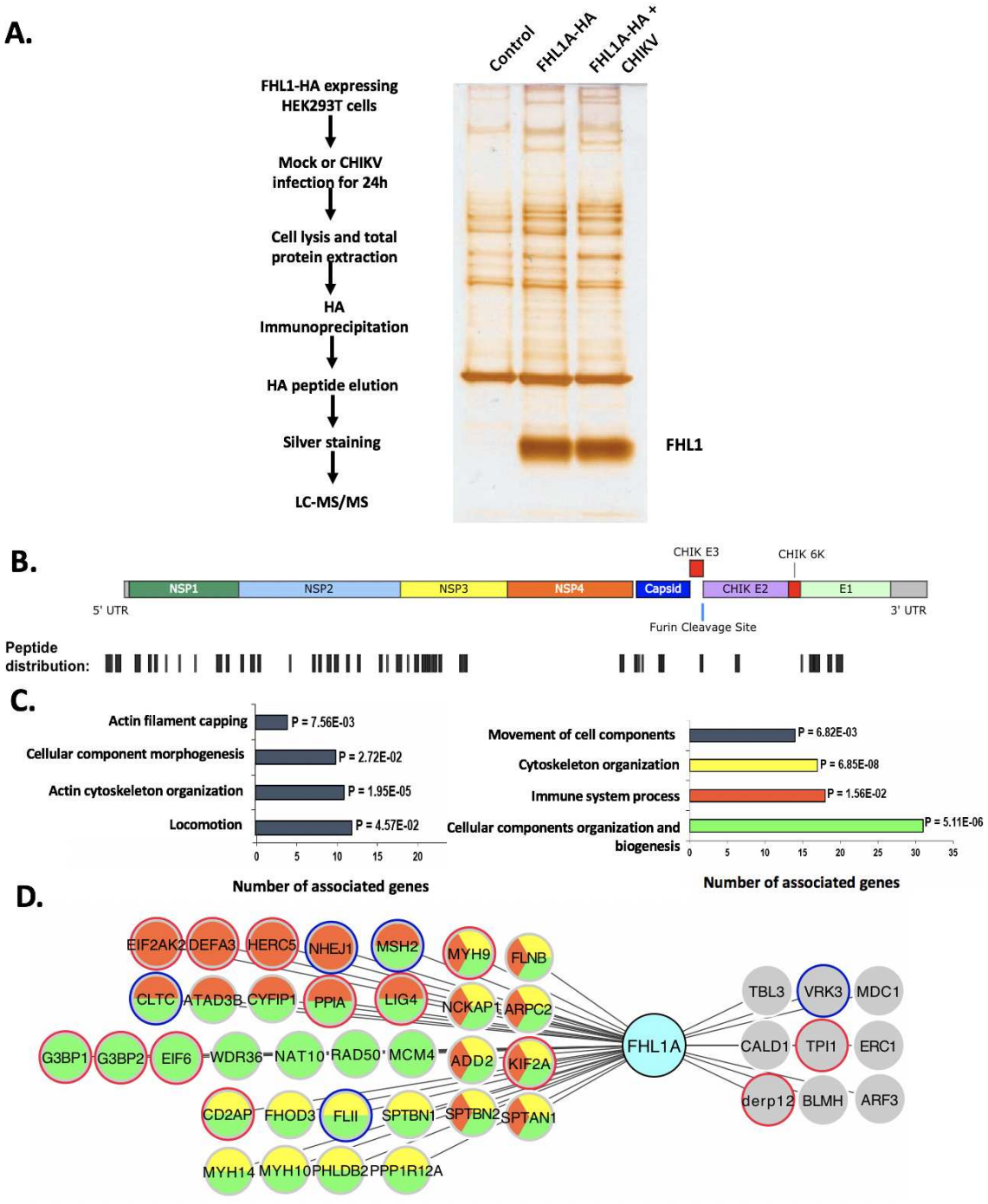

Figure 8: Characterization of FHL1 interactome. *A, Schematic representation of FHL1-affinity purification from control FHL1-KO, FHL1A-expressing uninfected and CHIKV infected cells (left panel). Separation of immunoprecipitated protein complexes by SDS-PAGE and visualization by silver staining (right panel). B, Schematic representation of peptides distribution (black bars) along the CHIKV genome, from three independent AP-MS analysis. C, Histogram indicating statistical enrichment for specific biological processes (BP) determined by Gene Ontology (GO) analysis. D,Clustering network of FHL1A-associated proteins identified by MS following additional analysis of the three independent IPs. One shot and individual analysis was also performed/ Protein find in two of three analysis or in all three analysis were encircled in blue and red respectively. The AP-MS experiments and network analysis were performed by Dr Lamine Hafirassou, and data served as a starting point for my PhD work.*

In addition, RNA and DNA metabolism proteins such as NAT10 (RNA metabolism), and LIG4, MCM4, MSH2 (involved in DNA ligation, replication, and mismatch repair) have been identified. Other proteins involved in mRNA translation (EIF6) or in the cellular response to viral infection (HERC5, PKR (EIF2AK2), DEFA3) were also identified (Figure 8D). Comparison between mock and infected conditions revealed that most of these factors were highly enriched in the infected condition. Proteins involved in cytoskeleton reorganization were already enriched in FHL1-complexes purified from mock-infected cells.

To further pinpoint the function of the 43 selected host factors interacting with the FHL1, we silenced their expression by RNA interference (RNAi) and determined the impact on CHIKV infection. 293T were transfected in triplicate with the siRNA library for 48H and then infected with CHIKV-GFP. (Figure 9A). Silencing of FHL1, MXRA8 (both used as positive controls), and G3BP2 led to a drastic reduction of viral infection with 80%, 55%, and 60%, respectively (Figure 9C). In two independent experiments, SPTBN1, MSH2, MCM4, and ADD2 knock-down were reduced by more than 50% CHIKV infection. EIF6 knockdown also drastically reduced viral infection, but this phenotype was expected as its catalysis 40S and 60S ribosomal subunits association to initiate translation, thus, its knockdown likely impaired viral mRNA translation. Further functional studies are now required to validate these potential candidates and investigate how they interact with FHL1 and nsP3.

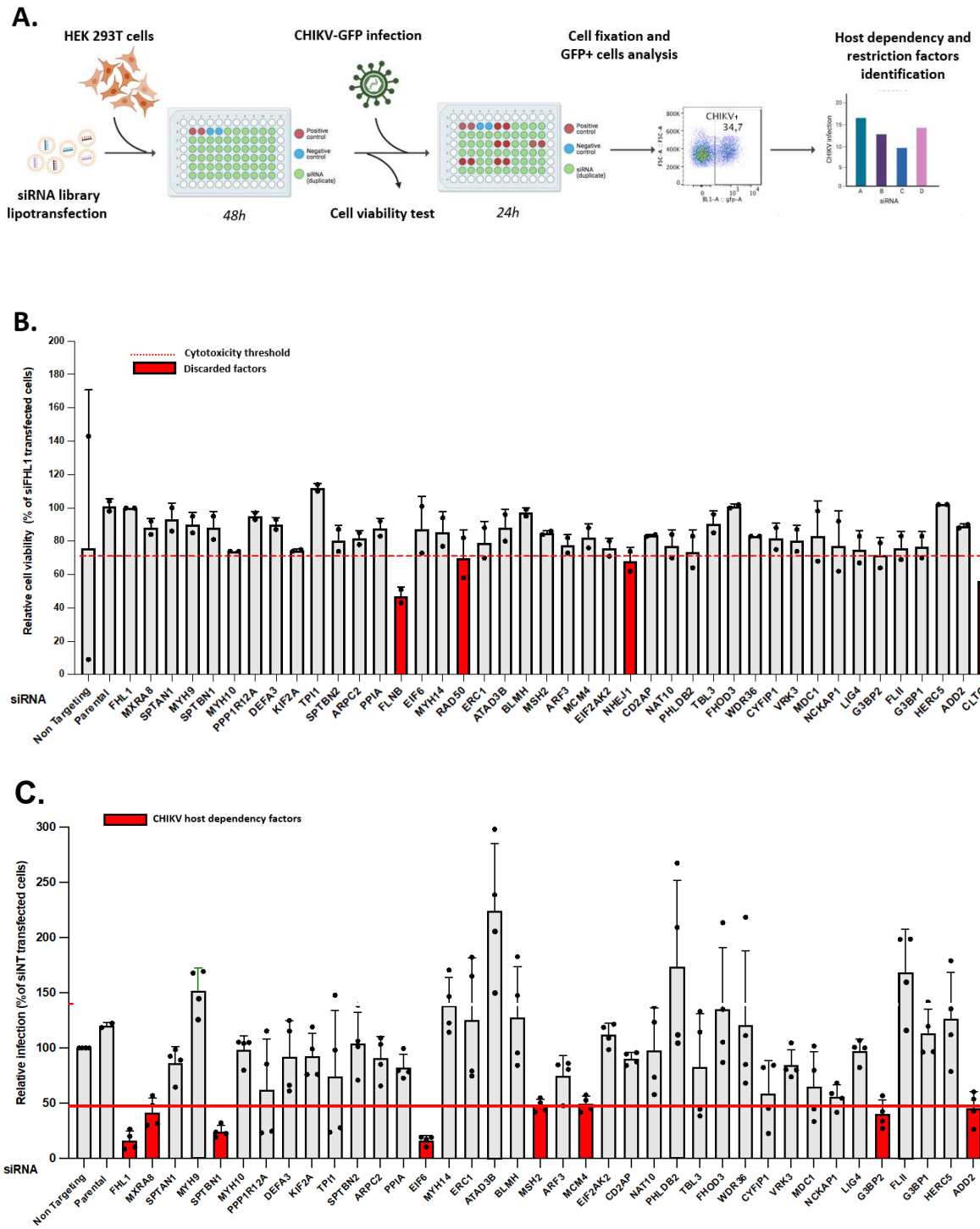

Figure 9: Functional validation of FHL1-interacting partners during CHIKV infection. *A, Schematic representation of the experimental procedure. B. 48 hours post-transfection, the impact of host-factor silencing on cell viability and proliferation was assessed. Data are mean ± s.d. of n =2 experiments. Host-factor which silencing diminishes cell viability with 25% were discarded. C, following 48h siRNA transfection, cells were challenged with CHIKV-GFP for another 24h. Levels of viral infection were assessed by flow cytometry. Host-factors which depletion inhibits 50% of CHIKV infection are depicted in red and are considered as CHIKV host-dependency factors. Data are mean ± s.d. of n =2 experiments.*

2) Conclusions

This study aimed to better understand how FHL1 interacts with CHIKV-nsP3 and how this molecule selectively mediates CHIKV infection.

NMR studies successfully determined the precise nsP3 HVD-amino acid sequence (R5 region) that mediates FHL1 interaction in vitro. The R5 region overlaps with the BIN1/Amph2-and CD2AP-binding motifs, suggesting cooperation between FHL1 and these molecules. Functional studies confirm that the R5 region is required for FHL1-relocalization to nsP3-complexes. Deletion of R5 completely abolished CHIKV replication in human 293T and U2OS cells, confirming that FHL1-nsP3 interaction is required for viral replication. Interestingly, the same phenotype was observed in Vero cells, which do not express FHL1. These results suggest that R5 is mediated interactions with other host factors, likely FHL2 or CD2AP and BIN1, which are expressed in these cell lines. Finally, CHIKV ΔR5 replicates efficiently in BHK cells, albeit not at WT levels. This indicates that FHL1, Bin1, and CD2AP are unnecessary for CHIKV infection in rodent cells.

A comparison of CHIKV replication and infection in $FHL1^{KO}$ cells versus $G3BP1/2^{KO}$ cells suggests that FHL1 and G3BPs fulfill different proviral functions. G3BP could be required at the very first stage of viral replication. One hypothesis is that G3BPs play a crucial role in vRC formation, supported by the confocal microscopy studies showing G3BP co-localizing with nsP3 and dsRNA. FHL1 is involved in post-entry steps, but its precise proviral function is still enigmatic. FHL1 has been proposed to play a role in minus-stranded RNA (Meertens et al. 2019). FHL1 may also participate in the subgenomic RNA and structural protein synthesis or regulate the host immune response against viral infection. FHL1 is recruited into nsP3 cytoplasmic aggregates, however, it is not directly involved in their formation.

Finally, we describe the first FHL1 interactome in mock or CHIKV-infected cells. For that purpose, I took advantage of results obtained by Dr. Lamine Hafirassou, who performed an affinity purification assay followed by mass spectrometry analysis performed on 293T cells expressing an HA-tagged version of FHL1. The results demonstrated that viral nsP, mainly nsP3, are found in complex with FHL1 at 24h post-infection. The MS analysis revealed that FHL1 interacts with actin cytoskeleton components, such as actin-binding proteins, spectrins, and non-muscle myosins. In addition, components of the cellular immune antiviral response were also found (PKR, HERC5, DEF3A) in our FHL1 interactome only in the context of infection. Knockdown

of each FHL1-interacting partner suggests a potential role of SPTBN1, MSH2, MCM4, and ADD2 factors in FHL1-mediated CHIKV infection. SPTBN1 (Spectrin beta, non-erythrocytic 1) is a top hit in our RNAi screen. SPTBN1 serves as both an actin crosslinking agent and a molecular scaffold protein. It establishes a connection between the plasma membrane and the actin cytoskeleton, playing a vital role in shaping cells, positioning transmembrane proteins, and arranging organelles within the cell (Panyu Yang et al. 2021). Further studies are required to validate these results.

3) Material and methods

Cell culture

HEK293T (ATCC, CRL-3216), Vero E6 (gift of Marc Lecuit, Pasteur Institute Paris, France), BHK-21 (ATCC, CCL-10) and U2OS cells (gift of Andres Merits, University of Tartu, Estonia) were cultured in DMEM supplemented with 10% FBS, 1% penicillin–streptomycin, and 25 mM HEPES. HAP1 cells (Horizon Discovery), which are derived from near-haploid chronic myeloid leukaemia KBM7 cells, were cultured in IMDM supplemented with 10% fetal bovine serum (FBS), 1% penicillin–streptomycin and GlutaMAX (Thermo Fisher Scientific) Fibroblast BJ-5ta cells (ATCC, CRL-4001) were cultured in DMEM supplemented with 20% Gibco Media 199, 10% FBS, 1% penicillin–streptomycin, 25 mM HEPES and 10 µg/mL Hygromycin D. Primary dermal fibroblasts, either from control or patient suffering from myopathy linked to *fhl1* gene mutation leading to deficiency in FHL1 expression were hTERT-immortalized (kind gift from Anne Bertrand). All cell lines were cultured at 37 °C in 5% CO2. All cell lines were routinely tested to be free of mycoplasma contamination.

Virus strains and production

CHIKV21 (strain 06-21 from Reunion Island) was previously described (Meertens et al. 2019) and obtained from Philippe Despres (Institut Pasteur, Paris, France). CHIKV West Africa (strain 37997), CHIKV St Martin (H20235 2013 Asian), CHIKV-Brazza-MRS1 2011 (ref EVA 8847), were obtained from the European Virus Archive (EVA) collection. Viruses were propagated with limited passages on Vero E6 cells. CHIKV 181/25 molecular clone (gift from Dr Gofinnet Christine, Institute of Virology Charité, Berlin, Germany) was derived from the parental Asian strain AF155561 and attenuated by two amino acid substitutions in the E2 glycoprotein (Levitt et al. 1986). Recombinant CHIKV CHIKV-Rluc molecular clones were derived from CHIKV isolate obtained during the Mauritius outbreak in 2006 (GenBank accession no. FJ959103) 32. To generate infectious viruses from CHIKV molecular clones, capped viral RNAs were generated from the NotI-linearized CHIKV plasmids using a mMESSAGE mMACHINE SP6 or T7 Transcription Kit (Thermo Fischer Scientific) according to manufacturer's instructions. Resulting RNAs were purified by phenol:chloroform extraction and isopropanol precipitation, resuspended in water, aliquoted and stored at -80°C until used. Thirty ug of purified RNAs were transfected in BHK21 with

lipofectamine 3000 reagent and supernatants harvested 72 hours later were used for viral propagation on Vero E6 cells. All virus stocks were purified through a 20% sucrose cushion by ultracentrifugation at 80,000g for 2 hours at 4°C. Pellets were resuspended in HNE1X pH7.4 (Hepes 5 mM, NaCl 150 mM, EDTA 0.1 mM), aliquoted and stored at -80°C. Viral titers were determined on Vero E6 cell by plaque assay and are expressed as PFU per mL

Plasmid constructions

The N-terminal FLAG-tagged full-length nsP3 WT, ΔHVD or ΔR4 constructs derived from CHIKV Sri Lanka/2006/SL15649 strain (Accession number: MK028838.1 synthesized and cloned into pcDNA 3.1 (-) mammalian expression vector by GenScript. 3Xflag nsP3 constructs are already described in (Meertens et al, 2019). To generate the C-terminal HA-tagged FHL1A, the cDNAs of FLH1A (NM_001449.4) was purchased from Genscript. Coding sequence (CDS) were amplified with a FHL1 Fwd primer 5'-CCGGAGAATTCGCCGCCATGGCGGAGAAGTTTGACTGCCACTACTGC-3'; and rev primer 5'-AATAGTTTAGCGGCCGCTCAAGCGTAATCTGGAACATCGTATGGGTATCCTCCAGCGGCCGACAGCTTTTTGGCACAGTCGGGACAATACACTTGCTCC-3'; and cloned into pLVX-IRES-ZsGreen1 vector (Takara).

Antibodies

The following primary antibodies were used: anti-Flag M2 mouse monoclonal antibody (F1804, Sigma), anti-dsRNA J2 mouse monoclonal antibody (Scicons), anti-nsP3 rabbit polyclonal antibodies (in-house from Andres Merits's laboratory), anti-CHIKV E2 mouse monoclonal antibody (3E4), anti-GAPDH mouse monoclonal antibody (SC-47724, Santa Cruz Biotechnology), anti-FHL1 mouse monoclonal antibody (MAB5938, R&D Systems) and anti-G3BP1 mouse monoclonal antibody (H-10 sc-365338, Santa Cruz Biotechnology), anti-CD2AP (51046-1-AP, Proteitech), anti-Bin1/Amphiphysin2 (ab182562, Abcam). The following secondary antibodies were used: Alexa Fluor 488-conjugated goat anti-rabbit IgG (A11034, Invitrogen), Alexa Fluor 488-conjugated goat anti-mouse IgG (A11001, Invitrogen), Alexa Fluor 647-conjugated donkey anti-rabbit IgG (A31573, Invitrogen), Alexa Fluor 647-conjugated donkey anti-mouse IgG (A31571, Invitrogen), Alexa Fluor 594-conjugated donkey anti-

rabbit IgG (21207, Invitrogen), peroxydase-conjugated donkey anti-rabbit IgG (711-035-152, Jackson ImmunoResearch), and anti-mouse/HRP (P0260, Dako Cytomotion).

Gene editing.

FHL1, CD2AP, G2BP1, G3BP2 and BIN1 were invalidated using two independent small guiding RNA (sgRNA) (see Table 1), cloned into the plasmid lentiCRISPR v2 according to Zhang lab's recommendation. HAP1 and 293FT cells were transiently transfected with the plasmid expressing individual sgRNA and selected with puromycin until all mock transfected cells died (approximately 72 hours). Transfected cells were used to ascertain gRNA-driven resistance to CHIKV cytopathic effect, and clonal cell lines were isolated by limiting dilution and assessed by immunoblot for protein expression.

Infection assay. For infection quantification by flow cytometry analysis, cells were plated in 24-well plates. Cells were inoculated with the indicated virus and MOI for 48 hours, then collected with trypsin, and fixed with 2% (v/v) paraformaldehyde (PFA) diluted in PBS for 15 min at room temperature. Cells were incubated for 30 min at 4°C with 1µg/ml of the 3E4 anti-CHIKV-E2 mAb diluted in permeabilization flow cytometry buffer (PBS supplemented with 5% FBS, 0.5% (w/v) saponin, 0.1% Sodium azide). After washing, cells were incubated with 1µg/ml of Alexa Fluor 488 or 647-conjugated goat anti-mouse IgG diluted in permeabilization flow cytometry buffer for 30 min at 4°C. Acquisition were performed on an Attune NxT Flow Cytometer (Thermo Fisher Scientific) and analyzed using Flowjo software (Tree Star).

Genomic viral RNA transfection and viral infection analysis

To assess wildtype and mutant CHIKV RNA replication, we transfected HEK293T cells with capped genomic viral RNA generated from pCHIKV-Rluc molecular clones (see 'Virus strains and production). Cells were plated on 48 well plates (5 x 104 cells) and transfected with 50 ng of purified RNA using the Lipofectamine MessengerMax reagent according to the manufacturer's instructions (Thermo Fisher Science). At 3 h after transfection, medium was removed and fresh medium was added. At specific time intervals, cell supernatant was collected and frozen at -80°C for plaque assay on VeroE6 cells, whilst cells were washed once with PBS and lysed with Passive lysis

buffer. Lysates were kept at −20 °C until all samples were collected. Luciferase activity was measured using the Renilla Luciferase Reporter Assay system (Promega) on a TriStar2 LB 942 with 20 □L of cell lysate, 20 uL of substrate and 2 s integration time. Each experiment was performed in quadruplicate.

Co-immunoprecipitation assay

HEK-293T cells were plated in 10 cm dishes (5.106 cells/ dish). Twenty-four hours later, the cells were transfected with a total of 15 ug of DNA expression plasmids (7.5 µg of each plasmid in co-transfection assays). Twenty-four hours post-transfection the cells washed once with PBS and collected with a cell scrapper. After 5 min centrifugation (400 x g for 5 min), cells pellets were lysed for 30 min in cold IP lysis buffer supplemented with Halt™ Protease and Phosphatase Inhibitor Cocktail, and then cleared by centrifugation for 15 min at 6,000 x g. Supernatants were incubated overnight at 4°C, with either anti-FLAG magnetic beads (see 'reagent' section above). Beads were washed three times with IP-lysis buffer. The retained complexes were eluted twice with either 3xFLAG-peptide (200 µg/ml; SIGMA F4799-4MG) for 30 min at room temperature. Samples were prepared and subjected to immunoblot as described below.

Identification and analysis of FHL1A-HA interactome in infectious context (*work performed by Dr Lamine Hafirassou, Post doc*)

FHL1A-HA immunoprecipitation was performed as previously described. Briefly, 5 × 108 293T cells expressing either the HA-tagged FHL1A protein, either mock or CHIKV infected for 24h, were lysed for 30 min in cold IP lysis buffer supplemented with complete protease and phosphatase inhibitors and then cleared by centrifugation for 30 min at 6,000 × g. Supernatants were incubated overnight at 4°C with anti-HA magnetic beads. Beads were washed three times with B015 buffer (20 mM Tris-HCl pH 7.4, 150 mM NaCl, 5 mM MgCl2, 10% glycerol, 0.5 mM EDTA, 0.05% Triton, 0.1% Tween-20) and immune complexes were eluted twice with HA-peptide (400 µg/mL) for 30 min at room temperature (RT). HA-IP complexes were further incubated with HA magnetic beads for 6 hr at 4°C, washed 3 times with B015, and immune complexes were eluted twice with HA peptide (400 µg/mL). Eluates were concentrated on a Pierce Concentrator, PES 10K, and stored at −20°C until used.

A total of 3 co-affinity purifications and MS analysis experiments were performed with; FHL1-KO 293T cells and, mock or CHIKV-infected FHL1A-HA

expressing 293T cells. Samples were analyzed at Taplin Biological Mass Spectrometry Facility (Harvard Medical School). Briefly, concentrated eluates issued from immunopurification are separated on 10% Tris-glycine SDS-PAGE gels (Invitrogen), and stained with Imperial Protein Stain (Thermo Fisher). Individual regions of the gel were cut into ~1 mm3 pieces and subjected to a modified in-gel trypsin digestion procedure (Shevchenko et al., 1996). Peptides were desalted and subjected to a nano-scale reverse-phase HPLC (Peng and Gygi, 2001). Eluted peptides are then subjected to electrospray ionization and then MS/MS analysis into an LTQ Orbitrap Velos Pro ion-trap mass spectrometer (Thermo Fisher Scientific, Waltham, MA). Peptides were detected, isolated, and fragmented to produce a tandem mass spectrum of specific fragment ions for each peptide. Peptide sequences were determined by matching protein databases with the acquired fragmentation pattern by the Sequest software program (Thermo Fisher Scientific, Waltham, MA) (Eng et al., 1994). All databases include a reversed version of all the sequences, and the data were filtered to ≤2% peptide false discovery rate.

Raw AP-MS dataset was analyzed with SAINTexpress, 43 proteins showed a probability score >0.8 with SAINTexpress and an average peptide count >2 in the CHIKV infected condition. Data were submitted two three type of analysis: additional IP1+IP2+IP3 analysis, One Shot analysis (one simultaneous analysis of the three IPs) and individual IP analysis. Host protein list was analyzed with DAVID 6.8 to identify statistical enrichments for specific GO terms from the “biological process” (BP) categories (Huang et al., 2009a, Huang et al., 2009b).

siRNA screen assay

The proteins identified by the AP-MS approach were targeted by an ON-TARGETplus SMARTpool siRNA library (Dharmacon). I use a siRNA pool instead of individual siRNA to improve silencing efficiency and drastically reduce off target effects. 293T cells were transfected using the Lipofectamine RNAiMax protocol (Life Technologies) with 20 nM final siRNA. 48 hr post-transfection, cells were infected CHIKV-GFP at MOI 0.2 for 24 hr and infection was quantified by flow cytometry. Three siRNA controls were included in the screen: (1) a non-targeting siRNA used as a reference, (2) a siFHL1 targeting the FHL1 gene expression, which we demonstrated as an important CHIKV host dependency factor, which serves as a positive control for host dependency factors (HDFs), and (3) a siMXRA8 for the knock down of the MXRA8

receptor expression, involved into alphavirus entry. Cutoffs criteria were for HDF to be <50% of the mean of infection and for HRF to be ≥200% of the mean of infection.

Cell viability

Cell viability and proliferation were assessed using CellTiter-Glo 2.0 assay (Promega) according to the manufacturer's protocol. The cells (3 × 104) were plated in 48-well plates. At the indicated times, 100 µL of CellTiter-Glo reagent were added to each well. After 10 min of incubation, 200 µL from each well was transferred in an opaque 96-well plate (Cellstar, Greiner Bio-One), and luminescence was measured on a TriStar2 LB 942 (Berthold) with a 0.1-s integration time.

Cell lines stably expressing CHIKV FLAG-nsP3

Empty lentiviral plasmid or 3xFLAG-tagged full-length nsP3 lentiviral plasmid (pLVX) were co-transfected in 293T cells by with psPAX2 (Kind gift from Nicolas Manel, Institut Curie, Paris, France) and pCMV-VSV-G at a ratio of 4:3:1 with lipofectamine 3000 (Thermo Fisher Scientific). Supernatants were collected 48 h and 72 h after transfection, cleared by centrifugation (750g for 10 min), filtered using a 0.45-µm filter and purified through a 20% sucrose cushion by ultracentrifugation (80,000g for 2 h at 4 °C). Pellets were resuspended in HNE 1X pH 7.4, aliquoted and stored at −80 °C. $FHL1^{KO}$ cells were transduced by spinoculation (750g for 2 h at 33 °C) using these lentiviruses and selected with puromycin (2 µg/mL).

Westernblot

Equal amount of protein, determined by DC™Protein Assay (BioRad), were prepared in LDS Sample Buffer 4X (Pierce™) containing 25 mM dithiothreitol (DTT) and heated at 95°C for 5 min. Samples were separated on Bolt™ 4-12% Bis-Tris gels in Bolt® MOPS SDS Running Buffer (Thermo Scientific), and proteins were transferred onto a PVDF membrane (BioRad) using the Power Blotter system (Thermo Fischer Scientific). Membranes were blocked with PBS containing 0.1% Tween-20 and 5% non-fat dry milk and incubated overnight at 4°C with primary antibody. Staining was revealed with corresponding horseradish peroxidase (HRP)-coupled secondary antibodies and developed using SuperSignal™ West Dura Extended Duration Substrate (Thermo Fisher Scientific) following manufacturer's instructions. The signals were acquired through Fusion Fx camera (VILBERT Lourmat).

Immunofluorescence

Human fibroblasts (1.1 x 10^4 cells per well) were grown on Lab-Tek CC2 chamber slides (Nunc) for 24 hours. Cells were inoculated with CHIKV21 at the indicated MOIs. At 7 and 24 hours post infection, cells were washed with PBS and fixed with 4% (v/v) of PFA diluted in PBS for 15 min at room temperature. Fixed cells were washed with PBS for 5 min, then incubated with 0.1 mM of glycine in PBS for 30 min at room temperature. Cells were permeabilized and blocked with 0.5% saponine and 3% (w/v) BSA in PBS for 45 min. Cells were incubated for 1 h at room temperature with primary antibodies, and washed with PBS. Cells were labelled with corresponding Alexa Fluor-conjugated secondary antibodies (1 ug.ml-1) for 30 min at room temperature. All antibodies were diluted in PBS supplemented with 3% (w/v) BSA. Slides were mounted with ProLong Gold antifade reagent containing DAPI for nuclear staining (Thermo Fisher Scientific). Fluorescence microscopy images were acquired using a LSM 800 confocal microscope with the following objectives: Plan-Apochromat 63x/1.40 Oil DIC M27 and Plan-Apochromat 40x/1.3 Oil DIC (UV) VIS-IR M27 (Zeiss).

Discussion and perspectives

A. Structure and function of the alphavirus nsP3

In this study, we reported the cryo-electron microscopy structure of CHIKV nsP3 protein for the first time and showed its intrinsic ability to oligomerize and form helical scaffolds. These scaffolds fit perfectly with previously identified but uncharacterized structures at the neck of CHIKV replicative spherules. We demonstrated that nsP3 forms tubular structures in infected cells corresponding to the in vitro helical scaffolds. Finally, functional data revealed that nsP3 oligomerization inhibition impairs viral replication, suggesting it is a prerequisite for its activity during the replicative cycle. Interestingly, in the late stages of the viral cycle, nsP3 organize in tubular assemblies that trap host factors FHL1 and G3BP and contain viral genomic RNA and capsid proteins. These data pinpoint a second, more tardive role of nsP3 during the viral cycle. This study reports new and valuable insights into nsP3 structure and function and reveals the architecture of a new type of virus-induced organelles.

1. nsP3 helical scaffolds are involved in vRC formation

a. AUD is a unique oligomerization module driving nsP3 oligomerization

The structural analysis performed by our collaborators (Dr. Michael Horns, Dr. Juan Reguera, and his team) of the CHIKV nsP3 revealed that this protein possesses the intrinsic ability to oligomerize into tubular structures with a well-defined internal channel delimited by a weakly structured matrix and surrounded by a jelly-like shield. The cryo-electron microscopy (cryoEM) at 2.52Å resolution revealed that the Alphavirus Unique Domain (AUD) is an oligomerization module organized into four alpha helixes with extensions (O-modules) in C-terminal and N-terminal, responsible for axial and lateral contacts between AUDs of neighboring nsP3 molecules. The O-modules are enriched in positively charged residues, mediating electrostatic interactions with a specific region called O-loop. The O-loop of AUD at position hA n mediates interactions with the lateral O-module of AUD at position hA (helix A) n-1 and the axial O-module of the AUD at the neighboring helix- hB n – position. In addition to the electrostatic charges, hydrogen bonds established by several residues seal the lateral and axial interactions. The AUD is an alphavirus-specific protein fold that does not have direct homologs in unrelated organisms or viruses (Gao et al. 2019; Götte, Liu, et McInerney 2018), in contrast with the alphavirus macrodomain, which is a well-conserved structural fold harboring a specific enzymatic ADP-ribose binding and hydrolase activities (Fehr et al. 2018). AUD-resembling domains have never been

reported in the literature so far, either in other viruses or unrelated organisms. Further investigations using protein databases coupled to artificial intelligence such as Alpha Fold can be helpful to identify protein folds similar to AUD.

b. nsP3 helical scaffolds form a supporting crown for spherule biogenesis

Multiple biochemical and immunofluorescence studies have reported that nsP3 is a fundamental component of the enzymatic machinery that mediates viral replication. Indeed, microscopy studies showed that nsP3 is found close to the dsRNA, a hallmark of vRC. However, the spatial organization of nsP3 and the other replicase proteins as well as the precise nsP3 activity during RNA synthesis remained poorly understood until recently. With the advent of single-particle cryo-EM and cryo-electron tomography (cryo-ET), we gained valuable information about the CHIKV nsP organization and stoichiometry within the vRC. In addition to the nsP1 dodecameric ring anchored to the plasma membrane and organizing the spherule pore, *in situ* cryo-ET, showed the presence of a cylinder-like structure below nsP1-ring. The cavity formed by this structure eventually displays linear density resembling RNA transported from the spherule to the cytoplasmic side of the cylinder (Tan et al. 2022). This protein density was also reported in another tomographic reconstruction of CHIKV vRC (Laurent et al. 2022), but the nature of this protein complex remained unknown. Interestingly, the same study showed inactive replication complexes core, tethered to the plasma membrane. Subtomogram averaging of the

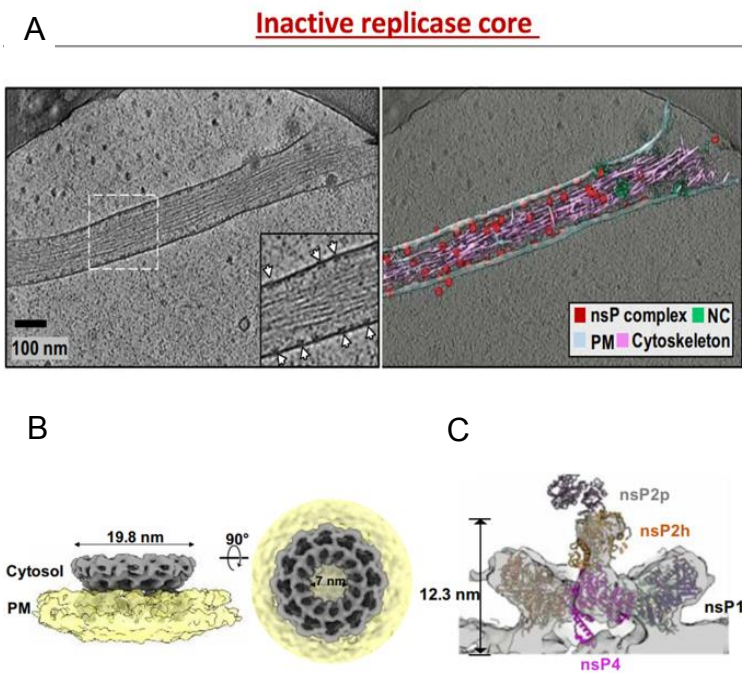

***Figure 1: Structure of inactive vRC**. A. Tomographic slice of cell periphery depicting a filopodia-like membrane protrusion structure extended from the PM. White arrows point to the membrane-associated nsP complexes. Scale bar, 100 nm. B (right) Corresponding 3D segmentation of cellular features. C, CHIKV nsP complex 3D volume determined by subtomogram averaging with imposed C12 symmetry. F, The RC core complex (nsP1 + 2 + 4) is fitted into the C1 subtomogram average map of the nsP complex. Note that the cytoplasmic ring as observed in Fig. 3C is absent in this inactive nsP complex. Consequently, there is no density observed for the C-terminal protease of nsP2. From Tan et al. 2022.*

reconstructed complexes revealed the nsP1-dodecameric ring, nsP4 in the vicinity of the nsP1-pore and nsP2 facing the cytoplasmic side of the complex, but no cytoplasmic cylinder density. Strikingly, this RC core was not generating spherules, and no RNA synthesis was observed.

The nsP3 helical scaffolds reported in our study fit remarkably in size and shape with the cytoplasmic cylinder-like (or crown-like) structure found in active CHIKV replicative complexes. In addition, the fact that no nsP3 could be assigned in the structure of inactive RC cores (Figure 1) pinpoints the formation of an nsP3 crown at the neck of the replicative spherules supporting their biogenesis. However, further direct evidence by in situ cryo-electron tomography on CHIKV and other alphavirus-infected cells is needed to confirm that the cytoplasmic cylinder-shaped complex corresponds to nsP3 oligomers.

Cryo-ET is a powerful tool to decipher the structural organization of alphavirus replication complexes, but it also can give insights into the host factors recruited at these sites. For instance, one of the well-documented nsP3 functions is to mediate interactions with multiple host factors required for efficient replication. G3BP proteins are the main nsP3 interactants that participate in vRC formation and clustering at the plasma membrane (Kim et al. 2016). Other host factors such as Bin1/Amphiphysin, which contains BAR-domains involved in membrane reshaping and curvature, are thought to be recruited to alphavirus vRC for spherule biogenesis. In light of these data, it is reasonable to propose that nsP3 helical scaffolds are formed at the cytoplasmic side of vRC to generate or stabilize membrane spherules and thus permit RNA synthesis. Our structural data suggest that nsP3 AUD forms the inner channel of the helix and that the MD and the HVD are projected toward the exterior. This highly suggests that the host factors could be quickly recruited by these domains, mainly the HVD and decorate the surface of the nsP3 cylinder.

c. nsP3 helices trigger vRC maturation and sgRNA synthesis

Once synthesized, P1234 and P123+nsP4 are addressed along with viral genomic RNA to the plasma membrane to establish vRC formation and RNA synthesis. The molecular mechanisms involved in this process are still unknown. Studies of alphavirus non-structural polyprotein processing and regulation of RNA synthesis (K. H. Kim et al. 2004; Gorchakov, Frolova, et al. 2008) demonstrated that active nsP4 and uncleaved P123 are required for spherule formation. In addition, the uncleaved P123+nsP4 complex can only synthesize the negative RNA strand that will

serve as a template for synthesizing new positive RNA species (K. H. Kim et al. 2004; Gorchakov, Frolova, et al. 2008). Subsequent nsP1 individualization leads to a short-lived nsP1+P23+nsP4 replicase complex, which switches its activity from negative RNA to positive genomic RNA synthesis. Finally, the P23 cleavage into fully individualized nsPs was proposed to induce major conformational changes that irreversibly switch off the negative RNA synthesis toward mainly sub-genomic RNA species synthesis (K. H. Kim et al. 2004; Gorchakov, Frolova, et al. 2008).

In a previous study focusing on nsP3 AUD's role during viral replication, Gao and colleagues demonstrated for the first time a link between nsP3 and sgRNA synthesis (Gao et al. 2019). The authors described that P247A/V248A substitutions within the AUD dramatically decreased sub-genomic RNA synthesis and subsequent structural protein production. In line with SINV P23 structural data, the authors showed that this phenotype is linked to a reduced capacity of the AUD to recognize the subgenomic promoter (in vitro assay) and to bind viral positive-stranded RNA (RNA pulldown assay) (Gao et al. 2019). Despite these results, there is no clear evidence of nsP3 binding viral RNA in the replicative spherules. In our study, the P247A/V249A mutant also displayed a significant decrease in viral replication with a principal reduction in structural protein synthesis, suggesting a defect in viral sgRNA synthesis or sgRNA translation.

Considering the data mentioned above and also the structural organization of active *versus* inactive vRC (Tan et al.2022, see section b.), it appears reasonable to propose that nsP3-helical scaffolds are required for a fully mature vRC that can efficiently synthesize genomic and subgenomic RNA. In addition, AUD's capacity to bind genomic viral RNA might have essential implications regarding nascent RNA export outside the replicative spherules. Indeed, it is still unknown how viral RNA traffics from replicative sites to 1) translation sites and 2) nucleocapsid assembly sites (see section A.2).

d. nsP3 oligomerization and P1234 polyprotein processing

The superposition of our AUD structure with a predicted uncleaved P23 complex suggested that, in the unprocessed folded configuration, nsP2 C-terminal protease domain completely blocks the AUD-O-loop, which mediates axial contacts and the subsequent nsP3 scaffold formation. In addition, our CHIKV AUD mutant viruses, which have a strong defect in the nsP3 oligomerization process, present a reduced viral replication and spread. While the inability of unprocessed nsP3 to form

helical scaffolds should be further validated, our observations raise questions about the spatiotemporal regulation of nsP3 processing, oligomerization, and activity during the early steps of the viral cycle.

As described in the introduction of this work, membrane spherules formation requires fully processed nsP4 (RdRp) combined with either uncleaved P123 or nsP1+ uncleaved P23 (Hellström et al. 2017). In addition to forming spherules, the nsP1+P23+nsP4 complex is able to synthesize viral RNA. In contrast, the expression of fully processed nsPs is not able to mediate RNA synthesis (Hellström et al. 2017). These data demonstrate that efficient viral replication complexes (vRC) formation requires unprocessed P23 precursor but fully processed nsP4.

Furthermore, uncleaved P123 or P23 activity was also assessed in mutated SINV and SFV viruses (K. H. Kim et al. 2004; Gorchakov, Frolova, et al. 2008). Uncleavable P23 viruses replicate and produce spreading infection near wildtype virus level but only in cells that are not immunocompetent (Gorchakov et al. 2008). However, cleavage-deficient P123 virus was dramatically impaired in new genomic and subgenomic-RNAs synthesis, and thus the producing of spreading infection on BHK-21 cells (Gorchakov et al. 2008). Interestingly, the study reported that the uncleavable P23 virus synthesized more genomic RNA but less subgenomic RNA. These results fit with other data demonstrating that in contrast to uncleavable P123+nsP4 complex, which only synthesizes negative-strand RNA, nsP1+P23+nsP4 is very inefficient in negative synthesis but allows genomic RNA production (K. H. Kim et al. 2004; Gorchakov, Frolova, et al. 2008).

Given the above data, our hypothesis that P23 cleavage is required for nsP3-helices formation and, thus, for viral RNA synthesis is inconsistent. Indeed, our results demonstrated that nsP3 oligomerization is a prerequisite for replication and production of infectious particles. However, processing-dead CHIKV viruses are viable (K. H. Kim et al. 2004; Gorchakov, Frolova, et al. 2008), suggesting that nsP3oligomerization could occur in the P23 precursor. Interestingly, it was proposed that P23 site cleavage is driven by conformational changes in the replicase complex rather than by the only nsP2-protease activity (Hardy et Strauss 1989; Lulla, Lulla, et Merits 2012; Gorchakov, Frolova, et al. 2008). These conformational changes could start when the P12 site is cleaved in *cis (Figure 2, step 2)*, which liberates the N-terminal domain of nsP2. This first cleavage may induce a conformational change that releases the nsP3-AUD oligomerization loop (O-loop), thus enabling nsP3 helical scaffold formation (Figure 2,

step 3). P23 processing likely occurs following AUD helices formation, liberating nsP2, which is finally able to recognize the sub-genomic promoter (Hahn, Strauss, et Strauss 1989; Lulla, Lulla, et Merits 2012), thus favoring sgRNA synthesis (Figure 2, step 4). Alternatively, replicase conformational changes could also result from the interaction between the replicase proteins (P123 and P23) and the viral genomic RNA. Indeed, structural data of SINV P23 predicted an RNA-binding region that extends from nsP2 to the AUD zinc finger motif (Malet et al. 2009).

e. Conclusions

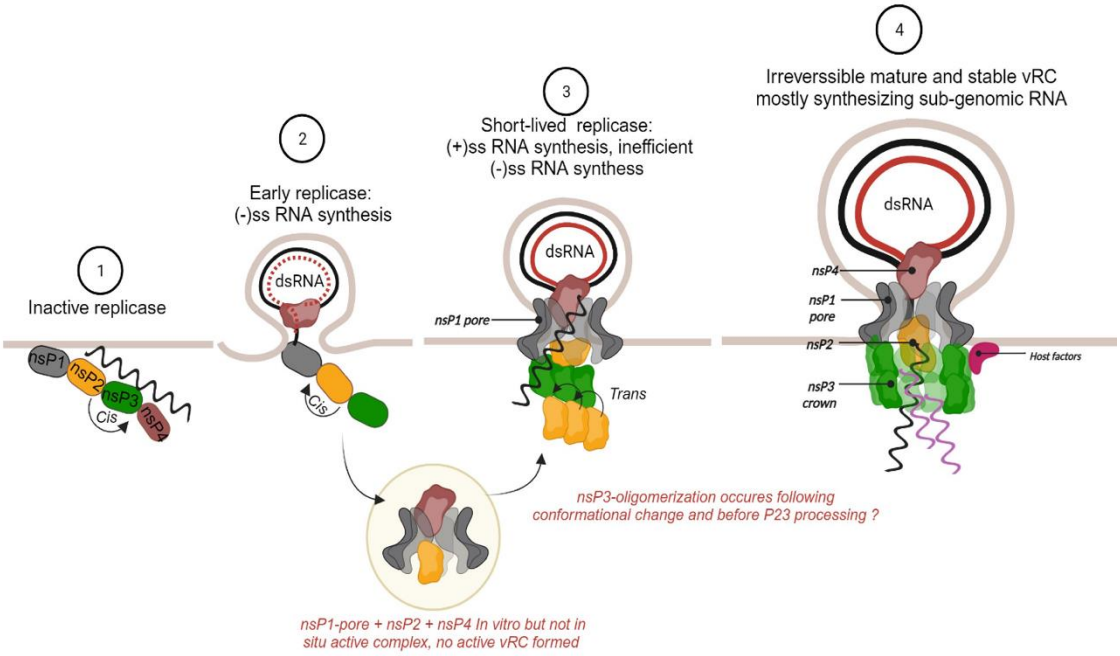

Figure 2: nsP3 forms a supporting crown below nsP1-dodecameric ring of vRC.

With the development of trans-replicase molecular systems, which allows us to decouple RNA synthesis and spherule biogenesis, and the amount of structural information we can obtain by cryo-electron microscopy and tomography, we can now explore in detail the formation of alphavirus vRC and investigate the importance of the polyprotein processing in this process. For instance, deciphering the structural organization of the P123+nsP4-induced spherules and the fully matured active spherules observed in infected cells will be of great interest. Questions remain to be assessed regarding the oligomerization of nsP1 and nsP3 in the context of the uncleaved P123 polyprotein. In vitro expression of the individualized nsPs and all the polyprotein precursors (P123, P23) and the characterization by electron microscopy of their capacity to organize into macromolecular assemblies could be valuable. In addition, the same experiments performed in situ could give us insights into the very

first stages of vRC formation.

Furthermore, it is commonly proposed that the alphavirus nsP3 protein recruits a set of host factors at the sites of replication in order to ensure spherule biogenesis and RNA synthesis. One reasonable interrogation concerns the importance of nsP3 scaffold formation for efficient clustering of host factors, such as G3BP, FHL1, CD2AP, and Bin1 for CHIKV. Preliminary data not shown here suggested that AUD-mutated nsP3 proteins, unable to polymerize and form scaffolds, can still interact with host factors (G3BP in our experiments). This suggests that in addition to interact with these factors, their aggregation at specific sites such as vRC is required for efficient viral replication.

2. Cytoplasmic nsP3 aggregates

We showed that CHIKV nsP3 form high-ordered helices that stuck together in a honeycomb network as the infection progresses. We propose that these networks are not active replicative comportments but rather support more tardive functions of alphavirus infectious cycle such as the selective packaging of viral RNA or viral assembly.

a. Structure and composition of nsP3 tubular assemblies

Electron micrographs of CHIKV-infected or nsP3-expressing cells showed the presence of highly ordered tubular networks. Specific nsP3-immunogold labelling confirmed that these structures are indeed nsP3 tubular assemblies. Electron micrographs of transversal sections revealed homogeneously spaced cylindric structures. The inner cylinders perfectly correspond in size to the channel formed by the AUD-helical arrangement in vitro. Densities surrounding the channel likely correspond to the AUD plus the MD. Additional extra-densities surrounding the tubes certainly correspond to host and viral factors recruited by the nsP3. The precise positioning of the HVD is still unknown. Interestingly, nsP3 tubes formed *in vitro* do not generate well-ordered assemblies' structures, as found in CHIKV-infected or nsP3-expressing cells. This suggests that independent nsP3 tubes can't stack together and that viral or host factors are probably required for the nsP3-tubular network formation. Whereas full-length nsP3 expression leads to the formation of well-structured tubes, AUD expression in the absence of the other two protein domains results in much

longer and disorganized filamentous structures resembling amyloid fibrils.

nsP3 cytoplasmic aggregates have been reported in multiple studies (Elena Frolova et al. 2006; D. Y. Kim et al. 2016b; Remenyi et al. 2017; 2018; Meshram et al. 2018; Jayabalan et al. 2021b). All of them used optical microscopy techniques to describe the morphology and composition of these aggregates. As they contain several components of stress granules (Marc D. Panas et al. 2012; Jayabalan et al. 2021b) and they appear as spherical membrane-less structures (Marc D. Panas et al. 2012; Jayabalan et al. 2021b; Remenyi et al. 2017), nsP3-aggregates have been proposed to be very similar to stress granules (Figure 3). In CHIKV-infected cells, nsP3 complexes close to the plasma membrane are formed in association with dsRNA and host factors such as G3BP (J. J. Fros et al. 2012; D. Y. Kim et al. 2016). As the infection progresses, larger, spherical nsP3 aggregates could be observed away from the plasma membrane, and 24h post-infection nsP3-aggregates showing a rod-like morphology could be observed. In the early stages of the infection, when stress granules are formed in response to viral infection, the nsP3 protein mediates their disassembly and sequester the RNA-binding proteins (G3BP) into nsP3-enriched aggregates. These nsP3 condensates are resistant to cycloheximide treatment suggesting that they are not *bona fide* SG (Jayabalan et al. 2021).

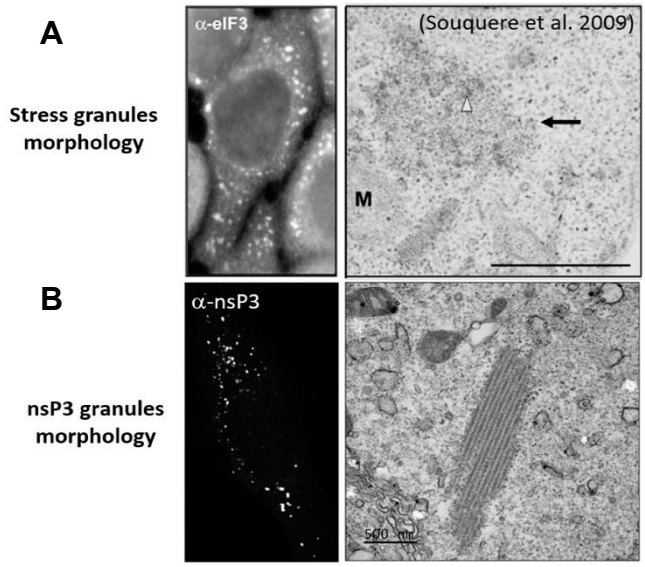

Figure 3: Comparison of SGs and nsP3-assemblies ultrastructure. *A, Fluorescence (left) and electron (right) micrographs showing stress granules ultrastructure (From Souquere et al. 2009). B. Fluorescence (left) and electron (right) micrographs of nsP3 in CHIKV infected human fibroblasts (From Kril et al. 2023 submitted).*

Stress granules are formed by liquid-liquid phase transition driven by protein-protein and RNA-protein interactions. These condensates are dynamic membrane-less structures that can exchange components with the cellular milieu. When observed by electron microscopy, SG are membrane-less condensates with irregular outlines, containing granular structures (likely ribosomes) within a loosely organized and non-uniform milieu (Figure 3A). Interestingly, whereas SGs ultrastructure agrees with their appearance in fluorescence microscopy, nsP3-cytoplasmic condensates exert a completely different organization (Figure 3B). These condensates are actually tubular structures closely tight one to another, forming a highly-ordered electron-dense

network. In contrast with SGs that assemble and disassemble rapidly, nsP3 tubular networks are apparently much more rigid and stable, as they can be observed even 48 hours post-infection.

Further investigations are required to understand the kinetics of nsP3 tube formation and their ability to exchange components with the surrounding milieu. It is possible to apply the Fluorescence Recovery After Photobleaching (FRAP) approach to get insights into nsP3 kinetics in an infectious or overexpression context. FRAP is a single molecule technique where a specific area of the cell is selectively photobleached so that recovery of fluorescence to that area can be observed. With this technique, we can eventually track nsP3 and its interactant motility. Applying live cell imaging could also be valuable to investigate whether the nsP3 structures come from the plasma membrane after viral RNA synthesis was achieved and then grow progressively while moving away from vRC, or nsP3cytoplasmic aggregates form from newly translated nsP3, which is not required for vRC formation. The latter hypothesis appears plausible because as the viral replication progresses, non-structural polyprotein concentration rises, and its processing becomes faster. Thus, it is possible that an important fraction of nsP3 is not addressed to the plasma membrane and is not used for vRC formation. Another important question is whether these assemblies are dynamic virus-induced organelles that exchange components with the cytoplasmic milieu.

Our data and other studies demonstrated that nsP3 cytoplasmic tubular structures recruit host factors (nsP3-interactants G3BP, FHL1, CD2AP, and likely other RNA-binding proteins)(Götte, Liu, et McInerney 2018; Meshram et al. 2018; Nowee et al. 2021). In addition, we and others also identified that nsP3 tubes recruit viral nsP2 protein and capsid but not nsP1 or envelop proteins (Zheng and Kielian 2013, Kril et al. 2023, submitted) (Figure 4) . Furthermore, genomic viral RNA was found to colocalize with these nsP3 assemblies in infected cells, but no replicative dsRNA intermediate, demonstrating that these are not active replicative complexes. Interestingly, the presence of nucleic acids is consistent with the structural features of the

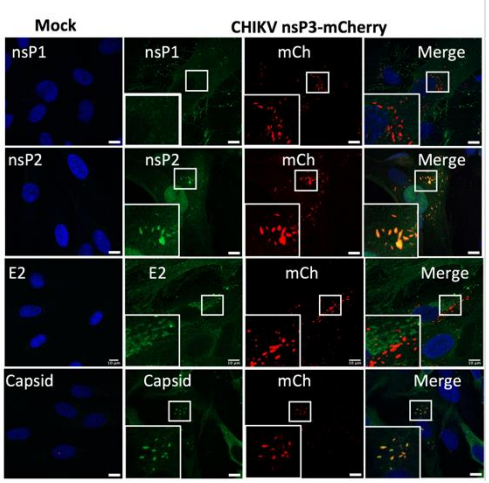

Figure 4: nsP3-tubular assemblies contain nsP2 and capsid but not nsP1 and E2 viral proteins.

nsP3helical scaffolds. Supplementary investigations are required to assess whether viral RNA molecules are found within the channel formed by the AUD, thus buried and protected from the cellular environment, and whether these nsP3 structures selectively trap and transport genomic and sub-genomic RNA species. We are currently trying to isolate and purify nsP3 tubes from infected cells to establish their protein and RNA composition.

b. Functions

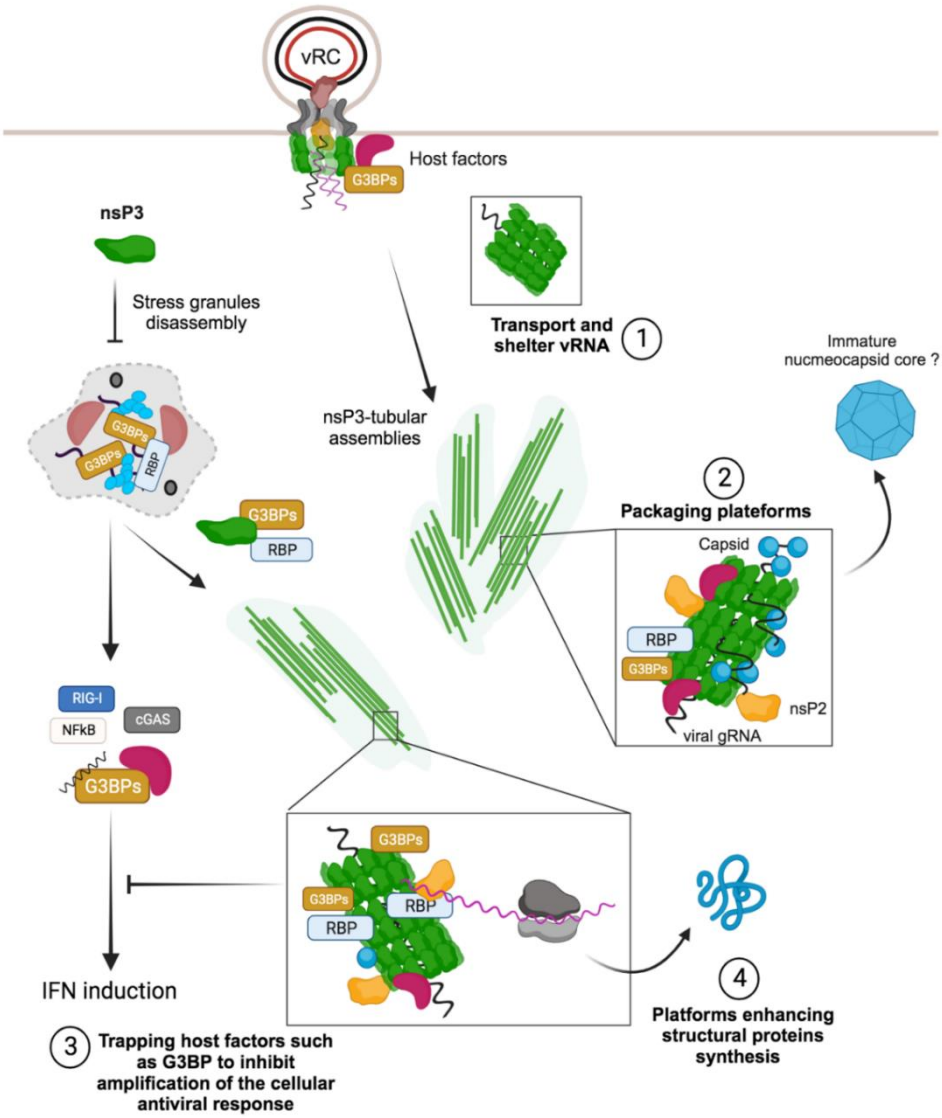

Figure 5. Overview of nsP3-tubular assemblies' potential functions during alphavirus replication. *vRC, viral replication complexes; RBP, RNA-binding proteins.*

Alphavirus nsP3 are obviously not active viral replication complexes, but they contain multiple viral and host factors. They differ from bona fide "viral factories" as they are neither membranous organelles nor viral inclusions formed by liquid-liquid phase separation. nsP3assemblies result from the oligomerization of the nsP3 AUD domain, which constitutes the core tubular structure. Each nsP3 mediates multiple interactions with cellular and viral host factors, which are recruited to these tubes and

likely mediate their well-ordered architecture in the cellular context. A fundamental question is whether these tubular assemblies are actively formed during the viral cycle or constitute an indirect consequence of excess viral material. Because nsP3 assemblies are not amorphous aggregates of viral proteins but rather extremely well-organized tubular networks, we suggest that they might be functional in contributing to an efficient alphavirus replicative cycle (Figure 5).

nsP3 tubular transport viral RNA and constitutes a platform for specific viral RNA packaging

How do alphaviral nascent genomes traffic from the vRC to packaging sites, and what is the precise subcellular localization of these sites is unclear. Recent cryo-electron tomography studies reported that immature nucleocapsids are formed into the cytoplasm and traffic to the plasma membrane for the assembly and budding (Chmielewski et al. 2022). In vitro studies of alphavirus genome packaging demonstrated that nucleic acids (RNA) are an absolute prerequisite for capsid oligomerization and assembly (Mukhopadhyay et al. 2002; Mendes et Kuhn 2018). Interestingly, in vitro, the nature of the RNA is not of great importance, suggesting that in the cellular context, viral RNA must be sorted and specifically addressed for packaging. Intracellular modeling of alphavirus packaging also suggests that alphavirus nsPs might play a role in viral RNA packaging. Indeed, nsP2 was found to harbor adaptive mutations when VEEV capsid sites involved in packaging were mutated (D. Y. Kim et al. 2013). Interestingly capsid proteins were found to colocalize with nsP3 “granules”, and newly synthesized capsid proteins were found to be continuously addressed to these sites (Zheng and Kielian 2013).

In light of these and our data, nsP3 helical scaffolds could be involved into the transport of viral RNA from the vRC to the sites where capsid proteins are produced. The organized nsP3 network could serve as a platform for specific viral RNA packaging, thus limiting unspecific packaging and protecting viral RNA from degradation and recognition by cellular immune sensors. Eventually, nsP3assemblies could create an optimal microenvironment connecting capsid to viral RNA (Figure 5 step 1,2,3).

nsP-tubular networks are negatively regulating stress response and cellular antiviral immunity

nsP3 tubular assemblies were shown to contain several host factors involved into CHIKV infection, such as FHL1, CD2AP or G3BP proteins. Whereas the precise role of FHL1 or CD2AP is unclear, G3BP proteins have been widely studied in physiological and infectious contexts. G3BP is known as a core component for stress granules (SGs) formation. SGs are disassembled through the macrodomain ADP-ribose binding and hydrolase activities in the early steps of alphavirus infection. It is proposed that SGs disassembly leads to the sequestration of G3BP, which is addressed to viral replication complexes that promote efficient vRC clustering and viral RNA synthesis. In addition, SG disassembly releases translation initiation factors that can be further used for viral protein synthesis. Interestingly, G3BPs organize SGs and amplify multiple immune signaling pathways (RIG-I, NF-kB, cGAS-STING, PI3K-akt-mTOR pathways), establishing an antiviral state. Thus, nsP3 tubular scaffolds might sequester G3BP and other antiviral or cellular stress factors to allow efficient replication, protein synthesis, and production of new infectious particles (Figure 5 step4). Finally, nsP3-assemblies could be also involved in the efficient translation of viral structural proteins (Figure 5 step 5). It was demonstrated that 2 to 4 hours post-infection, alphaviruses induce a general shutoff of protein synthesis. Interestingly viral sub-genomic RNAs are efficiently translated in this context. We still ignore if sub-genomic RNA species are found in the nsP3-assemblies. Interestingly, the presence of nsP2 and G3BP, which are known to interact with different ribosomal subunits, eventually pinpoint a role in protein synthesis.

Further experiments to establish nsP3 scaffold functions are required. We are conducting preliminary experiments to establish an efficient nsP3-tube purification protocol using a CHIKV virus expressing a dual-tagged HA/FLAG-tagged nsP3 protein (Figure 6). In our first attempt, we efficiently purified nsP3 from infected cells, as shown in the western blot analysis (Figure 6B). The purified complexes were subjected to mass spectrometry analysis, from which the 74 statistical hits are shown in Figure 6C. We efficiently co-immunoprecipitated nsP3 since the most statistically significant peptides belong to the nsP3. In addition, we also found in the complex nsP2 and nsP1 peptides. Finally, we also efficiently pulled down the major nsP3-interacting factors (G3BP, NAP1L1, FHL1). Consistently with our other data and the western blot (Figure 6B), we also identified the capsid protein. Surprisingly, peptides corresponding to the

E2 glycoprotein are also found. A preliminary gene ontology analysis revealed that most of the host factors in immunoprecipitated complexes are RNA metabolism or translational proteins. We also found a substantial part of the interactants belonging to the cytoskeleton network (Figure 6C, pie chart). Other experiments must be performed to validate these hits. In addition, we failed to show that the immunoprecipitated complexes are nsP3-oligomers. However, these preliminary data pinpoint a function of nsP3 in RNA metabolism and translation. Sequencing of RNAs found in complex with the nsP3 will be of great interest.

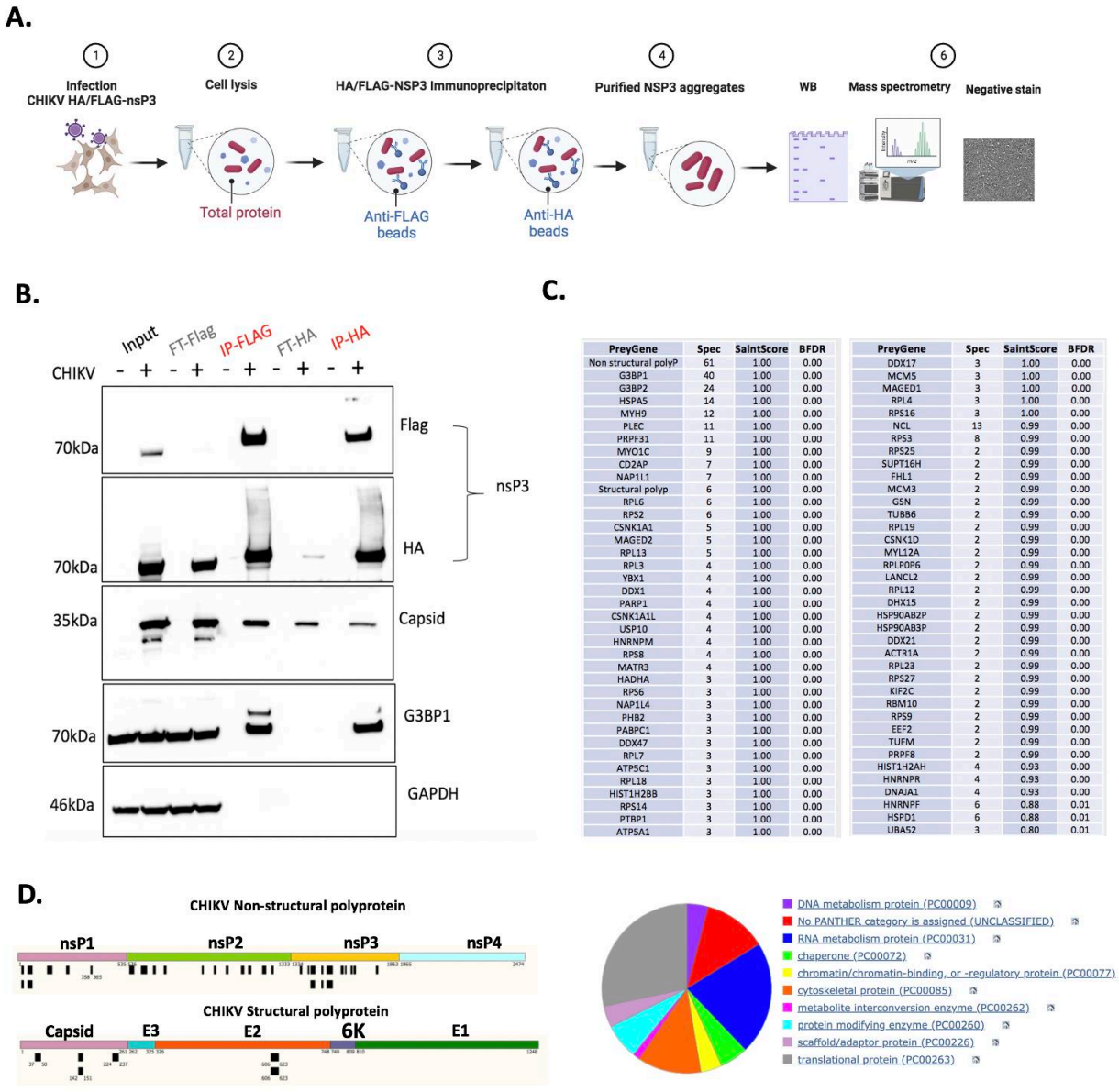

PreyGene	Spec	SaintScore	BFDR
Non structural polyP	61	1.00	0.00
G3BP1	40	1.00	0.00
G3BP2	24	1.00	0.00
HSPA5	14	1.00	0.00
MYH9	12	1.00	0.00
PLEC	11	1.00	0.00
PRPF31	11	1.00	0.00
MYO1C	9	1.00	0.00
CD2AP	7	1.00	0.00
NAP1L1	7	1.00	0.00
Structural polyp	6	1.00	0.00
RPL6	6	1.00	0.00
RPS2	6	1.00	0.00
CSNK1A1	5	1.00	0.00
MAGED2	5	1.00	0.00
RPL13	5	1.00	0.00
RPL3	4	1.00	0.00
YBX1	4	1.00	0.00
DDX1	4	1.00	0.00
PARP1	4	1.00	0.00
CSNK1A1L	4	1.00	0.00
USP10	4	1.00	0.00
HNRNPM	4	1.00	0.00
RPS8	4	1.00	0.00
MATR3	4	1.00	0.00
HADHA	3	1.00	0.00
RPS6	3	1.00	0.00
NAP1L4	3	1.00	0.00
PHB2	3	1.00	0.00
PABPC1	3	1.00	0.00
DDX47	3	1.00	0.00
RPL7	3	1.00	0.00
ATP5C1	3	1.00	0.00
RPL18	3	1.00	0.00
HIST1H2BB	3	1.00	0.00
RPS14	3	1.00	0.00
PTBP1	3	1.00	0.00
ATP5A1	3	1.00	0.00

PreyGene	Spec	SaintScore	BFDR
DDX17	3	1.00	0.00
MCM5	3	1.00	0.00
MAGED1	3	1.00	0.00
RPL4	3	1.00	0.00
RPS16	3	1.00	0.00
NCL	13	0.99	0.00
RPS3	8	0.99	0.00
RPS25	2	0.99	0.00
SUPT16H	2	0.99	0.00
FHL1	2	0.99	0.00
MCM3	2	0.99	0.00
GSN	2	0.99	0.00
TUBB6	2	0.99	0.00
RPL19	2	0.99	0.00
CSNK1D	2	0.99	0.00
MYL12A	2	0.99	0.00
RPLP0P6	2	0.99	0.00
LANCL2	2	0.99	0.00
RPL12	2	0.99	0.00
DHX15	2	0.99	0.00
HSP90AB2P	2	0.99	0.00
HSP90AB3P	2	0.99	0.00
DDX21	2	0.99	0.00
ACTR1A	2	0.99	0.00
RPL23	2	0.99	0.00
RPS27	2	0.99	0.00
KIF2C	2	0.99	0.00
RBM10	2	0.99	0.00
RPS9	2	0.99	0.00
EEF2	2	0.99	0.00
TUFM	2	0.99	0.00
PRPF8	2	0.99	0.00
HIST1H2AH	4	0.93	0.00
HNRNPR	4	0.93	0.00
DNAJA1	4	0.93	0.00
HNRNPF	6	0.88	0.01
HSPD1	6	0.88	0.01
UBA52	3	0.80	0.01

Figure 6: nsP3 tubular assemblies' purification and interactome analysis. *A. Experimental approach for nsP3 purification from infected cells. B, Western blot analysis of immunoprecipitated nsP3 complexes. C, statistically significant mass spectrometry (MS)-identified nsP3-interactants (table) and their corresponding molecular functions (pie chart). D, Mapping of the viral peptides identified in the MS.*

c. Structural characterization of nsP3 tubes by cryo-electron tomography

In order to reveal the precise structure and composition of these tubes, our lab has started to characterize the structural basis of nsP3 tubes by cryo-electron tomography in collaboration with the Nanoimaging facility of the Pasteur Institute (Dr Anna Sartori-Rupp, Stéphane Tachon, and Johannes Groen). The aim of these experiments was to characterize nsP3 tubes in a context as close as possible to what happens during CHIKV infection. In addition, to avoid structural artifacts due to the chemical fixation of the samples, we chose to work only on vitrified samples. However, we could not prepare and image cells infected with wild-type CHIKV because of technical and security limitations. Instead, we used single-round CHIKV viral particles (CHIKV RVPs) (Figure 7). These particles were assembled following the co-transfection of in vitro transcribed and capped CHIKV-GFP or CHIKV-nsP3 mCherry replicon RNA molecules, a capsid, and envelope proteins encoding RNA. Thus, the CHIKV-GFP RVPs can enter cells, produce non-structural proteins, and establish vRC and RNA synthesis without producing structural proteins and infectious virions (Figure 7, upper panel).

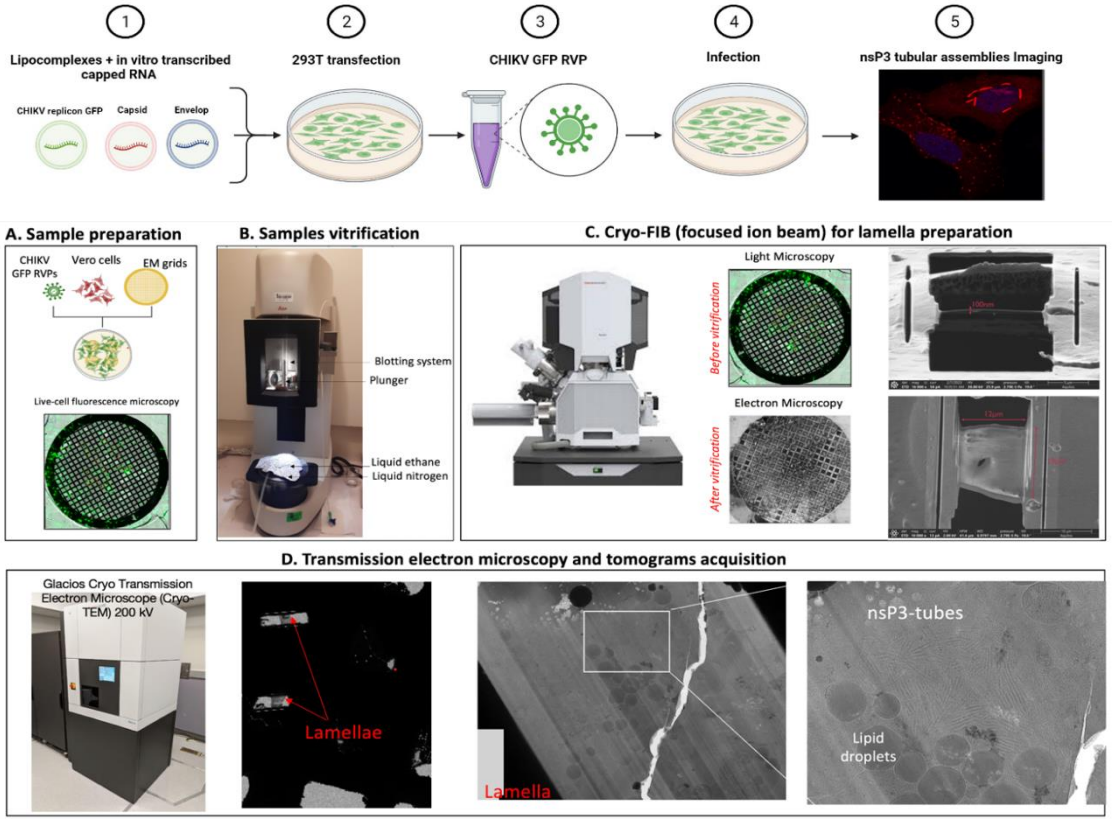

Figure 7: *Experimental approach for CHIKV non-infectious virus particle production (upper panel steps 1 to 5) and in situ characterization of nsP3-tubes by cryo-electron tomography (lower panel A. to D.).*

The experimental approach for cryo-electron tomography sample preparation and tomogram acquisition is illustrated on Figure 7, lower panel. Vero cells were infected with CHIKV RVP and seeded on cryo-electron microscopy grids. 24h post-infection cells were imaged under a fluorescence microscope and grids were vitrificated at -188°C. Grids were then transferred to the cryo-FIB microscope for lamellae preparation. Targeted cells were first rough mild, and most promising lamellae were thinned to obtain around 100nm thin sections. Grids were finally observed under a transmission cryo-electron microscope for analysis and tomogram acquisition.

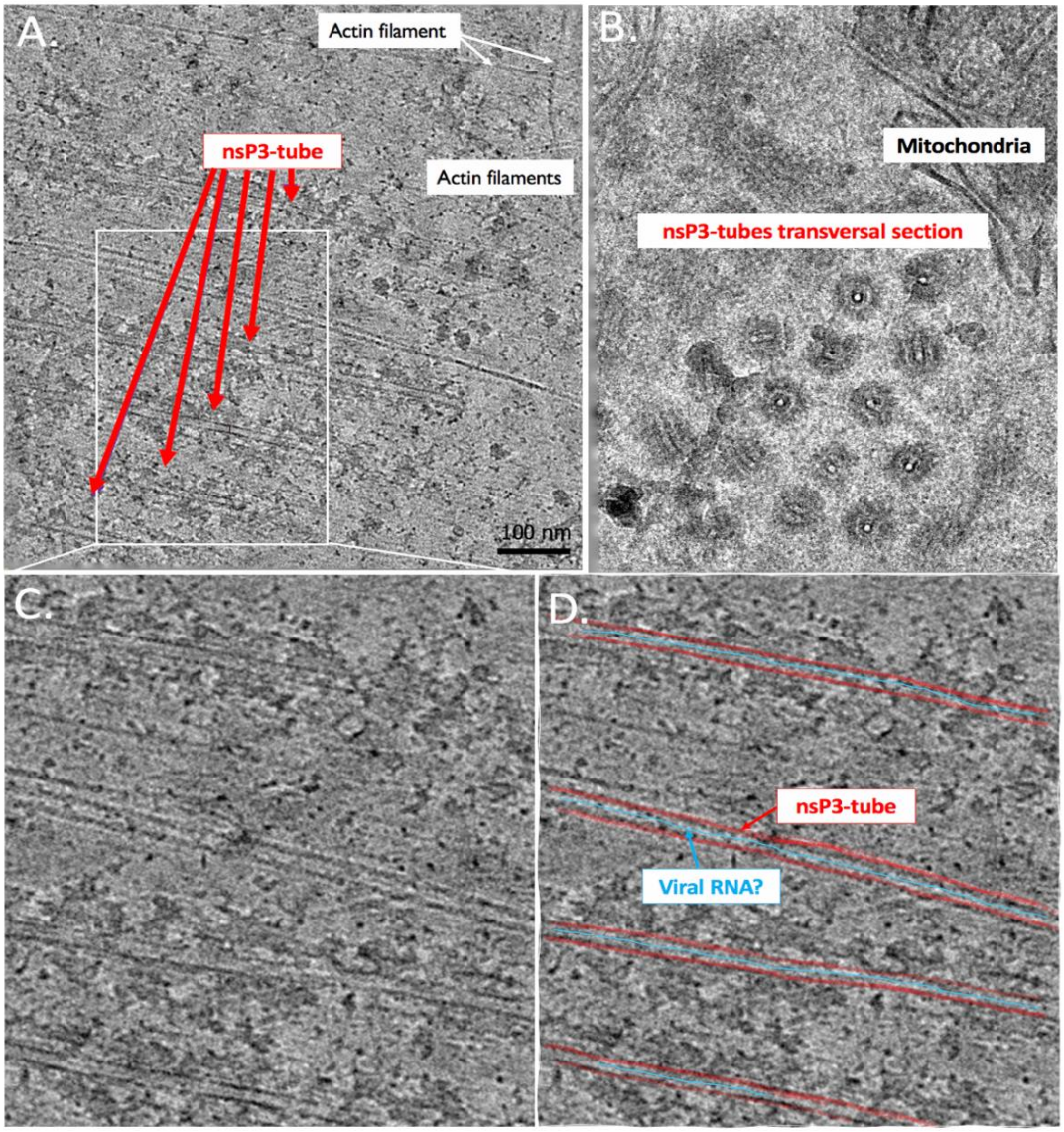

Figure 8. Cryo-electron tomography of nsP3-tubular structures in CHIKV single-round particles infected Vero cells

Using this experimental approach, we successfully detected nsP3 tubular networks in CHIKV-infected cells (Figure 8), albeit very few lamellae were positive, meaning that supplementary setups are required. Preliminary images from

reconstructed tomograms (reconstruction by Dr Anna Sartori-Rupp) are shown in Figure 8. Longitudinal section (Figure 8A) shows tubular structures arranged in parallel and close to actin filaments. The transversal section (Figure 8B) shows the inner channel, which appears empty, with surrounding extra-densities as observed by classic electron microscopy. Images also revealed that in the same assembly, all nsP3 tubes are not arranged in parallel but rather form a mesh of tubes. Interestingly, when observed lengthwise, the edge of each tube is dense and well-delineated (Figure 8C, D red lines), whereas in the space between, which correspond to the channel, a very thin line of dense material could be observed. Analysis of the acquired tomograms are ongoing to decipher nsP3 tube organization and composition.

One limitation to our approach was the use of a non-infectious system since infectious and unfixed samples could not be handled on the platform. Thus, the infected cells synthesize viral RNA but not viral structural proteins. This implies that the role of nsP3 assemblies in the later steps of CHIKV replication cycle could not be investigated. However, this system certainly will give us valuable information about the presence of nucleic acids in the nsP3 tubes channel or in the exterior in complex with other viral or host proteins. This approach could also demonstrate if other cellular components such as ribosomes are recruited to these sites, which could imply sites of active protein synthesis. Finally, we can also assess the interplay between nsP3 structures and the cytoskeleton network. We still don't know if these structures are anchored to the actin or microtubular cytoskeleton, and thus if it is able to from plasma membrane to deeper cytoplasmic sites.

d. Conclusions and further perspectives

This work presents a deep ultrastructural analysis of CHIKV nsP3-structures for the first time and proposes a functional role of these assemblies in the late steps of the infectious cycle. From a structural perspective, no other viral family is known to induce de formation of such highly-ordered assemblies. However, we can draw a parallel with the NSs protein, a major virulence factor of the Rift Valley Fever virus (RVFV) (Barski et al. 2017; Léger et al. 2020). This protein assembles spontaneously into of 12-nm width amyloid fibrils, which grow as the infection progresses. In contrast to the nsP3-tubes, RVFV-NSs likely assemble through their intrinsically disordered domain and their N-terminal, which is prone to form β-strands. Interestingly, this protein is involved in the inhibition of type I interferon (IFN)-induced antiviral response,

as well as cell cycle regulation (Barski et al. 2017; Léger et al. 2020). RVFV NSs amyloid fibrils are found in the nucleus and the cytoplasm, although shorter in length.

Whether nsP3 assemblies directly affect viral replication or not, studying their impact on cell viability and homeostasis is crucial. Indeed, previous studies suggested that nsP3 condensates formed following CHIKV infection or nsP3 overexpression are stable and persistent structures (Remenyi et al. 2017; 2018). In addition, it was demonstrated that in CHIKV-infected mice, some infected myofibers and fibroblasts survive acute infection and harbor viral RNA (Young et al. 2019). Altogether, investigating whether CHIKV-infection-surviving cells harbor nsP3-tubular assemblies, viral RNA, and proteins is of great interest. Indeed, if nsP3 tubular assemblies can persist in surviving muscle cells in infected patients, it could trigger a continuous induction of proinflammatory cytokines (IL-6, IL-1β, TNFα, and IP10) which are biomarkers of disease severity (Lentscher et al. 2020; Nair et al. 2017). This could have important implications regarding CHIKV- and alphavirus-induced chronic immunopathology and further development of specific therapeutic strategies.

B. Molecular mechanisms of FHL-1 mediated CHIKV infection

Different screens have been performed in the last years to identify host factors involved in CHIKV infection (Cristea et al. 2006; Bouraï et al. 2012; Meshram et al. 2018b; Lark, Keck, et Narayanan 2018; Kumar et al. 2018; Meertens et al. 2019). FHL1 is a recently discovered host determinant involved in CHIKV infection *in vitro* and *in vivo*. Importantly, FHL1 is, to our knowledge, the only CHIKV host-dependency factor whose expression pattern (muscle cells and fibroblasts) correlates with CHIKV tropism for musculoskeletal tissues (Cowling et al. 2008; Gueneau et al. 2009; Han et al. 2020; Meertens et al. 2019). FHL1 is one of the multiple CHIKV-nsP3 interacting partners along with G3BP and the SH3-domain containing proteins Bin1 and CD2AP. The work reported here aimed to characterize the interaction between FHL1 and nsP3 and to bring insights into how FHL1 mediates CHIKV infection

1. FHL1 interactions with the nsP3 HVD and implication in infection

NMR experiments performed by our collaborators demonstrated that all four FHL1-domains are involved in the interaction with the nsP3 HVD. Conversely, the HVD domain that mediates FHL1-binding extends beyond the already published region (Lukash et al. 2020; Meertens et al. 2019). Furthermore, this region contains residues

that mediate interactions with Bin1 and CD2AP. The interplay between FHL1 and the latter factors is unclear. Previous studies also demonstrated that FHL1-binding does not have any impact on CD2AP/nsP3 interaction, suggesting that there is no cooperative effect. From infection experiments on Bin1 and CD2AP^{KO} human cell lines, we established that CD2AP is not required for CHIKV infection, but Bin1 considerably participates. However, FHL1 depletion drastically reduced viral replication, although CHIKV remains viable when higher MOIs are applied. We can't rule out the possibility that Bin1 and FHL1 have additional proviral functions and that their importance depends on the infected cell type. However, in physiological conditions, FHL1 and Bin1 are not found in common cellular pathways, which can pinpoint a common function.

The deletion of the FHL1-binding domain (R5) reported by NMR, which is also mediating Bin1/CD2AP, led to a drastic reduction of viral replication in 293T, U20S (also human cell line), or Vero cells but not BHK21. Interestingly, Vero and BHK21 cells do not express FHL1 but express FHL2, albeit at a very low level for BHK21. Both cell lines support productive infection with the wild type CHIKV. FHL2 is another LIM-domain containing protein exerting comparable cell type and tissue expression pattern to that of FHL1. In addition, we and other groups showed that FHL2 could interact with the HVD and restore viral infection to some extent (Lukash et al. 2020; Meertens et al. 2019).

Altogether these data suggest that FHL1 is likely not involved in a fundamental step of the CHIKV replication cycle. In addition, in Vero cells, Bin1, CD2AP, and/or other FHL-family proteins recruited by the R5 region of nsP3 might fulfill the same functions as FHL1 in human cells. Levels of Bin1 and CD2AP expression in this cell line are unknown. Generating Vero knockout cells for Bin1, CD2AP, and FHL2 to test the ability of wildtype CHIKV to replicate could give us valuable information. In BHK21, the R5 deleted virus mediates productive infection, suggesting that the potential host factors recruited by this domain are not important for CHIKV replication in rodent cells. However, BHK21 cells are deficient in the production of IFN-type I (Stanwick et Hallum 1974; MacDonald et al. 2007) and barely express FHL2. Altogether, these results pinpoint a role of FHL1 in regulating or repressing the cellular antiviral response rather than a direct function in CHIKV replication (vRC formation, RNA synthesis). This is supported by other findings in Huh7.5 cells that express neither FHL1 nor FHL2 (Lukash et al. 2020), but are still susceptible to CHIKV. Huh7.5 cells are not fully

immunocompetent, as they possess a missense mutation in the RIG-I encoding gene. Assessing CHIKV infection in the original Huh7 cell line will likely be more informative. If FHL1 usage is linked to the antiviral response, parental Huh7, which can induce type-I IFN, must be less susceptible to CHIKV. Conversely, the trans-complementation with FHL1 must enhance CHIKV propagation in these cells.

Finally, the ability to productively infect hamster BHK21 but not human immunocompetent cells with the R5-deleted CHIKV represents a potential strategy for generating attenuated CHIKV. The next step of the project is to address whether this mutated R5 CHIKV replicates and induces musculoskeletal pathology in mice (collaboration with Pr. Marc Lecuit, Pasteur Institute)

2. Investigating the molecular mechanisms of FHL1-mediated CHIKV infection

Previous data published by our group demonstrated that FHL1 is required for post-entry steps, likely for the formation of viral replication complexes and RNA synthesis. Indeed, as soon as 6 hours post-infection, drastic effects of FHL1 depletion were observed on the synthesis of the negative RNA strand, suggesting that FHL1 is involved in the very early steps of RNA synthesis. Surprisingly, further experiments suggested that FHL1 is likely not a direct component of vRC. For instance, whereas transfected full-length CHIKV RNA failed to replicate efficiently in $FHL1^{KO}$ cells, CHIKV replicon system was able to fulfill viral synthesis, albeit not at wild-type levels. In contrast, G3BP protein depletion completely abolished RNA synthesis in both systems. Finally, subcellular localization of FHL1 and G3BP in the late steps of viral infection demonstrated that G3BP but not FHL1 is in close proximity to vRC. Altogether, our data suggest that FHL1 might indirectly enable viral RNA synthesis. Since FHL1 is a major nsP3-binding partner, one can speculate that it could regulate nsP3 expression, subcellular localizations, or tubular assemblies. However, FHL1 depletion did not impact either nsP3 expression, stability, or its oligomerization property. This was somehow expected as nsP3 oligomerization is driven by the nsP3 AUD, not the HVD. Furthermore, FHL1 is specifically used by CHIKV and its close relative ONNV but not by other alphaviruses, whereas all alphavirus nsP3 are able to oligomerize.

a. FHL1 as a scaffold connecting viral structures and the actin cytoskeleton

LIM-domain-containing proteins are known to interact with components of the actin cytoskeleton, such as actin-binding or membrane proteins (Sharma et al. 2011; L. Wang et al. 2013) The FHL1-interactome reported here also suggests that FHL1 complexes with several actin- and myosin binding factors (SPTBN1, SPTBN2, SPTAN1, MYH9, MYH10, MYH14, FLII, ADD2, KIF2A). Interestingly, the knockdown of SPTBN1 resulted in an important reduction of CHIKV replication. SPTBN1 (spectrin beta, non-erythrocytic 1) spectrin is an actin crosslinking agent and a molecular scaffold protein. It establishes a connection between the plasma membrane and the actin cytoskeleton, playing a vital role in shaping cells, positioning transmembrane proteins, and arranging organelles within the cell (Panyu Yang et al. 2021). There are only a few occurrences of SPTBN1 involved in viral infection. During HIV1 replication in macrophages, SPTBN1 was identified as a proviral host factor thought to associate with the viral capsid and matrix proteins to mediate the uncoating process (Dai et al. 2013; Havlicek, s. d.). Interestingly, recently SPTBN1 was also identified as an interactant of Semliki Forest virus (SFV) nsP2 interactant along with other cytoskeleton proteins. siRNA downregulation of SPTBN1 was shown to reduce viral SFV infection, suggesting that this protein is a proviral factor (Contu et al. 2021). Interestingly, SFV doesn't use FHL1 as a proviral factor, and in our experiments, SPTBN1 was found as an FHL1 interactant in the absence of viral infection. Given these results, we can speculate that FHL1 could mediate the transport of viral or cellular components between vRC and nsP3-tubular assemblies. FHL1 could be a scaffold for viral structures recruiting cytoskeleton-binding proteins required for nsP3 helical assemblies to traffic between different cellular sites.

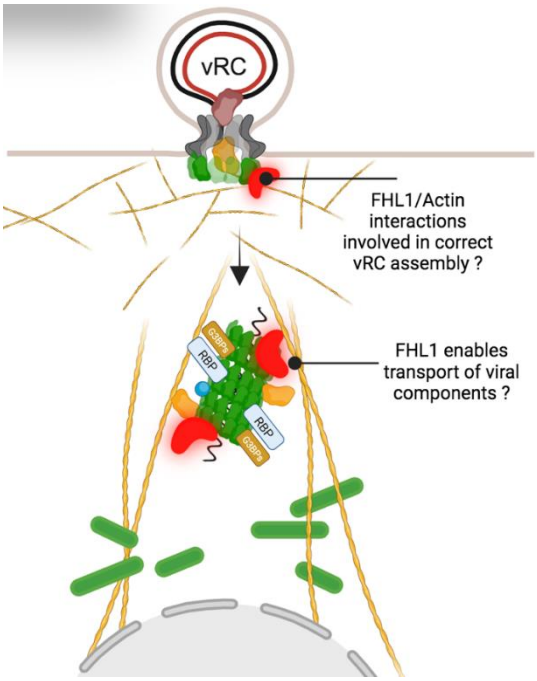

Figure 9: FHL1 as a scaffold for CHIKV interaction with the actin cytoskeleton.

b. FHL1 as an antiviral immunity repressor

Interestingly, FHL1 immunoprecipitation from CHIKV-infected cells demonstrated that this protein was found in a complex with cellular PKR and HERC5. PKR plays a dual role as a sensor and effector in the immune response against viral infections. Upon detecting double-stranded RNA molecules within infected cells, PKR undergoes self-activation (Cesaro et Michiels 2021). Its primary antiviral function involves impeding the translation process and triggering apoptosis. In the context of viral infections, HERC5 is known for its ability to inhibit viral replication (reviewed in Mathieu et al. 2021). It achieves this by adding ubiquitin-like molecules (ISG15, or interferon-stimulated gene 15) to viral proteins, a process known as ISGylation. HERC5 is the only human E3-ubiquitin ligase that is known to conjugate ISG15 to host and viral proteins. ISG15 modification interferes with various stages of the viral life cycle, such as viral transcription, translation, assembly, and release (Dzimianski et al. 2019; Mathieu et al. 2021). This modification can disrupt the proper functioning of viral components and thereby limit the ability of the virus to replicate and spread (Mathieu et al. 2021). In this context, one can speculate that FHL1 is able to repress or counteract such immune actors. A plausible explanation could be that FHL1 interacts with HERC5 and repress its ability to conjugate ISG15 moieties to viral non-structural or structural proteins. When FHL1 is depleted from immunocompetent cells, HERC5 can mediate viral proteins ISGylation and inhibit their functions. Additionally, ISGylation of immune sensors such as RIG-I, MDA5 or PKR can amplify the cellular antiviral state (Figure 10). Alternatively, FHL1 could be involved into the regulation or repression of antiviral long non-coding RNA (lncRNA). Indeed, recent studies identified the transcription of the lncRNA ALPHA, which is triggered upon infection with different alphaviruses, but also restricts CHIKV and ONNV infection. This is of great interest as FHL1 is specifically used by CHIKV and ONNV, but not the other alphaviruses (Basavappa et al. 2022). The lncRNA ALPHA was demonstrated to directly interact with CHIKV genome and to restrict viral replication in a IFN -independent manner (Basavappa et al. 2022). One can speculate that in absence of FHL1, such lncRNA -mediated restrictions of viral infection could be amplified leading to the inability of CHIKV to productively infect the cells. Further experiments are required to establish a link between FHL1 and the cellular antiviral state during CHIKV infection. Validating direct interaction between FHL1 and HERC5 or ISG15 will be important to validate the hypothesis. Additionally, sequencing cellular RNAs in both control and FHL1 deficient

cells will give us a global picture of the upregulated immune pathways that can affect CHIKV replication.

3. FHL1 usage and CHIKV tropism and pathogenesis

FHL1 is the only host factor identified so far that could explain, at least in part, CHIKV tropism for musculoskeletal tissues and joints. FHL1 regulates myogenesis, activating satellite cells and transforming them into myoblasts (Cowling et al. 2008; Wilding et al. 2014; Han et al. 2020). These myoblasts subsequently fuse to form myotubes, ultimately differentiating into mature myofibers (Cowling et al. 2008; Wilding et al. 2014; Han et al. 2020). The heightened expression of FHL1 in muscle satellite cells may make them more susceptible to CHIKV infection. When nsP3 recruits FHL1 into the tubular assemblies, it is plausible that infected muscle satellite cells may struggle to efficiently regenerate damaged muscle fibers, potentially contributing to musculoskeletal disorders induced by CHIKV. This hypothesis is further strengthened by studies focused on FHL1-linked myopathies. In addition to the Emery Dreifuss Muscle Disorder linked to a mutation in the *fhl1* gene leading to a reduced protein expression, other mutations can lead to the formation of abnormal aggregates or clumps of FHL1 proteins that accumulate within muscle cells, particularly in the subsarcolemmal and sarcoplasmic regions (Schessl et al. 2008; 2011; Cowling et al. 2011; Wilding et al. 2014). These aggregates are called reducing bodies. Mechanistic studies reported that FHL1-reducing bodies mutations lead to a loss of wild-type FHL1 function and a gain of new toxic function, impairing myoblasts fusion (Schessl et al. 2008; 2011; Cowling et al. 2011; Wilding et al. 2014). Thus, one can speculate that once FHL1 is trapped in the nsP3-tubular assemblies in infected myoblasts, it can no longer exert its physiological functions and further damages the muscle cell (Figure 10).

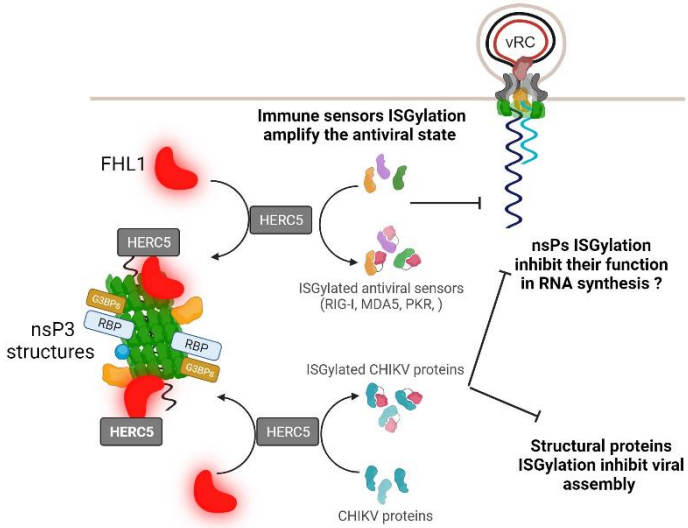

Figure 10: Model for FHL1-mediated repressing of HERC5 and its subsequent impact on viral infection

The connection between FHL1 and the severity of CHIKV-induced disease is indirectly supported, as various CHIKV strains appear to utilize FHL1 differently. Notably, the CHIKV-21 strain isolated during the 2005–2006 outbreak on Reunion Island heavily relies on FHL1 for in vitro infection and induced severe muscular pathology in mice. On the other hand, the necessity for FHL1 was not as noticeable for the sylvatic CHIKV 37997 strain from the West African genotype (Meertens et al. 2019) and the weakened CHIKV 181/25 strain (Lukash et al. 2020), both of which exhibit lower pathogenicity in mice (Rohatgi et al. 2014). Investigating the underlying molecular mechanisms governing FHL1 utilization by various CHIKV strains could offer valuable insights into the muscular complications linked to CHIKV infection. Moreover, a study examining FHL1 polymorphisms in cohorts of CHIKV-infected individuals could significantly underscore the relevance of this host factor to CHIKV pathogenesis in vivo.

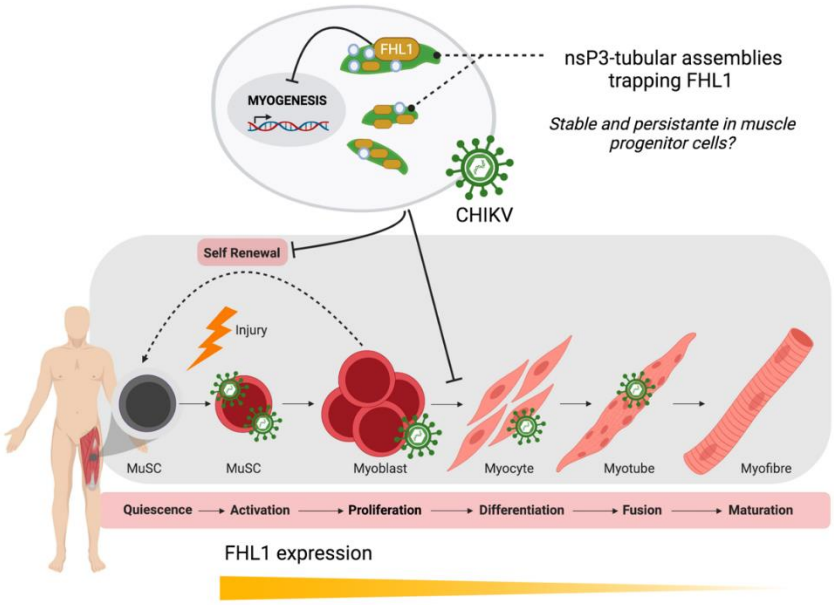

Figure 11: FHL1-hijacking and sequestration by CHIKV-nsP3 might be involved in impaired muscle cell regeneration and differentiation. *Modified from Nguyen et al. 2019*

C. Concluding remarks

Despite multiple studies on alphavirus nsP3 protein, little is known about how it orchestrates viral replication and counteracts the cellular antiviral response. The studies mainly focused on nsP3's ability to recruit multiple host factors required for the replication cycle. This function is fulfilled by the C-terminal HVD, an intrinsically disordered domain which by nature is prone to interact with multiple protein. During infection, nsP3 and host factors are recruited to replication complexes or cytoplasmic granules. nsP3 is critical for alphaviruses replication but its precise functioning at both vRC and cytoplasmic condensates is unclear. The results reported in this thesis

describe for the first time the structure of CHIKV nsP3. It is able of spontaneous helical arrangement through its AUD, leading to the formation of highly-ordered cytoplasmic tubular structures. nsP3-helices match perfectly with the crown-shaped structures found at the neck of vRC, thus supporting and stabilizing the complex required for positive RNA species synthesis. We also demonstrated that the nsP3 cytoplasmic condensates which were thought to be membrane-less organelles formed by liquid phase separation, are actually well-organized tubular networks of nsP3 oligomers. These networks appear as reservoirs for viral genomic RNA and proteins (capsid, nsP2) but also host factors such as FHL1 or G3BP. Disruption of the nsP3-helical arrangement has always a negative impact on viral RNA synthesis and production of infection virions, suggesting that nsP3 oligomeric state determines its activity. Whereas the other nsPs has precise enzymatic activities, the nsP3 also evolved as a structural organizer orchestrating early and late stages of the infection cycle. On one hand, the presence of the HVD domain ensures a great adaptability of alphaviruses to their host, as this domain is recruiting proteins in cell type-specific and host-specific manner. On the other hand, the AUD oligomerization offers a core structure preserved in all alphaviruses that serves as supporting platform for viral activities and protein recruitment.

The second part of my thesis work aimed to decipher the function of the FHL1 protein during CHIKV infection Although FHL1 is an important host factor for CHIKV replication, its mechanisms remain unclear. The accumulated data pinpoint an indirect role of FHL1 in viral RNA synthesis which could be linked to the repression of cellular stress or antiviral pathways. Despite its unknown function, FHL1 appears as a bridge between CHIKV replication, musculoskeletal tropism and pathogenesis. Indeed, the expression pattern of FHL1, mainly in skeletal muscle cells and fibroblasts, correlates with the very high susceptibility of these cells to CHIKV. In addition, the enhanced dependency on FHL1 of CHIKV strain inducing severe pathology on FHL1 is intriguing. Further studies are required to demonstrate a direct link between FHL1-use by CHIKV and the induced musculoskeletal damages.

Altogether, nsP3 oligomerization appears as target of interest to develop new antiviral strategies against CHIKV and alphavirus infection. In addition, the ability of nsP3 tubular assemblies to persist in infected cells and tissues must be investigated. These structures could have an important implication in arthritogenic viruses' acute and chronic physiopathology.

References

Abdelnabi, Rana, et Leen Delang. 2020. « Antiviral Strategies against Arthritogenic Alphaviruses ». *Microorganisms* 8 (9): 1365. https://doi.org/10.3390/microorganisms8091365.

Abere, Bizunesh, Nitwara Wikan, Sukathida Ubol, Prasert Auewarakul, Atchara Paemanee, Suthathip Kittisenachai, Sittiruk Roytrakul, et Duncan R. Smith. 2012. « Proteomic Analysis of Chikungunya Virus Infected Microgial Cells ». Édité par Lisa Ng Fong Poh. *PLoS ONE* 7 (4): e34800. https://doi.org/10.1371/journal.pone.0034800.

Abraham, Rachy, Debra Hauer, Robert Lyle McPherson, Age Utt, Ilsa T. Kirby, Michael S. Cohen, Andres Merits, Anthony K. L. Leung, et Diane E. Griffin. 2018. « ADP-ribosyl–binding and hydrolase activities of the alphavirus nsP3 macrodomain are critical for initiation of virus replication ». *Proceedings of the National Academy of Sciences* 115 (44): E10457-66. https://doi.org/10.1073/pnas.1812130115.

Abraham, Rachy, Prashant Mudaliar, Aiswaria Padmanabhan, et Easwaran Sreekumar. 2013. « Induction of Cytopathogenicity in Human Glioblastoma Cells by Chikungunya Virus ». Édité par Lisa Ng Fong Poh. *PLoS ONE* 8 (9): e75854. https://doi.org/10.1371/journal.pone.0075854.

Abraham, Rachy, Sneha Singh, Sreeja R. Nair, Neha Vijay Hulyalkar, Arun Surendran, Abdul Jaleel, et Easwaran Sreekumar. 2017. « Nucleophosmin (NPM1)/B23 in the Proteome of Human Astrocytic Cells Restricts Chikungunya Virus Replication ». *Journal of Proteome Research* 16 (11): 4144-55. https://doi.org/10.1021/acs.jproteome.7b00513.

Agback, Peter, Francisco Dominguez, Yulia Pustovalova, Tetyana Lukash, Nikita Shiliaev, Vladislav Yu Orekhov, Ilya Frolov, Tatiana Agback, et Elena I. Frolova. 2019. « Structural Characterization and Biological Function of Bivalent Binding of CD2AP to Intrinsically Disordered Domain of Chikungunya Virus nsP3 Protein ». *Virology* 537 (novembre): 130-42. https://doi.org/10.1016/j.virol.2019.08.022.

Ahola, Tero, et Andres Merits. 2016. « Functions of Chikungunya Virus Nonstructural Proteins ». In *Chikungunya Virus: Advances in Biology, Pathogenesis, and Treatment*, édité par Chioma M. Okeoma, 75-98. Cham: Springer International Publishing. https://doi.org/10.1007/978-3-319-42958-8_6.

Akhrymuk, Ivan, Sergey V. Kulemzin, et Elena I. Frolova. 2012. « Evasion of the Innate Immune Response: The Old World Alphavirus nsP2 Protein Induces Rapid Degradation of Rpb1, a Catalytic Subunit of RNA Polymerase II ». *Journal of Virology* 86 (13): 7180-91.

https://doi.org/10.1128/JVI.00541-12.

Albrecht, Inka, Cecilia Wick, Åsa Hallgren, Anna Tjärnlund, Kanneboyina Nagaraju, Felipe Andrade, Kathryn Thompson, et al. s. d. « Development of autoantibodies against muscle-specific FHL1 in severe inflammatory myopathies ». *The Journal of Clinical Investigation* 125 (12): 4612-24. https://doi.org/10.1172/JCI81031.

Amaral, J. Kennedy, Joshua B. Bilsborrow, et Robert T. Schoen. 2020. « Chronic Chikungunya Arthritis and Rheumatoid Arthritis: What They Have in Common ». *The American Journal of Medicine* 133 (3): e91-97. https://doi.org/10.1016/j.amjmed.2019.10.005.

Angelini, P., P. Macini, A. C. Finarelli, C. Pol, C. Venturelli, R. Bellini, et M. Dottori. 2008. « Chikungunya Epidemic Outbreak in Emilia-Romagna (Italy) during Summer 2007 ». *Parassitologia* 50 (1-2): 97-98.

Arankalle, Vidya A., Shubham Shrivastava, Sarah Cherian, Rashmi S. Gunjikar, Atul M. Walimbe, Santosh M. Jadhav, A. B. Sudeep, et Akhilesh C. Mishra. 2007. « Genetic Divergence of Chikungunya Viruses in India (1963-2006) with Special Reference to the 2005-2006 Explosive Epidemic ». *The Journal of General Virology* 88 (Pt 7): 1967-76. https://doi.org/10.1099/vir.0.82714-0.

Arias-Goeta, Camilo, Laurence Mousson, François Rougeon, et Anna-Bella Failloux. 2013. « Dissemination and Transmission of the E1-226V Variant of Chikungunya Virus in Aedes Albopictus Are Controlled at the Midgut Barrier Level ». Édité par Nikos Vasilakis. *PLoS ONE* 8 (2): e57548. https://doi.org/10.1371/journal.pone.0057548.

Auguste, Albert J., Jonathan Liria, Naomi L. Forrester, Dileyvic Giambalvo, Maria Moncada, Kanya C. Long, Dulce Morón, et al. 2015. « Evolutionary and Ecological Characterization of Mayaro Virus Strains Isolated during an Outbreak, Venezuela, 2010 ». *Emerging Infectious Diseases* 21 (10): 1742-50. https://doi.org/10.3201/eid2110.141660.

Azar, Sasha R., Rafael K. Campos, Nicholas A. Bergren, Vidyleison N. Camargos, et Shannan L. Rossi. 2020. « Epidemic Alphaviruses: Ecology, Emergence and Outbreaks ». *Microorganisms* 8 (8): 1167. https://doi.org/10.3390/microorganisms8081167.

B., Siva Raghavendhar, Ashok Kumar Patel, Sushil Kumar Kabra, Rakesh Lodha, Vinod H. Ratageri, et Pratima Ray. 2019. « Virus load and clinical features during the acute phase of Chikungunya infection in children ». *PLoS ONE* 14 (2): e0211036. https://doi.org/10.1371/journal.pone.0211036.

Babu, M. Madan. 2016. « The Contribution of Intrinsically Disordered Regions to Protein Function, Cellular Complexity, and Human Disease ». *Biochemical Society Transactions* 44 (5): 1185-1200. https://doi.org/10.1042/BST20160172.

Bae, Sojung, Jeong Yoon Lee, et Jinjong Myoung. 2020. « Chikungunya Virus nsP2 Impairs MDA5/RIG-I-Mediated Induction of NF-κB Promoter Activation: A Potential Target for Virus-Specific Therapeutics ». *Journal of Microbiology and Biotechnology* 30 (12): 1801-9. https://doi.org/10.4014/jmb.2012.12005.

Bakhache, William, Aymeric Neyret, Eric Bernard, Andres Merits, et Laurence Briant. 2020. « Palmitoylated Cysteines in Chikungunya Virus nsP1 Are Critical for Targeting to Cholesterol-Rich Plasma Membrane Microdomains with Functional Consequences for Viral Genome Replication ». *Journal of Virology* 94 (10): e02183-19. https://doi.org/10.1128/JVI.02183-19.

Barrera, Roberto. 2022. « New Tools for Aedes Control: Mass Trapping ». *Current Opinion in Insect Science* 52 (août): 100942. https://doi.org/10.1016/j.cois.2022.100942.

Barski, Michal, Benjamin Brennan, Ona K Miller, Jane A Potter, Swetha Vijayakrishnan, David Bhella, James H Naismith, Richard M Elliott, et Ulrich Schwarz-Linek. 2017. « Rift Valley fever phlebovirus NSs protein core domain structure suggests molecular basis for nuclear filaments ». Édité par John Kuriyan. *eLife* 6 (septembre): e29236. https://doi.org/10.7554/eLife.29236.

Bartholomeeusen, Koen, Matthieu Daniel, Desiree A. LaBeaud, Philippe Gasque, Rosanna W. Peeling, Kathryn E. Stephenson, Lisa F. P. Ng, et Kevin K. Ariën. 2023. « Chikungunya Fever ». *Nature Reviews Disease Primers* 9 (1): 1-21. https://doi.org/10.1038/s41572-023-00429-2.

Bartholomeeusen, Koen, Age Utt, Sandra Coppens, Kai Rausalu, Katleen Vereecken, Kevin K. Ariën, et Andres Merits. 2018. « A Chikungunya Virus trans-Replicase System Reveals the Importance of Delayed Nonstructural Polyprotein Processing for Efficient Replication Complex Formation in Mosquito Cells ». *Journal of Virology* 92 (14). https://doi.org/10.1128/JVI.00152-18.

Basavappa, Megha G., Max Ferretti, Mark Dittmar, Julian Stoute, Megan C. Sullivan, Kanupriya Whig, Hui Shen, et al. 2022. « The lncRNA ALPHA Specifically Targets Chikungunya Virus to Control Infection ». *Molecular Cell* 82 (19): 3729-3744.e10. https://doi.org/10.1016/j.molcel.2022.08.030.

Basore, Katherine, Arthur S. Kim, Christopher A. Nelson, Rong Zhang, Brittany K. Smith, Carla Uranga, Lo Vang, et al. 2019. « Cryo-EM Structure of Chikungunya Virus in Complex with the Mxra8 Receptor ». *Cell* 177 (7): 1725-1737.e16. https://doi.org/10.1016/j.cell.2019.04.006.

Battisti, Verena, Ernst Urban, et Thierry Langer. 2021. « Antivirals against the Chikungunya

Virus ». *Viruses* 13 (7): 1307. https://doi.org/10.3390/v13071307.

Beckham, Carla J., et Roy Parker. 2008. « P Bodies, Stress Granules, and Viral Life Cycles ». *Cell Host & Microbe* 3 (4): 206-12. https://doi.org/10.1016/j.chom.2008.03.004.

Belov, George A, et Frank JM van Kuppeveld. 2012. « (+)RNA viruses rewire cellular pathways to build replication organelles ». *Current Opinion in Virology*, Virus replication in animals and plants, 2 (6): 740-47. https://doi.org/10.1016/j.coviro.2012.09.006.

Bennett, Sean R., James M. McCarty, Roshan Ramanathan, Jason Mendy, Jason S. Richardson, Jonathan Smith, Jeff Alexander, et al. 2022. « Safety and Immunogenicity of PXVX0317, an Aluminium Hydroxide-Adjuvanted Chikungunya Virus-like Particle Vaccine: A Randomised, Double-Blind, Parallel-Group, Phase 2 Trial ». *The Lancet. Infectious Diseases* 22 (9): 1343-55. https://doi.org/10.1016/S1473-3099(22)00226-2.

Berg, J M. 1990. « Zinc Fingers and Other Metal-Binding Domains. Elements for Interactions between Macromolecules. » *Journal of Biological Chemistry* 265 (12): 6513-16. https://doi.org/10.1016/S0021-9258(19)39172-0.

Berman, Jules J. 2012. « Group IV Viruses ». *Taxonomic Guide to Infectious Diseases*, 237-46. https://doi.org/10.1016/B978-0-12-415895-5.00042-8.

Bernard, Eric, Rodolphe Hamel, Aymeric Neyret, Peeraya Ekchariyawat, Jean-Pierre Molès, Graham Simmons, Nathalie Chazal, Philippe Desprès, Dorothée Missé, et Laurence Briant. 2015. « Human Keratinocytes Restrict Chikungunya Virus Replication at a Post-Fusion Step ». *Virology* 476 (février): 1-10. https://doi.org/10.1016/j.virol.2014.11.013.

Bernard, Eric, Maxime Solignat, Bernard Gay, Nathalie Chazal, Stephen Higgs, Christian Devaux, et Laurence Briant. 2010. « Endocytosis of Chikungunya Virus into Mammalian Cells: Role of Clathrin and Early Endosomal Compartments ». Édité par Olivier Schwartz. *PLoS ONE* 5 (7): e11479. https://doi.org/10.1371/journal.pone.0011479.

Borch, Josefine d. S., Thomas Krag, Sonja D. Holm-Yildiz, Hakan Cetin, Tuva A. Solheim, Freja Fornander, Volker Straub, Morten Duno, et John Vissing. 2022. « Three Novel FHL1 Variants Cause a Mild Phenotype of Emery-Dreifuss Muscular Dystrophy ». *Human Mutation* 43 (9): 1234-38. https://doi.org/10.1002/humu.24415.

Bouraï, Mehdi, Marianne Lucas-Hourani, Hans Henrik Gad, Christian Drosten, Yves Jacob, Lionel Tafforeau, Patricia Cassonnet, et al. 2012. « Mapping of Chikungunya Virus Interactions with Host Proteins Identified nsP2 as a Highly Connected Viral Component ». *Journal of Virology* 86 (6): 3121-34. https://doi.org/10.1128/JVI.06390-11.

Brault, Aaron C., Robert B. Tesh, Ann M. Powers, et Scott C. Weaver. 2000. « Re-Emergence of Chikungunya and o'nyong-Nyong Viruses: Evidence for Distinct Geographical Lineages

and Distant Evolutionary Relationships ». *Journal of General Virology* 81 (2): 471-79. https://doi.org/10.1099/0022-1317-81-2-471.

Briant, Laurence, Philippe Desprès, Valérie Choumet, et Dorothée Missé. 2014. « Role of Skin Immune Cells on the Host Susceptibility to Mosquito-Borne Viruses ». *Virology* 464-465 (septembre): 26-32. https://doi.org/10.1016/j.virol.2014.06.023.

Brizzi, Kate. 2017. « Neurologic Manifestation of Chikungunya Virus ». *Current Infectious Disease Reports* 19 (2): 6. https://doi.org/10.1007/s11908-017-0561-1.

Brown, Rebecca S., Dimitrios G. Anastasakis, Markus Hafner, et Margaret Kielian. 2020. « Multiple Capsid Protein Binding Sites Mediate Selective Packaging of the Alphavirus Genomic RNA ». *Nature Communications* 11 (1): 4693. https://doi.org/10.1038/s41467-020-18447-z.

Brown, S., M. J. McGrath, L. M. Ooms, R. Gurung, M. M. Maimone, et C. A. Mitchell. 1999. « Characterization of Two Isoforms of the Skeletal Muscle LIM Protein 1, SLIM1. Localization of SLIM1 at Focal Adhesions and the Isoform Slimmer in the Nucleus of Myoblasts and Cytoplasm of Myotubes Suggests Distinct Roles in the Cytoskeleton and in Nuclear-Cytoplasmic Communication ». *The Journal of Biological Chemistry* 274 (38): 27083-91. https://doi.org/10.1074/jbc.274.38.27083.

Calisher, Charles H., Robert E. Shope, Walter Brandt, Jordi Casals, Nick Karabatsos, Frederick A. Murphy, Robert B. Tesh, et Michael E. Wiebe. 1980. « Proposed Antigenic Classification of Registered Arboviruses I. Togaviridae, Alphavirus ». *Intervirology* 14 (5-6): 229-32. https://doi.org/10.1159/000149190.

Cassadou, S., S. Boucau, M. Petit-Sinturel, P. Huc, I. Leparc-Goffart, et M. Ledrans. 2014. « Emergence of Chikungunya Fever on the French Side of Saint Martin Island, October to December 2013 ». *Eurosurveillance* 19 (13): 20752. https://doi.org/10.2807/1560-7917.ES2014.19.13.20752.

Catara, Giuliana, Giovanna Grimaldi, Laura Schembri, Daniela Spano, Gabriele Turacchio, Matteo Lo Monte, Andrea Rosario Beccari, Carmen Valente, et Daniela Corda. 2017. « PARP1-Produced Poly-ADP-Ribose Causes the PARP12 Translocation to Stress Granules and Impairment of Golgi Complex Functions ». *Scientific Reports* 7 (1): 14035. https://doi.org/10.1038/s41598-017-14156-8.

Centers for Disease Control and Prevention (CDC). 2006. « Chikungunya Fever Diagnosed among International Travelers--United States, 2005-2006 ». *MMWR. Morbidity and Mortality Weekly Report* 55 (38): 1040-42.

Cesaro, Teresa, et Thomas Michiels. 2021. « Inhibition of PKR by Viruses ». *Frontiers in*

Microbiology 12. https://www.frontiersin.org/articles/10.3389/fmicb.2021.757238.

Chen, Rubing, Suchetana Mukhopadhyay, Andres Merits, Bethany Bolling, Farooq Nasar, Lark L. Coffey, Ann Powers, Scott C. Weaver, et ICTV Report Consortium. 2018. « ICTV Virus Taxonomy Profile: Togaviridae ». *Journal of General Virology* 99 (6): 761-62. https://doi.org/10.1099/jgv.0.001072.

Chen, Weiqiang, Suan-Sin Foo, Ali Zaid, Terk-Shin Teng, Lara J. Herrero, Stefan Wolf, Kothila Tharmarajah, et al. 2017. « Specific Inhibition of NLRP3 in Chikungunya Disease Reveals a Role for Inflammasomes in Alphavirus-Induced Inflammation ». *Nature Microbiology* 2 (10): 1435-45. https://doi.org/10.1038/s41564-017-0015-4.

Chirathaworn, Chintana, Jira Chansaenroj, et Yong Poovorawan. 2020. « Cytokines and Chemokines in Chikungunya Virus Infection: Protection or Induction of Pathology ». *Pathogens* 9 (6): 415. https://doi.org/10.3390/pathogens9060415.

Chmielewski, David, Michael F. Schmid, Graham Simmons, Jing Jin, et Wah Chiu. 2022. « Chikungunya Virus Assembly and Budding Visualized in Situ Using Cryogenic Electron Tomography ». *Nature Microbiology* 7 (8): 1270-79. https://doi.org/10.1038/s41564-022-01164-2.

Choi, Hok-Kin, Liang Tong, Wladek Minor, Philippe Dumas, Ulrike Boege, Michael G. Rossmann, et Gerd Wengler. 1991. « Structure of Sindbis Virus Core Protein Reveals a Chymotrypsin-like Serine Proteinase and the Organization of the Virion ». *Nature* 354 (6348): 37-43. https://doi.org/10.1038/354037a0.

Choi, Young Ki. 2021. « Emerging and Re-Emerging Fatal Viral Diseases ». *Experimental & Molecular Medicine* 53 (5): 711-12. https://doi.org/10.1038/s12276-021-00608-9.

Chow, Angela, Zhisheng Her, Edward K. S. Ong, Jin-miao Chen, Frederico Dimatatac, Dyan J. C. Kwek, Timothy Barkham, et al. 2011. « Persistent Arthralgia Induced by Chikungunya Virus Infection is Associated with Interleukin-6 and Granulocyte Macrophage Colony-Stimulating Factor ». *The Journal of Infectious Diseases* 203 (2): 149-57. https://doi.org/10.1093/infdis/jiq042.

Chretien, Jean-Paul, Assaf Anyamba, Sheryl A. Bedno, Robert F. Breiman, Rosemary Sang, Kibet Sergon, Ann M. Powers, et al. 2007. « DROUGHT-ASSOCIATED CHIKUNGUNYA EMERGENCE ALONG COASTAL EAST AFRICA ». *The American Journal of Tropical Medicine and Hygiene* 76 (3): 405-7. https://doi.org/10.4269/ajtmh.2007.76.405.

Clark, Lars E., Sarah A. Clark, ChieYu Lin, Jianying Liu, Adrian Coscia, Katherine G. Nabel, Pan Yang, et al. 2022. « VLDLR and ApoER2 Are Receptors for Multiple Alphaviruses ». *Nature* 602 (7897): 475-80. https://doi.org/10.1038/s41586-021-04326-0.

Clavarino, Giovanna, Nuno Cláudio, Thérèse Couderc, Alexandre Dalet, Delphine Judith, Voahirana Camosseto, Enrico K. Schmidt, et al. 2012. « Induction of GADD34 Is Necessary for dsRNA-Dependent Interferon-β Production and Participates in the Control of Chikungunya Virus Infection ». Édité par Mark T. Heise. *PLoS Pathogens* 8 (5): e1002708. https://doi.org/10.1371/journal.ppat.1002708.

Clemens, M. J. 2001. « Initiation Factor eIF2 Alpha Phosphorylation in Stress Responses and Apoptosis ». *Progress in Molecular and Subcellular Biology* 27: 57-89. https://doi.org/10.1007/978-3-662-09889-9_3.

Contu, Lara, Giuseppe Balistreri, Michal Domanski, Anne-Christine Uldry, et Oliver Mühlemann. 2021. « Characterisation of the Semliki Forest Virus-Host Cell Interactome Reveals the Viral Capsid Protein as an Inhibitor of Nonsense-Mediated mRNA Decay ». *PLOS Pathogens* 17 (5): e1009603. https://doi.org/10.1371/journal.ppat.1009603.

Couderc, Thérèse, Fabrice Chrétien, Clémentine Schilte, Olivier Disson, Madly Brigitte, Florence Guivel-Benhassine, Yasmina Touret, et al. 2008. « A Mouse Model for Chikungunya: Young Age and Inefficient Type-I Interferon Signaling Are Risk Factors for Severe Disease ». *PLOS Pathogens* 4 (2): e29. https://doi.org/10.1371/journal.ppat.0040029.

Cowling, Belinda S., Denny L. Cottle, Brendan R. Wilding, Colleen E. D'Arcy, Christina A. Mitchell, et Meagan J. McGrath. 2011. « Four and a Half LIM Protein 1 Gene Mutations Cause Four Distinct Human Myopathies: A Comprehensive Review of the Clinical, Histological and Pathological Features ». *Neuromuscular Disorders* 21 (4): 237-51. https://doi.org/10.1016/j.nmd.2011.01.001.

Cowling, Belinda S., Meagan J. McGrath, Mai-Anh Nguyen, Denny L. Cottle, Anthony J. Kee, Susan Brown, Joachim Schessl, et al. 2008. « Identification of FHL1 as a regulator of skeletal muscle mass: implications for human myopathy ». *The Journal of Cell Biology* 183 (6): 1033-48. https://doi.org/10.1083/jcb.200804077.

Cristea, Ileana M., John-William N. Carroll, Michael P. Rout, Charles M. Rice, Brian T. Chait, et Margaret R. MacDonald. 2006. « Tracking and Elucidating Alphavirus-Host Protein Interactions ». *Journal of Biological Chemistry* 281 (40): 30269-78. https://doi.org/10.1074/jbc.M603980200.

Cristea, Ileana M., Heather Rozjabek, Kelly R. Molloy, Sophiya Karki, Laura L. White, Charles M. Rice, Michael P. Rout, Brian T. Chait, et Margaret R. MacDonald. 2010. « Host Factors Associated with the Sindbis Virus RNA-Dependent RNA Polymerase: Role for G3BP1 and G3BP2 in Virus Replication ». *Journal of Virology* 84 (13): 6720-32. https://doi.org/10.1128/JVI.01983-09.

Dai, Lue, Kristy B. Lidie, Qian Chen, Joseph W. Adelsberger, Xin Zheng, DaWei Huang, Jun Yang, et al. 2013. « IL-27 inhibits HIV-1 infection in human macrophages by down-regulating host factor SPTBN1 during monocyte to macrophage differentiation ». *Journal of Experimental Medicine* 210 (3): 517-34. https://doi.org/10.1084/jem.20120572.

Danis, Bénédicte, Thaddeus C. George, Stanislas Goriely, Binita Dutta, Joëlle Renneson, Laurent Gatto, Patricia Fitzgerald-Bocarsly, et al. 2008. « Interferon Regulatory Factor 7-Mediated Responses Are Defective in Cord Blood Plasmacytoid Dendritic Cells ». *European Journal of Immunology* 38 (2): 507-17. https://doi.org/10.1002/eji.200737760.

Delang, Leen, Rana Abdelnabi, et Johan Neyts. 2018. « Favipiravir as a Potential Countermeasure against Neglected and Emerging RNA Viruses ». *Antiviral Research* 153 (mai): 85-94. https://doi.org/10.1016/j.antiviral.2018.03.003.

Delisle, E., C. Rousseau, B. Broche, I. Leparc-Goffart, G. L'Ambert, A. Cochet, C. Prat, et al. 2015. « Chikungunya Outbreak in Montpellier, France, September to October 2014 ». *Euro Surveillance: Bulletin Europeen Sur Les Maladies Transmissibles = European Communicable Disease Bulletin* 20 (17). https://doi.org/10.2807/1560-7917.es2015.20.17.21108.

Diallo, Diawo, Amadou A. Sall, Michaela Buenemann, Rubing Chen, Oumar Faye, Cheikh T. Diagne, Ousmane Faye, et al. 2012. « Landscape Ecology of Sylvatic Chikungunya Virus and Mosquito Vectors in Southeastern Senegal ». Édité par Duane J. Gubler. *PLoS Neglected Tropical Diseases* 6 (6): e1649. https://doi.org/10.1371/journal.pntd.0001649.

Domenighetti, Andrea A., Pao-Hsien Chu, Tongbin Wu, Farah Sheikh, David S. Gokhin, Ling T. Guo, Ziyou Cui, et al. 2014. « Loss of FHL1 Induces an Age-Dependent Skeletal Muscle Myopathy Associated with Myofibrillar and Intermyofibrillar Disorganization in Mice ». *Human Molecular Genetics* 23 (1): 209-25. https://doi.org/10.1093/hmg/ddt412.

Dominguez, Francisco, Nikita Shiliaev, Tetyana Lukash, Peter Agback, Oksana Palchevska, Joseph R. Gould, Chetan D. Meshram, et al. 2021. « NAP1L1 and NAP1L4 Binding to Hypervariable Domain of Chikungunya Virus nsP3 Protein Is Bivalent and Requires Phosphorylation ». *Journal of Virology* 95 (16): e0083621. https://doi.org/10.1128/JVI.00836-21.

Dong, Shengzhang, Velmurugan Balaraman, Asher M. Kantor, Jingyi Lin, DeAna G. Grant, Nicole L. Held, et Alexander W. E. Franz. 2017. « Chikungunya Virus Dissemination from the Midgut of Aedes Aegypti Is Associated with Temporal Basal Lamina Degradation during Bloodmeal Digestion ». *PLoS Neglected Tropical Diseases* 11 (9): e0005976. https://doi.org/10.1371/journal.pntd.0005976.

Duan, Yongjia, Aiying Du, Jinge Gu, Gang Duan, Chen Wang, Xinrui Gui, Zhiwei Ma, et al.

2019. « PARylation Regulates Stress Granule Dynamics, Phase Separation, and Neurotoxicity of Disease-Related RNA-Binding Proteins ». *Cell Research* 29 (3): 233-47. https://doi.org/10.1038/s41422-019-0141-z.

Dutta, Sudip Kumar, Tithi Pal, Bibhuti Saha, Syamsundar Mandal, et Anusri Tripathi. 2014. « Copy Number Variation of Chikungunya ECSA Virus with Disease Symptoms among Indian Patients ». *Journal of Medical Virology* 86 (8): 1386-92. https://doi.org/10.1002/jmv.23794.

Duvignaud, A., A. Fianu, A. Bertolotti, J. Jaubert, A. Michault, P. Poubeau, A. Fred, et al. 2018. « Rheumatism and Chronic Fatigue, the Two Facets of Post-Chikungunya Disease: The TELECHIK Cohort Study on Reunion Island ». *Epidemiology and Infection* 146 (5): 633-41. https://doi.org/10.1017/S0950268818000031.

Dzimianski, John V., Florine E. M. Scholte, Éric Bergeron, et Scott D. Pegan. 2019. « ISG15: It's Complicated ». *Journal of Molecular Biology*, Mechanisms and Strategies of Host Response to Pathogens, 431 (21): 4203-16. https://doi.org/10.1016/j.jmb.2019.03.013.

Eckei, Laura, Sarah Krieg, Mareike Bütepage, Anne Lehmann, Annika Gross, Barbara Lippok, Alexander R. Grimm, et al. 2017. « The Conserved Macrodomains of the Non-Structural Proteins of Chikungunya Virus and Other Pathogenic Positive Strand RNA Viruses Function as Mono-ADP-Ribosylhydrolases ». *Scientific Reports* 7 (février): 41746. https://doi.org/10.1038/srep41746.

Edelman, R., C. O. Tacket, S. S. Wasserman, S. A. Bodison, J. G. Perry, et J. A. Mangiafico. 2000. « Phase II Safety and Immunogenicity Study of Live Chikungunya Virus Vaccine TSI-GSD-218 ». *The American Journal of Tropical Medicine and Hygiene* 62 (6): 681-85. https://doi.org/10.4269/ajtmh.2000.62.681.

Ekchariyawat, Peeraya, Rodolphe Hamel, Eric Bernard, Sineewanlaya Wichit, Pornapat Surasombatpattana, Loïc Talignani, Frédéric Thomas, et al. 2015. « Inflammasome Signaling Pathways Exert Antiviral Effect against Chikungunya Virus in Human Dermal Fibroblasts ». *Infection, Genetics and Evolution: Journal of Molecular Epidemiology and Evolutionary Genetics in Infectious Diseases* 32 (juin): 401-8. https://doi.org/10.1016/j.meegid.2015.03.025.

Ertel, Kenneth J., Desirée Benefield, Daniel Castaño-Diez, Janice G. Pennington, Mark Horswill, Johan A. den Boon, Marisa S. Otegui, et Paul Ahlquist. 2017. « Cryo-Electron Tomography Reveals Novel Features of a Viral RNA Replication Compartment ». *eLife* 6 (juin): e25940. https://doi.org/10.7554/eLife.25940.

Fehr, Anthony R., Gytis Jankevicius, Ivan Ahel, et Stanley Perlman. 2018. « Viral Macrodomains: Unique Mediators of Viral Replication and Pathogenesis ». *Trends in Microbiology* 26 (7): 598-610. https://doi.org/10.1016/j.tim.2017.11.011.

Fehr, Anthony R., Sasha A. Singh, Catherine M. Kerr, Shin Mukai, Hideyuki Higashi, et Masanori Aikawa. s. d. « The Impact of PARPs and ADP-Ribosylation on Inflammation and Host–Pathogen Interactions ». Cold Spring Harbor Lab. Consulté le 13 janvier 2021. https://doi.org/10.1101/gad.334425.119.

Ferreira, André C., Patrícia A. Reis, Caroline S. de Freitas, Carolina Q. Sacramento, Lucas Villas Bôas Hoelz, Mônica M. Bastos, Mayara Mattos, et al. 2019. « Beyond Members of the Flaviviridae Family, Sofosbuvir Also Inhibits Chikungunya Virus Replication ». *Antimicrobial Agents and Chemotherapy* 63 (2): e01389-18. https://doi.org/10.1128/AAC.01389-18.

Fong, Rachel H., Soma S. R. Banik, Kimberly Mattia, Trevor Barnes, David Tucker, Nathan Liss, Kai Lu, et al. 2014. « Exposure of Epitope Residues on the Outer Face of the Chikungunya Virus Envelope Trimer Determines Antibody Neutralizing Efficacy ». *Journal of Virology* 88 (24): 14364-79. https://doi.org/10.1128/JVI.01943-14.

Forrester, N. L., G. Palacios, R. B. Tesh, N. Savji, H. Guzman, M. Sherman, S. C. Weaver, et W. I. Lipkin. 2012. « Genome-Scale Phylogeny of the Alphavirus Genus Suggests a Marine Origin ». *Journal of Virology* 86 (5): 2729-38. https://doi.org/10.1128/jvi.05591-11.

Foy, N. J., M. Akhrymuk, I. Akhrymuk, S. Atasheva, A. Bopda-Waffo, I. Frolov, et E. I. Frolova. 2013. « Hypervariable Domains of nsP3 Proteins of New World and Old World Alphaviruses Mediate Formation of Distinct, Virus-Specific Protein Complexes ». *Journal of Virology* 87 (4): 1997-2010. https://doi.org/10.1128/JVI.02853-12.

Foy, Niall J., Maryna Akhrymuk, Alexander V. Shustov, Elena I. Frolova, et Ilya Frolov. 2013. « Hypervariable Domain of Nonstructural Protein nsP3 of Venezuelan Equine Encephalitis Virus Determines Cell-Specific Mode of Virus Replication ». *Journal of Virology* 87 (13): 7569-84. https://doi.org/10.1128/jvi.00720-13.

Frolov, Ilya, Natalia Garmashova, Svetlana Atasheva, et Elena I. Frolova. 2009. « Random Insertion Mutagenesis of Sindbis Virus Nonstructural Protein 2 and Selection of Variants Incapable of Downregulating Cellular Transcription ». *Journal of Virology* 83 (18): 9031-44. https://doi.org/10.1128/JVI.00850-09.

Frolov, Ilya, Dal Young Kim, Maryna Akhrymuk, James A. Mobley, et Elena I. Frolova. 2017. « Hypervariable Domain of Eastern Equine Encephalitis Virus nsP3 Redundantly Utilizes Multiple Cellular Proteins for Replication Complex Assembly ». *Journal of Virology* 91 (14). https://doi.org/10.1128/JVI.00371-17.

Frolova, E, I Frolov, et S Schlesinger. 1997. « Packaging signals in alphaviruses ». *Journal of Virology* 71 (1): 248-58. https://doi.org/10.1128/jvi.71.1.248-258.1997.

Frolova, E. I., R. Gorchakov, L. Pereboeva, S. Atasheva, et I. Frolov. 2010. « Functional

Sindbis Virus Replicative Complexes Are Formed at the Plasma Membrane ». *Journal of Virology* 84 (22): 11679-95. https://doi.org/10.1128/JVI.01441-10.

Frolova, Elena, Rodion Gorchakov, Natalia Garmashova, Svetlana Atasheva, Leoncio Vergara, et Ilya Frolov. 2006. « Formation of nsP3-Specific Protein Complexes during Sindbis Virus Replication ». *Journal of virology* 80 (mai): 4122-34. https://doi.org/10.1128/JVI.80.8.4122-4134.2006.

Fros, J. J., N. E. Domeradzka, J. Baggen, C. Geertsema, J. Flipse, J. M. Vlak, et G. P. Pijlman. 2012. « Chikungunya Virus nsP3 Blocks Stress Granule Assembly by Recruitment of G3BP into Cytoplasmic Foci ». *Journal of Virology* 86 (19): 10873-79. https://doi.org/10.1128/JVI.01506-12.

Fros, Jelke J., Lee D. Major, Florine E. M. Scholte, Joy Gardner, Martijn J. van Hemert, Andreas Suhrbier, et Gorben P. Pijlman. 2015. « Chikungunya Virus Non-Structural Protein 2-Mediated Host Shut-off Disables the Unfolded Protein Response ». *The Journal of General Virology* 96 (Pt 3): 580-89. https://doi.org/10.1099/vir.0.071845-0.

Fros, Jelke J., Erika van der Maten, Just M. Vlak, et Gorben P. Pijlman. 2013. « The C-Terminal Domain of Chikungunya Virus nsP2 Independently Governs Viral RNA Replication, Cytopathicity, and Inhibition of Interferon Signaling ». *Journal of Virology* 87 (18): 10394-400. https://doi.org/10.1128/JVI.00884-13.

Fros, Jelke J., et Gorben P. Pijlman. 2016. « Alphavirus Infection: Host Cell Shut-Off and Inhibition of Antiviral Responses ». *Viruses* 8 (6). https://doi.org/10.3390/v8060166.

Gao, Yanni, Niluka Goonawardane, Joseph Ward, Andrew Tuplin, et Mark Harris. 2019. « Multiple Roles of the Non-Structural Protein 3 (nsP3) Alphavirus Unique Domain (AUD) during Chikungunya Virus Genome Replication and Transcription ». *PLOS Pathogens* 15 (1): e1007239. https://doi.org/10.1371/journal.ppat.1007239.

Gardner, Joy, Itaru Anraku, Thuy T. Le, Thibaut Larcher, Lee Major, Pierre Roques, Wayne A. Schroder, Stephen Higgs, et Andreas Suhrbier. 2010. « Chikungunya Virus Arthritis in Adult Wild-Type Mice ». *Journal of Virology* 84 (16): 8021-32. https://doi.org/10.1128/JVI.02603-09.

Gérardin, Patrick, Thérèse Couderc, Marc Bintner, Patrice Tournebize, Michel Renouil, Jérome Lémant, Véronique Boisson, et al. 2016. « Chikungunya Virus-Associated Encephalitis: A Cohort Study on La Réunion Island, 2005-2009 ». *Neurology* 86 (1): 94-102. https://doi.org/10.1212/WNL.0000000000002234.

Gérardin, Patrick, Vanina Guernier, Joëlle Perrau, Adrian Fianu, Karin Le Roux, Philippe Grivard, Alain Michault, Xavier de Lamballerie, Antoine Flahault, et François Favier. 2008.

« Estimating Chikungunya prevalence in La Réunion Island outbreak by serosurveys: Two methods for two critical times of the epidemic ». *BMC Infectious Diseases* 8 (juillet): 99. https://doi.org/10.1186/1471-2334-8-99.

Girard, Justine, Olivier Le-Bihan, Joséphine Lai-Kee-Him, Maria Girleanu, Eric Bernard, Cedric Castellarin, Aymeric Neyret, et al. 2023. « In Situ Characterization of Late Chikungunya Virus Replication Organelle ». Preprint. Molecular Biology. https://doi.org/10.1101/2023.02.25.530016.

Göertz, Giel P., Kristin L. McNally, Shelly J. Robertson, Sonja M. Best, Gorben P. Pijlman, et Jelke J. Fros. 2018. « The Methyltransferase-Like Domain of Chikungunya Virus nsP2 Inhibits the Interferon Response by Promoting the Nuclear Export of STAT1 ». *Journal of Virology* 92 (17): e01008-18. https://doi.org/10.1128/JVI.01008-18.

Gorbalenya, Alexander E., Eugene V. Koonin, et Michael M.-C. Lai. 1991. « Putative Papain-Related Thiol Proteases of Positive-Strand RNA Viruses Identification of Rubi- and Aphthovirus Proteases and Delineation of a Novel Conserved Domain Associated with Proteases of Rubi-, α- and Coronaviruses ». *FEBS Letters* 288 (1-2): 201-5. https://doi.org/10.1016/0014-5793(91)81034-6.

Gorchakov, Rodion, Elena Frolova, et Ilya Frolov. 2005. « Inhibition of Transcription and Translation in Sindbis Virus-Infected Cells ». *Journal of Virology* 79 (15): 9397-9409. https://doi.org/10.1128/JVI.79.15.9397-9409.2005.

Gorchakov, Rodion, Elena Frolova, Stanley Sawicki, Svetlana Atasheva, Dorothea Sawicki, et Ilya Frolov. 2008. « A New Role for ns Polyprotein Cleavage in Sindbis Virus Replication ». *Journal of Virology* 82 (13): 6218-31. https://doi.org/10.1128/jvi.02624-07.

Gorchakov, Rodion, Elena Frolova, Bryan R. G. Williams, Charles M. Rice, et Ilya Frolov. 2004. « PKR-Dependent and -Independent Mechanisms Are Involved in Translational Shutoff during Sindbis Virus Infection ». *Journal of Virology* 78 (16): 8455-67. https://doi.org/10.1128/JVI.78.16.8455-8467.2004.

Gorchakov, Rodion, Natalia Garmashova, Elena Frolova, et Ilya Frolov. 2008. « Different Types of nsP3-Containing Protein Complexes in Sindbis Virus-Infected Cells ». *Journal of Virology* 82 (20): 10088-101. https://doi.org/10.1128/JVI.01011-08.

Gorchakov, Rodion, Eryu Wang, Grace Leal, Naomi L. Forrester, Kenneth Plante, Shannan L. Rossi, Charalambos D. Partidos, et al. 2012. « Attenuation of Chikungunya Virus Vaccine Strain 181/Clone 25 Is Determined by Two Amino Acid Substitutions in the E2 Envelope Glycoprotein ». *Journal of Virology* 86 (11): 6084-96. https://doi.org/10.1128/jvi.06449-11.

Götte, Benjamin, Lifeng Liu, et Gerald McInerney. 2018. « The Enigmatic Alphavirus Non-

Structural Protein 3 (nsP3) Revealing Its Secrets at Last ». *Viruses* 10 (3): 105. https://doi.org/10.3390/v10030105.

Götte, Benjamin, Marc D. Panas, Kirsi Hellström, Lifeng Liu, Baila Samreen, Ola Larsson, Tero Ahola, et Gerald M. McInerney. 2019. « Separate Domains of G3BP Promote Efficient Clustering of Alphavirus Replication Complexes and Recruitment of the Translation Initiation Machinery ». *PLOS Pathogens* 15 (6): e1007842. https://doi.org/10.1371/journal.ppat.1007842.

Gould, Ernest, John Pettersson, Stephen Higgs, Remi Charrel, et Xavier De Lamballerie. 2017. « Emerging Arboviruses: Why Today? » *One Health* 4 (décembre): 1-13. https://doi.org/10.1016/j.onehlt.2017.06.001.

Groot, R. J. de, T. Rümenapf, R. J. Kuhn, E. G. Strauss, et J. H. Strauss. 1991. « Sindbis Virus RNA Polymerase Is Degraded by the N-End Rule Pathway ». *Proceedings of the National Academy of Sciences of the United States of America* 88 (20): 8967-71. https://doi.org/10.1073/pnas.88.20.8967.

Gueneau, Lucie, Anne T. Bertrand, Jean-Philippe Jais, Mustafa A. Salih, Tanya Stojkovic, Manfred Wehnert, Maria Hoeltzenbein, et al. 2009. « Mutations of the FHL1 Gene Cause Emery-Dreifuss Muscular Dystrophy ». *The American Journal of Human Genetics* 85 (3): 338-53. https://doi.org/10.1016/j.ajhg.2009.07.015.

Guo, C., R. Fu, S. Wang, Y. Huang, X. Li, M. Zhou, J. Zhao, et N. Yang. 2018. « NLRP3 Inflammasome Activation Contributes to the Pathogenesis of Rheumatoid Arthritis ». *Clinical and Experimental Immunology* 194 (2): 231-43. https://doi.org/10.1111/cei.13167.

Gupte, Rebecca, Ziying Liu, et W. Lee Kraus. 2017. « PARPs and ADP-Ribosylation: Recent Advances Linking Molecular Functions to Biological Outcomes ». *Genes & Development* 31 (2): 101-26. https://doi.org/10.1101/gad.291518.116.

Hahn, Y S, E G Strauss, et J H Strauss. 1989. « Mapping of RNA- temperature-sensitive mutants of Sindbis virus: assignment of complementation groups A, B, and G to nonstructural proteins. » *Journal of Virology* 63 (7): 3142-50.

Halstead, S. B., et S. Udomsakdi. 1966. « Vertebrate Hosts of Chikungunya Virus ». *Bulletin of the World Health Organization* 35 (1): 89.

Hammon, W. McD., A. Rundnick, et G. E. Sather. 1960. « Viruses Associated with Epidemic Hemorrhagic Fevers of the Philippines and Thailand ». *Science* 131 (3407): 1102-3. https://doi.org/10.1126/science.131.3407.1102.

Han, Shunshun, Can Cui, Haorong He, Xiaoxu Shen, Yuqi Chen, Yan Wang, Diyan Li, Qing Zhu, et Huadong Yin. 2020. « FHL1 Regulates Myoblast Differentiation and Autophagy

through Its Interaction with LC3 ». *Journal of Cellular Physiology* 235 (5): 4667-78. https://doi.org/10.1002/jcp.29345.

Hardy, W. R., et J. H. Strauss. 1989. « Processing the Nonstructural Polyproteins of Sindbis Virus: Nonstructural Proteinase Is in the C-Terminal Half of nsP2 and Functions Both in Cis and in Trans ». *Journal of Virology* 63 (11): 4653-64. https://doi.org/10.1128/JVI.63.11.4653-4664.1989.

Hartman, Tiffiney Roberts, Shuiming Qian, Cheryl Bolinger, Soledad Fernandez, Daniel R. Schoenberg, et Kathleen Boris-Lawrie. 2006. « RNA Helicase A Is Necessary for Translation of Selected Messenger RNAs ». *Nature Structural & Molecular Biology* 13 (6): 509-16. https://doi.org/10.1038/nsmb1092.

Havlicek, Marc Gordon. s. d. « The Role of the Host Factor SPTBN1 in HIV-1 Infection of Microglial Cells ».

Hawman, D. W., K. A. Stoermer, S. A. Montgomery, P. Pal, L. Oko, M. S. Diamond, et T. E. Morrison. 2013. « Chronic Joint Disease Caused by Persistent Chikungunya Virus Infection Is Controlled by the Adaptive Immune Response ». *Journal of Virology* 87 (24): 13878-88. https://doi.org/10.1128/JVI.02666-13.

Heath, Claire J, Jason Lowther, Trevor P Noël, Idis Mark-George, Derek B Boothroyd, George Mitchell, Calum MacPherson, et A Desiree LaBeaud. 2018. « The Identification of Risk Factors for Chronic Chikungunya Arthralgia in Grenada, West Indies: A Cross-Sectional Cohort Study ». *Open Forum Infectious Diseases* 5 (1): ofx234. https://doi.org/10.1093/ofid/ofx234.

Hellström, Kirsi, Katri Kallio, Hanna-Mari Meriläinen, Eija Jokitalo, et Tero Ahola. 2016. « Ability of Minus Strands and Modified plus Strands to Act as Templates in Semliki Forest Virus RNA Replication ». *Journal of General Virology* 97 (6): 1395-1407. https://doi.org/10.1099/jgv.0.000448.

Hellström, Kirsi, Katri Kallio, Age Utt, Tania Quirin, Eija Jokitalo, Andres Merits, et Tero Ahola. 2017. « Partially Uncleaved Alphavirus Replicase Forms Spherule Structures in the Presence and Absence of RNA Template ». Édité par Anne E. Simon. *Journal of Virology* 91 (18): e00787-17. https://doi.org/10.1128/JVI.00787-17.

Hoarau, Jean-Jacques, Marie-Christine Jaffar Bandjee, Pascale Krejbich Trotot, Trina Das, Ghislaine Li-Pat-Yuen, Bérengère Dassa, Mélanie Denizot, et al. 2010. « Persistent Chronic Inflammation and Infection by Chikungunya Arthritogenic Alphavirus in Spite of a Robust Host Immune Response ». *The Journal of Immunology* 184 (10): 5914-27. https://doi.org/10.4049/jimmunol.0900255.

Hoarau, Jean-Jacques, Marie-Christine Jaffar Bandjee, Pascale Krejbich Trotot, Trina Das, Ghislaine Li-Pat-Yuen, Bérengère Dassa, Mélanie Denizot, et al. 2010. « Persistent Chronic Inflammation and Infection by Chikungunya Arthritogenic Alphavirus in Spite of a Robust Host Immune Response ». *The Journal of Immunology* 184 (10): 5914-27. https://doi.org/10.4049/jimmunol.0900255.

Hoornweg, Tabitha E., Mareike K. S. van Duijl-Richter, Nilda V. Ayala Nuñez, Irina C. Albulescu, Martijn J. van Hemert, et Jolanda M. Smit. 2016. « Dynamics of Chikungunya Virus Cell Entry Unraveled by Single-Virus Tracking in Living Cells ». *Journal of Virology* 90 (9): 4745-56. https://doi.org/10.1128/JVI.03184-15.

Hu, Siqi, Hong Sun, Lijuan Yin, Jian Li, Shan Mei, Fengwen Xu, Chao Wu, et al. 2019. « PKR-dependent cytosolic cGAS foci are necessary for intracellular DNA sensing ». *Science Signaling* 12 (609): eaav7934. https://doi.org/10.1126/scisignal.aav7934.

Hu, ZhenXian, Ying Zhu, Xiao Liu, Wei Zhang, Jing Liu, Shiwen Wu, Jiangxi Xiao, Yun Yuan, et Zhaoxia Wang. 2019. « FHL1-Related Clinical, Muscle MRI and Genetic Features in Six Chinese Patients with Reducing Body Myopathy ». *Journal of Human Genetics* 64 (9): 919-26. https://doi.org/10.1038/s10038-019-0627-z.

Ikeda, Naoki, Kenichi Asano, Kenta Kikuchi, Yoshimi Uchida, Hiroki Ikegami, Ryo Takagi, Satoshi Yotsumoto, et al. 2018. « Emergence of Immunoregulatory Ym1+Ly6Chi Monocytes during Recovery Phase of Tissue Injury ». *Science Immunology* 3 (28): eaat0207. https://doi.org/10.1126/sciimmunol.aat0207.

Inoue, S., K. Morita, R. R. Matias, J. V. Tuplano, R. R. G. Resuello, J. R. Candelario, D. J. M. Cruz, et al. 2003. « Distribution of Three Arbovirus Antibodies among Monkeys (Macaca Fascicularis) in the Philippines ». *Journal of Medical Primatology* 32 (2): 89-94. https://doi.org/10.1034/j.1600-0684.2003.00015.x.

Irvine, Katharine, Renee Stirling, David Hume, et Derek Kennedy. 2004. « Rasputin, More Promiscuous than Ever: A Review of G3BP ». *The International Journal of Developmental Biology* 48 (10): 1065-77. https://doi.org/10.1387/ijdb.041893ki.

Ivanov, Pavel, Nancy Kedersha, et Paul Anderson. 2019. « Stress Granules and Processing Bodies in Translational Control ». *Cold Spring Harbor Perspectives in Biology* 11 (5): a032813. https://doi.org/10.1101/cshperspect.a032813.

Jayabalan, Aravinth Kumar, Srivathsan Adivarahan, Aakash Koppula, Rachy Abraham, Mona Batish, Daniel Zenklusen, Diane E. Griffin, et Anthony K. L. Leung. 2021a. « Stress Granule Formation, Disassembly, and Composition Are Regulated by Alphavirus ADP-Ribosylhydrolase Activity ». *Proceedings of the National Academy of Sciences of the United*

States of America 118 (6). https://doi.org/10.1073/pnas.2021719118.

———. 2021b. « Stress Granule Formation, Disassembly, and Composition Are Regulated by Alphavirus ADP-Ribosylhydrolase Activity ». *Proceedings of the National Academy of Sciences* 118 (6): e2021719118. https://doi.org/10.1073/pnas.2021719118.

Jayabalan, Aravinth Kumar, Diane E. Griffin, et Anthony K. L. Leung. 2023. « Pro-Viral and Anti-Viral Roles of the RNA-Binding Protein G3BP1 ». *Viruses* 15 (2): 449. https://doi.org/10.3390/v15020449.

Jemielity, Stephanie, Jinyize J. Wang, Ying Kai Chan, Asim A. Ahmed, Wenhui Li, Sheena Monahan, Xia Bu, et al. 2013. « TIM-Family Proteins Promote Infection of Multiple Enveloped Viruses through Virion-Associated Phosphatidylserine ». Édité par Theodore C. Pierson. *PLoS Pathogens* 9 (3): e1003232. https://doi.org/10.1371/journal.ppat.1003232.

Jones, Jennifer E., Kristin M. Long, Alan C. Whitmore, Wes Sanders, Lance R. Thurlow, Julia A. Brown, Clayton R. Morrison, et al. 2017. « Disruption of the Opal Stop Codon Attenuates Chikungunya Virus-Induced Arthritis and Pathology ». *mBio* 8 (6): e01456-17. https://doi.org/10.1128/mBio.01456-17.

Jones, Rhian, Gabriel Bragagnolo, Rocío Arranz, et Juan Reguera. 2021. « Capping Pores of Alphavirus nsP1 Gate Membranous Viral Replication Factories ». *Nature* 589 (7843): 615-19. https://doi.org/10.1038/s41586-020-3036-8.

Jones, Rhian, Michael Hons, Nadia Rabah, Noelia Zamarreño, Rocío Arranz, et Juan Reguera. 2023. « Structural Basis and Dynamics of Chikungunya Alphavirus RNA Capping by nsP1 Capping Pores ». *Proceedings of the National Academy of Sciences* 120 (12): e2213934120. https://doi.org/10.1073/pnas.2213934120.

Jose, Joyce, Aaron B. Taylor, et Richard J. Kuhn. 2017. « Spatial and Temporal Analysis of Alphavirus Replication and Assembly in Mammalian and Mosquito Cells ». Édité par Terence S. Dermody. *mBio* 8 (1). https://doi.org/10.1128/mBio.02294-16.

Josseran, Loïc, Christophe Paquet, Abdelkrim Zehgnoun, Nadège Caillere, Alain Le Tertre, Jean-Louis Solet, et Martine Ledrans. 2006. « Chikungunya Disease Outbreak, Reunion Island ». *Emerging Infectious Diseases* 12 (12): 1994-95. https://doi.org/10.3201/eid1212.060710.

Jupp, P. G., et B. M. McIntosh. 1990. « Aedes Furcifer and Other Mosquitoes as Vectors of Chikungunya Virus at Mica, Northeastern Transvaal, South Africa ». *Journal of the American Mosquito Control Association* 6 (3): 415-20.

Kading, Rebekah C., Aaron C. Brault, et J. David Beckham. 2020. « Global Perspectives on Arbovirus Outbreaks: A 2020 Snapshot ». *Tropical Medicine and Infectious Disease* 5 (3): 142.

https://doi.org/10.3390/tropicalmed5030142.

Kadrmas, Julie L., et Mary C. Beckerle. 2004. « The LIM Domain: From the Cytoskeleton to the Nucleus ». *Nature Reviews Molecular Cell Biology* 5 (11): 920-31. https://doi.org/10.1038/nrm1499.

Kalkkinen, Nisse, Hans Söderlund, Hans Jörnvall, et Leevi Kääriäinen. 1980. « Analysis of Semliki-Forest-Virus Structural Proteins to Illustrate Polyprotein Processing of Alpha Viruses ». *European Journal of Biochemistry* 108 (1): 31-37. https://doi.org/10.1111/j.1432-1033.1980.tb04692.x.

Kallio, Katri, Kirsi Hellström, Eija Jokitalo, et Tero Ahola. 2016. « RNA Replication and Membrane Modification Require the Same Functions of Alphavirus Nonstructural Proteins ». Édité par A. Simon. *Journal of Virology* 90 (3): 1687-92. https://doi.org/10.1128/JVI.02484-15.

Kaneko, Tomonori, Lei Li, et Shawn S.-C. Li. 2008. « The SH3 Domain--a Family of Versatile Peptide- and Protein-Recognition Module ». *Frontiers in Bioscience: A Journal and Virtual Library* 13 (mai): 4938-52. https://doi.org/10.2741/3053.

Kariuki Njenga, M., L. Nderitu, J. P. Ledermann, A. Ndirangu, C. H. Logue, C. H. L. Kelly, R. Sang, K. Sergon, R. Breiman, et A. M. Powers. 2008. « Tracking Epidemic Chikungunya Virus into the Indian Ocean from East Africa ». *Journal of General Virology* 89 (11): 2754-60. https://doi.org/10.1099/vir.0.2008/005413-0.

Kedersha, Nancy, et Paul Anderson. 2007. « Mammalian Stress Granules and Processing Bodies ». In *Methods in Enzymology*, 431:61-81. Translation Initiation: Cell Biology, High-Throughput Methods, and Chemical-Based Approaches. Academic Press. https://doi.org/10.1016/S0076-6879(07)31005-7.

Kedersha, Nancy, Marc D. Panas, Christopher A. Achorn, Shawn Lyons, Sarah Tisdale, Tyler Hickman, Marshall Thomas, et al. 2016. « G3BP-Caprin1-USP10 Complexes Mediate Stress Granule Condensation and Associate with 40S Subunits ». *The Journal of Cell Biology* 212 (7): 845-60. https://doi.org/10.1083/jcb.201508028.

Keßler, M., A. Kieltsch, E. Kayvanpour, H. A. Katus, B. Schoser, J. Schessl, S. Just, et W. Rottbauer. 2018. « A Zebrafish Model for FHL1-Opathy Reveals Loss-of-Function Effects of Human FHL1 Mutations ». *Neuromuscular Disorders: NMD* 28 (6): 521-31. https://doi.org/10.1016/j.nmd.2018.03.001.

Khan, Afjal Hossain, Kouichi Morita, Maria Del Carmen Parquet, Futoshi Hasebe, Edward G. M. Mathenge, et Akira Igarashi. 2002. « Complete Nucleotide Sequence of Chikungunya Virus and Evidence for an Internal Polyadenylation Site ». *The Journal of General Virology* 83 (Pt

12): 3075-84. https://doi.org/10.1099/0022-1317-83-12-3075.

Kim, Arthur S., et Michael S. Diamond. 2022. « A Molecular Understanding of Alphavirus Entry and Antibody Protection ». *Nature Reviews Microbiology*, décembre. https://doi.org/10.1038/s41579-022-00825-7.

Kim, Dal Young, Svetlana Atasheva, Elena I. Frolova, et Ilya Frolov. 2013. « Venezuelan Equine Encephalitis Virus nsP2 Protein Regulates Packaging of the Viral Genome into Infectious Virions ». *Journal of Virology* 87 (8): 4202-13. https://doi.org/10.1128/JVI.03142-12.

Kim, Dal Young, Andrew E. Firth, Svetlana Atasheva, Elena I. Frolova, et Ilya Frolov. 2011. « Conservation of a Packaging Signal and the Viral Genome RNA Packaging Mechanism in Alphavirus Evolution ». *Journal of Virology* 85 (16): 8022-36. https://doi.org/10.1128/JVI.00644-11.

Kim, Dal Young, Josephine M. Reynaud, Aliaksandra Rasalouskaya, Ivan Akhrymuk, James A. Mobley, Ilya Frolov, et Elena I. Frolova. 2016a. « New World and Old World Alphaviruses Have Evolved to Exploit Different Components of Stress Granules, FXR and G3BP Proteins, for Assembly of Viral Replication Complexes ». Édité par Mark T. Heise. *PLOS Pathogens* 12 (8): e1005810. https://doi.org/10.1371/journal.ppat.1005810.

———. 2016b. « New World and Old World Alphaviruses Have Evolved to Exploit Different Components of Stress Granules, FXR and G3BP Proteins, for Assembly of Viral Replication Complexes ». Édité par Mark T. Heise. *PLOS Pathogens* 12 (8): e1005810. https://doi.org/10.1371/journal.ppat.1005810.

Kim, Kyongmin Hwang, Tillmann Rümenapf, Ellen G. Strauss, et James H. Strauss. 2004. « Regulation of Semliki Forest Virus RNA Replication: A Model for the Control of Alphavirus Pathogenesis in Invertebrate Hosts ». *Virology* 323 (1): 153-63. https://doi.org/10.1016/j.virol.2004.03.009.

Kim, Susana Soo-Yeon, Lynette Sze, et Kong-Peng Lam. 2019. « The Stress Granule Protein G3BP1 Binds Viral dsRNA and RIG-I to Enhance Interferon-β Response ». *Journal of Biological Chemistry* 294 (16): 6430-38. https://doi.org/10.1074/jbc.RA118.005868.

Klimstra, William B., Elizabeth M. Nangle, M. Shane Smith, Andrew D. Yurochko, et Kate D. Ryman. 2003. « DC-SIGN and L-SIGN Can Act as Attachment Receptors for Alphaviruses and Distinguish between Mosquito Cell- and Mammalian Cell-Derived Viruses ». *Journal of Virology* 77 (22): 12022-32. https://doi.org/10.1128/jvi.77.22.12022-12032.2003.

Kong, Y., J. M. Shelton, B. Rothermel, X. Li, J. A. Richardson, R. Bassel-Duby, et R. S. Williams. 2001. « Cardiac-Specific LIM Protein FHL2 Modifies the Hypertrophic Response

to Beta-Adrenergic Stimulation ». *Circulation* 103 (22): 2731-38. https://doi.org/10.1161/01.cir.103.22.2731.

Kraemer, Moritz U. G., Marianne E. Sinka, Kirsten A. Duda, Adrian Mylne, Freya M. Shearer, Oliver J. Brady, Jane P. Messina, et al. 2015. « The Global Compendium of Aedes Aegypti and Ae. Albopictus Occurrence ». *Scientific Data* 2: 150035. https://doi.org/10.1038/sdata.2015.35.

Kristensen, Ole. 2015. « Crystal Structure of the G3BP2 NTF2-like Domain in Complex with a Canonical FGDF Motif Peptide ». *Biochemical and Biophysical Research Communications* 467 (1): 53-57. https://doi.org/10.1016/j.bbrc.2015.09.123.

Kumar, Sameer, Abhishek Kumar, Prabhudutta Mamidi, Atul Tiwari, Sriram Kumar, Animamalar Mayavannan, Sagarika Mudulli, Ajit Kumar Singh, Bharat Bhusan Subudhi, et Soma Chattopadhyay. 2018. « Chikungunya Virus nsP1 Interacts Directly with nsP2 and Modulates Its ATPase Activity ». *Scientific Reports* 8 (1): 1045. https://doi.org/10.1038/s41598-018-19295-0.

Kurkela, Satu, Tytti Manni, Johanna Myllynen, Antti Vaheri, et Olli Vapalahti. 2005. « Clinical and Laboratory Manifestations of Sindbis Virus Infection: Prospective Study, Finland, 2002-2003 ». *The Journal of Infectious Diseases* 191 (11): 1820-29. https://doi.org/10.1086/430007.

Laakkonen, P., P. Auvinen, P. Kujala, et L. Kääriäinen. 1998. « Alphavirus Replicase Protein NSP1 Induces Filopodia and Rearrangement of Actin Filaments ». *Journal of Virology* 72 (12): 10265-69. https://doi.org/10.1128/JVI.72.12.10265-10269.1998.

Labadie, Karine, Thibaut Larcher, Christophe Joubert, Abdelkrim Mannioui, Benoit Delache, Patricia Brochard, Lydie Guigand, et al. 2010. « Chikungunya disease in nonhuman primates involves long-term viral persistence in macrophages ». *The Journal of Clinical Investigation* 120 (3): 894-906. https://doi.org/10.1172/JCI40104.

Lambrechts, Louis, Thomas W. Scott, et Duane J. Gubler. 2010. « Consequences of the Expanding Global Distribution of Aedes albopictus for Dengue Virus Transmission ». *PLoS Neglected Tropical Diseases* 4 (5): e646. https://doi.org/10.1371/journal.pntd.0000646.

Lark, Tyler, Forrest Keck, et Aarthi Narayanan. 2018. « Interactions of Alphavirus nsP3 Protein with Host Proteins ». *Frontiers in Microbiology* 8. https://doi.org/10.3389/fmicb.2017.02652.

Laurent, Timothée, Pravin Kumar, Susanne Liese, Farnaz Zare, Mattias Jonasson, Andreas Carlson, et Lars-Anders Carlson. 2022. « Architecture of the chikungunya virus replication organelle ». Édité par Giulia Zanetti et Vivek Malhotra. *eLife* 11 (octobre): e83042. https://doi.org/10.7554/eLife.83042.

Lee, Teresa, et Jerry Pelletier. 2016. « The Biology of DHX9 and Its Potential as a Therapeutic Target ». *Oncotarget* 7 (27): 42716-39. https://doi.org/10.18632/oncotarget.8446.

Léger, Psylvia, Eliana Nachman, Karsten Richter, Carole Tamietti, Jana Koch, Robin Burk, Susann Kummer, et al. 2020. « NSs Amyloid Formation Is Associated with the Virulence of Rift Valley Fever Virus in Mice ». *Nature Communications* 11 (1): 1-19. https://doi.org/10.1038/s41467-020-17101-y.

Lemant, Jérôme, Véronique Boisson, Arnaud Winer, Laure Thibault, Hélène André, François Tixier, Marie Lemercier, et al. 2008. « Serious Acute Chikungunya Virus Infection Requiring Intensive Care during the Reunion Island Outbreak in 2005–2006* ». *Critical Care Medicine* 36 (9): 2536. https://doi.org/10.1097/CCM.0b013e318183f2d2.

Lentscher, Anthony J., Mary K. McCarthy, Nicholas A. May, Bennett J. Davenport, Stephanie A. Montgomery, Krishnan Raghunathan, Nicole McAllister, Laurie A. Silva, Thomas E. Morrison, et Terence S. Dermody. 2020. « Chikungunya Virus Replication in Skeletal Muscle Cells Is Required for Disease Development ». *Journal of Clinical Investigation* 130 (3): 1466-78. https://doi.org/10.1172/JCI129893.

Leung, Anthony K. L., Robert Lyle McPherson, et Diane E. Griffin. 2018. « Macrodomain ADP-Ribosylhydrolase and the Pathogenesis of Infectious Diseases ». *PLOS Pathogens* 14 (3): e1006864. https://doi.org/10.1371/journal.ppat.1006864.

Leung, Anthony K. L., Sejal Vyas, Jennifer E. Rood, Arjun Bhutkar, Phillip A. Sharp, et Paul Chang. 2011. « Poly(ADP-Ribose) Regulates Stress Responses and microRNA Activity in the Cytoplasm ». *Molecular Cell* 42 (4): 489-99. https://doi.org/10.1016/j.molcel.2011.04.015.

Levi, Laura I., et Marco Vignuzzi. 2019. « Arthritogenic Alphaviruses: A Worldwide Emerging Threat? » *Microorganisms* 7 (5): 133. https://doi.org/10.3390/microorganisms7050133.

Levitt, N. H., H. H. Ramsburg, S. E. Hasty, P. M. Repik, F. E. Cole, et H. W. Lupton. 1986. « Development of an Attenuated Strain of Chikungunya Virus for Use in Vaccine Production ». *Vaccine* 4 (3): 157-62. https://doi.org/10.1016/0264-410x(86)90003-4.

Li, Changqing, Yannick Debing, Gytis Jankevicius, Johan Neyts, Ivan Ahel, Bruno Coutard, et Bruno Canard. 2016. « Viral Macro Domains Reverse Protein ADP-Ribosylation ». *Journal of Virology* 90 (19): 8478-86. https://doi.org/10.1128/JVI.00705-16.

Li, Guangpu, Mark W. La Starza, W. Reef Hardy, James H. Strauss, et Charles M. Rice. 1990. « Phosphorylation of Sindbis Virus nsP3 in Vivo and in Vitro ». *Virology* 179 (1): 416-27. https://doi.org/10.1016/0042-6822(90)90310-N.

Li, Lili, Hui Zhao, Ping Liu, Chunfeng Li, Natalie Quanquin, Xue Ji, Nina Sun, et al. 2018.

« *PARP12* Suppresses Zika Virus Infection through PARP-Dependent Degradation of NS1 and NS3 Viral Proteins ». *Science Signaling* 11 (535): eaas9332. https://doi.org/10.1126/scisignal.aas9332.

Li, Long, Joyce Jose, Ye Xiang, Richard J. Kuhn, et Michael G. Rossmann. 2010. « Structural Changes of Envelope Proteins during Alphavirus Fusion ». *Nature* 468 (7324): 705-8. https://doi.org/10.1038/nature09546.

Li, Shitao, Lingyan Wang, Michael Berman, Young-Yun Kong, et Martin E. Dorf. 2011. « Mapping a Dynamic Innate Immunity Protein Interaction Network Regulating Type I Interferon Production ». *Immunity* 35 (3): 426-40. https://doi.org/10.1016/j.immuni.2011.06.014.

Liljeström, P., et H. Garoff. 1991. « Internally Located Cleavable Signal Sequences Direct the Formation of Semliki Forest Virus Membrane Proteins from a Polyprotein Precursor ». *Journal of Virology* 65 (1): 147-54. https://doi.org/10.1128/JVI.65.1.147-154.1991.

Lim, Elisa X. Y., Wai Suet Lee, Eugene T. Madzokere, et Lara J. Herrero. 2018. « Mosquitoes as Suitable Vectors for Alphaviruses ». *Viruses* 10 (2): 84. https://doi.org/10.3390/v10020084.

Liu, Hainan, Yu Bai, Xun Zhang, Ting Gao, Yue Liu, Entao Li, Xuefeng Wang, et al. 2022. « SARS-CoV-2 N Protein Antagonizes Stress Granule Assembly and IFN Production by Interacting with G3BPs to Facilitate Viral Replication ». *Journal of Virology* 96 (12): e0041222. https://doi.org/10.1128/jvi.00412-22.

Liu, Zhao-Shan, Hong Cai, Wen Xue, Miao Wang, Tian Xia, Wan-Jin Li, Jia-Qing Xing, et al. 2019. « G3BP1 Promotes DNA Binding and Activation of cGAS ». *Nature Immunology* 20 (1): 18-28. https://doi.org/10.1038/s41590-018-0262-4.

Lloyd-Smith, James O., Dylan George, Kim M. Pepin, Virginia E. Pitzer, Juliet R. C. Pulliam, Andrew P. Dobson, Peter J. Hudson, et Bryan T. Grenfell. 2009. « Epidemic dynamics at the human-animal interface ». *Science (New York, N.Y.)* 326 (5958): 1362-67. https://doi.org/10.1126/science.1177345.

Lohachanakul, Jindarat, Weerawat Phuklia, Montri Thannagith, Tipparat Thongsakulprasert, Duncan R. Smith, et Sukathida Ubol. 2015. « Differences in Response of Primary Human Myoblasts to Infection with Recent Epidemic Strains of Chikungunya Virus Isolated from Patients with and without Myalgia: Viral Factor in CHIKV-Induced Myalgia ». *Journal of Medical Virology* 87 (5): 733-39. https://doi.org/10.1002/jmv.24081.

Lukash, Tetyana, Tatiana Agback, Francisco Dominguez, Nikita Shiliaev, Chetan Meshram, Elena I. Frolova, Peter Agback, et Ilya Frolov. 2020. « Structural and Functional Characterization of Host FHL1 Protein Interaction with Hypervariable Domain of

Chikungunya Virus nsP3 Protein ». *Journal of Virology* 95 (1). https://doi.org/10.1128/JVI.01672-20.

Lulla, A., V. Lulla, et A. Merits. 2012. « Macromolecular Assembly-Driven Processing of the 2/3 Cleavage Site in the Alphavirus Replicase Polyprotein ». *Journal of Virology* 86 (1): 553-65. https://doi.org/10.1128/JVI.05195-11.

Lumsden, W.H.R. 1955. « An Epidemic of Virus Disease in Southern Province, Tanganyika Territory, in 1952–1953 II. General Description and Epidemiology ». *Transactions of the Royal Society of Tropical Medicine and Hygiene* 49 (1): 33-57. https://doi.org/10.1016/0035-9203(55)90081-X.

Ma, Guoda, Yajun Wang, You Li, Lili Cui, Yujuan Zhao, Bin Zhao, et Keshen Li. 2015. « MiR-206, a Key Modulator of Skeletal Muscle Development and Disease ». *International Journal of Biological Sciences* 11 (3): 345-52. https://doi.org/10.7150/ijbs.10921.

Ma, Hongming, Arthur S. Kim, Natasha M. Kafai, James T. Earnest, Aadit P. Shah, James Brett Case, Katherine Basore, et al. 2020. « LDLRAD3 Is a Receptor for Venezuelan Equine Encephalitis Virus ». *Nature* 588 (7837): 308-14. https://doi.org/10.1038/s41586-020-2915-3.

MacDonald, Margaret R., Erica S. Machlin, Owen R. Albin, et David E. Levy. 2007. « The Zinc Finger Antiviral Protein Acts Synergistically with an Interferon-Induced Factor for Maximal Activity against Alphaviruses ». *Journal of Virology* 81 (24): 13509-18. https://doi.org/10.1128/JVI.00402-07.

Mackenzie, John S., Duane J. Gubler, et Lyle R. Petersen. 2004. « Emerging Flaviviruses: The Spread and Resurgence of Japanese Encephalitis, West Nile and Dengue Viruses ». *Nature Medicine* 10 (12 Suppl): S98-109. https://doi.org/10.1038/nm1144.

Madewell, Zachary J. 2020. « Arboviruses and Their Vectors ». *Southern Medical Journal* 113 (10): 520-23. https://doi.org/10.14423/SMJ.0000000000001152.

Malet, H., B. Coutard, S. Jamal, H. Dutartre, N. Papageorgiou, M. Neuvonen, T. Ahola, et al. 2009. « The Crystal Structures of Chikungunya and Venezuelan Equine Encephalitis Virus nsP3 Macro Domains Define a Conserved Adenosine Binding Pocket ». *Journal of Virology* 83 (13): 6534-45. https://doi.org/10.1128/JVI.00189-09.

Mangala Prasad, Vidya, Jelle S. Blijleven, Jolanda M. Smit, et Kelly K. Lee. 2022. « Visualization of Conformational Changes and Membrane Remodeling Leading to Genome Delivery by Viral Class-II Fusion Machinery ». *Nature Communications* 13 (1): 4772. https://doi.org/10.1038/s41467-022-32431-9.

Manimunda, Sathya Prakash, Paluru Vijayachari, Raghuraj Uppoor, Attayur Purushottaman Sugunan, Shiv Shankar Singh, Subhodh Kumar Rai, Anakkathil Balan Sudeep, Nagarajan

Muruganandam, Itta Krishna Chaitanya, et Dev Reddy Guruprasad. 2010. « Clinical Progression of Chikungunya Fever during Acute and Chronic Arthritic Stages and the Changes in Joint Morphology as Revealed by Imaging ». *Transactions of the Royal Society of Tropical Medicine and Hygiene* 104 (6): 392-99. https://doi.org/10.1016/j.trstmh.2010.01.011.

Manojlovic, Zarko, et Branko Stefanovic. 2012. « A Novel Role of RNA Helicase A in Regulation of Translation of Type I Collagen mRNAs ». *RNA (New York, N.Y.)* 18 (2): 321-34. https://doi.org/10.1261/rna.030288.111.

Marchette, N. J., A. Rudnick, R. Garcia, et D. W. MacVean. 1978. « Alphaviruses in Peninusular Malaysia: I. Virus Isolations and Animal Serology ». *The Southeast Asian Journal of Tropical Medicine and Public Health* 9 (3): 317-29.

Marr, Nico, Ting-I. Wang, Sarah H. Y. Kam, Yuan Shen Hu, Ashish A. Sharma, Angie Lam, Joy Markowski, Alfonso Solimano, Pascal M. Lavoie, et Stuart E. Turvey. 2014. « Attenuation of Respiratory Syncytial Virus-Induced and RIG-I-Dependent Type I IFN Responses in Human Neonates and Very Young Children ». *Journal of Immunology (Baltimore, Md.: 1950)* 192 (3): 948-57. https://doi.org/10.4049/jimmunol.1302007.

Mathieu, Nicholas A., Ermela Paparisto, Stephen D. Barr, et Donald E. Spratt. 2021. « HERC5 and the ISGylation Pathway: Critical Modulators of the Antiviral Immune Response ». *Viruses* 13 (6): 1102. https://doi.org/10.3390/v13061102.

Matkovic, Roy, Eric Bernard, Simon Fontanel, Patrick Eldin, Nathalie Chazal, Deka Hassan Hersi, Andres Merits, Jean-Marie Péloponèse, et Laurence Briant. 2018. « The Host DHX9 DExH-Box Helicase Is Recruited to Chikungunya Virus Replication Complexes for Optimal Genomic RNA Translation ». Édité par Terence S. Dermody. *Journal of Virology* 93 (4): e01764-18, /jvi/93/4/JVI.01764-18.atom. https://doi.org/10.1128/JVI.01764-18.

Matsuki, Hideaki, Masahiko Takahashi, Masaya Higuchi, Grace N Makokha, Masayasu Oie, et Masahiro Fujii. 2013. « Both G3BP1 and G3BP2 Contribute to Stress Granule Formation ». *Genes to Cells* 18 (2): 135-46. https://doi.org/10.1111/gtc.12023.

Matusali, Giulia, Francesca Colavita, Licia Bordi, Eleonora Lalle, Giuseppe Ippolito, Maria Capobianchi, et Concetta Castilletti. 2019. « Tropism of the Chikungunya Virus ». *Viruses* 11 (2): 175. https://doi.org/10.3390/v11020175.

Mayer, Sandra V., Robert B. Tesh, et Nikos Vasilakis. 2017. « The emergence of arthropod-borne viral diseases: A global prospective on dengue, chikungunya and zika fevers ». *Acta Tropica* 166 (février): 155-63. https://doi.org/10.1016/j.actatropica.2016.11.020.

Mazzon, Michela, Cecilia Castro, Bastian Thaa, Lifeng Liu, Margit Mutso, Xiang Liu, Suresh Mahalingam, Julian L. Griffin, Mark Marsh, et Gerald M. McInerney. 2018. « Alphavirus-

Induced Hyperactivation of PI3K/AKT Directs pro-Viral Metabolic Changes ». *PLoS Pathogens* 14 (1): e1006835. https://doi.org/10.1371/journal.ppat.1006835.

McAllister, Nicole, Yan Liu, Lisete M. Silva, Anthony J. Lentscher, Wengang Chai, Nian Wu, Kira A. Griswold, et al. 2020. « Chikungunya Virus Strains from Each Genetic Clade Bind Sulfated Glycosaminoglycans as Attachment Factors ». Édité par Tom Gallagher. *Journal of Virology* 94 (24): e01500-20. https://doi.org/10.1128/JVI.01500-20.

McCarthy, Mary K., Bennett J. J. Davenport, et Thomas E. Morrison. 2019. « Chronic Chikungunya Virus Disease ». *Current Topics in Microbiology and Immunology*, janvier. https://doi.org/10.1007/82_2018_147.

McGrath, Meagan J., Denny L. Cottle, Mai-Anh Nguyen, Jennifer M. Dyson, Imogen D. Coghill, Paul A. Robinson, Melissa Holdsworth, et al. 2006. « Four and a Half LIM Protein 1 Binds Myosin-Binding Protein C and Regulates Myosin Filament Formation and Sarcomere Assembly ». *Journal of Biological Chemistry* 281 (11): 7666-83. https://doi.org/10.1074/jbc.M512552200.

McGrath, Meagan J., Christina A. Mitchell, Imogen D. Coghill, Paul A. Robinson, et Susan Brown. 2003. « Skeletal muscle LIM protein 1 (SLIM1/FHL1) induces α5β1-integrin-dependent myocyte elongation ». *American Journal of Physiology-Cell Physiology* 285 (6): C1513-26. https://doi.org/10.1152/ajpcell.00207.2003.

McInerney, Gerald M., Nancy L. Kedersha, Randal J. Kaufman, Paul Anderson, et Peter Liljeström. 2005. « Importance of eIF2alpha Phosphorylation and Stress Granule Assembly in Alphavirus Translation Regulation ». *Molecular Biology of the Cell* 16 (8): 3753-63. https://doi.org/10.1091/mbc.e05-02-0124.

McIntosh, P. G. Jupp, B. M. 1988. « Chikungunya Virus Disease ». In *The Arboviruses*. CRC Press.

McPherson, Robert Lyle, Rachy Abraham, Easwaran Sreekumar, Shao-En Ong, Shang-Jung Cheng, Victoria K. Baxter, Hans A. V. Kistemaker, Dmitri V. Filippov, Diane E. Griffin, et Anthony K. L. Leung. 2017. « ADP-ribosylhydrolase activity of Chikungunya virus macrodomain is critical for virus replication and virulence ». *Proceedings of the National Academy of Sciences of the United States of America* 114 (7): 1666-71. https://doi.org/10.1073/pnas.1621485114.

Meertens, Laurent, Mohamed Lamine Hafirassou, Thérèse Couderc, Lucie Bonnet-Madin, Vasiliya Kril, Beate M. Kümmerer, Athena Labeau, et al. 2019. « FHL1 Is a Major Host Factor for Chikungunya Virus Infection ». *Nature* 574 (7777): 259-63. https://doi.org/10.1038/s41586-019-1578-4.

Mehta, Ravi, Patrick Gerardin, Carlos Alexandre Antunes de Brito, Cristiane Nascimento Soares, Maria Lucia Brito Ferreira, et Tom Solomon. 2018. « The neurological complications of chikungunya virus: A systematic review ». *Reviews in Medical Virology* 28 (3). https://doi.org/10.1002/rmv.1978.

Melancon, P., et H. Garoff. 1987. « Processing of the Semliki Forest Virus Structural Polyprotein: Role of the Capsid Protease ». *Journal of Virology* 61 (5): 1301-9. https://doi.org/10.1128/JVI.61.5.1301-1309.1987.

Mendes, Adriano, et Richard Kuhn. 2018. « Alphavirus Nucleocapsid Packaging and Assembly ». *Viruses* 10 (3): 138. https://doi.org/10.3390/v10030138.

Merits, Andres, Lidia Vasiljeva, Tero Ahola, Leevi Kääriäinen, et Petri Auvinen. 2001. « Proteolytic Processing of Semliki Forest Virus-Specific Non-Structural Polyprotein by nsP2 Protease ». *The Journal of General Virology* 82 (Pt 4): 765-73. https://doi.org/10.1099/0022-1317-82-4-765.

Meshram, Chetan D., Peter Agback, Nikita Shiliaev, Nadya Urakova, James A. Mobley, Tatiana Agback, Elena I. Frolova, et Ilya Frolov. 2018. « Multiple Host Factors Interact with the Hypervariable Domain of Chikungunya Virus nsP3 and Determine Viral Replication in Cell-Specific Mode ». *Journal of Virology* 92 (16). https://doi.org/10.1128/JVI.00838-18.

Messina, Jane P., Oliver J. Brady, Thomas W. Scott, Chenting Zou, David M. Pigott, Kirsten A. Duda, Samir Bhatt, et al. 2014. « Global Spread of Dengue Virus Types: Mapping the 70 Year History ». *Trends in Microbiology* 22 (3): 138-46. https://doi.org/10.1016/j.tim.2013.12.011.

Michelsen, J W, K L Schmeichel, M C Beckerle, et D R Winge. 1993. « The LIM motif defines a specific zinc-binding protein domain. » *Proceedings of the National Academy of Sciences of the United States of America* 90 (10): 4404-8.

Milligan, Gregg N., Barbara S. Schnierle, Alexander J. McAuley, et David W. C. Beasley. 2019. « Defining a Correlate of Protection for Chikungunya Virus Vaccines ». *Vaccine* 37 (50): 7427-36. https://doi.org/10.1016/j.vaccine.2018.10.033.

Mim, Carsten, et Vinzenz M. Unger. 2012. « Membrane Curvature and Its Generation by BAR Proteins ». *Trends in Biochemical Sciences* 37 (12): 526-33. https://doi.org/10.1016/j.tibs.2012.09.001.

Mohsen, Mona O., et Martin F. Bachmann. 2022. « Virus-like Particle Vaccinology, from Bench to Bedside ». *Cellular & Molecular Immunology* 19 (9): 993-1011. https://doi.org/10.1038/s41423-022-00897-8.

Moller-Tank, Sven, et Wendy Maury. 2014. « Phosphatidylserine Receptors: Enhancers of

Enveloped Virus Entry and Infection ». *Virology* 468-470 (novembre): 565-80. https://doi.org/10.1016/j.virol.2014.09.009.

Molony, Ryan D., Jenny T. Nguyen, Yong Kong, Ruth R. Montgomery, Albert C. Shaw, et Akiko Iwasaki. 2017. « Aging Impairs Both Primary and Secondary RIG-I Signaling for Interferon Induction in Human Monocytes ». *Science Signaling* 10 (509): eaan2392. https://doi.org/10.1126/scisignal.aan2392.

Monath, Thomas P. 2020. *The Arboviruses:: Epidemiology and Ecology*. CRC Press.

Morgan, M. J., et A. J. A. Madgwick. 1999. « The LIM Proteins FHL1 and FHL3 Are Expressed Differently in Skeletal Muscle ». *Biochemical and Biophysical Research Communications* 255 (2): 245-50. https://doi.org/10.1006/bbrc.1999.0179.

Morgan, M. J., A. J. Madgwick, B. Charleston, J. M. Pell, et P. T. Loughna. 1995. « The Developmental Regulation of a Novel Muscle LIM-Protein ». *Biochemical and Biophysical Research Communications* 212 (3): 840-46. https://doi.org/10.1006/bbrc.1995.2045.

Mukhopadhyay, Suchetana, Paul R. Chipman, Eunmee M. Hong, Richard J. Kuhn, et Michael G. Rossmann. 2002. « In Vitro-Assembled Alphavirus Core-Like Particles Maintain a Structure Similar to That of Nucleocapsid Cores in Mature Virus ». *Journal of Virology* 76 (21): 11128-32. https://doi.org/10.1128/JVI.76.21.11128-11132.2002.

Mulvey, M., et D. T. Brown. 1996. « Assembly of the Sindbis Virus Spike Protein Complex ». *Virology* 219 (1): 125-32. https://doi.org/10.1006/viro.1996.0229.

Mutso, Margit, Ainhoa Moliner Morro, Cecilia Smedberg, Sergo Kasvandik, Muriel Aquilimeba, Mona Teppor, Liisi Tarve, et al. 2018. « Mutation of CD2AP and SH3KBP1 Binding Motif in Alphavirus nsP3 Hypervariable Domain Results in Attenuated Virus ». *Viruses* 10 (5). https://doi.org/10.3390/v10050226.

Nair, Sharmila, Subhajit Poddar, Raeann M. Shimak, et Michael S. Diamond. 2017. « Interferon Regulatory Factor 1 Protects against Chikungunya Virus-Induced Immunopathology by Restricting Infection in Muscle Cells ». Édité par Julie K. Pfeiffer. *Journal of Virology* 91 (22): e01419-17, e01419-17. https://doi.org/10.1128/JVI.01419-17.

Natrajan, Muktha S., Alejandra Rojas, et Jesse J. Waggoner. 2019. « Beyond Fever and Pain: Diagnostic Methods for Chikungunya Virus ». Édité par Colleen Suzanne Kraft. *Journal of Clinical Microbiology* 57 (6): e00350-19, /jcm/57/6/JCM.00350-19.atom. https://doi.org/10.1128/JCM.00350-19.

Nayak, Tapas Kumar, Prabhudutta Mamidi, Subhransu Sekhar Sahoo, P. Sanjai Kumar, Chandan Mahish, Sanchari Chatterjee, Bharat Bhusan Subudhi, Soma Chattopadhyay, et Subhasis Chattopadhyay. 2019. « P38 and JNK Mitogen-Activated Protein Kinases Interact

With Chikungunya Virus Non-Structural Protein-2 and Regulate TNF Induction During Viral Infection in Macrophages ». *Frontiers in Immunology* 10: 786. https://doi.org/10.3389/fimmu.2019.00786.

Neufeldt, Christopher John, et Mirko Cortese. 2022. « Membrane architects: how positive-strand RNA viruses restructure the cell ». *Journal of General Virology* 103 (8): 001773. https://doi.org/10.1099/jgv.0.001773.

Neuvonen, Maarit, et Tero Ahola. 2009. « Differential Activities of Cellular and Viral Macro Domain Proteins in Binding of ADP-Ribose Metabolites ». *Journal of Molecular Biology* 385 (1): 212-25. https://doi.org/10.1016/j.jmb.2008.10.045.

Neuvonen, Maarit, Arunas Kazlauskas, Miika Martikainen, Ari Hinkkanen, Tero Ahola, et Kalle Saksela. 2011a. « SH3 Domain-Mediated Recruitment of Host Cell Amphiphysins by Alphavirus nsP3 Promotes Viral RNA Replication ». *PLoS Pathogens* 7 (11): e1002383. https://doi.org/10.1371/journal.ppat.1002383.

———. 2011b. « SH3 Domain-Mediated Recruitment of Host Cell Amphiphysins by Alphavirus nsP3 Promotes Viral RNA Replication ». *PLOS Pathogens* 7 (11): e1002383. https://doi.org/10.1371/journal.ppat.1002383.

Ng, Wern Hann, Xiang Liu, Zheng L. Ling, Camilla N. O. Santos, Lucas S. Magalhães, Andrew J. Kueh, Marco J. Herold, et al. 2023. « FHL1 Promotes Chikungunya and o'nyong-Nyong Virus Infection and Pathogenesis with Implications for Alphavirus Vaccine Design ». *Nature Communications* 14 (1): 6605. https://doi.org/10.1038/s41467-023-42330-2.

Noret, M., L. Herrero, N. Rulli, M. Rolph, P. N. Smith, R. W. Li, P. Roques, G. Gras, et S. Mahalingam. 2012. « Interleukin 6, RANKL, and Osteoprotegerin Expression by Chikungunya Virus-Infected Human Osteoblasts ». *Journal of Infectious Diseases* 206 (3): 455-57. https://doi.org/10.1093/infdis/jis368.

Nowee, Gwen, Julian W. Bakker, Corinne Geertsema, Vera I. D. Ros, Giel P. Göertz, Jelke J. Fros, et Gorben P. Pijlman. 2021. « A Tale of 20 Alphaviruses; Inter-species Diversity and Conserved Interactions Between Viral Non-structural Protein 3 and Stress Granule Proteins ». *Frontiers in Cell and Developmental Biology* 9. https://www.frontiersin.org/articles/10.3389/fcell.2021.625711.

Nsoesie, Elaine O., Moritz UG Kraemer, Nick Golding, David M. Pigott, Oliver J. Brady, Catherine L. Moyes, Michael A. Johansson, et al. 2016. « Global Distribution and Environmental Suitability for Chikungunya Virus, 1952 to 2015 ». *Eurosurveillance* 21 (20): 30234. https://doi.org/10.2807/1560-7917.ES.2016.21.20.30234.

Oldstone, Michael B. A. 2020. *Viruses, Plagues, and History: Past, Present, and Future*.

Second edition. New York: Oxford University Press.

Oliveira, Sandra, Jorge Rocha, Carla A. Sousa, et César Capinha. 2021. « Wide and Increasing Suitability for Aedes Albopictus in Europe Is Congruent across Distribution Models ». *Scientific Reports* 11 (1): 9916. https://doi.org/10.1038/s41598-021-89096-5.

Onyango, Clayton, Robert F. Breiman, Victor Ofula, Sheryl Bedno, Limbaso S. Konongoi, Heather Burke, Joseph Konde, et al. 2008. « Seroprevalence of Chikungunya Virus (CHIKV) Infection on Lamu Island, Kenya, October 2004 ». *The American Journal of Tropical Medicine and Hygiene* 78 (2): 333-37. https://doi.org/10.4269/ajtmh.2008.78.333.

Ozden, Simona, Michel Huerre, Jean-Pierre Riviere, Lark L. Coffey, Philippe V. Afonso, Vincent Mouly, Jean de Monredon, et al. 2007. « Human Muscle Satellite Cells as Targets of Chikungunya Virus Infection ». *PloS One* 2 (6): e527. https://doi.org/10.1371/journal.pone.0000527.

Panas, M. D., T. Ahola, et G. M. McInerney. 2014. « The C-Terminal Repeat Domains of nsP3 from the Old World Alphaviruses Bind Directly to G3BP ». *Journal of Virology* 88 (10): 5888-93. https://doi.org/10.1128/JVI.00439-14.

Panas, Marc D., Tim Schulte, Bastian Thaa, Tatiana Sandalova, Nancy Kedersha, Adnane Achour, et Gerald M. McInerney. 2015. « Viral and Cellular Proteins Containing FGDF Motifs Bind G3BP to Block Stress Granule Formation ». *PLOS Pathogens* 11 (2): e1004659. https://doi.org/10.1371/journal.ppat.1004659.

Panas, Marc D., Margus Varjak, Aleksei Lulla, Kai Er Eng, Andres Merits, Gunilla B. Karlsson Hedestam, et Gerald M. McInerney. 2012. « Sequestration of G3BP Coupled with Efficient Translation Inhibits Stress Granules in Semliki Forest Virus Infection ». Édité par Sandra Wolin. *Molecular Biology of the Cell* 23 (24): 4701-12. https://doi.org/10.1091/mbc.e12-08-0619.

Park, Young-Eun, Dae-Seong Kim, et Jin-Hong Shin. 2019. « Myofibrillar Myopathy Caused by a Novel FHL1 Mutation Presenting a Mild Myopathy with Ankle Contracture ». *Clinical Neurology and Neurosurgery* 180 (mai): 48-51. https://doi.org/10.1016/j.clineuro.2019.03.015.

Park, Young-Jun, et Karolin Luger. 2006. « Structure and Function of Nucleosome Assembly Proteins ». *Biochemistry and Cell Biology = Biochimie Et Biologie Cellulaire* 84 (4): 549-58. https://doi.org/10.1139/o06-088.

Paul, Binoy J., et Shajit Sadanand. 2018. « Chikungunya Infection: A Re-Emerging Epidemic ». *Rheumatology and Therapy* 5 (2): 317-26. https://doi.org/10.1007/s40744-018-0121-7.

Paul, David, et Ralf Bartenschlager. 2013. « Architecture and Biogenesis of Plus-Strand RNA Virus Replication Factories ». *World Journal of Virology* 2 (2): 32-48. https://doi.org/10.5501/wjv.v2.i2.32.

Paul, S. D., et K. R. P. Singh. 1968. « Experimental Infection of Macaca Radiala with Chikungunya Virus and Transmission of Virus by Mosquitoes. » *Indian Journal of Medical Research* 56 (6): 802-11.

Peränen, J., K. Takkinen, N. Kalkkinen, et L. Kääriäinen. 1988. « Semliki Forest Virus-Specific Non-Structural Protein nsP3 Is a Phosphoprotein ». *The Journal of General Virology* 69 (Pt 9) (septembre): 2165-78. https://doi.org/10.1099/0022-1317-69-9-2165.

Peranen, J., K. Takkinen, N. Kalkkinen, et L. Kaariainen. 1988. « Semliki Forest Virus-Specific Non-Structural Protein nsP3 Is a Phosphoprotein ». *Journal of General Virology* 69 (9): 2165-78. https://doi.org/10.1099/0022-1317-69-9-2165.

Perera, Rushika, Katherine E. Owen, Timothy L. Tellinghuisen, Alexander E. Gorbalenya, et Richard J. Kuhn. 2001. « Alphavirus Nucleocapsid Protein Contains a Putative Coiled Coil α-Helix Important for Core Assembly ». *Journal of Virology* 75 (1): 1-10. https://doi.org/10.1128/jvi.75.1.1-10.2001.

Perich, M. J., G. Davila, A. Turner, A. Garcia, et M. Nelson. 2000. « Behavior of Resting Aedes Aegypti (Culicidae: Diptera) and Its Relation to Ultra-Low Volume Adulticide Efficacy in Panama City, Panama ». *Journal of Medical Entomology* 37 (4): 541-46. https://doi.org/10.1603/0022-2585-37.4.541.

Phuklia, Weerawat, Jitra Kasisith, Naphak Modhiran, Ekkarat Rodpai, Montri Thannagith, Tipparat Thongsakulprasert, Duncan R. Smith, et Sukathida Ubol. 2013. « Osteoclastogenesis Induced by CHIKV-Infected Fibroblast-like Synoviocytes: A Possible Interplay between Synoviocytes and Monocytes/Macrophages in CHIKV-Induced Arthralgia/Arthritis ». *Virus Research* 177 (2): 179-88. https://doi.org/10.1016/j.virusres.2013.08.011.

Poo, Yee Suan, Penny A. Rudd, Joy Gardner, Jane A. C. Wilson, Thibaut Larcher, Marie-Anne Colle, Thuy T. Le, et al. 2014. « Multiple Immune Factors Are Involved in Controlling Acute and Chronic Chikungunya Virus Infection ». Édité par Ann M. Powers. *PLoS Neglected Tropical Diseases* 8 (12): e3354. https://doi.org/10.1371/journal.pntd.0003354.

Powers, Ann M., Aaron C. Brault, Yukio Shirako, Ellen G. Strauss, WenLi Kang, James H. Strauss, et Scott C. Weaver. 2001. « Evolutionary Relationships and Systematics of the Alphaviruses ». *Journal of Virology* 75 (21): 10118-31. https://doi.org/10.1128/JVI.75.21.10118-10131.2001.

Prow, Natalie A., Bing Tang, Joy Gardner, Thuy T. Le, Adam Taylor, Yee S. Poo, Eri

Nakayama, et al. 2017. « Lower Temperatures Reduce Type I Interferon Activity and Promote Alphaviral Arthritis ». *PLoS Pathogens* 13 (12): e1006788. https://doi.org/10.1371/journal.ppat.1006788.

Quinzii, Catarina M., Tuan H. Vu, K. Christopher Min, Kurenai Tanji, Sandra Barral, Raji P. Grewal, Andrea Kattah, et al. 2008. « X-Linked Dominant Scapuloperoneal Myopathy Is Due to a Mutation in the Gene Encoding Four-and-a-Half-LIM Protein 1 ». *American Journal of Human Genetics* 82 (1): 208-13. https://doi.org/10.1016/j.ajhg.2007.09.013.

Rack, Johannes Gregor Matthias, Dragutin Perina, et Ivan Ahel. 2016. « Macrodomains: Structure, Function, Evolution, and Catalytic Activities ». *Annual Review of Biochemistry* 85 (1): 431-54. https://doi.org/10.1146/annurev-biochem-060815-014935.

Rall, Glenn F., Vincent R. Racaniello, Anna Marie Skalka, et Jane Flint. 2015. *Principles of Virology, Volume II: Pathogenesis & Control*. Vol. II. American Society of Microbiology. https://doi.org/10.1128/9781555818968.

Rathore, Abhay P S, Mah-Lee Ng, et Subhash G Vasudevan. 2013. « Differential Unfolded Protein Response during Chikungunya and Sindbis Virus Infection: CHIKV nsP4 Suppresses eIF2α Phosphorylation ». *Virology Journal* 10 (1): 36. https://doi.org/10.1186/1743-422X-10-36.

Rausalu, Kai, Age Utt, Tania Quirin, Finny S. Varghese, Eva Žusinaite, Pratyush Kumar Das, Tero Ahola, et Andres Merits. 2016. « Chikungunya Virus Infectivity, RNA Replication and Non-Structural Polyprotein Processing Depend on the nsP2 Protease's Active Site Cysteine Residue ». *Scientific Reports* 6 (1): 37124. https://doi.org/10.1038/srep37124.

Reis, Erik V. S., Beatriz M. Damas, Diogo C. Mendonça, Jônatas S. Abrahão, et Cláudio A. Bonjardim. 2022. « In-Depth Characterization of the Chikungunya Virus Replication Cycle ». *Journal of Virology* 96 (3): e0173221. https://doi.org/10.1128/JVI.01732-21.

———. s. d. « In-Depth Characterization of the Chikungunya Virus Replication Cycle ». *Journal of Virology* 96 (3): e01732-21. https://doi.org/10.1128/JVI.01732-21.

Remenyi, Roland, Yanni Gao, Ruth E. Hughes, Alistair Curd, Carsten Zothner, Michelle Peckham, Andres Merits, et Mark Harris. 2018. « Persistent Replication of a Chikungunya Virus Replicon in Human Cells Is Associated with Presence of Stable Cytoplasmic Granules Containing Nonstructural Protein 3 ». Édité par Michael S. Diamond. *Journal of Virology* 92 (16): e00477-18, /jvi/92/16/e00477-18.atom. https://doi.org/10.1128/JVI.00477-18.

Remenyi, Roland, Grace C. Roberts, Carsten Zothner, Andres Merits, et Mark Harris. 2017. « SNAP-Tagged Chikungunya Virus Replicons Improve Visualisation of Non-Structural Protein 3 by Fluorescence Microscopy ». *Scientific Reports* 7 (1): 1-15.

https://doi.org/10.1038/s41598-017-05820-0.

Renault, Philippe, Jean-Louis Solet, Daouda Sissoko, Elsa Balleydier, Sophie Larrieu, Laurent Filleul, Christian Lassalle, et al. 2007. « A Major Epidemic of Chikungunya Virus Infection on Reunion Island, France, 2005-2006 ». *The American Journal of Tropical Medicine and Hygiene* 77 (4): 727-31.

Risco, Cristina, Isabel Fernández de Castro, Laura Sanz-Sánchez, Kedar Narayan, Giovanna Grandinetti, et Sriram Subramaniam. 2014. « Three-Dimensional Imaging of Viral Infections ». *Annual Review of Virology* 1 (1): 453-73. https://doi.org/10.1146/annurev-virology-031413-085351.

Roberts, Grace C., Carsten Zothner, Roland Remenyi, Andres Merits, Nicola J. Stonehouse, et Mark Harris. 2017. « Evaluation of a Range of Mammalian and Mosquito Cell Lines for Use in Chikungunya Virus Research ». *Scientific Reports* 7 (1): 14641. https://doi.org/10.1038/s41598-017-15269-w.

Robinson, Marion C. 1955. « An Epidemic of Virus Disease in Southern Province, Tanganyika Territory, in 1952–1953 ». *Transactions of the Royal Society of Tropical Medicine and Hygiene* 49 (1): 28-32. https://doi.org/10.1016/0035-9203(55)90080-8.

Robinson, Paul A., Susan Brown, Meagan J. McGrath, Imogen D. Coghill, Rajendra Gurung, et Christina A. Mitchell. 2003. « Skeletal muscle LIM protein 1 regulates integrin-mediated myoblast adhesion, spreading, and migration ». *American Journal of Physiology-Cell Physiology* 284 (3): C681-95. https://doi.org/10.1152/ajpcell.00370.2002.

Rodríguez-Morales, Alfonso J., Jaime A. Cardona-Ospina, Sivia Fernanda Urbano-Garzón, et Juan Sebastian Hurtado-Zapata. 2016. « Prevalence of Post-Chikungunya Infection Chronic Inflammatory Arthritis: A Systematic Review and Meta-Analysis ». *Arthritis Care & Research* 68 (12): 1849-58. https://doi.org/10.1002/acr.22900.

Rohatgi, A., J. C. Corbo, K. Monte, S. Higgs, D. L. Vanlandingham, G. Kardon, D. J. Lenschow, et S. Perlman. 2014. « Infection of Myofibers Contributes to Increased Pathogenicity during Infection with an Epidemic Strain of Chikungunya Virus ». *Journal of Virology* 88 (5): 2414-25. https://doi.org/10.1128/JVI.02716-13.

Ross, R. W. 1956. « The Newala Epidemic: III. The Virus: Isolation, Pathogenic Properties and Relationship to the Epidemic ». *Journal of Hygiene* 54 (2): 177-91. https://doi.org/10.1017/S0022172400044442.

Roy, Enakshi, Wen Shi, Bin Duan, et St Patrick Reid. 2020. « Chikungunya Virus Infection Impairs the Function of Osteogenic Cells ». *mSphere* 5 (3): e00347-20. https://doi.org/10.1128/mSphere.00347-20.

Rudd, Penny A., Jane Wilson, Joy Gardner, Thibaut Larcher, Candice Babarit, Thuy T. Le, Itaru Anraku, et al. 2012. « Interferon Response Factors 3 and 7 Protect against Chikungunya Virus Hemorrhagic Fever and Shock ». *Journal of Virology* 86 (18): 9888-98. https://doi.org/10.1128/JVI.00956-12.

Ruggieri, Alessia, Eva Dazert, Philippe Metz, Sarah Hofmann, Jan-Philip Bergeest, Johanna Mazur, Peter Bankhead, et al. 2012. « Dynamic Oscillation of Translation and Stress Granule Formation Mark the Cellular Response to Virus Infection ». *Cell Host & Microbe* 12 (1): 71-85. https://doi.org/10.1016/j.chom.2012.05.013.

Rümenapf, T., E. G. Strauss, et J. H. Strauss. 1994. « Subgenomic mRNA of Aura Alphavirus Is Packaged into Virions ». *Journal of Virology* 68 (1): 56-62. https://doi.org/10.1128/JVI.68.1.56-62.1994.

Rupp, Jonathan C., Kevin J. Sokoloski, Natasha N. Gebhart, et Richard W. Hardy. 2015. « Alphavirus RNA synthesis and non-structural protein functions ». *The Journal of General Virology* 96 (Pt 9): 2483-2500. https://doi.org/10.1099/jgv.0.000249.

Sahoo, Bibekananda, et Tirumala Kumar Chowdary. 2019. « Conformational Changes in Chikungunya Virus E2 Protein upon Heparan Sulfate Receptor Binding Explain Mechanism of E2-E1 Dissociation during Viral Entry ». *Bioscience Reports* 39 (6): BSR20191077. https://doi.org/10.1042/BSR20191077.

Saisawang, Chonticha, Sawanan Saitornuang, Pornpan Sillapee, Sukathida Ubol, Duncan R. Smith, et Albert J. Ketterman. 2015. « Chikungunya nsP2 Protease Is Not a Papain-like Cysteine Protease and the Catalytic Dyad Cysteine Is Interchangeable with a Proximal Serine ». *Scientific Reports* 5 (1): 17125. https://doi.org/10.1038/srep17125.

Salonen, A., L. Vasiljeva, A. Merits, J. Magden, E. Jokitalo, et L. Kaariainen. 2003. « Properly Folded Nonstructural Polyprotein Directs the Semliki Forest Virus Replication Complex to the Endosomal Compartment ». *Journal of Virology* 77 (3): 1691-1702. https://doi.org/10.1128/JVI.77.3.1691-1702.2003.

Sang, Rosemary, Jennifer Brown, Clayton Onyango, Ann M. Powers, Naphtali Agata, M. Kariuki Njenga, Said A. Bedja, et al. 2007. « SEROPREVALENCE OF CHIKUNGUNYA VIRUS INFECTION ON GRANDE COMORE ISLAND, UNION OF THE COMOROS, 2005 ». *The American Journal of Tropical Medicine and Hygiene* 76 (6): 1189-93. https://doi.org/10.4269/ajtmh.2007.76.1189.

Sanz, M. A., et L. Carrasco. 2001. « Sindbis Virus Variant with a Deletion in the 6K Gene Shows Defects in Glycoprotein Processing and Trafficking: Lack of Complementation by a Wild-Type 6K Gene in Trans ». *Journal of Virology* 75 (16): 7778-84.

https://doi.org/10.1128/JVI.75.16.7778-7784.2001.

Schessl, Joachim, Sarah Feldkirchner, Christiana Kubny, et Benedikt Schoser. 2011. « Reducing Body Myopathy and Other FHL1-Related Muscular Disorders ». *Seminars in Pediatric Neurology* 18 (4): 257-63. https://doi.org/10.1016/j.spen.2011.10.007.

Schessl, Joachim, Yaqun Zou, Meagan J. McGrath, Belinda S. Cowling, Baijayanta Maiti, Steven S. Chin, Caroline Sewry, et al. 2008. « Proteomic Identification of FHL1 as the Protein Mutated in Human Reducing Body Myopathy ». *Journal of Clinical Investigation*, février, JCI34450. https://doi.org/10.1172/JCI34450.

Schmeichel, K. L., et M. C. Beckerle. 1994. « The LIM Domain Is a Modular Protein-Binding Interface ». *Cell* 79 (2): 211-19. https://doi.org/10.1016/0092-8674(94)90191-0.

———. 1997. « Molecular Dissection of a LIM Domain ». *Molecular Biology of the Cell* 8 (2): 219-30. https://doi.org/10.1091/mbc.8.2.219.

Schneider, Martina, Marivic Narciso-Abraham, Sandra Hadl, Robert McMahon, Sebastian Toepfer, Ulrike Fuchs, Romana Hochreiter, et al. 2023. « Safety and Immunogenicity of a Single-Shot Live-Attenuated Chikungunya Vaccine: A Double-Blind, Multicentre, Randomised, Placebo-Controlled, Phase 3 Trial ». *Lancet (London, England)* 401 (10394): 2138-47. https://doi.org/10.1016/S0140-6736(23)00641-4.

Scholte, Florine E. M., Ali Tas, Irina C. Albulescu, Eva Žusinaite, Andres Merits, Eric J. Snijder, et Martijn J. van Hemert. 2015. « Stress Granule Components G3BP1 and G3BP2 Play a Proviral Role Early in Chikungunya Virus Replication ». Édité par M. S. Diamond. *Journal of Virology* 89 (8): 4457-69. https://doi.org/10.1128/JVI.03612-14.

Schulte, Tim, Lifeng Liu, Marc D. Panas, Bastian Thaa, Nicole Dickson, Benjamin Götte, Adnane Achour, et Gerald M. McInerney. 2016. « Combined Structural, Biochemical and Cellular Evidence Demonstrates That Both FGDF Motifs in Alphavirus nsP3 Are Required for Efficient Replication ». *Open Biology* 6 (7): 160078. https://doi.org/10.1098/rsob.160078.

Schwartz, Olivier, et Matthew L. Albert. 2010. « Biology and Pathogenesis of Chikungunya Virus ». *Nature Reviews Microbiology* 8 (7): 491-500. https://doi.org/10.1038/nrmicro2368.

Sharma, Parveen, Thiruchelvi Shathasivam, Vladimir Ignatchenko, Thomas Kislinger, et Anthony O. Gramolini. 2011. « Identification of an FHL1 Protein Complex Containing ACTN1, ACTN4, and PDLIM1 Using Affinity Purifications and MS-Based Protein–Protein Interaction Analysis ». *Molecular BioSystems* 7 (4): 1185. https://doi.org/10.1039/c0mb00235f.

Sharp, Tyler M., M. Kelly Keating, Wun-Ju Shieh, Julu Bhatnagar, Brigid C. Bollweg, Rebecca Levine, Dianna M. Blau, et al. 2021. « Clinical Characteristics, Histopathology, and Tissue

Immunolocalization of Chikungunya Virus Antigen in Fatal Cases ». *Clinical Infectious Diseases: An Official Publication of the Infectious Diseases Society of America* 73 (2): e345-54. https://doi.org/10.1093/cid/ciaa837.

Shathasivam, Thiruchelvi, Thomas Kislinger, et Anthony O. Gramolini. 2010. « Genes, Proteins and Complexes: The Multifaceted Nature of FHL Family Proteins in Diverse Tissues ». *Journal of Cellular and Molecular Medicine* 14 (12): 2702-20. https://doi.org/10.1111/j.1582-4934.2010.01176.x.

Shin, G., S. A. Yost, M. T. Miller, E. J. Elrod, A. Grakoui, et J. Marcotrigiano. 2012. « Structural and Functional Insights into Alphavirus Polyprotein Processing and Pathogenesis ». *Proceedings of the National Academy of Sciences* 109 (41): 16534-39. https://doi.org/10.1073/pnas.1210418109.

Shupliakov, Oleg, Peter Löw, Detlev Grabs, Helge Gad, Hong Chen, Carol David, Kohji Takei, Pietro De Camilli, et Lennart Brodin. 1997. « Synaptic Vesicle Endocytosis Impaired by Disruption of Dynamin-SH3 Domain Interactions ». *Science* 276 (5310): 259-63. https://doi.org/10.1126/science.276.5310.259.

Simon, F., E. Javelle, A. Cabie, E. Bouquillard, O. Troisgros, G. Gentile, I. Leparc-Goffart, et al. 2015. « French Guidelines for the Management of Chikungunya (Acute and Persistent Presentations). November 2014 ». *Medecine Et Maladies Infectieuses* 45 (7): 243-63. https://doi.org/10.1016/j.medmal.2015.05.007.

Singer, Zakary S., Pradeep M. Ambrose, Tal Danino, et Charles M. Rice. 2021. « Quantitative Measurements of Early Alphaviral Replication Dynamics in Single Cells Reveals the Basis for Superinfection Exclusion ». *Cell Systems* 12 (3): 210-219.e3. https://doi.org/10.1016/j.cels.2020.12.005.

Sissoko, Daouda, Denis Malvy, Khaled Ezzedine, Philippe Renault, Frederic Moscetti, Martine Ledrans, et Vincent Pierre. 2009. « Post-Epidemic Chikungunya Disease on Reunion Island: Course of Rheumatic Manifestations and Associated Factors over a 15-Month Period ». *PLoS Neglected Tropical Diseases* 3 (3): e389. https://doi.org/10.1371/journal.pntd.0000389.

Skidmore, Andrew M., et Steven B. Bradfute. 2023. « The Life Cycle of the Alphaviruses: From an Antiviral Perspective ». *Antiviral Research* 209 (janvier): 105476. https://doi.org/10.1016/j.antiviral.2022.105476.

Smith, Scott A., Laurie A. Silva, Julie M. Fox, Andrew I. Flyak, Nurgun Kose, Gopal Sapparapu, Solomiia Khomandiak, et al. 2015. « Isolation and Characterization of Broad and Ultrapotent Human Monoclonal Antibodies with Therapeutic Activity against Chikungunya Virus ». *Cell Host & Microbe* 18 (1): 86-95. https://doi.org/10.1016/j.chom.2015.06.009.

Song, Hao, Zhennan Zhao, Yan Chai, Xiyue Jin, Changyao Li, Fei Yuan, Sheng Liu, et al. 2019. « Molecular Basis of Arthritogenic Alphavirus Receptor MXRA8 Binding to Chikungunya Virus Envelope Protein ». *Cell* 177 (7): 1714-1724.e12. https://doi.org/10.1016/j.cell.2019.04.008.

Sourisseau, Marion, Clémentine Schilte, Nicoletta Casartelli, Céline Trouillet, Florence Guivel-Benhassine, Dominika Rudnicka, Nathalie Sol-Foulon, et al. 2007. « Characterization of Reemerging Chikungunya Virus ». *PLoS Pathogens* 3 (6): e89. https://doi.org/10.1371/journal.ppat.0030089.

Spence, L. P., et L. Thomas. 1959. « Application of Haemagglutination and Complement-Fixation Techniques to the Identification and Serological Classification of Arthropod-Borne Viruses ». *Transactions of The Royal Society of Tropical Medicine and Hygiene* 53 (3): 248-55. https://doi.org/10.1016/0035-9203(59)90004-5.

Spuul, Pirjo, Giuseppe Balistreri, Kirsi Hellström, Andrey V. Golubtsov, Eija Jokitalo, et Tero Ahola. 2011. « Assembly of Alphavirus Replication Complexes from RNA and Protein Components in a Novel *Trans* -Replication System in Mammalian Cells ». *Journal of Virology* 85 (10): 4739-51. https://doi.org/10.1128/JVI.00085-11.

Spuul, Pirjo, Anne Salonen, Andres Merits, Eija Jokitalo, Leevi Kääriäinen, et Tero Ahola. 2007. « Role of the Amphipathic Peptide of Semliki Forest Virus Replicase Protein nsP1 in Membrane Association and Virus Replication ». *Journal of Virology* 81 (2): 872-83. https://doi.org/10.1128/JVI.01785-06.

Stanwick, T. L., et J. V. Hallum. 1974. « Role of Interferon in Six Cell Lines Persistently Infected with Rubella Virus ». *Infection and Immunity* 10 (4): 810-15. https://doi.org/10.1128/iai.10.4.810-815.1974.

Strassburg, M. A. 1982. « The Global Eradication of Smallpox ». *American Journal of Infection Control* 10 (2): 53-59. https://doi.org/10.1016/0196-6553(82)90003-7.

Strauss, Ellen G., Raoul J. De Groot, Randy Levinson, et James H. Strauss. 1992. « Identification of the active site residues in the nsP2 proteinase of sindbis virus ». *Virology* 191 (2): 932-40. https://doi.org/10.1016/0042-6822(92)90268-T.

Strauss, Ellen G., Randy Levinson, Charles M. Rice, Joel Dalrymple, et James H. Strauss. 1988. « Nonstructural Proteins nsP3 and nsP4 of Ross River and O'Nyong-Nyong Viruses: Sequence and Comparison with Those of Other Alphaviruses ». *Virology* 164 (1): 265-74. https://doi.org/10.1016/0042-6822(88)90644-7.

Strauss, J. H., et E. G. Strauss. 1994. « The Alphaviruses: Gene Expression, Replication, and Evolution ». *Microbiological Reviews* 58 (3): 491-562.

Suhrbier, Andreas. 2019a. « Rheumatic Manifestations of Chikungunya: Emerging Concepts and Interventions ». *Nature Reviews Rheumatology* 15 (10): 597-611. https://doi.org/10.1038/s41584-019-0276-9.

———. 2019b. « Rheumatic Manifestations of Chikungunya: Emerging Concepts and Interventions ». *Nature Reviews Rheumatology* 15 (10): 597-611. https://doi.org/10.1038/s41584-019-0276-9.

Suhrbier, Andreas, Marie-Christine Jaffar-Bandjee, et Philippe Gasque. 2012a. « Arthritogenic Alphaviruses--an Overview ». *Nature Reviews. Rheumatology* 8 (7): 420-29. https://doi.org/10.1038/nrrheum.2012.64.

———. 2012b. « Arthritogenic Alphaviruses—an Overview ». *Nature Reviews Rheumatology* 8 (7): 420-29. https://doi.org/10.1038/nrrheum.2012.64.

Suhrbier, Andreas, et Suresh Mahalingam. 2009. « The Immunobiology of Viral Arthritides ». *Pharmacology & Therapeutics* 124 (3): 301-8. https://doi.org/10.1016/j.pharmthera.2009.09.005.

Sun, Siyang, Ye Xiang, Wataru Akahata, Heather Holdaway, Pankaj Pal, Xinzheng Zhang, Michael S Diamond, Gary J Nabel, et Michael G Rossmann. 2013. « Structural analyses at pseudo atomic resolution of Chikungunya virus and antibodies show mechanisms of neutralization ». Édité par Werner Kühlbrandt. *eLife* 2 (avril): e00435. https://doi.org/10.7554/eLife.00435.

Tan, Yaw Bia, David Chmielewski, Michelle Cheok Yien Law, Kuo Zhang, Yu He, Muyuan Chen, Jing Jin, Dahai Luo, et Wah Chiu. 2022. « Molecular Architecture of the Chikungunya Virus Replication Complex ». Preprint. Microbiology. https://doi.org/10.1101/2022.04.08.487651.

Tanaka, Atsushi, Uranan Tumkosit, Shota Nakamura, Daisuke Motooka, Natsuko Kishishita, Thongkoon Priengprom, Areerat Sa-Ngasang, Taroh Kinoshita, Naokazu Takeda, et Yusuke Maeda. 2017. « Genome-Wide Screening Uncovers the Significance of N-Sulfation of Heparan Sulfate as a Host Cell Factor for Chikungunya Virus Infection ». *Journal of Virology* 91 (13): e00432-17. https://doi.org/10.1128/JVI.00432-17.

Teo, Teck-Hui, Fok-Moon Lum, Wendy W. L. Lee, et Lisa F. P. Ng. 2012. « Mouse Models for Chikungunya Virus: Deciphering Immune Mechanisms Responsible for Disease and Pathology ». *Immunologic Research* 53 (1-3): 136-47. https://doi.org/10.1007/s12026-012-8266-x.

Teppor, Mona, Eva Žusinaite, et Andres Merits. 2021a. « Phosphorylation Sites in the Hypervariable Domain in Chikungunya Virus nsP3 Are Crucial for Viral Replication ».

Journal of Virology 95 (9): 10.1128/jvi.02276-20. https://doi.org/10.1128/jvi.02276-20.

———. 2021b. « Phosphorylation Sites in the Hypervariable Domain in Chikungunya Virus nsP3 Are Crucial for Viral Replication ». Édité par Mark T. Heise. *Journal of Virology* 95 (9). https://doi.org/10.1128/JVI.02276-20.

Thaa, Bastian, Roberta Biasiotto, Kai Eng, Maarit Neuvonen, Benjamin Götte, Lara Rheinemann, Margit Mutso, et al. 2015. « Differential Phosphatidylinositol-3-Kinase-Akt-mTOR Activation by Semliki Forest and Chikungunya Viruses Is Dependent on nsP3 and Connected to Replication Complex Internalization ». *Journal of Virology* 89 (22): 11420-37. https://doi.org/10.1128/JVI.01579-15.

Tossavainen, Helena, Olli Aitio, Maarit Hellman, Kalle Saksela, et Perttu Permi. 2016. « Structural Basis of the High Affinity Interaction between the Alphavirus Nonstructural Protein-3 (nsP3) and the SH3 Domain of Amphiphysin-2 ». *The Journal of Biological Chemistry* 291 (31): 16307-17. https://doi.org/10.1074/jbc.M116.732412.

Tourrière, Hélène, Karim Chebli, Latifa Zekri, Brice Courselaud, Jean Marie Blanchard, Edouard Bertrand, et Jamal Tazi. 2003. « The RasGAP-associated endoribonuclease G3BP assembles stress granules ». *The Journal of Cell Biology* 160 (6): 823-31. https://doi.org/10.1083/jcb.200212128.

Traore-Lamizana, M, D Fontenille, M Diallo, et J Thonnon. 1999. « Vectors of Chikungunya Virus in Senegal: Current Data and Transmission Cycles. » *The American Journal of Tropical Medicine and Hygiene* 60 (2): 281-86. https://doi.org/10.4269/ajtmh.1999.60.281.

Treffers, Emmely E., Ali Tas, Florine E. M. Scholte, Arnoud H. de Ru, Eric J. Snijder, Peter A. van Veelen, et Martijn J. van Hemert. 2023. « The alphavirus nonstructural protein 2 NTPase induces a host translational shut-off through phosphorylation of eEF2 via cAMP-PKA-eEF2K signaling ». *PLOS Pathogens* 19 (2): e1011179. https://doi.org/10.1371/journal.ppat.1011179.

Tripathi, Praveen Kumar, Anjali Soni, Shiv Pratap Singh Yadav, Ankit Kumar, Nitika Gaurav, Siva Raghavendhar, Pradeep Sharma, et al. 2020. « Evaluation of Novobiocin and Telmisartan for Anti-CHIKV Activity ». *Virology* 548 (septembre): 250-60. https://doi.org/10.1016/j.virol.2020.05.010.

Tsetsarkin, Konstantin A, Rubing Chen, et Scott C Weaver. 2016. « Interspecies transmission and chikungunya virus emergence ». *Current opinion in virology* 16 (février): 143-50. https://doi.org/10.1016/j.coviro.2016.02.007.

Tsetsarkin, Konstantin A., Charles E. McGee, Sara M. Volk, Dana L. Vanlandingham, Scott C. Weaver, et Stephen Higgs. 2009. « Epistatic Roles of E2 Glycoprotein Mutations in

Adaption of Chikungunya Virus to Aedes Albopictus and Ae. Aegypti Mosquitoes ». *PLOS ONE* 4 (8): e6835. https://doi.org/10.1371/journal.pone.0006835.

Tsetsarkin, Konstantin A., Dana L. Vanlandingham, Charles E. McGee, et Stephen Higgs. 2007. « A Single Mutation in Chikungunya Virus Affects Vector Specificity and Epidemic Potential ». *PLoS Pathogens* 3 (12): e201. https://doi.org/10.1371/journal.ppat.0030201.

Tsetsarkin, Konstantin A., et Scott C. Weaver. 2011. « Sequential Adaptive Mutations Enhance Efficient Vector Switching by Chikungunya Virus and Its Epidemic Emergence ». *PLoS Pathogens* 7 (12): e1002412. https://doi.org/10.1371/journal.ppat.1002412.

Uchime, Onyinyechukwu, Whitney Fields, et Margaret Kielian. 2013. « The Role of E3 in pH Protection during Alphavirus Assembly and Exit ». *Journal of Virology* 87 (18): 10255-62. https://doi.org/10.1128/JVI.01507-13.

Unchwaniwala, Nuruddin, Hong Zhan, Johan A den Boon, et Paul Ahlquist. 2021. « Cryo-electron microscopy of nodavirus RNA replication organelles illuminates positive-strand RNA virus genome replication ». *Current Opinion in Virology* 51 (décembre): 74-79. https://doi.org/10.1016/j.coviro.2021.09.008.

Utt, Age, Pratyush Kumar Das, Margus Varjak, Valeria Lulla, Aleksei Lulla, et Andres Merits. 2015. « Mutations Conferring a Noncytotoxic Phenotype on Chikungunya Virus Replicons Compromise Enzymatic Properties of Nonstructural Protein 2 ». Édité par S. Perlman. *Journal of Virology* 89 (6): 3145-62. https://doi.org/10.1128/JVI.03213-14.

Van Bortel, W., F. Dorleans, J. Rosine, A. Blateau, D. Rousset, S. Matheus, I. Leparc-Goffart, et al. 2014. « Chikungunya Outbreak in the Caribbean Region, December 2013 to March 2014, and the Significance for Europe ». *Euro Surveillance: Bulletin Europeen Sur Les Maladies Transmissibles = European Communicable Disease Bulletin* 19 (13). https://doi.org/10.2807/1560-7917.es2014.19.13.20759.

Van Huizen, Eline, et Gerald M. McInerney. 2020. « Activation of the PI3K-AKT Pathway by Old World Alphaviruses ». *Cells* 9 (4): 970. https://doi.org/10.3390/cells9040970.

Varjak, Margus, Sirle Saul, Liisa Arike, Aleksei Lulla, Lauri Peil, et Andres Merits. 2013. « Magnetic Fractionation and Proteomic Dissection of Cellular Organelles Occupied by the Late Replication Complexes of Semliki Forest Virus ». *Journal of Virology* 87 (18): 10295-312. https://doi.org/10.1128/JVI.01105-13.

Vasiljeva, Lidia, Andres Merits, Andrey Golubtsov, Valeria Sizemskaja, Leevi Kääriäinen, et Tero Ahola. 2003. « Regulation of the Sequential Processing of Semliki Forest Virus Replicase Polyprotein ». *The Journal of Biological Chemistry* 278 (43): 41636-45. https://doi.org/10.1074/jbc.M307481200.

Vazeille, Marie, Sara Moutailler, Daniel Coudrier, Claudine Rousseaux, Huot Khun, Michel Huerre, Julien Thiria, et al. 2007. « Two Chikungunya Isolates from the Outbreak of La Reunion (Indian Ocean) Exhibit Different Patterns of Infection in the Mosquito, Aedes Albopictus ». Édité par Joel Montgomery. *PLoS ONE* 2 (11): e1168. https://doi.org/10.1371/journal.pone.0001168.

« Vector-Borne Diseases ». s. d. Consulté le 29 août 2023. https://www.who.int/news-room/fact-sheets/detail/vector-borne-diseases.

Ventoso, Iván, Miguel Angel Sanz, Susana Molina, Juan José Berlanga, Luis Carrasco, et Mariano Esteban. 2006. « Translational Resistance of Late Alphavirus mRNA to eIF2α Phosphorylation: A Strategy to Overcome the Antiviral Effect of Protein Kinase PKR ». *Genes & Development* 20 (1): 87-100. https://doi.org/10.1101/gad.357006.

Vihinen, Helena, et Juhani Saarinen. 2000. « Phosphorylation Site Analysis of Semliki Forest Virus Nonstructural Protein 3 * ». *Journal of Biological Chemistry* 275 (36): 27775-83. https://doi.org/10.1074/jbc.M002195200.

Volk, Sara M., Rubing Chen, Konstantin A. Tsetsarkin, A. Paige Adams, Tzintzuni I. Garcia, Amadou A. Sall, Farooq Nasar, et al. 2010. « Genome-Scale Phylogenetic Analyses of Chikungunya Virus Reveal Independent Emergences of Recent Epidemics and Various Evolutionary Rates ». *Journal of Virology* 84 (13): 6497-6504. https://doi.org/10.1128/JVI.01603-09.

Voss, James E., Marie-Christine Vaney, Stéphane Duquerroy, Clemens Vonrhein, Christine Girard-Blanc, Elodie Crublet, Andrew Thompson, Gérard Bricogne, et Félix A. Rey. 2010a. « Glycoprotein Organization of Chikungunya Virus Particles Revealed by X-Ray Crystallography ». *Nature* 468 (7324): 709-12. https://doi.org/10.1038/nature09555.

———. 2010b. « Glycoprotein Organization of Chikungunya Virus Particles Revealed by X-Ray Crystallography ». *Nature* 468 (7324): 709-12. https://doi.org/10.1038/nature09555.

Waggoner, Jesse J., Lionel Gresh, Maria Jose Vargas, Gabriela Ballesteros, Yolanda Tellez, K. James Soda, Malaya K. Sahoo, et al. 2016. « Viremia and Clinical Presentation in Nicaraguan Patients Infected With Zika Virus, Chikungunya Virus, and Dengue Virus ». *Clinical Infectious Diseases: An Official Publication of the Infectious Diseases Society of America* 63 (12): 1584-90. https://doi.org/10.1093/cid/ciw589.

Wahid, Braira, Amjad Ali, Shazia Rafique, et Muhammad Idrees. 2017a. « Global Expansion of Chikungunya Virus: Mapping the 64-Year History ». *International Journal of Infectious Diseases* 58 (mai): 69-76. https://doi.org/10.1016/j.ijid.2017.03.006.

———. 2017b. « Global Expansion of Chikungunya Virus: Mapping the 64-Year History ».

International Journal of Infectious Diseases 58 (mai): 69-76. https://doi.org/10.1016/j.ijid.2017.03.006.

Wang, Guan-Hong, Stephanie Gamez, Robyn R. Raban, John M. Marshall, Luke Alphey, Ming Li, Jason L. Rasgon, et Omar S. Akbari. 2021. « Combating Mosquito-Borne Diseases Using Genetic Control Technologies ». *Nature Communications* 12 (1): 4388. https://doi.org/10.1038/s41467-021-24654-z.

Wang, Lili, Jianing Miao, Lianyong Li, Di Wu, Yi Zhang, Zhaohong Peng, Lijun Zhang, Zhengwei Yuan, et Kailai Sun. 2013. « Identification of an FHL1 Protein Complex Containing Gamma-Actin and Non-Muscle Myosin IIB by Analysis of Protein-Protein Interactions ». Édité par Leonard Eisenberg. *PLoS ONE* 8 (11): e79551. https://doi.org/10.1371/journal.pone.0079551.

Wang, Xiang, Xiaofan Wei, Yang Yuan, Qingrui Sun, Jun Zhan, Jing Zhang, Yan Tang, et al. 2018. « Src-Mediated Phosphorylation Converts FHL1 from Tumor Suppressor to Tumor Promoter ». *The Journal of Cell Biology* 217 (4): 1335-51. https://doi.org/10.1083/jcb.201708064.

Wang, Y. F., S. G. Sawicki, et D. L. Sawicki. 1994a. « Alphavirus nsP3 Functions to Form Replication Complexes Transcribing Negative-Strand RNA ». *Journal of Virology* 68 (10): 6466-75. https://doi.org/10.1128/JVI.68.10.6466-6475.1994.

———. 1994b. « Alphavirus nsP3 Functions to Form Replication Complexes Transcribing Negative-Strand RNA ». *Journal of Virology* 68 (10): 6466-75. https://doi.org/10.1128/JVI.68.10.6466-6475.1994.

Weaver, S C, W Kang, Y Shirako, T Rumenapf, E G Strauss, et J H Strauss. 1997. « Recombinational history and molecular evolution of western equine encephalomyelitis complex alphaviruses ». *Journal of Virology* 71 (1): 613-23. https://doi.org/10.1128/jvi.71.1.613-623.1997.

Weaver, S.C., W.B. Klimstra, et K.D. Ryman. 2008. « Togaviruses: General Features ». In *Encyclopedia of Virology*, 107-16. Elsevier. https://doi.org/10.1016/B978-012374410-4.00627-0.

Weaver, Scott C., Caroline Charlier, Nikos Vasilakis, et Marc Lecuit. 2018. « Zika, Chikungunya, and Other Emerging Vector-Borne Viral Diseases ». *Annual Review of Medicine* 69 (1): 395-408. https://doi.org/10.1146/annurev-med-050715-105122.

Weaver, Scott C., Rubing Chen, et Mawlouth Diallo. 2020. « Chikungunya Virus: Role of Vectors in Emergence from Enzootic Cycles ». *Annual Review of Entomology* 65 (1): 313-32. https://doi.org/10.1146/annurev-ento-011019-025207.

Weaver, Scott C., et Naomi L. Forrester. 2015. « Chikungunya: Evolutionary History and Recent Epidemic Spread ». *Antiviral Research* 120 (août): 32-39. https://doi.org/10.1016/j.antiviral.2015.04.016.

Weaver, Scott C., et Marc Lecuit. 2015. « Chikungunya Virus and the Global Spread of a Mosquito-Borne Disease ». Édité par Edward W. Campion. *New England Journal of Medicine* 372 (13): 1231-39. https://doi.org/10.1056/NEJMra1406035.

Weaver, Scott C., Richard Winegar, Ian D. Manger, et Naomi L. Forrester. 2012. « Alphaviruses: Population Genetics and Determinants of Emergence ». *Antiviral Research* 94 (3): 242-57. https://doi.org/10.1016/j.antiviral.2012.04.002.

Webb, L. G., J. Veloz, J. Pintado-Silva, T. Zhu, M. V. Rangel, T. Mutetwa, L. Zhang, et al. 2020. « Chikungunya Virus Antagonizes cGAS-STING Mediated Type-I Interferon Responses by Degrading cGAS ». *PLoS Pathogens* 16 (10): e1008999. https://doi.org/10.1371/journal.ppat.1008999.

Wei, Xiaofan, et Hongquan Zhang. 2020. « Four and a half LIM domains protein 1 can be as a double-edged sword in cancer progression ». *Cancer Biology & Medicine* 17 (2): 270-81. https://doi.org/10.20892/j.issn.2095-3941.2019.0420.

Weinbren, M.P, A.J Haddow, et M.C Williams. 1958. « The Occurrence of Chikungunya Virus in Uganda I. Isolation from Mosquitoes ». *Transactions of the Royal Society of Tropical Medicine and Hygiene* 52 (3): 253-62. https://doi.org/10.1016/0035-9203(58)90084-1.

White, Laura K., Tina Sali, David Alvarado, Evelina Gatti, Philippe Pierre, Daniel Streblow, et Victor R. DeFilippis. 2011. « Chikungunya Virus Induces IPS-1-Dependent Innate Immune Activation and Protein Kinase R-Independent Translational Shutoff ». *Journal of Virology* 85 (1): 606-20. https://doi.org/10.1128/JVI.00767-10.

Wikan, Nitwara, Prirayapak Sakoonwatanyoo, Sukathida Ubol, Sutee Yoksan, et Duncan R. Smith. 2012. « Chikungunya Virus Infection of Cell Lines: Analysis of the East, Central and South African Lineage ». Édité par Lisa Ng Fong Poh. *PLoS ONE* 7 (1): e31102. https://doi.org/10.1371/journal.pone.0031102.

Wilding, Brendan R., Meagan J. McGrath, Gisèle Bonne, et Christina A. Mitchell. 2014. « FHL1 Mutants That Cause Clinically Distinct Human Myopathies Form Protein Aggregates and Impair Myoblast Differentiation ». *Journal of Cell Science* 127 (10): 2269-81. https://doi.org/10.1242/jcs.140905.

Wolfe, N. D., A. M. Kilbourn, W. B. Karesh, H. A. Rahman, E. J. Bosi, B. C. Cropp, M. Andau, A. Spielman, et D. J. Gubler. 2001. « Sylvatic Transmission of Arboviruses among Bornean Orangutans ». *The American Journal of Tropical Medicine and Hygiene* 64 (5-6): 310-16.

https://doi.org/10.4269/ajtmh.2001.64.310.

Wolff, Georg, et Montserrat Bárcena. 2021. « Multiscale Electron Microscopy for the Study of Viral Replication Organelles ». *Viruses* 13 (2): 197. https://doi.org/10.3390/v13020197.

Wolff, Georg, Charlotte E. Melia, Eric J. Snijder, et Montserrat Bárcena. 2020. « Double-Membrane Vesicles as Platforms for Viral Replication ». *Trends in Microbiology* 28 (12): 1022-33. https://doi.org/10.1016/j.tim.2020.05.009.

Wong, Kai Zhi, et Justin Jang Hann Chu. 2018. « The Interplay of Viral and Host Factors in Chikungunya Virus Infection: Targets for Antiviral Strategies ». *Viruses* 10 (6). https://doi.org/10.3390/v10060294.

Wressnigg, Nina, Romana Hochreiter, Oliver Zoihsl, Andrea Fritzer, Nicole Bézay, Anton Klingler, Karen Lingnau, et al. 2020. « Single-Shot Live-Attenuated Chikungunya Vaccine in Healthy Adults: A Phase 1, Randomised Controlled Trial ». *The Lancet. Infectious Diseases* 20 (10): 1193-1203. https://doi.org/10.1016/S1473-3099(20)30238-3.

Yang, Panyu, Yanyan Yang, Pin Sun, Yu Tian, Fang Gao, Chen Wang, Tingyu Zong, et al. 2021. « βII spectrin (SPTBN1): biological function and clinical potential in cancer and other diseases ». *International Journal of Biological Sciences* 17 (1): 32-49. https://doi.org/10.7150/ijbs.52375.

Yang, Peiguo, Cécile Mathieu, Regina-Maria Kolaitis, Peipei Zhang, James Messing, Ugur Yurtsever, Zemin Yang, et al. 2020. « G3BP1 Is a Tunable Switch that Triggers Phase Separation to Assemble Stress Granules ». *Cell* 181 (2): 325-345.e28. https://doi.org/10.1016/j.cell.2020.03.046.

Yap, Moh Lan, Thomas Klose, Akane Urakami, S. Saif Hasan, Wataru Akahata, et Michael G. Rossmann. 2017. « Structural Studies of Chikungunya Virus Maturation ». *Proceedings of the National Academy of Sciences* 114 (52): 13703-7. https://doi.org/10.1073/pnas.1713166114.

Yergolkar, Prasanna N., Babasaheb V. Tandale, Vidya A. Arankalle, Padmakar S. Sathe, Swati S. Gandhe, Mangesh D. Gokhle, George P. Jacob, Supriya L. Hundekar, et Akhilesh C. Mishra. 2006. « Chikungunya Outbreaks Caused by African Genotype, India ». *Emerging Infectious Diseases* 12 (10): 1580-83. https://doi.org/10.3201/eid1210.060529.

Yin, Peiqi, Xia Jian, Yihan Liu, Yuwen Liu, Lu Lv, Haoran Cui, et Leiliang Zhang. 2023. « Elucidating Cellular Interactome of Chikungunya Virus Identifies Host Dependency Factors ». *Virologica Sinica* 38 (4): 497-507. https://doi.org/10.1016/j.virs.2023.05.007.

Yoneyama, Mitsutoshi, Michihiko Jogi, et Koji Onomoto. 2016. « Regulation of Antiviral Innate Immune Signaling by Stress-Induced RNA Granules ». *Journal of Biochemistry* 159 (3): 279-86. https://doi.org/10.1093/jb/mvv122.

Young, Alissa R., Marissa C. Locke, Lindsey E. Cook, Bradley E. Hiller, Rong Zhang, Matthew L. Hedberg, Kristen J. Monte, Deborah J. Veis, Michael S. Diamond, et Deborah J. Lenschow. 2019. « Dermal and Muscle Fibroblasts and Skeletal Myofibers Survive Chikungunya Virus Infection and Harbor Persistent RNA ». Édité par Janko Nikolich-Žugich. *PLOS Pathogens* 15 (8): e1007993. https://doi.org/10.1371/journal.ppat.1007993.

Zacks, Michele A., et Slobodan Paessler. 2010. « Encephalitic Alphaviruses ». *Veterinary Microbiology* 140 (3-4): 281-86. https://doi.org/10.1016/j.vetmic.2009.08.023.

Zaid, Ali, Patrick Gérardin, Adam Taylor, Helen Mostafavi, Denis Malvy, et Suresh Mahalingam. 2018. « Review: Chikungunya Arthritis: Implications of Acute and Chronic Inflammation Mechanisms on Disease Management ». *Arthritis & Rheumatology* 70 (4): 484-95. https://doi.org/10.1002/art.40403.

Zaid, Ali, Kothila Tharmarajah, Helen Mostafavi, Joseph R. Freitas, Kuo-Ching Sheng, Suan-Sin Foo, Weiqiang Chen, et al. 2020. « Modulation of Monocyte-Driven Myositis in Alphavirus Infection Reveals a Role for CX3CR1+ Macrophages in Tissue Repair ». *mBio* 11 (2). https://doi.org/10.1128/mBio.03353-19.

Zhang, Kuo, Yee-Song Law, Michelle Cheok Yien Law, Yaw Bia Tan, Melissa Wirawan, et Dahai Luo. 2021. « Structural Insights into Viral RNA Capping and Plasma Membrane Targeting by Chikungunya Virus Nonstructural Protein 1 ». *Cell Host & Microbe* 29 (5): 757-764.e3. https://doi.org/10.1016/j.chom.2021.02.018.

Zhang, Na, Hongjian Zhao, et Leiliang Zhang. 2019. « Fatty Acid Synthase Promotes the Palmitoylation of Chikungunya Virus nsP1 ». *Journal of Virology* 93 (3). https://doi.org/10.1128/JVI.01747-18.

Zhang, Rong, James T. Earnest, Arthur S. Kim, Emma S. Winkler, Pritesh Desai, Lucas J. Adams, Gaowei Hu, et al. 2019. « Expression of the Mxra8 Receptor Promotes Alphavirus Infection and Pathogenesis in Mice and Drosophila ». *Cell Reports* 28 (10): 2647-2658.e5. https://doi.org/10.1016/j.celrep.2019.07.105.

Zhang, Rong, Arthur S. Kim, Julie M. Fox, Sharmila Nair, Katherine Basore, William B. Klimstra, Rebecca Rimkunas, et al. 2018. « Mxra8 Is a Receptor for Multiple Arthritogenic Alphaviruses ». *Nature* 557 (7706): 570-74. https://doi.org/10.1038/s41586-018-0121-3.

Zhang, S., et F. Grosse. 1997. « Domain Structure of Human Nuclear DNA Helicase II (RNA Helicase A) ». *The Journal of Biological Chemistry* 272 (17): 11487-94. https://doi.org/10.1074/jbc.272.17.11487.

Zhang, Suisheng, et Frank Grosse. 2004. « Multiple Functions of Nuclear DNA Helicase II (RNA Helicase A) in Nucleic Acid Metabolism ». *Acta Biochimica Et Biophysica Sinica* 36

(3): 177-83. https://doi.org/10.1093/abbs/36.3.177.

Zhang, Xinyong, Martin Fugère, Robert Day, et Margaret Kielian. 2003. « Furin Processing and Proteolytic Activation of Semliki Forest Virus ». *Journal of Virology* 77 (5): 2981-89. https://doi.org/10.1128/jvi.77.5.2981-2989.2003.

Zhang, Ya-Nan, Cheng-Lin Deng, Jia-Qi Li, Na Li, Qiu-Yan Zhang, Han-Qing Ye, Zhi-Ming Yuan, et Bo Zhang. 2019. « Infectious Chikungunya Virus (CHIKV) with a Complete Capsid Deletion: A New Approach for a CHIKV Vaccine ». Édité par Mark T. Heise. *Journal of Virology* 93 (15): e00504-19. https://doi.org/10.1128/JVI.00504-19.

Zhang, Zhiqiang, Bin Yuan, Ning Lu, Valeria Facchinetti, et Yong-Jun Liu. 2011. « DHX9 Pairs with IPS-1 to Sense Double-Stranded RNA in Myeloid Dendritic Cells ». *Journal of Immunology (Baltimore, Md.: 1950)* 187 (9): 4501-8. https://doi.org/10.4049/jimmunol.1101307.

Zheng, Yan, et Margaret Kielian. 2013. « Imaging of the Alphavirus Capsid Protein during Virus Replication ». *Journal of Virology* 87 (17): 9579-89. https://doi.org/10.1128/JVI.01299-13.

Annexes

Annual Review of Virology

New Insights into Chikungunya Virus Infection and Pathogenesis

Vasiliya Kril,[1,*] Olivier Aïqui-Reboul-Paviet,[2,*] Laurence Briant,[2] and Ali Amara[1]

[1]Biology of Emerging Viruses Team, INSERM U944, CNRS UMR 7212, Institut de Recherche Saint-Louis, Université de Paris, Hôpital Saint-Louis, 75010 Paris, France; email: ali.amara@inserm.fr

[2]RNA Viruses and Metabolism Team, CNRS UMR 9004, Institut de Recherche en Infectiologie de Montpellier, University of Montpellier, 34090 Montpellier, France; email: laurence.briant@irim.cnrs.fr

Annu. Rev. Virol. 2021. 8:327–47

First published as a Review in Advance on July 13, 2021

The *Annual Review of Virology* is online at virology.annualreviews.org

https://doi.org/10.1146/annurev-virology-091919-102021

*These authors contributed equally to this article

Keywords

chikungunya virus, host cell interactions, nonstructural proteins, pathogenesis, musculoskeletal tissues, immune evasion

Abstract

Chikungunya virus (CHIKV) is a re-emerging mosquito-borne alphavirus responsible for major outbreaks of disease since 2004 in the Indian Ocean islands, South east Asia, and the Americas. CHIKV causes debilitating musculoskeletal disorders in humans that are characterized by fever, rash, polyarthralgia, and myalgia. The disease is often self-limiting and nonlethal; however, some patients experience atypical or severe clinical manifestations, as well as a chronic rheumatic syndrome. Unfortunately, no efficient antivirals against CHIKV infection are available so far, highlighting the importance of deepening our knowledge of CHIKV host cell interactions and viral replication strategies. In this review, we discuss recent breakthroughs in the molecular mechanisms that regulate CHIKV infection and lay down the foundations to understand viral pathogenesis. We describe the role of the recently identified host factors co-opted by the virus for infection and pathogenesis, and emphasize the importance of CHIKV nonstructural proteins in both replication complex assembly and host immune response evasion.

INTRODUCTION

CHIKV: chikungunya virus

IOL: Indian Ocean Lineage

nsP: nonstructural protein

ORF: open reading frame

Chikungunya virus (CHIKV) is a mosquito-borne virus that belongs to the *Alphavirus* genus, a group of enveloped RNA viruses that cause severe diseases in humans and animals. CHIKV is the epidemiologically most prevalent alphavirus that is transmitted to humans by *Aedes* mosquitoes during the blood meal. Phylogenetic analysis identified three distinct lineages of CHIKV corresponding to their respective geographical origins: the West African, the East-Central-South African (ECSA), and the Asian lineages (1, 2). Before 2000, CHIKV circulation was restricted to Sub-Saharan Africa, where sporadic outbreaks have been described (2, 3). CHIKV transmission remained silent until 2004, when an ECSA strain re-emerged in Kenya (4), evolved, and rapidly disseminated to the Indian Ocean islands, causing outbreaks of unprecedented magnitude particularly on Reunion Island (5, 6). This epidemic strain, assigned now to a new lineage termed Indian Ocean Lineage (IOL), spread to Southeast Asia and India, causing more than 1.3 million cases (7), and autochthonous transmission was reported in southern Europe (Italy and France) (8, 9). A second major outbreak occurred when a strain from the Asian lineage emerged in the Caribbean Sea (Saint Martin Island) in December 2013 (10), causing more than one million cases in 50 countries of the South American continent (11). Prior to the 2004 Indian Ocean outbreak, CHIKV was vectored mainly by *Aedes aegypti* mosquitoes. However, the IOL strain contains an adaptive mutation within the sequence coding the E1 glycoprotein, causing an alanine-to-valine substitution at position 226 (E1-A226V), which is responsible for a 40-fold increase in transmission by *Aedes albopictus* without affecting viral fitness in the *A. aegypti* vector (12, 13). This and other *A. albopictus*–adaptive mutations (reviewed in 14) in the IOL CHIKV strain have promoted viral expansion in temperate regions colonized by this mosquito vector.

CHIKV belongs to the arthritogenic Old World alphaviruses (15, 16). CHIKV-infected persons experience a syndrome characterized by fever, rash, arthralgia, and myalgia (reviewed in 17). Importantly, CHIKV-infected patients develop chronic muscle and joint pains that last for months to years after acute infection (17). Currently, there is no CHIKV-specific antiviral or vaccine. Patient management relies only on symptom relief with antalgics (paracetamol) and steroidal and nonsteroidal anti-inflammatory drugs. The identification of new antiviral strategies relies on a better understanding of CHIKV host cell interactions and on the elucidation of the molecular mechanisms and cellular pathways co-opted by the virus to become a successful human pathogen. In recent years, significant progress has been made in the fields of CHIKV molecular and structural virology, immunology, entomology, and epidemiology. However, many aspects of CHIKV biology, including tissue tropism and pathogenesis, remain poorly understood. In this review, we focus on important insights that have emerged into how CHIKV interacts with the host cell and subverts host cellular pathways for productive infection. We discuss the molecular determinants of viral replication and persistence in musculoskeletal tissues and their effect on CHIKV pathogenesis. We also emphasize the recently discovered cellular factors mediating CHIKV infection and discuss the emerging roles of the CHIKV nonstructural proteins (nsPs) in viral replication and immune evasion.

CHIKUNGUNYA VIRUS: GENOMIC ORGANIZATION AND INFECTIOUS CYCLE

CHIKV is a small (70 nm in diameter) enveloped virus with a single-stranded, message-sense, 5′-capped and 3′-polyadenylated RNA genome (11.8 kb) that is separated into two open reading frames (ORFs) (**Figure 1*a***). The 5′ ORF encodes a CHIKV nonstructural polyprotein (P1234) that is translated and cleaved in four nsPs forming the RNA replicase complex (18, 19). The 3′ ORF is transcribed into a subgenomic positive-stranded RNA and encodes, after subsequent cleavage

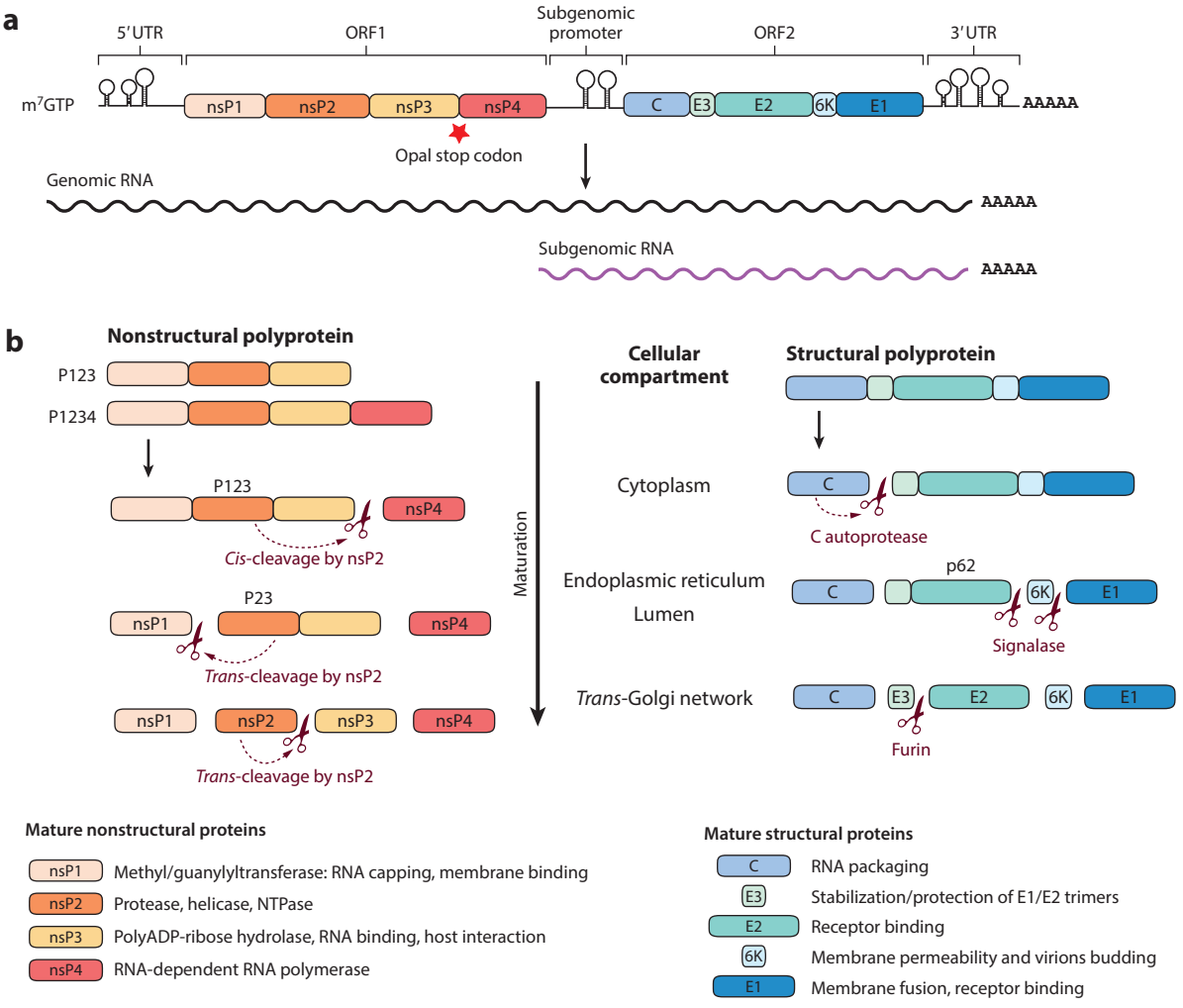

Figure 1

CHIKV genomic organization and viral proteins. (*a*) The CHIKV genome consists of a 5′-capped and 3′-polyadenylated positive-stranded RNA molecule divided into two ORFs. Expression of ORF1 and ORF2, encoding for the nonstructural and structural polyproteins, is controlled by the genomic promoter in the 5′ UTR and the internal subgenomic promoter, respectively. Genome replication and transcription are *cis*-regulated by RNA stem loops, referred to as conserved sequence elements, located in the 5′ UTR, subgenomic promoter, and 3′ UTR regions. CHIKV replication results in the accumulation of full-length RNA used as a genome for CHIKV progeny assembly. Subgenomic RNA is transcribed and used as a template for translation of structural polyproteins. (*b*) Translation of the CHIKV genome and subgenomic RNA results in the accumulation of nonstructural (P1234) and structural (C-E3-E2-6K-E1) polyproteins. The presence of a leaky opal stop codon at the end of the nsP3 sequence directs the translation of a partial nonstructural polyprotein (P123). P123 and P1234 are sequentially processed in *cis*- and *trans*-reactions by the cysteine protease nsP2 to produce mature nsPs (nsP1–4) forming the replication complex. The structural precursor is first maturated by the C protein that possesses *cis*-proteolytic activity and then by cellular proteases (signalases and furin), resulting in the production of E1, E2, and E3 glycoproteins and 6K protein, all contributing to viral particle assembly and budding. Abbreviations: C, nucleocapsid; CHIKV, chikungunya virus; E, envelope; nsP, nonstructural protein; ORF, open reading frame; UTR, untranslated region.

and maturation steps, six structural proteins: C (nucleocapsid); E1, E2, and E3 envelope viral glycoproteins; 6K and its translational frameshift product, TF (transframe) (**Figure 1*b***). A CHIKV virion consists of the viral RNA genome that is surrounded by 240 copies of the C protein and a host lipid bilayer with 80 embedded trimeric glycoprotein spikes. Each spike is formed by three E1-E2 heterodimers that are essential for receptor recognition and binding (E2) and membrane fusion (E1) (20).

C: nucleocapsid

E: envelope protein

vRC: viral replication complex

dsRNA: double-stranded RNA

CPV-I: type I cytopathic vacuole

CPV-II: type II cytopathic vacuole

CHIKV enters target cells by receptor-mediated endocytosis. Within the endosome, pH acidification triggers major conformational reorganization of E1/E2 heterodimers and unmasks the buried E1 fusion loop, leading to fusion of the viral and endosomal membrane (18, 19). Subsequently, the nucleocapsid disassembles in the cytoplasm, releasing the viral genomic RNA, which is directly translated into the P123 and P1234 precursors. (**Figure 2**). The P1234 polyprotein is rapidly processed at the nsP3/nsP4 junction by the nsP2 protease to release the active nsP4 RNA-dependent RNA polymerase. P123 and nsP4, along with the viral RNA, are recruited to the plasma membrane where, in association with host factors, they form an early short-lived replicase complex. A negative-stranded RNA complementary to the viral genome is synthesized and serves as an intermediate for viral replication (21, 22) (**Figure 2**). P123 accumulation leads to the complete polyprotein processing, and the replicase activity switches to the transcription of new positive-stranded RNA genomes and subgenomic RNA-encoding viral structural proteins. These steps take place in bulb-shaped, viral-induced vesicular structures formed at the plasma membrane, termed replicative spherules or viral replication complexes (vRCs), which isolate the accumulating double-stranded RNA (dsRNA) from innate immune sensing (**Figure 2**). Upon internalization, these compartments can fuse with endosomes, resulting in the formation of large vacuolar structures of 600 to 2,000 nm in diameter, termed type I cytopathic vacuoles (CPV-I), where RNA synthesis continues before diffusion to the cytoplasm through a connecting pore (23). Once in the cytoplasm, the subgenomic RNA is translated into a structural polyprotein. It is processed by the autocatalytical activity of the C protein, which is released in its mature form (22). Direct interaction with the newly synthesized genomes catalyzes C oligomerization and nucleocapsid assembly. The remaining polyprotein (pE3-E2-6K-E1) is translocated and inserted in the endoplasmic reticulum (ER) membrane for processing (**Figure 2**). Release of the accessory 6K protein mediated by host ER signalases allows the association of E1, E2, and E3 into an immature trimeric spike complex, which traffics through the secretory pathway while undergoing conformational changes and post-translational modifications (palmitoylation, N-linked glycosylation). Alternatively, E glycoproteins are arranged and transported from the *trans*-Golgi network to the plasma membrane in type II cytopathic vacuoles (CPV-II), which recruit assembled nucleocapsids on their cytoplasmic face (24). The E3 protein, which stabilizes the E2/E1 trimers by preventing the activation of the E1, is released by a furin-dependent cleavage in the *trans*-Golgi (22). At the plasma membrane, CHIKV particle budding is finally promoted by the interaction of the E2 cytoplasmic domain with the hydrophobic domain of the C protein (**Figure 2**).

THE KEY ROLE OF THE MUSCULOSKELETAL TISSUE IN CHIKUNGUNYA VIRUS PATHOGENESIS

Viral tropism has a direct effect on pathogenesis, including the nature of symptoms, the duration of infection, and the establishment of a chronic phase (25). In vertebrates, CHIKV displays a large cell and tissue tropism that covers endothelial cells, fibroblasts from almost all organs, and brain cells (26–30). However, viral pathogenesis mainly reflects CHIKV capacity to actively replicate in joints and muscle tissues (29, 31–37). In joints, chondrocytes, osteoblasts, and bone marrow mesenchymal stem cells, which serve as precursors for osteogenic cells, are susceptible to CHIKV

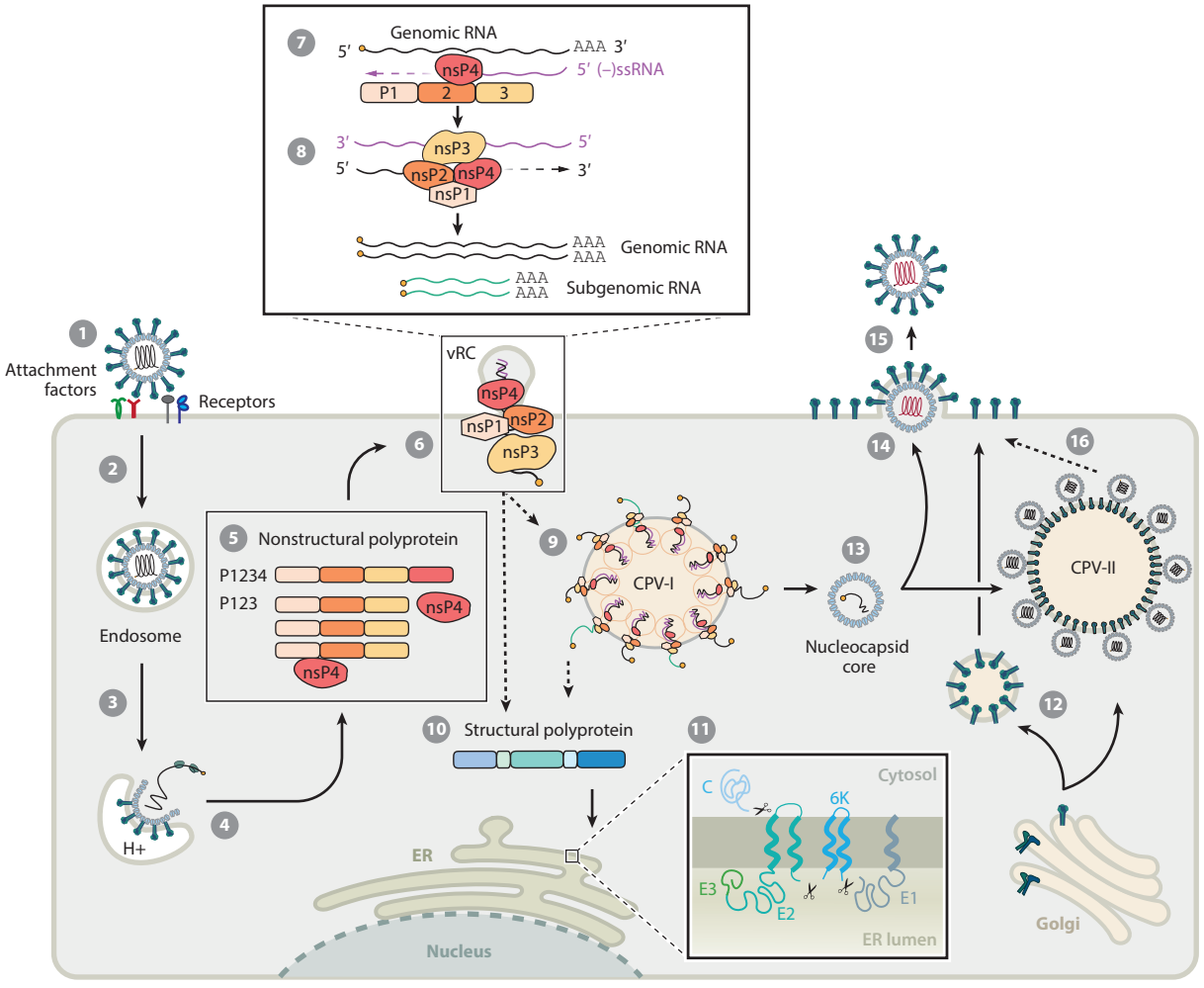

Figure 2

CHIKV replication cycle in vertebrate cells. CHIKV infection is initiated by the interaction of E1/E2 glycoprotein heterodimers with cell surface Mxra8 receptor and attachment factors (*Step 1*). The viral particle is internalized by endocytosis and trafficked to endosomes (*Step 2*). Acidification of the vacuolar pH results in the unmasking of the E1 fusion peptide and fusion of viral and endosomal membranes (*Step 3*). The viral C is released in the cytoplasm and rapidly uncoated (*Step 4*). The CHIKV genome is translated to produce P123 and P1234 polyproteins (*Step 5*). nsP4 is maturated and forms a complex with P123 and an RNA template that traffics to the plasma membrane. This complex reshapes the cell membrane to promote the formation of replication organelles, or spherules (*Step 6*), in which a negative-stranded full-length RNA [(–)RNA] is synthesized (*Step 7*). Then, P123 is sequentially processed to produce the four mature nsPs, resulting in a shift of replication complex activity toward the synthesis of a positive-stranded RNA [(+)RNA] genome and subgenomic RNA (*Step 8*). To some extent, CHIKV replication compartments are endocyted and fused with endo-lysosomes to form CPV-I in which internalized spherules remain active (*Step 9*). Structural proteins are translated from subgenomic RNA in the form of a polyprotein translocated to the ER (*Step 10*). C is liberated by autocatalytic processing. E glycoproteins and 6K protein are maturated by host proteases (*Step 11*) and trafficked to the plasma membrane through the secretory pathway (*Step 12*). The C protein and RNA genome form an icosahedral nucleocapsid (*Step 13*). Viral assembly takes place at the plasma membrane where mature E glycoproteins and nucleocapsids are targeted (*Step 14*). C/E2 interaction promotes CHIKV particle budding and release (*Step 15*). Alternative recruitment of assembled nucleocapsids and E glycoproteins to CPV-II additionally contributes to CHIKV virion assembly and budding (*Step 16*). Abbreviations: C, nucleocapsid; CHIKV, chikungunya virus; CPV-I, type I cytopathic vacuole; CPV-II, type II cytopathic vacuole; E, envelope; ER, endoplasmic reticulum; nsP, nonstructural protein; ORF, open reading frame; ssRNA, single-stranded RNA; UTR, untranslated region; vRC, viral replication complex. Figure adapted from Cell Background Straight by BioRender.com (2020), retrieved from **https://app.biorender.com/biorender-templates**.

infection (38–40). Cellular damages account for CHIKV-induced arthritis and joint pain. As an example, infection of osteogenic cells impairs mineralization and repair capacity, resulting in the dysregulated dynamics of bone homeostasis often reported in patients (40). Muscles are also a privileged site for CHIKV replication as supported by the presence of viral antigens and signs of necrosis, vacuolization, and fibrosis from patients with acute and chronic CHIKV disease (41). In vitro, muscle fibroblasts, satellite cells, and myoblasts (muscle progenitors) are highly susceptible to CHIKV infection (37, 41, 42). Initial reports suggested that terminally differentiated myotubes are poorly infected by CHIKV (41). However, murine skeletal muscle fibers were recently proven to be efficiently infected with effect on the severity of CHIKV infection in mice (43–45). A few studies also suggested that recent epidemic strains could differ in their ability to infect muscle cells and to induce a myopathic syndrome, although it is not formally demonstrated (42, 45). The isolate from the Reunion Island outbreak was shown to induce more severe muscle disease in neonatal mice as compared to an isolate from Senegal circulating in 1983 (45). Whereas both strains equally spread from the inoculation site to distal muscle by infecting connective tissue fibroblasts, the epidemic strain replicates more efficiently in myofibers, resulting in increased muscle disease characterized by severe myonecrosis (45). Whether the increased muscle pathology is due to a more robust immune response is not clear, as no differences were observed in the induction of type I interferon (IFN-I) and proinflammatory cytokines such as IL-1β or IL-6 (45). Recently, Lentscher and colleagues (44) definitively established that viral replication in muscle cells is determinant for CHIKV disease pathogenesis. They engineered a CHIKV strain exhibiting restricted replication in muscles via incorporation of target sequences for skeletal muscle cell–specific miR-206. This microRNA is expressed at detectable levels in skeletal muscle progenitor satellite cells, strongly induced upon differentiation, and then stably expressed at high levels throughout the life of the muscle fiber. Using this tool, Lentscher and colleagues demonstrated that replication in skeletal muscle cells does not affect the overall viral titers and the global inflammatory status. Instead, it results in attenuated muscle damages reflected by diminished necrosis and local induction of IL-6, IL-1β, TNFα, and IP10, which are biomarkers of disease severity in humans and mice (44, 46).

Besides tissue damage, the attraction of infiltrating monocytes/macrophages is also critical to local inflammation and viral persistence (39, 47–49). More specifically, infection of fibroblast-like synoviocytes results in the secretion of IL-6, IL-8, and CCL2, which attracts phagocytes. It also stimulates secretion of RANKL (receptor activator of nuclear factor κB), which may contribute to bone loss and to the occurrence of arthritis/arthralgia by stimulating the differentiation of monocytes into bone-resorbing osteoclasts (39, 50). In muscles, monocytes/macrophages could be part of the dynamics of CHIKV-induced myositis. The modulation of the monocyte-driven infiltration reduces muscle inflammation while allowing the accumulation of a macrophage subset enhancing muscle repair and recovery (48).

Musculoskeletal tissues are also proposed to participate in CHIKV persistence and chronic condition (34, 38, 51–53). Multiple studies reported that CHIKV RNA persists long after viremia declines (38, 53, 54). Besides synovial macrophages, which are proposed to be a niche for viral persistence (38, 54), muscle fibroblasts and also myofibers that survive acute infection are potential reservoirs for persistent CHIKV RNA in mice (34). Nevertheless, actively replicating CHIKV has not been evidenced so far in tissues exhibiting chronic inflammation, and CHIKV surface antigens failed to be detected in muscle fibroblasts harboring persistent viral RNA (17, 34, 55). Instead, the chronic CHIKV-induced immunopathology seems to be the prolongation of the acute inflammatory process, which persists until clearing of the viral material (17, 56). It is still unknown how CHIKV RNA persists in joints and muscles and to what extent it contributes to chronic CHIKV disease.

IFN: interferon

RANKL: receptor activator of nuclear factor κB

Mxra8, AN IMPORTANT BUT NOT EXCLUSIVE DETERMINANT OF CHIKUNGUNYA VIRUS ENTRY AND PATHOGENESIS

CHIKV entry into target cells is a complex multistep process that begins with the interaction of the viral E2 glycoprotein with specific receptor(s) expressed on the host cell surface. The cellular receptor mediating viral entry remained elusive until Zhang and colleagues (57) identified Mxra8 (also called limitrin, DICAM, or ASP3) as a CHIKV entry factor using a CRISPR/Cas9 genome-wide screening strategy. Mxra8 is an adhesion molecule mainly expressed on epithelial and mesenchymal cell types targeted by CHIKV (dermal and synovial fibroblasts, osteoblasts, chondrocytes, and skeletal muscle cells). Mxra8 is the first CHIKV entry molecule identified so far that fulfills the criteria of a virus receptor. Structural studies have revealed that it interacts with the envelope spike in a complex 3:3 binding interaction (58, 59). In this complex, Mxra8 contacts both E2 and E1 proteins to facilitate virus attachment and internalization in the cell. Overexpression of Mxra8 in poorly susceptible cells renders them permissive to CHIKV (57). Conversely, preventing the Mxra8-CHIKV interaction by CRISPR-Cas9-mediated depletion of the *Mxra8* gene or by using neutralizing antibodies or fusion of extracellular Mxra8 domains with an immunoglobulin Fc fragment (Mxra8-Fc) blocked infection in both murine and human cells and reduced CHIKV pathogenesis in experimentally infected mice (57, 60, 61). This indicates that Mxra8 is required for optimal infection, dissemination, and articular pathogenesis (joint swelling and neutrophil infiltration). Interestingly, this function is conserved for arthritogenic alphaviruses, such as Ross River, Mayaro, and o'nyong-nyong viruses (57). The lack of Mxra8 on the surface of some CHIKV permissive cells (57) strongly indicates that other CHIKV receptors exist and remain to be discovered. Consistent with this, some pathogenic IOL strains (e.g., LR-2006) display limited dependency on Mxra8, conversely to Asian CHIKV strains (181/25 and AF15561 strains) (57). Glycosaminoglycans (GAGs), a family of negatively charged polysaccharides, interact with a structurally conserved and positively charged domain in E2. These membrane proteins were proposed to enhance infection by promoting E1/E2 dissociation (62, 63). The functional importance of GAGs was recently reassessed in genome-wide loss of function screens performed in HAP1 cells that identified GAGs' biosynthesis enzymes (B3GAT3, SLC35B2, PAPSS1, NDST1) as critical factors for CHIKV infectivity (64, 65). The need for GAGs binding in order to achieve efficient infection was recently demonstrated for all CHIKV clades (62). Interestingly, the comparison of viruses from the ECSA and Asian lineages revealed that the requirement of GAGs for CHIKV binding and infection was inversely correlated with Mxra8 dependency (62). This suggests that GAG binding may be a compensatory mechanism for the entry of CHIKV strains poorly interacting with Mxra8 (62). However, this model does not seem to be the only scenario allowing for viral entry, as infection was still observed to some extent in the absence of GAGs and Mxra8 (62). The vast array of cell factors reported to facilitate CHIKV entry, including C-type lectins (DC-SIGN and L-SIGN), immunoglobulin and mucin domain-containing proteins 1 and 4 (hTIM1 and hTIM4), and the AXL receptor, which all have also been described to stimulate CHIKV infection (66–68), could be part of the complex mechanism accounting for CHIKV entry and wide tropism.

BUILDING MEMBRANE SPHERULES TO ENSURE VIRAL REPLICATION

Like other alphaviruses, CHIKV remodels the host plasma membrane into bulb-shaped protrusions of approximately 50 nm in diameter, referred to as spherules. These compartments create an optimal microenvironment for viral replication because they concentrate the viral nsP, genomic RNA, and dsRNA used as genome replication forms (69). Spherules are also supposed to protect

dsRNA and nascent uncapped RNAs from innate sensing and degradation by cellular RNases (69, 70). In this context, the inner spherule is connected to the cytosol by a 7-nm opening that allows the import of metabolites and cofactors and the export of newly synthesized genomic and subgenomic RNAs. Inside the spherule, the CHIKV replication complex (RC) associates with the inner face of membranes through nsP1, the viral capping enzyme that contains unique membrane binding capacity and displays membrane-dependent methyl/guanylyltransferase activities (71–74). Three-dimensional (3D) cryo-electron tomography was successfully applied to resolve the complex spatial organization of replication membranes formed by many positive-stranded RNA viruses (75–81). Conversely, the 3D architecture and biogenesis of alphavirus spherules remain enigmatic. Particularly, the exact localization of the RC within the spherule, stoichiometries of the nsPs in these compartments, and the nature of cellular factors contributing in spherule biogenesis are all questions that remain unanswered.

Jones and colleagues (82) recently solved the structure of the CHIKV nsP1 assembly by single-particle cryo-electron microscopy. They found that, upon membrane binding, recombinant nsP1 assembles in a dodecameric ring, forming a pore-like structure compatible with the trafficking of globular proteins up to 70–90 kDa in size. In this membrane-bound complex, nsP1 is switched from an enzymatically inactive monomer to a methyl/guanylyltansferase dodecameric active form, NsP1, a monotopic membrane protein. Therefore, by interacting with the inner phospholipid leaflet, nsP1 forms a capping pore that may corral the replication vesicle neck and therefore be critical for spherule structure maintenance (**Figure 3**). Further, nsP1 macroassembly might potentially function as a bioreactor simultaneously capping 12 nascent RNA molecules during their export to the cytosol, thereby contributing to the exceptionally high alphavirus replication rate. Striking similarities also exist with the crown-like assembly of nodavirus-encoded replicase at the neck of Flock House virus spherules, which favors the hypothesis of an evolutionarily conserved replication organelle pore structure among alpha-like viruses (83, 84). This information, which provides an incomparable breakthrough to our understanding of alphavirus replication compartment assembly, needs to be refined in CHIKV-infected cells, considering the simultaneous expression of all four nsPs in the context of a sequential maturated nonstructural polyprotein. Overall, this model questions the stoichiometry of other nsPs within and near the spherules. It also raises new important questions regarding the role of nsP1 in spherule biogenesis. Indeed, the minimal requirement for alphavirus spherule formation is the expression of a partially cleaved nonstructural polyprotein in the form of nsP4 + P123 (85) (**Figure 3**). This process is modulated to some extent by the viral RNA template length that determines the spherule shape and size (86). nsP1, whose complex interaction with membranes dramatically reshapes synthetic lipid bilayers or cell membranes in the absence of any other viral factor, is certainly pivotal to spherule creation (72, 82, 87–89). Nevertheless, morphological differences in CHIKV spherules and nsP1-induced membrane deformation, seen as filopodia-like protrusions, suggest additional players (**Figure 3**). For instance, the contribution of nsP1-interacting cellular factors in membrane reshaping during spherule biogenesis awaits investigation (90, 91). CHIKV nsP3 was proposed to be involved in spherule assembly by recruiting BIN1/amphiphysin 2, an F-BAR protein involved in membrane curvature, but there is still a lack of clear evidence (92) (**Figure 3**). Furthermore, the contribution of defined membrane lipid species should be considered with a special attention to fatty acid molecular species that determine the fluidity or curvature of the lipid bilayer, depending on the length and saturation of their fatty acyl chains, and to negatively charged phospholipids and cholesterol that regulate nsP1 capping activity and membrane affinity, respectively (74, 93), and could alternatively promote host cofactor coalescence to the replication site to assist spherule assembly.

Finally, the exact replication steps taking place in proximity to CHIKV spherules at the plasma membrane remain poorly defined. In contrast with other alphaviruses, which internalize

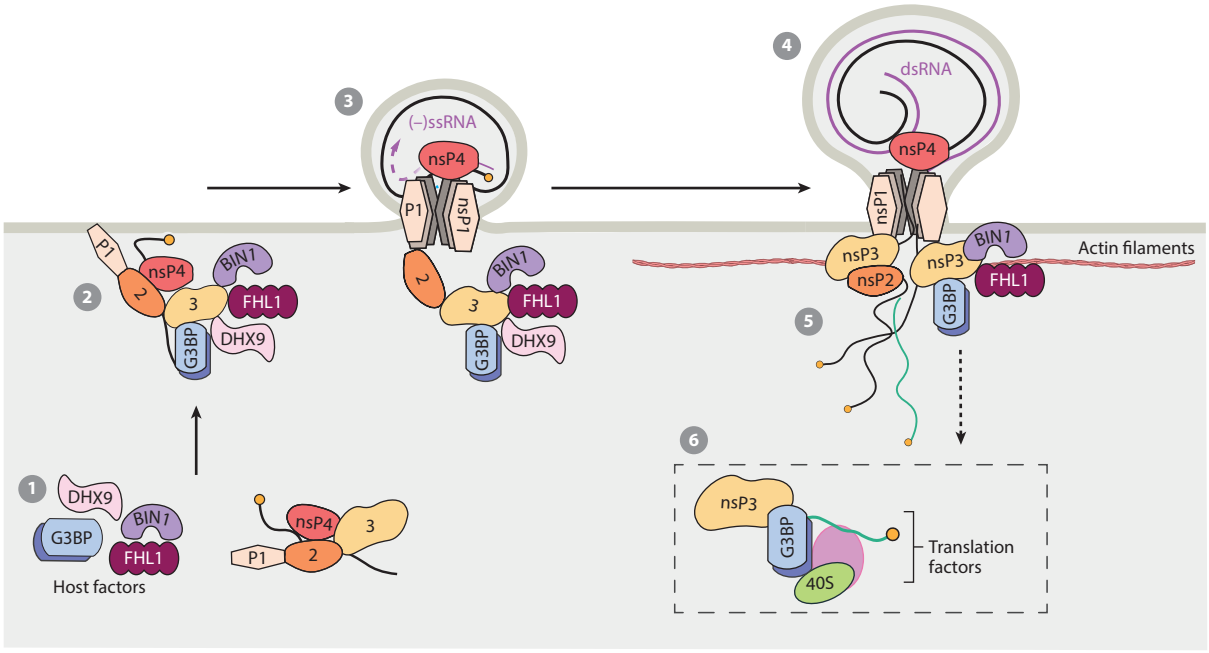

Figure 3

Model of CHIKV replication complex assembly. (*Step 1*) G3BP, FHL1, DHX9, and BIN1/Amphiphysin2 (and other SH3 domain replicase and associated host factors) anchor to the plasma membrane through nsP1 membrane-binding properties. (*Step 3*) This complex starts replicating the RNA genome-containing proteins such as CD2AP and SH3KBP1 are recruited to the CHIKV replication complex through interaction with the nsP3 hypervariable domain, which serves as a hub for host/pathogen interactions. (*Step 2*) CHIKV replicase and associated host factors anchor to the plasma membrane through nsP1 membrane-binding properties. (*Step 3*) This complex starts replicating the RNA genome, assisted by DHX9, which is proposed to regulate the early RNA translation-to-replication switch. (*Step 4*) BIN1/Amphiphysin2, CD2AP, SH3KBP1 and FHL1 involved in membrane bending and/or actin cytoskeleton organization may assist the biogenesis of bulb-shaped spherules separating the dsRNA replication intermediate from host innate immune recognition. (*Step 5*) Genomic and subgenomic RNAs synthesized in the replication organelle are then massively exported to the cytoplasm and capped by the nsP1 dodecameric ring connecting the spherule to the cytoplasm. (*Step 6*) G3BP molecules recruited to the cytoplasmic face of these organelles are proposed to recruit the cellular translation machinery in close proximity to membrane vRCs to ensure optimal viral protein synthesis. Abbreviations: CHIKV, chikungunya virus; dsRNA, double-stranded RNA; nsP, nonstructural protein; ssRNA, single-stranded RNA; UTR, untranslated region; vRC, viral replication complex. Figure adapted from images created with BioRender.com.

membrane spherules by activation of the phosphatidylinositol-3-kinase-Akt-mammalian target of rapamycin signaling, CHIKV replication compartments are mostly maintained at the plasma membrane. This feature was assigned to the poor capacity of CHIKV to activate this pathway (94). Currently, the clear benefit of spherule endocytosis is not clearly understood (23). Altogether, viral protein assembly, contributing cell factors, and metabolism pathways involved in spherule biogenesis and architecture represent new promising targets for the development of therapeutics to control CHIKV infection in humans.

CHIKUNGUNYA VIRUS NONSTRUCTURAL PROTEIN 3: A MULTIFACETED VIRAL PROTEIN ESSENTIAL FOR VIRUS INFECTION AND PATHOGENESIS

The nsP3 molecule is probably the most fascinating and enigmatic CHIKV-encoded protein and has been recognized as essential for both viral replication and adaptation to its host. This viral

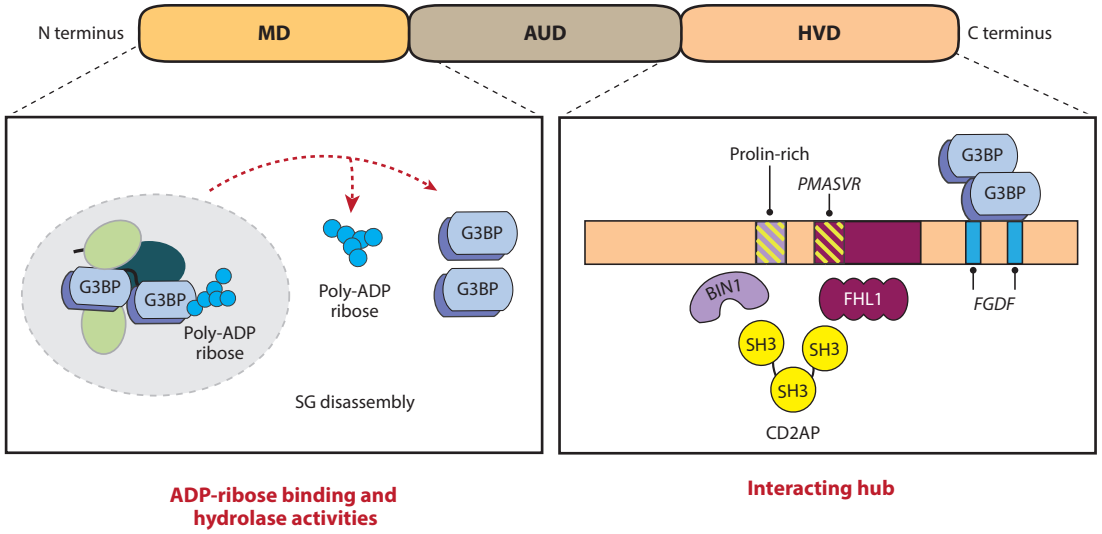

Figure 4

Organization of CHIKV nsP3 and associated functions. CHIKV nsP3 is structurally separated into three domains: an N-terminal MD that binds and hydrolyzes ADPr and poly-ADPr, a central zinc-finger-containing AUD, and a C-terminal HVD identified as a hub for host factor binding. Mapped binding domains in HVD are indicated. The concerted action of MD-associated ribosylhydrolase activity and HVD results in the removal of poly-ADPr conjugated to G3BP, dissociation of G3BP-positive SGs, and redirection of G3BP to the CHIKV replication complex and nsP3 aggregates. Abbreviations: ADPr, ADP-ribose, AUD, alphavirus unique domain; CHIKV, chikungunya virus; HVD, hypervariable domain; MD, macrodomain; nsP, nonstructural protein; SG, stress granule.

factor is a tripartite phospho-protein composed of a highly conserved N-terminal globular domain termed macrodomain (MD), a central domain forming the alphavirus unique domain (AUD) conserved among alphaviruses, and a C-terminal hypervariable domain (HVD) (**Figure 4**). During the early phase of the CHIKV life cycle, nsP3 localizes within the vRC and plays a critical role in viral replication (95–98). Several studies showed that nsP3 acts as a platform for the recruitment of multiple host factors through its HVD (91, 92, 95, 99–101). The HVD is intrinsically disordered and consists of multiple small peptides that interact with distinct sets of cellular proteins, which vary depending on both the alphavirus species and the infected cell type (101) (**Figure 4**). For CHIKV, the major HVD binding molecules identified so far are the G3BP (Ras-GAP SH3 domain-binding proteins, G3BP1 and G3BP2) family proteins, FHL1, DHX9, and several SH3 domain-containing proteins including BIN1/Amphiphysin2, CD2AP, and SH3KBP1, which are involved in membrane bending and cytoskeleton regulation. The roles of G3BP family members during CHIKV replication have been extensively studied. These are essential factors in the assembly of stress granules (SGs), which control viral replication by arresting viral protein translation (reviewed in 102). G3BPs contain RNA-binding domains that self-assemble in macromolecular complexes (103), driving the nucleation of cellular SGs. Disruption of the G3BP-nsP3 HVD interaction or the depletion of both G3BP1 and G3BP2 blocks CHIKV replication (98, 104, 105). According to the current model, in CHIKV-infected cells, G3BPs may interact with the viral P123 precursor and in turn bind the viral genomic RNA to form prereplicative complexes that drive membrane spherule formation and viral RNA synthesis (104). Furthermore, G3BPs interact with the 40S ribosomal subunit, which is thought to recruit the cellular translational machinery in the vicinity of the vRCs for viral protein synthesis (106).

MD: macrodomain

AUD: alphavirus unique domain

HVD: hypervariable domain

G3BPs: Ras-GAP SH3 domain-binding proteins

SG: stress granule

Emerging evidence indicates that nsP3 may accomplish a yet-unknown function during the CHIKV life cycle that is distinct from its role in RNA replication and vRC assembly. Several studies showed that a large proportion of nsP3 proteins, expressed either alone or in the context of CHIKV infection, aggregate to form high-density rod-like structures and large spherical granules distinct from the vRC (95, 107, 108). These nsP3 condensates rapidly increase in size and number during virus replication (108). Importantly, CHIKV nsP3 aggregates also contain G3BPs, yet they are different from SGs in morphology and composition (97, 109). Moreover, cells harboring nsP3 aggregates are not able to form bona fide SGs in response to cellular stress, suggesting a role of nsP3 in SG disassembly by trapping G3BPs (97, 98). Importantly, other nsP3 binding proteins such as FHL1, CD2AP, and SH3KBP1 are also found within these condensates (64, 110, 111). By using subdiffractional multicolor microscopy and human cells persistently replicating a CHIKV replicon, Remenyi and colleagues (108, 112) assessed nsP3 spatial and temporal distribution. They demonstrated that nsP3 clusters of different sizes and morphology coexist in cells and can persist for hours to days. The nsP3 clusters contain genomic RNA and are localized either near dsRNA- and nsP1-enriched foci or close to the nuclear envelop and nucleoporins. Moreover, they are detergent resistant and exert liquid-liquid phase separation properties also proposed for SGs (108, 113). Recent studies revealed that, besides the HVD region, the nsP3 MD is important for aggregate formations (**Figures 4** and **5**). The N-terminal MD of nsP3 binds and removes ADP-ribose (ADPr) or poly-ADPr (114, 115), a reversible post-translational modification known to regulate SG formation/disassembly. In CHIKV-infected cells, this activity reverses G3BP-ribosylation, and favors SG disassembly, and recruitment of translation initiation factors within nsP3 condensates (109). Indeed, in the absence of MD ribosylhydrolase activity, nsP3 condensates contain both RNA-binding proteins (G3BPs, TIA-1, TIAR, and others) and translation initiation factors (eIF3, RACK1, and others), thereby corresponding to SGs (109). An important question raised by the abovementioned studies is how these nsP3 aggregates contribute to virus pathogenesis (**Figure 5**). One possibility is that these nsP3 structures might participate in viral persistence by trapping CHIKV RNA or contribute in the attenuation of the antiviral responses by sequestering key players of the innate immunity, thereby facilitating CHIKV replication. Given the importance of nsP3 in CHIKV replication, further studies providing a precise description of the formation, composition, and functions of the nsP3 condensates are required to understand their biological relevance in CHIKV pathogenesis.

ADPr: ADP-ribose

FHL1, A BRIDGE BETWEEN CHIKUNGUNYA VIRUS REPLICATION AND PATHOGENESIS?

Little is known about the host cellular factors that dictate CHIKV tropism for muscles and joints. A recent genome-wide CRISPR-Cas9 screen identified the FHL1 protein as an important host factor for CHIKV infection and pathogenesis (64). FHL1 is a member of the FHL protein family, which is characterized by the presence of an N-terminal half LIM domain followed by four complete LIM domains (116, 117) (**Figure 6**). Infection studies in FHL1 knock-out cell lines, as well as in primary cells from patients suffering from Emery–Dreifuss muscular dystrophy that lack functional FHL1 proteins, demonstrated that FHL1 is important for CHIKV replication and cell permissiveness (64). Interestingly among the *alphavirus* genus, only CHIKV and its close relative o'nyong-nyong virus use FHL1 for infection. These observations suggest that FHL1 dependency was acquired late during alphavirus evolution. FHL1 interacts with the nsP3 HVD and is important for viral RNA amplification (64). Indeed, ablation of the *fhl1* gene severely reduced both CHIKV negative-stranded RNA synthesis and viral spherule formation. Further investigation is required to decipher the exact molecular mechanisms by which FHL1 mediates CHIKV infection

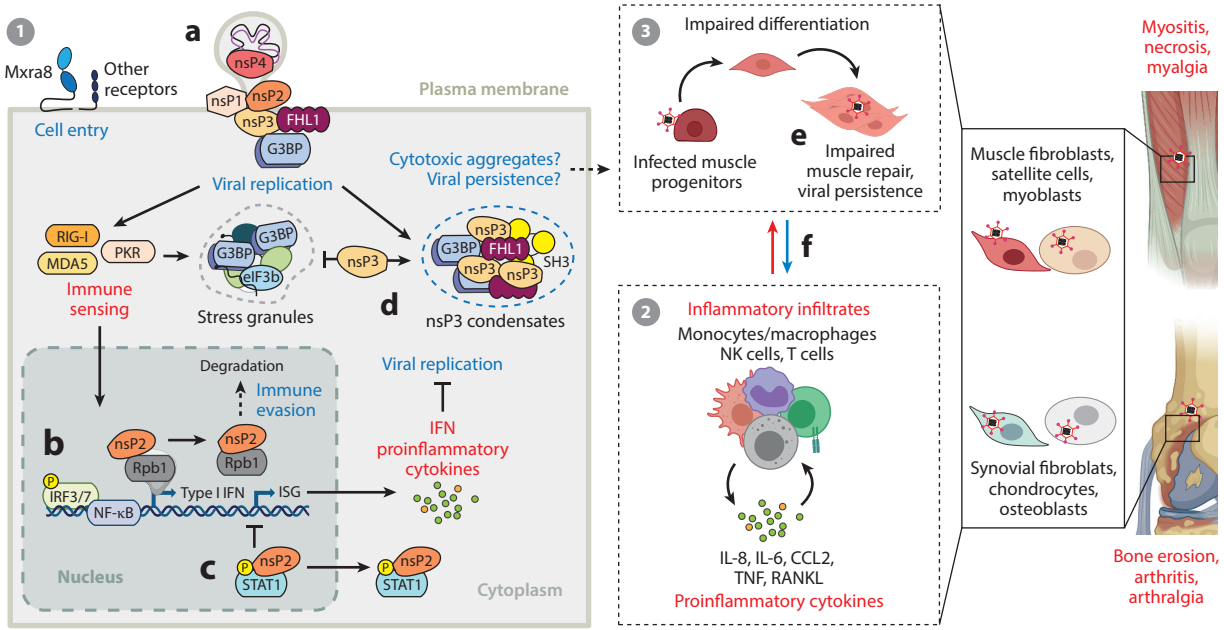

Figure 5

Hypothetical model for CHIKV-induced muscular and articular pathogenesis. (*Step 1*) Successful CHIKV replication in muscle and joint cells relies on the concerted action of host factors and viral proteins. CHIKV nsPs allow efficient viral RNA synthesis within the replicative spherules (*a*). CHIKV nsP2, translocated to the nucleus of infected cells, shuts down antiviral genes transcription by (*b*) redirecting the RNA polymerase II Rpb1 subunit to proteasomal degradation and (*c*) inhibiting phospho-STAT1 nuclear accumulation. By sequestrating G3BPs, nsP3 counteracts the assembly of cytosolic stress granules and contributes to translational shutoff (*d*). (*Step 2*) The release of cytokines and immune mediators by infected cells attracts monocytes/macrophages to muscles and joints, leading to local inflammation, muscle myositis, and bone resorption. (*Step 3*) CHIKV replication and persistence in muscle progenitor cells impairs muscle repair, contributing to musculoskeletal disease (*e*). Viral material persistence in infected tissues can exacerbate host immune responses, leading to chronic rheumatic symptoms (*f*). Abbreviations: CHIKV, chikungunya virus; IFN, interferon; IRF, interferon regulatory factor; ISG, interferon-stimulated gene; nsP, nonstructural protein; NF-κB, nuclear factor κB; NK, natural killer; PKR, protein kinase R; RANKL, receptor activator of nuclear factor κB; STAT1, signal transducer and activator of transcription 1. Figure adapted from images created with BioRender.com.

and to determine whether FHL1 is directly involved in the assembly of spherules or regulates a step in the viral RNA synthesis process. The importance of FHL1 in CHIKV pathogenesis is further supported by in vivo studies showing that FHL1 knock-out mice are resistant to CHIKV infection and do not develop disease. Interestingly, FHL1 tissue expression reflects CHIKV tropism. Indeed, FHL1 protein is highly abundant in skeletal muscle and fibroblasts (118, 119). FHL1 is known to participate in muscle development and homeostasis. It is involved in myogenesis, which consists of the activation of satellite cells and their differentiation in myoblasts, which then fuse to create myotubes that finally differentiate in mature myofibers. Muscle satellite cells express high levels of FHL1, which could explain their susceptibility to CHIKV infection. One can speculate that, upon FHL1 hijacking by nsP3, infected muscle satellite cells might be unable to properly regenerate damaged muscle fibers, contributing to CHIKV-induced musculoskeletal disorders (**Figure 5**). An indirect link between FHL1 expression and CHIKV disease severity is supported by the observation that FHL1 seems to be differentially used by CHIKV strains (64, 111). For instance, the pathogenic CHIKV-21 strain isolated from a patient infected during the 2005–2006 CHIKV outbreak on Reunion Island is highly dependent on FHL1 for infection in vitro and

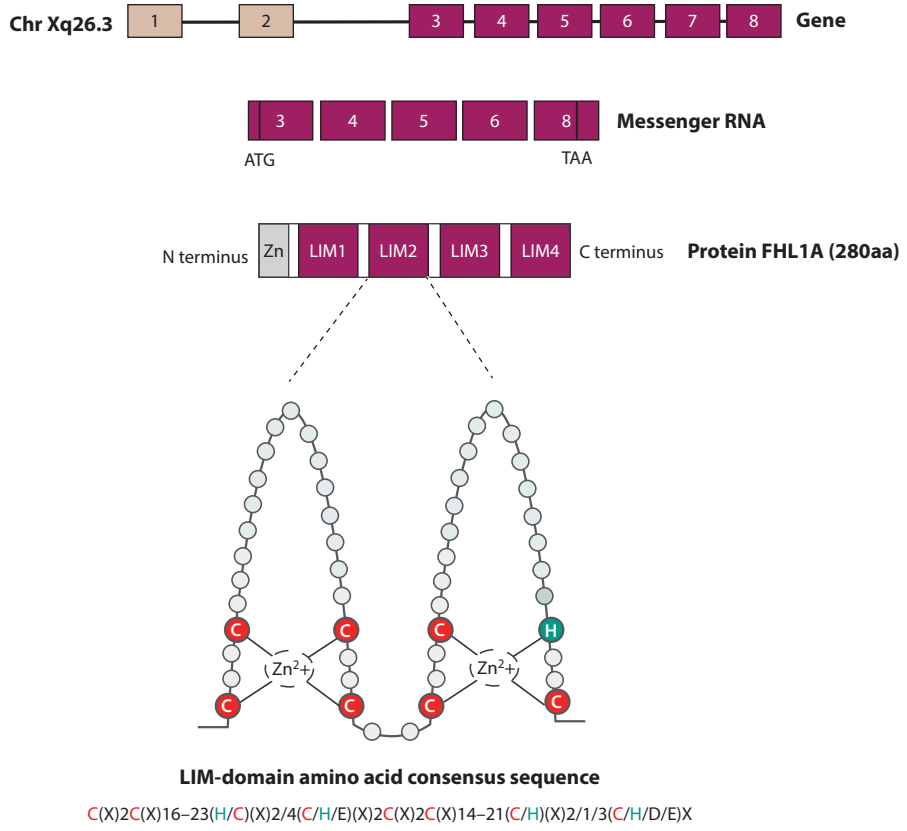

Figure 6

FHL1 gene and protein organization. FHL1A is encoded by human chromosome Xq26.3 and is expressed with high levels in striated muscle cells and fibroblasts. Exons 1 and 2 (*beige boxes*) are noncoding; exons 3 to 8 (*purple boxes*) encode the full-length FHL1 protein, organized into an N-terminal half LIM domain followed by four complete LIM domains. Each domain consists of two zinc-finger motifs, proposed to be a protein/protein binding interface ensuring the assembly of multimeric protein complexes. The LIM domain amino acid consensus sequence is indicated.

induces severe muscular pathology in mice (64). Conversely, the requirement for FHL1 was less pronounced for the sylvatic CHIKV 37997 strain from the West African genotype (64) and the attenuated CHIKV 181/25 strain (111), which are less pathogenic in mice (45). Understanding the molecular basis for FHL1 usage by CHIKV strains may provide important insights into the muscular pathology associated with CHIKV infection. Furthermore, a study on FHL1 polymorphisms in cohorts of CHIKV-infected individuals could add considerable weight to the in vivo relevance of this host factor to CHIKV pathogenesis.

INHIBITION OF HOST INNATE IMMUNITY BY THE CHIKUNGUNYA VIRUS NONSTRUCTURAL PROTEINS

The ability of CHIKV to successfully establish infection and pathogenesis in its host hinges upon its capacity to counteract the host immune responses. Early after infection, CHIKV elicits the massive secretion of IFNs and numerous proinflammatory chemokines and cytokines that are

ISG: interferon-stimulated gene

STAT1: signal transducer and activator of transcription 1

critical to the control of viremia and pathogenesis (37, 120) (**Figure 5**). Mice deficient for the IFN α/β receptor rapidly succumb to CHIKV infection, showing that IFN-I signaling is critical in controlling infection (121). This response, initiated by primary sensing of viral RNA via pattern recognition receptors (PRRs) of the RIG-1-like helicase family (RIG-1 and MDA5), controls the expression of hundreds of interferon-stimulated genes (ISGs) (e.g., ISG15, BST2) capable of interrupting CHIKV replication (121–124) (**Figure 5**). As a countermeasure, CHIKV has evolved various strategies to disrupt IFN signaling. In contrast to New World alphaviruses that usually use their C protein to evade innate immunity, the strategies developed by CHIKV to prevent IFN signaling and ISG antiviral effects have been mainly assigned to the viral protease nsP2. In infected cells, CHIKV nsP2 is detected close to the plasma membrane, where it takes part in the RC, and in the nucleus, where it translocates early after infection, thanks to the presence of a noncanonical nuclear localization motif (125, 126). In the nucleus, nsP2 rapidly targets the Rpb1 catalytic subunit of the RNA polymerase II to proteasomal degradation, thereby shutting down cellular gene transcription and avoiding activation of innate immune genes (127) (**Figure 5**). NsP2-mediated Rpb1 degradation is independent of nsP2 enzymatic activities but is abolished by mutation of Proline 718 in the nsP2 C terminus (90, 125–127). Besides this mechanism, proposed as the main strategy to evade the cellular antiviral response, it now appears that nsP2 specifically interrupts IFN signaling independent of general transcriptional shutoff. The nuclear fraction of nsP2 was indeed found to prevent the nuclear accumulation of signal transducer and activator of transcription 1 (STAT1) (128) by promoting its re-export in the cytoplasm through the chromosome region maintenance 1–mediated pathway. This activity involves the nsP2 methyltransferase-like domain (129) (**Figure 5**). Besides nsP2, recent evidence suggests that other nsPs, namely nsP1 and nsP3, also play a role in immune evasion. In this context, nsP3-MD ADP-ribose hydrolase activity was recently reported to reverse nsP2 mono-ADP-ribosylation by the ADP-ribosyltransferase ARTD10, interfering with its auto-proteolytic function (130). In this model, nsP3 ADP-ribose hydrolysis activity would therefore be critical for immune evasion by antagonizing the antiviral activity of the IFN-inducible ARTD10 that efficiently restricts CHIKV protein maturation and efficient replication. nsP1 also appears as one of the countermeasures deployed by CHIKV to avoid the cellular antiviral system, thus contributing to CHIKV-induced musculoskeletal inflammation in mice (131). nsP1 has recently been described as counteracting the IFN-I response by interacting with the cyclic GMP-AMP synthase (cGas), an effector of the cGas-stimulator of IFN genes signaling axis that restricts CHIKV infection (132). Considering these recent reports, CHIKV has seemingly acquired diverse countermeasures to limit host antiviral responses (**Figure 5**). While the most recent investigations suggest redundant mechanisms, the respective importance of nsP1-, nsP2- and nsP3-dependent scenarios in CHIKV global control strategy remains unknown.

CONCLUDING REMARKS

CHIKV causes a debilitating acute disease that results in persisting arthralgia and myalgia in a large proportion of infected individuals. The mechanisms of CHIKV pathogenesis are complicated and multifactorial, involving both viral and host factors. In the past decades, genomics, proteomics, and structural studies as well as forward genetic screens have generated a plethora of new information about the CHIKV host cell molecular interactions, leading to the identification of several key host molecules important for viral infection. Most of these studies have been performed in immortalized cell lines. In the future, exploring the function of these cellular factors in relevant cellular systems such as primary fibroblasts, musculoskeletal tissues, and animal models of disease will undoubtedly unlock new paradigms of viral pathogenesis. In addition, research will need to uncover the mechanisms of viral RNA persistence in musculoskeletal tissues and joints in

order to uncover at a molecular level why CHIKV frequently evolves to a chronic phase. Studies on CHIKV immunobiology have outlined several elegant mechanisms developed by the virus to counteract host innate immune responses. A detailed understanding of the involved molecular processes and the identification of novel immune evasion strategies would certainly refine our understanding of CHIKV pathogenesis and may be the starting point for the generation of attenuated vaccine candidates and therapeutics to combat CHIKV disease.

DISCLOSURE STATEMENT

The authors are not aware of any affiliations, memberships, funding, or financial holdings that might be perceived as affecting the objectivity of this review.

ACKNOWLEDGMENTS

We apologize to all authors whose work could not be cited due to space restrictions. A.A.'s lab received funding from the French Government's Investissement d'Avenir program, Laboratoire d'Excellence "Integrative Biology of Emerging Infectious Diseases" (grant n°ANR-10-LABX-62-IBEID), the Fondation pour la Recherche Medicale (grant FRM - EQU202003010193), the AFM-Téléthon (grant R20082HH), the Agence Nationale de la Recherche (ANR-AAPG2020 Projet CHIKHOST), and the consortium REACTing. L.B.'s team is funded by the Agence Nationale de la Recherche TOMOCHIKV grant (ANR-18-CE11-0026-01) and by the CNRS. V.K. and O.A.-R.-P. are funded by a scholarship from the French Ministry of Research.

LITERATURE CITED

1. Brault AC, Tesh RB, Powers AM, Weaver SC. 2000. Re-emergence of chikungunya and o'nyong-nyong viruses: evidence for distinct geographical lineages and distant evolutionary relationships. *J. Gen. Virol.* 81(2):471–79
2. Schuffenecker I, Iteman I, Michault A, Murri S, Frangeul L, et al. 2006. Genome microevolution of chikungunya viruses causing the Indian Ocean outbreak. *PLOS Med.* 3(7):e263
3. Powers AM, Logue CH. 2007. Changing patterns of chikungunya virus: re-emergence of a zoonotic arbovirus. *J. Gen. Virol.* 88(9):2363–77
4. Chretien J-P, Anyamba A, Bedno SA, Breiman RF, Sang R, et al. 2007. Drought-associated chikungunya emergence along coastal East Africa. *Am. J. Trop. Med. Hyg.* 76(3):405–7
5. Gérardin P, Guernier V, Perrau J, Fianu A, Le Roux K, et al. 2008. Estimating Chikungunya prevalence in La Réunion Island outbreak by serosurveys: two methods for two critical times of the epidemic. *BMC Infect. Dis.* 8:99
6. Josseran L, Paquet C, Zehgnoun A, Caillere N, Le Tertre A, et al. 2006. Chikungunya disease outbreak, Reunion Island. *Emerg. Infect. Dis.* 12(12):1994–95
7. Arankalle VA, Shrivastava S, Cherian S, Gunjikar RS, Walimbe AM, et al. 2007. Genetic divergence of Chikungunya viruses in India (1963–2006) with special reference to the 2005–2006 explosive epidemic. *J. Gen. Virol.* 88(7):1967–76
8. Angelini P, Macini P, Finarelli AC, Pol C, Venturelli C, et al. 2008. Chikungunya epidemic outbreak in Emilia-Romagna (Italy) during summer 2007. *Parassitologia* 50(1–2):97–98
9. Delisle E, Rousseau C, Broche B, Leparc-Goffart I, L'Ambert G, et al. 2015. Chikungunya outbreak in Montpellier, France, September to October 2014. *Eurosurveillance* 20(17):21108
10. Cassadou S, Boucau S, Petit-Sinturel M, Huc P, Leparc-Goffart I, Ledrans M. 2014. Emergence of chikungunya fever on the French side of Saint Martin island, October to December 2013. *Eurosurveillance* 19(13):20752

11. Van Bortel W, Dorleans F, Rosine J, Blateau A, Rousset D, et al. 2014. Chikungunya outbreak in the Caribbean region, December 2013 to March 2014, and the significance for Europe. *Eurosurveillance* 19(13):20759
12. Tsetsarkin KA, Vanlandingham DL, McGee CE, Higgs S. 2007. A single mutation in chikungunya virus affects vector specificity and epidemic potential. *PLOS Pathog.* 3(12):e201
13. Volk SM, Chen R, Tsetsarkin KA, Adams AP, Garcia TI, et al. 2010. Genome-scale phylogenetic analyses of chikungunya virus reveal independent emergences of recent epidemics and various evolutionary rates. *J. Virol.* 84(13):6497–504
14. Weaver SC, Chen R, Diallo M. 2020. Chikungunya virus: role of vectors in emergence from enzootic cycles. *Annu. Rev. Entomol.* 65:313–32
15. Azar SR, Campos RK, Bergren NA, Camargos VN, Rossi SL. 2020. Epidemic alphaviruses: ecology, emergence and outbreaks. *Microorganisms* 8(8):1167
16. Chen R, Mukhopadhyay S, Merits A, Bolling B, Nasar F, et al. 2018. ICTV virus taxonomy profile: *Togaviridae*. *J. Gen. Virol.* 99(6):761–62
17. Suhrbier A. 2019. Rheumatic manifestations of chikungunya: emerging concepts and interventions. *Nat. Rev. Rheumatol.* 15(10):597–611
18. Khan AH, Morita K, Parquet MDC, Hasebe F, Mathenge EGM, Igarashi A. 2002. Complete nucleotide sequence of chikungunya virus and evidence for an internal polyadenylation site. *J. Gen. Virol.* 83(12):3075–84
19. Solignat M, Gay B, Higgs S, Briant L, Devaux C. 2009. Replication cycle of chikungunya: a re-emerging arbovirus. *Virology* 393(2):183–97
20. Voss JE, Vaney MC, Duquerroy S, Vonrhein C, Girard-Blanc C, et al. 2010. Glycoprotein organization of Chikungunya virus particles revealed by X-ray crystallography. *Nature* 468(7324):709–12
21. Ahola T, Merits A. 2016. Functions of chikungunya virus nonstructural proteins. In *Chikungunya Virus: Advances in Biology, Pathogenesis, and Treatment*, ed. CM Okeoma, pp. 75–98. Cham, Switz.: Springer
22. Okeoma CM, ed. 2016. *Chikungunya Virus: Advances in Biology, Pathogenesis, and Treatment*. Cham, Switz.: Springer
23. Thaa B, Biasiotto R, Eng K, Neuvonen M, Gotte B, et al. 2015. Differential phosphatidylinositol-3-kinase-Akt-mTOR activation by Semliki Forest and chikungunya viruses is dependent on nsP3 and connected to replication complex internalization. *J. Virol.* 89(22):11420–37
24. Soonsawad P, Xing L, Milla E, Espinoza JM, Kawano M, et al. 2010. Structural evidence of glycoprotein assembly in cellular membrane compartments prior to alphavirus budding. *J. Virol.* 84(21):11145–51
25. Rall GF, Racaniello VR, Skalka AM, Flint J. 2015. *Principles of Virology*, Vol. 2: *Pathogenesis & Control*. Washington, DC: Am. Soc. Microbiol.
26. Abraham R, Mudaliar P, Padmanabhan A, Sreekumar E. 2013. Induction of cytopathogenicity in human glioblastoma cells by chikungunya virus. *PLOS ONE* 8(9):e75854
27. Abraham R, Singh S, Nair SR, Hulyalkar NV, Surendran A, et al. 2017. Nucleophosmin (NPM1)/B23 in the proteome of human astrocytic cells restricts chikungunya virus replication. *J. Proteome Res.* 16(11):4144–55
28. Abere B, Wikan N, Ubol S, Auewarakul P, Paemanee A, et al. 2012. Proteomic analysis of chikungunya virus infected microgial cells. *PLOS ONE* 7(4):e34800
29. Sourisseau M, Schilte C, Casartelli N, Trouillet C, Guivel-Benhassine F, et al. 2007. Characterization of reemerging chikungunya virus. *PLOS Pathog.* 3(6):e89
30. Wikan N, Sakoonwatanyoo P, Ubol S, Yoksan S, Smith DR. 2012. Chikungunya virus infection of cell lines: analysis of the East, Central and South African lineage. *PLOS ONE* 7(1):e31102
31. Briant L, Desprès P, Choumet V, Missé D. 2014. Role of skin immune cells on the host susceptibility to mosquito-borne viruses. *Virology* 464–465:26–32
32. Bernard E, Hamel R, Neyret A, Ekchariyawat P, Molès J-P, et al. 2015. Human keratinocytes restrict chikungunya virus replication at a post-fusion step. *Virology* 476:1–10
33. Ekchariyawat P, Hamel R, Bernard E, Wichit S, Surasombatpattana P, et al. 2015. Inflammasome signaling pathways exert antiviral effect against Chikungunya virus in human dermal fibroblasts. *Infect. Genet. Evol.* 32:401–8

34. Young AR, Locke MC, Cook LE, Hiller BE, Zhang R, et al. 2019. Dermal and muscle fibroblasts and skeletal myofibers survive chikungunya virus infection and harbor persistent RNA. *PLOS Pathog.* 15(8):e1007993
35. Wichit S, Diop F, Hamel R, Talignani L, Ferraris P, et al. 2017. *Aedes Aegypti* saliva enhances chikungunya virus replication in human skin fibroblasts via inhibition of the type I interferon signaling pathway. *Infect. Genet. Evol.* 55:68–70
36. Broeckel R, Haese N, Messaoudi I, Streblow D. 2015. Nonhuman primate models of Chikungunya virus infection and disease (CHIKV NHP model). *Pathogens* 4(3):662–81
37. Couderc T, Chrétien F, Schilte C, Disson O, Brigitte M, et al. 2008. A mouse model for Chikungunya: Young age and inefficient type-I interferon signaling are risk factors for severe disease. *PLOS Pathog.* 4(2):e29
38. Hoarau J-J, Bandjee M-CJ, Trotot PK, Das T, Li-Pat-Yuen G, et al. 2010. Persistent chronic inflammation and infection by Chikungunya arthritogenic alphavirus in spite of a robust host immune response. *J. Immunol.* 184(10):5914–27
39. Phuklia W, Kasisith J, Modhiran N, Rodpai E, Thannagith M, et al. 2013. Osteoclastogenesis induced by CHIKV-infected fibroblast-like synoviocytes: a possible interplay between synoviocytes and monocytes/macrophages in CHIKV-induced arthralgia/arthritis. *Virus Res.* 177(2):179–88
40. Roy E, Shi W, Duan B, Reid SP. 2020. Chikungunya virus infection impairs the function of osteogenic cells. *mSphere* 5(3):e00347-20
41. Ozden S, Huerre M, Riviere J-P, Coffey LL, Afonso PV, et al. 2007. Human muscle satellite cells as targets of Chikungunya virus infection. *PLOS ONE* 2(6):e527
42. Lohachanakul J, Phuklia W, Thannagith M, Thongsakulprasert T, Smith DR, Ubol S. 2015. Differences in response of primary human myoblasts to infection with recent epidemic strains of Chikungunya virus isolated from patients with and without myalgia: viral factor in CHIKV-induced myalgia. *J. Med. Virol.* 87(5):733–39
43. Roberts GC, Zothner C, Remenyi R, Merits A, Stonehouse NJ, Harris M. 2017. Evaluation of a range of mammalian and mosquito cell lines for use in Chikungunya virus research. *Sci. Rep.* 7(1):14641
44. Lentscher AJ, McCarthy MK, May NA, Davenport BJ, Montgomery SA, et al. 2020. Chikungunya virus replication in skeletal muscle cells is required for disease development. *J. Clin. Invest.* 130(3):1466–78
45. Rohatgi A, Corbo JC, Monte K, Higgs S, Vanlandingham DL, et al. 2014. Infection of myofibers contributes to increased pathogenicity during infection with an epidemic strain of chikungunya virus. *J. Virol.* 88(5):2414–25
46. Nair S, Poddar S, Shimak RM, Diamond MS. 2017. Interferon regulatory factor 1 protects against chikungunya virus-induced immunopathology by restricting infection in muscle cells. *J. Virol.* 91(22):e01419-17
47. Herrero LJ, Nelson M, Srikiatkhachorn A, Gu R, Anantapreecha S, et al. 2011. Critical role for macrophage migration inhibitory factor (MIF) in Ross River virus-induced arthritis and myositis. *PNAS* 108(29):12048–53
48. Zaid A, Tharmarajah K, Mostafavi H, Freitas JR, Sheng K-C, et al. 2020. Modulation of monocyte-driven myositis in alphavirus infection reveals a role for CX_3CR1^+ macrophages in tissue repair. *mBio* 11(2):e03353-19
49. Chow A, Her Z, Ong EKS, Chen J, Dimatatac F, et al. 2011. Persistent arthralgia induced by Chikungunya virus infection is associated with interleukin-6 and granulocyte macrophage colony-stimulating factor. *J. Infect. Dis.* 203(2):149–57
50. Chen W, Foo S-S, Rulli NE, Taylor A, Sheng K-C, et al. 2014. Arthritogenic alphaviral infection perturbs osteoblast function and triggers pathologic bone loss. *PNAS* 111(16):6040–45
51. Borgherini G, Poubeau P, Jossaume A, Gouix A, Cotte L, et al. 2008. Persistent arthralgia associated with chikungunya virus: a study of 88 adult patients on Reunion Island. *Clin. Infect. Dis.* 47(4):469–75
52. Davenport BJ, Bullock C, McCarthy MK, Hawman DW, Murphy KM, et al. 2020. Chikungunya virus evades antiviral $CD8^+$ T cell responses to establish persistent infection in joint-associated tissues. *J. Virol.* 94(9):e02036-19

53. Hawman DW, Stoermer KA, Montgomery SA, Pal P, Oko L, et al. 2013. Chronic joint disease caused by persistent Chikungunya virus infection is controlled by the adaptive immune response. *J. Virol.* 87(24):13878–88
54. Labadie K, Larcher T, Joubert C, Manniou A, Delache B, et al. 2010. Chikungunya disease in nonhuman primates involves long-term viral persistence in macrophages. *J. Clin. Invest.* 120(3):894–906
55. Couderc T, Lecuit M. 2015. Chikungunya virus pathogenesis: from bedside to bench. *Antivir. Res.* 121:120–31
56. Wilson JAC, Prow NA, Schroder WA, Ellis JJ, Cumming HE, et al. 2017. RNA-Seq analysis of chikungunya virus infection and identification of granzyme A as a major promoter of arthritic inflammation. *PLOS Pathog.* 13(2):e1006155
57. Zhang R, Kim AS, Fox JM, Nair S, Basore K, et al. 2018. Mxra8 is a receptor for multiple arthritogenic alphaviruses. *Nature* 557(7706):570–74
58. Basore K, Kim AS, Nelson CA, Zhang R, Smith BK, et al. 2019. Cryo-EM structure of chikungunya virus in complex with the Mxra8 receptor. *Cell* 177(7):1725–37.e16
59. Song H, Zhao Z, Chai Y, Jin X, Li C, et al. 2019. Molecular basis of arthritogenic alphavirus receptor MXRA8 binding to chikungunya virus envelope protein. *Cell* 177(7):1714–24.e12
60. Zhang R, Earnest JT, Kim AS, Winkler ES, Desai P, et al. 2019. Expression of the Mxra8 receptor promotes alphavirus infection and pathogenesis in mice and *Drosophila*. *Cell Rep.* 28(10):2647–58.e5
61. Powell LA, Miller A, Fox JM, Kose N, Klose T, et al. 2020. Human mAbs broadly protect against arthritogenic alphaviruses by recognizing conserved elements of the Mxra8 receptor-binding site. *Cell Host Microbe* 28(5):699–711.e7
62. McAllister N, Liu Y, Silva LM, Lentscher AJ, Chai W, et al. 2020. Chikungunya virus strains from each genetic clade bind sulfated glycosaminoglycans as attachment factors. *J. Virol.* 94(24):e01500-20
63. Sahoo B, Chowdary TK. 2019. Conformational changes in Chikungunya virus E2 protein upon heparan sulfate receptor binding explain mechanism of E2–E1 dissociation during viral entry. *Biosci. Rep.* 39(6):BSR20191077
64. Meertens L, Hafirassou ML, Couderc T, Bonnet-Madin L, Kril V, et al. 2019. FHL1 is a major host factor for chikungunya virus infection. *Nature* 574(7777):259–63
65. Tanaka A, Tumkosit U, Nakamura S, Motooka D, Kishishita N, et al. 2017. Genome-wide screening uncovers the significance of N-sulfation of heparan sulfate as a host cell factor for chikungunya virus infection. *J. Virol.* 91(13):e00432-17
66. Klimstra WB, Nangle EM, Smith MS, Yurochko AD, Ryman KD. 2003. DC-SIGN and L-SIGN can act as attachment receptors for alphaviruses and distinguish between mosquito cell- and mammalian cell-derived viruses. *J. Virol.* 77(22):12022–32
67. Jemielity S, Wang JJ, Chan YK, Ahmed AA, Li W, et al. 2013. TIM-family proteins promote infection of multiple enveloped viruses through virion-associated phosphatidylserine. *PLOS Pathog.* 9(3):e1003232
68. Moller-Tank S, Maury W. 2014. Phosphatidylserine receptors: enhancers of enveloped virus entry and infection. *Virology* 468–470:565–80
69. Grimley PM, Berezesky IK, Friedman RM. 1968. Cytoplasmic structures associated with an arbovirus infection: loci of viral ribonucleic acid synthesis. *J. Virol.* 2(11):1326–38
70. Salonen A, Ahola T, Kääriäinen L. 2005. Viral RNA replication in association with cellular membranes. *Membr. Traffick. Viral Replication* 285:139–73
71. Decroly E, Ferron F, Lescar J, Canard B. 2011. Conventional and unconventional mechanisms for capping viral mRNA. *Nat. Rev. Microbiol.* 10(1):51–65
72. Peranen J, Laakkonen P, Hyvonen M, Kaariainen L. 1995. The alphavirus replicase protein nsP1 is membrane-associated and has affinity to endocytic organelles. *Virology* 208(2):610–20
73. Tomar S, Narwal M, Harms E, Smith JL, Kuhn RJ. 2011. Heterologous production, purification and characterization of enzymatically active Sindbis virus nonstructural protein nsP1. *Protein Expr. Purif.* 79(2):277–84
74. Ahola T, Lampio A, Auvinen P, Kaariainen L. 1999. Semliki Forest virus mRNA capping enzyme requires association with anionic membrane phospholipids for activity. *EMBO J.* 18(11):3164–72
75. Belov GA, Nair V, Hansen BT, Hoyt FH, Fischer ER, Ehrenfeld E. 2012. Complex dynamic development of poliovirus membranous replication complexes. *J. Virol.* 86(1):302–12

76. Knoops K, Kikkert M, Worm SH, Zevenhoven-Dobbe JC, van der Meer Y, et al. 2008. SARS-coronavirus replication is supported by a reticulovesicular network of modified endoplasmic reticulum. *PLOS Biol.* 6(9):e226
77. Kopek BG, Perkins G, Miller DJ, Ellisman MH, Ahlquist P. 2007. Three-dimensional analysis of a viral RNA replication complex reveals a virus-induced mini-organelle. *PLOS Biol.* 5(9):e220
78. Romero-Brey I, Merz A, Chiramel A, Lee JY, Chlanda P, et al. 2012. Three-dimensional architecture and biogenesis of membrane structures associated with hepatitis C virus replication. *PLOS Pathog.* 8(12):e1003056
79. Sachse M, Fernández de Castro I, Tenorio R, Risco C. 2019. The viral replication organelles within cells studied by electron microscopy. *Adv. Virus Res.* 105:1–33
80. Snijder EJ, Limpens RWAL, de Wilde AH, de Jong AWM, Zevenhoven-Dobbe JC, et al. 2020. A unifying structural and functional model of the coronavirus replication organelle: tracking down RNA synthesis. *PLOS Biol.* 18(6):e3000715
81. Welsch S, Miller S, Romero-Brey I, Merz A, Bleck CK, et al. 2009. Composition and three-dimensional architecture of the dengue virus replication and assembly sites. *Cell Host Microbe* 5(4):365–75
82. Jones R, Bragagnolo G, Arranz R, Reguera J. 2021. Capping pores of alphavirus nsP1 gate membranous viral replication factories. *Nature* 589(7843):615–19
83. Ertel KJ, Benefield D, Castano-Diez D, Pennington JG, Horswill M, et al. 2017. Cryo-electron tomography reveals novel features of a viral RNA replication compartment. *eLife* 6:e25940
84. Unchwaniwala N, Zhan H, Pennington J, Horswill M, den Boon JA, Ahlquist P. 2020. Subdomain cryo-EM structure of nodaviral replication protein A crown complex provides mechanistic insights into RNA genome replication. *PNAS* 117(31):18680–91
85. Hellstrom K, Kallio K, Utt A, Quirin T, Jokitalo E, et al. 2017. Partially uncleaved alphavirus replicase forms spherule structures in the presence and absence of RNA template. *J. Virol.* 91(18):e00787-17
86. Kallio K, Hellstrom K, Balistreri G, Spuul P, Jokitalo E, Ahola T. 2013. Template RNA length determines the size of replication complex spherules for Semliki Forest virus. *J. Virol.* 87(16):9125–34
87. Ahola T, Kujala P, Tuittila M, Blom T, Laakkonen P, et al. 2000. Effects of palmitoylation of replicase protein nsP1 on alphavirus infection. *J. Virol.* 74(15):6725–33
88. Gottipati K, Woodson M, Choi KH. 2020. Membrane binding and rearrangement by chikungunya virus capping enzyme nsP1. *Virology* 544:31–41
89. Laakkonen P, Ahola T, Kaariainen L. 1996. The effects of palmitoylation on membrane association of Semliki Forest virus RNA capping enzyme. *J. Biol. Chem.* 271(45):28567–71
90. Bouraï M, Lucas-Hourani M, Gad HH, Drosten C, Jacob Y, et al. 2012. Mapping of Chikungunya virus interactions with host proteins identified nsP2 as a highly connected viral component. *J. Virol.* 86(6):3121–34
91. Cristea IM, Carroll JW, Rout MP, Rice CM, Chait BT, MacDonald MR. 2006. Tracking and elucidating alphavirus-host protein interactions. *J. Biol. Chem.* 281(40):30269–78
92. Neuvonen M, Kazlauskas A, Martikainen M, Hinkkanen A, Ahola T, Saksela K. 2011. SH3 domain-mediated recruitment of host cell amphiphysins by alphavirus nsP3 promotes viral RNA replication. *PLOS Pathog.* 7(11):e1002383
93. Bakhache W, Neyret A, Bernard E, Merits A, Briant L. 2020. Palmitoylated cysteines in chikungunya virus nsP1 are critical for targeting to cholesterol-rich plasma membrane microdomains with functional consequences for viral genome replication. *J. Virol.* 94(10):e02183-19
94. Van Huizen E, McInerney GM. 2020. Activation of the PI3K-AKT pathway by Old World alphaviruses. *Cells* 9(4):970
95. Gorchakov R, Garmashova N, Frolova E, Frolov I. 2008. Different types of nsP3-containing protein complexes in Sindbis virus-infected cells. *J. Virol.* 82(20):10088–101
96. Wang YF, Sawicki SG, Sawicki DL. 1994. Alphavirus nsP3 functions to form replication complexes transcribing negative-strand RNA. *J. Virol.* 68(10):6466–75
97. Fros JJ, Domeradzka NE, Baggen J, Geertsema C, Flipse J, et al. 2012. Chikungunya virus nsP3 blocks stress granule assembly by recruitment of G3BP into cytoplasmic foci. *J. Virol.* 86(19):10873–79
98. Scholte FEM, Tas A, Albulescu IC, Žusinaite E, Merits A, et al. 2015. Stress granule components G3BP1 and G3BP2 play a proviral role early in Chikungunya virus replication. *J. Virol.* 89(8):4457–69

99. Varjak M, Saul S, Arike L, Lulla A, Peil L, Merits A. 2013. Magnetic fractionation and proteomic dissection of cellular organelles occupied by the late replication complexes of Semliki Forest virus. *J. Virol.* 87(18):10295–312
100. Frolova E, Gorchakov R, Garmashova N, Atasheva S, Vergara LA, Frolov I. 2006. Formation of nsP3-specific protein complexes during Sindbis virus replication. *J. Virol.* 80(8):4122–34
101. Meshram CD, Agback P, Shiliaev N, Urakova N, Mobley JA, et al. 2018. Multiple host factors interact with the hypervariable domain of chikungunya virus nsP3 and determine viral replication in cell-specific mode. *J. Virol.* 92(16):e00838-18
102. Onomoto K, Yoneyama M, Fung G, Kato H, Fujita T. 2014. Antiviral innate immunity and stress granule responses. *Trends Immunol.* 35(9):420–28
103. Tourrière H, Chebli K, Zekri L, Courselaud B, Blanchard JM, et al. 2003. The RasGAP-associated endoribonuclease G3BP assembles stress granules. *J. Cell Biol.* 160(6):823–31
104. Kim DY, Reynaud JM, Rasalouskaya A, Akhrymuk I, Mobley JA, et al. 2016. New World and Old World alphaviruses have evolved to exploit different components of stress granules, FXR and G3BP proteins, for assembly of viral replication complexes. *PLOS Pathog.* 12(8):e1005810
105. Götte B, Utt A, Fragkoudis R, Merits A, McInerney GM. 2020. Sensitivity of alphaviruses to G3BP deletion correlates with efficiency of replicase polyprotein processing. *J. Virol.* 94(7):e01681-19
106. Götte B, Panas MD, Hellström K, Liu L, Samreen B, et al. 2019. Separate domains of G3BP promote efficient clustering of alphavirus replication complexes and recruitment of the translation initiation machinery. *PLOS Pathog.* 15(6):e1007842
107. Foy NJ, Akhrymuk M, Akhrymuk I, Atasheva S, Bopda-Waffo A, et al. 2013. Hypervariable domains of nsP3 proteins of New World and Old World alphaviruses mediate formation of distinct, virus-specific protein complexes. *J. Virol.* 87(4):1997–2010
108. Remenyi R, Gao Y, Hughes RE, Curd A, Zothner C, et al. 2018. Persistent replication of a chikungunya virus replicon in human cells is associated with presence of stable cytoplasmic granules containing nonstructural protein 3. *J. Virol.* 92(16):e00477-18
109. Jayabalan AK, Adivarahan S, Koppula A, Abraham R, Batish M, et al. 2021. Stress granule formation, disassembly, and composition are regulated by alphavirus ADP-ribosylhydrolase activity. *PNAS* 118(6):e2021719118
110. Mutso M, Morro AM, Smedberg C, Kasvandik S, Aquilimeba M, et al. 2018. Mutation of CD2AP and SH3KBP1 binding motif in alphavirus nsP3 hypervariable domain results in attenuated virus. *Viruses* 10(5):226
111. Lukash T, Agback T, Dominguez F, Shiliaev N, Meshram C, et al. 2020. Structural and functional characterization of host FHL1 protein interaction with hypervariable domain of chikungunya virus nsP3 protein. *J. Virol.* 95(1):e01672-20
112. Remenyi R, Roberts GC, Zothner C, Merits A, Harris M. 2017. SNAP-tagged chikungunya virus replicons improve visualisation of non-structural protein 3 by fluorescence microscopy. *Sci. Rep.* 7:5682
113. Molliex A, Temirov J, Lee J, Coughlin M, Kanagaraj AP, et al. 2015. Phase separation by low complexity domains promotes stress granule assembly and drives pathological fibrillization. *Cell* 163(1):123–33
114. Abraham R, Hauer D, McPherson RL, Utt A, Kirby IT, et al. 2018. ADP-ribosyl-binding and hydrolase activities of the alphavirus nsP3 macrodomain are critical for initiation of virus replication. *PNAS* 115(44):E10457–66
115. Eckei L, Krieg S, Butepage M, Lehmann A, Gross A, et al. 2017. The conserved macrodomains of the non-structural proteins of Chikungunya virus and other pathogenic positive strand RNA viruses function as mono-ADP-ribosylhydrolases. *Sci. Rep.* 7:41746
116. Kadrmas JL, Beckerle MC. 2004. The LIM domain: from the cytoskeleton to the nucleus. *Nat. Rev. Mol. Cell Biol.* 5(11):920–31
117. Zheng Q, Zhao Y. 2007. The diverse biofunctions of LIM domain proteins: determined by subcellular localization and protein–protein interaction. *Biol. Cell* 99(9):489–502
118. Cowling BS, McGrath MJ, Nguyen M-A, Cottle DL, Kee AJ, et al. 2008. Identification of FHL1 as a regulator of skeletal muscle mass: implications for human myopathy. *J. Cell Biol.* 183(6):1033–48

119. Domenighetti AA, Chu P-H, Wu T, Sheikh F, Gokhin DS, et al. 2014. Loss of FHL1 induces an age-dependent skeletal muscle myopathy associated with myofibrillar and intermyofibrillar disorganization in mice. *Hum. Mol. Genet.* 23(1):209–25
120. Ng LFP, Chow A, Sun Y-J, Kwek DJC, Lim P-L, et al. 2009. IL-1β, IL-6, and RANTES as biomarkers of Chikungunya severity. *PLOS ONE* 4(1):e4261
121. Schilte C, Couderc T, Chretien F, Sourisseau M, Gangneux N, et al. 2010. Type I IFN controls chikungunya virus via its action on nonhematopoietic cells. *J. Exp. Med.* 207(2):429–42
122. Akhrymuk I, Frolov I, Frolova EI. 2016. Both RIG-I and MDA5 detect alphavirus replication in concentration-dependent mode. *Virology* 487:230–41
123. Olagnier D, Scholte FEM, Chiang C, Albulescu IC, Nichols C, et al. 2014. Inhibition of dengue and chikungunya virus infections by RIG-I-mediated type I interferon-independent stimulation of the innate antiviral response. *J. Virol.* 88(8):4180–94
124. White LK, Sali T, Alvarado D, Gatti E, Pierre P, et al. 2011. Chikungunya virus induces IPS-1-dependent innate immune activation and protein kinase R-independent translational shutoff. *J. Virol.* 85(1):606–20
125. Fros JJ, van der Maten E, Vlak JM, Pijlman GP. 2013. The C-terminal domain of chikungunya virus nsP2 independently governs viral RNA replication, cytopathicity, and inhibition of interferon signaling. *J. Virol.* 87(18):10394–400
126. Utt A, Das PK, Varjak M, Lulla V, Lulla A, Merits A. 2015. Mutations conferring a noncytotoxic phenotype on chikungunya virus replicons compromise enzymatic properties of nonstructural protein 2. *J. Virol.* 89(6):3145–62. Erratum. 2016. *J. Virol.* 90(17):8030
127. Akhrymuk I, Kulemzin SV, Frolova EI. 2012. Evasion of the innate immune response: The Old World alphavirus nsP2 protein induces rapid degradation of Rpb1, a catalytic subunit of RNA polymerase II. *J. Virol.* 86(13):7180–91
128. Fros JJ, Liu WJ, Prow NA, Geertsema C, Ligtenberg M, et al. 2010. Chikungunya virus nonstructural protein 2 inhibits type I/II interferon-stimulated JAK-STAT signaling. *J. Virol.* 84(20):10877–87
129. Goertz GP, McNally KL, Robertson SJ, Best SM, Pijlman GP, Fros JJ. 2018. The methyltransferase-like domain of chikungunya virus nsP2 inhibits the interferon response by promoting the nuclear export of STAT1. *J. Virol.* 92(17):e01008-18
130. Krieg S, Pott F, Eckei L, Verheirstraeten M, Bütepage M, et al. 2020. Mono-ADP-ribosylation by ARTD10 restricts Chikungunya virus replication by interfering with the proteolytic activity of nsP2. bioRxiv 2020.01.07.896977. **https://doi.org/10.1101/2020.01.07.896977**
131. Jupille HJ, Oko L, Stoermer KA, Heise MT, Mahalingam S, et al. 2011. Mutations in nsP1 and PE2 are critical determinants of Ross River virus-induced musculoskeletal inflammatory disease in a mouse model. *Virology* 410(1):216–27
132. Webb LG, Veloz J, Pintado-Silva J, Zhu T, Rangel MV, et al. 2020. Chikungunya virus antagonizes cGAS-STING mediated type-I interferon responses by degrading cGAS. *PLOS Pathog.* 16(10):e100899

LETTER

https://doi.org/10.1038/s41586-019-1578-4

FHL1 is a major host factor for chikungunya virus infection

Laurent Meertens[1,13]*, Mohamed Lamine Hafirassou[1], Thérèse Couderc[2], Lucie Bonnet-Madin[1], Vasiliya Kril[1], Beate M. Kümmerer[3], Athena Labeau[1], Alexis Brugier[1], Etienne Simon-Loriere[4], Julien Burlaud-Gaillard[5], Cécile Doyen[6], Laura Pezzi[7], Thibaud Goupil[2], Sophia Rafasse[2], Pierre-Olivier Vidalain[8], Anne Bertrand-Legout[9], Lucie Gueneau[9], Raul Juntas-Morales[10], Rabah Ben Yaou[9], Gisèle Bonne[9], Xavier de Lamballerie[7], Monsef Benkirane[6], Philippe Roingeard[5], Constance Delaugerre[1,11], Marc Lecuit[2,12] & Ali Amara[1,13]*

Chikungunya virus (CHIKV) is a re-emerging alphavirus that is transmitted to humans by mosquito bites and causes musculoskeletal and joint pain[1,2]. Despite intensive investigations, the human cellular factors that are critical for CHIKV infection remain unknown, hampering the understanding of viral pathogenesis and the development of anti-CHIKV therapies. Here we identified the four-and-a-half LIM domain protein 1 (FHL1)[3] as a host factor that is required for CHIKV permissiveness and pathogenesis in humans and mice. Ablation of FHL1 expression results in the inhibition of infection by several CHIKV strains and o'nyong-nyong virus, but not by other alphaviruses and flaviviruses. Conversely, expression of FHL1 promotes CHIKV infection in cells that do not normally express it. FHL1 interacts directly with the hypervariable domain of the nsP3 protein of CHIKV and is essential for the replication of viral RNA. FHL1 is highly expressed in CHIKV-target cells and is particularly abundant in muscles[3,4]. Dermal fibroblasts and muscle cells derived from patients with Emery–Dreifuss muscular dystrophy that lack functional FHL1[5] are resistant to CHIKV infection. Furthermore, CHIKV infection is undetectable in Fhl1-knockout mice. Overall, this study shows that FHL1 is a key factor expressed by the host that enables CHIKV infection and identifies the interaction between nsP3 and FHL1 as a promising target for the development of anti-CHIKV therapies.

Several host factors involved in mediating infection with CHIKV have been identified[6–9]; however, none of these factors accounts for the tropism of CHIKV for joint and muscle tissues. To uncover host genes required for CHIKV infection, we performed a genome-wide CRISPR–Cas9 screen in near haploid human HAP1 cells using CHIKV21, a strain isolated from a patient infected during the 2005–2006 CHIKV outbreak in La Reunion Island[10] (Fig. 1a, Extended Data Fig. 1 and Supplementary Table 1). The top hit of our screen was the gene encoding FHL1 (Fig. 1a and Extended Data Fig. 2a–c), the founding member of the FHL protein family[11]. FHL1 is characterized by four-and-a-half highly conserved LIM domains with two zinc fingers arranged in tandem[11]. FHL1 is highly expressed in skeletal muscles and heart[3,11]. There are three human FHL1 splice variants: FHL1A, FHL1B and FHL1C[3,12,13]. FHL1A is most-abundantly expressed in striated muscles[3] and fibroblasts[14]. The two other variants, FHL1B and FHL1C, are expressed in muscles, brain and testis[12,13]. We validated the requirement of FHL1 in CHIKV21 infection with two distinct guide (g)RNAs targeting the three *FHL1* isoforms (Extended Data Fig. 2a). We generated HAP1 and HEK293T *FHL1*-knockout clones (ΔFHL1) and confirmed gene editing (Extended Data Fig. 2d–f). *FHL1* knockout did not alter cell proliferation and viability (Extended Data Fig. 2g). CHIKV21 infection and release of infectious particles was markedly inhibited in ΔFHL1 cells (Fig. 1b and Extended Data Fig. 3a–d). Trans-complementation of ΔFHL1 cells with a human cDNA encoding FHL1A, but not FHL1B or FHL1C, restored both the susceptibility to CHIKV21 and release of the virus (Fig. 1c and Extended Data Fig. 4a, b). Expression of FHL2, a member of the FHL family that is expressed in the heart[15], restored CHIKV infection in ΔFHL1 cells, albeit with a lower efficiency than FHL1 (Extended Data Fig. 4c). FHL1 is important for infection by CHIKV strains belonging to the Asian (strain St Martin H20235 2013), the east, central, and south African strains Ross and Brazza (MRS1 2011) and the Indian Ocean (strain M-899) lineages (Fig. 1d). Notably, the requirement for FHL1 was less pronounced with CHIKV 37997, a strain from the West African genotype (Fig. 1d). We next tested the requirement of FHL1 for infection by other alphaviruses. O'nyong-nyong virus (ONNV), an Old World alphavirus that is phylogenetically close to CHIKV, showed a markedly reduced infection level in ΔFHL1 cells (Fig. 1e and Extended Data Fig. 3e). By contrast, other alphaviruses—such as Mayaro virus (MAYV), Sindbis virus (SINV), Semliki Forest Virus (SFV), Ross River virus, eastern equine encephalitis virus, western equine encephalitis virus and Venezuelan equine encephalitis virus—infected HAP1 cells in a FHL1-independent manner (Fig. 1e, f and Extended Data Fig. 3e). FHL1 is not necessary for infection by the flaviviruses dengue virus (DENV) or Zika virus (ZIKV) (Fig. 1g and Extended Data Fig. 3f). BeWo or HepG2 cells, which are poorly susceptible to CHIKV infection[16,17] and lack FHL1 (Extended Data Fig. 5a), became permissive to infection after expression of FHL1A (Fig. 1h and Extended Data Fig. 5b–d). This highlights the major role of FHL1A in the permissiveness of human cells to CHIKV.

To determine which step in the CHIKV life cycle requires FHL1, we challenged parental and ΔFHL1 cells with CHIKV and quantified the viral RNA at different time points (Fig. 2a). We did not observe any significant difference in CHIKV RNA levels in ΔFHL1 cells compared to wild-type cells at 2 h after infection (Fig. 2a). By contrast, a large reduction in CHIKV RNA was observed in ΔFHL1 cells as early as 6 h after infection (Fig. 2a) and this reduction was greater at 24 h after infection. We bypassed virus entry and uncoating by transfecting CHIKV RNA into controls or ΔFHL1 cells in the presence of NH_4Cl to inhibit further rounds of infection[8]. Viral replication was markedly impaired in ΔFHL1 cells compared to wild-type cells

[1]INSERM U944, CNRS UMR 7212, Genomes & Cell Biology of Disease Unit, Institut de Recherche Saint-Louis, Université de Paris, Hôpital Saint-Louis, Paris, France. [2]Institut Pasteur, Inserm U1117, Biology of Infection Unit, Paris, France. [3]Institute of Virology, University of Bonn Medical Centre, Bonn, Germany. [4]Institut Pasteur, G5 Evolutionary Genomics of RNA Viruses, Paris, France. [5]INSERM U1259 MAVIVH et Plateforme IBiSA de Microscopie Electronique, Université de Tours et CHRU de Tours, Tours, France. [6]Institut de Génétique Humaine, Laboratoire de Virologie Moléculaire, CNRS-Université de Montpellier, Montpellier, France. [7]Unité des Virus Émergents, Aix-Marseille Univ, IRD190, Inserm 1207, EFS-IRBA, Marseille, France. [8]Equipe Chimie & Biologie, Modélisation et Immunologie pour la Thérapie, Université Paris Descartes, CNRS UMR 8601, Paris, France. [9]Center of Research in Myology, Sorbonne Université, INSERM UMRS974, Paris, France. [10]Département de Neurologie, Centre Hospitalier Universitaire de Montpellier, Montpellier, France. [11]Laboratoire de Virologie et Département des Maladies Infectieuses, Hôpital Saint-Louis, APHP, Paris, France. [12]Université de Paris, Department of Infectious Diseases and Tropical Medicine, Necker-Enfants Malades University Hospital, APHP, Institut Imagine, Paris, France. [13]These authors contributed equally: Laurent Meertens, Ali Amara. *e-mail: laurent.meertens@inserm.fr; ali.amara@inserm.fr

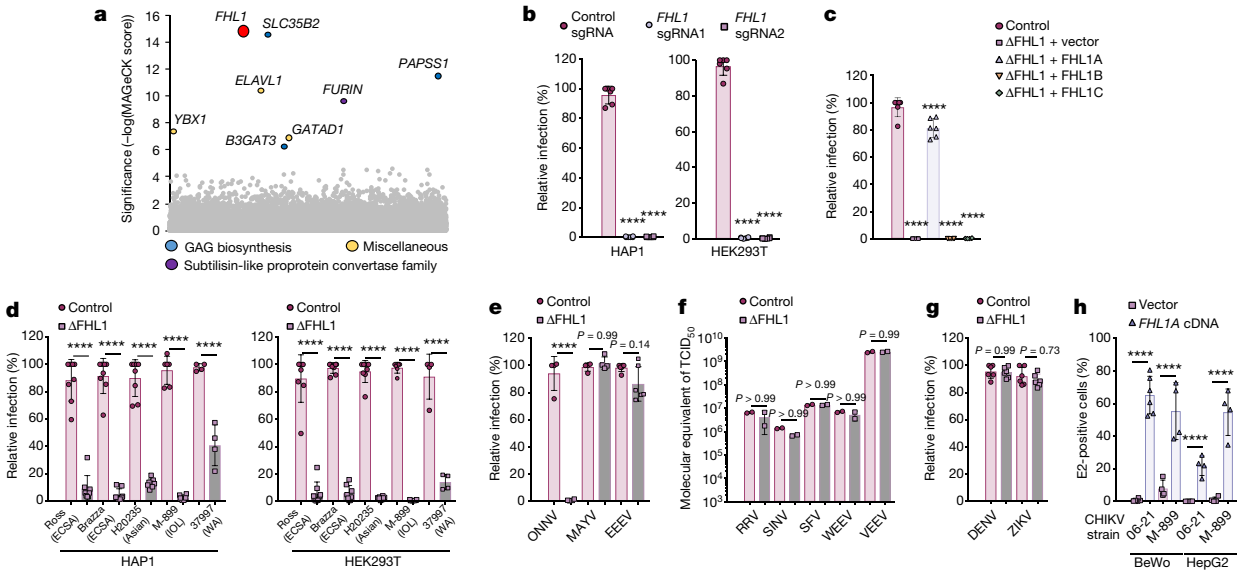

Fig. 1 | FHL1 is important for infection by CHIKV and ONNV. **a**, Results of the CHIKV screen analysed by MAGeCK. Each circle represents an individual gene. The *y* axis shows the significance of sgRNA enrichment of genes in the selected population compared to the unselected control population. The *x* axis represents a random distribution of the genes. All genes with a false-discovery rate-adjust $P < 0.05$ are coloured (Benjamini-Hochberg procedure). **b**, E2 protein expression in control or ΔFHL1 cells infected with the CHIKV21 strain (multiplicity of infection (MOI) of 10). **c**, ΔFHL1 HAP1 cells were complemented with FHL1A, FHL1B or FHL1C isoforms, infected with CHIKV21 (MOI of 10) and stained for E2 protein expression at 48 h after infection. **b**, **c**, Data are mean ± s.d. $n = 3$ independent experiments performed in duplicate. One-way analysis of variance (ANOVA) with Dunnett's multiple comparison test. **d**, ΔFHL1 and control cells were inoculated with CHIKV Ross (MOI of 10), CHIKV Brazza (MOI of 10), CHIKV 20235 (MOI of 10), CHIKV-M (M-899) (MOI of 10) or CHIKV 37997 (MOI of 10) and analysed at 24 (HEK293T cells) or 48 h (HAP1 cells) after infection for E2 expression. ECSA, east, central, and south African strains; IOL, Indian Ocean strain; WA, west African strain. Data are mean ± s.d. $n = 4$ independent experiments performed in duplicate, except for CHIKV 37997, for which $n = 2$ independent experiments were performed in duplicate. One-way ANOVA with Tukey's multiple comparison test. **e**–**g**, ΔFHL1 and control HAP1 cells were inoculated with ONNV (MOI of 2), MAYV (MOI of 50), eastern equine encephalitis virus (EEEV) (MOI of 2), SINV, SFV, Ross River virus (RRV), western equine encephalitis virus (WEEV), Venezuelan equine encephalitis virus (VEEV), DENV (MOI of 0.4) or ZIKV (MOI of 50). **e**, Infection was quantified 48 h after infection by flow cytometry using the anti-E2 3E4, 265 CHIKV monoclonal antibody or the anti-EEEV monoclonal antibody 1A4B6. $n = 2$ independent experiments performed in duplicate. One-way ANOVA with Tukey's multiple comparison test. **f**, Virus growth was assessed on day 4 after infection using RT–qPCR. Serial dilutions of infected supernatants titrated using the 50% tissue culture infectious dose ($TCID_{50}$) were used as quantification standards for RT–qPCR. Accordingly, results were expressed for each virus as 'molecular equivalents of $TCID_{50}$'. Data are representative of two independent experiments performed in duplicates. **g**, DENV or ZIKV infection was assessed by flow cytometry 48 h after infection using the anti-E protein 4G2 monoclonal antibody. $n = 3$ independent experiments performed in duplicate. **e**–**g**, Data are mean ± s.d. One-way ANOVA with Tukey's multiple comparison test. **h**, BeWo and HepG2 cells were transduced with FHL1A or a control vector and challenged with CHIKV21 (MOI of 5) or CHIKV M-899 (MOI of 2). Infection was quantified 2 days later by flow cytometry using the 3E4 monoclonal antibody. Data are mean ± s.d. $n = 2$ independent experiments performed in duplicate, except for BeWo cells infected with CHIKV21, for which $n = 3$ independent experiments were performed in duplicate. One-way ANOVA with Tukey's multiple comparison test. ****$P < 0.0001$.

(Fig. 2b and Extended Data Fig. 6a). To evaluate the contribution of FHL1 in viral RNA translation versus replication, we generated a replication-deficient CHIKV molecular clone (the GDD motif of the polymerase nsP4 was mutated to GAA), which encoded a *Renilla* luciferase (Rluc) fused to nsP3. Transfection of CHIKV(GAA) RNA in ΔFHL1 or control cells resulted in similar Rluc activities (Fig. 2c), indicating that FHL1 is dispensable for viral RNA translation. When similar experiments were performed with wild-type CHIKV RNA, a large increase in Rluc activity was observed in control—but not ΔFHL1—cells 24 h after infection (Fig. 2d), demonstrating that FHL1 is essential for viral RNA replication. Quantitative reverse-transcription PCR (RT–qPCR) experiments showed that ablation of FHL1 resulted in severely reduced synthesis of CHIKV negative-strand RNA (Fig. 2e). We investigated the effect of FHL1 in the production of dsRNA intermediates, which are a marker of viral replication complex assembly[18]. At 6 h after infection, a massive reduction in dsRNA-containing complexes was observed in ΔFHL1 cells stained with an anti-dsRNA monoclonal antibody compared to parental cells (Fig. 2f). Transmission electron microscopy analyses showed that the formation of plasma-membrane-associated spherules and cytoplasmic vacuolar membrane structures, which are alphavirus-induced platforms that are required for viral RNA synthesis[19], are absent in ΔFHL1 cells (Fig. 2g).

Confocal microscopy imaging showed that FHL1 displays a diffuse cytoplasmic distribution in uninfected human fibroblasts. In cells infected for 6 h, FHL1-containing foci appeared and colocalized with nsP3 (Extended Data Fig. 6b), a CHIKV non-structural protein that organizes viral replication in the cytoplasm[20,21]. CHIKV nsP3 contains a large C-terminal hypervariable domain (HVD)[20] that is known to mediate assembly of protein complexes and regulate RNA amplification[20,21]. Notably, FHL1 and FHL2 have been reported as putative nsP3(HVD)-binding partners in mass spectrometry analyses[21,22]. We experimentally validated the interaction between FHL1 and nsP3 (Fig. 2h, i and Extended Data Fig. 6c–g) and found that endogenous FHL1 co-immunoprecipitates with nsP3 from CHIKV-infected cells (Fig. 2h). Both FHL1A and FHL2 co-precipitated with CHIKV nsP3 (Extended Data Fig. 6d). The interaction between FHL1A and nsP3 is specific to CHIKV, as it was not observed with nsP3 from SINV or SFV (Extended Data Fig. 6e). In ΔFHL1 cells, nsP3 retained its ability to bind to G3BP1 and G3BP2, two components of the stress granules that have been implicated in CHIKV replication[21,23] (Extended Data Fig. 6e). We generated chimeric proteins in which the HVD region of CHIKV nsP3 is swapped with the corresponding domain of SINV nsP3 and vice versa. Whereas the CHIKV–SINV(HVD) chimeric protein lost its ability to bind to FHL1, the HVD of CHIKV in the context of the SINV nsP3 protein conferred binding to FHL1 (Extended Data Fig. 6f).

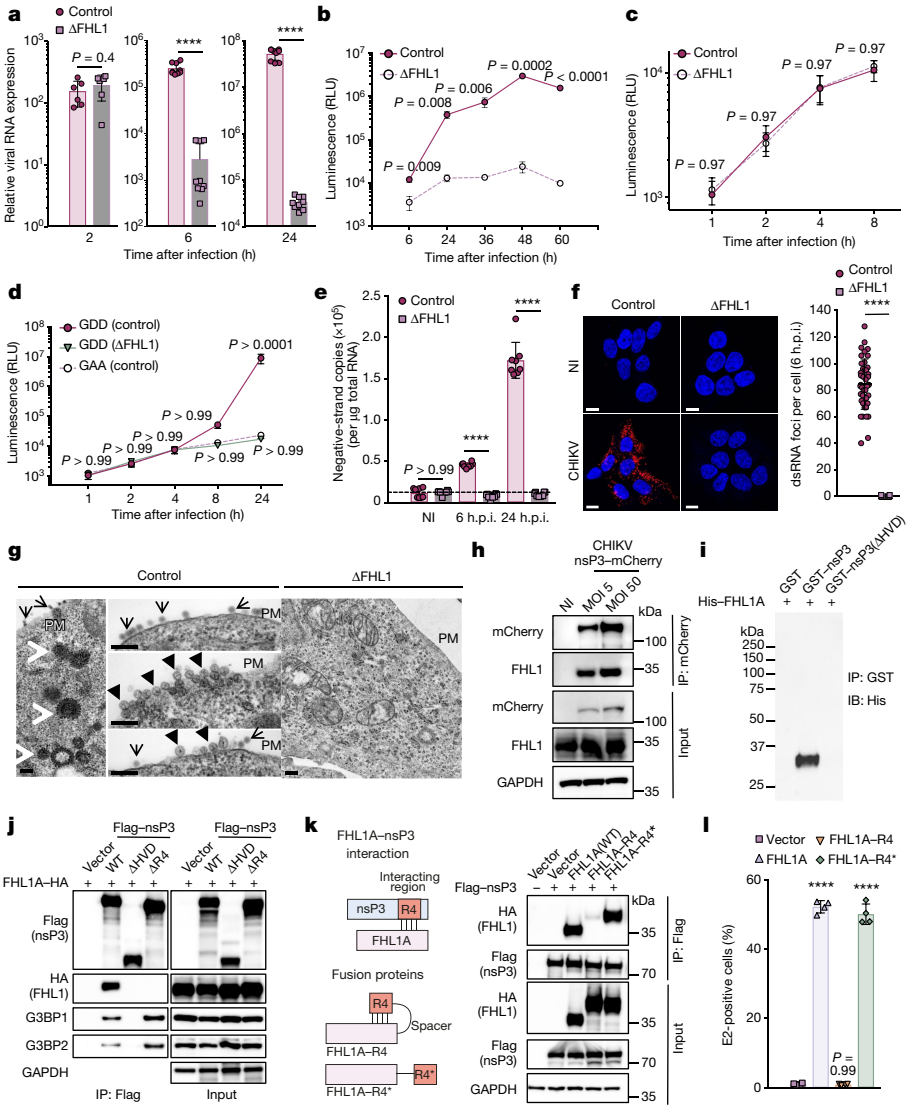

Fig. 2 | FHL1 interacts with CHIKV nsP3 and is required for CHIKV RNA replication. a, Control and ΔFHL1 HAP1 cells were inoculated with CHIKV21 (MOI of 10). At the indicated time points, cells were treated with trypsin to remove cell-surface-bound virus and viral RNA was quantified by RT–qPCR. Data are mean ± s.d. $n = 3$ independent experiments performed in triplicate, except for 2 h after infection, for which $n = 2$ independent experiments were performed. Two-tailed Student's *t*-test. **b**, Control or ΔFHL1 HEK293T cells were transfected with in vitro transcribed CHIKV-M RNA, expressing Gaussia luciferase (Gluc). Gluc activity was monitored at the indicated time points. RLU, relative light units. Data are mean ± s.e.m. $n = 3$ independent experiments performed in quadruplicate. Two-tailed multiple *t*-tests with Holm–Sidak correction. **c**, Control or ΔFHL1 HEK293T cells were transfected with a replication-deficient mutant CHIKV (CHIKV(GAA)) RNA, expressing Rluc and Rluc activity was monitored at the indicated time points. Data are mean ± s.e.m. $n = 3$ independent experiments performed in quadruplicate. Two-tailed multiple *t*-tests with Holm-Sidak correction). **d**, Control or ΔFHL1 HEK293T cells were transfected with a replication-competent (CHIKV(GDD)) or a replication-deficient mutant CHIKV (CHIKV(GAA)) capped RNA expressing Rluc. The Rluc activity was monitored at described in **c**. Data are mean ± s.e.m. $n = 3$ independent experiments performed in quadruplicate. Two-way ANOVA with Tukey's multiple comparison test. **e**, Negative-stranded viral RNA quantification by RT–qPCR from samples collected in **a**. h.p.i., hours post-infection; NI, not infected. Data are mean ± s.d. $n = 2$ independent experiments in quadruplicate. One-way ANOVA with a Tukey's multiple comparison test. Dashed line represents the experimental background threshold. **f**, Control and ΔFHL1 HEK293T cells were inoculated with CHIKV21 (MOI of 50). Left, representative images of infected cells stained with anti-dsRNA monoclonal antibody 6 h after infection. Scale bars, 10 µm. Right, number of foci per cell was quantified using the Icy software. Data are from 2 experiments, $n = 42$ cells in control and $n = 45$ cells in ΔFHL1 cells. Data are mean ± s.d. Two-tailed Student's *t*-test. **g**, Transmission electron microscopy of control and ΔFHL1 HAP1 cells challenged with CHIKV21 (MOI of 100) at 24 h after infection. Data are representative of two independent experiments. Left, CPV-II structures containing attached nucleocapsids at their cytoplasmic side (white arrows) as well as viral particles at the cell surface (thin black arrows). Middle, replication spherules (arrowheads) together with viral particles (thin black arrows) at the plasma membrane (PM). Scale bars, 200 nm. **h**, Co-immunoprecipitation of endogenous FHL1 and CHIKV nsP3 from cell lysates of HEK293T cells infected with a CHIKV nsP3-mCherry reporter virus at MOI of 5 or 50. **i**, In vitro co-immunoprecipitation (IP) analysis of the direct interaction between CHIKV nsP3 and FHL1A through the HVD domain. Glutathione *S*-transferase (GST) precipitation of wild-type GST–nsP3 or GST–nsP3(ΔHVD) and immunoblot (IB) analysis of 6×His–FHL1A. **j**, HEK293T cells were co-transfected with plasmids encoding haemagglutinin (HA)-tagged FHL1A (FHL1A–HA) and Flag-tagged wild-type CHIKV nsP3, CHIKV nsP3(ΔHVD) or CHIKV lacking the amino acid region 423–454 (ΔR4). Proteins from cell lysates were immunoprecipitated with anti-Flag beads followed by immunoblot analysis with Flag, HA and G3BP1 and G3BP2 antibodies. **k**, Left, schematic representation of FHL1A fused to the nsP3 interacting region (FHL1A–R4) or a similar randomized sequence (FHL1A–R4*). Right, immunoassay of the interaction between CHIKV nsP3 and FHL1A fusion proteins in HEK293T cells co-transfected with Flag-tagged CHIKV nsP3 and HA-tagged FHL1A, FHL1A–R4 or FHL1A–R4* constructs. Proteins from cell lysates were immunoprecipitated with Flag antibody followed by immunoblot analysis with Flag and HA antibodies. **g**–**k**, Data are representative of three independent experiments. **l**, ΔFHL1 HEK293T cells were transfected with an empty vector or plasmids encoding FHL1A, FHL1A–R4 or FHL1A–R4*. Cells were incubated with CHIKV21 (MOI of 5) and infection was quantified 24 h after infection by flow cytometry. Data are mean ± s.d. $n = 2$ independent experiments performed in duplicate. One-way ANOVA with Dunnett's multiple comparison test. ****$P < 0.0001$.

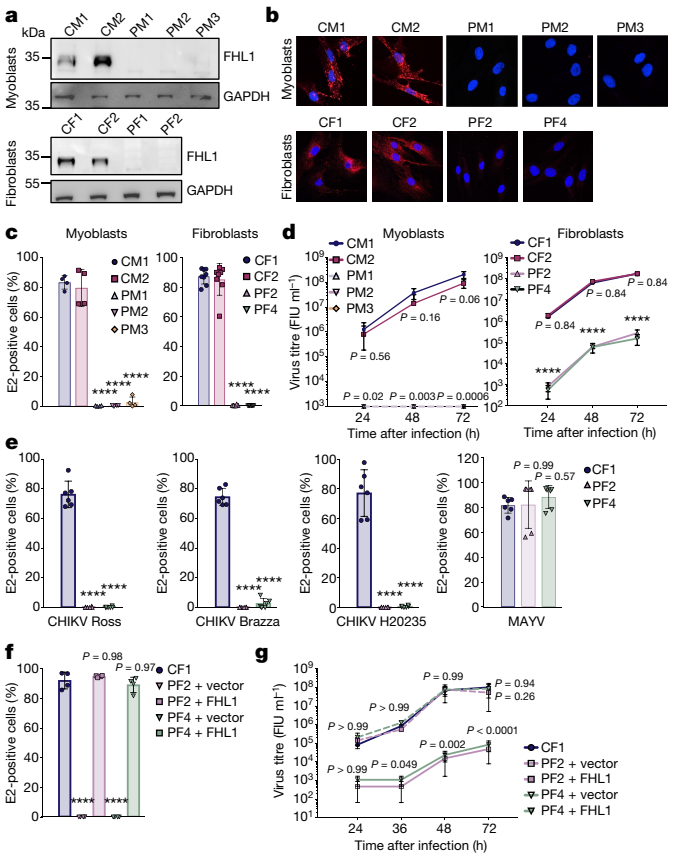

Fig. 3 | Primary cells from patients with FHL1 deficiency are resistant to CHIKV infection. a, FHL1 expression in primary myoblasts and fibroblasts from healthy donors or patients with EDMD. CF1, CF2, control fibroblasts from healthy donors; CM1, CM2, control myoblasts from healthy donors, PF2, PF4, fibroblasts from patients with EDMD; PM1–PM3, myoblasts from patients with EDMD. Data are representative of two independent experiments. **b**, Cells from healthy donors (control) or patients with EMDM were inoculated with CHIKV expressing nsP3–mCherry. At 48 h after infection, cells were fixed and images were taken using a fluorescence microscope. Images are representative of three experiments. **c**, E2 protein expression in primary cells from healthy donors (control) or patients with EDMD infected with CHIKV21 (MOI of 2). Data are mean ± s.d. $n = 2$ independent experiments performed in duplicate for myoblasts; $n = 3$ independent experiments performed in duplicate for fibroblasts. One-way ANOVA with Tukey's multiple comparison test. **d**, Quantification of viral particles released in the supernatant of infected cells collected at 24, 48 and 72 h after infection. FIU, flow cytometry infectious units. Data are mean ± s.e.m. 2 independent experiments performed in duplicates for myoblasts; $n = 3$ independent experiments performed in duplicate for fibroblasts. Two-tailed multiple *t*-test with Holm–Sidak correction. **e**, Primary fibroblasts from a control (CF1) or from two patients with EDMD (PF2, PF4) were inoculated with CHIKV Ross, CHIKV Brazza, CHIKV H20235 strains or MAYV (MOI of 2) and analysed for E2 expression. Data are mean ± s.d. $n = 3$ independent experiments performed in duplicate. One-way ANOVA with Dunnett's multiple comparison test). **f**, **g**, Fibroblasts from control (CF1) or patients with EDMD (PF2, PF4) were transduced with a lentiviral vector encoding FHL1A or a control vector and then challenged with CHIKV21 (MOI of 2). **f**, Infection was quantified as described in **c**. Data are mean ± s.d. $n = 2$ independent experiments performed in duplicate. One-way ANOVA with Tukey's multiple comparison test. **g**, Supernatants were collected from infected cells at the indicated time points and viral titres were measured on VeroE6 cells. Data are mean ± s.e.m. $n = 2$ independent experiments performed in duplicate. Two-way ANOVA with Dunnett's multiple comparison test. ****$P < 0.0001$.

Pull-down experiments showed that FHL1A directly binds to wild-type nsP3 but not to the HVD-deficient variant (Fig. 2i and Extended Data Fig. 6g). We then mapped the binding region within CHIKV nsP3(HVD) that is responsible for interaction with FHL1A (Fig. 2j and Extended Data Fig. 7). The FHL1-binding domain, referred as HVD R4, is present in all CHIKV and ONNV strains, located upstream of the G3BP1- and G3BP2-binding sites[21] (Fig. 2j and Extended Data Fig. 7a). Deletion of the HVD R4 region strongly impaired the interaction of FHL1 with nsP3, without affecting G3BP1 and/or G3BP2 binding to the viral protein (Fig. 2j and Extended Data Fig. 7b). We generated two chimeric FHL1A proteins that were fused either to the HVD R4 peptide (FHL1A–R4) or to a randomized peptide sequence of HVD R4 (FHL1A–R4*) as a positive control (Fig. 2k and Extended Data Fig. 7c), and assessed their ability to bind to nsP3. Whereas FHL1A-R4 failed to bind to nsP3 (Fig. 2k), FHL1A–R4* interacted with nsP3 as efficiently as wild-type FHL1A (Fig. 2k), indicating that the fused HVD R4 peptide probably hides the binding site of FHL1A to nsP3, inhibiting their interaction. Trans-complementation of ΔFHL1 cells with a cDNA encoding FHL1A–R4 did not restore CHIKV21 infection compared to

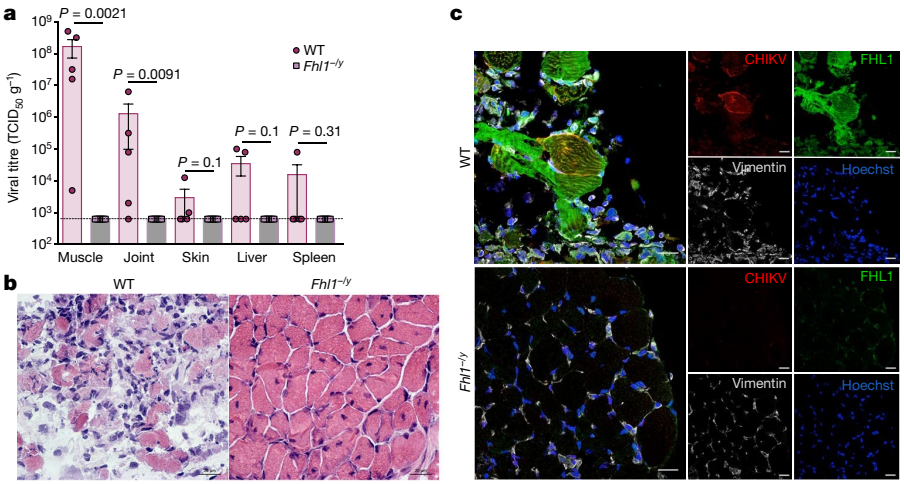

Fig. 4 | FHL1 is a factor of susceptibility to CHIKV infection in mice. a, Viral titres in tissues of 9-day-old mice. Wild-type (WT) male littermates ($n = 5$) and *Fhl1*$^{-/y}$ mice ($n = 7$) were inoculated with 10^5 plaque-forming units of CHIKV by intradermal injection and euthanized 7 days after infection. The amount of infectious virus in tissues was quantified as the $TCID_{50}$. The dashed line indicates the detection threshold. Data are mean ± s.e.m. Two-tailed *t*-test. **b**, Haematoxylin and eosin staining of transversal sections of skeletal muscle of CHIKV-inoculated mice. **c**, Immunostaining of nuclei (Hoechst), FHL1, vimentin and CHIKV in skeletal muscle of CHIKV-inoculated mice. **b**, **c**, Data are representative of $n = 3$ independent experiments.

FHL1A–R4* or wild-type FHL1A (Fig. 2l). In vitro transcribed RNA from a CHIKV molecular clone with a mutation in the FHL1-binding site (ΔR4 or R4*) showed a strong defect in replication in transfected HEK293T cells (Extended Data Fig. 7d). Together, these data show that the interaction between nsP3(HVD) and FHL1 is critical for the proviral function of FHL1.

Mutations in *FHL1* have been associated with X-linked myopathies[4,24], including Emery–Dreifuss muscular dystrophy (EDMD)[5], a rare genetic disorder characterized by early joint contractures, muscular wasting and adult-onset cardiac disease[25]. We studied the permissiveness of dermal fibroblasts and myoblasts to CHIKV that were obtained from four male patients with EDMD who carried mutations in *FHL1* as well as from two healthy donors (Extended Data Fig. 8a, b). FHL1 expression is severely reduced in primary cells from all four patients with EDMD (Fig. 3a). Infection studies showed that fibroblasts and myoblasts from patients with EDMD are resistant to CHIKV infection (Fig. 3b–e and Extended Data Fig. 8c, d) and exhibit a marked defect in the release of infectious particles (Fig. 3d). Cells of patients with EDMD remained highly susceptible to MAYV, which does not rely on FHL1 for replication (Fig. 3e). Trans-complementation of fibroblasts derived from patients with EDMD with a lentivirus that encodes FHL1A restored CHIKV viral antigen synthesis (Fig. 3f and Extended Data Fig. 8e) and the release of infectious particles (Fig. 3g).

To directly assess the role of FHL1 in the pathogenesis of CHIKV, we experimentally infected mice that did or did not express FHL1. Human and mouse FHL1 orthologues are highly conserved (Extended Data Fig. 9a). Mouse FHL1 interacts with CHIKV nsP3 and enhances viral infection, albeit less efficiently than its human orthologue (Extended Data Fig. 9b–d). Moreover, CHIKV infection is strongly impaired in the mouse muscle cell line C2C12 in which *Fhl1* is edited (Extended Data Fig. 9e, f). Susceptibility to CHIKV infection was tested in young male mice that were deficient in FHL1 expression and in young wild-type littermate male mice. CHIKV actively replicated in tissues of wild-type littermates as previously reported[16], but no infectious particles were detected in tissues of $Fhl1^{-/y}$ mice (Fig. 4a). Moreover, necrotizing myositis with large infiltrates and necrosis of the muscle fibres were observed in the skeletal muscle of wild-type littermates, whereas skeletal muscle of $Fhl1^{-/y}$ mice showed no detectable pathology (Fig. 4b). Immunolabelling against CHIKV E2 protein, FHL1 and vimentin in muscles revealed that in young wild-type mice, CHIKV mainly targets muscle fibres that express FHL1, whereas muscle cells of $Fhl1^{-/y}$ mice showed no labelling for CHIKV nor for FHL1 (Fig. 4c). These experiments demonstrate that $Fhl1^{-/y}$ mice are resistant to CHIKV infection.

In conclusion, our study identifies FHL1 as a critical host factor for CHIKV infection and pathogenesis. Indeed, the expression pattern of FHL1 reflects CHIKV tissue tropism. In addition to its direct implication for viral replication, hijacking of FHL1 by CHIKV may lead to cellular dysfunctions that contribute to the muscular and joint pains that are the hallmark of CHIKV disease. FHL1 interacts with CHIKV nsP3 to promote viral RNA synthesis. Deciphering the underlying mechanisms and understanding FHL1 selectivity for CHIKV will be essential to fully understand its pathogenesis and to develop novel therapeutic strategies to combat CHIKV disease.

Online content

Any methods, additional references, Nature Research reporting summaries, source data, extended data, supplementary information, acknowledgements, peer review information; details of author contributions and competing interests; and statements of data and code availability are available at https://doi.org/10.1038/s41586-019-1578-4.

Received: 19 February 2019; Accepted: 19 August 2019;
Published online 25 September 2019.

1. Burt, F. J. et al. Chikungunya virus: an update on the biology and pathogenesis of this emerging pathogen. *Lancet Infect. Dis.* **17**, e107–e117 (2017).
2. Silva, L. A. & Dermody, T. S. Chikungunya virus: epidemiology, replication, disease mechanisms, and prospective intervention strategies. *J. Clin. Invest.* **127**, 737–749 (2017).
3. Greene, W. K., Baker, E., Rabbitts, T. H. & Kees, U. R. Genomic structure, tissue expression and chromosomal location of the LIM-only gene, *SLIM1*. *Gene* **232**, 203–207 (1999).
4. Schessl, J., Feldkirchner, S., Kubny, C. & Schoser, B. Reducing body myopathy and other FHL1-related muscular disorders. *Semin. Pediatr. Neurol.* **18**, 257–263 (2011).
5. Gueneau, L. et al. Mutations of the *FHL1* gene cause Emery–Dreifuss muscular dystrophy. *Am. J. Hum. Genet.* **85**, 338–353 (2009).
6. Ooi, Y. S., Stiles, K. M., Liu, C. Y., Taylor, G. M. & Kielian, M. Genome-wide RNAi screen identifies novel host proteins required for alphavirus entry. *PLoS Pathog.* **9**, e1003835 (2013).
7. Karlas, A. et al. A human genome-wide loss-of-function screen identifies effective chikungunya antiviral drugs. *Nat. Commun.* **7**, 11320 (2016).
8. Zhang, R. et al. Mxra8 is a receptor for multiple arthritogenic alphaviruses. *Nature* **557**, 570–574 (2018).
9. Tanaka, A. et al. Genome-wide screening uncovers the significance of *N*-sulfation of heparan sulfate as a host cell factor for chikungunya virus infection. *J. Virol.* **91**, 1–22 (2017).
10. Schuffenecker, I. et al. Genome microevolution of chikungunya viruses causing the Indian Ocean outbreak. *PLoS Med.* **3**, e263 (2006).
11. Shathasivam, T., Kislinger, T. & Gramolini, A. O. Genes, proteins and complexes: the multifaceted nature of FHL family proteins in diverse tissues. *J. Cell. Mol. Med.* **14**, 2702–2720 (2010).
12. Brown, S. et al. Characterization of two isoforms of the skeletal muscle LIM protein 1, SLIM1. Localization of SLIM1 at focal adhesions and the isoform slimmer in the nucleus of myoblasts and cytoplasm of myotubes suggests distinct roles in the cytoskeleton and in nuclear–cytoplasmic communication. *J. Biol. Chem.* **274**, 27083–27091 (1999).
13. Krempler, A., Kollers, S., Fries, R. & Brenig, B. Isolation and characterization of a new FHL1 variant (FHL1C) from porcine skeletal muscle. *Cytogenet. Cell Genet.* **90**, 106–114 (2000).
14. Pen, A. E. et al. A novel single nucleotide splice site mutation in *FHL1* confirms an Emery–Dreifuss plus phenotype with pulmonary artery hypoplasia and facial dysmorphology. *Eur. J. Med. Genet.* **58**, 222–229 (2015).
15. Chan, K. K. et al. Molecular cloning and characterization of FHL2, a novel LIM domain protein preferentially expressed in human heart. *Gene* **210**, 345–350 (1998).
16. Couderc, T. et al. A mouse model for chikungunya: young age and inefficient type-I interferon signaling are risk factors for severe disease. *PLoS Pathog.* **4**, e29 (2008).
17. Roberts, G. C. et al. Evaluation of a range of mammalian and mosquito cell lines for use in Chikungunya virus research. *Sci. Rep.* **7**, 14641 (2017).
18. Kim, D. Y. et al. New World and Old World Alphaviruses have evolved to exploit different components of stress granules, FXR and G3BP proteins, for assembly of viral replication complexes. *PLoS Pathog.* **12**, e1005810 (2016).
19. Jose, J., Taylor, A. B. & Kuhn, R. J. Spatial and temporal analysis of alphavirus replication and assembly in mammalian and mosquito cells. *mBio* **8**, e02294-16 (2017).
20. Götte, B., Liu, L. & Mclnerney, G. M. The enigmatic alphavirus non-structural protein 3 (nsP3) revealing its secrets at last. *Viruses* **10**, 105 (2018).
21. Meshram, C. D. et al. Multiple host factors interact with the hypervariable domain of chikungunya virus nsP3 and determine viral replication in cell-specific mode. *J. Virol.* **92**, e00838-18 (2018).
22. Mutso, M. et al. Mutation of CD2AP and SH3KBP1 binding motif in alphavirus nsP3 hypervariable domain results in attenuated virus. *Viruses* **10**, 226 (2018).
23. Scholte, F. E. M. et al. Stress granule components G3BP1 and G3BP2 play a proviral role early in chikungunya virus replication. *J. Virol.* **89**, 4457–4469 (2015).
24. Schessl, J. et al. Proteomic identification of FHL1 as the protein mutated in human reducing body myopathy. *J. Clin. Invest.* **118**, 904–912 (2008).
25. Bonne, G., Leturcq, F. & Ben Yaou, R. in *GeneReviews* (eds Adam, M. P. et al.) (University of Washington, 1993).

METHODS

Cell culture. HAP1 cells (Horizon Discovery), which are derived from near-haploid chronic myeloid leukaemia KBM7 cells, were cultured in IMDM supplemented with 10% fetal bovine serum (FBS), 1% penicillin–streptomycin and GlutaMAX (Thermo Fisher Scientific). HEK293FT (Thermo Fisher Scientific), HEK293T (ATCC), Vero E6 (ATCC), BHK-21 (ATCC), HepG2 (gift of O. Schwartz), primary myoblasts and primary fibroblasts were cultured in DMEM supplemented with 10% FBS, 1% penicillin–streptomycin, 1% GlutaMAX and 25 mM HEPES. Human placenta choriocarcinoma BeWo cells were cultured in DMEM supplemented with 5% FBS, 1% penicillin–streptomycin, 1% GlutaMAX and 25 mM HEPES. AP61 mosquito (*Aedes pseudoscutellaris*) cells (gift from P. Despres) were cultured at 28 °C in Leibovitz medium supplemented with 10% FBS, 1% penicillin–streptomycin, 1% glutamine, 1× non-essential amino acids, 1× Tryptose phosphate and 10 mM HEPES. All cell lines were cultured at 37 °C in 5% CO_2 with the exception of AP61 cells, which were maintained at 28 °C without CO_2. Cell lines from ATCC were authenticated by the provider. HepG2, BeWo and AP61 were not further authenticated. All cell lines were tested for mycoplasma contamination.

Virus strains and culture. CHIKV21 (strain 06-21), ZIKV (HD78788) (gifts from P. Despres), CHIKV West Africa (strain 37997, accession AY726732.1) and DENV serotype 2 (16681) were propagated in mosquito AP61 cell monolayers with limited cell passages. CHIKV Brazza-MRS1 2011, CHIKV Ross, CHIKV St Martin H20235 2013 Asian, Ross River virus (strain 528v), MAYV (strain TC 625), ONNV (strain Dakar 234), SINV (strain Egypt 339), EEEV (strain H178/99), VEEV (strain TV83 vaccine), western equine encephalitis virus (strain 47A), SFV (strain 1745) were obtained from the European Virus Archive (EVA) collection and propagated with limited passages on Vero E6 cells.

pCHIKV-M-Gluc (see 'Plasmid constructions') and pCHIKV-mCherry molecular clones were derived from pCHIKV-M899, which is constructed from a CHIKV (strain BNI-CHIKV_899) strain isolated from a patient during the Mauritius outbreak in 2006. To generate infectious virus from CHIKV molecular clones, capped viral RNAs were generated from the NotI-linearized CHIKV plasmids using a mMESSAGE mMACHINE SP6 or T7 Transcription Kit (Thermo Fischer Scientific) according to the manufacturer's instructions. Resulting RNAs were purified by phenol:chloroform extraction and isopropanol precipitation, resuspended in water, aliquoted and stored at −80 °C until use. Subsequently 30 μg of purified RNAs were transfected in BHK21 cells with Lipofectamine 3000 reagent and supernatants were collected 72 h later were used for viral propagation on Vero E6 cells.

For all of the viral stocks used in flow cytometry experiments, viruses were purified through a 20% sucrose cushion by ultracentrifugation at 80,000*g* for 2 h at 4 °C. Pellets were resuspended in HNE1X pH 7.4 (HEPES 5 mM, NaCl 150 mM, EDTA 0.1 mM), aliquoted and stored at −80 °C. Viral stock titres were determined on Vero E6 cells by plaque-forming assay and are expressed as plaque-forming units (PFU) per ml. Virus stocks were also determined by flow cytometry as previously described[26,27]. In brief, Vero E6 cells were incubated for 1 h with 100 μl of tenfold serial dilutions of viral stocks. The inoculum was then replaced with 500 μl of culture medium and the percentage of E2-expressing cells was quantified by flow cytometry at 8 h after infection. Viral titres were calculated using the following formula and expressed as FIU per ml: Titre = (average percentage of infection) × (number of cells in well) × (dilution factor)/(ml of inoculum added to cells).

Reagents. The following antibodies were used: anti-FHL1 monoclonal antibody (MAB5938, R&D Systems), anti-FHL1 rabbit antibody (NBP1-88745, Novus Biologicals), anti-vimentin antibody (ab24525, Abcam), anti-GAPDH monoclonal antibody (SC-47724, Santa Cruz Biotechnology), polyclonal rabbit anti-HA (3724, Cell Signaling Technology), anti-Flag M2 monoclonal antibody (F1804, Sigma), anti-RFP (6G6, Chromotek), anti-CHIKV E2 monoclonal antibody (3E4 and 3E4 conjugated to Cy3), anti-alphavirus E2 monoclonal antibody (CHIK-265; gift from M. Diamonds), anti-EEEV E1 monoclonal antibody (MAB8754, Sigma), anti-pan-flavivirus E protein monoclonal antibody (4G2), anti-dsRNA J2 monoclonal antibody (Scicons), Alexa Fluor 488-conjugated goat anti-rabbit IgG (A11034, Invitrogen), Alexa Fluor-647-conjugated goat anti-chicken IgG (ab150175, Abcam), Alexa Fluor 488-conjugated goat anti-mouse IgG (115-545-003, Jackson ImmunoResearch), Alexa Fluor 647-conjugated goat anti-mouse IgG (115-606-062, Jackson ImmunoResearch), peroxydase-conjugated donkey anti-rabbit IgG (711-035-152, Jackson ImmunoResearch) and anti-mouse/HRP (P0260, DAKO Cytomotion). Flag magnetic beads (M8823, Sigma), HA magnetic beads (88837, Thermo Fisher Scientific) and anti-RFP coupled to magnetic agarose beads (RFP-Trap MA, Chromotek) were used for immunoprecipitation experiments.

CRISPR genetic screen. The GeCKO v.2 human CRISPR pooled libraries (A and B) encompassing 123,411 different sgRNA targeting 19,050 genes and cloned in the plentiCRISPR v.2[28] were purchased from GenScript. Lentiviral production was prepared independently for each half-library in HEK293FT cells by co-transfecting sgRNA plasmids with psPAX2 (from N. Manel) and pCMV-VSV-G at a ratio of 4:3:1 with Lipofectamine 3000 (Thermo Fisher Scientific). Supernatants were collected 48 h after transfection, cleared by centrifugation (750*g* for 10 min), filtered using a 0.45-μm filter and purified through a 20% sucrose cushion by ultracentrifugation (80,000*g* for 2 h at 4 °C). Pellets were resuspended in HNE1X pH 7.4, aliquoted and stored at −80 °C. HAP1 cells were transduced by spinoculation (750*g* for 2 h at 32 °C) with each CRISPR–sgRNA lentiviral library at a multiplicity of infection (MOI) of 0.3 and a coverage of 500× the sgRNA representation. Cells were selected with puromycin for 8 days and expanded. Then, 60 million cells from each library were pooled and inoculated with CHIKV21, a viral strain isolated during the 2005–2006 CHIKV outbreak in La Reunion Island[10]. Approximately 5 days after infection, cytopathic effects were detectable and surviving cells were collected 2 weeks later. Genomic DNA was extracted from selected cells or uninfected pooled cells using a QIAamp DNA column (Qiagen), and inserted gRNA sequences were amplified and sequenced using next-generation sequencing on an Illumina MiSeq (Plateforme MGX, Institut Génomique Fonctionelle). gRNA sequences were analysed using the MAGeCK software[29]. Additionaly, gRNA sequences were analysed using the RIGER software following previously published recommendations[30].

FHL1 editing. FHL1 was validated using two independent sgRNAs targeting exon 3 and exon 4, which are common to all FHL1 isoforms. sgRNA1 (5′-GAGGACTCCCCCAAGTGCAA-3′) and sgRNA2 (5′-GCAGTCAAACTTCTCCGCCA-3′) were cloned into the plasmid lentiCRISPR v.2 according to the recommendations of members of the Zhang laboratory. HAP1 and HEK293FT cells were transiently transfected with the plasmid expressing individual sgRNAs and selected with puromycin until all mock-transfected cells died (approximately 72 h). Transfected cells were used to ascertain gRNA-driven resistance to the cytopathic effects caused by CHIKV, and clonal cell lines were isolated by limiting dilution and assessed by immunoblot for FHL1 expression.

Infection assay. For infection quantification by flow cytometry analysis, cells were plated in 24-well plates. Cells were infected for 24 h (HEK293T cells) or 48 h (HAP1 cells), trypsinized and fixed with 2% (v/v) paraformaldehyde (PFA) diluted in PBS for 15 min at room temperature. Cells were incubated for 30 min at 4 °C with 1 μg ml^{-1} of the 3E4 anti-E2 monoclonal antibody (for CHIKV strains and ONNV), the CHIKV 265 anti-E2 monoclonal antibody (for MAYV), the anti-E1 monoclonal antibody (for EEEV) or anti-pan-flavivirus E 4G2 antibody (for DENV and ZIKV). Antibodies were diluted in permeabilization flow cytometry buffer (PBS supplemented with 5% FBS, 0.5% (w/v) saponin, 0.1% sodium azide). After washing, cells were incubated with 1 μg ml^{-1} of Alexa Fluor 488- or 647-conjugated goat anti-mouse IgG diluted in permeabilization flow cytometry buffer for 30 min at 4 °C. Acquisition was performed on an Attune NxT Flow Cytometer (Thermo Fisher Scientific) and analysis was done by using FlowJo software (TreeStar). To assess the release of infectious viral particles during infection, cells were inoculated for 3 h with viruses, washed once and then maintained in culture medium over a 72-h period. At the indicated time points, supernatants were collected and kept at −80 °C. Vero E6 cells were incubated with tenfold serial dilutions of supernatant for 24 h and E2 expression was quantified by flow cytometry as described above.

For detection of infected cells by immunofluorescence, control and ΔFHL1 HAP1 cells were plated on Laboratory-Tek II CC2 8-well glass slides (Nunc). Cells were inoculated with CHIKV21 (MOI of 20) or CHIKV nsP3–mCherry (MOI of 20) for 48 h, washed three times with cold PBS and fixed with 4% (v/v) PFA diluted in PBS for 20 min at room temperature. CHIKV E2 protein was stained with the 3E4 monoclonal antibody at 5 μg ml^{-1}, followed by a secondary staining with 1 μg ml^{-1} of Alexa 488-conjugated goat anti-mouse IgG. Both antibodies were diluted in PBS supplemented with 3% (w/v) BSA and 0.1% saponin. Slides were mounted with ProLong Gold antifade reagent containing DAPI for nuclear staining (Thermo Fisher Scientific).

For colocalization experiments, cells infected with CHIKV nsP3–mCherry (MOI of 20) were stained with 10 μg ml^{-1} of the anti-FHL1 monoclonal antibody, followed by secondary antibody staining with 1 μg ml^{-1} of Alexa 488-conjugated goat anti-mouse IgG.

For detection of dsRNA foci, control and ΔFHL1 HEK293T cells were plated on Laboratory-Tek II CC2 8-well glass slides (Nunc) and infected with CHIKV21 (MOI of 50) for 4 or 6 h. After fixation with 4% (v/v) PFA diluted in PBS, cells were stained with 5 μg ml^{-1} of the anti-dsRNA monoclonal antibody, followed by a secondary staining with 1 μg ml^{-1} of Alexa 488-conjugated goat anti-mouse IgG. Both antibodies were diluted in PBS supplemented with 3% (w/v) BSA and 0.1% Triton X-100. Of note, no dsRNA foci were detectable at 4 h after infection.

Fluorescence microscopy images were acquired using a LSM 800 confocal microscope (Zeiss).

Plasmid constructions. To generate the C-terminal HA-tagged FHL1 isoforms, the cDNAs of *FHL1A* (NM_001449.4), *FHL1B* (XM_006724746.2) and *FHL1C* (NM_001159703.1) were purchased from Genscript. Coding sequences were amplified with a common FHL1 forward primer (5′-CC**GGAGAATTC**GCCGCCATGGCGGAGAAGTTTGACTGCCACTACTGC-3′); and specific *FHL1A* reverse primer (5′-AATAGTTTA**GCGGCCGC**TCAAGCG TAATCTGGAACATCGTATGGGTATCCTCCAGCGGCCGACAGCTTTTTG GCACAGTCGGGACAATACACTTGCTCC-3′); or specific *FHL1B* and *FHL1C*

reverse primer (5′-AATAGTTTA**GCGGCCGC**TCAAGCGTAATCTGGAACATCGTATGGGTATCCTCCAGCGGCCGACGGAGCATTTTTTGCAGTGGAAGCAGTAGTCGTGCC-3′) (segments hybridizing with the target sequence are underlined; restriction endonuclease sites for cloning are highlighted in bold); and cloned into a pLVX-IRES-ZsGreen1 vector (Takara). Using the same approach, the coding sequence of mouse *Fhl1* (NM_001077362.2) was amplified with a mouse *Fhl1* forward primer (5′-CCGGAGAATTCGCCGCCATGGCTTCTCAAAGACACTCAGGTCCCTCC-3′) and mouse *Fhl1* reverse primer (5′-AATAGTTTAGCGGCCGCTCAAGCGTAATCTGGAACATCGTATGGGTATCCTCCAGCGGCCGACAGCTTTTTGGCACAGTCAGGGCAATACACCGCTC-3′), and cloned into a pLVX-IRES-ZsGreen1 vector. The C-terminal HA-tagged human *FHL2* coding sequence was synthesized by Genscript and subcloned into a pLVX-IRES-ZsGreen1 vector. The pCI-neo-3×Flag plasmids expressing CHIKV nsP3 and nsP4, SINV and SFV nsP3 proteins were previously described[31]. The CHIKV nsP3(ΔHVD), ΔR1 to ΔR4 proteins were generated by site-directed mutagenesis (QuickChange XL Site-Directed Mutagenesis Kit, Agilent) using the following sets of primers: ΔHVD forward (5′-CGTAAGTCCAAGGGAATATTGATGATCTTCCCAGGAGTCTGC-3′) and ΔHVD reverse (5′-GCAGACTCCTGGGAAGATCATCAATATTCCCTTGGACTTACG-3′); ΔR1 forward (5′-GTACCTGTCGCGCCGCCCAGAGAGCTGTGTCCGGTCGTACAAGAAAC-3′) and ΔR1 reverse (5′-GTTTCTTGTACGACCGGACACAGCTCTCTGGGCGGCGCGACAGGTAC-3′); ΔR2 forward (5′-GAAACAGCGGAGACGCGTGACAGTACCGCCACGGAACCGAATC-3′) and ΔR2 reverse (5′-GATTCGGTTCCGTGGCGGTACTGTCACGCGTCTCCGCTGTTTC-3′); ΔR3 forward (5′-CTTCTTACCAGGAGAAGTGTGATGACTTGACAGACAGC-3′) and ΔR3 reverse (5′-GCTGTCTGTCAAGTCATCACACTTCTCCTGGTAAGAAG-3′); ΔR4 forward (5′-GACGAGAGAAGGGAATATAACACCGAGTACCGCCACGGAACCGAATC-3′) and ΔR4 reverse (5′-GATTCGGTTCCGTGGCGGTACTCGGTGTTATATTCCCTTCTCTCTCTCGTC-3′).

The plasmids expressing chimeric nsP3 CHIKV–HVD SINV and nsP3 SINV–HVD CHIKV were obtained as follows. First, the DNA sequence encoding the N-terminal parts of the CHIKV or SINV nsP3 (MD-AUD region) were obtained by PCR using the pCI-neo-3×Flag expression plasmids as templates and the following sets of primers: 3×Flag NotI forward (5′-ACTGAGCGGCCGCATGGACTACAAAGACCATGAC-3′) and overlap CHIKV–SINV reverse (5′-GCTGTTCTGGCACTTCTATATATTCCCTTGGACTTACG-3′), or 3×Flag NotI forward and overlap SINV–CHIKV reverse (5′-CAGACTCCTGGGAAGATCTGTACTTACGGGCGGGAAC-3′) for CHIKV and SINV constructs, respectively. HVD coding sequences were also generated by PCR using the following primers: overlap CHIKV–SINV forward (5′-CGTAAGTCCAAGGGAATATATAGAAGTGCCAGAACAGC-3′) and nsP3 SINV BamHI reverse (5′-ACTGAGGATCCTTAGTATTCAGTCCTCCTGCTC-3′) for SINV HVD; and overlap SINV–CHIKV forward (5′-GTTCCCGCCCGTAAGTACAGATCTTCCCAGGAGTCTG-3′) and nsP3 CHIKV BamHI reverse (5′-ACTGAGGATCCTCATAACTCGTCGTCCGTG-3′) for CHIKV HVD. Next, the CHIKV–HVD–SINV and SINV–HVD–CHIKV PCR fragments were obtained by overlap extension PCR using the previously obtained PCR products and the following sets of primers: 3×Flag NotI forward and nsP3 SINV BamHI reverse, or nsP3 CHIKV BamHI reverse. Finally, the chimeric PCR fragments were cloned into a NotI–BamHI-digested pLVX-IRES-ZsGreen1 vector (Takara).

The plasmid expressing FHL1A–R4 and FHL1A–R4* fusion proteins were also obtained by overlap extension PCR approach. First, the *FHL1A* part, which is common to both constructs, was amplified from a cDNA template (Genscript, NM_001449.4) using the common *FHL1* forward primer (5′-CCGGAGAATTCGCCGCCATGGCGGAGAAGTTTGACTGCCACTACTGC-3′) and the overlap *FHL1A* fusion reverse primer (5′-CGCCCTGGAAGTACAGGTTCTCGCCGCCGCCCAGCTTTTTGGCACAGTCGGGACAATAC-3′). Second, nsP3 R4 and R4* portions were obtained by PCR using either the pCI-neo-3×Flag-nsP3 expression plasmid or the pCHIKV-SG45-R4* plasmid (containing the randomized R4 region) as templates and the following set of primers: overlap *FHL1* fusion forward (5′-CGAGAACCTGTACTTCCAGGGCGGCGGCGGCCCCATGGCTAGCGTCCGATTCTTTAG-3′) and *FHL1* fusion reverse (5′-AATAGTTTAGCGGCCGCTCAAGCGTAATCTGGAACATCGTATGGGTAGCCGCCGCCCCGGTGGTGCCTGAAGAGACATTGCTG-3′) for the R4 construct; or *FHL1* fusion Random reverse primer (5′-AATAGTTTAGCGGCCGCTCAAGCGTAATCTGGAACATCGTATGGGTAGCCGCCGCCCCTCACCTCGGCGCACATGG-3′) for the randomized R4* construct. Next, the FHL1A–R4 and FHL1A–R4* PCR fragments were obtained by PCR using the previously obtained PCR products and the outer sets of primers: *FHL1A* forward and *FHL1* fusion reverse or *FHL1* fusion Rand reverse. Amplification fragments were cloned into a NotI–EcoRI-digested pLVX-IRES-ZsGreen1 vector (Takara).

To obtain pCHIKV-M-Gluc, a viral sequence encompassing the CHIKV 26S promoter and part of the capsid protein sequence was amplified from pCHIKV-M using primers (5′-TATGCGTTTAAACCATGGCCACCTTTGCAAGCTCCAGATC-3′) and (5′-GCTTCTTATTCTTCCGATTCCTGCGTGG-3′), cut with PmeI and BssHII and assembled together with an AgeI–PmeI fragment from pCHIKVRepl-Gluc[32] into an AgeI–BssHII cut vector. From the resulting plasmid the AgeI–BssHII fragment was released and ligated together with a BssHII–SfiI fragment from pCHIKV-M[33] into pCHIKV-M cut with AgeI and SfiI.

To establish pCHKV-Rluc-GAA, two PCR fragments were amplified from wild-type CHIKV using primers CHIKV 5590 F (5′-AGACTTCTTACCAGGAGAAGTG-3′) and Bo422 (5′-CGACTCCATGTATTATGTTACCCGCTGCGATGAAGGCCGCGCACGCGG-3′) or Bo421 (5′-CCGCGTGCGCGGCCTTCATCGCAGCGGGTAACATAATACATGGAGTCG-3′) and CHIKV 8512 R (5′-GAAGTTGTCCTTGGTGCTGC-3′), respectively. The obtained fragments were fused via PCR amplification using the outer primers CHIKV 5590 forward and CHIKV 8512 reverse. The resulting fragment was cut with AgeI and BglI and inserted into pCHIKV-Rluc cut with the same restriction enzymes.

For generation of CHIKV-Rluc-ΔR4 and CHIKV-Rluc-R4*, PCR fragments encompassing the desired changes were first amplified and assembled as follows. For CHIKV-Rluc-ΔR4, two fragments were amplified from CHIKV-Rluc using Bo408 (5′-CACCACGTGCTCCTGGTCAGTG-3′) and Bo1259 (5′-GATTCGGTTCCGTGGCGGTACTCGGTGTTATATTCCCTTCTCTCTCGTCA-3′) or Bo1258 (5′-tGACGAGAGAGAAGGGAATATAACACCGAGTACCGCCACGGAACCGAATC-3′) and Bo409 (5′-GACTTCCTCCAGGGTGTTCACC-3′) and Bo409 (5′-GACTTCCTCCAGGGTGTTCACC-3′), respectively, and were fused together using the outer primers Bo408 and Bo409. For CHIKV-Rluc-R4*, the randomized sequence cassette was obtained sequentially from three successive PCRs. First, the PCR fragment was generated using primers Bo1260 (5′-AGCACCGTGCCCCTGCCCGCCCTGAGGAGGGCCAGCTTCGCCGACACCATGGAGCAGACC-3′) and Bo1261 (5′-CCTCACCTCGGCGCACATGGGGAACTGCTCGGCCACGGTCTGCTCCATGGTGTCGGCGAA-3′). Then, it was fused at the 5′ end with a PCR fragment amplified from CHIKV-Rluc with Bo408 and Bo1262 (5′-TCAGGGCGGGCAGGGGCACGGTGCTtgttatattcccttctctctcgtca-3′). Next, the resulting fragment was further fused at the 3′ end with a PCR fragment amplified from CHIKV-Rluc with Bo1263 (5′-GTTCCCCATGTGCGCCGAGGTGAGGccgagtaccgccacggaaccgaatc-3′) and Bo409, using the outer primers Bo408 and Bo409. Finally, the PCR fragments containing the ΔR4 and R4* mutations were cut with SacII and AgeI and fused with a NgoMIV–SacII fragment derived from CHIKV-Rluc (SG45) and cloned into a NgoMIV–AgeI-digested SG45 plasmid.

Trans-complementation and overexpression experiments. The lentiviral plasmids containing FHL1 isoforms were packaged as described above (see 'CRISPR genetic screen'). Cells of interest were stably transduced by spinoculation (750*g* for 2 h at 32 °C) with these lentiviruses and, when necessary, sorted for GFP-positive cells by flow cytometry. For trans-complementation assays, cells were inoculated with CHIKV21 for 48 h. Cells were then collected and processed for E2 expression by flow cytometry. For ectopic expression, cells were plated on 24-well plates (5×10^4) and incubated with CHIKV-M-Gluc and CHIKV21, and either processed for E2 expression by flow cytometry or infectious virus yield quantification on Vero E6 cells.

Kinetic of infection by RT–qPCR assay. Control and ΔFHL1 HAP1 cells were plated on 60-mm dishes (400,000 cells) and inoculated with CHIKV21 (MOI of 5). At the indicated time points, cells were washed three times with PBS, incubated with 0.25% trypsin for 5 min at 37 °C to remove cell-surface-bound particles, and total RNA was extracted using the RNeasy Plus Mini kit (Qiagen) according to the manufacturer's instructions. cDNAs were generated from 500 ng total RNA using the Maxima First Strand Synthesis Kit following the manufacturer's instructions (Thermo Fisher Scientific). Amplification products were incubated with 1 unit of RNase H for 20 min at 37 °C, followed by 10 min at 72 °C for enzyme inactivation, and diluted tenfold in DNase/RNase-free water. RT–qPCR was performed using a Power Syber green PCR master Mix (Fisher Thermo Scientific) on a Light Cycler 480 (Roche). The primers used for RT–qPCR were: E1-C21 forward (5′-ACGCAGTTGAGCGAAGCAC-3′), E1-C21 reverse (5′-CTGAAGACATTGGCCCCAC-3′) for viral RNA quantification, and Quantitect primers for *GAPDH* were purchased from Qiagen. Quantification using relative expression was performed based on the comparative threshold cycle (C_t) method, using *GAPDH* as endogenous reference control. CHIKV negative-strand RNA was quantified as previously described[34]. In brief, cDNA was generated from 1 μg total RNA using a primer containing a 5′ tag sequence CHIKV(−) tag (5′-GGCAGTATCGTGAATTCGATGCCGCTGTACCGTCCCCATTCC-3′) and the SuperScript II reverse transcriptase following the manufacturer's instructions (Thermo Fisher Scientific). Amplifications products were diluted tenfold and used for RT–qPCR with the following primers CHIKV(−) forward (5′-GGCAGTATCGTGAATTCGATGC-3′) and CHIKV(−) reverse

(5′-ACTGCTGAGTCCAAAGTGGG-3′). The 133-bp sequence corresponding to the amplified cDNA was synthesized by Genescript and serially diluted (650 to 6.5×10^9 genes copies μl^{-1}) to generate standard curves.

Genomic viral RNA transfection and kinetic of viral amplification. To assess CHIKV RNA replication within the cells, we transfected control and ΔFHL1 cells with capped genomic viral RNA generated from pCHIKV-M-Gluc (see 'Virus strains and culture'). Cells were plated on 48 well plate (3×10^4 cells) and transfected with 100 ng of purified RNA using the Lipofectamine MessengerMax reagent according to the manufacturer's instructions (Thermo Fisher Science), and cells were cultured in the absence or presence of 15 mM NH_4Cl to prevent subsequent viral propagation. At specific times, cells were washed once with PBS and lysed with *Gaussia* lysis buffer. Lysates were kept at −20 °C until all samples were collected. Luciferase activity was measured using the Pierce *Gaussia* Luciferase Glow assay kit on a TriStar2 LB 942 with 20 µl of cell lysate, 20 µl of substrate and 2 s integration time.

The same experimental approach was used to monitor luciferase activity from capped genomic viral RNA generated from wild-type pCHIKV-Rluc (SG45), pCHIKV-Rluc-GAA, pCHIKV-Rluc-ΔR4 and pCHIKV-Rluc-R4* mutants. Luciferase activity was measured using the *Renilla* luciferase assay system (Promega) on a TriStar2 LB 942 with 20 µl of cell lysate, 20 µl of substrate and 2.5 s integration time.

Immunoblots. Cell pellet were lysed in Pierce IP Lysis Buffer (Thermo Fisher Scientific) containing Halt protease and phosphatase inhibitor cocktails (Thermo Fischer Scientific) for 30 min at 4 °C. Equal amounts of protein, determined by DC Protein Assay (BioRad), were prepared in LDS sample buffer 4× (Pierce) containing 25 mM dithiothreitol (DTT) and heated at 95 °C for 5 min. Samples were separated on Bolt 4–12% Bis-Tris gels in Bolt MOPS SDS Running Buffer (Thermo Scientific), and proteins were transferred onto a PVDF membrane (BioRad) using the Power Blotter system (Thermo Fischer Scientific). Membranes were blocked with PBS containing 0.1% Tween-20 and 5% non-fat dry milk and incubated overnight at 4 °C with primary antibodies. Staining was revealed with corresponding horseradish peroxidase (HRP)-coupled secondary antibodies and developed using SuperSignal West Dura Extended Duration Substrate (Thermo Fisher Scientific) following the manufacturer's instructions. The signals were acquired through Fusion Fx camera (VILBERT Lourmat).

Co-immunoprecipitation assay. HEK293T cells were plated in 10-cm dishes (5×10^6 cells per dish). After 24 h, the cells were transfected with a total of 15 µg DNA expression plasmids (7.5 µg of each plasmid in co-transfection assays). After 24 h of transfection, the cells were washed once with PBS and collected with a cell scraper. After centrifugation (400*g* for 5 min), cell pellets were lysed for 30 min in cold immunoprecipitation lysis buffer supplemented with Halt protease and phosphatase inhibitor cocktails, and then cleared by centrifugation for 15 min at 6,000*g*. Supernatants were incubated overnight at 4 °C, with either anti-Flag magnetic beads or anti-HA magnetic beads (see 'Reagents'). Beads were washed three times with BO15 buffer (20 mM Tris-HCl pH 7.4, 150 mM NaCl, 5 mM $MgCl_2$, 10% glycerol, 0.5 mM EDTA, 0.05% Triton X-100, 0.1% Tween-20). The retained complexes were eluted twice with either 3×Flag peptide (200 µg ml^{-1}; Sigma-Aldrich F4799-4MG) or HA peptide (400 µg ml^{-1}; Roche 11666975001) for 30 min at room temperature. Samples were prepared and immunoblotted as described above. For input, 1% of whole-cell lysates was loaded on the gel.

Bacterial expression, purification and GST pull-down assay. To express nsP3 and nsP3(ΔHVD) as GST fusion proteins, their respective open reading frames were subcloned into pGEX-4T-1. Similarly, *FHL1A* cDNA was subcloned into pET47b(+) and expressed as a 6×His fusion protein. The following oligonucleotides were used to amplify nsP3 and nsP3ΔHVD cDNAs (sense, 5′-CCCCGGAATTCATGGCACCGTCGTACCGGGTAA-3′; antisense, 5′-CCGCTCGAGTCATAACTCGTCGTCCGTGTCTG-3′) and *FHL1A* (sense, 5′-CCGGAATTCCATGGCGGAGAAGTTTGACTGCC-3′; antisense, 5′-CCGCTCGAGTTACAGCTTTTTGGCACAGTC-3′). *Escherichia coli* strain BL21 Star (Invitrogen) was transformed with recombinant expression vectors encoding GST−nsP3, GST−nsP3(ΔHVD) or 6×His–FHL1A recombinant proteins. Transformed bacteria were induced with isopropylthio-β-Dgalactoside (IPTG) for 3 h at 37 °C. Cells were collected by centrifugation and the pellets were resuspended in lysis buffer containing lysozyme (1 mg ml^{-1}), incubated for 30 min at 4 °C followed by three subsequent freeze–thaw cycles and sonication. The bacterial lysates were centrifuged at 13,000 r.p.m for 20 min and the supernatants were incubated with glutathione-sepharose beads for GST–nsP3 and GST–nsP3(ΔHVD) or on a Ni-NTA column (Qiagen) for 6×His–FHL1A. Column washing and recombinant protein elution were performed according to the manufacturer's instructions. In brief, 5 µl of eluted GST-fusion proteins and 3 µl of Ni-NTA-eluted 6×His–FHL1A were analysed by SDS–PAGE and proteins were visualized by Coomassie staining. For pull-down assays, GST-, GST–nsP3- or GST–nsP3(ΔHVD)-bound beads were incubated with 6×His–FHL1A for 1 h at 4 °C in the presence of 100 µM $ZnSO_4$. The resin was washed extensively with a buffer containing 500 mM KCl. The beads were then resuspended in Laemmli buffer, resolved by SDS–PAGE and the presence of 6×His–FHL1A was assessed by western blot using the anti-FHL1 antibody.

Genetic analysis, fibroblasts and myoblasts from patients with EDMD. Dermal fibroblasts and myoblasts were taken from four patients carrying *FHL1* mutations. *FHL1* was analysed as previously reported[5], as the patients had, among other symptoms, features that were reminiscent of EDMD. Patients P1, P2 and P3 have been previously reported[5] with detailed clinical descriptions (respectively as patient F321-3, F997-8 and F1328-4), whereas information for patient P4 was not previously published. In brief, patient P4 had myopathy with joint contractures, hypertrophic cardiomyopathy, vocal cord palsy, short stature, alopecia, skin abnormalities and facial dysmorphism. In this patient, *FHL1* analysis revealed an insertion of a full-length LINE-1 retrotransposon sequence together with poly(A) tail of unknown length (indicated by a '?' thereafter) after 27 bp of the start of exon 4 (c.183–184ins, *LINE1*; ?; 171–183) that results at the mRNA level in altered splicing with retention of 108 bp of the inserted LINE sequence leading to a predicted premature termination codon and shorter *FHL1A* (Extended Data Fig. 8b).

Ethics statement. All materials (skin and/or muscle biopsies) from patients and controls included in this study were taken with the informed consent of the donors and with approval of the local ethical boards (that is, P1, Tokyo Women's Medical University, Japan; P2, King Saudi University, Saudi Arabia; P3, University Hospital of Lille, France; P4, University Hospital of Montpellier, France). All procedures were followed alongside the usual molecular diagnostic procedure during patient follow-up, and in accordance with the ethical standards of the responsible national committee on human experimentation.

In vivo studies. Animals were housed in the Institut Pasteur animal facilities accredited by the French Ministry of Agriculture for performing experiments on live rodents. Work on animals was performed in compliance with French and European regulations on care and protection of laboratory animals (EC Directive 2010/63, French Law 2013-118, 6 February 2013). All experiments were approved by the Ethics Committee 89 (and registered under the reference APAFIS#6954-2016091410257906 v.2). FHL1-deficient male mice (*Fhl1*$^{-/y}$) or wild-type male littermates were obtained by crossing *Fhl1* heterozygous females[35] with wild-type male Black Swiss mice. Subsequently, 9-day-old *Fhl1*$^{-/y}$ and wild-type male littermates, were injected with CHIKV21 (10^5 PFU per 20 µl) by intradermal route and viral load was determined in tissues on day 7 after inoculation. Virus titres in tissue samples were determined on Vero E6 cells as $TCID_{50}$ g^{-1}. For histology experiments, muscles were snap-frozen in isopentane cooled by liquid nitrogen for cryo-sectioning then processed for histological staining (haematoxylin and eosin) or immunolabelling.

Transmission electron microscopy. Cells were scraped and fixed for 24 h in 1% glutaraldehyde, 4% PFA (Sigma) in 0.1 M phosphate buffer (pH 7.2). Samples were then washed in PBS and post-fixed for 1 h by incubation with 2% osmium tetroxide (Agar Scientific). Cells were subsequently fully dehydrated in a graded series of ethanol solutions and propylene oxide. An impregnation step was performed with a mixture of (1:1) propylene oxide/Epon resin (Sigma) and then left overnight in pure resin. Samples were embedded in Epon resin (Sigma), which was allowed to polymerize for 48 h at 60 °C. Ultra-thin sections (90 nm) of these blocks were obtained with a Leica EM UC7 ultramicrotome. Sections were stained with 2% uranyl acetate (Agar Scientific), 5% lead citrate (Sigma) and observations were made with a transmission electron microscope (JEOL 1011).

Cell viability assay. Cell viability and proliferation were assessed using the CellTiter-Glo 2.0 assay (Promega) according to the manufacturer's protocol. In brief, cells were plated in 48-well plates (3×10^4). At specific times, 100 µl of CellTiter-Glo reagent were added to each well. After a 10-min incubation, 200 µl from each well was transferred to an opaque 96-well plate (Cellstar, Greiner Bio-One) and luminescence was measured on a TriStar2 LB 942 (Berthold) with 0.1 s integration time.

Statistical analysis. Graphical representation and statistical analyses were performed using Prism 7 software (GraphPad software). Unless otherwise stated, results are shown as mean ± s.d. from at least two independent experiments in duplicates. Differences were tested for statistical significance using an unpaired two-tailed *t*-test, or one-way or two-way ANOVA with multiple comparison post hoc test.

Reporting Summary. Further information on research design is available in the Nature Research Reporting Summary linked to this paper.

Data availability

The authors declare that the data supporting the findings are available within the paper and its Supplementary Information. Source Data for Figs. 1–4 are provided with the paper. All other data are available from the corresponding authors upon request.

26. Medina, F. et al. Dengue virus: isolation, propagation, quantification, and storage. *Curr. Protoc. Microbiol*. **15**, 15D.2.1–15D.2.24 (2012).
27. Meertens, L. et al. The TIM and TAM families of phosphatidylserine receptors mediate dengue virus entry. *Cell Host Microbe* **12**, 544–557 (2012).
28. Shalem, O. et al. Genome-scale CRISPR–Cas9 knockout screening in human cells. *Science* **343**, 84–87 (2014).
29. Li, W. et al. MAGeCK enables robust identification of essential genes from genome-scale CRISPR/Cas9 knockout screens. *Genome Biol*. **15**, 554 (2014).
30. Joung, J. et al. Genome-scale CRISPR–Cas9 knockout and transcriptional activation screening. *Nat. Protoc.* **12**, 828–863 (2017).
31. Pellet, J. et al. ViralORFeome: an integrated database to generate a versatile collection of viral ORFs. *Nucleic Acids Res*. **38**, D371–D378 (2010).
32. Gläsker, S. et al. Virus replicon particle based chikungunya virus neutralization assay using *Gaussia* luciferase as readout. *Virol. J*. **10**, 235 (2013).
33. Kümmerer, B. M., Grywna, K., Gläsker, S., Wieseler, J. & Drosten, C. Construction of an infectious chikungunya virus cDNA clone and stable insertion of mCherry reporter genes at two different sites. *J. Gen. Virol*. **93**, 1991–1995 (2012).
34. Plaskon, N. E., Adelman, Z. N. & Myles, K. M. Accurate strand-specific quantification of viral RNA. *PLoS ONE* **4**, e7468 (2009).
35. Domenighetti, A. A. et al. Loss of FHL1 induces an age-dependent skeletal muscle myopathy associated with myofibrillar and intermyofibrillar disorganization in mice. *Hum. Mol. Genet.* **23**, 209–225 (2014).

Acknowledgements This study received funding from the French Government's Investissement d'Avenir program, Laboratoire d'Excellence 'Integrative Biology of Emerging Infectious Diseases' (ANR-10-LABX-62-IBEID), the 'Investissements d'Avenir' program (ANR-10-IHUB-0002, ANR-15-CE15-00029 ZIKAHOST and the INCEPTION program ANR-16-CONV-0005), Institut Pasteur, Inserm and European Research Council. Viruses were provided by the Europe and Virus Archive, which has received funding from the EU Horizon 2020 research and innovation program under grant agreement 653316. The authors thank the EA7310, Laboratoire de Virologie, Université de Corse-Inserm for funding the doctoral position of L.P. We thank F. Rey, O. Schwartz, N. Manel, H. de Thé, Y. Gaudin, J. Hellert, M.-L. Chaix, S. Marot, S. Chawki, A. Canat, A. Zamborlini, A. Saïb, F. Sigaux, S. Emiliani and F. Bachelerie for reading the manuscript and discussions; P. Thouvenot and D. Hardy for technical assistance; J. Chen and J. Bogomolovas for providing *Fhl1*$^{-/-}$ mice; M. Diamond and J. Fox, A. Merit and F. Tangy for providing the CHIKV 265 monoclonal antibody, the nsP3 antibodies and the alphavirus nsP1-4 constructs, respectively; and MGX-Montpellier facility for sequencing.

Author contributions L.M. and A.A. conceived the study. L.M., M.L.H., T.C., V.K., A.B., L.B.-M., C. Delaugerre, M.L. and A.A. designed the experiments. L.M. performed the CRISPR–Cas9 screening and infection studies with L.B.-M. M.L.H. characterized the FHL1 and nsP3 interactions and performed the immunoprecipitation and western blot studies with help of V.K. A.L. validated the gRNA targeting human and mouse FHL1 and generated the *FHL1*-knockout cells described in this study and performed infection studies. A.B. performed the immunofluorescence microscopy experiments and some infection studies. L.M. and E.S.-L. analysed the gRNA sequencing studies and identified the hits. J.B.-G. and P.R. performed the electron microscopy experiments. C. Doyen and M.B. performed the GST pull-down experiments. B.M.K. generated the CHIKV molecular clones described in this study and P.-O.V. provided key CHIKV reagents. L.P. and X.d.L. provided the alphavirus strains and performed infection studies. T.C. and M.L. conceived and performed the in vivo studies and provided expertise in the design of CHIKV experiments. S.R. performed virus titration assays and mice genotyping. T.G. performed immunofluorescence experiments in mouse tissues with T.C. A.B.-L., R.B.Y., L.G., R.J.-M. and G.B. provided myoblasts and fibroblasts from patients with EDMD and the description of a new *FHL1* mutation in EDMD disease. L.M. and A.A. wrote the initial manuscript draft, M.L. edited the draft and the other authors contributed to editing it in its final form.

Competing interests The authors declare no competing interests.

Additional information

Supplementary information is available for this paper at https://doi.org/10.1038/s41586-019-1578-4.

Correspondence and requests for materials should be addressed to L.M. or A.A.

Peer review information *Nature* thanks Laurie A. Silva and the other, anonymous, reviewer(s) for their contribution to the peer review of this work.

a

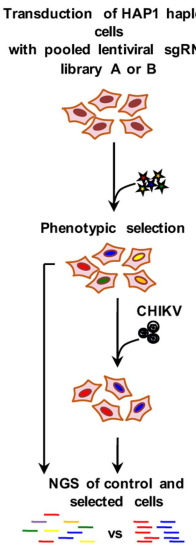

b

Ranked Genes	MAGeCK rank	RIGER Rank
FHL1	1	1
SLC35B2	2	2
PAPSS1	3	3
ELAVL1	4	4
FURIN	5	7
YBX1	6	6
GATAD1	7	5
B3GAT3	8	9
OR10W1	9	217
MTRNR2L5	11	18
COA5	12	436
POMT2	13	641
ELP5	14	47
PRIM2	16	337
NRCAM	17	238
PDE8B	18	78
EXT1	19	26
ELF2	20	10
MYT1L	21	381
CUL5	22	956
MAP4K3	23	37
ALDH18A1	24	107
ACTR10	25	13544
SLC7A6OS	26	2704
C11orf30	27	11
BID	28	8
SMOC1	30	507
SCGB1D1	32	84
RPE65	33	75
FAM124B	34	459

c

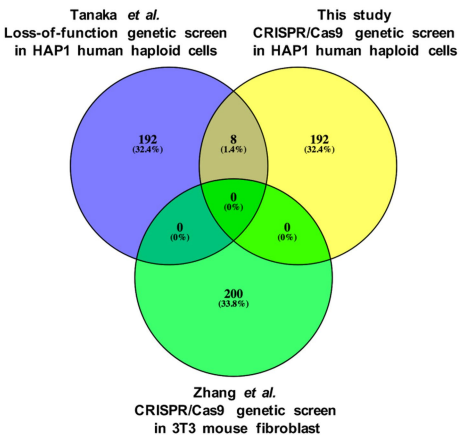

Extended Data Fig. 1 | CRISPR–Cas9 genetic screen identifies essential host factors of CHIKV infection. a, Schematic of CRISPR–Cas9 genome-wide screen in HAP1 haploid cells. **b**, Ranked list of the top 30 genes identified using the MAGeCK algorithm and their corresponding rank in RIGER analysis. **c**, Venn diagram comparing the top 200 hits from our screen and previously published CRISPR and haploid screens[8,9] for CHIKV host factors.

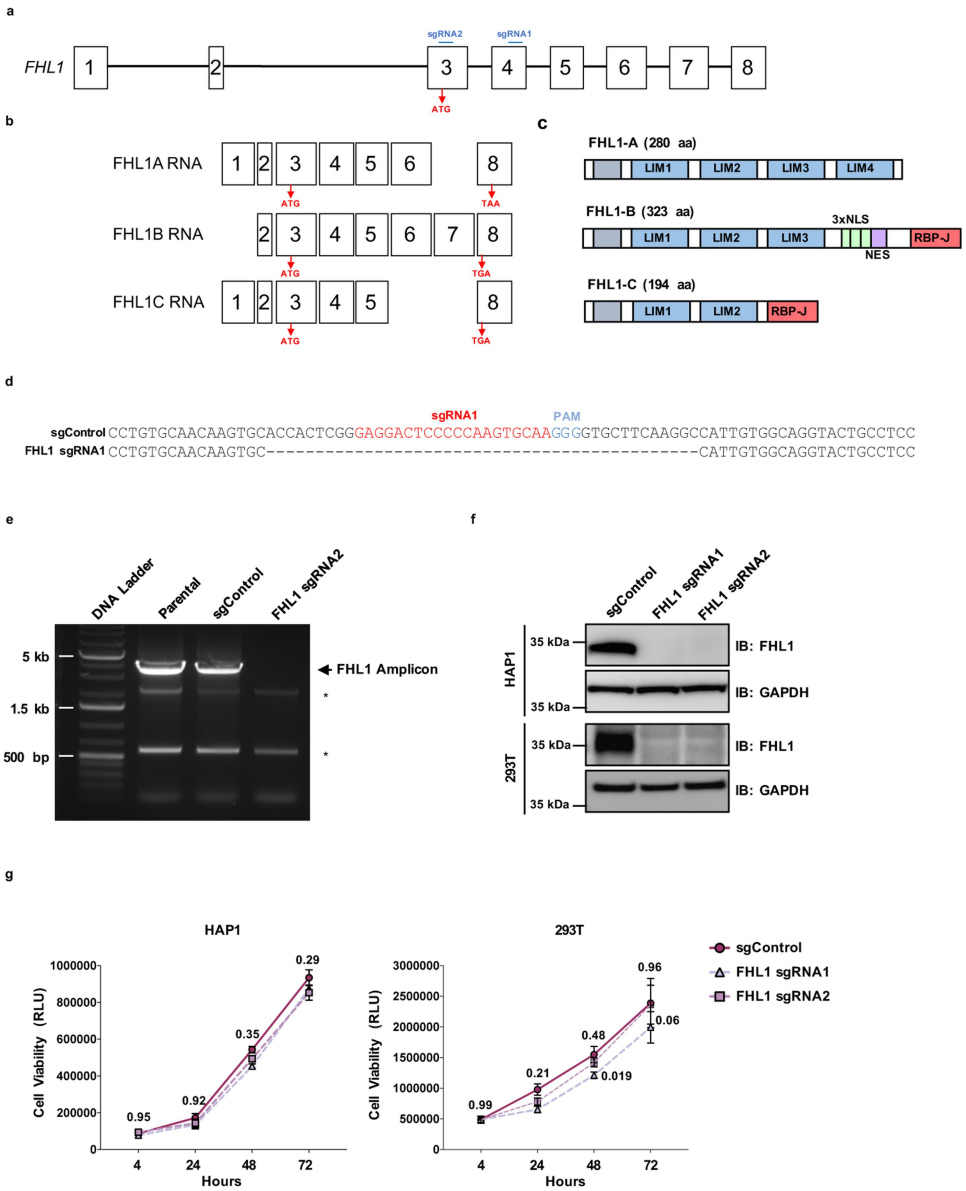

Extended Data Fig. 2 | Validation of *FHL1* gene edition by CRISPR–Cas9. a–**c**, Schematic of the genomic organization of *FHL1* (**a**), alternative splicing of the isoforms *FHL1A*, *FHL1B* and *FHL1C* (**b**) and their corresponding proteins (**c**). Initiation and stop codons are indicated in red and relative positions of the sequence targeted by the sgRNA are indicated in blue. **d**, Sanger sequencing of FHL1 in control and ΔFHL1 HAP1 cells. **e**, Genomic DNA was used for PCR amplification using primers flanking the sequence targeted by *FHL1* sgRNA2. The absence of an amplification product of 3.9 kb (black arrow) in the HAP1 clone suggests that a large indel is responsible for the absence of FHL1 expression. Asterisks indicate unspecific PCR products. Data are representative of two experiments. **f**, Immunoblot of FHL1 in control and ΔFHL1 cells. One representative experiment of three experiments is shown. **g**, Control and ΔFHL1 cells were plated and viability was assessed over a 72-h period using the CellTiter-Glo assay. Data shown are mean ± s.e.m. $n = 2$ independent experiments were performed in quadruplicate. Two-way ANOVA with Dunnett's multiple comparison test; *P* values are indicated.

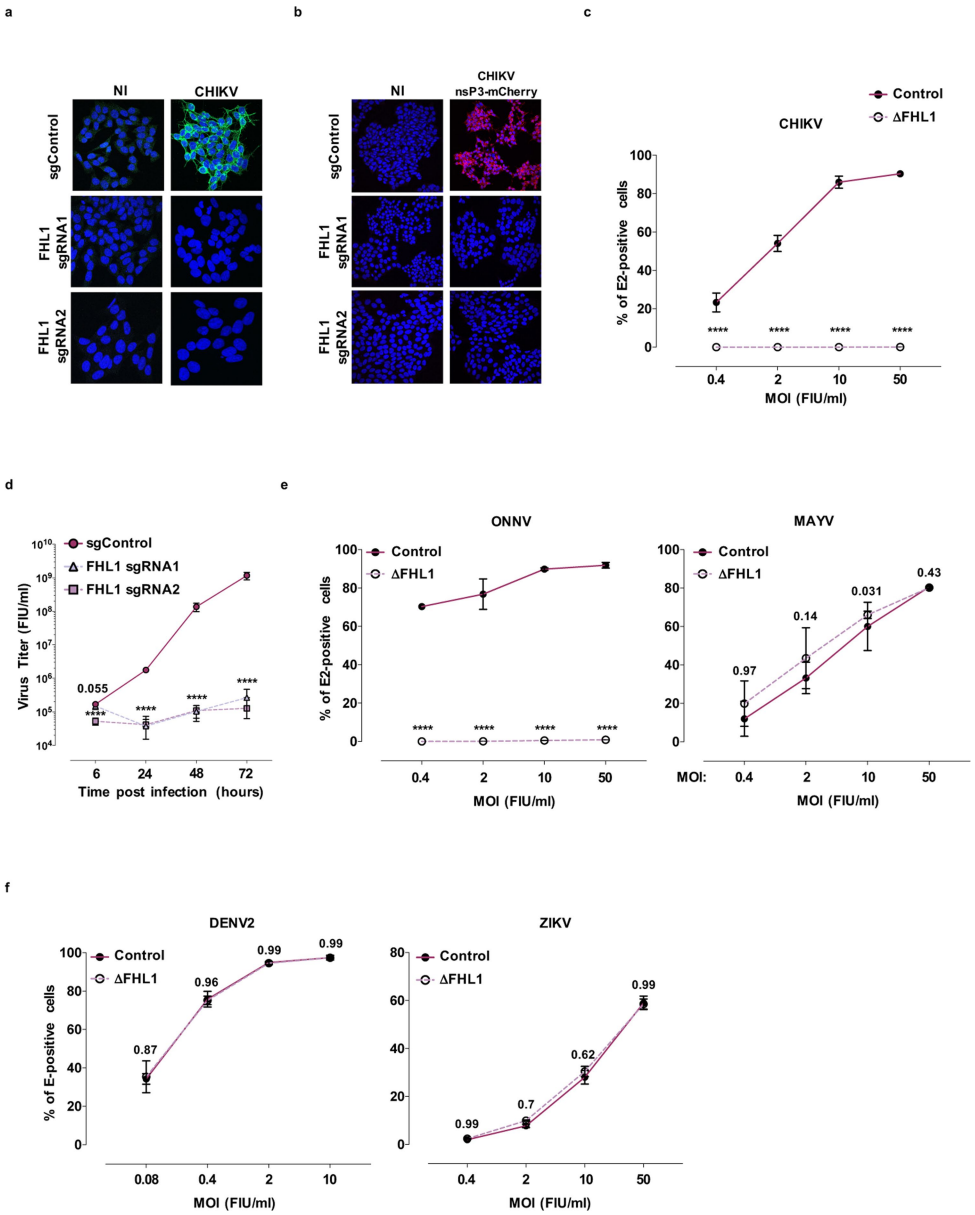

Extended Data Fig. 3 | FHL1 is an essential host factor for CHIKV and ONNV infection. a, Immunofluorescence images of control and ΔFHL1 HAP1 cells inoculated with CHIKV21 (MOI of 10), fixed 48 h after infection and stained for E2 expression. NI, not infected. **b**, Immunofluorescence images of control and ΔFHL1 HAP1 cells inoculated with CHIKV expressing nsP3–mCherry (MOI of 10) and fixed 48 h after infection. **a**, **b**, Images were taken on a fluorescence microscope and are representative of three experiments. **c**, Control and ΔFHL1 HAP1 cells were inoculated with increasing MOIs of CHIKV21, and infection was quantified 48 h after infection by flow cytometry using the anti-E2 3E4 monoclonal antibody. Data are mean ± s.d. $n = 3$ independent experiments performed in duplicate. Two-way ANOVA with Tukey's multiple comparison test. **d**, Multi-step growth curves with the CHIKV21 strain in control or ΔFHL1 cells. Data are mean ± s.e.m. $n = 2$ independent experiments performed in duplicate. Two-tailed multiple *t*-tests with Holm–Sidak correction. **e**, Control and ΔFHL1 HAP1 cells were inoculated with increasing MOIs of ONNV or MAYV, and infection was quantified 48 h later by flow cytometry using anti-E2 3E4 and 265 monoclonal antibodies. Data are mean ± s.e.m. $n = 2$ independent experiments performed in duplicate. Two-way ANOVA with Tukey's multiple comparison test. **f**, Control and ΔFHL1 HAP1 cells were inoculated with increasing MOIs of DENV or ZIKV, and infection was quantified 48 h later by flow cytometry using the anti-E 4G2 monoclonal antibody. Data are mean ± s.e.m. $n = 3$ independent experiments performed in duplicate. Two-way ANOVA with Tukey's multiple comparison test. ****$P < 0.0001$.

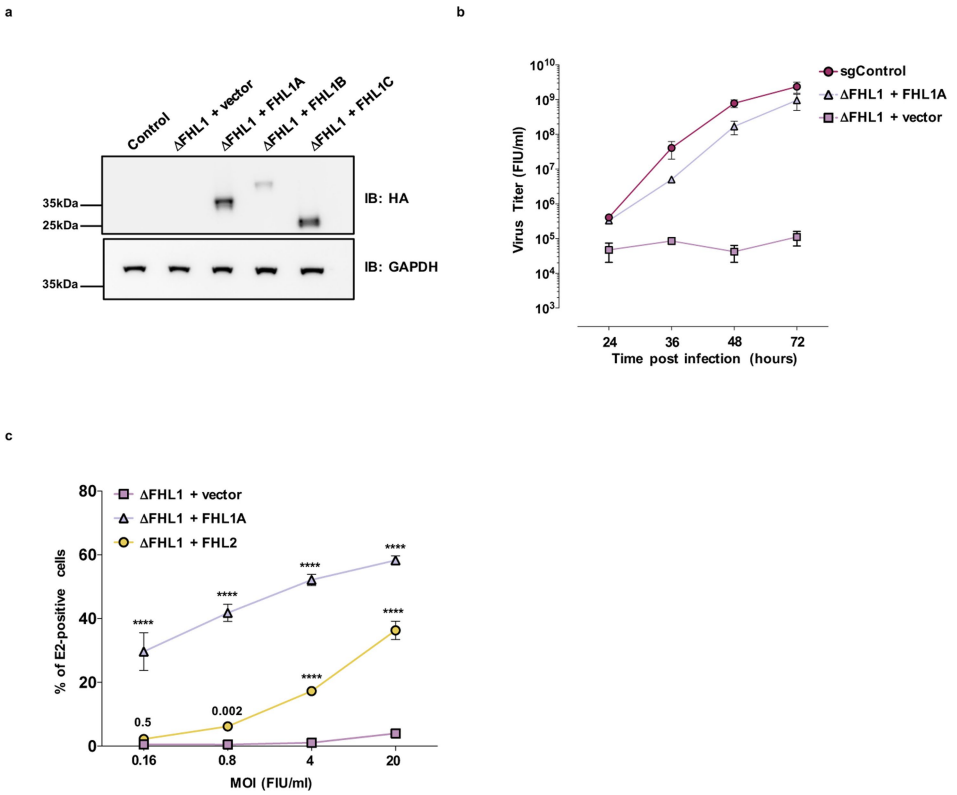

Extended Data Fig. 4 | FHL1A and FHL2 expression in ΔFHL1 cells restores CHIKV infection. a, Immunoblot (IB) of ectopic FHL1 expression in HAP1 cells stably transduced with an empty vector or FHL1A, FHL1B or FHL1C isoform. Data are representative of three experiments. **b**, Quantification in the supernatant of infected HAP1 cells of viral particles released by measuring the viral titre on Vero E6 cells. Data are representative of three experiments performed in duplicate. Data are mean ± s.e.m. **c**, ΔFHL1 HEK293T cells transfected with an empty vector or HA-tagged plasmids encoding FHL1A and FHL2 were infected with increasing MOIs of CHIKV21. Infection was quantified 24 h after infection by flow cytometry. Data are mean ± s.d. $n = 3$ experiments performed in duplicate. Two-way ANOVA with Dunnett's multiple comparison test. ****$P < 0.0001$.

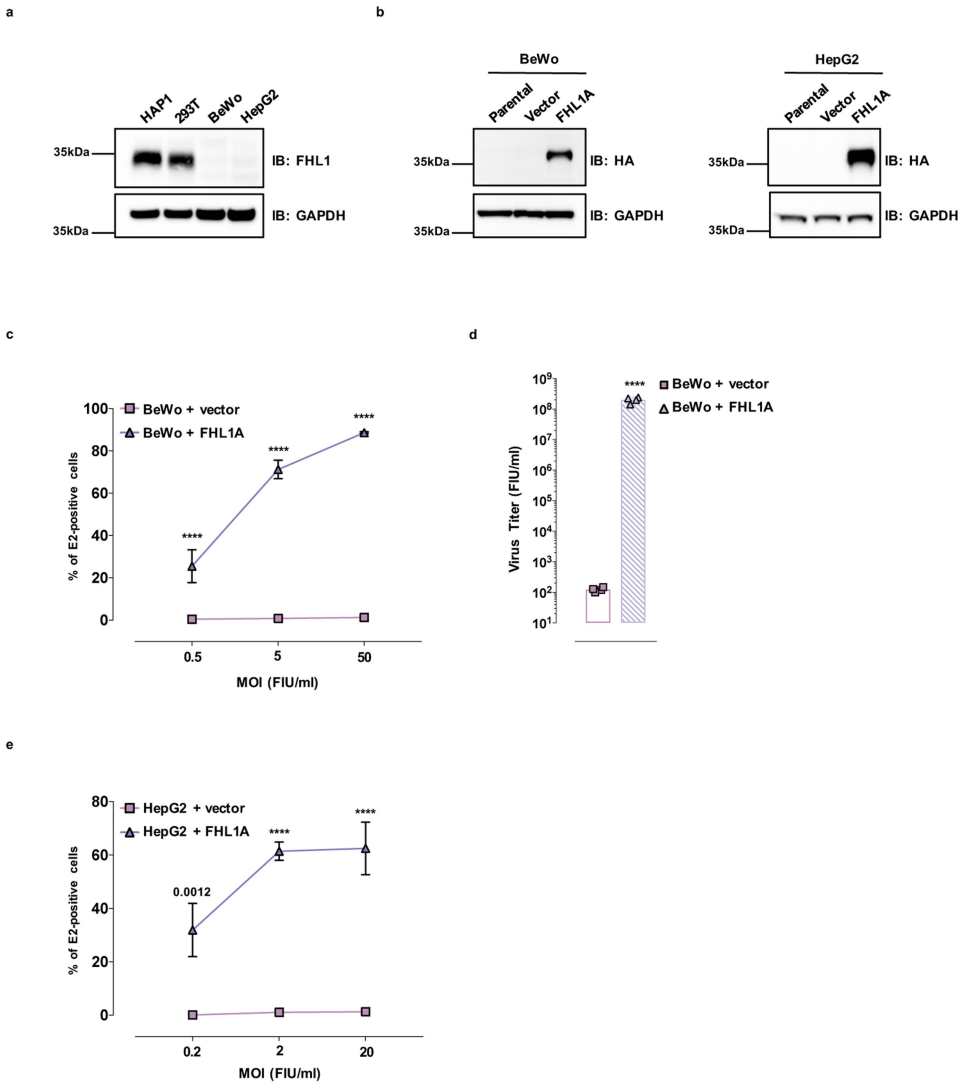

Extended Data Fig. 5 | FHL1A overexpression in BeWo and HepG2 cells enhances CHIKV infection. a, Expression of endogenous FHL1 in HAP1, HEK293T, BeWo and HepG2 cells. **b**, Immunoblot of ectopic FHL1 expression in Bewo and HepG2 cells stably transduced with an empty vector or HA-tagged FHL1A. **a**, **b**, Data are representative of three experiments. **c**, **d**, Bewo cells stably transduced with an empty vector or HA-tagged FHL1A were inoculated with increasing MOIs of CHIKV21. **c**, Infection was quantified 48 h after infection by flow cytometry using the anti-E2 3E4 monoclonal antibody. Data are mean ± s.e.m. $n = 3$ independent experiments performed in duplicate. Two-way ANOVA with Tukey's multiple comparison test. **d**, Quantification of the viral particles released into the supernatants of infected cells, measured as the viral titre on Vero E6 cells. Data are mean ± s.d. $n = 2$ independent experiments performed in duplicate. Two-tailed Student's *t*-test. **e**, HepG2 cells stably transduced with an empty vector or FHL1A were inoculated with increasing MOIs of CHIKV-M-Gluc. Infection was quantified 48 h later as indicated in **c**. Data shown are mean ± s.e.m. $n = 2$ independent experiments performed in duplicate. Two-way ANOVA with Tukey's multiple comparison test. ****$P < 0.0001$.

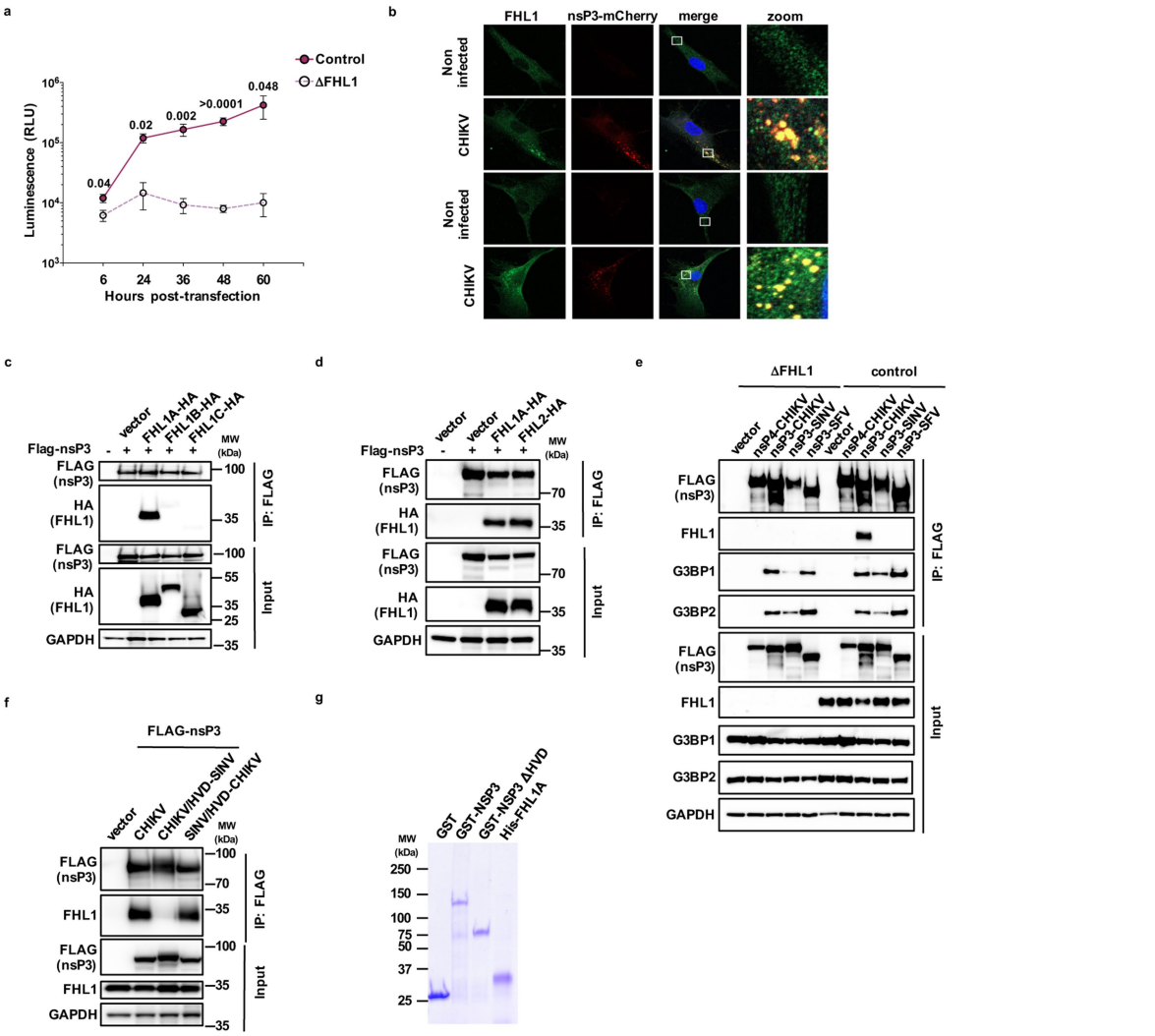

Extended Data Fig. 6 | CHIKV nsP3 interacts with FHL1A and FHL2. **a**, Control or ΔFHL1 HAP1 cells were transfected with CHIKV-M-Gluc capped genomic RNA expressing *Gaussia* luciferase (Gluc). Gluc activity was monitored at the indicated time points. RLU, relative light units. Data are mean ± s.e.m. $n = 3$ independent experiments performed in quadruplicate. Two-tailed multiple *t*-tests with Holm-Sidak correction. **b**, Confocal microscopy of the colocalization of CHIKV nsP3 with FHL1 in fibroblasts inoculated with CHIKV nsP3–mCherry (MOI of 2), fixed 48 h after infection and stained with anti-FHL1 antibody. Images are representative of three experiments. **c**, Immunoassay of the interaction between CHIKV nsP3 and FHL1 isoforms in HEK293T cells transfected with Flag-tagged CHIKV nsP3 and either an empty vector or plasmids encoding the three HA-tagged FHL1 isoforms. Proteins from cell lysates were immunoprecipitated with anti-Flag antibody followed by immunoblot analysis with anti-Flag and anti-HA antibodies. **d**, Immunoassay of the interaction between CHIKV nsP3 and FHL2 in HEK293T cells transfected with Flag-tagged CHIKV nsP3 and either an empty vector or plasmids encoding HA-tagged FHL1 and FHL2. Proteins from cell lysates were immunoprecipitated with anti-Flag followed by immunoblot analysis with anti-Flag and anti-HA. **e**, Endogenous FHL1, G3BP1 or G3BP2 immunoprecipitation from control and ΔFHL1 HEK293T cells transfected with plasmids encoding Flag-tagged CHIKV, Sindbis (SINV) or Semliki forest virus (SFV) nsP3. Proteins from cell lysates were immunoprecipitated with anti-Flag antibody followed by immunoblot analysis with anti-Flag, anti-FHL1, anti-G3BP1 and anti-G3BP2 antibodies. **f**, Endogenous FHL1 immunoprecipitation from HEK293T cells transfected with plasmids encoding Flag-tagged full length CHIKV nsP3, CHIKV nsP3 carrying the SINV HVD (CHIKV/HVD-SINV) or Sindbis nsP3 carrying CHIKV HVD (SINV/HVD-CHIKV). Proteins from cell lysates were immunoprecipitated with anti-Flag antibody followed by immunoblot analysis with anti-Flag and anti-FHL1 antibodies. **g**, Purified GST-tagged nsP3 constructs and HA-tagged FHL1A detected by Coomassie blue staining. **c**–**i**, One representative experiment of three experiments is shown.

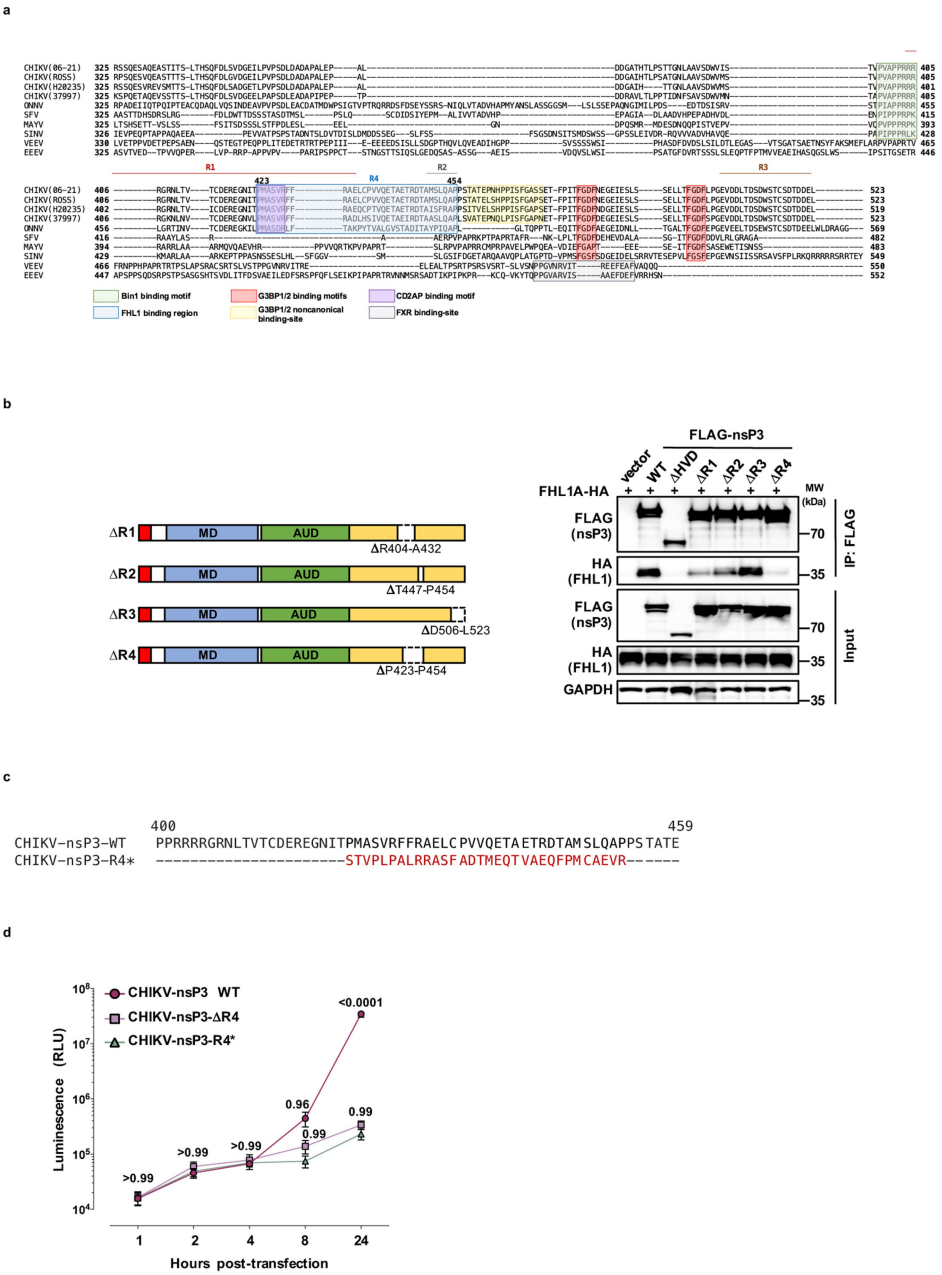

Extended Data Fig. 7 | Mapping the FHL1–nsP3 interaction. a, The sequence alignment of nsP3 protein HVD domains of representative members of New and Old World alphaviruses. Sequence alignment was performed with Clustal Omega and edited with Jalview. R1, R2 and R3 sequences of high homology between CHIKV strains and ONNV are defined by coloured lines. CHIKV(06–21) (GenBank accession number AM258992.1); CHIKV Ross (GenBank accession number MG280943.1); CHIKV H20235 (GenBank accession number MG208125.1); CHIKV 37997 (GenBank accession number AY726732.1); ONNV (GenBank accession number MF409176.1); SFV (GenBank accession number HQ848388.1); MAYV (GenBank accession number KY618137.1); SINV (GenBank accession number MF409178.1); EEEV (GenBank accession number Q4QXJ8.2); VEEV (GenBank accession number P27282.2). **b**, Left, schematic representation of CHIKV nsP3 constructs in which the R1, R2, R3 or R4 sequence was deleted. Right, HEK293T cells were transfected with FHL1A–HA and either an empty vector or plasmids encoding Flag-tagged nsP3 constructs. Cell lysates were immunoprecipitated with anti-Flag antibody followed by immunoblot analysis with anti-HA or anti-Flag antibodies. One experiment representative of three experiments is shown. **c**, Alignment of nsP3 regions containing the wild-type R4 sequence or the corresponding randomized sequence. Dashes represent identical amino acids. **d**, Control HEK293T cells were transfected with the indicated CHIKV capped in vitro transcribed RNA-expressing *Renilla* luciferase (Rluc). Rluc activity was monitored at indicated time points. RLU, relative light units. Data are mean ± s.e.m. $n = 2$ independent experiments performed in quadruplicate. Two-way ANOVA with Tukey's multiple comparison test.

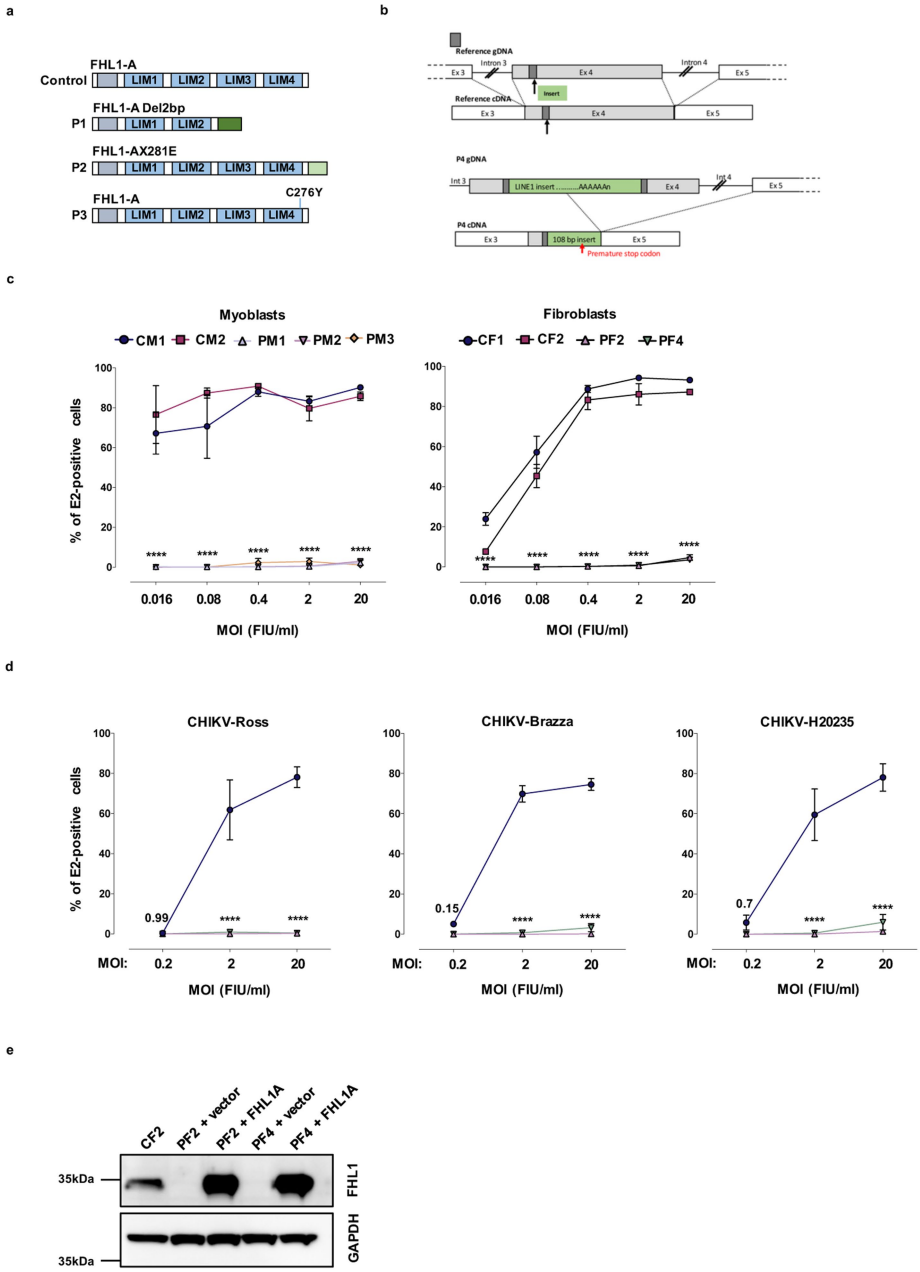

Extended Data Fig. 8 | CHIKV infection of myoblasts and fibroblasts derived from patients with EDMD. a, Schematic of FHL1A proteins from three patients with EDMD (P1, P2 and P3). **b**, Schematic of FHL1 genomic organization in the patient with a LINE1 insertion within exon 4 (P4). **c**, Myoblasts and fibroblasts from patients with EDMD or healthy donors were infected with increasing MOIs of CHIKV21, and infection was quantified 24 h later by flow cytometry using the anti-E2 3E4 monoclonal antibody. Data are mean ± s.e.m. $n = 2$ experiments performed in duplicate for myoblasts; $n = 3$ independent experiments performed in duplicate for fibroblasts. Two-way ANOVA with Dunnett's multiple comparison test. **d**, Fibroblasts from patients with EDMD or healthy donors were inoculated with increasing MOIs of CHIKV Ross, CHIKV Brazza, CHIKV H20235, and infection was quantified 24 h later by flow cytometry using the anti-E2 3E4 monoclonal antibody. Data are mean ± s.e.m. $n = 3$ independent experiments performed in duplicate. Two-way ANOVA with Dunnett's multiple comparison test. **e**, Immunoblot of ectopic FHL1 expression in primary fibroblasts (PF2 and PF4) obtained from patients that were stably transduced with an empty vector or a plasmid encoding HA–FHL1A. One representative of two experiments performed in duplicate is shown. Data are mean ± s.d. $^{****}P < 0.0001$.

a

```
Human FHL1A     ----------------MAEKFDCHYCRDPLQGKKYVQKDGHHCCLKCFDKFCANTCVECR    44
Murine FHL1     MASQRHSGPSSYKVGTMSEKFDCHYCRDPLQGKKYVQKDGRHCCLKCFDKFCANTCVDCR    60

Human FHL1A     KPIGADSKEVHYKNRFWHDTCFRCAKCLHPLANETFVAKDNKILCNKCTTREDSPKCKGC    104
Murine FHL1     KPISADAKEVHYKNRYWHDNCFRCAKCLHPLASETFVSKDGKILCNKCATREDSPRCKGC    120

Human FHL1A     FKAIVAGDQNVEYKGTVWHKDCFTCSNCKQVIGTGSFFPKGEDFYCVTCHETKFAKHCVK    164
Murine FHL1     FKAIVAGDQNVEYKGTVWHKDCFTCSNCKQVIGTGSFFPKGEDFYCVTCHETKFAKHCVK    180

Human FHL1A     CNKAITSGGITYQDQPWHADCFVCVTCSKKLAGQRFTAVEDQYYCVDCYKNFVAKKCAGC    224
Murine FHL1     CNKAITSGGITYQDQPWHAECFVCVTCSKKLAGQRFTAVEDQYYCVDCYKNFVAKKCAGC    240

Human FHL1A     KNPITGFGKGSSVVAYEGQSWHDYCFHCKKCSVNLANKRFVFHQEQVYCPDCAKKL        280
Murine FHL1     KNPITGFGKGSSVVAYEGQSWHDYCFHCKKCSVNLANKRFVFHNEQVYCPDCAKKL        297
```

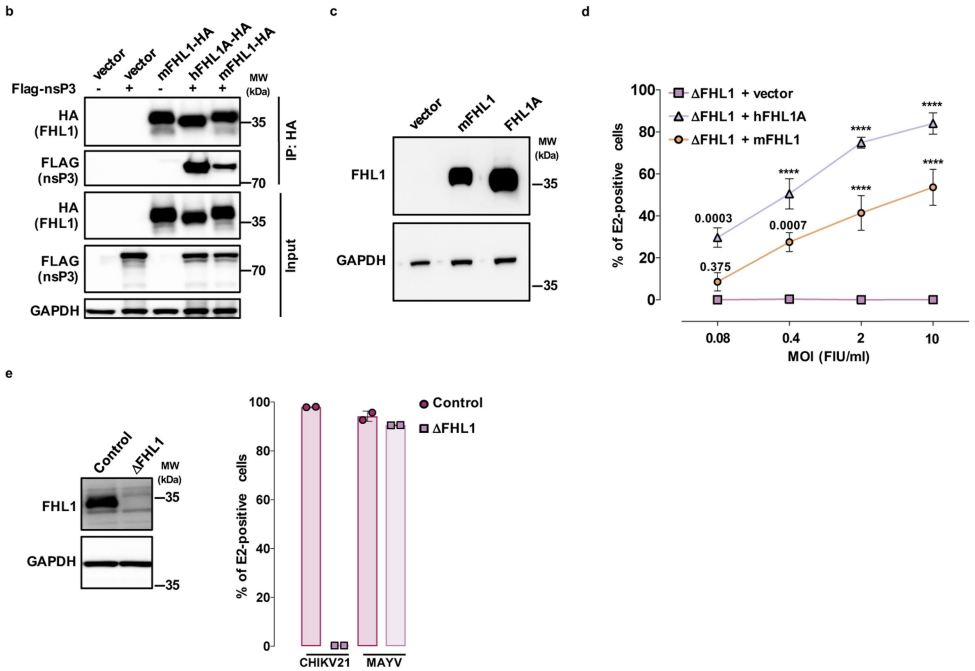

Extended Data Fig. 9 | Mouse FHL1 interacts with CHIKV nsP3 and restores infection in ΔFHL1 cells. a, Sequence alignment of mouse and human FHL1A proteins. **b**, HEK293T cells were co-transfected with Flag-tagged CHIKV nsP3 and plasmids encoding HA-tagged mouse FHL1 (mFHL1) or human FHL1A (hFHL1A). Proteins from cell lysates were immunoprecipitated with anti-HA antibody followed by immunoblot analysis with anti-Flag (nsP3) and anti-HA (FHL1) antibodies. **c**, Immunoblot of FHL1 ectopic expression in ΔFHL1 HEK293T cells stably transduced with a plasmid encoding mouse FHL1 or human FHL1A. **b**, **c**, Data are representative of three experiments. **d**, Cells showed in **c** were inoculated with increasing MOIs of CHIKV21. Infection was quantified by flow cytometry at 24 h after infection using anti-E2 3E4 monoclonal antibody. Data are mean ± s.d. $n = 3$ independent experiments performed in duplicate. Two-way ANOVA with Dunnett's multiple comparison test. **e**, Left, immunoblot of endogenous FHL1 in control and ΔFHL1 C2C12 mouse cells. Right, control and ΔFHL1 cells were inoculated with CHIKV21 or MAYV (MOI of 2) and infection was quantified at 24 h after infection by flow cytometry using anti-E2 3E4 or anti-E2 265 monoclonal antibodies. One representative experiment of three experiments is shown. ****$P < 0.0001$.

AMERICAN SOCIETY FOR MICROBIOLOGY | Journal of Virology®

VIRUS-CELL INTERACTIONS

RACK1 Associates with RNA-Binding Proteins Vigilin and SERBP1 to Facilitate Dengue Virus Replication

Alexis Brugier,[a] Mohamed Lamine Hafirrassou,[a] Marie Pourcelot,[a] Morgane Baldaccini,[b] Vasiliya Kril,[a] Laurine Couture,[a] Beate M. Kümmerer,[c] Sarah Gallois-Montbrun,[d] Lucie Bonnet-Madin,[a] Pierre-Olivier Vidalain,[e] Constance Delaugerre,[a,f] Sébastien Pfeffer,[b] Laurent Meertens,[a] Ali Amara[a]

[a]Université de Paris, INSERM U944, CNRS 7212, Biology of Emerging Viruses Team, Institut de Recherche Saint-Louis, Hôpital Saint-Louis, Paris, France
[b]Université de Strasbourg, Architecture et Réactivité de l'ARN, Institut de Biologie Moléculaire et Cellulaire du CNRS, Strasbourg, France
[c]Institute of Virology, Medical Faculty, University of Bonn, Bonn, Germany
[d]Université de Paris, Institut Cochin, INSERM U1016, CNRS UMR8104, Paris, France
[e]Centre International de Recherche en Infectiologie, Team Viral Infection, Metabolism and Immunity, INSERM U1111, CNRS UMR5308, ENS de Lyon, Université Claude Bernard Lyon 1, Lyon, France
[f]Laboratoire de Virologie et Département des Maladies Infectieuses, Hôpital Saint-Louis, Assistance Publique–Hôpitaux de Paris, Paris, France

Alexis Brugier and Mohamed Lamine Hafirrassou contributed equally to this article. Author order was determined by the corresponding author after negotiation.

ABSTRACT Dengue virus (DENV) is a mosquito-borne flavivirus responsible for dengue disease, a major human health concern for which no effective treatment is available. DENV relies heavily on the host cellular machinery for productive infection. Here, we show that the scaffold protein RACK1, which is part of the DENV replication complex, mediates infection by binding to the 40S ribosomal subunit. Mass spectrometry analysis of RACK1 partners coupled to an RNA interference screen-identified Vigilin and SERBP1 as DENV host-dependency factors. Both are RNA-binding proteins that interact with the DENV genome. Genetic ablation of Vigilin or SERBP1 rendered cells poorly susceptible to DENV, as well as related flaviviruses, by hampering the translation and replication steps. Finally, we established that a Vigilin or SERBP1 mutant lacking RACK1 binding but still interacting with the viral RNA is unable to mediate DENV infection. We propose that RACK1 recruits Vigilin and SERBP1, linking the DENV genome to the translation machinery for efficient infection.

IMPORTANCE We recently identified the scaffolding RACK1 protein as an important host-dependency factor for dengue virus (DENV), a positive-stranded RNA virus responsible for the most prevalent mosquito-borne viral disease worldwide. Here, we have performed the first RACK1 interactome in human cells and identified Vigilin and SERBP1 as DENV host-dependency factors. Both are RNA-binding proteins that interact with the DENV RNA to regulate viral replication. Importantly, Vigilin and SERBP1 interact with RACK1 and the DENV viral RNA (vRNA) to mediate viral replication. Overall, our results suggest that RACK1 acts as a binding platform at the surface of the 40S ribosomal subunit to recruit Vigilin and SERBP1, which may therefore function as linkers between the viral RNA and the translation machinery to facilitate infection.

KEYWORDS dengue virus, host factors, RACK1, RNA-binding proteins, SERBP1, Vigilin

Dengue virus (DENV) belongs to the genus *Flavivirus* of the family *Flaviviridae*, which includes important emerging and reemerging viruses such as West Nile virus (WNV), yellow fever virus (YFV), Zika virus (ZIKV), and tick-borne encephalitis virus (TBEV) (1). DENV is transmitted to humans by an *Aedes* mosquito bite and may lead to a variety of diseases ranging from mild fever to lethal dengue hemorrhagic fever and dengue shock syndrome (2). Recent estimations indicate that half of the world's

Editor Anice C. Lowen, Emory University School of Medicine

Address correspondence to Ali Amara, ali.amara@inserm.fr.

The authors declare no conflict of interest.

Received 16 November 2021
Accepted 24 January 2022
Published 10 March 2022

population lives in areas where dengue fever is endemic (3), with 100 million symptomatic infections, including 500,000 cases of severe manifestations of the disease per year (4). There are currently no approved antiviral therapies against DENV, although a promising inhibitor targeting the viral NS3-NS4B interaction was recently described (5). Conversely, the recently approved tetravalent live attenuated vaccine showed disappointing efficacy (6, 7).

DENV is an enveloped virus containing a positive-stranded RNA genome of ~11 kb. Upon entry into the host cell, the viral genome is released in the cytoplasm and translated by the host machinery into a large polyprotein precursor that is processed by host and viral proteases. Co- and posttranslational processing gives rise to three structural proteins: the C (core), prM (precursor of the M protein), and E (envelope) glycoproteins, which form the viral particle and seven nonstructural proteins (NS) called NS1, NS2A, NS2B, NS3, NS4A, NS4B, and NS5 (8) that play central roles in viral genome replication, assembly, and modulation of innate immune responses (9). Like other flaviviruses, DENV genome replication takes place within virus-induced vesicles (Ve) derived from invaginations of the endoplasmic reticulum (ER) membrane (10, 11). These structures consist of 90-nm-wide vesicles containing a ±11-nm pore that allows exchanges between the Ve lumen and the cytosol (11). Within the Ve, viral NS proteins, viral RNA (vRNA), and some host factors assemble to form the viral replication complex (RC) that is essential for viral RNA synthesis. We have recently purified the DENV RC in human cells, using a tagged DENV subgenomic replicon, and determined its composition by mass spectrometry (12). Our study provided an unprecedented mapping of the DENV RC host interactome and identified cellular modules exploited by DENV during active replication. By combining these proteomics data with gene silencing experiments, we identified a set of host-dependency factors (HDFs) that have a critical impact on DENV infection and established an important role for RACK1 (receptor for activated C kinase 1) in DENV vRNA amplification (12), which was recently confirmed by others (13).

RACK1 is a core component of the 40S ribosomal subunit (14, 15), containing seven WD40 domains that mediate protein-protein interactions (16, 17). RACK1 is a scaffold protein (18, 19) described to interact with many cellular pathways such as Sarcoma (Src) tyrosine kinase (20, 21), cAMP/protein kinase A (PKA) (22), or receptor tyrosine kinase (23). Ribosomal RACK1 has also been shown to be involved in the association of mRNAs with polysomes (24), in the recruitment and phosphorylation of translational initiation factors (25–27), and in quality control during translation (28). The nonribosomal form of RACK1 is involved in innate immunity, by recruiting the PP2A phosphatase (29) or by targeting the VISA/TRAF complexes (30), and participates in the assembly and activation of the NLRP3 inflammasome (31). To date, only one proteomic study aiming to identify RACK1 cofactors has been performed in *Drosophila* S2 cells (32). RACK1 cellular partners in human cells are largely unknown.

Several viruses depend on RACK1 to complete their infectious cycle[31–35]. For instance, RACK1 is involved in internal ribosome entry site (IRES)-mediated translation of viruses possessing a type I IRES such as cricket paralysis virus or hepatitis C virus (33). RACK1 also contributes to poxvirus infection through a ribosome customization mechanism. Indeed, poxviruses trigger the phosphorylation of the serine 278 of RACK1 (34) to promote the selective translation of viral RNAs.

In this work, we have investigated the function of RACK1 during DENV life cycle. We performed the first interactome of RACK1 in human cells. Functional studies revealed that RACK1 interacts with the RNA-binding proteins Vigilin and SERBP1 to facilitate DENV replication.

RESULTS AND DISCUSSION

RACK1 interaction with the 40S ribosomal subunit is required for DENV infection. To confirm the role of RACK1 in DENV infection, we challenged parental and RACK1 knockout (RACK1^{KO}) HAP1 cells with DENV2-16681 particles at different multiplicities of infection (MOIs) and measured viral infection by quantifying the percentage of cells

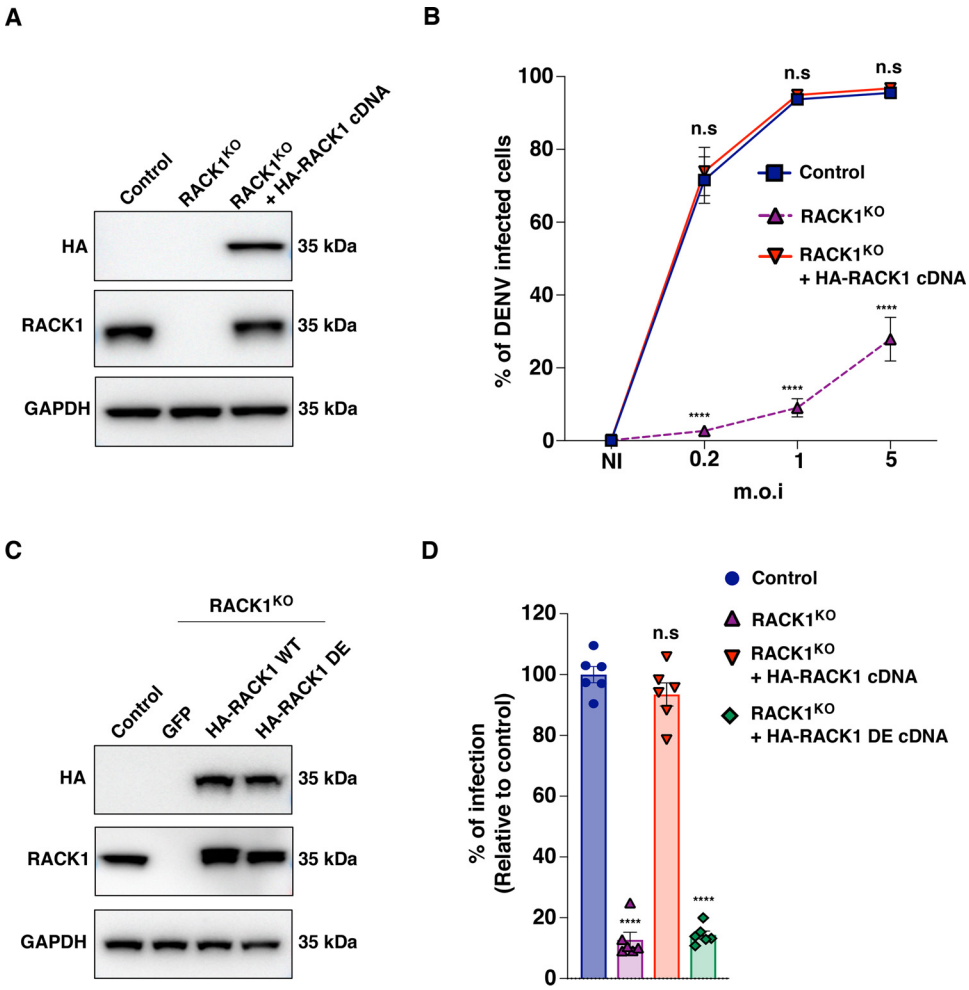

FIG 1 The interaction between RACK1 and the 40S ribosome is required for dengue virus (DENV) infection. (A) Western blot analysis of RACK1 expression in control, RACK1^{KO}, and RACK1^{KO} HAP1 cells transcomplemented with a hemagglutinin (HA)-RACK1 cDNA. Cell lysates were probed with the indicated antibodies. Shown is a representative Western blot of $n = 3$ technically independent experiments. (B) Role of RACK1 in DENV infection. Control, RACK1^{KO}, or RACK1^{KO} cells transcomplemented with a cDNA encoding wild-type (WT) HA-RACK1 were infected at different multiplicities of infection (m.o.i) with DENV2-16681. Levels of infection were determined by flow cytometry using the 2H2 prM monoclonal antibody (MAb) at 48 h postinfection (hpi). The data shown are the means ± stardard error of the mean (SEM) of four independent experiments performed in duplicate. Significance was calculated using two-way analysis of variance (ANOVA) with Dunnett's multiple-comparison test. (C) Western blot analysis of RACK1 expression in RACK1^{KO} HAP1 transcomplemented with cDNA encoding WT HA-RACK1 or the HA-RACK1 D/E mutant (HA-RACK1 DE cDNA). Cell lysates were probed with the indicated antibodies. Shown is a representative Western blot of three independent experiments. (D) Impact of RACK1 association to the 40S subunit of the ribosome in DENV infection. Control, RACK1^{KO}, and RACK1^{KO} HAP1 cells transcomplemented with cDNA encoding WT HA-RACK1 or the HA-RACK1 DE mutant were infected at MOI 1 with DENV2-16681 and harvested at 48 hpi. Levels of infection were determined by flow cytometry as described above. The data shown are the means ± SEM of three independent experiments performed in duplicate. Significance was calculated using one-way ANOVA with Dunnett's multiple-comparison test. ****, $P < 0.0001$; n.s, not significant; GAPDH, glyceraldehyde-3-phosphate dehydrogenase; GFP, green fluorescent protein; NI, not infected.

expressing the DENV antigen PrM. In agreement with our previous studies (12), DENV infection was severely impaired in HAP1 cells lacking RACK1 (Fig. 1A and B). Importantly, transcomplementation of the HAP1 RACK1^{KO} cells with a plasmid encoding human RACK1 rescued cell susceptibility to DENV infection (Fig. 1A and B), ruling out CRISPR-Cas9-mediated off-target effects and demonstrating that RACK1 is an important host factor for DENV.

RACK1 is a component of the 40S subunit of the ribosome and is located near the mRNA exit channel (17). To test whether DENV infection requires RACK1 association

with the 40S ribosome, we transcomplemented RACK1^{KO} cells with a RACK1 mutant defective for ribosome-binding (RACK1R36D/K38E, DE mutant) (34, 35). The RACK1 DE mutant, which displayed a wild-type (WT) expression level and was unable to associated with polysomes (data not shown and Ref. 36), failed to rescue DENV2-16681 infection (Fig. 1C and D). These results indicate that the interaction with the 40S ribosomal subunit is important for RACK1 proviral function.

Mapping the RACK1 interactome. Because RACK1 is a scaffold protein, we hypothesized that its proviral activity may rely on its ability to recruit host proteins near the ribosome for optimal translation. To characterize the RACK1 interactome in mammalian cells, we transfected 293T cells with a plasmid encoding an hemagglutinin (HA)-tagged version of human RACK1. We pulled down RACK1 and its binding partners using HA beads and eluted purified proteins with HA peptide according to the experimental procedures that we recently described (12). Immunoprecipitated proteins were separated by SDS-PAGE, visualized by silver staining, and subjected to mass spectrometry (MS) analysis (Fig. 2A). By analyzing the raw affinity purification-mass spectrometry (AP-MS) data set with SAINT express and MiST softwares (37), we identified 135 high-confidence host factors that copurified with RACK1 and showed a SAINT express score greater than 0.8 (supplemental material). Next, we analyzed the list of 135 high-confidence interactors with DAVID 6.8 to identify statistical enrichments for specific Gene Ontology (GO) terms from the "cellular component" (CC) annotation (38, 39) (Fig. 2B) and built the corresponding interaction network using Cytoscape 3.4.0 (40) (Fig. 2C). The 135 RACK1-interacting proteins were clustered into functional modules using enriched GO terms as a guideline and literature mining (Fig. 2C). As expected, the RACK1 interactome was significantly enriched in proteins associated with ribosome/polysome and mRNA translation (Rps3, eIF3, eIF4G, and eIF4J), stress granules (G3BP2 and LARP1), P-Bodies (Ago1 and 2), and RNA splicing factors (HNRNPA2B1 and U2AF2) (Fig. 2C). Interestingly, several proteins found in our study, such as Ago2, LARP1 and 2, and eIF3A, were also identified in a RACK1 interactome done in *Drosophila* S2 cells (32).

Vigilin, SERBP1, and ZNF598 are DENV host-dependency factors. To pinpoint the function of the RACK1 binding partners during DENV infection, we silenced by RNA interference (RNAi) the expression of the 49 highest ranked hits with an average peptide count of more than 28 and determined the consequences on viral infection (Fig. 3A; supplemental material). Four proteins, namely HNRNPA2B1, Vigilin, SERBP1, and ZNF598, whose silencing decreased infection by at least 50% without affecting cell viability in the two cell lines were considered for further investigation (Fig. 3A; supplemental material). These factors are RNA-binding proteins (RBP) involved in RNA splicing (HNRNPA2B1) (41) or translation regulation (Vigilin, SERBP1, and ZNF598) (28, 42, 43). HNRNPA2B1 was already described to interact with the 3′-untranslated region (UTR) part of the virus (44). Because HNRNPA2B1 is a nuclear protein (45), it was not further considered in our study. Vigilin is a multiple K-homology (KH) domain protein implicated in translation regulation and lipidic metabolism (24, 43, 46). This protein was recently described to bind the DENV RNA and, in association with the ribosomal-binding protein 1 (RRBP1), to facilitate viral RNA translation and replication (47). However, how this protein interacts with RACK1 to regulate DENV infection is still unknown. SERBP1 is a RACK1 cofactor (48) that is located at the entry channel of ribosomes (49) and enhances translation by promoting the association of mRNAs with polysomes (42). SERBP1 was also described to interact with DENV RNA. However, its role in DENV replication remains unclear (50). Finally, ZNF598 is an E3 ubiquitin-protein ligase known to interact with RACK1 and playing a key role in the ribosome quality control (28). ZNF598 was also described to play a role in innate immunity (51). However, its role in DENV infection is unknown.

We first confirmed that endogenous Vigilin, ZNF598, and SERBP1 proteins coimmunoprecipitated with HA-RACK1 ectopically expressed in 293T cells (Fig. 3B). Next, we validated the requirement of Vigilin, SERBP1, and ZNF598 using two approaches. On one hand, we found that knocking down by RNA interference Vigilin, SERBP1, or ZNF598 (Fig. 3C) significantly impaired DENV infection but not viability of primary human fibroblasts, which are DENV target cells (Fig. 3D and E). On the other hand, we

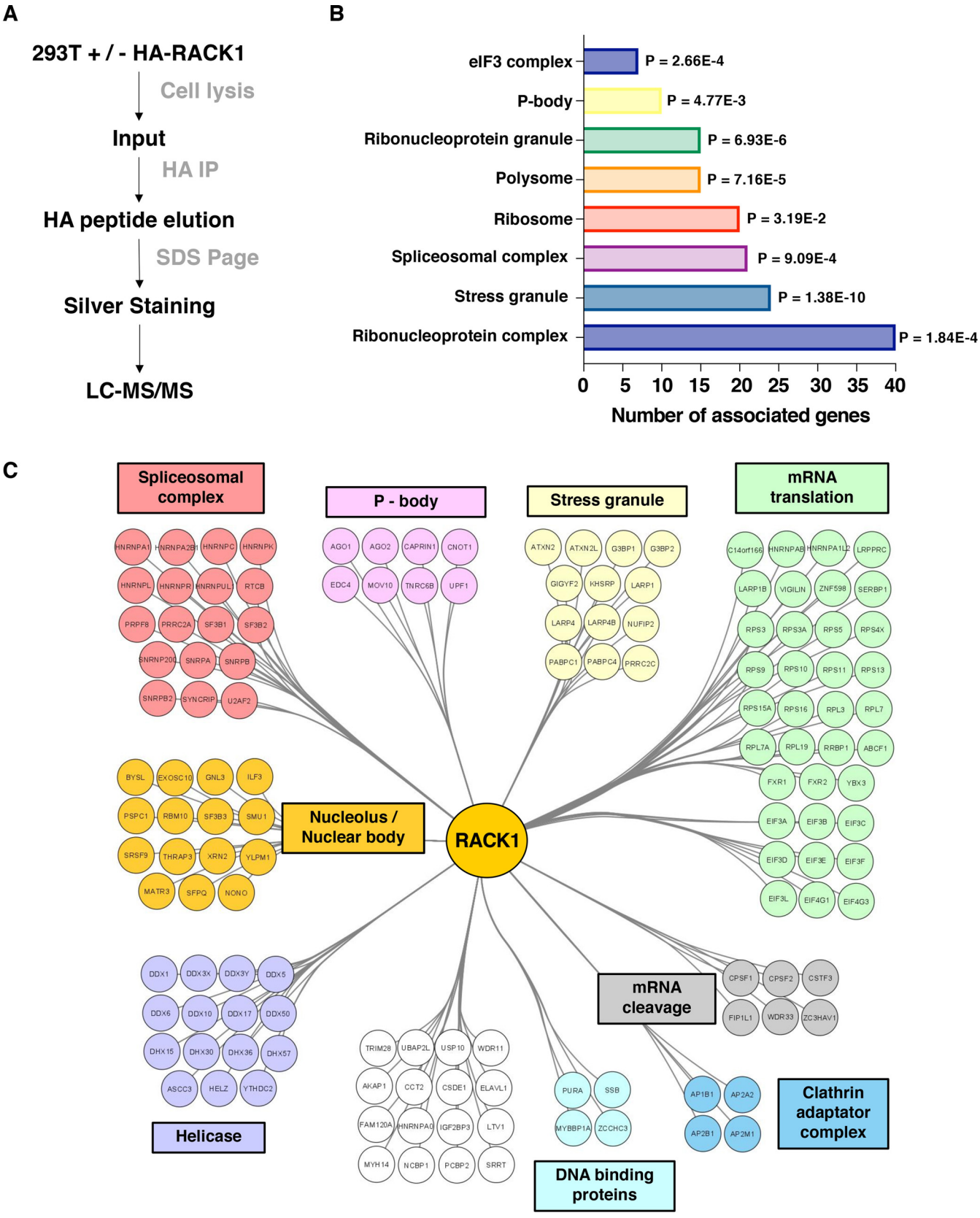

FIG 2 Global map of the RACK1 interactome in human cells. (A) Experimental scheme of our RACK1 immunoprecipitation approach. 293T cells expressing RACK1 or HA-RACK1 were lysed, and extracts were purified with anti-HA-coated beads before SDS-PAGE and mass spectrometry (MS) analysis. (B) Histogram indicating statistical enrichment for specific biological processes and cellular components, determined by Gene Ontology (GO) analysis.

(Continued on next page)

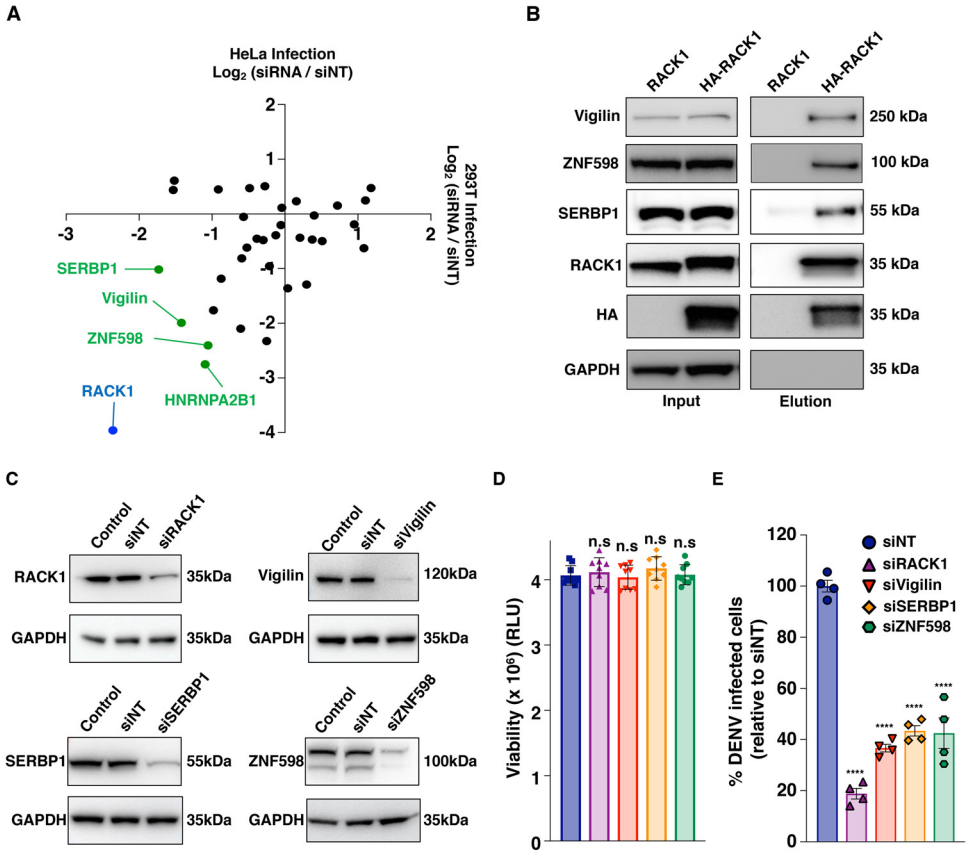

FIG 3 RNA interference (RNAi) screen-identified Vigilin, SERBP1, and ZNF598 are DENV host-dependency factors. (A) Host-dependency factors (HDFs) found in our RNAi screen. The data shown are representative of three independent experiments. Host-dependency factors are marked in green. The positive control (small interfering RNA [siRNA] pool targeting RACK1) is highlighted in blue. (B) Validation of the interaction between RACK1 and endogenous Vigilin or SERBP1 in 293T cells by immunoprecipitation. Cell extracts from 293T cells expressing RACK1 or HA-RACK1 were subjected to affinity purification using anti-HA beads, and interacting proteins were revealed by Western blotting. The data shown are representative of three independent experiments. (C) Human primary fibroblasts were transfected with the indicated siRNA pools. RACK1, Vigilin, SERBP1, and ZNF598 expression in siRNA transfected cells was assessed by Western blot analysis 48 h posttransfection. (D) The viability of siRNA transfected fibroblasts described in B was monitored by cell titer glow analysis. The data shown are the means ± SEM of three independent experiments performed in triplicate. Significance was calculated using two-way ANOVA with Dunnett's multiple-comparison test. (E) siRNA transfected fibroblasts described for panel B were challenged with DENV2-16681 at MOI 1. At 48 h posttransfection, the levels of infection were determined by flow cytometry using 2H2 MAb at 48 hpi. The data shown are the means ± SEM of three independent experiments performed in duplicate. Significance was calculated using one-way ANOVA with Dunnett's multiple-comparison test. RLU, relative light units; siNT, nontargeting siRNA.

used the CRISPR-Cas9 technology to edit the corresponding genes in HAP1 cells (Vigilin ^{KO}, SERBP1 ^{KO}, and ZNF598 ^{KO}) (Fig. 4). Gene editing and knockout generation were confirmed by genomic DNA sequencing (Fig. 4A) and Western blot analysis (Fig. 4B), respectively. In agreement with our previous findings, lack of RACK1, Vigilin, SERBP1, and ZNF598 expression had no impact on cell growth and viability as assessed by quantification of ATP levels in culture wells at different time points (Fig. 4C). HAP1 cells lacking Vigilin, SERBP1, or ZNF598 expression were poorly permissive to DENV infection as shown by the quantification of viral progeny in supernatants of infected cells (Fig. 4D), Western blot analysis of the DENV protein expression (NS3, E, and PrM)

FIG 2 Legend (Continued)
(C) Interaction network of RACK1-associated proteins identified by MS in 293T cells. Proteins were clustered into functional modules using enriched GO terms as a guideline and manual mining of literature. This panel is a representative network of $n = 3$ independent experiments showing similar results. LC-MS/MS, liquid chromatography-tandem MS.

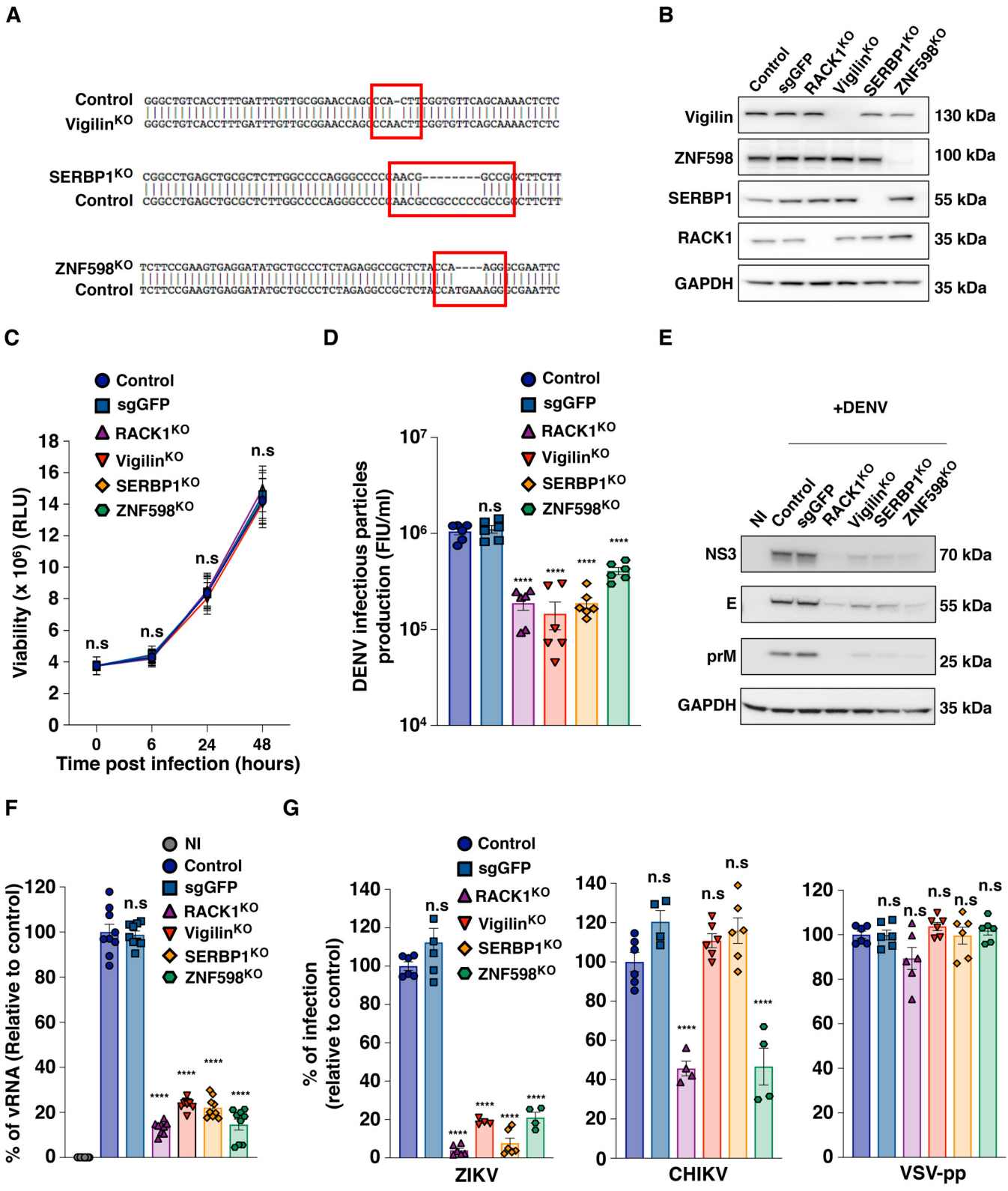

FIG 4 Impact of RACK1, Vigilin, SERBP1, and ZNF598 gene editing on infection by DENV and other enveloped viruses. (A) Sanger sequencing of *VIGILIN*, *SERBP1*, and *ZNF598* in control and Vigilin^{KO}, SERBP1^{KO}, or ZNF598^{KO} HAP1 cells, respectively. (B) Validation of Vigilin, SERBP1, and ZNF598 gene editing by Western blot analysis. Shown is a representative Western blot of three independent experiments. (C) Impact of RACK1, Vigilin, SERBP1, and ZNF598 gene editing on cell viability in HAP1 cells by cell titer glow analysis. The data shown are the means ± SEM of three independent experiments performed in duplicate. Significance was calculated using two-way ANOVA with Dunnett's multiple-comparison test. (D to G) Impact of RACK1/Vigilin/SERBP1/ZNF598 gene editing on DENV infectious cycle. The indicated cells were infected for 48 h at MOI 1 with DENV2-16681. (D) Supernatants from infected cells were

(Continued on next page)

(Fig. 4E), and quantification of the viral RNA (Fig. 4F). Parental (control) and HAP1 cells transfected with a nonspecific single guide RNA (targeting the green fluorescent protein [GFP]) were used as negative controls (Fig. 4), while RACK1^{KO} HAP1 cells were used as positive controls (Fig. 4). We then investigated whether these phenotypes were specific to DENV2-16681 or could be observed with other flaviviruses. We found that Vigilin, SERBP1, and ZNF598 mediate infection by other DENV serotypes (data not shown), as well as by Zika virus (ZIKV), a related flavivirus (Fig. 4G). In contrast, infections by the *Alphavirus* chikungunya virus (CHIKV) or the vesicular stomatitis virus G protein (VSV-G)-pseudotyped human immunodeficiency virus (VSVpp) were unaffected in Viligin^{KO} and SERBP1^{KO} cells (Fig. 4G). CHIKV infection but not VSVpp was significantly reduced in RACK1^{KO} and ZNF598^{KO} cells (Fig. 4G). Altogether, our data indicate that Vigilin, SERBP1, and ZNF598 are important host factors for DENV. ZNF598 is required for DENV and CHIKV infection, while Vigilin and SERBP1 are exclusively exploited by DENV and other related flaviviruses.

Vigilin and SERBP1 regulate DENV translation and replication. To determine whether Vigilin and SERBP1 impact initial vRNA translation or amplification, Vigilin^{KO} and SERPB1^{KO} cells were challenged with DENV2 *Renilla* luciferase (Luc) reporter virus (DV-R2A) through a time-course experiment to monitor the kinetic of viral infection (Fig. 5A). RACK1 ^{KO} cells were used as a positive control. A weak Luc activity was detected at 6 h postinfection, reflecting the initial translation of the incoming vRNA. This was followed by a marked increase in Luc activity caused by a combination of translation and replication of the viral genome (Fig. 5A). Depletion of RACK1, Vigilin, and SERBP1 had no impact on initial translation step but strongly impaired DENV translation and replication at later time points (Fig. 5A). Importantly, viral genome replication was completely restored in KO cells transduced with RACK1, SERBP1, or Vigilin cDNAs (Fig. 5A). CHIKV expressing the *Gaussia* luciferase replicated as efficiently in Vigilin or SERBP1 ^{KO} cells as in control cells, while its replication in RACK1^{KO} was impaired (Fig. 5B). To assess further the effect of Vigilin and SERBP1 on DENV vRNA replication, we used a *Renilla* luciferase (Rluc) reporter subgenomic replicon (sgDVR2A), which is a self-replicating DENV RNA containing a large in-frame deletion in the structural genes and represents a useful tool to exclusively monitor DENV translation and RNA amplification. Control, Vigilin^{KO}, SERBP1^{KO}, and RACK1^{KO} HAP1 cells were transfected with the *in vitro* transcribed DENVR2A subgenomic RNA, and vRNA replication was monitored over time by quantifying the Rluc activity in infected cell lysates (Fig. 5C). Depletion of RACK1, Vigilin, or SERBP1 had no impact during the early phase of DENV RNA translation. At 12 h posttransfection, the RLuc signal increased over time in control cells, while a strong reduction was observed (more than 10-fold reduction at 48 h postinfection [hpi]) in Vigilin^{KO} and SERBP1^{KO} cells (Fig. 5C). The RLuc signal was restored in Vigilin^{KO} or SERBP1^{KO} transcomplemented with their corresponding cDNAs (Fig. 5C).

Vigilin has been previously shown to mediate, in association with the host factor RRBP1, the stability of DENV vRNA (47). Since SERBP1 also binds the DENV RNA (50), we reasoned that it might play a similar role. To assess this hypothesis, RACK1^{KO}, Vigilin^{KO}, or SERBP1^{KO} HAP1 cells were challenged with DENV followed by treatment with MK0608 to inhibit viral replication (47). Then, we monitored the decay of the vRNA overtime by Northern blotting analysis using a probe that targets the DENV 3′-UTR (Fig. 6). We observed that the levels of the DENV genomic RNA were similar in control,

FIG 4 Legend (Continued)
harvested, and then the titer was determined by flow cytometry on Vero cells and expressed as fluorescence-activated cell sorter infectious unit (FIU)/mL. (E) Infection was assessed by immunoblot using anti-NS3, anti-prM, and anti-E DENV MAbs. The data shown are representative of three independent experiments. (F) Levels of infection were assessed by quantification of DENV viral RNA (vRNA) by quantitative reverse transcription-PCR using NS3 primers. The data shown are the means ± SEM of three independent experiments performed in duplicate. Significance was calculated using one-way ANOVA. (G) The indicated cells were infected with Zika virus (ZIKV) HD78 at MOI 2 (left), chikungunya virus (CHIKV) 21 at MOI 2 (middle), and vesicular stomatitis virus G protein-pseudotyped human immunodeficiency virus (VSV-pp) at MOI 2 (right). Levels of infection were determined by flow cytometry at 48 hpi. The data shown are the means ± SEM of at least two independent experiments performed in duplicate. Significance was calculated using one-way ANOVA with Dunnett's multiple-comparison test. n.s, not significant; ****, $P < 0.0001$.

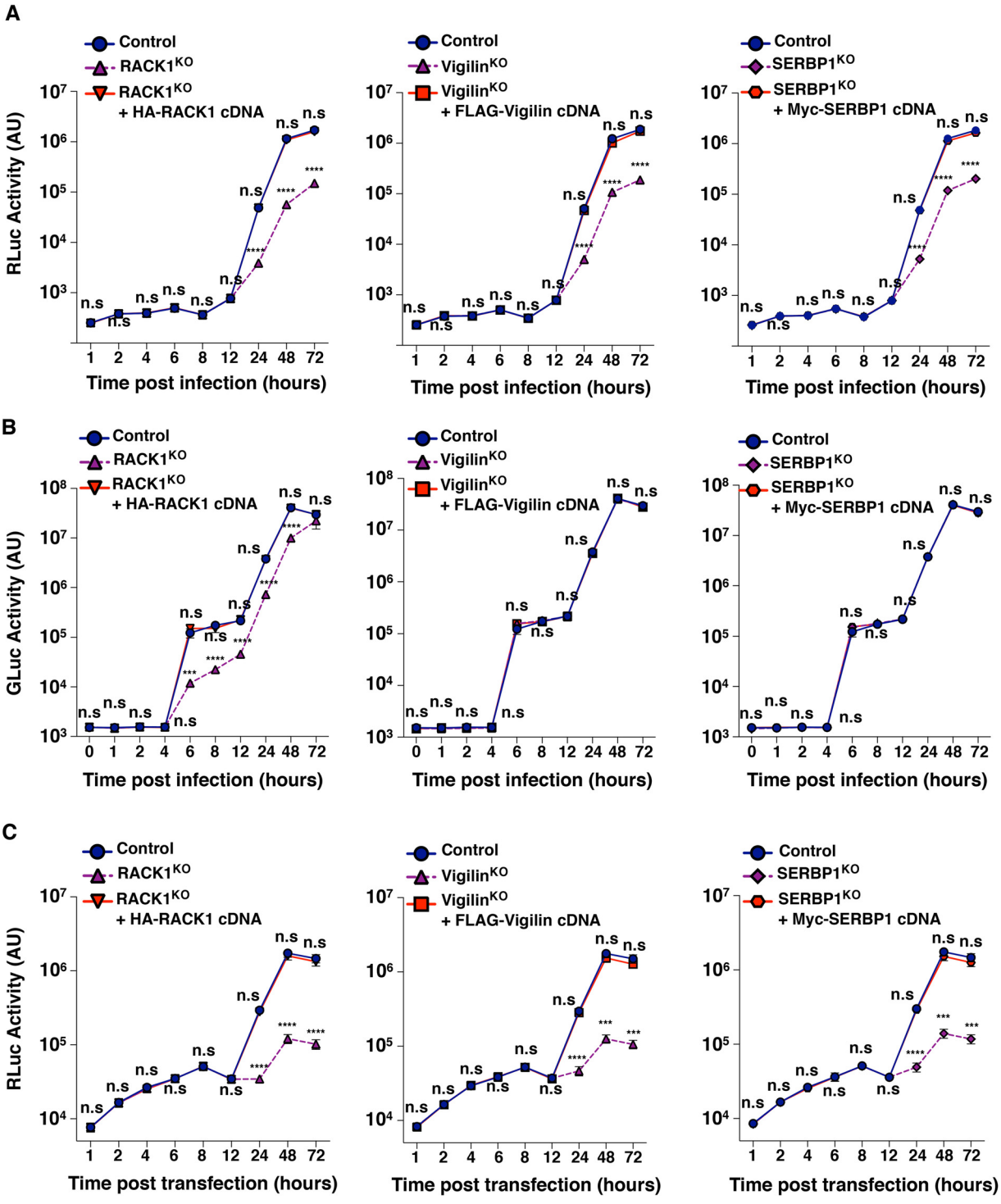

FIG 5 Vigilin and SERBP1 regulate DENV translation and replication. (A) The indicated cells were infected at MOI 1 with DENV-Luc. At the indicated time points, *Renilla* luciferase activity reflecting RNA translation (1 to 8 hpi) and replication (12 to 72 hpi) was measured. The data shown are the means ± SEM of three independent experiments performed in triplicate. Significance was calculated using two-way ANOVA with Dunnett's multiple-comparison test. (B) The indicated cells were infected at MOI 1 with CHIKV-Luc. *Gaussia* luciferase activity was monitored at the indicated time points. The data shown are the means ± SEM of three independent experiments performed in triplicate. Significance was calculated using two-way ANOVA with Dunnett's multiple-comparison test. (C) Impact of RACK1/Vigilin/SERBP1 KO on DENV life cycle in HAP1 cells transfected with a DENV replicon RNA expressing *Renilla* luciferase. *Renilla* luciferase activity was monitored at the indicated time point. The data shown are the means ± SEM of three independent experiments performed in triplicate. Significance was calculated using two-way ANOVA with Dunnett's multiple-comparison test. n.s, not significant; ****, $P < 0.0001$; AU, arbitrary units; Gluc, *Gaussia* luciferase; Rluc, *Renilla* luciferase.

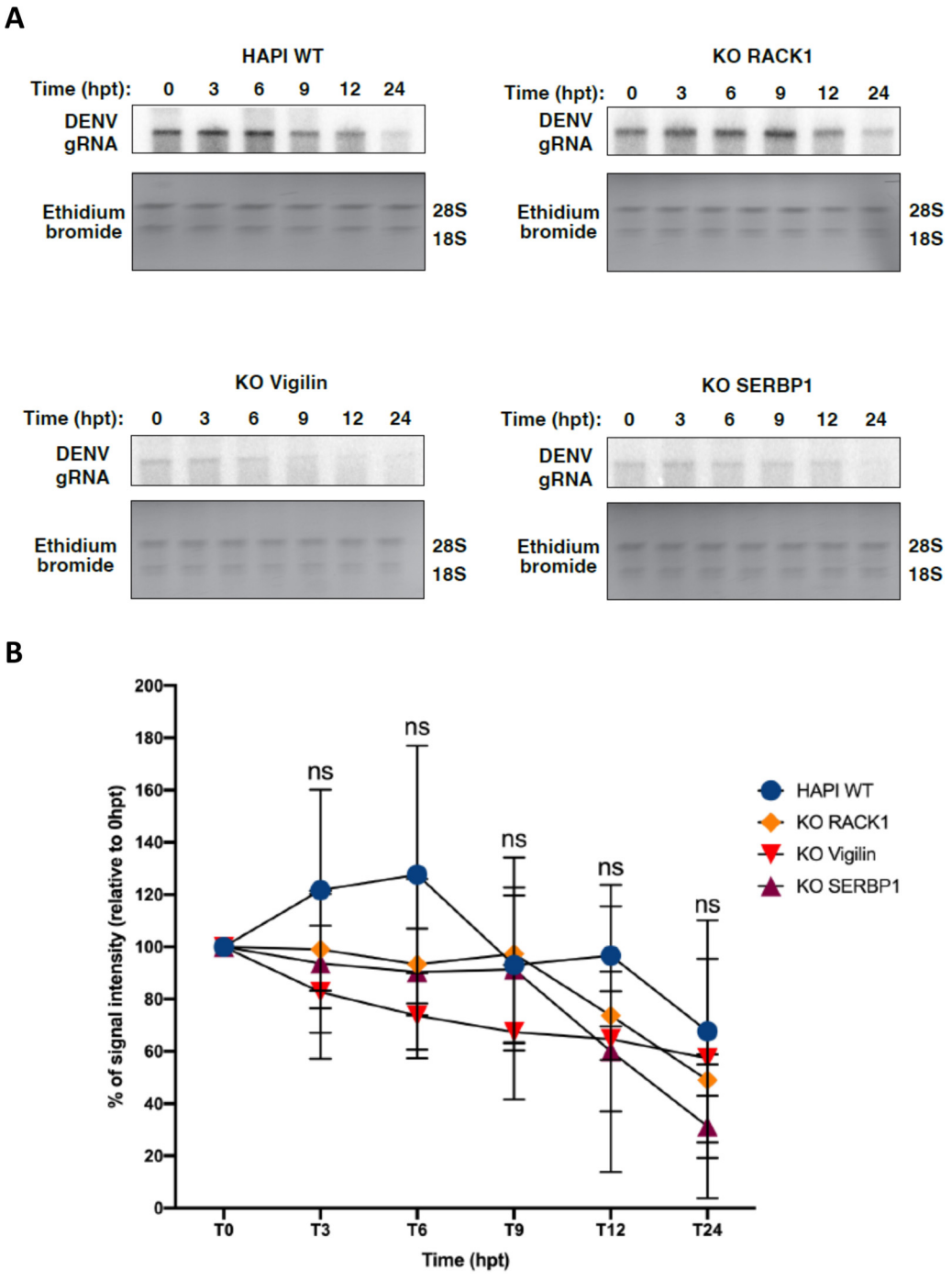

FIG 6 Northern blot analysis of the impact of RACK1, Vigilin, and SERBP1 knockout on DENV genomic RNA (gRNA) stability. (A) Indicated cells were infected at an MOI of 1 with DENV2-16681. Total RNA was extracted 48 h.p.i. at the indicated time after treatment with MK0608 replication inhibitor. The data shown are the means ± SEM of three independent experiments performed in triplicate. (B) vRNA stability is expressed as a percentage relative to the signal monitored at time point 0 h after MK0608 treatment. Ethidium bromide serves as a loading control, showing 28S and 18S rRNA. Statistics were performed using two-way ANOVA. hpt, h posttransfection; ns, nonsignificant.

RACK1^{KO}, and SERBP1^{KO} HAP1 cells up to 24 h after MK0608 treatment (Fig. 6). Surprisingly, a lack of Vigilin expression had a very mild effect on DENV RNA stability (Fig. 6). Together, these results show that RACK1, Vigilin, and SERBP1 promote viral replication without a major impact on the stability of DENV vRNA.

Vigilin and SERBP1 interactions with RACK1 are important for DENV infection. Scp160p and Asc1p, the yeast homologs of Vigilin and RACK1, respectively, have

been shown to interact each other (24). This interaction is thought to promote translation of specific mRNAs linked to Scp160p by mediating their association with polysomes (24). Because Vigilin is very well-conserved among different species, a similar interaction with RACK1 might occur in mammalian cells. Having established that Vigilin and SERBP1 do not have a major influence on the stability of the vRNA, we hypothesized that their proviral effect might be linked to their interaction with RACK1. Previous studies showed that Scp160p interacts with Asc1p via the KH 13 and 14 domains located in its C-terminal region (24, 52), while SERBP1 interacts directly with RACK1 through a motif (amino acids [aa] 354 to 474) that contains the RGG domain (48) (Fig. 7A). On the basis of these observations, we generated the corresponding deletion mutants of FLAG-tagged Vigilin (FLAG-Vigilin Mut) and Myc-tagged SERBP1 (Myc-SERPB1 Mut) (Fig. 7A) and tested their ability to interact with RACK1 (Fig. 7B). Pulldown experiments showed that RACK1 binds both WT FLAG Vigilin or WT Myc SERBP1 ectopically expressed in HEK-293T cells (Fig. 7B). In contrast, RACK1 failed to associate with mutant forms of Vigilin and SERBP1 (Fig. 7B). We next assessed the ability of the mutant forms to interact with DENV vRNA by performing an RNA immunoprecipitation (IP) assay after UV irradiation (Fig. 7C). For both RNA-binding proteins, the WT and mutant forms were able to specifically enrich the vRNA (at least 10-fold more than actin enrichment). Furthermore, we did not observe any significant differences in vRNA enrichment between the mutant and WT forms of the RBPs. These data demonstrate that Vigilin Mut and SERBP1 Mut bind the DENV vRNA to the same extent as their WT counterparts.

Finally, we investigated whether Vigilin and SERBP1 binding to RACK1 impacts DENV infection. For this, we stably expressed Mut Vigilin or Mut SERBP1 in Vigilin ^{KO} or SERBP1 ^{KO} cells, respectively (Fig. 8A). Infection studies showed that expression of Mut Vigilin or Mut SERBP1 in Vigilin ^{KO} or SERBP1 ^{KO} cells did not restore DENV2-16681 infection in contrast to their WT counterparts (Fig. 8B). Together, these data indicate that Vigilin and SERBP1 interaction with RACK1 is important for DENV infection

Conclusions. Our results provide new insights into the molecular mechanisms of DENV replication. We performed the first RACK1 interactome in human cells and identified Vigilin and SERBP1 as host factors for DENV infection. Both are RNA-binding proteins that interact with the DENV RNA and regulate viral replication. Importantly, our data suggest that the interaction of Vigilin and SERBP1 with RACK1 are important for DENV infection. The proviral function of RACK1 depends on its association with the 40S ribosomal subunit. Furthermore, mutants of SERBP1 or Vigilin that lost their ability to interact with RACK1 were unable to support infection. We propose a model in which RACK1 acts as a binding platform at the surface of the 40S ribosomal subunit to recruit Vigilin and SERBP1, which may therefore function as linkers between the viral RNA and the translation machinery to facilitate DENV infection. Strategies that interfere with RACK1-ribosome association or disturb the RACK1-Vigilin-SERBP1 complex may represent new ways to combat DENV-induced disease.

MATERIALS AND METHODS

Cell lines. HAP1 cells (Horizon Discovery) and HAP1 RACK1^{KO} (provided by Gabriele Fuchs, University at Albany) were cultured in Iscove's modified Dulbecco's medium (IMDM) supplemented with 10% fetal bovine serum (FBS), 1% penicillin-streptomycin, 1% GlutaMAX, and 25 mM HEPES. HEK293T (ATCC), Vero E6 (ATCC), BHK-21 (ATCC), and HeLa (ATCC) cells were cultured in Dulbecco's modified Eagle's medium (DMEM) supplemented with 10% FBS, 1% penicillin-streptomycin, 1% GlutaMAX, and 25 mM HEPES. Fibroblast BJ-5ta cells (ATCC) were cultured according to the manufacturer's instructions. A final concentration of 50 μM MK0608 was used in this study. All of the cell lines were cultured at 37°C and 5% CO_2.

Virus strains and replicons. DENV1-KDH0026A (gift from L. Lambrechts, Pasteur Institute, Paris, France), DENV2-16681 (Thailand/16681/84), DENV4 (H241), and ZIKV HD78788 were propagated in mosquito AP61 cell monolayers with limited cell passages. DENV2 Rluc reporter virus (DVR2A) was provided by Ralf Bartenschlager (University of Heidelberg). The CHIKV Luc reporter virus was described previously (53).To generate infectious virus, capped viral RNAs were generated from the NotI-linearized plasmids using a mMessage mMachine T7 transcription kit (Thermo Fisher Scientific) according to the manufacturer's instructions. RNAs were purified (see RNA IP protocol), resuspended in DNase/RNase-free water, aliquoted, and stored at −80°C until used. 30 μg of purified RNAs were transfected in BHK21 cells using Lipofectamine 3000 reagent. Supernatants were collected 72 h later and used for viral propagation on

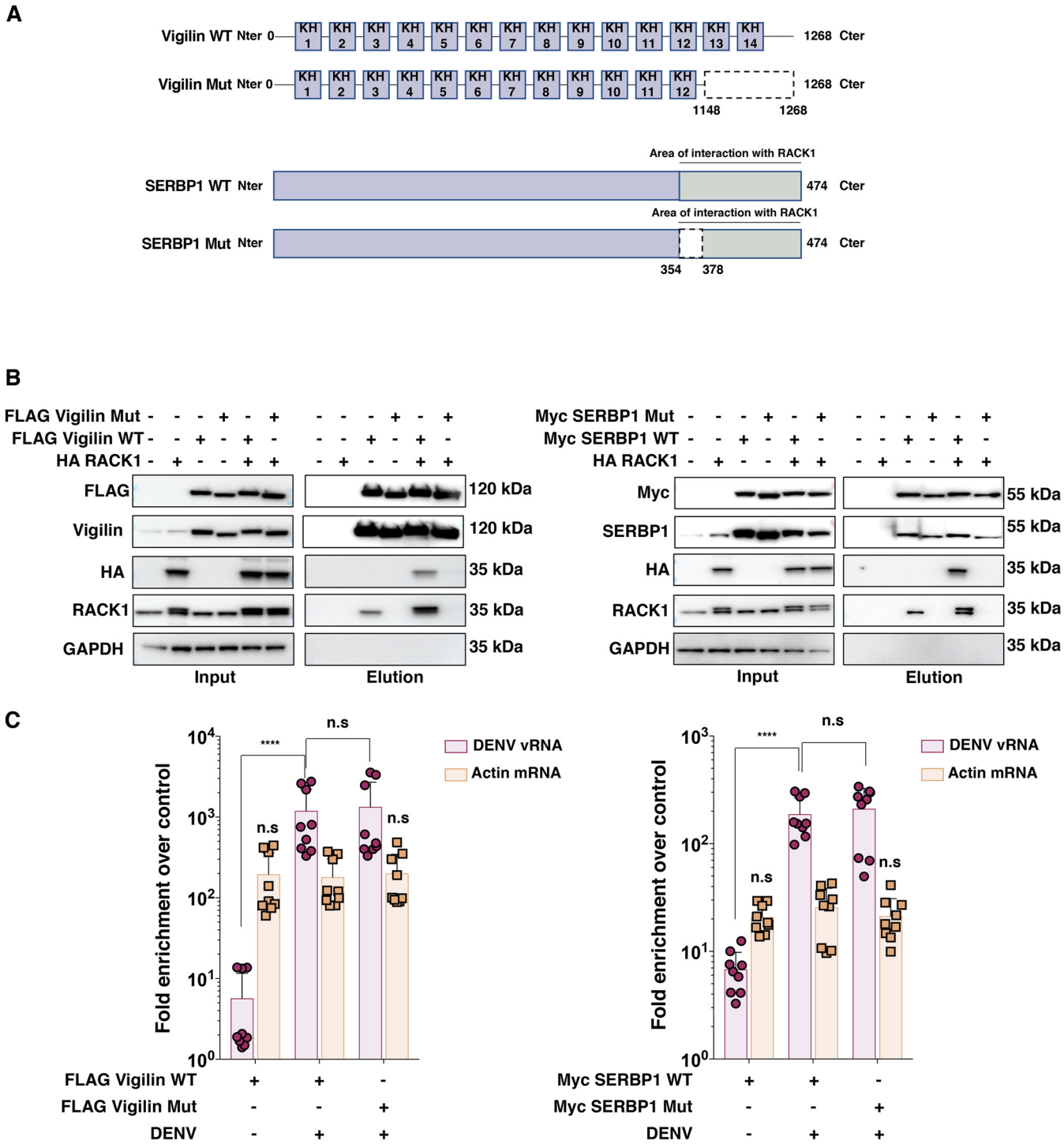

FIG 7 Characterization of Vigilin and SERBP1 mutants (Mut) deficient for RACK1 binding. (A) Schematic representations of Vigilin mutant (upper diagram) and SERBP1 mutant (lower diagram) constructs. (B) Evaluation of FLAG-Vigilin mutant (left) or Myc-SERBP1 mutant (right) interaction with RACK1. Cell extracts from 293T expressing the WT or mutated forms of Vigilin and SERBP1 were subjected to affinity purification using anti-FLAG- or -Myc-coated beads, respectively. Input and eluates were resolved by SDS-PAGE, and interacting proteins were revealed by Western blotting using corresponding antibodies. Shown is a representative Western blot of three independent experiments. (C) Analysis of Vigilin (WT and Mut) and SERBP1 (WT and Mut) interactions with the DENV RNA by RNA immunoprecipitation assay (RIP). The cells were infected at MOI 1 by DENV2-16681 and harvested 48 hpi. Tagged proteins were immunoprecipitated after UV cross-link at 254 nm using anti-FLAG- or -Myc-coated beads. The enrichment of DENV RNA or Actin RNA over the negative-control condition were determined by quantitative reverse transcription-PCR using specific primers and quantified using the ΔΔCt method. The data shown are the means ± SEM of three independent experiments performed in triplicate. Significance was calculated using a two-way ANOVA with Dunnett's multiple-comparison test. Cter, C terminus; Nter, N terminus; n.s, not significant; ****, $P < 0.0001$.

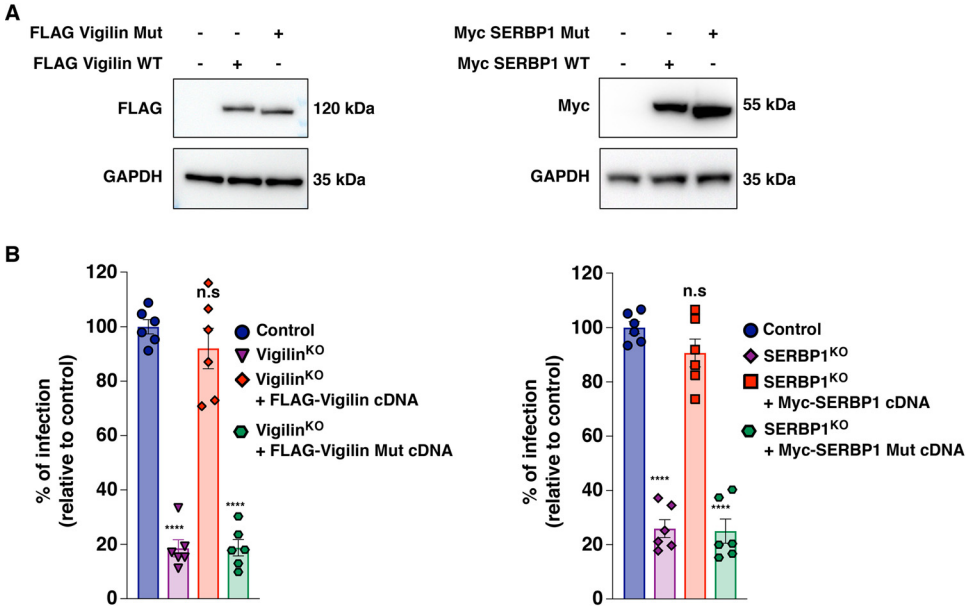

FIG 8 Vigilin and SERBP1 interaction with RACK1 is important in DENV infection. (A) Stable expression of Vigilin WT or Mut and SERBP1 WT or Mut in Vigilin ^{KO} or SERBP1 ^{KO} HAP1 cells, respectively. Western blot analysis of Vigilin or SERBP1 expression is shown. The data shown are representative of three independent experiments. (B) The indicated cells were infected at MOI 1 with DENV2-16681. Levels of infection were determined by flow cytometry at 48 hpi using the 2H2 MAb. The data shown are the means ± SEM of three technically independent experiments performed in duplicate. Significance was calculated using one-way ANOVA with Dunnett's multiple-comparison test. n.s, not significant; ****, $P < 0.0001$.

Vero E6 cells. For all of the viral stocks used in flow cytometry experiments, the viruses were purified through a 20% sucrose cushion by ultracentrifugation at 80,000 × *g* for 2 h at 4°C. The pellets were resuspended in HNE1X pH 7.4 (5 mM HEPES, 150 mM NaCl, 0.1 mM EDTA), aliquoted, and stored at −80°C. Viral stock titers were determined on Vero E6 cells by plaque-forming assay and were expressed as PFU/mL. Virus stocks were also determined by flow cytometry as described (54). Vero E6 cells were incubated 1 h with 100 μL of 10-fold serial dilutions of viral stocks. The inoculum was then replaced with 500 μL of culture medium, and the percentage of infected cells was quantified by flow cytometry using the 2H2 anti-PrM monoclonal antibody (MAb) at 8 h after infection. Viral titers were calculated and expressed as the number of fluorescence-activated cell sorter infectious units (FIU)/mL: titer = (average percentage of infection) × (number of cells in well) × (dilution factor)/(mL of inoculum added to cells).

To establish a DENV replicon plasmid, based on the infectious DENV2-16681 cDNA clone, the region encoding the structural proteins was mostly deleted and replaced by a cassette encoding ubiquitin-*Renilla* luciferase-foot-and-mouth disease virus (FMDV) 2A. DENV replicon RNA was generated as previously described (12). Infection or replication was determined by measuring the luciferase activity using TriStar LB942 microplate reader (Berthold Technologies). Red fluorescent protein (RFP)-expressing lentiviral vector pseudotyped with vesicular stomatitis virus glycoprotein G (VSV-G) were generated by transfecting HEK293FT cells with pNL4.3 Luc RFP ΔEnv, psPAX2, and pVSV-G (4:3:1 ratio) using Lipofectamine 3000. The ;Supernatants were harvested 48 h after transfection, cleared by centrifugation, filtered, and frozen at –80°C.

Polysome profiling. A total of 2 × 10^8 of indicated cells were incubated with 100 μg/mL of cycloheximide (CHX) for 10 min at 37°C and washed twice with cold phosphate-buffered saline (PBS) + 100 μg/mL CHX. The cells were pelleted by centrifugation at 4°C at 300 × *g* for 10 min and washed once with cold PBS + 100 μg/mL CHX. The pellet was resuspended in 2 mL lysis buffer (10 mM Tris-HCl, pH 7.5, 100 mM KCl, 10 mM magnesium acetate, 1% Triton X-100, 2 mM dithiothreitol [DTT]) containing 100 μg/mL CHX. The cells were pulverized by adding glass beads and vortexed for 5 min at 4°C. Cells debris were removed by centrifugation at 4°C at 3,000 × rpm for 10 min, and the supernatant was transferred to a 2 mL cryovial. The determination of polysome concentration was done by spectrophotometric estimation, based on the fact that ribosomes are ribonucleoprotein particles. Supernatant was quickly flash-frozen in liquid nitrogen and stored in a −80°C freezer. The supernatant was loaded on a 10 to 50% sucrose gradient (31% sucrose, 50 mM Tris-acetate, pH 7.6, 50 mM NH_4Cl, 12 mM $MgCl_2$, 1 mM DTT) and spun for 3 h at 39,000 rpm at 4°C in an SW41 swing-out rotor. The gradient was fractionated by hand and analyzed by immunoblotting.

Mass spectrometry analysis. HAP1 cells (5 × 10^8), expressing either the WT or the HA-tagged RACK1 proteins, were lysed in Pierce IP lysis buffer (Thermo Scientific) in the presence of Halt protease inhibitor cocktail (Thermo Scientific) for 30 min at 4°C and then cleared by centrifugation for 30 min at 6,000 × *g*. The supernatants were incubated overnight at 4°C with anti-HA magnetic beads. The beads

were washed three times with B015 buffer (20 mM Tris-HCl, pH 7.4, 150 mM NaCl, 5 mM $MgCl_2$, 10% glycerol, 0.5 mM EDTA, 0.05% Triton, 0.1% Tween 20), and the immune complexes were eluted twice with HA peptide (400 mg/mL) for 30 min at room temperature (RT). The eluates were concentrated on a Pierce concentrator (PES 10K) and stored at −20°C until used. A total of three coaffinity purifications and MS analysis experiments were performed with the HA-tagged RACK1 protein or the untagged RACK1 protein as a control in 293T cells. The samples were analyzed at Taplin Biological Mass Spectrometry Facility (Harvard Medical School). Briefly, concentrated eluates issued from immunopurification of endogenous and RACK1-HA-tagged protein were separated on 10% Tris-glycine SDS-PAGE gels (Invitrogen) and stained with Imperial Protein Stain (Thermo Fisher). Individual regions of the gel were cut into 1-mm^3 pieces and subjected to a modified in-gel trypsin digestion procedure (55). The peptides were desalted and subjected to a nanoscale reverse-phase high-performance liquid chromatography (HPLC) (56). Eluted peptides were then subjected to electrospray ionization and then tandem mass spectrometry (MS/MS) analysis into an LTQ Orbitrap Velos Pro ion-trap mass spectrometer (Thermo Fisher Scientific, Waltham, MA). The peptides were detected, isolated, and fragmented to produce a tandem mass spectrum of specific fragment ions for each peptide. The peptide sequences were determined by matching protein databases with the acquired fragmentation pattern by the Sequest software program (Thermo Fisher Scientific, Waltham, MA) (57). All databases include a reversed version of all the sequences, and the data were filtered to less than 2% peptide false discovery rate.

Network analysis. The AP-MS data set was analyzed with SAINTexpress and MIST software (37). Of the 1,671 proteins selected in our pipeline, 193 of 1,671 showed a probability score greater than 0.80 with SAINTexpress, and 135 of 193 showed an average peptide count greater than 10. This list of 135 host proteins was analyzed with DAVID 6.8 to identify statistical enrichments for specific GO terms from the cellular component (CC) annotation (38, 39). The interaction network was built using Cytoscape 3.4.0 (40), and the proteins were clustered into functional modules using enriched GO terms as a guideline and manual curation of literature.

Small interfering RNA (siRNA) screen assay. An arrayed ON-TARGETplus SMARTpool siRNA library targeting 49 of 135 proteins of our RACK1 network, which had an average peptide count great than 28, was purchased from Horizon Discovery. To this end, HeLa or 293T cells were transfected with a 30 nM final concentration of siRNA using the Lipofectamine RNAiMax (Life Technologies). 48 h posttransfection, the cells were infected with DENV2-16681 at MOI 5. Infection was quantified 48 h postinfection by flow cytometry and viability by CellTiter-Glo 2.0 assay (Promega). Two siRNA controls were included in the screen: a nontargeting siRNA used as a reference (siNT) and a siRNA targeting RACK1 (siRACK1) as a positive control for host-dependency factors (HDFs) (12). HDFs were defined as factors whose inhibition in both cell types decreases infection by at least 50% compared to siNT and viability by at most 20% of the siNT.

Gene editing and transcomplementation experiments. Single guide RNA (sgRNA) targeting Vigilin, SERBP1, and ZNF598 were designed using the CRISPOR software (58). Sequences for all the sgRNAs are listed in Table 1. The sgRNAs were cloned into the plasmid lentiCRISPR v2 (Addgene) according to the recommendations provided by the members of the Zhang's laboratory (Broad Institute, Cambridge, MA). HAP1 cells were transiently transfected with the plasmid expressing sgRNAs and selected with puromycin until all mock-transfected cells died. Clonal cell lines were isolated by limiting dilution and assessed by DNA sequencing and immunoblot for gene editing. The human HA-RACK1 WT and HA-RACK1 DE mutant plasmids were provided by Catherine Schuster (University of Strasbourg), the FLAG-tagged Vigilin cDNA was purchased from Genscript (clone OHu17734), and the Myc-tagged SERBP1 cDNA was purchased from Genscript (clone OHu26811C). After PCR, amplification products were cloned into a SpeI-NotI-digested (RACK1), NotI-XhoI-digested (Vigilin), or EcoRI-BamHI-digested (SERBP1) pLVX-IRES-ZsGreen1 vector. SERBP1 mutant and Vigilin mutant were obtained using the Q5 site-directed mutagenesis kit (E0554) (NEB) with deletion primers using the WT cDNA in pLVX as the template. All of the primers are listed in Table 1. Lentivirus-like particles for transduction were prepared in 293T cells by cotransfecting the plasmid of interest with psPAX2 (from N. Manel's lab, Curie Institute, Paris, France) and pCMV-VSV-G at a ratio of 4:3:1 with Lipofectamine 3000 (Thermo Fisher Scientific). The supernatants were collected 48 h after transfection, centrifuged (750 × *g*, 10 min), filtered using a 0.45-μm filter, and purified through a 20% sucrose cushion by ultracentrifugation (80,000 × *g* for 2 h at 4°C). The pellets were resuspended in HNE1X, pH 7.4, aliquoted, and stored at −80°C. Cells of interest were transduced by spinoculation (750 × *g* for 2 h at 32°C) and sorted for GFP-positive cells by flow cytometry if necessary.

Flow cytometry analysis. The indicated cells were plated in 24-well plates and infected. At indicated times, the cells were trypsinized and fixed with 2% paraformaldehyde (PFA) diluted in PBS for 15 min at room temperature. The cells were incubated for 1 h at 4°C with 1 μg/mL of 3E4 anti-E2 monoclonal antibody (CHIKV), 2H2 anti-prM monoclonal antibody (MAb) (DENV), or the anti-E protein MAb 4G2 (ZIKV). Antibodies were diluted in permeabilization flow cytometry buffer (PBS supplemented with 5% FBS, 0.5% saponin, 0.1% sodium azide). After washing, the cells were incubated with 1 μg/mL of Alexa Fluor 488- or 647-conjugated goat anti-mouse IgG diluted in permeabilization flow cytometry buffer for 30 min at 4°C. Acquisition was performed with an Attune NxT flow cytometer (Thermo Fisher Scientific), and the data were analyzed by FlowJo software (TreeStar).

Infectious virus yield assay. To assess the release of infectious particles during infection, the indicated cells were inoculated for 3 h with DENV2-16681, washed once with PBS, and maintained in the culture medium for 48 h. At the indicated time points, the supernatants were collected and kept at −80°C. Vero E6 cells were incubated with 3-fold serial dilutions of supernatant for 24 h, and prM expression was quantified by flow cytometry as previously described (54).

TABLE 1 Antibodies and reagents[a]

Reagent or resource	Source or sequence	Identifier
Antibodies		
Mouse anti-RACK1 (B-3)	Santa Cruz Biotechnology	sc-17754
Rabbit anti-HA tag (C29F4)	Cell Signaling	3724S
Mouse anti-β-tubulin (D-10)	Santa Cruz Biotechnology	sc-5274
Rabbit anti-Vigilin	Bethyl	A303-971A
Mouse anti-Vigilin (H-3)	Santa Cruz Biotechnology	sc-271523
Rabbit anti-ZNF598	Bethyl	A305-108A
Mouse anti-SERBP1 (1B9)	Santa Cruz Biotechnology	sc-100800
Rabbit anti-RPS3	Bethyl	A303-841A
Mouse anti-GAPDH (0411)	Santa Cruz Biotechnology	sc-47724
Mouse anti-dengue virus NS3 protein antibody	GeneTex	GTX629477
Rabbit anti-dengue virus envelope protein antibody	GeneTex	GTX127277
Rabbit anti-dengue virus prM protein antibody	GeneTex	GTX128093
Mouse anti-FLAG (M2)	Sigma-Aldrich	F1804
Mouse anti-Myc tag (9B11)	Cell Signaling	2276S
Polyclonal rabbit anti-mouse immunoglobulins/HRP	Agilent Technologies	P0260
Peroxidase AffiniPure donkey anti-rabbit IgG (H + L)	Jackson ImmunoResearch	711-035-152
Chemicals and reagents		
DMEM	Gibco	12440-053
IMDM	Gibco	41966-029
Paraformaldehyde (32%) aqueous solution	Electron Microscopy Sciences	15714
Lipofectamine RNAiMAX	Invitrogen	13778150
Lipofectamine 3000 transfection kit	Invitrogen	L3000-015
Halt protease and phosphatase inhibitor cocktail	Thermo Scientific	1861281
Bolt 4 to 12% Bis-Tris Plus gels	Invitrogen	NW04120BOX
Bolt 10% Bis-Tris Plus gel	Invitrogen	NW00100BOX
Tampon RIPA Pierce lysis buffer	Thermo Scientific	89900
20$\times$ Bolt MOPS SDS running buffer	Invitrogen	B0001
Pierce 1-Step transfer buffer	Thermo Scientific	84731
SuperSignal West Dura extended duration substrate	Thermo Scientific	34076
Maxima first-strand cDNA synthesis kit for reverse transcription-qPCR	Thermo Scientific	K1671
RNase H, recombinant	New England BioLabs	M0297S
TRIzol LS reagent	Ambion	10296010
RNeasy minikit	Qiagen	74106
Tampon RIPA Pierce lysis buffer	Thermo Scientific	87788
Q5 site-directed mutagenesis kit	NEB	E0554S
7-Deaza-2′-C-methyladenosine (MK0608, 50 μM final concn)	Biosynth Carbosynth	ND08351
Power SYBR Green PCR master mix	Life Technologies, Inc.	4367659
Critical commercial assay		
Pierce *Gaussia* luciferase glow assay kit	Thermo Scientific	16160
Renilla luciferase assay system	Promega	E2810
CellTiter-Glo 2.0 assay	Promega	G9242
Protein assay reagent A	Bio-Rad	500-0113
Protein assay reagent B	Bio-Rad	500-0114
Protein assay reagent S	Bio-Rad	500-0115
gRNA for CRISPR/Cas9 KO		
Control	GAGCTGGACGGCGACGTAAA	
Vigilin	GTTTTGCTGAACACCGAAGTGGGGGG	
SERBP1	AAGCCGGCGGGGGCGGCGTTGGG	
ZNF598	GGGGGCCGGATCCCGGACCATGG	
Plasmids		
pLentiCRISPRv2	Addgene	98290
pLentiCRISPRv2 sgRNA Vigilin	This paper	NA
pLentiCRISPRv2 sgRNA SERBP1	This paper	NA
pLentiCRISPRv2 sgRNA ZNF598	This paper	NA
pLVX-IRES-ZsGreen1	Takara	632187
pLVX-IRES-ZsGreen1 HA-RACK1 WT	This paper	NA
pLVX-IRES-ZsGreen1 HA-RACK1 D/E	This paper	NA
pLVX-IRES-ZsGreen1 FLAG-Vigilin	This paper	NA

(Continued on next page)

Structure et fonction de la protéine nsP3 du virus chikungunya et son impact sur la biologie des alphavirus

Les alphavirus, tels que le virus du chikungunya (CHIKV), constituent un groupe de virus à ARN simple brin de polarité positive, représentant un défi constant pour la médecine et la santé publique. Selon les symptômes provoqués, les alphavirus peuvent être regroupés en virus arthritogènes, conduisant à des atteintes articulaires et musculaires, et en virus encéphalitiques induisant des encéphalomyélites principalement chez les équidés. Le CHIKV est un virus arthritogène qui a réémergé en 2004 au Kenya et s'est rapidement propagé, provoquant de multiples épidémies dans le monde. Entre 2005 et 2006, plus de 30 % de la population de l'île de La Réunion a été infectée par le CHIKV. Depuis 2007, des cas autochtones ont été enregistrés dans le sud de l'Europe (Italie, France). À partir de 2013, le virus a atteint les Caraïbes et s'est propagé sur le continent américain. À ce jour, des cas de CHIKV ont été enregistrés dans plus de cent pays, totalisant plus de dix millions de cas. Chez l'homme, l'infection par le CHIKV est responsable de douleurs articulaires et musculaires invalidantes, pouvant persister de plusieurs semaines à plusieurs mois. À ce jour, les mécanismes précis menant à une persistance de la maladie liée à l'infection virale ne sont pas entièrement compris. Malgré des efforts considérables pour développer des traitements, aucun antiviral ou vaccin homologué n'existe. Comprendre les mécanismes fondamentaux régissant la réplication et le tropisme du CHIKV constitue donc une étape significative dans le développement de nouvelles stratégies antivirales et thérapeutiques.

Les alphavirus répliquent leur génome ARN simple brin dans le cytoplasme de la cellule infectée. Une étape cruciale du cycle de réplication est l'établissement de complexes réplicatifs viraux (CRv). Les CRv représentent des déformations viro-induites de la membrane plasmique appelées « sphérules ». Ces structures sont nécessaires à la réplication et à la transcription de l'ARN viral, et protègent l'intermédiaire réplicatif ARN double-brin des récepteurs de reconnaissance de motifs moléculaires pathogènes et de l'activation de la réponse cellulaire antivirale. L'établissement des CRv et la synthèse de l'ARN viral reposent sur l'activité synergique de quatre protéines non-structurales virales (nsP1 à nsP4). Les quatre protéines non-structurales sont exprimées à partir d'une seule polyprotéine, dont le clivage séquentiel en protéines individualisées détermine la maturation des CRv. La

protéine nsP1 est nécessaire à l'ancrage du complexe viral enzymatique à la membrane plasmique. De plus, cette protéine est nécessaire à la formation de la structure de la coiffe en 5' des ARN viraux synthétisés. La protéine nsP2 possède une activité hélicase et méthyltransférase, ainsi qu'une activité protéase servant au clivage des différentes protéines. La nsP4 possède l'activité ARN-polymérase ARN-dépendante. Enfin, la nsP3 est la plus énigmatique des protéines alphavirales. Elle est essentielle à la formation des CRv et à la synthèse de l'ARN, mais aussi à la neutralisation de la réponse antivirale cellulaire. Au cours de l'infection, la nsP3 est retrouvée à proximité des CRv mais aussi au sein de condensats protéiques cytoplasmiques de fonction inconnue. La nsP3 est organisée en trois domaines distincts, exerçant des fonctions spécifiques contribuant au cycle viral. Le macrodomaine (MD), codé par l'extrémité N-terminale de la protéine, possède une activité ADP-ribosylhydrolase permettant l'hydrolyse des résidus ADP-ribose de différents facteurs cellulaires. Cette activité sert au désassemblage des granules de stress qui sont des complexes ribonucléoprotéiques formés en réponse au stress cellulaire et jouant un rôle antiviral. Le domaine central unique des alphavirus (AUD) possède un motif en doigt de zinc et est essentiel au fonctionnement de la protéine ainsi qu'à la synthèse de l'ARN viral. Enfin, le domaine C-terminal hypervariable (HVD) est le plus étudié et aurait pour principale fonction celle d'une plateforme d'interaction recrutant de multiples facteurs cellulaires. Parmi ces facteurs, les protéines G3BP (Ras-GAP SH3 domain binding protein) participant à l'assemblage des granules de stress sont recrutées par le domaine HVD de CHIKV, ainsi que par d'autres alphavirus arthritogènes de l'ancien monde. Cette interaction est essentielle pour la viabilité de CHIKV. Plus récemment, notre laboratoire a identifié la protéine cellulaire FHL1 (Four-and-a-half LIM domain protein 1) comme un facteur spécifique important pour l'infection par CHIKV, ainsi que pour un autre alphavirus génétiquement proche, O'nyong-nyong (ONNV). FHL1 est une protéine majeure dans la réplication de CHIKV, participant à son tropisme pour le tissu musculaire et articulaire (cellules musculaires, fibroblastes), ainsi qu'à la pathogenèse liée à l'infection virale. Les mécanismes moléculaires précis par lesquels la protéine virale nsP3 ainsi que les facteurs cellulaires recrutés tels que FHL1 assurent la réplication virale et participent à la pathogénèse restent à déterminer.

L'objectif de cette thèse est donc de déterminer les mécanismes moléculaires mis en action par la nsP3 du CHIKV, afin d'assurer la mise en place des complexes de réplication et le bon déroulement du cycle infectieux. La première partie de ce travail de thèse tente de décrypter la structure et la fonction de la nsP3 du virus chikungunya au cours de son cycle réplicatif. Ce travail collaboratif effectué avec l'équipe du Dr Juan Reguera (Viral Macromolecular Complexes team, AFMB, Marseille, France) et Dr Michael Hons (EMBL) nous a permis de caractériser pour la première fois la structure de la nsP3 de CHIKV en cryo-microscopie électronique à une résolution de 2,35 Å. Nous avons démontré que la nsP3 possède la capacité intrinsèque à oligomériser en structures tubulaires et que cette fonction est assurée par le domaine AUD. La pertinence de ces oligomères a été validée dans le contexte infectieux ou par expression ectopique de la protéine seule dans différentes lignées cellulaires. En combinant des techniques d'imagerie en microscopie confocale et électronique, nous avons identifié que la nsP3 est recrutée sur les sites réplicatifs au niveau de la membrane cellulaire dès les étapes précoces du cycle viral. Dans les étapes tardives, la nsP3 s'autoassemble en structures tubulaires cytoplasmiques, formant un réseau en « nid d'abeilles ». Ces structures contiennent aussi les interactants majeurs de la nsP3 comme FHL1 et G3BP, ainsi que la protéine virale capside. Par des techniques d'hybridation fluorescente in situ, nous avons aussi identifié la présence d'ARN génomique viral. La double localisation de la nsP3, ainsi que la présence de génome viral et de la protéine capside, suggèrent que les oligomères de nsP3 peuvent être à la fois impliqués dans les complexes de réplication, ainsi que dans des étapes post-réplicatives telles que le transport du génome viral au site d'assemblage de la nucléocapside.

Enfin, sur la base des études structurales réalisées, nous avons identifié des résidus impliqués dans des interactions axiales et latérales entre différents domaines AUD. Leur mutagenèse conduit à la déstructuration ou à l'inhibition complète de l'oligomérisation in vivo et in situ. Nous avons montré que l'oligomérisation tubulaire de nsP3 est une caractéristique des alphavirus et détermine l'activité virale de la protéine. La perturbation ou l'inhibition complète de la polymérisation de nsP3 affecte négativement la formation des complexes de réplication, la synthèse de l'ARN et la production de particules infectieuses. En plus d'une réduction de la synthèse de protéines virales structurales, l'inhibition de la formation des oligomères de nsP3

induit aussi un changement de la localisation subcellulaire de la protéine capside. Les données suggèrent que ces structures seraient aussi impliquées dans les étapes tardives du cycle de réplication. Différentes hypothèses restent à exploiter quant aux rôles tardifs de ces structures : régulation de l'environnement cellulaire pour assurer la traduction de nouvelles protéines structurales, l'assemblage de la nucléoprotéine ou l'inhibition de l'immunité cellulaire antivirale. Enfin, une étude approfondie de la persistance de ces structures au sein des tissus musculaires et articulaires infectés par CHIKV, pourrait contribuer à la compréhension de la pathogénèse chronique liée à l'infection virale.

Dans un précédent travail publié par notre équipe (Meertens et al. 2019), nous avions identifié FHL1 par un crible génomique CRISPR/Cas9. Cette protéine cellulaire, abondamment exprimée dans les tissus musculaires par les cellules musculaires et fibroblastes, est un facteur déterminant le tropisme, la réplication et le développement de la pathologie liée au CHIKV dans les cellules humaines (lignées et cellules musculaires primaires) et chez le modèle murin. De manière intéressante, FHL1 est spécifiquement utilisée par CHIKV et ONNV, qui est phylogénétiquement le plus proche du CHIKV. En utilisant différents outils moléculaires, nous avons établi que FHL1 n'est pas impliquée dans l'entrée du virus dans la cellule cible, mais est nécessaire à la synthèse de l'intermédiaire de réplication ARN double-brin. Par quels mécanismes cette protéine cellulaire participe à la réplication du CHIKV et à sa propagation, n'est pas connu.

La deuxième partie de ce travail de thèse vise donc à aborder l'importance de l'interaction de nsP3 avec FHL1, et à apporter de nouvelles informations concernant les mécanismes moléculaires mis à l'œuvre au cours de la réplication virale. Tout d'abord, un travail collaboratif mené avec l'équipe de Virologie Structurale du Professeur Félix Rey a identifié la région précise du HVD de nsP3 interagissant avec FHL1. Cette région d'interaction contient aussi des motifs permettant le recrutement d'autres facteurs cellulaires connus, comme Bin1 ou CD2AP. Des études fonctionnelles impliquant un CHIKV délété de cette région du HVD, démontrent l'importance de celle-ci dans la réplication du CHIKV. Nos données ont également montré que FHL1 est recrutée de manière cellule- et hôte-spécifique lors de l'infection par CHIKV. De plus, nous avons découvert que toutes les souches de CHIKV dépendent de FHL1, en particulier la souche isolée au cours de l'épidémie de

l'Île de La Réunion. Celle-ci est associée à une pathologie musculaire plus sévère, en comparaison avec la souche sylvatique isolée chez le moustique Aedes furcifer.

Enfin, des études mécanistiques préliminaires ont indiqué que FHL1 facilite la réplication du CHIKV. De manière intéressante, l'utilisation d'outils moléculaires tels que de petits génomes autoréplicatifs, autrement appelés systèmes réplicons, montre que l'amplification du génome viral peut avoir lieu dans les cellules déficientes pour FHL1 mais pas dans les cellules déplétées de G3BP1 et G3BP2. De plus, des techniques d'imagerie par microscopie confocale sur des cellules infectées par le CHIKV montrent la colocalisation des CRv avec les protéines G3BP mais échouent à montrer la même colocalisation avec FHL1 dans les étapes précoces de la réplication. Ces résultats suggèrent que FHL1 ne serait pas directement impliqué dans la synthèse de l'ARN viral mais agirait de manière indirecte. L'absence d'activité enzymatique propre et la structure en quatre domaines LIM de FHL1 suggèrent que celle-ci pourrait être une protéine d'échafaudage, permettant l'interaction de la nsP3 avec d'autres facteurs cellulaires impliqués dans la mise en place d'une infection virale productive. Plus tardivement dans le cycle, FHL1 est recruté au sein des structures tubulaires formées par la nsP3, mais ne participe pas directement à leur formation. Le rôle de FHL1 au sein de ces structures n'est pas encore établi. Pour répondre à cette question, nous avons tenté d'établir l'interactome de FHL1 en présence ou en absence d'infection virale. Les résultats obtenus corroborent les données de la littérature, montrant que FHL1 interagit avec des protéines du cytosquelette d'actine, des spectrines ainsi que des myosines. L'inhibition de l'expression de certains de ces facteurs, notamment les spectrines bêta, par de petits ARN interférents (siRNA), montre un effet délétère sur l'infection virale.

Dans l'ensemble, les données présentées dans ce travail de thèse démontrent la polyvalence structurelle et fonctionnelle de la nsP3 des alphavirus, faisant d'elle une cible majeure d'intérêt pour le développement de nouvelles thérapeutiques antivirales.

Mots-clés : Chikungunya, alphavirus, nsP3, compléxes de réplication, facteurs cellulaires, FHL1